Transition Metal Catalyzed Polymerization of Olefins and Depolymerization of Polyolefins

by

Birajdar Rajkumar Swaminath

10CC19J26014

A thesis submitted to the

Academy of Scientific & Innovative Research

for the award of the degree of

DOCTOR OF PHILOSOPHY

in

SCIENCE

Under the supervision of

Dr. Samir H. Chikkali (Supervisor),

Dr. Ashootosh V. Ambade (Co-Supervisor)

Academy of Scientific and Innovative Research

AcSIR Headquarters, CSIR-HRDC campus

Sector 19, Kamla Nehru Nagar,

Ghaziabad, U.P. – 201 002, India

May 2024

Certificate

This is to certify that the work incorporated in this Ph.D. thesis entitled, "**Transition Metal Catalyzed Polymerization of Olefins and Depolymerization of Polyolefins**", submitted by **Birajdar Rajkumar Swaminath** to the Academy of Scientific and Innovative Research (AcSIR) in fulfillment of the requirements for the award of the Degree of **Doctor of Philosophy in Science**, embodies original research work carried-out by the student. We, further certify that this work has not been submitted to any other University or Institution in part or full for the award of any degree or diploma. Research material(s) obtained from other source(s) and used in this research work has/have been duly acknowledged in the thesis. Image(s), illustration(s), figure(s), table(s) etc., used in the thesis from other source(s), have also been duly cited and acknowledged.

(Signature of Student)	(Signature of Co-Supervisor)	(Signature of Supervisor)
Rajkumar S. Birajdar	**Dr. Ashootosh V. Ambade**	**Dr. Samir H. Chikkali**
Date: 29-05-2024	Date: 29-05-2024	Date: 29-05-2024

STATEMENTS OF ACADEMIC INTEGRITY

I **Birajdar Rajkumar Swaminath**, a Ph.D. student of the Academy of Scientific and Innovative Research (AcSIR) with Registration No. **10CC19J26014** hereby undertake that, the thesis entitled "**Transition Metal Catalyzed Polymerization of Olefins and Depolymerization of Polyolefins**" has been prepared by me and that the document reports original work carried out by me and is free of any plagiarism in compliance with the UGC Regulations on *"Promotion of Academic Integrity and Prevention of Plagiarism in Higher Educational Institutions (2018)"* and the CSIR Guidelines for "*Ethics in Research and in Governance (2020)".*

Signature of the Student
Date : 29-05-2024
Place : Pune

It is hereby certified that the work done by the student, under my/our supervision, is plagiarism-free in accordance with the UGC Regulations on *"Promotion of Academic Integrity and Prevention of Plagiarism in Higher Educational Institutions (2018)"* and the CSIR Guidelines for "*Ethics in Research and in Governance (2020)".*

Signature of the Co-supervisor
Name : Dr. Ashootosh V. Ambade
Date : 29-05-2024
Place : Pune

Signature of the Supervisor
Name : Dr. Samir H. Chikkali
Date : 29-05-2024
Place : Pune

Dedicated to

My Father

The Late Swaminath D. Birajdar

Acknowledgements

This thesis brings together all my work from the past five years at the Polyolefin Laboratory at CSIR-NCL. Many people have greatly supported me throughout my Ph.D. journey. I want to take this chance to thank all of them.

First and foremost, I would like to express my enormous gratitude to my research supervisor, Dr. Samir H. Chikkali, for his valuable guidance and scholarly input. His enthusiasm, encouragement, and faith in me have been extremely helpful throughout this journey. My sincere regards and reverence for him will remain forever, as he has moulded me into a competent researcher. I am deeply thankful to him for giving me the opportunity to work under his invaluable guidance. Our discussions have always been fruitful, allowing me the freedom to plan and execute my research ideas without pressure. The disciplines he has imparted to me are lessons I will carry throughout my life.

I would also like to thank my co-supervisor, Dr. Ashootosh V. Ambade for his advice, guidance, supports and encouragements during every stage of this research work. I would also like to thank Dr. Anu Raghunathan, Dr. Sakya Sen and Dr. S.Kiran for being my doctoral advisory committee (DAC) members and providing me valuable suggestions during the DAC meetings.

I am grateful to Dr. Ashish Lele, Director, CSIR-NCL, Prof. A. K. Nangia, (Former Director, NCL), Dr. Suresh Bhat, HoD, PSE Division, and Dr. Asha S. K., (Former HoD, PSE Division) for giving me this opportunity and providing all necessary infrastructure and facilities. I also acknowledge the DST-INSPIRE for the financial support in terms of junior and senior research fellowships.

I would like to thank all my Seniors Dr. Vijay Koshti, Dr. Shahaji Gaikwad, Dr. Ketan Patel, Dr. Swechcha pandey, Bhausaheb Rajput, Dr. Satej Deshmukh, Dr. Nilesh Mote, Dr. Shailaja Jawoor, Dr. Sandip Pawal, Dr. Ravi Gote, Dr. Anirban Sen, Dnyaneshwar Bodkhe, Rohit Kumar, Amol Chandanshive, Kishor Khopade, and Tanuja Tewari for their valuable scientific advice and help in lab practices which I greatly acknowledge and other lab colleagues Poonam Gupta, Manisha Singh, Suhas Parit, Dr. Neha Kathewad, Dr. Palash Banerjee, Dr. Raghuvendra Rangappa, Maulali Shaikh, Nikhita Rajput, Rohan Ramekar and Uday Paulbudhe for keeping

healthy environment in the lab and for their valuable scientific discussions. A special thanks to Tanuja, Dnyaneshwar, Kishor and Amol for their encouragement, scientific discussions, help, and unwavering support throughout my Ph.D.

I extend my thanks to our collaborators Dr. Rajesh Gonnade and his group for single crystal XRD analysis, Dinesh Shinde, Satish Pandole and Meghna for the suggestions with NMR measurements. Also I am thankful to Dr. Harshawardhan V. Pol and his research group for the fruitful collaboration. A special thanks to Dnyaneshwar Bodkhe and Poorvi Purohit for the GPC measurement and data analysis. I would also like to thank Mrs. B. Santhakumari, for HRMS analysis, Dr. Sapna Ravindranathan, Dr. Ajit Kumar and Dr. Uday Kiran for NMR facilities.

Also, I am thankful to Dr. Punji and his group members Dr. Shrikant, Dr. Hanumanprasad, Dr. Vineeta, Dr. Ulhas, Dr. Dilip, Dr. Rahul Jagtap, Dr. Dipesh, Dr. Sidhheshwar, Anand, Sadhana, Suryadev, Dr. Vijaykumar and Shana, for their time and cooperation. Also I would like to thank research trainee's of the polyolefin lab Abhijit, Yash, Shafi, Aakansha and Pradip for their cooperation.

My sincere thanks to the people in various parts of the institute, AcSIR and SAC office staff for their cooperation. I would also like to acknowledge all the staff members of X-ray single crystal analysis, NMR, Mass spectroscopy, Microanalysis, IR, Library, Administration and technical divisions of NCL for their assistance during the course of my work.

A special thanks goes to all my friends from CSIR-NCL for the cherished friendships and creating wonderful atmosphere around me outside the lab. I would like to extend my gratitude to all my friends who have supported me from postgraduation to my Ph.D. Special thanks to Akash, Parshuram, Vishal, Anand, Gaurishankar and Laxmikant for their invaluable help. Further, I would like to thank my college friends for always being there for me.

My family is always source of inspiration and great moral support for me in perceiving my education, I am thankful to God for having me such a supportive family. The words are insufficient to express my gratitude towards my family. I would like to take this opportunity to express my gratitude to my parents, the late Swaminath Birajdar and Surekha Birajdar, for their immense love, sacrifice, blessings, unconditional support, and encouragement. I express my deep and

paramount gratitude to my brothers and sisters Sachin, Iranna, Laxmi, Vikas, Ajay, Pallavi, Payal, Akshay and Saksham who stood up behind me throughout my Ph.D. career and became my strong moral support. Without their constant support and encouragement, I could not stand with this dissertation. I extend my deepest gratitude to my one-year-old nephew, Satvik, whose innocent laughter and pure spirit have brought immense joy, love, and comfort while writing this thesis. I would also like to thank my fiancé, Radhika, for her care and understanding. I would also like to show my deep gratitude to my relatives.

Above all, I owe it all to Almighty God for granting me the wisdom, health and strength to undertake this research task and enabling me to its completion.

Rajkumar…

Table of content

ABBREVIATIONS

aq	Aqueous
BF_4	Tetrafluoroborate
$B(C_6F_5)_3$	Tris(pentafluorophenyl)borane
$Ni(COD)_2$	Bis(cyclooctadiene)nickel(0)
CCDC	Cambridge Crystallographic Data Centre
$CDCl_3$	Deuterated chloroform
cm	Centimeter
conv	Conversion
CSD	Cambridge Structural Database
d	Doublet
Da	Dalton
DCM	Dichloromethane
DEPT	Distortionless enhancement by polarization transfer
DFT	Density functional theory
DMF	Dimethylformamide
DMSO	Dimethyl sulfoxide
DSC	Differential scanning calorimeter
eq	Equivalent
ESI-MS	Electro-Spray Ionization Mass-Spectroscopic
Et_2O	Diethylether
EtOH	Ethanol
EtOAc	Ethyl acetate
etc	et cetera
Fig.	Figure
FTIR	Fourier-transform infrared spectroscopy
g	Grams
GC	Gas chromatography
HCl	Hydrochloric acid
hr	Hour
Hz	Hertz
K_2CO_3	Potassium carbonate

LN_2	Liquid nitrogen
m	Multiplet
M^+	Molecular ion
MeOH	Methanol
mg	Milligrams
$MgSO_4$	Magnesium sulfate
MHz	Megahertz
min	Minutes
mL	Milliliter
mmol	Millimole
NaOAc	Sodium acetate
n-BuLi	n-Butyllithium
Na_2SO_4	Sodium sulfate
NEt_3	Triethyl amine
NMR	Nuclear Magnetic Resonance
PPh_3	Triphenylphosphine
Py	Pyridine
q	Quartet
RT(rt)	Room temperature
Rt	Retention time
Rf	Retention factor
br	Broad
s	Singlet
t	Triplet
TMEDA	Tetramethylethylenediamine
THF	Tetrahydrofuran
TLC	Thin layer chromatography
GPC	Gel Permeation Chromatography
WAXD	Wide-angle X-ray diffraction
TOF	Turnover frequency
TON	Turnover number

SYNOPSIS

Transition Metal Catalyzed Polymerization of Olefins and Depolymerization of Polyolefins

Synopsis of the Thesis to be submitted to the Academy of Scientific and Innovative Research for Award of the Degree of Doctor of Philosophy in Chemistry	
Name of the Candidate	Rajkumar S. Birajdar
Degree Enrolment No. & Date	Ph.D. in Chemical Sciences (10CC19J26014); January-2019
Title of the Thesis	**Transition Metal Catalyzed Polymerization of Olefins and Depolymerization of Polyolefins**
Research Supervisor	Dr. Samir H. Chikkali
Research Co-Supervisor	Dr. Ashootosh V. Ambade

1. Introduction:

The thesis titled "*Transition Metal Catalyzed Polymerization of Olefins and Depolymerization of Polyolefins*" comprises six distinct chapters. **Chapter 1** provides detailed literature review on olefin polymerization using various late transition metal-based catalysts. It emphasizes the important role of ligands to control parameters such as molecular weight, branching, and crystallinity.[1,2,3] Additionally, we reviewed the issue of substantial waste generation due to the large-scale production of polyolefins, underscoring the importance of depolymerization and recyclability. **Chapter 1** thus sets the objectives and defines ligands and metal complexes synthesis for olefin polymerization, along with the synthesis of chemically recyclable polyethylene. **Chapter-2** deals with the synthesis and characterization of a naphthoxy imine ligands and its corresponding neutral palladium catalysts. These catalyst were utilized in ethylene oligomerization, and post-functionalization of these results into hyperbranched functional ethylene oligomers. These hyperbranched oligomers were then employed as compatibilizers for Nylon-6 and LLDPE.[4] **Chapter-3** describes the synthesis and characterization of sterically tuned naphthoxy imine ligated neutral nickel complexes.[5] It highlights the performance differences between sterically more crowded Ni3 catalysts and less crowded counterparts in terms of activity and molecular weight. Furthermore, the complex with higher steric hindrance yields lower branching and produces linear polyethylene, resulting in a highly crystalline polymer. **Chapter 4** describes the synthesis and characterization of electronically tuned four imine phenoxy-ligated palladium complexes. The ligand with pentafluoro substituents forms a more electron-deficient metal center, whereas the 2,4,6-trimethoxy substituted ligand results in an electron-rich palladium, as confirmed by NMR and

Rajkumar S. Birajdar **Dr. Samir H. Chikkali** **Dr. Ashootosh V. Ambade**

XRD analyses. These complexes were utilized to produce polynorbornene through insertion polymerization, even at ambient temperature, both without and with cocatalysts [$B(C_6F_5)_3$, Trityl tetrakis(pentafluorophenyl)borate, MMAO]. **Chapter 5** delves into the synthesis and characterization of chemically recyclable polyethylene-like materials. These polymers are synthesized via ADMET and condensation polymerization, incorporating in-chain olefin and ester groups along with long hydrophobic methylene groups. **Chapter-6** concludes the work and provides future direction.

2. Methodology and Results

Chapter-2 Palladium-catalyzed polar solvent empowered synthesis of hyper-branched ethylene oligomers and their applications.

Synthesis of low-molecular weight (M_w) ethylene oligomers with hyperbranched microstructures is very difficult to achieve using a traditional Ziegler-Natta catalyst. Such hyperbranched ethylene oligomers can be used as functional additives in lubricants, surface treatments, compatibilizers, waxes, etc. For producing hyperbranched ethylene oligomers, the choice of catalysts is decisive. Catalysts with significant chain walking abilities can produce highly branched structures.[6,7]

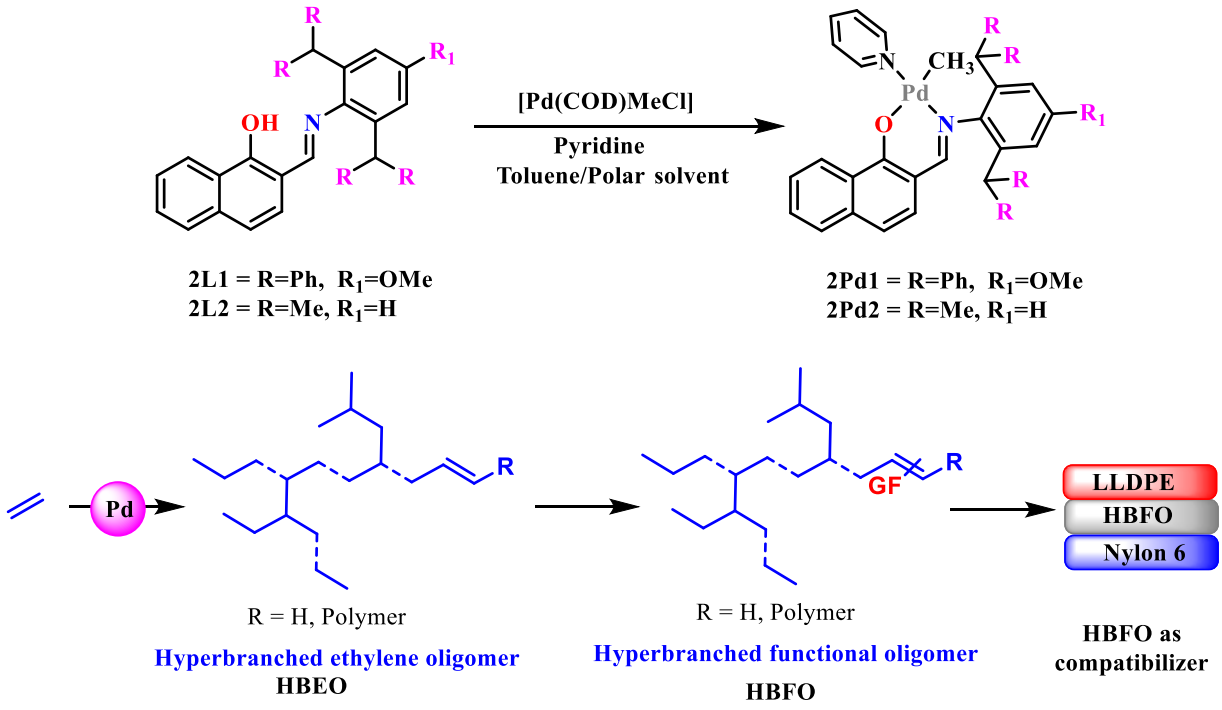

Rajkumar S. Birajdar Dr. Samir H. Chikkali Dr. Ashootosh V. Ambade

In this chapter, we report the synthesis of two naphthoxy imine ligands, 2-(((2,6-dibenzhydryl-4-methoxyphenyl)imino)methyl)naphthalen-1-ol (**2L1**) and 2-(((2,6-diisopropylphenyl)imino)methyl)naphthalen-1-ol (**2L2**), with different steric and electronic features. **2L1** and **2L2** were treated with [(TMEDA)$PdMe_2$] to obtain the corresponding neutral palladium(II) complexes **2Pd1** and **2Pd2** in excellent yields. The identity of **2Pd1** and **2Pd2** was unambiguously ascertained using a combination of spectroscopic and analytical methods, including single-crystal X-ray diffraction. When exposed to 5 bar ethylene pressure, **2Pd1** produced hyperbranched ethylene oligomers. The microstructure analysis of ethylene oligomers confirmed the existence of methyl, ethyl, propyl, and sec-butyl branches, with a molecular weight (M_n) of 500–1400 g mol^{-1}, a PDI of 1.46–2.10, and 67–106 branches per 1000 carbon atoms. The use of a polar solvent, tetrahydrofuran, led to a remarkable 3-fold increase in oligomerization activity without compromising the branching and molecular weight. The resultant hyperbranched ethylene oligomers were selectively monofunctionalized using industrially practiced hydroformylation, ozonolysis, and epoxidation, almost quantitatively. The hydroxy functionalized ethylene oligomer (**F4**) (5 wt%) was melt-compounded with LLDPE and Nylon-6 to produce a tough yet flexible blend with a higher strain-to-failure as compared to an uncompatibilized blend.

Chapter-3 Regulating the polyethylene microstructure by increasing steric crowding in naphthoxy imine-ligated Ni(II) complexes.

LDPE, LLDPE, and HDPE are commonly used polymers in everyday life, produced industrially. These polymers vary in their microstructure, including branching and molecular weight, distinguishing them from one another. Controlling these aspects is crucial for achieving desired polymer properties.

Ligands play a prominent role in ethylene polymerization. However, it is a highly challenging task to regulate branching and molecular weight through ligand modifications. In this chapter we report the synthesis of systematically sterically tailored naphthoxy imine-ligated nickel complexes (**Ni1, Ni2,** and **Ni3**), their performance in ethylene polymerization, and how the ligand steric controls branching in the resultant PE. **Ni1–Ni3** were prepared in one step with an excellent yield (73–93%). The identity of these complexes was unambiguously ascertained using ^{1}H, ^{13}C, 2D NMR spectroscopy, mass analysis, and single-crystal X-ray diffraction. The molecular structure revealed a cis arrangement of alkyl/aryl and donor groups (C–Ni–D), which is necessary for initiating ethylene polymerization.

Rajkumar S. Birajdar **Dr. Samir H. Chikkali** **Dr. Ashootosh V. Ambade**

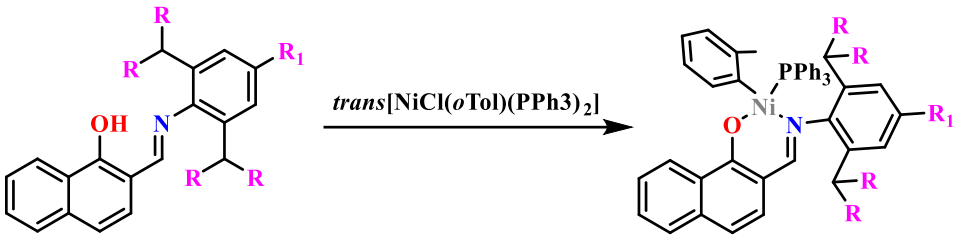

3L1 = R=H, R_1=Me
2L2 = R=Me, R_1=H
2L1 = R=Ph, R_1=OMe

Ni1 = R=H, R_1=Me
Ni2 = R=Me, R_1=H
Ni3 = R=Ph, R_1=OMe

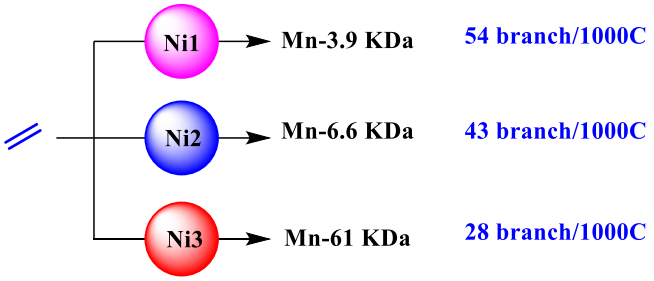

Buried volume contours suggested Ni3 to be sterically the most bulky among the three. When exposed to ethylene, the three nickel complexes **Ni1, Ni2,** and **Ni3** produced polyethylene with excellent activity. As predicted by buried volume calculations, dibenzhydryl-substituted **Ni3** outperformed sterically less crowded **Ni1** and **Ni2**. Careful analysis of the resultant PE disclosed that sterically less encumbered **Ni1** and **Ni2** produce PE with high branching (43–54 branches/1000-C atoms) density. However, the bulkiest **Ni3** revealed much lower branching (28 branches/1000-C atoms) and a high TOF of 35400 mol of PE per mol of Ni per h, along with a high molecular weight of PE (61000 Da). The steric bulk in Ni3, most likely, reduces chain-walking and thus lowers branching in the resultant PE. As compared to the literature-reported analogous Pd1 catalyst, the Ni3 catalyst discloses high TOF, high molecular weight, and less branched, linear polyethylene.

Chapter-4 Norbornene polymerization catalyzed by imine-phenoxy ligated palladium complexes.

Vinyl addition norbornene polymer (PNB) stands as a notable class of specialty polymers renowned for its remarkable optical and mechanical properties, including a high glass transition temperature, exceptional optical transparency, and low dielectric constant, rendering it highly attractive for a diverse range of industrial applications.[8] Metal complexes have been successfully used as pre-catalysts for the polymerization of norbornene, and can be divided into early and late transition metal catalysts.[9,] Nickel and palladium catalysts were studied for NB polymerization; however, these catalyst systems require hundreds or even thousands of

equivalents of the MAO/MMAO cocatalyst to exhibit any activity in NB homopolymerization. Hence, developing a palladium catalyst is highly sought after to improve polymerization efficiency, reduce cocatalyst ratios, and eliminate the need for highly pyrophoric aluminum alkyls.

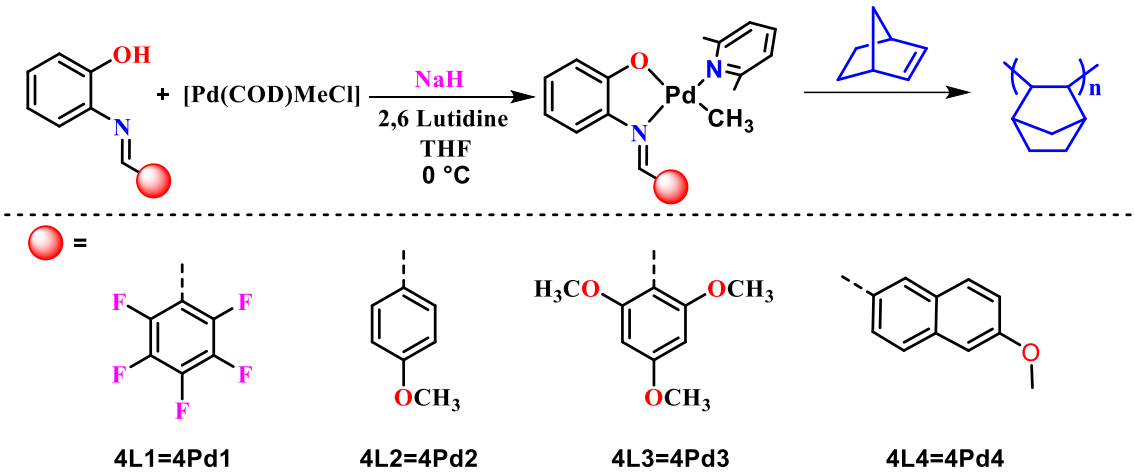

In this chapter, we present the synthesis of imine phenoxy ligands via condensation reactions between 2-aminophenol and electronically tuned aniline derivatives. These ligands were treated with [Pd(COD)MeCl] and 2,6-lutidine, resulting in the formation of **4Pd1-4Pd4** complexes in a single step with excellent yields. Characterization and confirmation of these complexes were achieved through NMR, mass analysis, and single-crystal X-ray diffraction. The square planar geometry around the palladium was observed in these complexes **(4Pd1-4Pd4)**. Molecular arrangement analysis revealed the crucial cis configuration between the methyl group of palladium and 2,6-lutidine, essential for insertion polymerization. Proton NMR and X-ray data analysis of **4Pd1** indicated deshielding, suggesting electronically deficient palladium metal compared to other complexes. Buried volume contours suggested **4Pd1** to be sterically the most bulky among the four metal complexes. When these palladium catalyst were exposed to norbornene, they produced polynorbornene (PNB) with trace amount and low activity. Furthermore, these complexes, in combination with the cocatalyst $B(C_6F_5)_3$, Trityl tetrakis(pentafluorophenyl)borate and MMAO, produces the polynorbornene with high catalytic activity. The combination of **4Pd1** and 25 equivalent of Trityl tetrakis(pentafluorophenyl)borate exhibited high catalytic activity and >99% conversion to PNB.

Rajkumar S. Birajdar Dr. Samir H. Chikkali Dr. Ashootosh V. Ambade

Chapter-5 Depolymerization and repolymerization of polyethylene-like polymers.

Polyolefins, a prominent class of synthetic polymers, have garnered widespread attention due to their exceptional versatility, durability, and cost-effectiveness. The substantial utilization of polyolefins leads to a significant amount of waste generation. Therefore, it is crucial to prioritize the depolymerization and recyclability of polyolefins. In polyethylene, the absence of functional groups makes it challenging to degrade or depolymerize. Polyolefins featuring unsaturation in their backbone are desired for the production of chemically recyclable polymers or chain end functionalized polyolefin macromonomers.

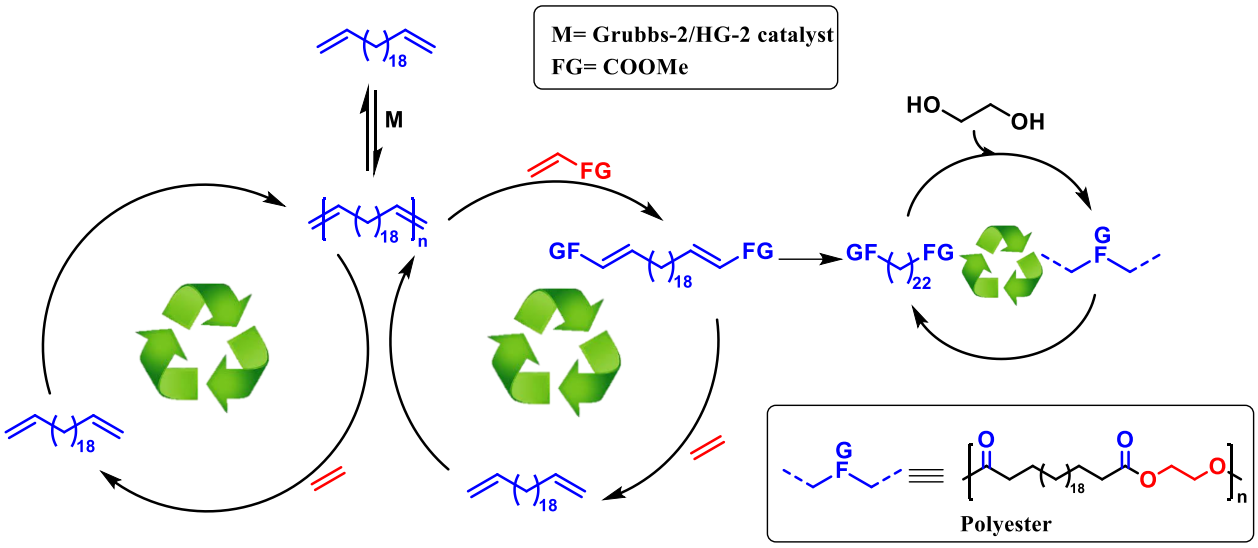

In this chapter we demonstrate a sustainable paradigm shift in polymer science, embodying the principles of a circular economy. This chapter outlines the synthesis of docosa-1,21-diene monomer, which is subsequently polymerized into a polymer (P1) through ADMET polymerization, resulting in a molecular weight (M_w) of up to 18 kDa. Analysis through DSC, TGA and WAXS shows data closely resembling to commercial polyethylene. Furthermore, in depolymerization experiments, exposure of the synthesized polymer (P1) to ethylene with HG-2 catalyst effectively converts the polymer back into its original monomer, and oligomers. Obtained monomers and oligomers are repolymerized to its parent polymer (P1) to achieve a closed loop system. The versatility of this research is underscored by the generation of a functionalized monomer through depolymerisation of polymer (P1) with acrylates. The functionalized monomer takes center stage as it undergoes a transformative process, culminating in the synthesis of a polyester with polyethylene-like material (P2). In the spirit of a circular economy, the study delves into the depolymerization and subsequent repolymerization of the polyester, demonstrating a closed-loop system.

Rajkumar S. Birajdar **Dr. Samir H. Chikkali** **Dr. Ashootosh V. Ambade**

3. Conclusions and outlook

In conclusion, naphthoxy imine-ligated palladium and nickel complexes were synthesized with excellent yields. The palladium complexes produced hyperbranched polyethylene in hydrocarbon solvents, with a significant increase in activity in polar solvents. These hyperbranched polymers were post-functionalized and utilized as compatibilizers for LLDPE and Nylon-6. The corresponding nickel complexes produced high molecular weight branched polyethylene. The less sterically hindered **Ni1** and **Ni2** catalysts produced branched polyethylene with molecular weights of up to 6.6 kDa, whereas the dibenzhydryl-substituted, sterically hindered **Ni3** catalyst produced high molecular weight linear polyethylene (up to 114 kDa).

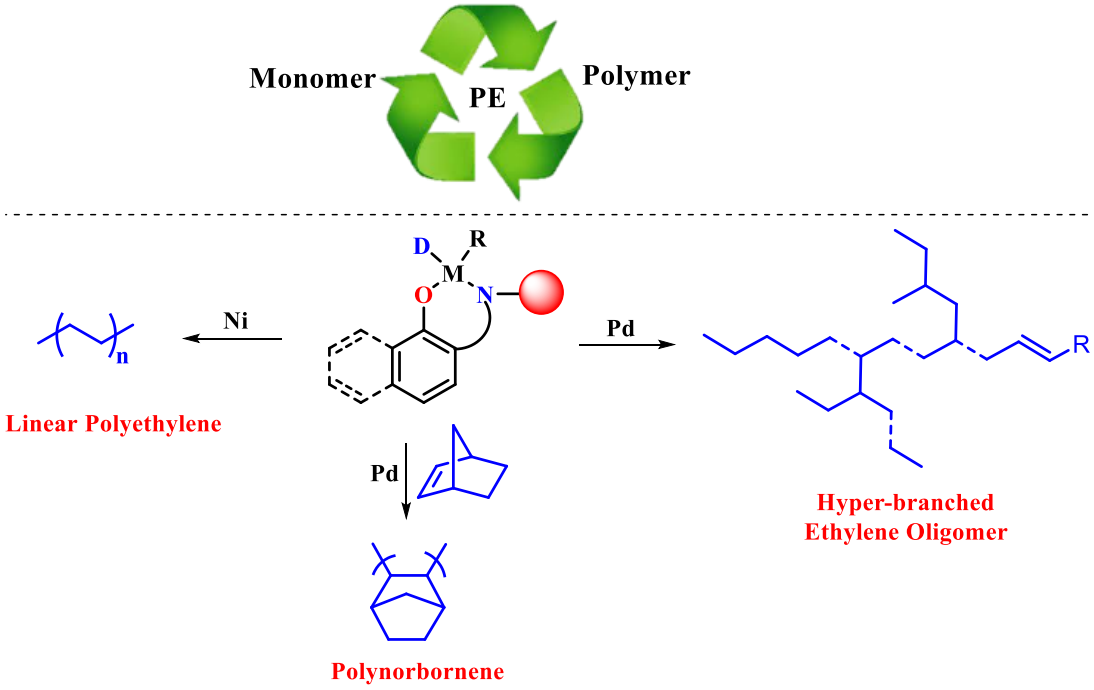

Imine phenoxy palladium complexes were active in norbornene polymerization, with and without aluminum alkyl cocatalysts. The palladium catalyst, in combination with Trityl tetrakis(pentafluorophenyl)borate, produced PNB with >99% conversion. The substantial production of polyolefins leads to waste generation. To address this issue, ADMET polymerization and condensation polymerization were employed to synthesize in chain olefin/ester-functionalized polyethylene-like polymers, which are chemically recyclable. These polymers can undergo depolymerization and repolymerization thereby circumventing waste generation.

Rajkumar S. Birajdar **Dr. Samir H. Chikkali** **Dr. Ashootosh V. Ambade**

4. Publications:

1. **Birajdar, R. S**.; Gonnade, R. G.; Chikkali, S. H. Regulating the polyethylene microstructure by increasing steric crowding in naphthoxy imine-ligated Ni(II) complexes. *Polym. Chem.*, **2024**, *15*, 292-302.
2. **Birajdar, R. S.;** Bodkhe, D.; Gupta, P.; Shaikh, M. H.; Ramekar, R.; Chikkali, S. H. Emerging trends in olefin polymerization: a perspective. *J. Macromol. Sci. A,* **2023**, *60*(11), 731-750.
3. **Birajdar, R. S**; Gonnade, R. G.; Pol, H. V.; Basava Prabhu M.; Rokade, D.; Nandimatha, S.; Chikkali, S. H. Palladium-catalyzed polar solvent empowered synthesis of hyper-branched ethylene oligomers and their applications. *Polym. Chem*., **2023**, *14*, 3239-3251.
4. **Birajdar, R. S.;** Chikkali, S. H. Insertion copolymerization of functional olefins: Quo Vadis?. *Eur. Polym. J.,* **2021**, *143*, 110183.
5. **Birajdar, R. S.;** Khopade, K. V.; Chikkali, S. H. Depolymerization and repolymerization of polyethylene-like material. (*Manuscript under preparation).*
6. **Birajdar, R. S**.; Chikkali, S. H. Exploring homopolymerization of norbornene by imine-ihenoxy ligated palladium complexes. (*Manuscript under preparation).*
7. Chatterjee, D.; Sajeevan, A.; Jana, S.; **Birajdar, R. S.;** Chikkali, S. H.; Sivaram, S.; Gupta, S. S. Solvent-free hydroxylation of C-H bonds by Fe-complex: A green approach for activation of small molecules and macromolecules. *ChemRxiv.* **2024**; (doi:10.26434/chemrxiv-2024-7f3dr).
8. Gaikwad, S. R.; Patel, K.; Deshmukh, S. S.; Mote, N. R.; **Birajdar, R. S.;** Pandole, S. P.; Chugh, J.; Chikkali, S. H. Palladium-catalyzed insertion of ethylene and 1, 1-disubstituted difunctional olefins: an experimental and computational study. *ChemPlusChem*, **2020**, *85*(6), 1200-1209.
9. Khopade, K. V.; Sen, A.; **Birajdar, R. S**.; Paulbudhe, U. P.; Kavale, D. S.; Shinde, P. S.; Mhaske, S. B.; Chikkali, S. H. Highly enantioselective synthesis of sitagliptin. *Asian J. Org. Chem.*, **2020**, *9*(2), 189-191.
10. Shaikh, M. H.; Ramekar, R. V.; Jawoor, S.; Dash, S. R.; **Birajdar, R. S.**; Pawal, S. B.; Thenmani, N.; Vanka, K.; Chikkali, S. H. Rational sesigning of imine thiophene-ligated Cr-complex and implication in ethylene polymerization. (*Manuscript communicated).*

5. Patents:

1. Chikkali, S. H.; **Birajdar, R. S.** Synthesis of dibenzhydryl substituted phenoxy imine ligated Pd(II) and Ni (II) catalyst for ethylene (co)polymerization. **(IN2022-NF-0181).**

Rajkumar S. Birajdar **Dr. Samir H. Chikkali** **Dr. Ashootosh V. Ambade**

2. Chikkali, S. H.; Jawoor, S.; **Birajdar, R. S.**; Pawal, S. B.; Thenmani, N.; Chugh, P. Homogeneous single site catalyst and its use in preparing linear polyethylene. **EP4157527A1; JP2023529101A; US2023201815A1; WO2021240549A1.**

6. References:

1. Birajdar, R. S.; Chikkali, S. H. Insertion copolymerization of functional olefins: Quo Vadis?. *Eur. Polym. J.*, **2021**, *143*, 110183.

2. Birajdar, R. S.; Bodkhe, D.; Gupta, P.; Shaikh, M. H.; Ramekar, R.; Chikkali, S. H. Emerging trends in olefin polymerization: a perspective. *J. Macromol. Sci. A*, **2023**, *60*(11), 731-750.

3. Khopade, K. V.; Chikkali, S. H.; Barsu, N. Metal-catalyzed plastic depolymerization. *Cell Rep. Phys. Sci.* **2023**, *4*(5), 101341.

4. Birajdar, R. S; Gonnade, R. G.; Pol, H. V.; Basava Prabhu M.; Rokade, D.; Nandimatha, S.; Chikkali, S. H. Palladium-catalyzed polar solvent empowered synthesis of hyper-branched ethylene oligomers and their applications. *Polym. Chem.,* **2023**, *14*, 3239-3251.

5. Birajdar, R. S.; Gonnade, R. G.; Chikkali, S. H. Regulating the polyethylene microstructure by increasing steric crowding in naphthoxy imine-ligated Ni(II) complexes. *Polym. Chem.*, **2024**, *15*, 292-302.

6. Johnson, L. K.; Killian, C. M.; Brookhart, M. New Pd (II)-and Ni (II)-based catalysts for polymerization of ethylene and. alpha.-olefins. *J. Am. Chem. Soc.* **1995**, *117*, 6414–6415.

7. Johnson, L. K.; Mecking, S.; Brookhart, M. Copolymerization of ethylene and propylene with functionalized vinyl monomers by palladium (II) catalysts. *J. Am. Chem. Soc.*, **1996**, *118* , 267 -268.

8. Xu, Y. M.; Li, K.; Wang, Y.; Deng, W.; Yao, Z. J. Mononuclear Nickel (II) Complexes with Schiff Base Ligands: Synthesis, Characterization, and Catalytic Activity in Norbornene Polymerization. *Polymers*, **2017**, *9*(3), 105.

9. Janiak, C.; Lassahn, P. G. The vinyl homopolymerization of norbornene. *Macromol. rapid commun.*, **2001**, *22*(7), 479-493.

Rajkumar S. Birajdar **Dr. Samir H. Chikkali** **Dr. Ashootosh V. Ambade**

Chapter 1

Introduction

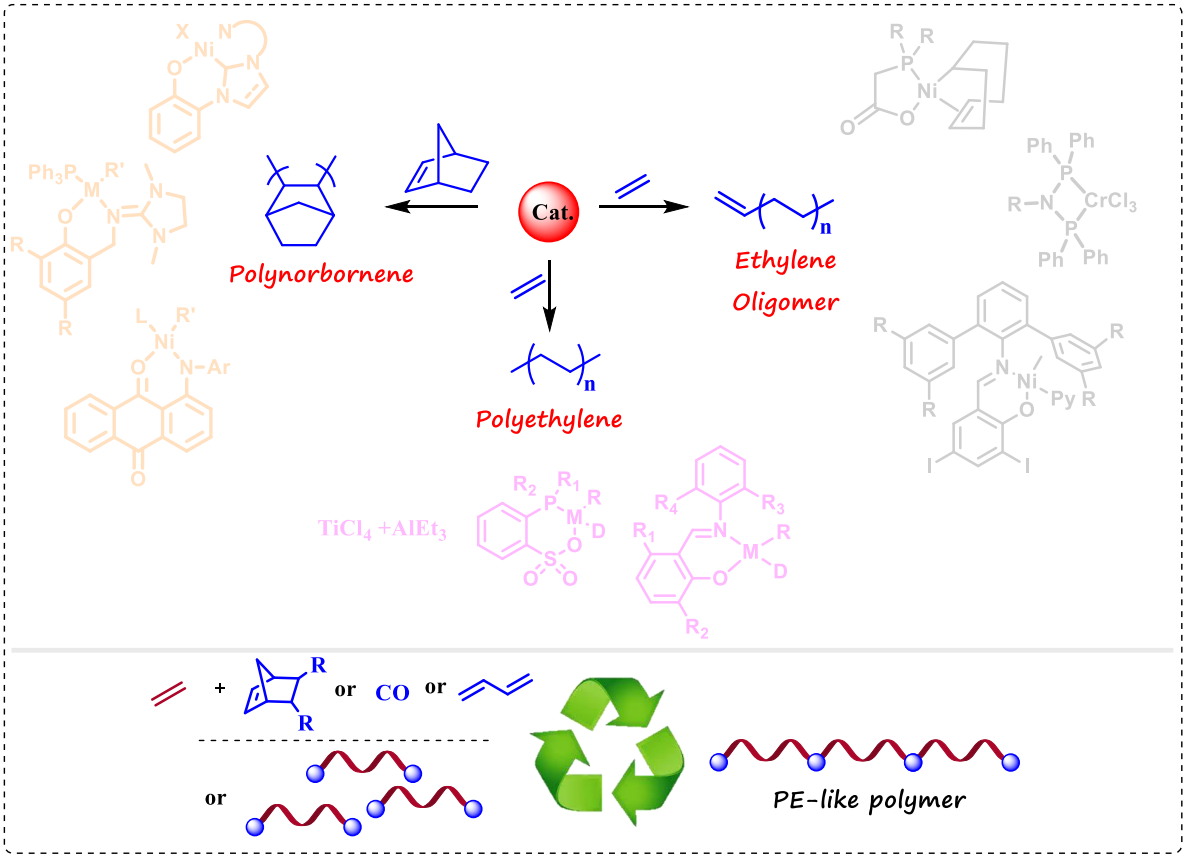

1.1. Abstract:

The chapter provides an overview of both historical and recent developments in the field of ethylene polymerization and oligomerization. It explains the evolution of ethylene polymerization, from high-pressure processes to low-pressure catalytic insertion polymerization. In catalytic olefin polymerization, steric and electronic effects of ligands play a crucial role. Higher steric hindrance around the metal center helps generate linear, high-molecular-weight polymers by reducing β-hydride elimination reactions. Traditional α-diimine catalyst, with moderate steric hindrance, tend to exhibit a higher degree of chain-walking, leading to branched or hyperbranched polymers or oligomers. Industrially, phosphine phenoxide-based catalysts are used to produce linear α-olefins. This catalyst shows a higher β-hydride elimination. The chapter also highlights significant discoveries in ligand and catalyst design, particularly in the context of norbornene polymerization. Additionally, the inclusion of carbonyl groups or olefins during polymerization can yield degradable polyethylene-like polymers, which are chemically recyclable. These degradable polymers offer a more sustainable option for polyethylene-based materials.

1.2. Introduction:

Catalysis plays a crucial role in both polymerization and oligomerization of ethylene/norbornene, enabling the transformation of ethylene/norbornene molecules into valuable products with tailored properties.[1,2] Ethylene polymerization yields polyethylene (PE) which is one of the most widely used polymers in the world.[3] These versatile materials have revolutionized various industries, including packaging, automotive, construction, and textiles. Polyethylene offer exceptional properties and therefore is widely used.[4] Polyethylene possess a unique combination of strength, flexibility, chemical resistance, and thermal stability, making it an ideal material for a wide range of applications. The low cost, light weight, and ease of processing further contributes to its popularity. Also, vinyl addition norbornene polymer (PNB) stands as a notable class of specialty polymers renowned for its remarkable optical and mechanical properties, including a high glass transition temperature, exceptional optical transparency, and low dielectric constant, rendering it highly attractive for a diverse range of industrial applications.[5,6] For the polymerization of norbornene, both early and late transition metal catalysts are utilized.

Similar to polyethylene, its low molecular weight counterpart, ethylene oligomers, are equally important and have been extensively studied. Ethylene oligomerization holds both academic and industrial importance due to its role in producing branched and linear long-chain olefins.

Higher olefins are crucial in multiple industries. In the plastics industry, C_4-C_6 olefins are used as comonomer.[7] For plasticizers, hydroformylation products of C_6-C_{10} olefins are used.[8] Also these are used as lubricants (C_{10}-C_{12} olefins) and surfactants (C_{12}-C_{16} olefins, which are processed through arylation or sulfonation). Additionally, they serve as starting materials for propylene, alcohols, amines, acids, and other essential chemicals. Notably, C_{10+} higher olefins are particularly used for jet fuel applications.

The demand for both polyethylene and its oligomers continues to grow steadily due to their wide range of applications. Global polyethylene production currently stands at close to 100 million tons per annum, while 3 million ton ethylene oligomers are synthesized annually. This demand is anticipated to further rise in the near future. Industrially used Ziegler catalyst and SHOP (Shell Higher Olefin Process) catalyst follows the coordination insertion mechanism which is discussed in detail in section 1.2.6.

1.2.1. Early years in olefin polymerization:

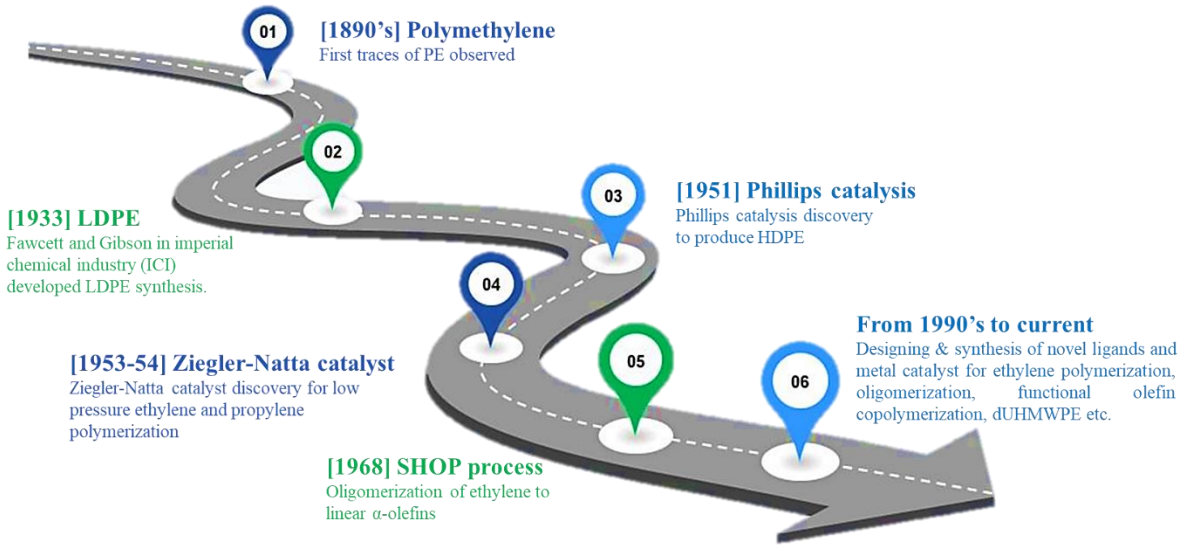

Figure 1.1: Significant advancements in the development of polyolefins.

Moving back in time, we may follow the history of the synthesis of polyethylene, which has an intriguing tale before we take stock of the most recent advancements in olefin polymerization. Around the end of the 19th century, for the first time, traces of polyethylene was observed during a thermal decomposition reaction of diazomethane, which was named "polymethylene".[1] During that period, the field of polymer science was underdeveloped and was not accepted by the community. German chemist Hermann Staudinger proposed that polymers consist of long chains, connected through covalent bonds.[1] This theory was initially met with skepticism, but it was eventually widely accepted and laid the foundation of rational polymer science. In 1933, Fawcett and Gibson at the Imperial Chemical Industry (ICI) found

a white powdery material on the reactor wall while performing a high-pressure condensation reaction of ethylene and benzaldehyde (Figure 1, top). When they were repeating the experiment without benzaldehyde, the reactor exploded and the project was halted. It took a couple of years to understand this and develop radical polymerization of ethylene to polyethylene. The ICI process operates at high pressure (1000-4000 bars) and high temperature (200-300 °C). After this discovery, several academic groups initiated research programs on ethylene polymerization to make polyethylene.

The major breakthroughs were reported in the early 1950s. The first one was by Hogan and Banks at the Phillips Petroleum Company who reported low molecular weight oligomer from gaseous olefin using nickel oxide supported on silica or alumina.[1] In 1951, while studying the effect of nickel oxide and chromium oxide supported on silica or alumina they found solid HDPE in their reactor. In the 1950s, Ziegler, at the Max Planck Institute in Mülheim, Germany, made a significant breakthrough in ethylene polymerization. Before embarking on the journey of polyethylene, he was investigating the reactivity of alkyl lithium/alkyl aluminum compounds with ethylene.[1] These organometallic reagents formed the foundation for his development of the "Aufbaureaktion," a process enabling the synthesis of 1-olefins, aliphatic alcohols (known as alfol synthesis), and high-purity alumina through the oxidation of alkyl aluminum compounds. Ziegler discovered that the presence of nickel had a profound effect on the "Aufbaureaktion" leading to chain termination and the production of 1-butene. This unexpected phenomenon, known as "the nickel effect," was attributed to the presence of nickel in the autoclave resulting from previous hydrogenation reactions. Ziegler's chance discovery of "the nickel effect" showed that nickel's presence during "Aufbaureaktion" led to chain termination and the production of 1-butene. This effect was traced to residual nickel in the autoclave from prior hydrogenation processes. Ziegler's students then began an extensive screening of different metal precursors with alkyl aluminum compounds to explore this unexpected behavior.[1] In 1953, Ziegler's team evaluated the combination of triethyl aluminum with various transition metal compounds, including chromium, vanadium, manganese, and platinum. The most notable result was achieved by combining zirconium acetylacetonate with triethyl aluminum, resulting in a conversion rate of over 90% for the introduced ethylene. The patent application claimed “a process for the production of a high molar mass polyethylene” which involved the association of triethyl aluminum with complexes containing metals from group 6 (Cr, Mo), 5 (V, Nb, Ta), and 4 (Ti, Zr, Hf).[1] This process operates at lower temperatures and with ethylene pressure below 55 bars and is widely known as the “Mülheim Atmospheric Process”.[1] In Mid 1954, Natta, an Italian chemist, successfully synthesized the stereospecific

propylene using a Ziegler catalyst composed of titanium trichloride and triethyl aluminum.[1] For this groundbreaking discovery, Ziegler and Natta were bestowed with the Nobel Prize in 1963. Subsequent to this discovery, several developments such as metallocene, MAO, postmetallocenes, etc. have been reported.[9,10]

1.2.2. Catalyst advancement in olefin polymerization:

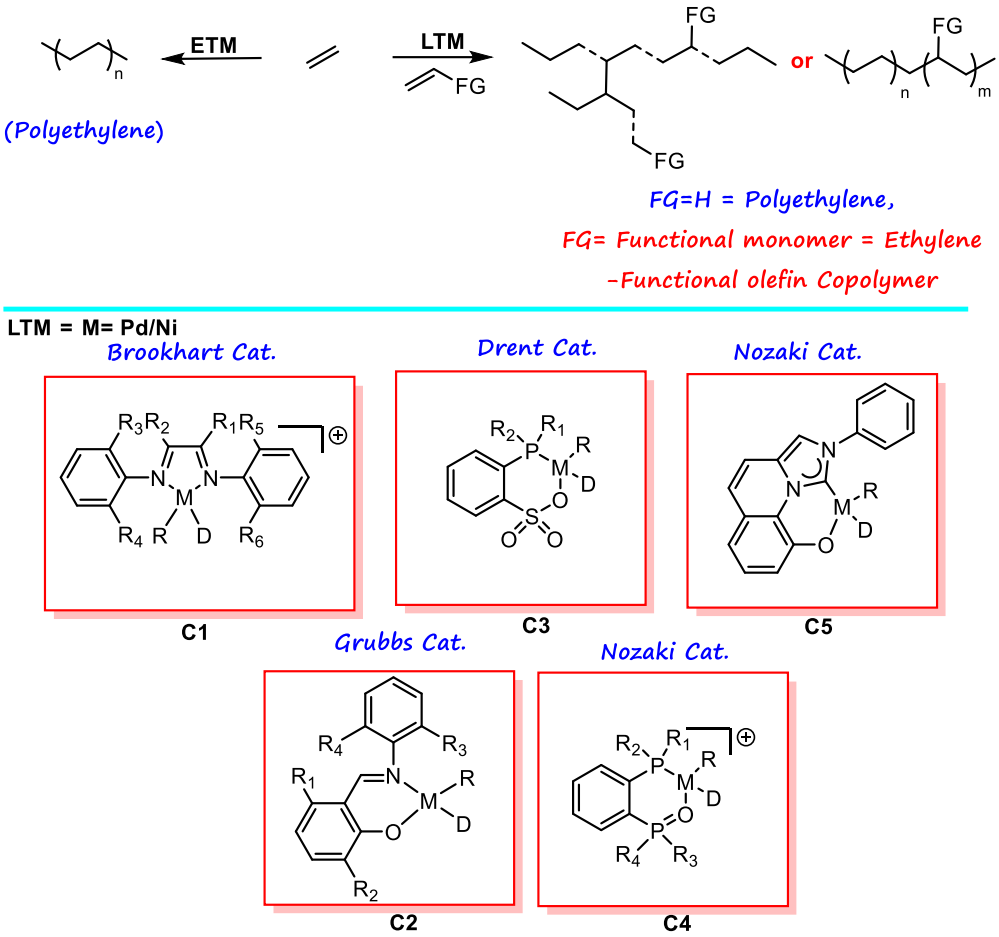

Figure 1.2: Ethylene polymerization by early transition metal (ETM) and (co)polymerization by late transition metal catalyst (LTM).

Ligands play a crucial role in olefin polymerization and control the molecular weight, crystallinity, and stereo-regularity of the resultant oligomer or polymer. Over the past three decades, there has been extensive research in the area of ligands and catalyst development for olefin polymerization. This research has led to the development of new types of ligands and their early and late transition metal complexes, designed for both homopolymerization and copolymerization of olefins. There has also been significant focus on ethylene polymerization and copolymerization with late transition metal (LTM) catalysts over early transition metal (ETM) catalysts. As Early transition metal (ETM) catalysts are highly sensitive to air and moisture, their synthesis and handling is quite tedious. Even small amounts of polar impurities

or polar comonomer can poison these catalysts. Additionally, activating early transition metal catalysts requires high concentrations or thousands of equivalents of aluminum alkyls to generate the metal alkyl species needed for catalysis. Furthermore, the industrially practiced Ziegler catalyst, a heterogeneous catalyst formed in combination with a co-catalyst, typically yields polymers with a high polydispersity index.

In contrast, late transition metal catalysts are generally more stable and less sensitive to air and moisture, making them easier to handle and less likely to be poisoned by impurities. This stability has contributed to their growing popularity in olefin polymerization.

In 1995, Brookhart and co-workers reported a rational design approach, an α-diimine ligated palladium complex **C1** (Figure 1.2) was employed for the ethylene homopolymerization and copolymerization of ethylene with methyl acrylate was successfully achieved for the first time.[11,12] The catalyst was activated using co-catalysts such as methyl aluminoxane (MAO) or boron-based activators.[13,14,15] The most distinctive property of these catalysts is the chain-walking process, which leads to the formation of highly branched polyolefins. The catalytic system features two neutral imine-donors, which form coordination bonds with a cationic metal (LTM) center, and the fourth coordination is satisfied by a weakly coordinating donor solvent (D). Since its discovery in the 1990s, this catalytic system has been rigorously tailored on several occasions and has been utilized in the insertion (co)polymerization of various functional olefins.[16,17] Although a large variation is reported in the ligand backbone, the metal of choice has been mainly nickel and palladium.[18]

Chain walking follows a mechanism as presented in figure 1.3 and explained below. During polymerization, ethylene coordination and subsequent insertion between the metal alkyl bond leads to metal alkyl species with longer chain. During this process, growing polymer chain can undergo β-hydride elimination to form a metal hydride complex (**2**) (figure 1.3, path b) and alkene (**2**), then further reinsertion of the formed olefin takes place. This creates either the same primary alkyl complex (**1**) or a new secondary alkyl complex (**3**) (figure 1.3, path c). This is the initial step in the chain-walking process. Ethylene coordination to metal center (**3a**) having secondary alkyl species and further insertion results in a methyl branch (**3b**) on the polymer backbone. Further chain walking along the polymer backbone creates longer branches. This process can happen several times during polymerization to yield branched polymer. Literature results suggest that in an α-diimine Pd(II) catalyst, the rate of chain-walking is 100 times faster compared to the chain-propagation reaction.[19]

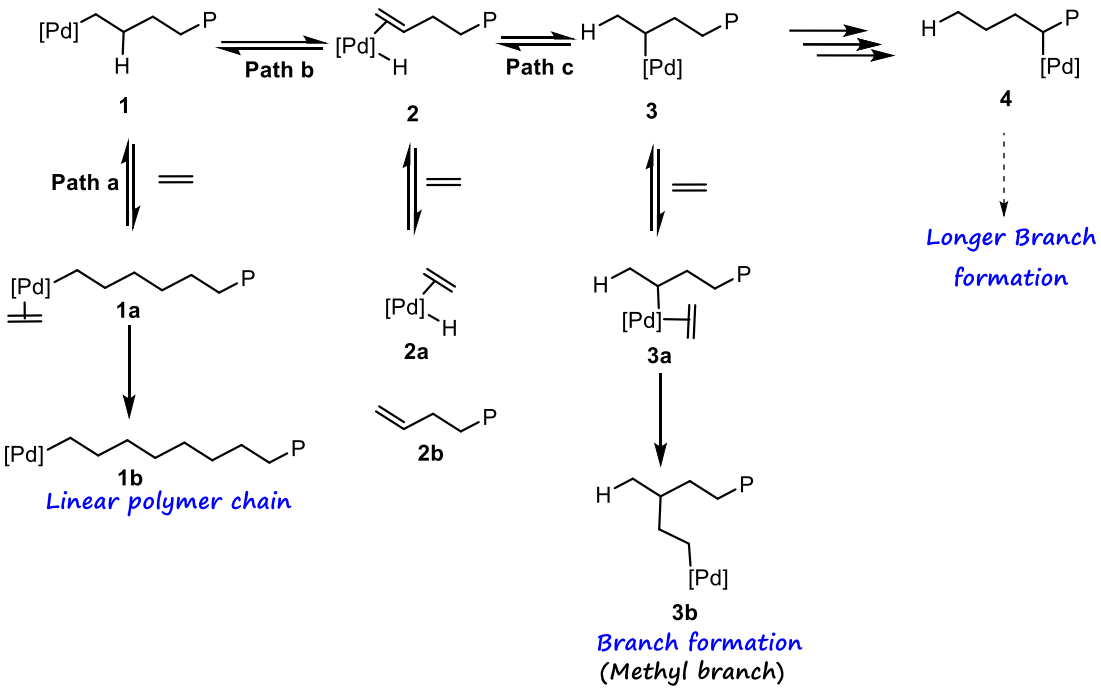

Figure 1.3: Chain walking mechanism for ethylene polymerization/oligomerization leads to short and long chain branches.

A neutral, single component phenoxy-imine nickel complex was reported by Grubbs and co-workers in 2000 (Figure 1.2, **C2**). It was demonstrated that **C2** could also tolerate functional groups such as ester and could copolymerize functional olefins with ethylene.[20] Subsequently, the phenoxy-imine catalyst has been tested by different research groups in olefin and functional olefin (co)polymerization.[21] In 2002, Drent and co-workers reported a palladium complex **C3** (Figure 1.2) derived from *ortho*-phosphinobenzenesulfonate ligand. Unlike **C1** catalyst, **C3** catalyst produces the linear polyethylene. **C3** has been the most successful catalytic system in polar olefin copolymerization and the characteristic ligand design is credited for its success. The *ortho*-phosphinobenzenesulfonate ligand features a neutral phosphine donor and an anionic sulfonate group. There are two parameters that empower **C3** to outperform other catalytic systems; the charge effect and the orbital interactions. 1) **C3** is a neutral palladium (II) system and therefore it is a relatively electron-rich system compared to catalysts with a metal center in lower oxidations or cationic metal complexes. Since it is (**C3**) electron-rich, it has a lower affinity towards functional groups and therefore functional olefins are tolerated by **C3**. 2) Theoretical investigations point that the lone pair of the ligated oxygen (in sulfonate group) repels π-electron on palladium, which facilitates palladium back-donation to π-acceptor olefin monomer.[22] This metal back-donation further strengthens monomer-metal π-complex formation, which promotes insertion of olefins. Thus, the characteristic ligand feature enables **C3** for olefin insertion and functional olefin copolymerization.

In the last decade, Nozaki and coworkers introduced two catalytic systems that show high catalytic activity in ethylene polymerization and these catalyst are capable of incorporating functional olefins in the polyolefin backbone. A bidentate ligand called bisphosphine monoxide (BPMO), disposing two neutral donors, was ligated on to LTM to produce complex **C4** (Figure 1.2).[23] Unlike **C3**, **C4** is a cationic system with a counter anion and the vacant fourth coordination is occupied by a donor solvent. The BPMO ligand with aliphatic substituents on phosphine met with limited success, subsequent ligand tailoring enabled **C4** (with aromatic substituents on phosphine) to initiate insertion copolymerization of functional olefins. Jordan and co-worker attempted replacing phosphine in **C3** with an *N*-heterocyclic-carbene (NHC) and prepared corresponding neutral palladium complex.[24] However, this palladium complex could not react with ethylene and polymerization could not take place. In a rational ligand design approach, Nozaki and co-workers reported palladium complex bearing imidazo[1,5-a]quinolin-9-olate-1-ylidene (IzQO) ligand. In the IzQO ligand, the neutral phosphine donor is replaced with isoelectronic *N*-heterocyclic-carbene (NHC) and the anionic SO_3^- is replaced by an anionic O^- donor. The orientation of NHC-plane appears to be very crucial in creating desired congestion around the active metal center. A carefully crafted, IzQO ligated, neutral, palladium complex **C5** (Figure 1.2) was found to be a very active catalyst in the insertion copolymerization of functional olefins.[25] Thus, **C1-C5** are the work-horse catalytic systems, that are most successful in the insertion (co)polymerization of functional olefins, among others.[26,27]

Similar to ethylene polymerization, metal complexes are also well-established as pre-catalysts for the vinyl polymerization of norbornene (NB). These catalysts can be classified into two main groups: early transition metal catalysts and late transition metal catalysts. The early transition metal catalysts, particularly metallocene catalyst, Ziegler–Natta catalysts and zirconium catalysts, are known for producing crystalline polymers with very high glass-transition temperatures.[28,29] This can lead to poor solubility in organic solvents and challenges in processability.

Recent research has shown the potential of various nickel-based catalysts for vinyl NB polymerization. These include bis(imino)pyridine Ni(II) catalysts, [30] α-diimine Ni(II) catalysts, [31] salicylaldimine Ni(II) catalysts,[32] phosphine-sulfonate Ni(II) catalysts, β-enaminoketonato Ni(II) catalysts,[33] aryloxide-NHC Ni(II) catalysts,[34] and (anilino)anthraquinone Ni(II)[35] catalysts. These Ni(II) catalysts have proven effective in copolymerizing norbornene with ethylene, α-olefins, and polar monomers. However, palladium catalysts have traditionally been used for homopolymerization of NB.[36,37] A common drawback of many palladium complexes

bearing bidentate or tridentate ligands is that they often require a significant excess of aluminum-based compounds as cocatalysts.[38,39,40]

1.2.3. Sterically and electronically modified catalyst:

In 1995 Brookhart and coworkers reported catalyst (C1) which shows a most distinctive property that is the chain-walking process, that leads to the formation of highly branched polyolefins. In the late-transition metal-catalysts, controlling the ratio of chain-walking/chain-transfer to chain propagation is crucial. This ratio determines the branching, crystallinity, and molecular weight of the resultant polyolefin.[41] This work opened doors to a flood of publications and several ligand and catalyst modifications to control the polymer branching crystallinity and molecular weight have been reported to date.

In 2016, Chen and co-worker synthesized a series of sterically tailored α–diimine ligated Pd(II) complexes.[42] They demonstrated that as steric hindrance increased, the molecular weight and activity also increased, while branching decreased. Similarly, Min Chen and colleagues studied the effect of ligand steric bulk on catalytic activity, molecular weight, and polymer microstructure in α-diimine nickel catalysts with ortho-dibenzhydryl or ortho-sec-phenyl substitutions.[43] They found that the dibenzhydryl-substituted species exhibited higher activity [(0.98–1.58) × 10^6 g (mol Ni h) $^{-1}$], higher molecular weight [Mn: (8.0–13.1) × 10^5 g mol^{-1}], and lower branch density (55-64 per 1000 carbon atoms) compared to methyl-substituted nickel complexes, which had lower activity [(0.63–0.44) × 10^6 g $(mol\ Ni\ h)^{-1}$], lower molecular weight [Mn: (0.8–0.6) × 10^5 g mol^{-1}], and higher branch density (90-95 per 1000 carbon atoms).

Steric factors are not the only important aspect; ligand symmetry also plays a crucial role in determining polymer microstructure. Recently, Dai and colleagues synthesized α–diimine Ni(II) complexes with dibenzobarrelenedione and dibenzhydrylanilines ligands.[44] They found that complexes with a quasi-centrosymmetric structure yielded semi-crystalline polyethylene with very high molecular weight and low branching densities (11-34 per 1000 carbon atoms). In contrast, planar-symmetric complexes with similar steric bulk produced highly branched polymers (110-115 per 1000 carbon atoms) with no discernible melting point under the same polymerization conditions.

Literature reports indicate that the bulkiness on the N-aryl moiety in imine-ligated metal catalysts, along with substituents in the ortho position relative to the oxygen-donor group, plays a significant role in controlling the behavior of phenoxy imine-ligated metal catalysts. These structural features contribute to higher molecular weights in the resulting polymers by reducing chain transfer processes and inhibiting β-hydride elimination. This, in turn, helps to increase

polymerization activity by preventing the formation of inactive bis-ligated complexes. By optimizing the steric hindrance in these key positions, researchers aim to improve catalyst performance and enhance the properties of the resulting polymers.[45]

In 2014, Brookhart and coworkers synthesized ultrahigh-molecular-weight polyethylene with a high degree of branching by employing a Ni(II) complex ligated with sterically hindered 2,8-diaryl naphthyl-substituted salicylaldimine.[46] In addition to steric effects, the electronic effect of ligands can significantly impact polymerization activity. Marks and coworker explored the influence of fluorine substituents in ethylene polymerization, discovering that a CF_3-substituted catalyst exhibited greater stability and catalytic activity compared to its CH_3-substituted counterpart.[47] The resultant polymers from CF_3-substituted catalysts demonstrated higher molecular weight and lower branch density (Mw = 9.2×10^4 g/mol; branching = 7/1000 carbon atoms) compared to those from CH_3-substituted catalysts (Mw = 1.4×10^3 g/mol; branching = 88/1000 carbon atoms). The researchers hypothesized that a weak interaction between the C-F bond in the ligand and the C-H bond in the growing polymer chain suppressed the β-hydride elimination reaction, leading to increased polymerization activity and reduced branching. In 2022, Jian and coworkers reported a sterically hindered sandwich-like neutral salicylaldiminato nickel catalyst with 8-aryl naphthyl and dibenzosuberyl groups as part of its N-aryl moiety. This catalyst yielded linear ultrahigh-molecular-weight polyethylene (UHMWPE) even at high temperatures of 90 °C.[48]

1.2.4. Early years in olefin oligomerization:

Ethylene oligomers are as important as polyethylene due to their wide range of applications. The initial discovery of ethylene oligomerization by the Ziegler process was a significant milestone in the field of polymer chemistry. The Ziegler alcohol synthesis, also referred to as the Ziegler higher alcohol synthesis or simply Alfol process, was first reported in 1955. The Ziegler alcohol synthesis is a significant industrial process utilized for the production of higher and linear primary alcohols featuring an even number of carbon atoms. This method encompasses several sequential steps to achieve the desired alcohol products.

Initially, the process begins with the synthesis of triethylaluminum, which serves as a key precursor in the subsequent reactions. Triethylaluminum is synthesized through the reaction of aluminum, hydrogen, and ethylene under controlled conditions. This step is crucial as it provides the necessary alkyl aluminum compound required for the chain growth reaction. The chain growth reaction involves the interaction between triethylaluminum and ethylene, leading to the elongation of the alkyl aluminum chain. This reaction serves as the foundation for the

subsequent formation of the desired alcohols. Following the chain growth reaction, the resulting trialkylaluminum species undergo oxidation to yield aluminum alkoxides. This oxidation step is typically carried out using suitable oxidizing agents under controlled conditions. Subsequently, the aluminum alkoxides are subjected to hydrolysis, resulting in the formation of aluminum hydroxide and the desired primary alcohols. Hydrolysis of aluminum alkoxides involves the reaction with water to break down the aluminum-oxygen bonds, ultimately releasing the desired alcohols. Since its discovery, this process has found widespread industrial application due to its efficiency in producing linear primary alcohols with specific carbon chain lengths.

After the alfol process, the "nickel effect" is a pivotal discovery in the realm of ethylene oligomerization, contributing significantly to the understanding and advancement of this industrial process. In 1953, while conducting a reaction at 100°C and 100 atm of ethylene in a high-pressure autoclave, Ziegler and Holzkamp encountered an unexpected phenomenon. They found that the majority of the product was 1-butene. The cause was traced back to the accidental presence of a nickel compound, which had been used in earlier hydrogenation experiments, in the reactor. This led Ziegler and Holzkamp to realize that this nickel compound sped up the chain termination process, thereby leading to the excessive production of 1-butene. This unusual outcome became known as "the nickel effect."

This discovery laid the groundwork for further exploration into the use of nickel complexes as pre-catalysts in ethylene oligomerization processes. Subsequent research efforts, particularly by W. Keim and co-worker in the late 1960s, led to the development of nickel(0) complexes with P,O-ligands. These complexes proved to be highly effective in catalyzing ethylene oligomerization reactions. The utilization of nickel complexes in ethylene oligomerization processes revolutionized the production of linear alpha-olefins (LAOs) on an industrial scale. Notably, these nickel complexes are integral components of various industrial processes, including the "SHOP" (Shell Higher Olefin Process) for ethylene oligomerization, which generates a wide range of alpha-olefins from C_4 (1-butene) to C_{20+}.

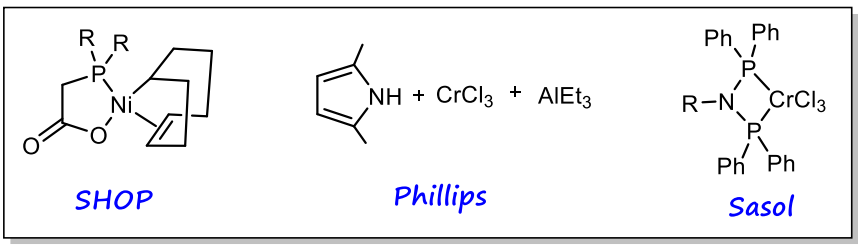

Figure 1.4: Industrially applied catalyst for the ethylene oligomerization.

In 1987, IFP-SABIC pioneered an innovative ethylene dimerization process, successfully transitioning it to industrial-scale production of 1-butene.[49,50] Chevron-Phillips operates a chromium-based ethylene trimerization process, leading to the production of 1-hexene.[51] Additionally, Sasol recently announced a chromium-based ethylene tetramerization process, yielding 1-octene.[52]

1.2.5. Catalyst advancement in ethylene oligomerization:

Based on the literature reports, it was observed that the choice of catalyst is crucial to achieving low molecular weight ethylene oligomers or hyperbranched ethylene oligomers. The catalyst must exhibit high β-hydride elimination relative to chain propagation. It should also promote a high degree of chain-walking, which leads to the formation of hyperbranched ethylene oligomers. Similar to the traditional SHOP (Shell Higher Olefin Process) catalyst, LTM (late transition metal) catalysts such as palladium, nickel, and iron have been extensively studied for ethylene oligomerization to linear as well as branched oligomers.[53]

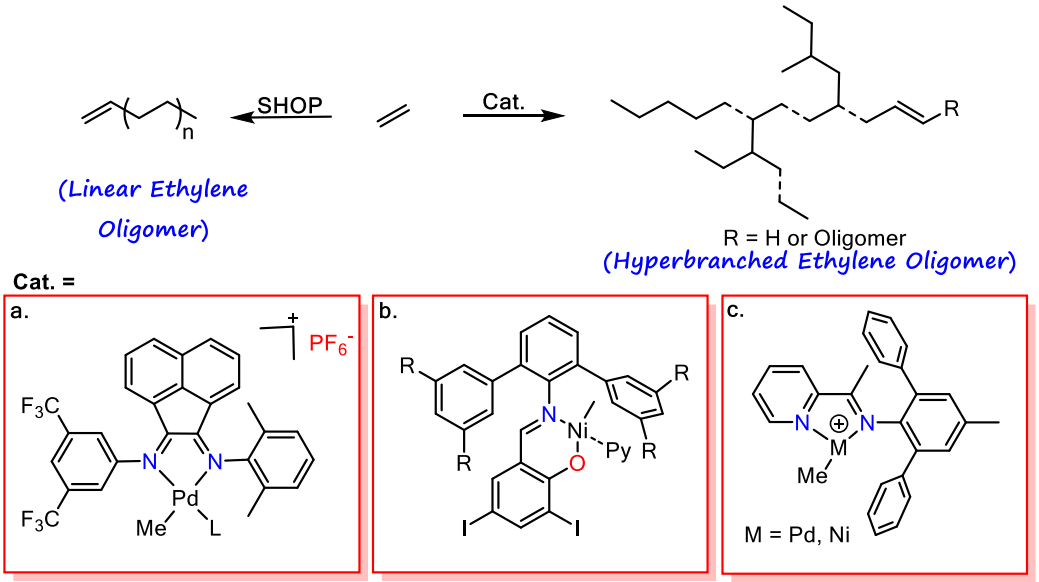

Figure 1.5: Recently developed catalyst for the synthesis of hyperbranched ethylene oligomer.

However, the synthesis of low-molecular-weight (Mw) ethylene oligomers with hyperbranched microstructures was very difficult to achieve using the above catalysts. Such hyperbranched ethylene oligomers can be used as, functional additives in lubricants, surface treatments, compatibilizer, waxes, etc. For producing hyperbranched ethylene oligomers, the choice of catalysts is decisive. Catalysts with significant chain walking abilities can produce highly branched structures.[54] As presented earlier, Brookhart catalyst reported in 1995 that is late transition metal catalysts based on Ni(II) and Pd(II) with bidentate α-diimine ligands [N,N] as efficient catalysts for ethylene polymerization.[11] These cationic complexes display extensive

chain walking during polymerization. Though the Pd-catalyst yields a highly branched structure, the molecular weight is high and leads to the production of amorphous rubbery material. In these α-diimine ligated metal catalysts, the bulky substituents on ligand reduce the chain transfer and yield a high molecular weight polymer. While, less bulky substituents display low activity and produce hyperbranched low molecular weight oligomers.[55,56]

Similar to α-diimine ligands, following the discovery of metal complexes with salicylaldimine (also known as phenoxy-imine) ligands for olefin polymerization in the 1990s, researchers have extensively modified these ligands to study their impact on olefin oligomerization/polymerization.[32] Ethylene oligomers or polymers with <10 branches per 1000 carbon atoms are considered as low branching material. While 75-100 branches per 1000 carbon atom is considered high branching, >150 branches per 1000 carbon atom is termed as ultrahigh branching number.[57] Producing ethylene oligomers with hyperbranched microstructure requires the catalysts to chainwalk and display high propensity for chain transfer. Catalysts that can chain walk without chain transfer will produce highly branched but high molecular weight polyethylene. Thus, synthesizing hyperbranched ethylene oligomers is challenging, and only a handful of catalysts could achieve this feat (Figure 1.5, cat.).

1.2.6. Mechanism of coordination insertion polymerization/ oligomerization:

Ethylene oligomerization and polymerization with early and late transition metal catalysts typically follow a coordination insertion mechanism, known as the Cossee-Arlman mechanism. This involves successive coordination and single insertion of ethylene by a metal hydride species [M−H]. Each insertion event leads to the formation of longer metal alkyl species, such as [M−Et], [M−Bu], and so on. The successive insertion of ethylene leads to the formation of high molecular weight polyethylene. Chain termination occurs through a β -hydride elimination mechanism. In the ethylene polymerization the rate of insertion and chain growth step is higher over the chain transfer by β -hydride elimination mechanism.

While in ethylene oligomerization the rate of termination or β-H elimination is competing with chain growth or rate of insertion. This termination process results in the release of alpha-olefins with low molecular weight. The insertion polymerization of norbornene also follows a similar coordination-insertion pathway results into a polynorbornene.

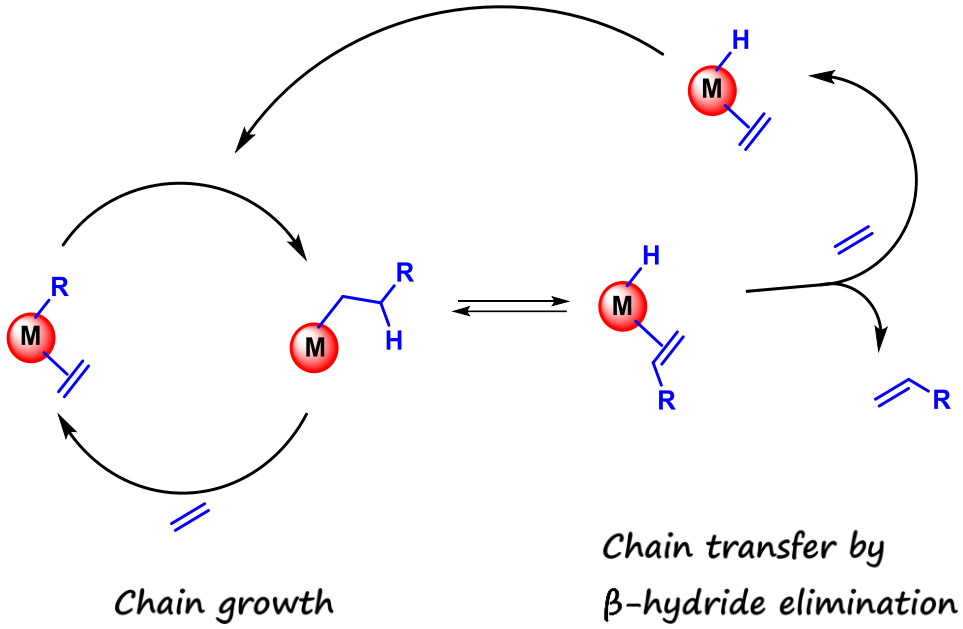

Figure 1.6: Cossee–Arlman mechanism for insertion polymerization/oligomerization of ethylene.

1.2.7. Polyethylene-like polymer:

Polyethylene reigns as the foremost synthetic polymer, boasting an annual production exceeding 100 million tons and constituting approximately one-third of the total plastic output. Despite its prevalence, the lifecycle of polyethylene from crude oil extraction to incineration with energy recovery leaves a significant carbon footprint, generating about 4.4 kg of CO_2 equivalents for every kilogram of polyethylene produced.[58]

Polyethylene is used in everyday products, from food packaging films and milk or detergent bottles to textiles, coating films, fibres, and freshwater pipes. Some polyethylene products, like single-use packaging made from low-density polyethylene (LDPE), have shorter life spans, leading to significant waste generation in a short period. Polyethylene waste generation is a significant environmental concern due to its widespread use and disposal practices. As the most produced synthetic polymer, polyethylene contributes substantially to plastic waste accumulation globally. Its harmful effects on the environment are multifaceted and include pollution of land, waterways, and oceans, as well as adverse impacts on wildlife and ecosystems. When polyethylene waste is improperly disposed of, whether through littering or inadequate waste management systems, it can persist in the environment for hundreds of years. This longevity exacerbates its harmful effects, as polyethylene does not readily degrade and can accumulate over time, posing ingestion and entanglement hazards to marine life and terrestrial animals. Moreover, the breakdown of polyethylene waste into microplastics further

amplifies its ecological impact, as these tiny particles can be ingested by organisms throughout the food chain, potentially leading to bioaccumulation and biomagnification of toxic substances.

In response to the challenges posed by polyethylene waste, various recycling methods have been developed to mitigate its environmental footprint. Mechanical recycling is one such approach, where polyethylene waste is sorted, cleaned, and processed into recycled pellets for use in new products. This method is relatively well-established and offers the potential for reducing the demand for virgin polyethylene, thus conserving resources and reducing waste.

Despite the potential benefits of recycling, there are several reasons why current recycling practices do not adequately address the waste polyethylene problem. One major challenge in recycling polyethylene is that repeated processing and usage lead to a decline in the polymer's properties. Another complication arises from the wide range of polyethylene grades, which makes mechanical recycling more complex. Additionally, different polyethylene products contain varying amounts of stabilizers, processing aids, and other additives, further complicating the recycling process. These factors contribute to the difficulty of achieving efficient and effective recycling for polyethylene. Furthermore, mechanical recycling may result in degraded material properties compared to virgin polyethylene, limiting its applicability in certain high-performance applications.

Chemical recycling, another technique, involves breaking down polyethylene into its constituent oligomers or other useful chemicals through processes like pyrolysis or depolymerization. Chemical recycling holds potential but is still in its early stages. Challenges include scalability, cost, and product purity. The main issue is the stable nature of polyethylene's C-C bonds, which makes it hard to break down into ethylene monomers or oligomers. This stability complicates recycling and adds to the hurdles for scaling and cost-effectiveness. The transformation of saturated chains into olefinic monomers is hindered kinetically and thermodynamically disfavored. Consequently, processes such as pyrolysis to convert polyethylene into liquid hydrocarbons require high temperatures (500-600 °C).

To establish a circular plastics economy, one effective approach involves synthesizing polymers specifically engineered for deconstruction. This entails introducing predetermined breaking points in the polymer chain, typically in the form of functional groups. By maintaining a low density of such in-chain functional groups, various deconstruction pathways can be enabled without compromising the highly crystalline nature and desirable material properties of polyethylene (PE). Predetermined break points can be incarporated into polymers via copolymerization of ethylene with functional comonomers during chain growth polymerization

(Figure 1.7). Another approach to create polyethylene-like polymer with in-chain functional groups is through step-growth polycondensation reactions (Figure 1.9) with long-chain difunctional monomers or through ring-opening polymerizations of macrocycles (Figure 1.8). Considering all of the above factors, a new class of polymers known as "polyethylene-type" polymers has been developed. These polymers are defined by their hydrocarbon-dominated polymer crystallinity, which is a key feature that unifies them with various traditional polyethylene types. This characteristic makes them highly valuable for addressing issues related to polymer recycling, plastic waste, and environmental sustainability, as it provides a common ground for developing recycling processes and reducing environmental impact.

1.2.8. In-chain carbonyl group functionalization:

Incorporating in-chain functional groups containing heteroatoms that could facilitate deconstruction has long been pursued. Traditional catalysts for olefin polymerization tend to be quite sensitive to polar substances or impurities.[59] Post-polymerization backbone oxidation reactions offer another avenue for introducing in chain ketone or hydroxyl functional groups. However, these reactions may encounter drawbacks such as uncontrolled chain cleavage and selectivity issues.[60,61] The synthesis of polymers exclusively containing keto groups via this pathway has been reported. However, it necessitates an additional oxidation step of mixed "oxo-polyethylenes" using Cp*Ir-catalyzed transfer dehydrogenation, with acetone serving as the oxidant.[62] While copper (Cu) catalysts paired with benzaldehyde as a reagent achieve high selectivity for keto groups (>99%), the C-H oxidation process leads to a notable decrease in molecular weight compared to the original material.[63]

Early studies have reported the incarporation of carbon monoxide (CO) in free-radical ethylene polymerization at high pressure, around 1000 atmospheres, which leads to the production of low-density polyethylene (LDPE) with ketone groups.[64,65] This process involves the relatively stable acyl radical formed after CO incorporation, leading to a decrease in the chain-growth rate compared to ethylene homopolymerization.[66] Through radical polymerization, branched polymer (LDPE) is obtained. On the other hand, traditional catalysts based on early transition metals, which typically produce linear polymers, are easily deactivated when they come into contact with carbon monoxide. Late transition-metal catalysts do not face such limitations as these metals are less oxophilic in nature and display good functional group tolerance. Nonalternating ethylene-CO copolymerizations are preferred when the catalyst carries a neutral charge.

This neutral charge leads to a lower binding affinity for carbon monoxide compared to ethylene, particularly in contrast with cationic catalysts. [67,68] Notably, the presence of various ethylene-based repeat units and alternating patterns was first observed when neutral Pd(II) phosphinosulfonate catalysts (Figure 1.7, a) were used.[69] However, subsequent studies have reported materials with low keto incorporations. Unfortunately, these materials tended to be low molecular weight brittle polymers or oligomers, which hindered investigations into their mechanical properties. Additionally, other catalysts have been utilized for nonalternating ethylene-CO copolymerization.[70,71,72,73,74]

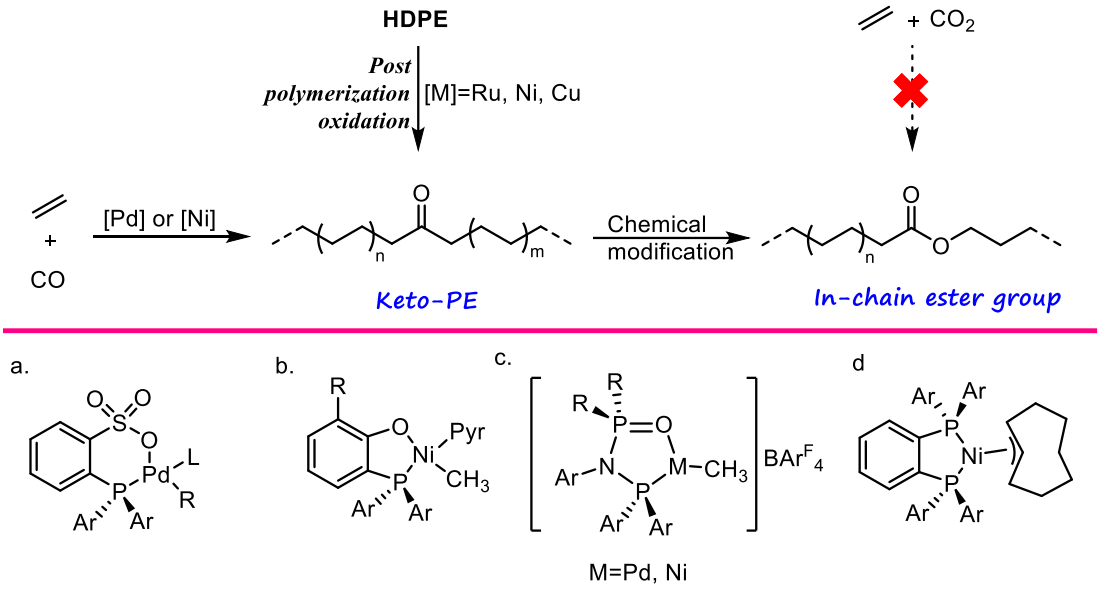

Figure 1.7: Routes for the synthesis of in-chain keto and ester functionalized polyethylene (top) and reported catalyst for the nonalternative copolymerization of ethylene and CO.

Although ethylene/carbon monoxide copolymerization offers an effective way to insert carbonyl groups into the polymer chain and provides photodegradability, the resulting keto-polyethylene (keto-PE) materials are not readily broken down through basic chemical processes, such as ester solvolysis. Despite this, the presence of keto groups within the polymer structure creates opportunities for additional chemical modifications, which could eventually make polyolefins easier to break down through targeted chemical reactions.[75,76] For example, recent research has shown that the Baeyer-Villiger oxidation of keto-polyethylenes (keto-PEs) can produce polyethylenes with a mix of in-chain keto and ester groups. [77,78] Although these keto-ester-polyethylenes (keto-ester-PEs) maintain material properties similar to high-density polyethylene (HDPE), their functional groups offer added benefits. The keto groups facilitate photolytic degradation, while the ester groups can be chemically deconstructed through methanolysis. To achive an direct ester groups in polymer chain, the use of CO_2 as a

comonomer with olefins has been a topic of discussion for some time, but it faces challenges due to thermodynamic and kinetic limitations.[79,80]

1.2.9. Polyethylene with low degree in-chain unsaturation:

An alternative approach to introduce in-chain groups for eventual deconstruction is by incorporating unsaturation during polymer synthesis. This can be achieved through catalytic insertion copolymerization of ethylene with butadiene or by using ring-opening metathesis polymerization (ROMP) of cycloolefins.

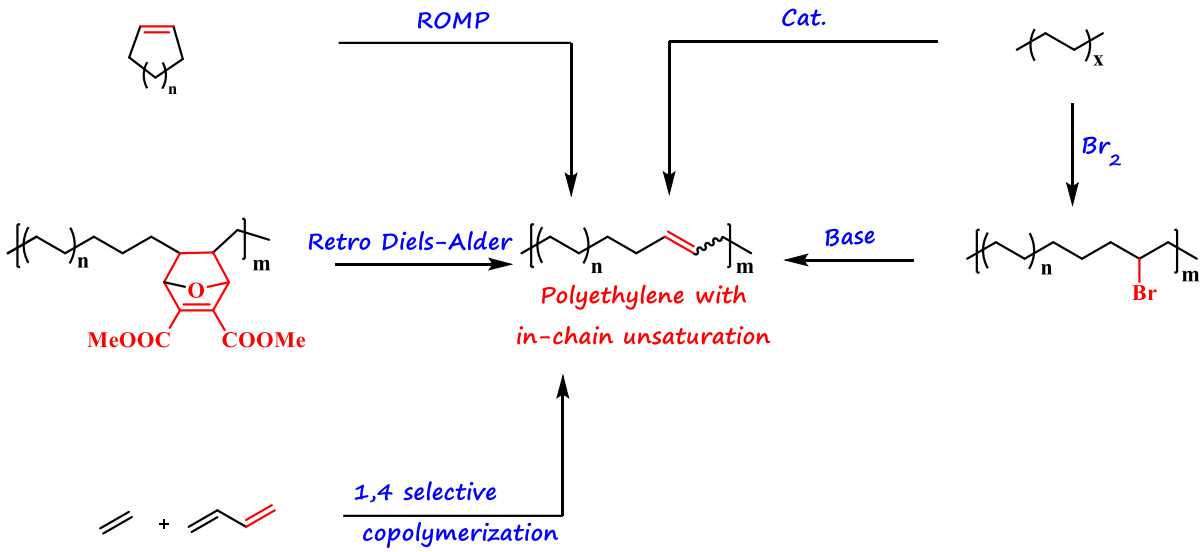

Figure 1.8: Routes for the synthesis of polyethylene with in-chain unsaturation.

Adding butadiene as a comonomer in a 1,4-fashion during catalytic copolymerization of ethylene (or propylene) can create double bonds within the polymer chain (Figure1.8). [81,82] The level of unsaturation in the polyolefin can be controlled by changing the ratio of monomers used. Moreover, terpolymerization with other α-olefins can produce structures that resemble linear low-density polyethylene (LLDPE) with in chain unsaturation. [83] Various catalysts have been reported for ethylene-butadiene copolymerization.[84,85]

A recent study has shown that "blocked" olefin groups can be incorporated into the polymer chain through palladium-catalyzed copolymerization of ethylene with oxanorbornadienes (Figure1.8).[86] These groups can later be unblocked through retro Diels-Alder cleavage by applying heat to a solution or polymer melt. The outcome is unsaturated high-density polyethylene (HDPE) chains containing up to 2.2 mol% in-chain olefins. Additionally, high molecular weights are achieved after unblocking, with M_n approximately around 3×10^4 g mol^{-1}.

Additionally, in-chain olefins can also be synthesized through ring-opening metathesis polymerization (ROMP) of cyclic monomers (Figure 1.8).[87,88] However, the resulting polymers typically exhibit a high degree of unsaturation, making them distinct from polyethylenes. Larger ring-size monomers are often not readily available and require multistep syntheses, making their utilization in ring-opening metathesis polymerization (ROMP) less feasible.[89,90] However, an alternative approach involves subjecting unsaturated polymers obtained from ROMP to partial hydrogenation. This process reduces the degree of unsaturation, resulting in polymers that more closely resemble the thermal and solid-state properties of polyethylene. This methodology has been demonstrated in the ROMP of cyclopentene.[91]

A condensation reaction of difunctionalized telechelic macromonomers is another effective method for creating a polyethylene-like polymer. This macromonomer synthesized via ring-opening metathesis polymerization (ROMP) with a functionalized acyclic alkene serving as a chain transfer agent (CTA).[92] Carboxyl-functionalized telechelic long-chain monomers can be precisely synthesized using unsaturated diacids like maleic acid (Figure1.9, A).[93] Hydroxyl-terminated telechelic molecules are generated by using diacetyl alkenes as the CTA in ROMP; these molecules can later be transformed into free alcohols through hydrolysis.[94,95] Hydrogenating unsaturated α,ω-telechelic molecules leads to saturated polyethylene-like segments, which can then be used as long-chain monomers for polycondensation reactions, resulting in recyclable polyethylene-like polymers.[96] This approach has been applied to produce both linear, high-density polyethylene (HDPE)-like segments, as well as branched, linear low-density polyethylene (LLDPE)-like building blocks. [97,98]

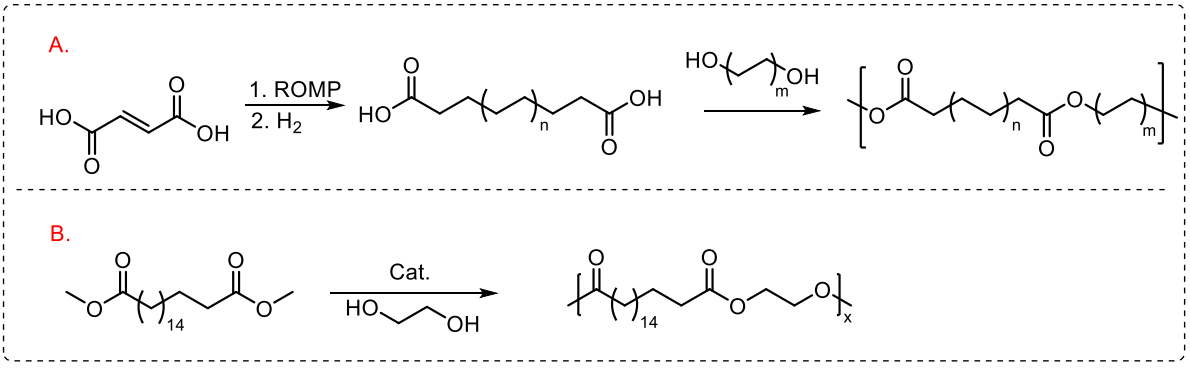

Figure 1.9: Synthesis of deconstructable in-chain ester functionalized polyethylene like material.

Mecking and co-worker introduced a newly developed polyester material derived from easily accessible biobased 1,18-octadecanedi-carboxylic acid and ethylene glycol (Figure1.9, B). This polyester has a solid-state structure that resembles polyethylene and shows tensile properties similar to those of high-density polyethylene (HDPE).[99] In this polymer, functional

groups are situated after the long [$(CH_2)_{16}$] hydrophobic repeating units, so it is behaving like polyethylene. Also they studied the biodegradation of this material were more than 95% of degradation was observed within 2 months.

1.3. Summary:

The seemingly matured field of olefin polymerization still poses several challenges and holds enormous potential to meet contemporary material requirements. In olefin polymerization ligands plays an important role to control the molecular weight, crystallinity, branching and tacticity. In this chapter, we highlighted the historical context and recent advancements in metal-catalyzed olefin polymerization. Emphasizing the pivotal role of transition metal complexes as catalysts, the chapter elucidates their mode of action and highlights the factors influencing polymerization and activity. A significant portion of this chapter is devoted to exploring ethylene oligomerization processes catalyzed by transition metal complexes. The chapter outlined the industrially practiced catalyst for ethylene oligomerization.

Furthermore, this chapter also investigates the synthesis of depolymerizable polyethylene-like polymers, a burgeoning area with promising implications for sustainability and recycling. By employing innovative strategies, such as incorporating cleavable linkages or functional groups into the polymer backbone, novel polyethylene analogs are synthesized that exhibit enhanced degradability without compromising the material properties.

1.4. Aim of the thesis:

The microstructure of a polymer plays a crucial role in determining its properties, and it is majorly controlled by the tuning the ligands used in the catalytic polymerization. Over the last three decades, significant progress has been made in developing ligands for various applications, but there is a limited selection of catalysts capable of producing hyperbranched ethylene oligomers.

To create hyperbranched microstructures, catalysts must exhibit a high chain-walking rather than favoring chain-propagation reactions. This behavior is influenced by the catalyst's design and, specifically, the steric hindrance introduced by the ligands. Traditional catalysts like phenoxy-imine and α-diimine have demonstrated only moderate to low catalytic activity in ethylene oligomerization. To address this, we designed naphthoxy-imine ligands with varied steric hindrance to decrease the formation of bisligated monometallic complexes, ensuring catalyst remains active for the longer time. Additionally, using larger 4d transition metals (Palldium) with higher β-hydride elimination can further encourage hyperbranched ethylene oligomer production. These new ligated catalyst designs not only extend the catalyst's lifespan

but also allow for greater tolerance to polar solvents and functional groups, expanding the range of possible reaction environments beyond the traditional toluene.

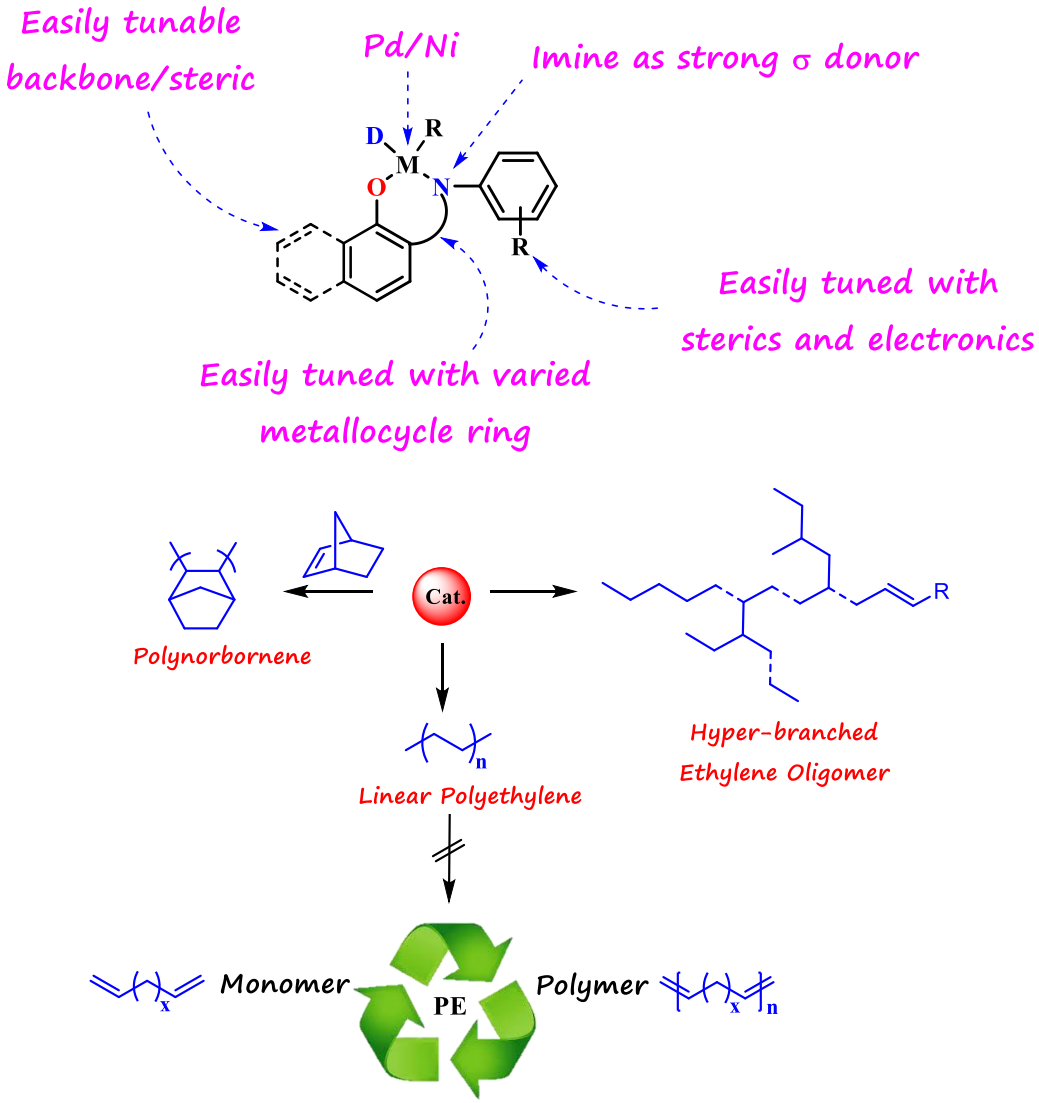

Figure 1.10: Designing metal catalyst (top) and proposed reactions with the catalyst (bottom).

Beyond hyperbranched polymers, it's also crucial to control the branching and molecular weight to produce linear high molecular weight polyethylene. Ligand sterics play a vital role in this process, along with selecting metal precursors (3d metals like Nickel) that allows high coordination and insertion affinity. Literature report suggest that the effect of steric bulk on ethylene polymerization has been investigated for two ligand systems: α–diamine and phenoxy-imine. Therefore, there's a need for more comprehensive analysis of naphthoxy-imine ligand systems to understand how steric and electronic factors influence polymerization outcomes.

Another key focus of this thesis is investigating the electronic effects of ligands on metal catalyst and their role in norbornene homopolymerization. Although norbornene

homopolymerization is challenging, despite this several catalysts have been developed. However, comprehensive studies on the electronic effects on metal catalysts remain scarce. Our research aims to fill this gap by exploring the impact of electronic characteristics on metal catalysts, contributing to a deeper understanding of the polymerization process.

Additionally, the substantial use of polyolefins has resulted in significant waste generation, underscoring the need to prioritize their depolymerization and recyclability. Polyethylene, for example, lacks functional groups, making it challenging to degrade or depolymerize. To address this issue, we focus on synthesizing polyethylene-like polymers with predetermined breaking points in the polymer backbone. These polymers can be chemically recycled back to their monomers and then reconverted to polymers, offering a sustainable solution for polyolefin waste. By integrating these depolymerization capabilities, we can move toward more sustainable polyolefin production and recycling processes, addressing both environmental and economic challenges.

Thus the overall aim of this thesis is the synthesis of electronically and sterically tuned ligands and its corresponding palladium and nickel catalyst for the olefin polymerization. Also, we demonstrate the synthesis of chemically recyclable polyethylene like polymers.

1.5. References:

1. Chikkali S. H. (Ed.) Metal catalyzed polymerization: fundamentals to applications. CRC Press, Taylor and Francis Group, FL, USA, 2017 and the references therein.
2. Blank, F.; Janiak, C. Metal catalysts for the vinyl/addition polymerization of norbornene. *Coord. Chem. Rev.* **2009**, *253*, 827-861.
3. Hustad, P. D. Frontiers in olefin polymerization: reinventing the world's most common synthetic polymers. *Science* **2009**, *325*, 704−707.
4. Severn, J. R.; Chadwick, J. C. (Eds.) Tailor-Made Polymers; Wiley-VCH Verlag GmbH & Co. KGaA: Weinheim, Germany, 2008.
5. Tritto, I.; Boggioni L.; Ferro, D. R. Metallocene catalyzed ethene-and propene co-norbornene polymerization: Mechanisms from a detailed microstructural analysis. *Coord. Chem. Rev.* **2006**, *250*, 212.
6. M. R. Buchmeiser, Homogeneous metathesis polymerization by well-defined group VI and group VIII transition-metal alkylidenes: Fundamentals and applications in the preparation of advanced materials. *Chem. Rev*. **2000**, *100*, 1565-1604.

7. Karanjia, H.; Kheterpal, N.; Morgan, M; Sood, M. Linear Alpha Olefins Market Study : Chemical Strategic Report. September 2023.
8. Godwin, A. D.; Lyman, D. M. High performance plasticizers from branched oxo alcohols 1999. AU752777B2.
9. Sauter, D. W.; Taoufik, M.; Boisson, C. Polyolefins, a success story. *Polymers* **2017**, *9*, 185.
10. Nakamura, A.; Ito, S.; Nozaki, K. Coordination-insertion copolymerization of fundamental polar monomers. *Chem. Rev.* **2009**, *109*, 5215-5244.
11. Johnson, L. K.; Mecking, S.; Brookhart, M. Copolymerization of Ethylene and Propylene with Functionalized Vinyl Monomers by Palladium(II) Catalysts. *J. Am. Chem. Soc*. **1996**, *118*, 267-268.
12. Mecking, S.; Johnson, L. K.; Wang, L.; Brookhart, M. Mechanistic Studies of the Palladium-catalyzed copolymerization of ethylene and α-Olefins with methyl acrylate. *J. Am. Chem. Soc.* **1998**, *120*, 888-899.
13. Chen, E. Y. X.; Marks, T. J. Cocatalysts for metal-catalyzed olefin polymerization: Activators, activation processes, and structure-activity relationships. *Chem. Rev.* **2000**, *100*, 1391-1434.
14. Zijlstra, H. S.; Harder, S. Methylalumoxane–history, production, properties, and Applications. *Eur. J. Inorg. Chem.* **2015,** 19-43.
15. Velthoen, M. E. Z.; Munoz-Murillo, A.; Bouhmadi, A.; Cecius, M.; Diefenbach, S.; Weckhuysen, B. M. The multifaceted role of methylaluminoxane in metallocene-based olefin polymerization catalysis. *Macromolecules* **2018**, *51*, 343-355.
16. Camacho, D. H.; Guan, Z. Designing late-transition metal catalysts for olefin insertion polymerization and copolymerization. *Chem. Commun.* **2010**, *46*, 7879-7893.
17. Wang, F.; Chen, C. A continuing legend: The Brookhart-type α-diimine nickel and palladium catalysts. *Polym. Chem.* **2019**, *10*, 2354-2369.
18. Ittel, S. D.; Johnson, L. K.; Brookhart, M. Late-metal catalysts for ethylene homo- and copolymerization. *Chem. Rev.* **2000**, *100*, 1169-1204.
19. Tempel, D. J.; Johnson, L. K.; Huff, R. L.; White, P. S.; Brookhart, M. Mechanistic studies of Pd(II)−α-diimine-catalyzed olefin polymerizations. *J. Am. Chem. Soc.* **2000**, *122*, 6686−6700.

20. Younkin, T. R.; Connor, E. F.; Henderson, J. I.; Friedrich, S. K.; Grubbs, R. H.; Bansleben, D. A. Neutral, Single-component Nickel (II) polyolefin catalysts that tolerate heteroatoms. *Science* **2000**, *287*, 460-462.

21. Mu, H.; Pan, L.; Song, D.; Li, Y. Neutral nickel catalysts for olefin homo- and copolymerization: relationships between catalyst structures and catalytic properties. *Chem. Rev.* **2015**, *115*, 12091-12137.

22. Nozaki, K.; Kusumoto, S.; Noda, S.; Kochi, T.; Chung, L. W.; Morokuma, K. Why did incorporation of acrylonitrile to a linear polyethylene become possible? Comparison of phosphine-sulfonate ligand with diphosphine and imine-phenolate ligands in the Pd-catalyzed ethylene/acrylonitrile copolymerization. *J. Am. Chem. Soc.* **2010**, *132*, 16030-16042.

23. Carrow, B. P.; Nozaki, K. Synthesis of functional polyolefins using cationic bisphosphine monoxide−palladium complexes. *J. Am. Chem. Soc.* **2012**, *134*, 8802-8805.

24. Zhou, X.; Jordan, R. F. Synthesis, cis/trans isomerization, and reactivity of palladium alkyl complexes that contain a chelating N-heterocyclic-carbene sulfonate ligand. *Organometallics* **2011**, *30*, 4632-4642.

25. Nakano, R.; Nozaki, K. Copolymerization of propylene and polar monomers using Pd/IzQO catalysts. *J. Am. Chem. Soc.* **2015**, *137*, 10934-10937.

26. Black, R. E.; Jordan, R. F. Synthesis and reactivity of palladium(II) alkyl complexes that contain phosphine-cyclopentanesulfonate ligands. *Organometallics* **2017**, *36*, 3415-3428.

27. Contrella, N. D.; Sampson, J. R.; Jordan, R. F. Copolymerization of ethylene and methyl acrylate by cationic palladium catalysts that contain phosphine-diethyl phosphonate ancillary ligands. *Organometallics* **2014**, *33*, 3546-3555.

28. Hasan, T.; Ikeda T.; Shiono, T. Highly efficient Ti-based catalyst systems for vinyl addition polymerization of norbornene. *Macromolecules* **2004**, *37*, 7432-7436.

29. Ziegler, K.; Holzkamp, E.; Breil H.; Martin, H. Das mülheimer normaldruck-polyäthylen-verfahren. *Angew. Chem., Int. Ed. Engl.* **1955**, *67*, 541–547.

30. Antonov, A. A.; Semikolenova, N. V.; Zakharov, V. A.; Zhang, W.; Wang, Y.; Sun, W. H.; Talsi, E. P.; Bryliakov, K. P. Vinyl polymerization of norbornene on nickel complexes with bis (imino) pyridine ligands containing electron-withdrawing groups. *Organometallics* **2012**, *31*, 1143–1149.

31. He, X.; Deng, Y.; Jiang, X.; Wang, Z.; Yang, Y.; Han, Z.; Chen, D. Copolymerization of norbornene and butyl methacrylate at elevated temperatures by a single centre nickel catalyst bearing bulky bis (α-diimine) ligand with strong electron-withdrawing groups. *Polym. Chem.* **2017**, *8*, 2390–2396 and references therein.

32. Makio, H.; Terao, H.; Iwashita A.; Fujita, T. FI Catalysts for olefin polymerization- A comprehensive treatment. *Chem. Rev.* **2011**, *111*, 2363–2449.

33. Wang, H. Y.; Zhang, J.; Meng, X.; Jin, G. X. Nickel (II) complexes with β-enaminoketonato chelate ligands: Synthesis, solid-structure characterization and reactivity toward the addition polymerization of norbornene. *J. Organomet. Chem.* **2006**, *691*, 1275–1281.

34. Yang, D.; Dong, J.; Wang, B. Homo-and copolymerization of norbornene with tridentate nickel complexes bearing o-aryloxide-N-heterocyclic carbene ligands. *Dalton Trans*. **2018**, *47*, 180–189 and the references therein.

35. Cheng, H.; Cai, Z. (Anilino) anthraquinone Nickel-catalyzed random copolymerization of norbornene and ethylene. *ChemCatChem* **2018**, *10*, 497–500 and the references therein.

36. Dang, L.; Guo, J.; Song, H.; Liu B.; Wang, B. Synthesis, structures, and norbornene polymerization behavior of C (sp^3), N-chelated palladacycles bearing o-aryloxide-N-heterocyclic carbene ligands. *Dalton Trans.* **2014**, *43*, 17177–17183.

37. Li, M.; Zhang, H.; Cai, Z.; Eisen, M. S. Norbornene polymerization and copolymerization with 1-alkenes by neutral palladium complexes bearing aryloxide imidazolin-2-imine ligand. *Polym. Chem*. **2019**, *10*, 2741-2748 and the references therein.

36. Dang, L.; Guo, J.; Song, H.; Liu B.; Wang, B. Synthesis, structures, and norbornene polymerization behavior of C (sp^3), N-chelated palladacycles bearing o-aryloxide-N-heterocyclic carbene ligands. *Dalton Trans.* **2014**, *43*, 17177–17183.

38. Zhuang, R.; Liu, H.; Guo, J.; Dong, B.; Zhao, W.; Hu, Y.; Zhang, X. Highly active nickel (II) and palladium (II) complexes bearing N, N, P tridentate ligand for vinyl addition polymerization of norbornene. *Eur. Polym. J.* **2017**, *93*, 358–367 and the references therein

39. Zheng, T.; Liao, H.; Gao, J.; Zhong, L.; Gao, H.; Wu, Q. Synthesis and characterization of α-diamine palladium complexes and insight into hybridization effects of nitrogen donor atoms on norbornene (co) polymerizations. *Polym. Chem.* **2018**, *9*, 3088–3097.

40. Dang, L.; Song, H.; Wang, B. Synthesis, structures, and norbornene polymerization behavior of o-aryloxide-substituted NHC-ligated σ, π-cycloalkenyl palladium complexes. *Organometallics* **2014**, *33*, 6812–6818 and the references therein.

41. Mahmood, Q.; Li, X.; Qin, L.; Wang, L.; Sun, W. H. Structural evolution of iminopyridine support for nickel/palladium catalysts in ethylene (oligo) polymerization. *Dalton Trans.* **2022**, *51*, 14375 – 14407.

42. Dai, S.; Zhou, S.; Zhang, W.; Chen, C. Systematic investigations of ligand steric effects on α-diimine palladium catalyzed olefin polymerization and copolymerization. *Macromolecules* **2016**, *49*, 8855−8862.

43. Sun, J.; Wang, F.; Li, W.; Chen, M. Ligand steric effects on α-diimine nickel catalyzed ethylene and 1-hexene polymerization. *RSC Adv.* **2017**, *7***,** 55051-55059.

44. Lu, Z.; Xu, X.; Luo, Y.; He, S.; Fan, W.; Dai, S. Unexpected effect of catalyst's structural symmetry on the branching microstructure of polyethylene in late transition metal polymerization catalysis. *ACS Catal.* **2023**, *13***,** 725−734.

45. Younkin, T. R.; Connor, E. F.; Henderson, J. I.; Friedrich, S. K.; Grubbs, R. H.; Bansleben, D. A. Neutral, single-component nickel (II) polyolefin catalysts that tolerate heteroatoms. *Science* **2000**, *287***,** 460-462.

46. Chen, Z.; Mesgar, M.; White, P. S.; Daugulis, O.; Brookhart, M. Synthesis of branched ultrahigh-molecular-weight polyethylene using highly active neutral, single-component Ni (II) catalysts. *ACS Catal.* **2015**, *5*, 631-636.

47. Weberski Jr, M. P.; Chen, C.; Delferro, M.; Zuccaccia, C.; Macchioni, A.; Marks, T. J. Suppression of β-hydride chain transfer in nickel (II)-catalyzed ethylene polymerization via weak fluorocarbon ligand–product interactions. *Organometallics* **2012**, *31*, 3773-3789.

48. Wang, C.; Kang, X.; Mu, H.; Jian, Z. Positive effect of polar solvents in olefin polymerization catalysis. *Macromolecules* **2022**, *55*, 5441-5447.

49. Alsherehy, F. A. IFP-SABIC process for the selective ethylene dimerization to butene-1. *Stud. Surf. Sci. Catal.* **1996**, *100*, 515–523.

50. Britovsek, G. J.; Malinowski, R.; McGuinness, D. S.; Nobbs, J. D.; Tomov, A. K.; Wadsley, A. W.; Young, C. T. Ethylene oligomerization beyond Schulz–Flory distributions. *ACS Catal.* **2015**, *5*, 6922–6925.

51. Van Leeuwen, P. W. N. M.; Clément, N. D.; Tschan, M. J. L. New processes for the selective production of 1-octene. *Coord. Chem. Rev.* **2011**, *255*, 1499.

52. McGuinness, D. S. Olefin oligomerization via metallacycles: dimerization, trimerization, tetramerization, and beyond. *Chem. Rev.* **2011**, *111*, 2321.

53. Wang, M.; Wu, W.; Wang, X.; Huang, X.; Nai, Y.; Wei, X.; Mao, G. Research progress of iron-based catalysts for selective oligomerization of ethylene. *RSC Adv.* **2020**, *10*, 43640.

54. Wiedemann, T.; Voit, G.; Tchernook, A.; Roesle, P.; Göttker-Schnetmann, I.; Mecking, S. Monofunctional hyperbranched ethylene oligomers. *J. Am. Chem. Soc*. **2014,** *136*, 2078–2085.

55. Deng, L.; Woo, T. K.; Cavallo, L.; Margl, P. M.; Ziegler, T. The role of bulky substituents in Brookhart-type Ni (II) diimine catalyzed olefin polymerization: a combined density functional theory and molecular mechanics study. *J. Am. Chem. Soc*. **1997**, *119*, 6177–6186.

56. Xiang, P.; Ye, Z.; Subramanian, R. Synthesis and characterization of low-and medium-molecular-weight hyperbranched polyethylenes by chain walking ethylene polymerization with Pd–diimine catalysts. *Polymer* **2011**, *52*, 5027–5039.

57. Zhang, Y.; Zhang, Y.; Hu, X.; Wang, C.; Jian, Z. Advances on controlled chain walking and suppression of chain transfer in catalytic olefin polymerization. *ACS Catal*. **2022**, *12*, 14304–14320.

58. Zheng, J.; Suh, S. Strategies to reduce the global carbon footprint of plastics. *Nat. Clim. Chang*. 2**019**, *9*, 374−378.

59. Nakamura, A.; Ito, S.; Nozaki, K. Coordination-insertion copolymerization of fundamental polar monomers. *Chem. Rev*. **2009**, *109*, 5215−5244.

60. Gloor, P.; Tang, Y.; Kostanska, A.; Hamielec, A. Chemical modification of polyolefins by free radical mechanisms: A modelling and experimental study of simultaneous random scission, branching and crosslinking. *Polymer* **1994**, *35*, 1012−1030.

61. Moad, G. The synthesis of polyolefin graft copolymers by reactive extrusion. *Prog. Polym. Sci*. **1999**, *24*, 81−142.

62. Shi, J. X.; Ciccia, N. R.; Pal, S.; Kim, D. D.; Brunn, J. N.; Lizandara-Pueyo, C.; Ernst, M.; Haydl, A. M.; Messersmith, P. B.; Helms, B. A. Chemical modification of oxidized polyethylene enables access to functional polyethylenes with greater reuse. *J. Am. Chem. Soc*. **2023**, *145*, 21527−21537.

63. Teo, J. Y. Q.; Yeung, C. W. S.; Tan, T. T. Y.; Loh, W. W.; Loh, X. J.; Lim, J. Y. C. Benzaldehyde-mediated selective aerobic polyethylene functionalisation with isolated backbone ketones. *Green Chem*. **2022**, *24*, 6287−6294.

64. Coffman, D. D.; Pinkney, P. S.; Wall, F. T.; Wood, W. H.; Young, H. S. Compositional relationships in the copolymerization of ethylene with carbon monoxide. *J. Am. Chem. Soc*. **1952**, *74*, 3391− 3393.

65. Brubaker, M. M.; Coffman, D. D.; Hoehn, H. H. Synthesis and characterization of ethylene/carbon monoxide copolymers, a new class of polyketones. *J. Am. Chem. Soc.* **1952**, *74*, 1509−1515.

66. Morgen, T. O.; Baur, M.; Göttker, I.; Mecking, S. Photodegradable branched polyethylenes from carbon monoxide copolymerization under benign conditions. *Nat. Commun*. **2020**, *11*, 3693.

67. Drent, E.; van Dijk, R.; van Ginkel, R.; van Oort, B.; Pugh, R. I. The first example of palladium catalysed non-perfectly alternating copolymerisation of ethene and carbon monoxide. *Chem. Commun*. **2002**, 964−965.

68. Bettucci, L.; Bianchini, C.; Claver, C.; Suarez, E. J. G.; Ruiz, A.; Meli, A.; Oberhauser, W. Ligand effects in the non-alternating CO ethylene copolymerization by palladium(II) Catalysis. *Dalton Trans.* **2007**, 5590−5602.

69. Luo, R.; Newsham, D. K.; Sen, A. Palladium-catalyzed nonalternating copolymerization of ethene and carbon monoxide: scope and mechanism. *Organometallics* **2009**, *28*, 6994−7000.

70. Baur, M.; Lin, F.; Morgen, T. O.; Odenwald, L.; Mecking, S. Polyethylene materials with in-chain ketones from nonalternating catalytic copolymerization. *Science* **2021**, *374*, 604−607.

71. Voccia, M.; Odenwald, L.; Baur, M.; Lin, F.; Falivene, L.; Mecking, S.; Caporaso, L. Mechanistic insights into Ni(II)-catalyzed nonalternating ethylene-carbon monoxide copolymerization. *J. Am. Chem. Soc.* **2022**, *144*, 15111−15117.

72. Tang, S.; Seidel, F. W.; Nozaki, K. High Density Polyethylenes Bearing Isolated In-Chain Carbonyls. *Angew. Chem. Int. Ed.* **2021**, *133*, 26710−26714.

73. Chen, S. Y.; Pan, R. C.; Chen, M.; Liu, Y.; Chen, C.; Lu, X. B. Synthesis of nonalternating polyketones using cationic diphosphazane monoxide-palladium complexes. *J. Am. Chem. Soc.* **2021**, *143*, 10743−10750.

74. Zhu, L.; Gaire, S.; Ziegler, C. J.; Jia, L. Nickel catalysts for non-alternating CO-ethylene copolymerization. *ChemCatChem*. **2022**, *14*, e202200974.

75. Kosaka, N.; Hiyama, T.; Nozaki, K. Baeyer-Villiger oxidation of an optically active 1,4-polyketone. *Macromolecules* **2004**, *37*, 4484−4487.

76. Yuan, H.; Takahashi, K.; Hayashi, S.; Suzuki, M.; Fujikake, N.; Kasuya, K. I.; Zhou, J.; Nakagawa, S.; Yoshie, N.; Li, C. Synthesis of novel polymers with biodegradability from propylene and carbon monoxide. ChemRxiv2023. DOI: 10.26434/chemrxiv2023-wj0p6.

77. Sobkowicz, M. J. Polymer design for the circular economy. *Science* **2021**, *374*, 540.

78. Baur, M.; Mast, N. K.; Brahm, J. P.; Habé, R.; Morgen, T. O.; Mecking, S. High-density polyethylene with in-chain photolyzable and hydrolyzable groups enabling recycling and degradation. *Angew. Chem., Int. Ed. Engl.* **2023**, *62*, No. e202310990.

79. Nakano, R.; Ito, S.; Nozaki, K. Copolymerization of carbon dioxide and butadiene via a lactone intermediate. *Nat. Chem.* **2014**, *6*, 325−331.

80. Price, C. J.; Reich, B. J. E.; Miller, S. A. Thermodynamic and kinetic considerations in the copolymerization of ethylene and carbon dioxide. *Macromolecules* **2006**, *39*, 2751−2756.

81. Barbotin, F.; Monteil, V.; Llauro, M. F.; Boisson, C.; Spitz, R. First synthesis of poly(ethene- co −1,3-butadiene) with neodymocene catalysts. *Macromolecules* **2000**, *33*, 8.

82. Shiono, T.; Yoshino, O.; Ikeda, T. Synthesis and oxidative degradation of poly(ethene-ran-1,3-butadiene). *Macromol. Rapid Commun.* **2000**, *21*, 1297−1301.

83. Adnan Akram, M.; Liu, X.; Fu, Z.; Fan, Z. Ethylene-butadiene copolymerization and ethylene-1-hexene-butadiene terpolymerization with a $MgCl_2$ supported Ziegler-Natta catalyst: polymer structure and active centers. *ChemistrySelect* **2021**, *6*, 8288−8298.

84. Belaid, I.; Monteil, V.; Boisson, C. Copolymerization of ethylene with conjugated dienes. in handbook of transition metal polymerization catalysts; Hoff, R., Hoff, R. E., Mathers, R. T., Eds.; Wiley: Hoboken, NJ, 2010; pp 661−692.

85. Schwab, S. T.; Baur, M.; Nelson, T. F.; Mecking, S. Synthesis and deconstruction of polyethylene-type materials. *Chem. Rev.* **2024**, *124*, 2327−2351.

86. Parke, S. M.; Lopez, J. C.; Cui, S.; LaPointe, A. M.; Coates, G. W. Polyethylene oncorporating Diels-Alder comonomers: A ″Trojan Horse″ strategy for chemically recyclable polyolefins. *Angew. Chem., Int. Ed.* **2023**, *62*, e202301927.

87. Walker, R.; Conrad, R. M.; Grubbs, R. H. The Living ROMP of trans-Cyclooctene. *Macromolecules* **2009**, *42*, 599−605.

88. Schrock, R. R. Living Ring-Opening Metathesis Polymerization catalyzed by well-characterized transition-Metal alkylidene complexes. *Acc. Chem. Res.* **1990**, *23*, 158−165.

89. Cho, I. Ring-Opening polymerizations for the synthesis of sequence-controlled copolymers. *Macromol. Symp.* **2003**, *195*, 89− 94.

90. Hlil, A. R.; Balogh, J.; Moncho, S.; Su, H. L.; Tuba, R.; Brothers, E. N.; Al-Hashimi, M.; Bazzi, H. S. Ring Opening Metathesis Polymerization (ROMP) of five- to eight-membered cyclic olefins: computational, thermodynamic, and experimental approach. *J. Polym. Sci., Part A: Polym. Chem.* **2017**, *55*, 3137−3145.

91. Naga, N.; Arai, R.; Kikuchi, G.; Toyota, A.; Noguchi, K.; Sone, M.; Shirae, F.; Gotoh, T.; Kurosu, H. Crystalline structure of polyethylene containing vinylene units in the main chain. *Polymer* **2011**, *52*, 4857−4866.

92. Yan, T.; Guironnet, D. Synthesis of telechelic polyolefins. *Polym. Chem.* **2021**, *12*, 5126−5138.

93. Pitet, L. M.; Hillmyer, M. A. Carboxy-telechelic polyolefins by ROMP using maleic acid as a chain transfer agent. *Macromolecules* **2011**, *44*, 2378−2381.

94. Hillmyer, M. A.; Grubbs, R. H. Preparation of hydroxytelechelic poly(butadiene) via Ring-Opening Metathesis Polymerization employing a well-defined metathesis catalyst. *Macromolecules* **1993**, *26*, 872−874.

95. Bielawski, C. W.; Scherman, O. A.; Grubbs, R. H. Highly efficient syntheses of acetoxy- and hydroxy-terminated telechelic poly(butadiene)s using ruthenium catalysts containing N -heterocyclic ligands. *Polymer* **2001**, *42*, 4939−4945.

96. Pitet, L. M.; Hillmyer, M. A. Carboxy-telechelic polyolefins by ROMP using maleic acid as a chain transfer agent. *Macromolecules* **2011**, *44*, 2378−2381.

97. Arrington, A. S.; Brown, J. R.; Win, M. S.; Winey, K. I.; Long, T. E. Melt polycondensation of carboxytelechelic polyethylene for the design of degradable segmented copolyester polyolefins. *Polym. Chem.* **2022**, *13*, 3116−3125.

98. Zhao, Y.; Rettner, E. M.; Harry, K. L.; Hu, Z.; Miscall, J.; Rorrer, N. A.; Miyake, G. M. Chemically recyclable polyolefin-like multiblock polymers. *Science* **2023**, *382*, 310−314.

99. Eck, M.; Schwab, S. T.; Nelson, T. F.; Wurst, K.; Iberl, S.; Schleheck, D.; Mecking, S. Biodegradable high-density polyethylene-like material. *Angew. Chem.* **2023** *135*, e202213438.

Chapter 2

Palladium-Catalyzed Polar Solvent Empowered Synthesis of Hyper-Branched Ethylene Oligomers and their Application

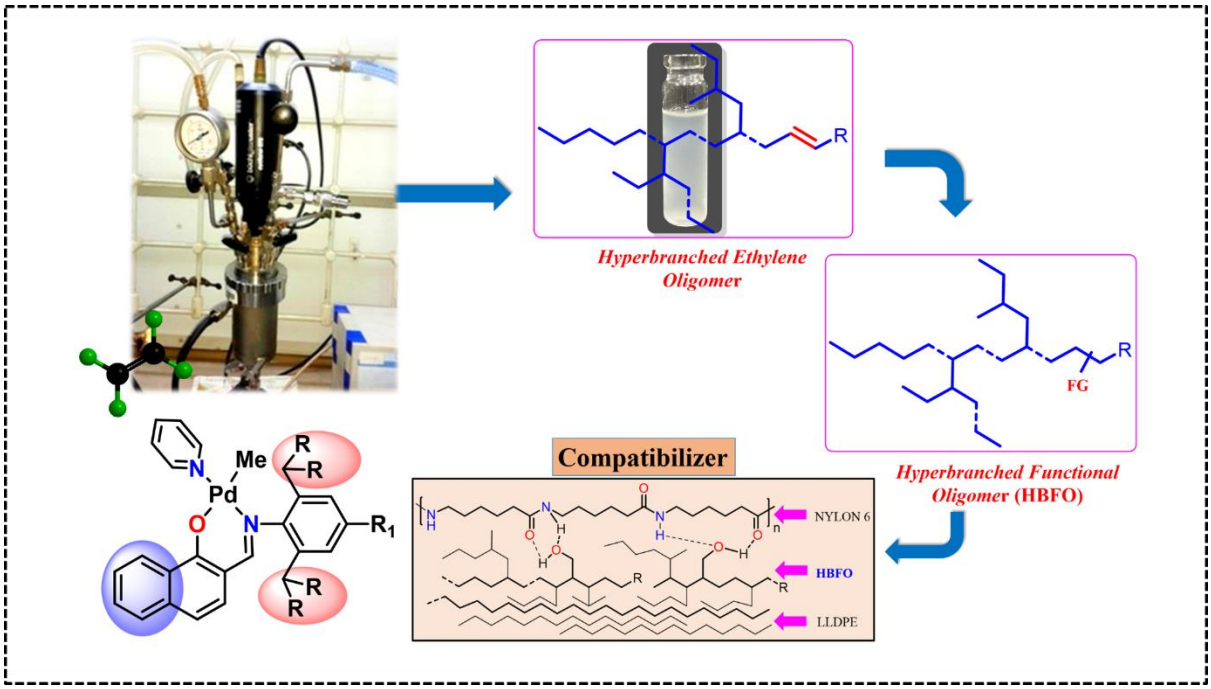

Birajdar, R. S; Gonnade, R. G.; Pol, H. V.; Basava Prabhu M.; Rokade, D.; Nandimatha, S.; Chikkali, S. H. *Polym. Chem*. **2023**, *14*, 3239-3251.

2.1. Abstract:

In this contribution, we report the synthesis of two naphthoxy imine ligands, 2-(((2,6-dibenzhydryl-4-methoxyphenyl)imino) methyl) naphthalen-1-ol (2L1), and 2-(((2,6-diisopropylphenyl)imino) methyl) naphthalen-1-ol (2L2) with different steric and electronic features. 2L1 and 2L2 were treated with [(TMEDA)$PdMe_2$] to obtain corresponding neutral palladium (II) complexes 2Pd1 and 2Pd2 in excellent yield. The identity of 2Pd1 and 2Pd2 was unambiguously ascertained using a combination of spectroscopic and analytical methods, including single-crystal X-ray diffraction. When exposed to 5 bar ethylene pressure, 2Pd1 produced hyperbranched ethylene oligomers. Microstructure analysis of ethylene oligomers confirmed the existence of methyl, ethyl, propyl, and sec-butyl branches, with a molecular weight (M_n) of 500-1400 g/mol, PDI of 1.46-2.10, and 67-106 branches per 1000 carbon atoms. The use of polar solvent, tetrahydrofuran, led to a remarkable 3 fold increase in oligomerization activity without compromising the branching and molecular weight. The resultant hyperbranched ethylene oligomers were selectively monofunctionalized using industrially practiced hydroformylation, ozonolysis, and epoxidation, almost quantitatively. The hydroxy functionalized ethylene oligomer (F4) (5 wt%) was melt-compounded with LLDPE and Nylon-6 to produce a tough yet flexible blend with a higher strain-to-failure as compared to an un-compatibilized blend.

2.2. Introduction:

Metal-catalyzed polymerization of olefins to polyolefins, such as polyethylene, polypropylene, etc. is well established, and today the world produces ~180 million tonnes of polyolefin per year.[1-4] The current polyolefin manufacturing technologies mainly use heterogeneous Ziegler-type catalysts with donors and additives.[5] Over the years, the interest in homogenously catalyzed olefin polymerization has attracted significant attention as these catalysts may offer an opportunity to improve specific properties of the resultant polymer.[6,7] Transition metal-catalyzed functional olefin polymerization resulting in the formation of functional polyolefin represents one of the most important reactions.[8-11] Ziegler's initial work on homogeneous alkyl aluminum catalysts and ethylene produced low molecular weight ethylene oligomers, which led to the development of an industrial process named "Alfol" process.[12-14] Apart from aluminium, nickel has been used to prepare ethylene oligomers. The commercial SHOP-type catalysts described in 1968 are the most noteworthy examples.[15] Since then, numerous other bidentate Ni-based catalysts have been reported.[16-19] Most of these catalysts produce highly linear ethylene oligomers.

However, the synthesis of low-molecular weight (M_w) ethylene oligomers with hyperbranched microstructures was very difficult to achieve using the above catalysts. Such hyperbranched ethylene oligomers can be used as functional additives in lubricants, surface treatments, compatibilizer, waxes, etc. For producing hyperbranched ethylene oligomers, the choice of catalysts is decisive. Catalysts with significant chain walking abilities can produce highly branched structures.[20] In 1995 Brookhart reported late metal catalysts based on Ni(II) and Pd(II) with bidentate α-diimine ligands [N,N] as efficient catalysts for ethylene polymerization.[21,22] These cationic complexes display extensive chain walking during polymerization. Though the Pd-catalyst yields a highly branched structure, the molecular weight is high and produces amorphous rubbery material.[21,23-26] In these α-diimine ligated metal catalysts, the bulky substituents on ligand reduce the chain transfer and yield a high molecular weight polymer.[27-30] While less bulky substituents display low activity and produce hyperbranched low molecular weight oligomers.[31,32]

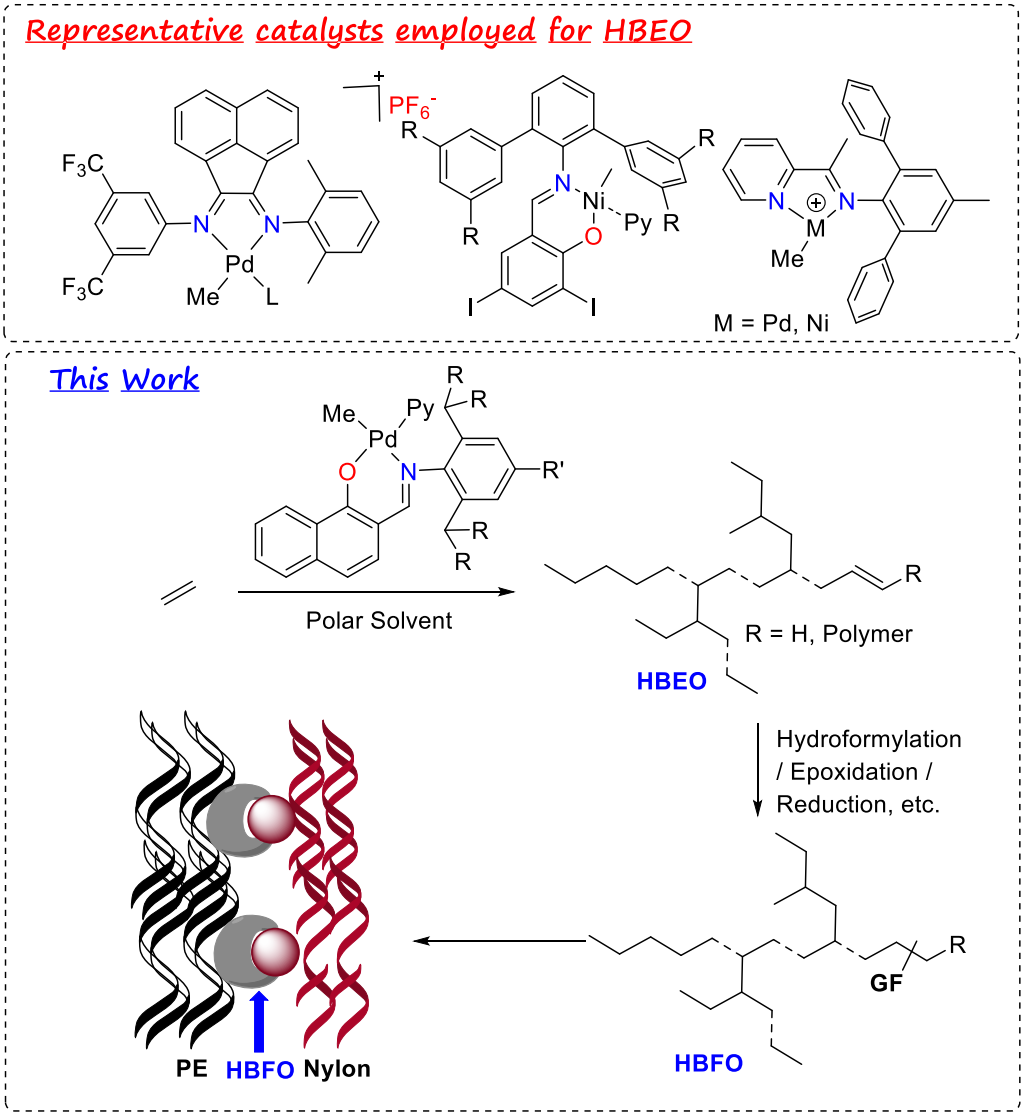

Figure 2.1: Representative catalysts utilized in the synthesis of hyper-branched ethylene oligomers (HBEO) (top) and this work (bottom), hyperbranched functional ethylene oligomers (HBFO).

In the 1990s, metal complexes with the salicylaldimine (phenoxy imine) ligands were reported to be active in olefin polymerization.[33-36] After this discovery, researchers modified this ligand and investigated olefin polymerization, and phenomenal work has been done on the ligand modification with early as well as late transition metals.[37,38] In 2014 Mecking and co-workers reported the neutral Ni(II) salicyldiminato complex that converts ethylene into a hyperbranched low molecular weight ethylene oligomer with high activity.[20]

Ethylene oligomers or polymers with <10 branches per 1000 carbon atoms are considered as low branching material. While 75-100 branches per 1000 carbon atom is considered high branching, >150 branches per 1000 carbon atom is termed as ultrahigh branching number.[39] Producing ethylene oligomers with hyperbranched microstructure requires the catalysts to chain walk and display high propensity for chain transfer. Catalysts that can chain walk without chain transfer will produce highly branched but high molecular weight polyethylene. Thus, synthesizing hyperbranched ethylene oligomers is challenging, and only a handful of catalysts could achieve this feat (Figure 2.1, top).

Herein we report a neutral Pd(II) naphthoxyimine ligated complex that produces hyperbranched ethylene oligomers (Figure 2.1, bottom). Surprisingly, the use of polar solvent produced a highly active catalyst, tripling activity without affecting branching and molecular weight. The resultant hyperbranched ethylene oligomer was functionalized using hydroformylation, epoxidation, etc., and was found to be an excellent compatibilizer for two non-miscible polymers.

2.3. Results and discussion:

2.3.1. Ligand synthesis:

The synthesis of starting aldehyde, 1-hydroxy 2-naphthaldehyde, is reported. We identified a single-step synthetic protocol, and 1-hydroxy 2-naphthaldehyde was prepared by modifying the literature procedure.[40] 1-Naphthol was treated with paraformaldehyde to obtain 1-hydroxy 2-naphthaldehyde (**1**) in 56% isolated yield (Scheme 2.1). The reaction between diphenyl methanol, *p*-anisidine and zinc chloride in HCl produced an aniline derivative **2**.[41]

The starting aldehyde **1** was treated with a 2,6-dibenzhydryl-4-methoxyaniline (**2**) in toluene, and the reaction mixture was refluxed for 6 hours. During the reflux, the color of the reaction mixture changed from dark brown to yellowish-brown. After completion of the reaction,

volatiles were evaporated, and pure ligand 2-(((2,6-dibenzhydryl-4-methoxyphenyl)imino) methyl) naphthalen-1-ol (**2L1**) was obtained in 69% isolated yield after column chromatography (Scheme 2.1). A proton NMR of the above solid revealed a characteristic singlet at 6.65 ppm (Figure S2.2 and S2.6), which can be easily assigned to an imine N=C−*H* proton. The proton NMR findings were further corroborated by ^{13}C NMR, which revealed an imine carbon at 168 ppm. Furthermore, the existence of **2L1** was expressed by using a combination of 1-2D NMR spectroscopy, and cross peaks confirmed the presence of compound **2L1**. An IR of **2L1** revealed the presence of an imine CN band at 1605 cm^{-1} and OH at 3385 cm^{-1}. The NMR and IR findings were corroborated by mass spectrometry analysis, which revealed a molecular ion peak at m/z = 610.27 Da $[M+H]^+$. The observed mass and isotopic pattern exactly match with the simulated pattern (Figure S2.7).

Along the same line, sterically less bulky ligand 2-(((2,6-diisopropylphenyl)imino) methyl) naphthalen-1-ol (**2L2**) was prepared. Compound **1** was treated with 2,6-diisopropylaniline in toluene at 110 °C for 6 hours. After completion of the reaction, the desired ligand 2L2 was purified by column chromatography in 51% isolated yield. The Proton NMR spectrum of this compound disclosed a characteristic imine proton at 8.49 ppm, and a corresponding carbon appeared at 165 ppm in a ^{13}C NMR spectrum. The NMR data was further supported by an IR band at 1604 cm^{-1} (CN) and an ESI-MS molecular ion peak at m/z = 332.20 Da $[M+H]^+$.

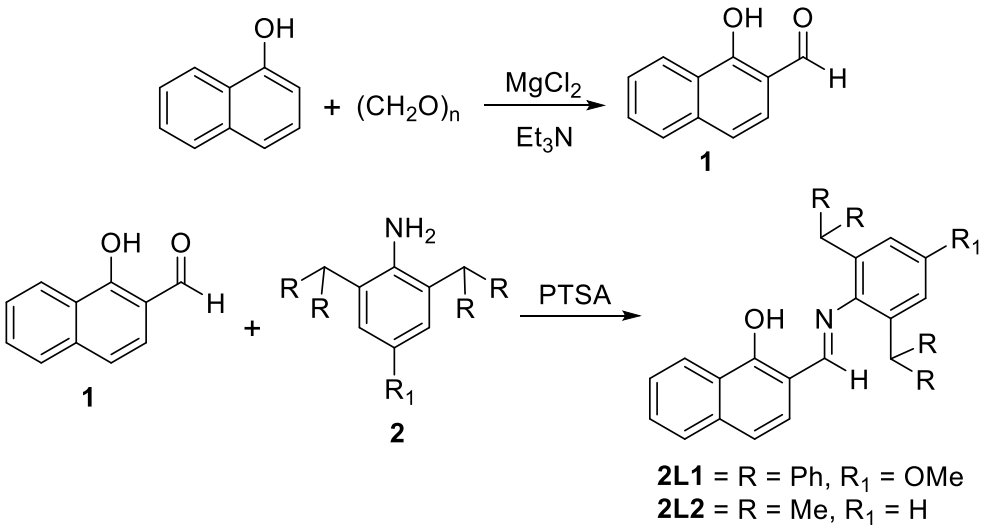

Scheme 2.1: Synthesis of ligand **2L1** and **2L2**.

2.3.2. Pd-Complex synthesis:

The naphthoxy imine ligand (**2L1**) was treated with a palladium precursor [(TMEDA)PdMe$_2$] in pyridine (Scheme 2.2). The progress of the reaction was monitored by ^{1}H NMR, which revealed a signal at 0.44 ppm after 2 hours, indicating the completion of the reaction. The

evaporation of unreacted pyridine and washing with hexane produced a solid compound with a 69% isolated yield. The characteristic resonance at 0.44 ppm, and a ^{13}C NMR peak at 1.9 ppm can be assigned to the Pd–Me group in **2Pd1**. The existence of the **2Pd1** was further corroborated by short (HSQC) and long (HMBC) range C-H correlation spectra. ESI-MS also supported the presence of **2Pd1,** and a molecular ion peak was observed at m/z = 809.20 $[2Pd1+H]^+$ (Figure S2.19). The observed mass and isotopic pattern exactly match the simulated pattern. The existence of **2Pd1** was unambiguously ascertained by single crystal X-ray diffraction. Suitable crystals of **2Pd1** were obtained from a mixture of dichloromethane and hexane at 0 °C, and the structure of the resultant crystals was determined by X-ray diffraction. The palladium complex **2Pd1** crystalizes in a monoclinic unit cell in space group $P2_{1/n}$. The single crystal consists of a central palladium atom with bis-chelated naphthoxy imine ligand (**2L1**), a coordinating pyridine, and a methyl group (Figure 2.2). The geometry around the palladium is distorted square planar. The methyl group is placed *cis* to the imine nitrogen, while the pyridine is located *trans* to the imine nitrogen. The oxygen is trans to the methyl group. The Pd1-N2 (imine) distance of 2.01 Å confirms the formation of a coordinate bond, while the Pd1-O1 distance of 2.07 Å suggests the formation of covalent bond.[42] The coordinating solvent pyridine revealed a Pd1-N1 distance of 2.03 Å. A C6-Pd1-N1 *cis* angle of 90.55° suggests that **2Pd1** can potentially initiate ethylene insertion and polymerization.

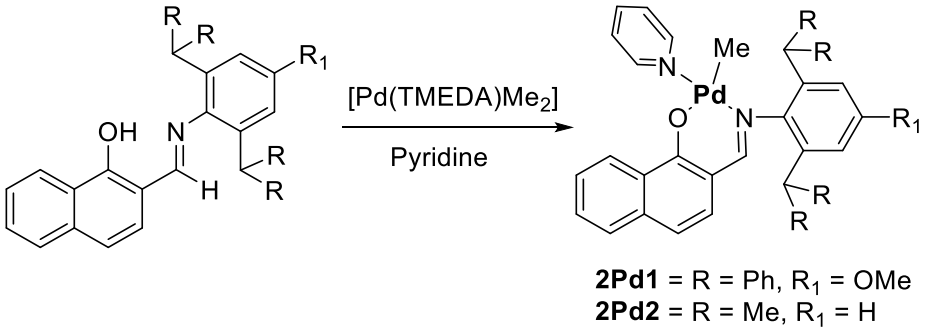

Scheme 2.2: Synthesis of palladium complexes **2Pd1** and **2Pd2**.

Along the same line, naphthoxy imine ligand **2L2** was treated with a palladium precursor [(TMEDA)$PdMe_2$] in pyridine (Scheme 2.2) to obtain palladium complex **2Pd2**. **2Pd2** will allow us to investigate the effect of ortho-substituents on the imine arm. The existence of **2Pd2** was confirmed by spectroscopic and analytical methods. The ^1H NMR spectrum disclosed singlet at 0.02 ppm which can be assigned to the Pd-Me protons. The corresponding methyl carbon was observed at 0.7 ppm. 1-2D NMR and ESI-MS data confirm the presence of complex **2Pd2**. A similar palladium complex was reported earlier as a control catalyst. The literature protocol involves two steps; initially preparing a sodium salt of ligand and then treating it with

[Pd(COD)MeCl].[43,44] While, we have used [Pd(TMEDA)Me_2] as a Pd-precursor and prepared **2Pd2** in one step.

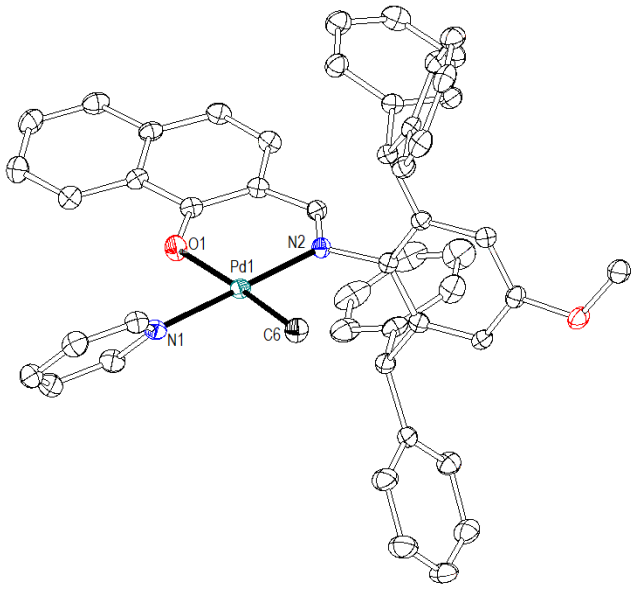

Figure 2.2: Molecular structure of **2Pd1**. H-atoms have been omitted for clarity; thermal ellipsoids are drawn at the 50% probability level. Important bond distances and angles; Pd1-N2 2.01 Å, Pd1-N1 2.03 Å, Pd1-O1 2.07 Å, N2-Pd1-O1 91.70 °, C6-Pd1-N1 90.55 ° CCDC 2225185.

2.3.3. Reactivity of 2Pd1 with ethylene:

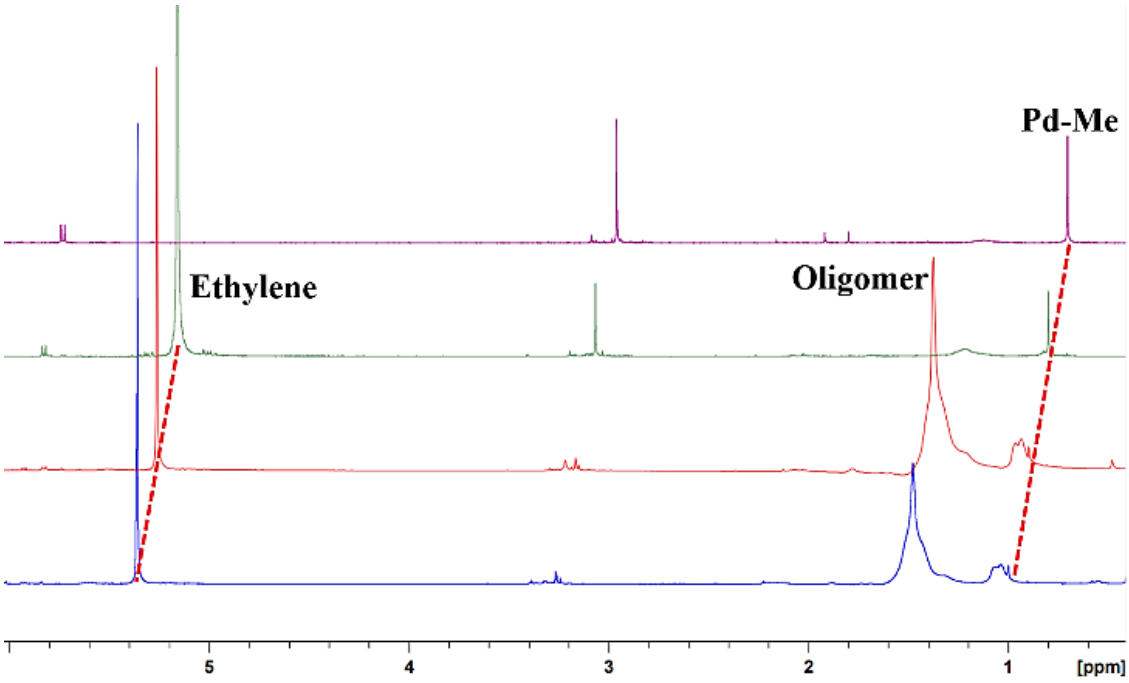

Figure 2.3. Stacked high-pressure ^{1}H NMR spectra of **2Pd1** in the presence of 4 bar ethylene at 0 (top) and 20 minutes, 4 and 24 hours (bottom) (at room temperature).

Before we embark on polymerization, it was crucial to investigate the reactivity of **2Pd1** towards ethylene. This is especially necessary, as the previous report on a similar complex suggests that such catalysts are incapable of homopolymerizing ethylene.[44] In a high-pressure NMR tube experiment, **2Pd1** was dissolved in benzene-d_6, and ^{1}H NMR spectrum was recorded. Subsequently, the NMR tube was charged with 4 bar of ethylene gas, and a proton NMR was recorded after 20 minutes, 4 and 24 hours. As depicted in figure 2.3, the initial Pd-Me resonance at 1.00 ppm slowly disappears, with the concomitant appearance of methylene (-CH_2-) resonance at 1.47 ppm. These mechanistic investigations suggest that the ethylene inserts in a Pd-Me bond and 2Pd1 is capable of ethylene insertion and oligomerization or polymerization, even at room temperature.

2.3.4. Ethylene oligomerization:

As **2Pd1** was found to initiate ethylene insertion, we set out to test its performance in ethylene oligomerization. In our initial effort, **2Pd1** was exposed to 25 bar ethylene at 60 °C (Table 2.1, entry 1). After 90 minutes, the reaction was quenched (see experimental part), and 0.171 g of highly viscous material was isolated. The ethylene oligomerization was performed at 70, 80, and 90 °C (Table 2.1, entries 2-4). As evident, the best yield of 0.385 g was observed at 80 °C (Table 2.1, entry 3), suggesting this is an optimal reaction temperature. After optimizing the reaction temperature, we turned our attention to ethylene pressure. The same experiment as above was repeated at 25, 20, 15, 10, and 5 bars of ethylene (Table 2.1, entries 5-8). As the ethylene pressure decreased, the yield of the oligomer reduced. This could be due to the lower availability (concentration) of ethylene monomer at lower pressure. Surprisingly, at 5 bar ethylene pressure, the highest yield of 0.452 g was obtained (Table 2.1, entry 8).

This could be due to the reduced rate of chain transfer to monomer at lower ethylene pressure. The lower chain transfer may allow the ethylene to insert and grow into oligomers. The number of branches per 1000 carbon atom at 5 bar was found to be similar to those at higher pressure (25-10 bars), suggesting that the chain-walking is unaffected. The molecular weight was determined by NMR and GPC, and was found to be in the range of 500-1400 g/mol. The polydispersity is around 2, suggesting well defined single-site catalyst.

The performance of **2Pd2** was examined in ethylene oligomerization. Under the optimized condition of 5 bar ethylene pressure, 80 °C temperature, and 90 minutes, **2Pd2** produced 0.194 g ethylene oligomers (Table 2.1, entry 9). When ethylene pressure was increased to 10 bars, only 0.148 g of ethylene oligomer was obtained. While, reducing the temperature to 60 °C, further reduced the oligomer yield to 0.073 g. Interestingly, **2Pd2** disclosed higher branching

(~90/1000 carbon atoms) as compared to **2Pd1** (Figure 2.4). These observations suggest that **2Pd2** is susceptible to higher β-H transfer and it is less active than **2Pd1**. Therefore, sterically hindered **2Pd1** potentially reduces β-H elimination and allows sufficient ethylene insertion to obtain hyperbranched ethylene oligomers. 2Pd2, being sterically less demanding, shows higher branching than sterically hindered 2Pd1. The electron-rich (relatively) 2Pd1 disclosed better activity and molecular weight as compared to 2Pd2. A comparative performance with respect to TOF, M_n, and branching is presented in figure 2.4.

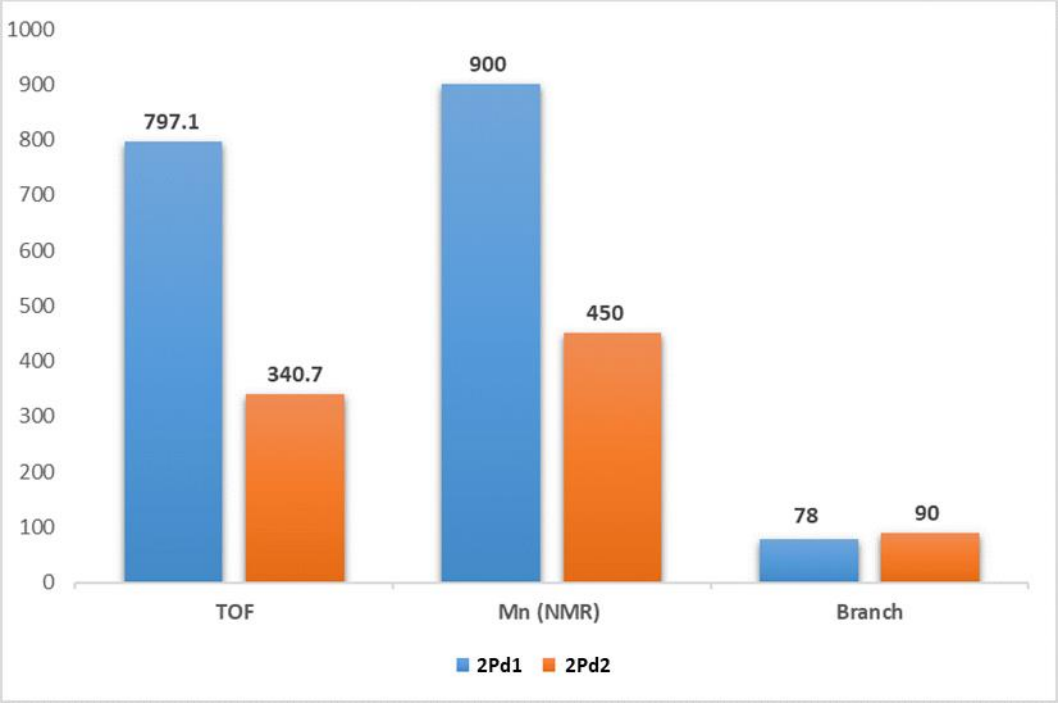

Figure 2.4: Comparison of TOF, molecular weight, and branches per 1000 carbon atoms for ethylene oligomers produced by **2Pd1** and **2Pd2**.

2.3.5. Ethylene oligomer microstructure analysis:

The microstructure of ethylene oligomers and polymers influences the properties and defines the application of the material.[45-47] Therefore, the resultant hyperbranched ethylene oligomers were subjected to a detailed NMR analysis.[20] ^{1}H NMR spectrum of an oligomer sample disclosed resonances at 5.78-5.85 ppm and 4.92-5.02 ppm. These can be assigned to terminal or chain end olefinic protons that are formed after the termination of a growing chain via β-H elimination (Figure 2.5, a). The other peak at 5.41 ppm (Figure 2.5, b) can be assigned to internal alkenes generated via the extensive chain walking of the catalyst. The minor resonances at 5.21 and 5.13 ppm can be assigned to substituted in-chain olefins such as c and d (Figure 2.5). A broad resonance at 4.7 ppm may correspond to a rare olefinic peak, as depicted in e (Figure 2.5).

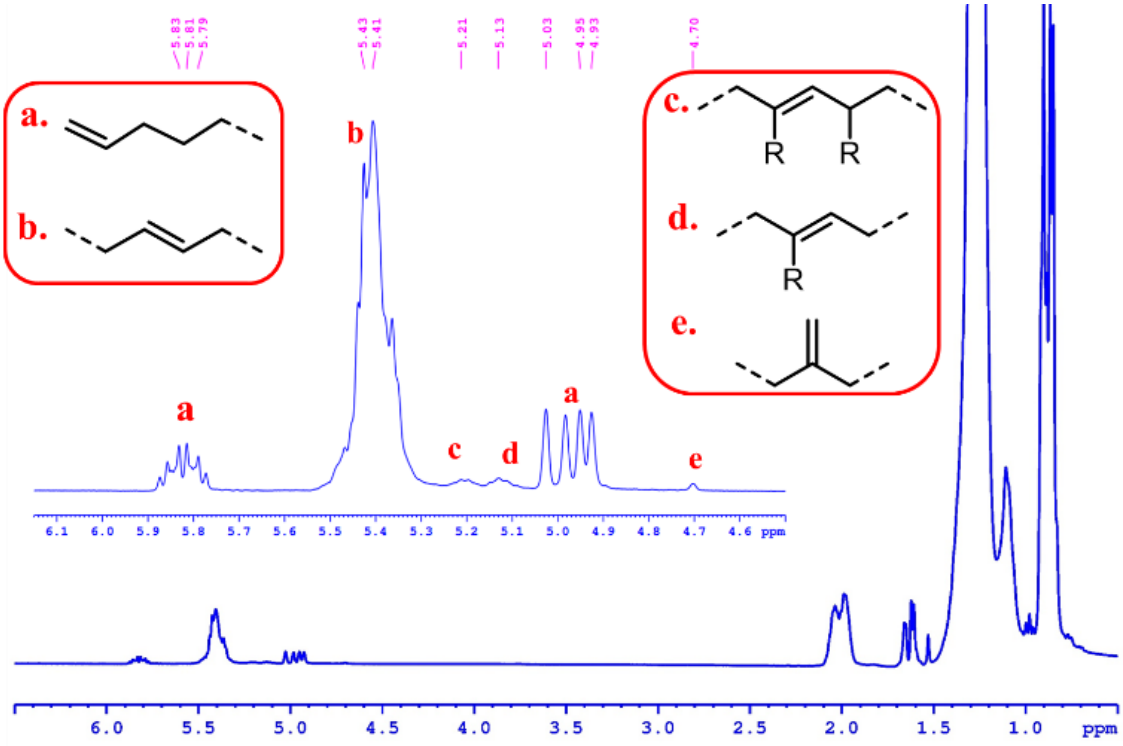

Figure 2.5: ^{1}H NMR spectrum of ethylene oligomer in $CDCl_3$ (olefinic region in sets).

The ^{13}C NMR spectroscopy is routinely used to determine branching in polyethylene and ethylene oligomers.[20, 48-50] Therefore, ^{13}C NMR of the ethylene oligomers obtained in our studies was recorded, and figure 2.6 depicts the spectrum. A resonance at 19.9 ppm can be assigned to a methyl branch, while peaks at 11.1, 26.1 ppm can be ascribed to ethyl branch. The ^{13}C NMR resonance at 14.8 ppm can be allotted to a methyl group in a propyl branch. Remarkably, the ^{13}C NMR revealed the presence of *sec*-butyl group at 19.4 and 11.6 ppm. The presence of these *sec*-butyl branches suggests the existence of branch-on-branch in the ethylene oligomers resulting in a hyperbranched microstructure. ^{1}H-^{13}C HSQC NMR spectrum disclosed cross-peaks between olefinic protons and double-bond carbons, confirming the existence of internal and terminal double bonds (Figure S2.31). These hyperbranched ethylene oligomers are highly viscous fluids and do not show crystallization or melting transitions.

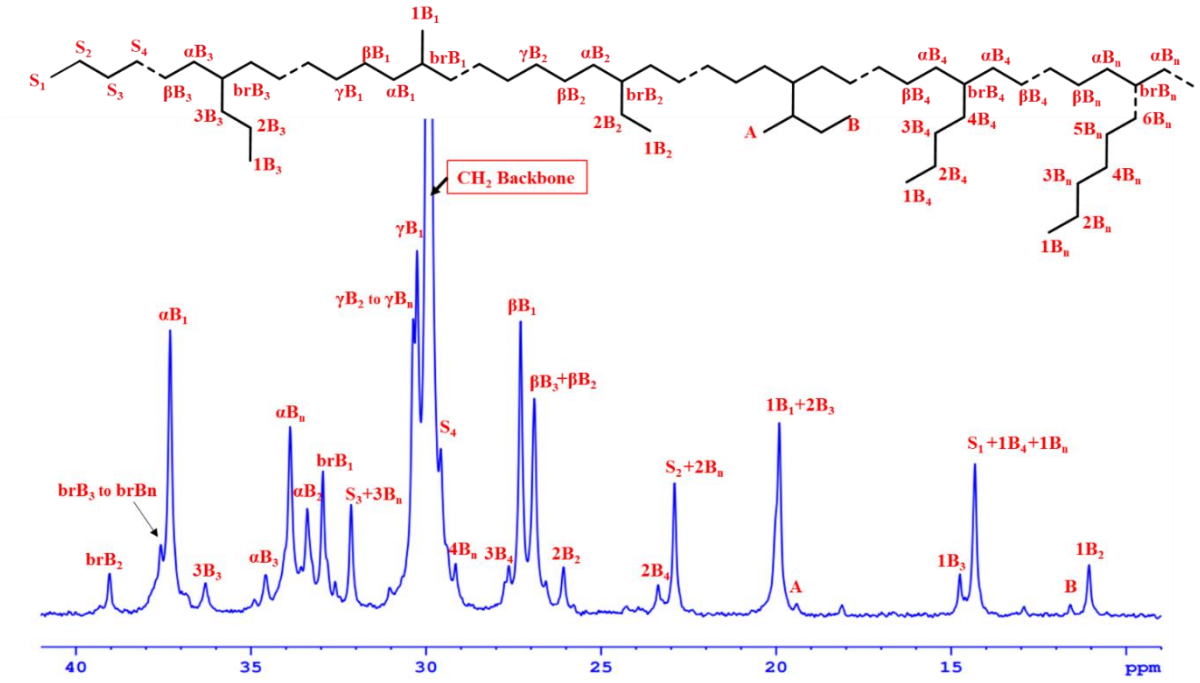

Figure 2.6: ^{13}C NMR spectrum of ethylene oligomer in $CDCl_3$.

Table 2.1: Ethylene oligomerization using 2Pd1 and 2Pd2.[a]

Entry	Cat.	Temperature (°C)	Pressure (bar)	Yield (g)	Branches/ 1000 carbon atom[b]	M_n[b] by NMR	TOF (h^{-1})
1	2Pd1	60	25	0.171	74	1350	301
2	2Pd1	70	25	0.206	67	1100	363
3	2Pd1	80	25	0.385	71	1000	679
4	2Pd1	90	25	0.168	76	800	296.2
5	2Pd1	80	20	0.298	85	950	525.5
6	2Pd1	80	15	0.240	87	1000	423.2
7	2Pd1	80	10	0.180	82	950	329.6
8	2Pd1	80	5	0.452	78	900	797.1
9	2Pd2	80	5	0.194	90	450	340.7
10	2Pd2	80	10	0.148	93	450	261
11.	2Pd2	60	5	0.073	106	500	128.7

[a]**Reaction conditions**: Toluene- 100 mL, Catalyst- 13.6 µmol., Time- 90 min, Ethylene pressure- 5 to 25 bar, TOF in (mol of PE / mol of Pd h^{-1}); the reported yield is after subtracting catalyst quantity from the final weight of oligomers; [b]M_n & branches /1000 C-atoms was

calculated by using ^{1}H NMR (for calculation and figures see S2.31 to S2.45 for oligomer NMR).

2.3.6. Ethylene oligomerization in polar solvents:

Solvents or monomers that possess heteroatoms or functional groups can poison a catalyst in olefin polymerization.[37,51-57] Therefore, olefin polymerization is routinely carried out in hydrocarbon solvents without heteroatoms or functional groups. In fact, Marks and co-workers employed very nonpolar solvents to prepare highly branched ethylene oligomers.[58] However, a few recent reports suggest that the polar solvent may enable chain growth and increase the molecular weight of polyethylene to ultrahigh molecular weight polyethylene (UHMWPE).[59-61] Although these reports do not provide a conclusive direction, solvent seems to play a pivotal role in ethylene polymerization. In the backdrop of the above reports, we pondered if the solvent influences our ethylene oligomerization.

The effect of polar solvents on the activity, branching and molecular weight was examined, and table 2.2 presents important results. When **2Pd1** was exposed to ethylene under optimized conditions in polar solvent DME (Dimethoxyethane), 0.655 g of ethylene oligomer was obtained. This is an increase of 44% yield of oligomers as compared to the highest yield achieved using nonpolar toluene (Table 2.1, entry 8). Similarly, **2Pd2** too displayed increased yield in the presence of polar DME (Table 2.2, entry 2). Subsequently, 1,4-dioxane was used as a solvent, and a remarkable increase in ethylene oligomer yield was observed (Table 2.2, entry 3).

Table 2.2: Ethylene oligomerization in the presence of polar solvents.[a]

Entry	Cat.	Solvent	Yield (g)	Branches/ 1000 C-atoms	TOF (h^{-1})	M_n NMR
1	2Pd1	DME	0.655	78	1155.2	750
2	2Pd2	DME	0.466	86	821.8	350
3	2Pd1	1,4 dioxane	1.124	75	1982.3	650
4	2Pd2	1,4 dioxane	0.738	97	1301	350
5	2Pd1	Et_2O	0.812	100	1421.5	800
6[b]	2Pd1	DCM	0.092	100	162.5	1250
7	2Pd1	ACN	0.141	99	248.6	400
8	2Pd1	THF	1.323	77	2333	650
9	2Pd2	THF	0.612	83	1079	350

[a]**Reaction conditions:** Solvent- 100 mL, catalyst- 13.6 µmol., Time- 90 min, Ethylene pressure- 5 bar, Temperature- 80 °C, TOF in (mol of PE / mol of Pd h^{-1}), the reported yield is

after subtracting catalyst quantity from the final weight of oligomer, branches /1000 C-atoms was calculated using ^{1}H NMR (for calculation and NMR see figures S2.49 to S2.57 for oligomer NMR); [b]Reaction temperature was 45 °C. DME: Dimethoxyethane; Et_2O: Diethyl ether; DCM: Dichloromethane; ACN: Acetonitrile; THF: Tetrahydrofuran.

Similar to DME and 1,4 dioxane, diethylether also produced 0.812 g of ethylene oligomer (Table 2.2, entry 5). While, dichloromethane, and acetonitrile were found to reduce the oligomer yield and TOF (Figure 2.7). To our delight, the use of tetrahydrofuran (THF) as a solvent produced almost 3 times more ethylene oligomer yield under identical conditions (Table 2.2, entry 8). Unlike the increased molecular weight noted by Mecking and Jian in polar solvents,[62,63] the number average molecular weight remained in the ethylene oligomer range of 350-1250 g/mol, but the activity increased by multifold. The branching, too, did not change in THF and remained at 77-83 branches/1000 C-atoms.

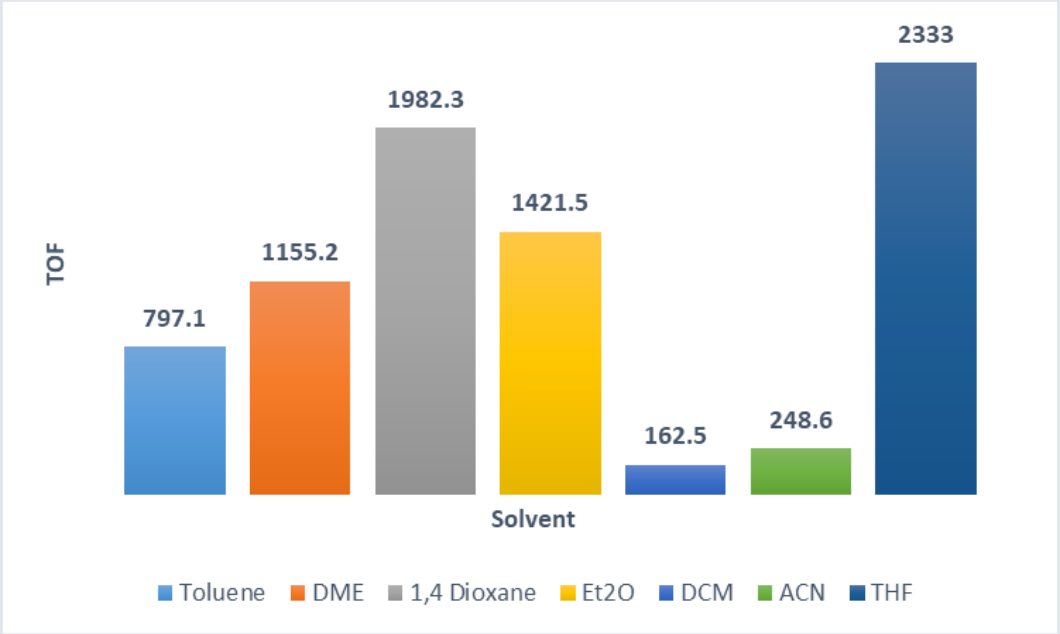

Figure 2.7: Comparison of TOF (for **2Pd1**) in polar and hydrocarbon solvents.

2.3.7. Understanding the effect of polar solvents:

The three-fold increase in ethylene oligomerization activity in the presence of THF was unexpected. Therefore, understanding such effects is crucial for the further development of the field. To get more insight into the role of THF, we performed NMR tube experiments. An NMR tube was charged with **2Pd1** in C_6D_6, and a proton NMR was recorded. The Pd-Me peak was observed at 1.00 ppm. When 50 equivalent of anhydrous THF was added to the above NMR tube, the Pd-Me resonance shifted upfield and appeared at 0.95 ppm. Although this is a small change in chemical shift, the observation suggests that the THF competes with pyridine for

metal coordination and might be in equilibrium (Scheme 2.3). To understand pyridine de-coordination further, **2Pd1** was treated with $B(C_6F_5)_3$ and 50 equivalent of THF was added to the NMR tube. Here, the Pd-Me resonance shifted further upfield and appeared at 0.92 ppm. The corresponding ^{11}B NMR disclosed a peak at -2.67 ppm, which can be assigned to pyridine-$B(C_6F_5)_3$ adduct.[62] The formation of pyridine-$B(C_6F_5)_3$ adduct suggests that pyridine is susceptible to de-coordination from the palladium center in the presence of an excess of polar solvent (THF), and a THF-coordinated intermediate is likely formed. The coordination of THF to the palladium center is weaker than pyridine, and therefore a [Pd.THF] adduct is proposed to be more active than the parent [Pd-Py] adduct (**2Pd1**). To validate this statement, we prepared [Pd.THF] complex *in-situ* using [Pd(COD)MeCl] and [(TMEDA)$PdMe_2$] precursors, and directly employed for the ethylene oligomerization (for details, see section 2.5.6.3). These in-situ prepared [Pd.THF] complexes disclosed comparable activity to **2Pd1** in THF. These observations suggest that THF replaces pyridine from **2Pd1** *in-situ* and generates a relatively more active [Pd.THF] catalyst. It is also proposed that the presence of an excess of THF (as solvent) during oligomerization reaction might stabilize the catalyst by forming a [Pd-X(THF)] species (see Scheme 2.3).[63]

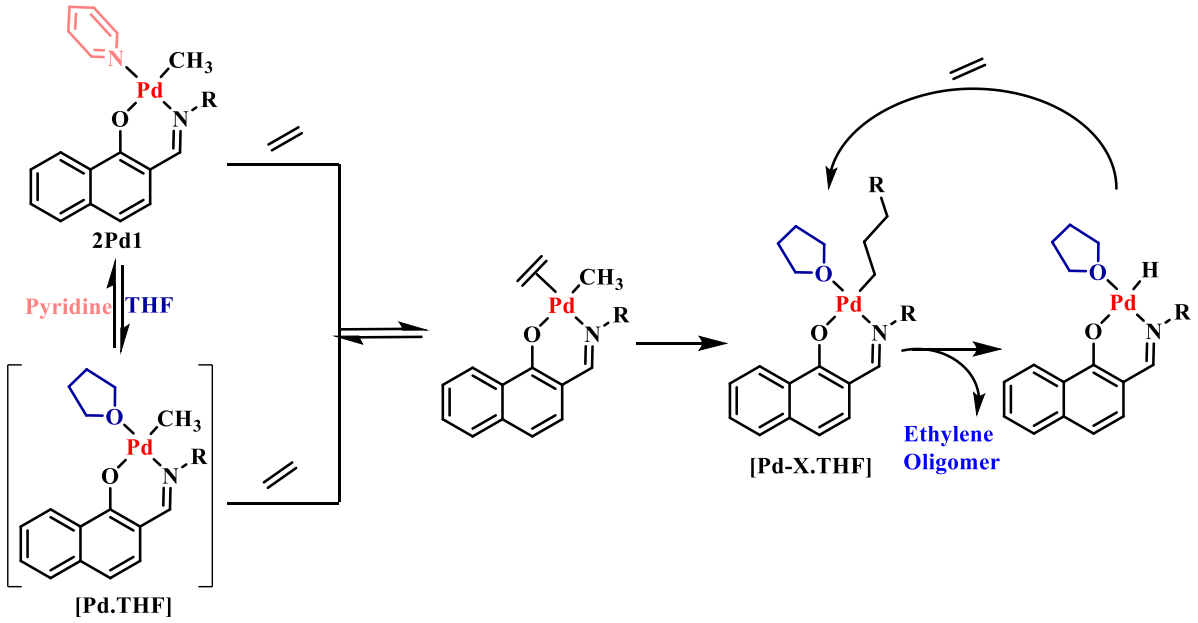

Scheme 2.3: Ethylene oligomerization in polar solvent.

2.3.8. Functionalization of ethylene oligomer:

The NMR analysis of the ethylene oligomers (Figure 2.5) suggested the presence of internal and terminal double bonds. Due to extensive chain walking, internal double bonds were found to dominate the terminal double bond, and the ratio between the two was about 3:1, respectively. As such, a C=C double bond is an important functional group and is known to

undergo several transformations. The presence of internal and terminal double bonds in ethylene oligomers offers tremendous potential for the post-polymerization functionalization of these oligomers. The resultant functional ethylene oligomers can be used as compatibilizers, in inks, interface active agents, adhesives, viscosity modifiers, nanoparticles, etc.[64]

Aldehydes and alcohols are versatile functional groups in organic synthesis. Therefore, the primary focus was to convert ethylene oligomers' internal and terminal double bonds into aldehyde or alcohol. This can be easily achieved by ozonolysis, hydroformylation and epoxidation. Thus, the resultant ethylene oligomers were directly used for further functionalization without any purification. Ethylene oligomers were dissolved in dry dichloromethane and cooled to -78 °C and ozone gas was bubbled in the reaction mixture for 5 minutes. Excess ozone gas was vented, the round bottom flask was purged with argon, and the reaction was quenched by adding dimethyl sulfide.[65] Volatiles were evaporated using a high vacuum pump to yield aldehyde functionalized ethylene oligomer (**F1**) (Scheme 2.4).

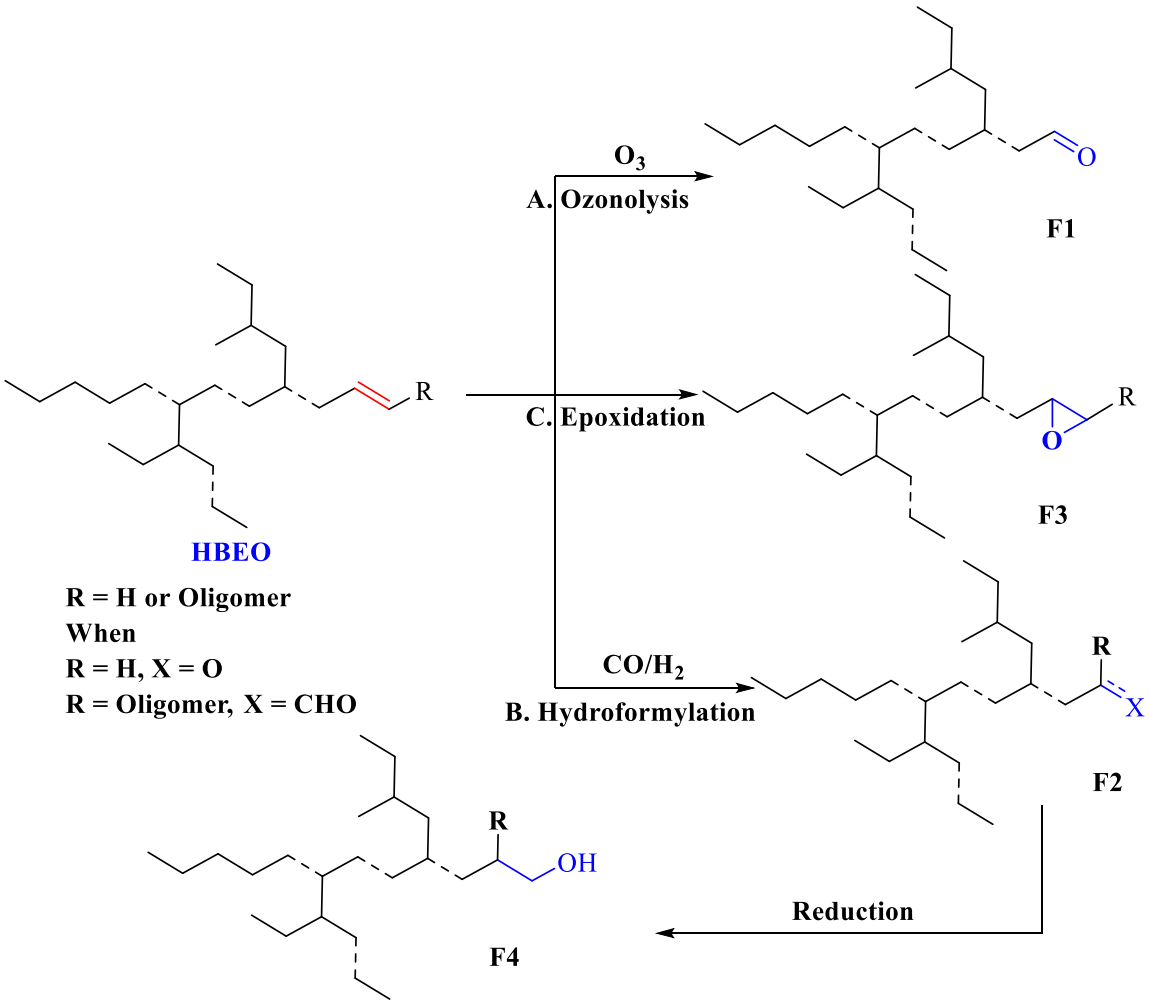

Scheme 2.4: Post oligomerization functionalization.

The identity of the aldehyde product was confirmed by ^{1}H and ^{13}C NMR spectra. A proton NMR spectroscopy revealed a single peak at 9.76 ppm (Fig. S2.62), while ^{13}C NMR disclosed a resonance at 203.0 ppm (Fig. S2.63) corresponding to the aldehydic group. The NMR findings were further corroborated by IR, which displayed a carbonyl stretching band at 1706 cm^{-1}. While, a THF GPC disclosed the molecular weight of functionalized oligomer to be 1600 Da. Although ozonolysis produced aldehyde, the molecular weight (GPC) was found to be lower than the starting HBEO. This is most likely due to the cleavage of internal double bonds in ozonolysis reaction. Hydroformylation of HBEO can produce same aldehyde without sacrificing the molecular weight. Therefore, hydroformylation of ethylene oligomers was performed in the presence of $[Rh(acac)(CO)_2]$ and triphenylphosphine in toluene.[66] The reaction was performed in a high-pressure autoclave at 10 bar syngas pressure and 100 °C temperature for 18 hours. This resulted in more than 99% conversion to product **F2** as observed by ^{1}H NMR spectrum (Figure S2.66A). The ^{1}H NMR revealed three broad peaks in the deshielded region; the resonance at 9.76 ppm can be assigned to the linear aldehyde, and other peaks correspond to branched aldehydes (Figure S2.66A). As shown in figure S2.66B, the olefinic peaks completely diminished, and new peaks were observed at 2.0-2.6 ppm, which corresponds to the C-H protons adjacent to the aldehyde. The ^{13}C NMR spectrum of the same sample displayed multiple peaks in the region of 203.2 to 205.9 ppm (Figure S2.67). These assignments are based on literature data for linear and branched aldehydes.[67-69]

The epoxide-functionalized ethylene oligomer (**F3**) was prepared by treating the ethylene oligomer with mCPBA in dichloromethane for 14 hours.[70] The conversion of an olefin into epoxide was confirmed by ^{1}H NMR spectroscopy. The protons next to epoxide-oxygen were observed between 2.48-3.09 ppm (Figure S2.69). While the corresponding ^{13}C NMR spectrum disclosed methylene carbon in the range of 45-60 ppm (Figure S2.70). The IR spectroscopy revealed an epoxide CO stretching band at 1215 cm^{-1}. Figure 8 depicts a stacked ^{1}H NMR spectra of **F1**, **F2, F3,** and **F4**.

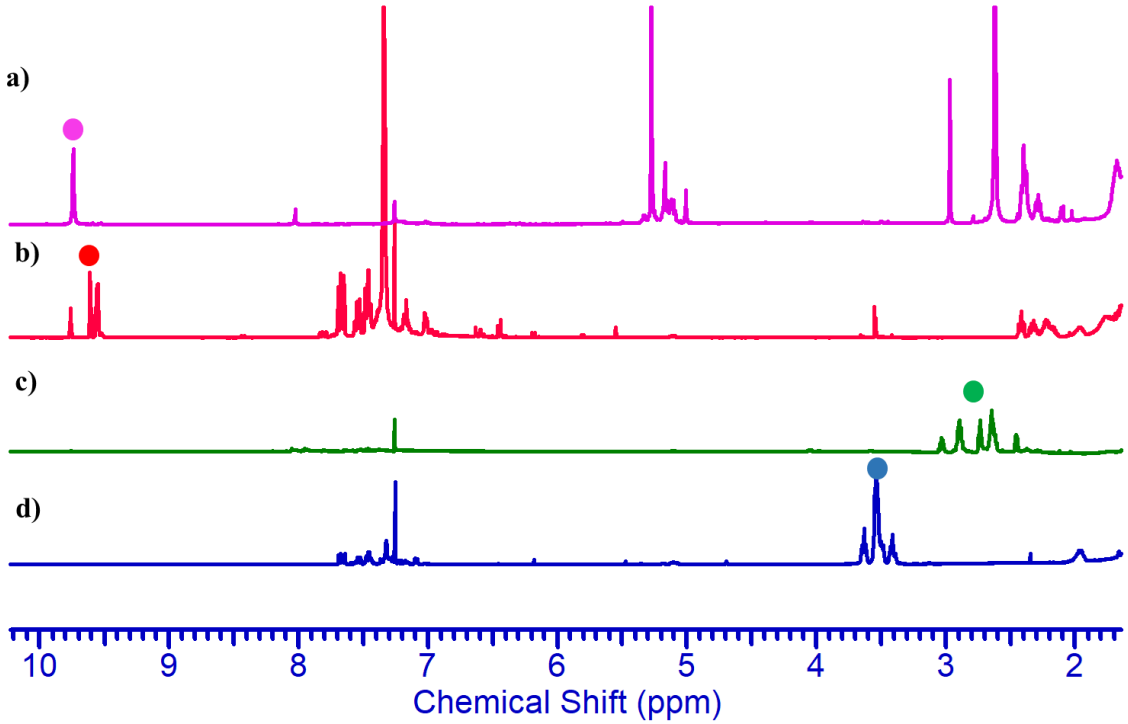

Figure 2.8: Stacked ^{1}H NMR spectra of functional ethylene oligomers; **a**) ozonolysis product (**F1**); **b**) hydroformylation product (**F2**); **c)** epoxide functionalized ethylene oligomer (**F3**); and **d)** hydroxy functionalized oligomer (**F4**).

The aldehyde product (**F2**) obtained from the hydroformylation reaction was treated with sodium borohydride ($NaBH_4$) at 0 °C in methanol-toluene (1:1). After 14 hours of stirring at room temperature, volatiles were evaporated, and oligomers were extracted using hexane. The aldehyde was fully (<99%) reduced to the corresponding hydroxyl functionalized ethylene oligomer (**F4**) as confirmed by the ^{1}H NMR spectroscopy (Figure 2.8,d). The proton NMR revealed that the aldehyde peaks disappeared, and new peaks appeared in the region of 3.39-3.77 ppm. These proton chemical shifts can be assigned to methylene groups generated after the reduction of aldehyde to alcohol (Fig. 2.8b versus d).

2.3.9. Functional oligomer as compatibilizer:

The presence of a polar functional group (OH), as well as non-polar hydrophobic unit (methylene backbone) in the ethylene oligomer **F4**, will help to serve as a compatibilizer for two immiscible polymers, one polar and the other non-polar.[71] We choose linear low density polyethylene (LLDPE) as the non-polar polymer and Nylon-6 as a polar polymer. A DSM MICRO 5 twin screw micro-compounder was used to melt-compound the two polymers with and without the presence of the compatibilizer (**F4**) at screw RPM of 100 at 250 °C for 5 minutes. Prior to melt compounding, the materials were dried in a vacuum oven at 80 °C for 4 hours to remove any traces of moisture. Additionally, 2000 ppm of anti-oxidant (Irganox 1010

from BASF) was added to prevent any thermal degradation during processing. The material ratios are shown in table 2.3. The non-polar LLDPE was obtained from Reliance Ind. Ltd. (grade: F18020), while the polar polymer Nylon-6 was obtained from Honeywell (grade Aegis H73QP). The melt mixed or compounded blends were molded into tensile specimens in a DSM micro injection molding machine and subjected to tensile testing at room temperature. Minimum 5-6 samples were tested for each blend formulation. A representative tensile test data is plotted below for the compatibilized and non-compatibilized blend samples (Figure 2.9 bottom). It is clear from the tensile test data that while the un-compatibilized blend formulation displays a higher tensile strength, the compatibilized blend formulation displays equivalent Young's modulus and, more importantly, higher strain-to failure vis-à-vis that for un-compatibilized blend formulation. The toughness of the blends increases with increasing compatibilizer content and reaches an optimum at 5 wt.% (see Table 2.3).

Table 2.3: Weight percentage formulation of LLDPE, Nylon-6 and compatibilizer (F4).

Sr. No	LLDPE (wt%)	Nylon 6 (wt%)	Compatibilizer (wt%)	Tensile Strength at break (MPa)	Young's Modulus (MPa)	Strain-to failure (mm/mm)	Toughness (J/mm^2)
1	80	20	0	9.8±0.9	422±13	1.0±0.17	9.08
2	79	20	1	9.6±0.31	327±9	1.6±0.19	14.77
3	78	20	2	10.5±0.68	362±30	1.8±0.36	16.80
4	75	20	5	8.5±0.15	294±17	2.3±0.8	24.07
5	70	20	10	2.3±0.65	282±21	1.4±0.32	10.38

The small dip in the tensile stress-strain data is the point where the clip-on extensometer was physically removed and the test was continued. It is evident that the functional ethylene oligomer **F4** as a compatibilizer played an important role in creating a tough yet flexible blend formulation that will also have good applications in packaging requiring a good oxygen barrier property in addition to water vapor barrier.

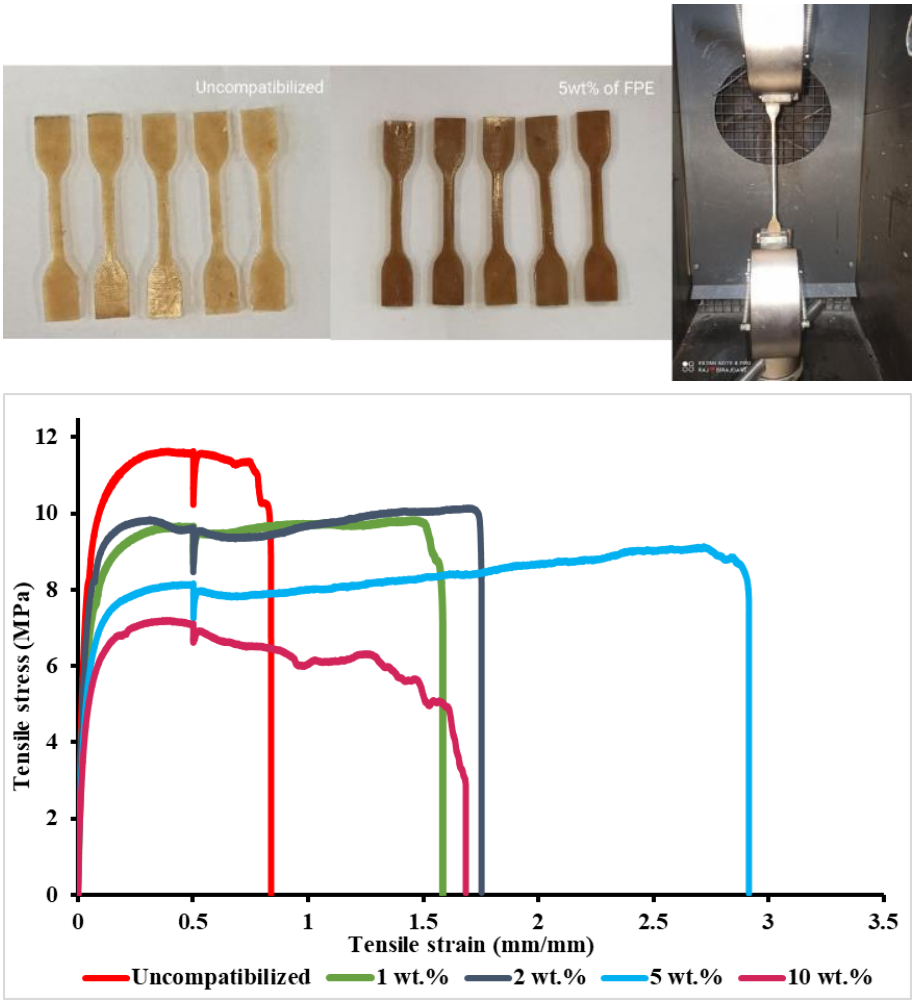

Figure 2.9: Polymer compatibility study; specimen for the tensile test (top); stress versus strain data (bottom).

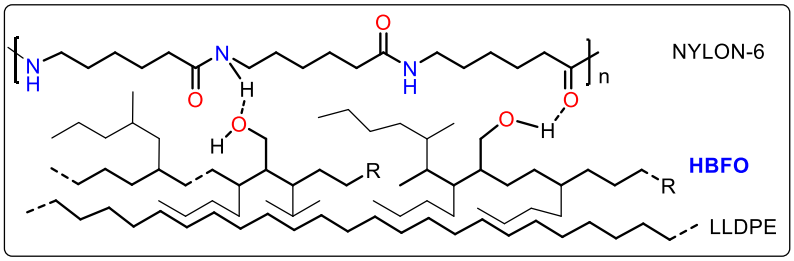

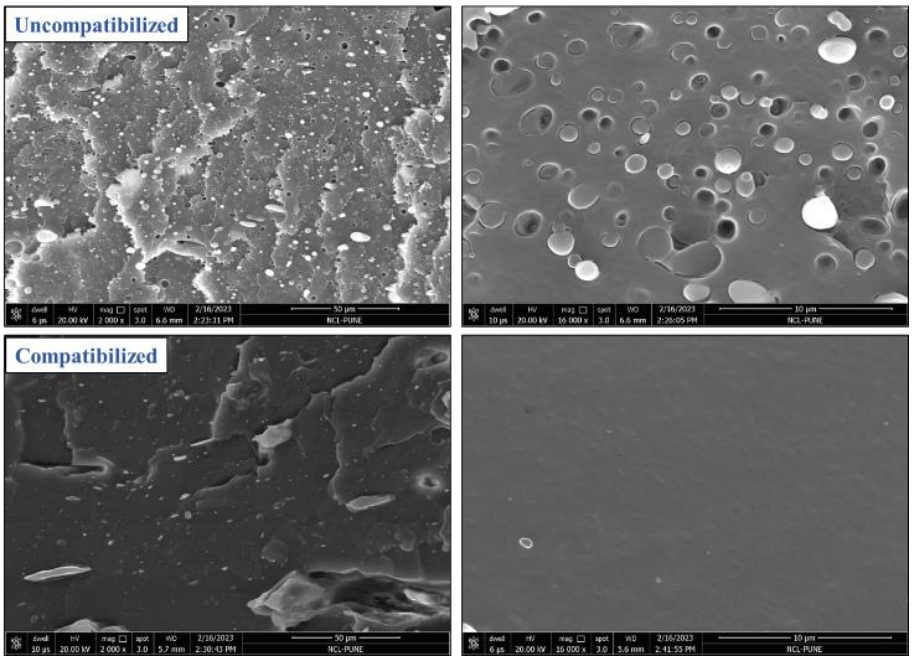

Figure 2.10: Proposed hydrogen-bonding interaction between Nylon-6 and HBFO, F4 (top); SEM images for un-compatibilized and compatibilized polymer blend.

The enhanced performance of the blend can be ascribed to the compatibilizing property of functionalized ethylene oligomer **F4**. It is proposed that the hydroxyl group in **F4** forms a hydrogen-bonding interaction with Nylon-6 and the alkyl chain mixes with LLDPE (Figure 2.10 top), leading to a compatible blend. The proposed interactions are based on literature reports for PE-PLA blends with functional polyethylene.[72,73] The blend morphologies of the compatibilized (5 wt%) and un-compatibilized blends were characterized by SEM analysis (Figure 2.10, bottom). The particle size of the dispersed phase is smaller in compatibilized blends (~200 nm) compared to the un-compatibilized blends (~800 to 900 nm). The void between the dispersed nylon phase and the PE matrix caused during cryofracturing due to poor interfacial adhesion is clearly visible in un-compatibilized blends. Similarly, due to poor interfacial adhesion in un-compatibilized blends, the nylon phase is pulled away from the PE matrix. In the case of compatibilized blends, as interfacial adhesion is increased, leading to a homogeneous phase (Figure 2.10, bottom-left).

2.4. Conclusions:

In summary, 1-hydroxy 2-naphthaldehyde was treated with aniline derivatives to obtain 2-(((2,6-dibenzhydryl-4-methoxyphenyl)imino) methyl) naphthalen-1-ol (**2L1**) and 2-(((2,6-diisopropylphenyl)imino) methyl) naphthalen-1-ol (**2L2**). The ligands **2L1** and **2L2** were isolated in good to excellent yield (51-69%). Ligand **2L1** was treated with [Pd(TMEDA)Me_2] in pyridine to obtain the corresponding palladium complex **2Pd1** in a 69% isolated yield. The

identity of **2Pd1** was established using a combination of 1-2D NMR, IR, and mass spectroscopy. A single crystal X-ray diffraction unambiguously ascertained the coordination of **2L1** to palladium and the existence of **2Pd1**. **2Pd2** was prepared along the same lines and was isolated in 89% yield. **2Pd1** and **2Pd2** were treated with ethylene, and their performance in ethylene oligomerization was examined. Initial screening using **2Pd1** suggested that 5 bar ethylene pressure, 80 °C temperature, and 90 minutes is the optimal condition to obtain the highest ToF of 797 mol of PE/mol of Pd h^{-1}. The molecular weight was found to be 500-1400 g/mol, with PDI of 1.46-2.10 and 71-106 branches per 1000 C-atoms. Detailed microstructure analysis revealed the existence of branch-on-branch or hyperbranched ethylene oligomers. **2Pd2** was also active and produced hyperbranched ethylene oligomers but was less reactive than **2Pd1**.

To our surprise, **2Pd1** was thrice more active in polar THF than non-polar toluene under identical conditions. Interestingly, though the productivity increased to 3 times higher, the molecular weight remained in the oligomer range, and the branching remained unchanged. The resultant hyperbranched ethylene oligomers were almost quantitatively functionalized to corresponding aldehydes, alcohols, and epoxides using industrially practiced transformations. The hydroxy functionalized hyperbranched ethylene oligomer **F4** was used as a compatibilizer. The addition of 5 wt.% of **F4** to non-polar LLDPE and polar Nylon-6, produced a tough yet flexible blend with higher strain-to-failure as compared to an un-compatibilized blend. This is, most likely, the first report on the use of functionalized hyperbranched ethylene oligomer as a compatibilizing agent.

2.5. Experimental section:

2.5.1. Methods and materials:

Unless noted otherwise, all manipulations were carried out under an inert atmosphere using standard Schlenk line techniques or M-Braun glove box. Toluene, diethyl ether, 1,4 dioxane, dimethoxyethane, and THF were distilled from sodium/benzophenone under an argon atmosphere. Acetonitrile, methylene chloride, and pyridine were distilled on calcium-hydride. Ethylene (3.5 grade) was supplied by Praxiar India Ltd., India. 1-Naphthol, diisopropyl aniline, and m-chloroperbenzoic acid, were supplied by Loba chemie and were used as received. Sodium borohydride was supplied by Avra Synthesis Pvt. Ltd. and was used as received. *p*-Anisidine and paraformaldehyde were supplied by Alfa Aesar and were used as received [$PdMe_2$(TMEDA)],[74] 1-hydroxy 2-napthaldehyde,[40] aniline derivative[41] were synthesized following known procedures. The insertion polymerization was run in a Büchi glasuster

cyclone 075 high-pressure reactor equipped with an overhead mechanical stirrer, heating/cooling jacket, and pressure regulators.

Solution NMR spectra were recorded on Bruker Avance 200, 400 and 500 MHz instruments. Chemical shifts are referenced to external reference TMS (^{1}H and ^{13}C). Coupling constants are given as absolute values. Multiplicities are given as follows s: singlet, d: doublet, t: triplet, m: multiplet. Mass spectra were recorded on Thermo Scientific Q-Exactive mass spectrometer, the column specification is Hypersil gold C18 column 150 x 4.6 mm diameter 8 µm particle size mobile phase used is 90 % methanol + 10 % water + 0.1 % formic acid. Infrared (IR) spectra were recorded on a Bruker Alpha II instrument and Fourier transform infrared spectrometer as a thin film. Gel Permeation Chromatography (GPC) was performed on a system equipped with an isocratic pump (Viscotek VE 1122 pump) and a differential refractometer (DRI) detector (Viscotek VE 3580 RI). For GPC with THF as the eluent, separations were performed using serially connected size exclusion columns (two T6000M, General Mixed Organic 8 × 300 mm, from Viscotek) at 25 °C and at a flow rate of 1.0 mL/min, and molecular weights were determined from the calibration curve generated from narrow polystyrene standards. DSM MICRO 5 twin screw microcompounder was used for compounding LLDPE, Nylon-6. Tensile specimen were prepared using a DSM micro injection molding machine. Tensile testing was done on a universal testing machine (Instron 33R4204). Single crystal X-ray diffraction measurement for 2Pd1 was carried out on a Bruker D8 VENTURE Kappa Duo PHOTON II CPAD diffractometer equipped with Incoatech multilayer mirrors optics. The intensity measurements were carried out with Mo micro-focus sealed tube diffraction source (MoKα = 0.71073 Å) at 100 K temperature. The X-ray generator was operated at 50 kV and 1.4 mA. SEM data was recorded on Field Emission Scanning Electron Microscope (FESEM), FEI -NOVA NANO 450.

2.5.2. Synthesis of ligands:

2.5.2.1. Synthesis of 1-hydroxy-2-naphthaldehyde:

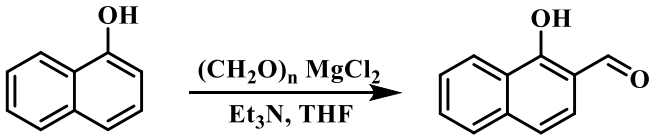

Scheme S2.1: Synthesis of 1-hydroxy-2-naphthaldehyde

In an oven-dried round bottom flask, 1-naphthol (13.8 mmol, 2 g), paraformaldehyde (138 mmol, 4.14 g), magnesium chloride (36 mmol, 3.43 g) and triethyl amine (63.4 mmol, 6.42 g), were added in 50 mL THF. The resultant reaction mixture was refluxed at 80 °C temperature

for 6 hours, the reaction was monitored by TLC analysis. After completion, the reaction mixture was cooled to room temperature and 2N.HCl (30 mL) was added, and the compound was extracted using 50 × 3 mL of ethyl acetate. Solvents were evaporated by using a rotary evaporator and the product was purified by using column chromatography (ethyl acetate 3%: petroleum ether 97%) to produce 1.34 g (56%) of 1-hydroxy-2-naphthaldehyde (**1**).

^{1}H NMR (200 MHz,$CDCl_3$) δ = 12.68 (s, 1 H), 9.97 (s, 1 H), 8.45 (d,1 H), 7.79 (d, 1 H), 7.71 - 7.63 (m, 1 H), 7.59 - 7.53 (m, 1 H), 7.49 (d, 1 H), 7.38 (d, 1 H).

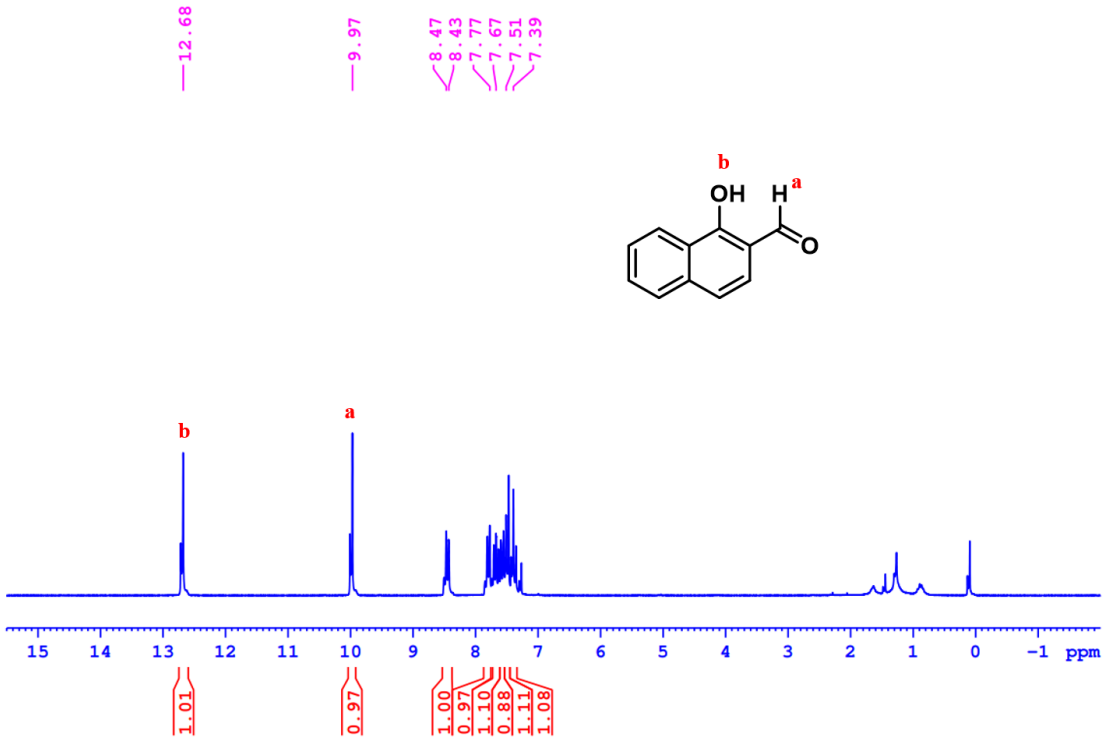

Figure S2.1: ^{1}H NMR spectrum of the 1-hydroxy-2-naphthaldehyde (**1**) in $CDCl_3$ (200 MHz, 298 K).

2.5.2.2. Synthesis of 2-(((2,6-dibenzhydryl-4-methoxyphenyl)imino) methyl) naphthalen-1-ol (2L1): In an oven-dried Schlenk flask, 1-hydroxy 2-naphthaldehyde (0.5 g, 2.90 mmol) and 2,6-dibenzhydryl-4-methoxyaniline (1.32 g, 2.90 mmol) were dissolved in 25 mL toluene, and a catalytic amount of PTSA (15 mg, 0.087 mmol) was added. The resulting reaction mixture was refluxed for 6 hours at 120 °C (bath temperature). The reaction mixture was cooled to room temperature, volatiles were evaporated, and the resultant residue was purified by column chromatography (1 % ethyl acetate and 99% Petroleum ether) to yield an orange-colored compound (1.22 g, 69%).

^{1}H NMR (500 MHz, $CDCl_3$) δ = 14.35 (br. s., 1 H), 8.42 (d, *J* = 7.6 Hz, 1 H), 7.64 (d, *J* = 7.9 Hz, 1 H), 7.59 - 7.50 (m, 1 H), 7.50 - 7.43 (m, 1 H), 7.25 (d, *J* = 7.6 Hz, 1 H), 7.21 - 7.12 (m,

12 H), 7.01 (d, *J* = 6.6 Hz, 7 H), 6.92 (d, *J* = 8.5 Hz, 1 H), 6.65 (br. s., 1 H), 6.45 (s, 2 H), 6.18 (s, 1 H), 5.56 (br. s., 2 H), 3.53 (s, 3 H). **^{13}C NMR (125 MHz, $CDCl_3$)** δ = 168.0, 165.3, 156.8, 143.1, 138.9, 138.3, 136.4, 129.7, 129.6, 129.2, 128.6, 128.4, 127.6, 127.4, 126.8, 126.5, 125.3, 124.3, 116.9, 114.2, 110.8, 55.2, 52.7. **ESI-MS** (positive mode)**:** m/z = 610.27 Da $[M+H]^+$ (observed); 610.27 Da $[M+H]^+$ (calculated), (calculated). IR (cm^{-1}) 1605.

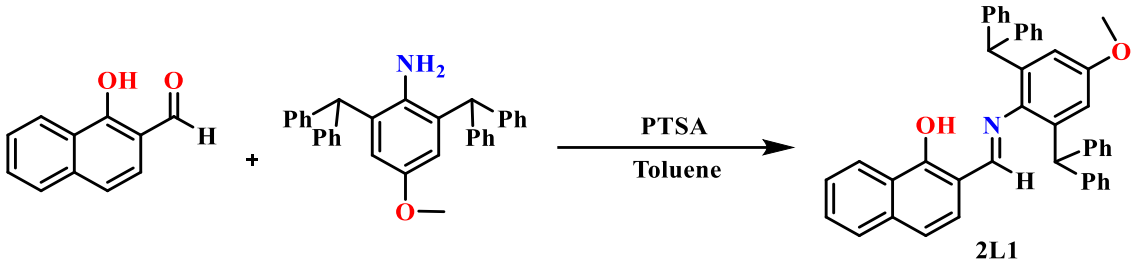

Scheme S2.2: Synthesis of **2L1**.

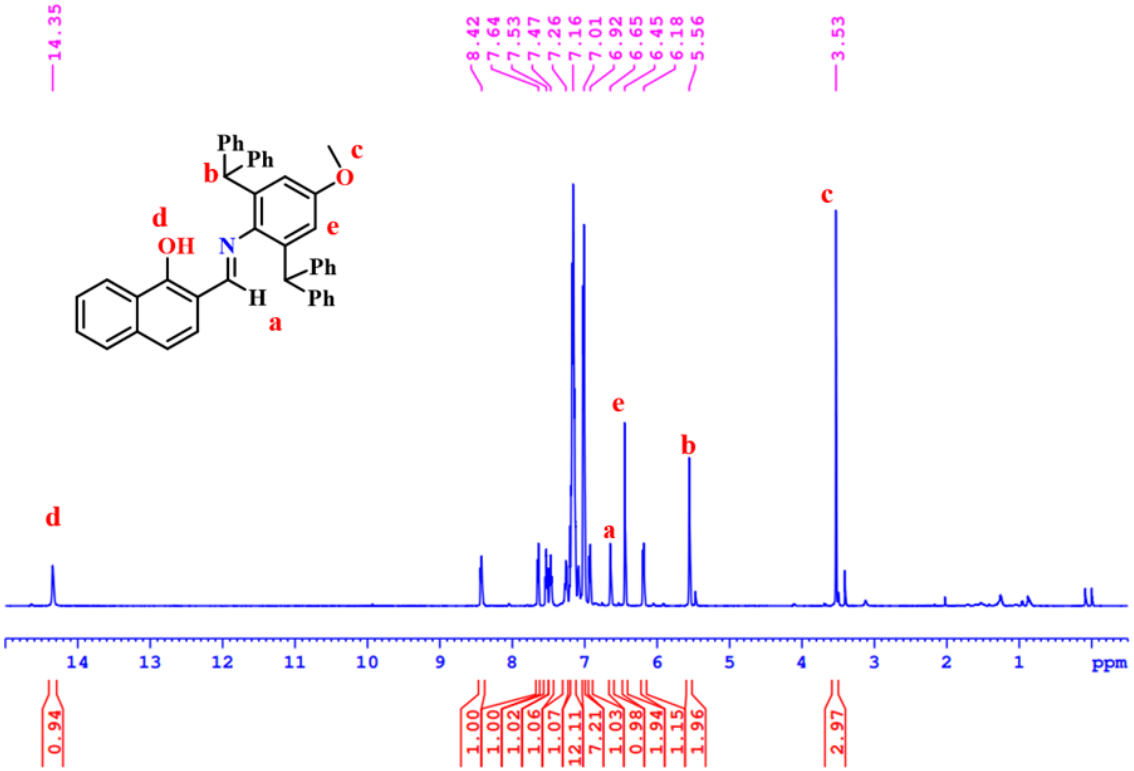

Figure S2.2: ^{1}H NMR spectrum of the **2L1** in $CDCl_3$ (500 MHz, 298 K).

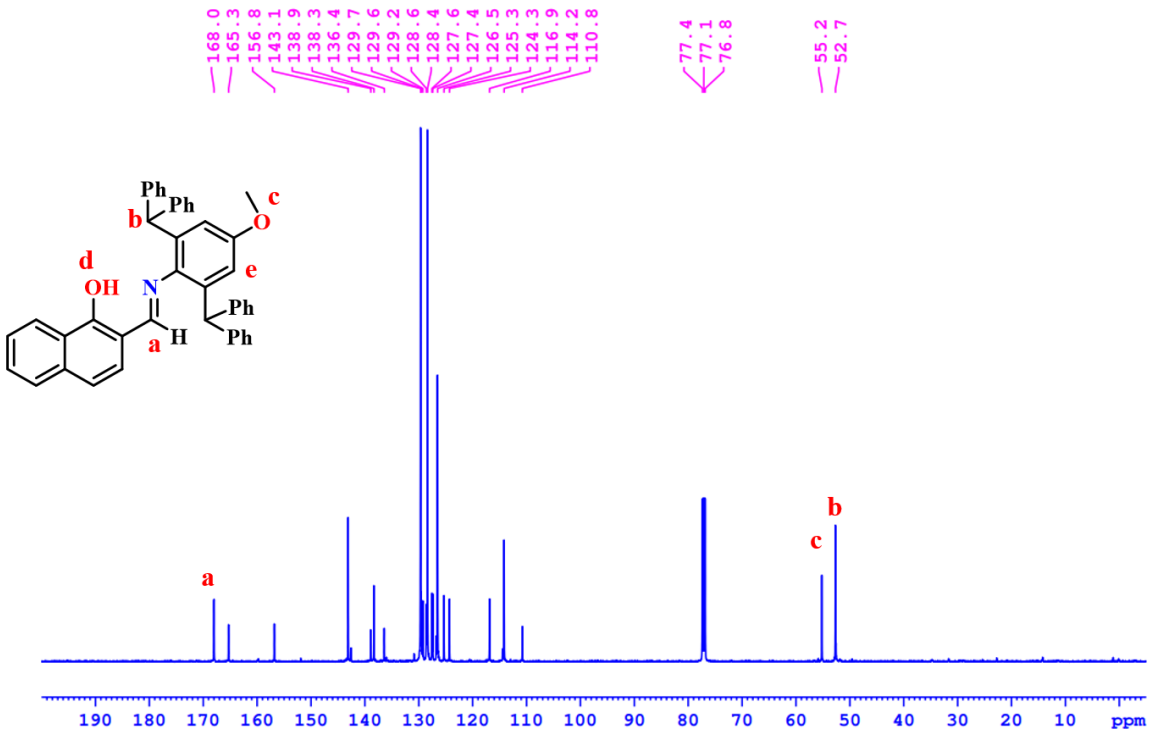

Figure S2.3: ^{13}C NMR spectrum of **2L1** in $CDCl_3$ (125 MHz, 298 K).

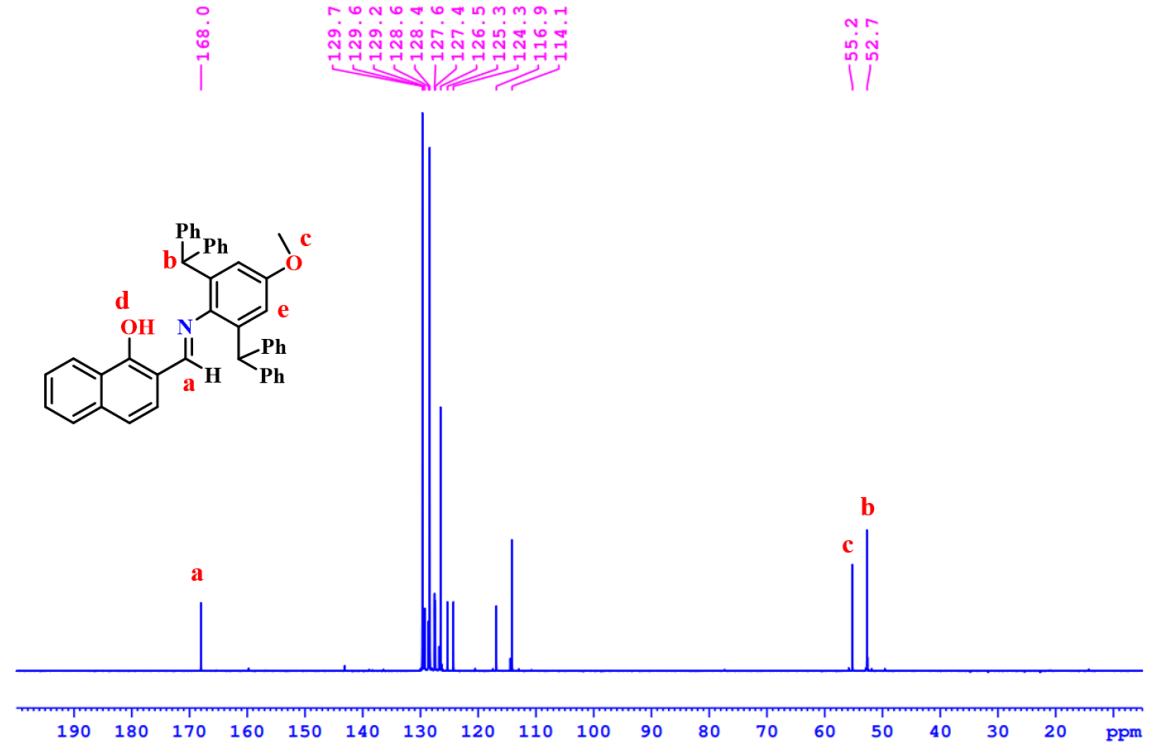

Figure S2.4: ^{13}C DEPT NMR spectrum of **2L1** in $CDCl_3$ (125 MHz, 298 K).

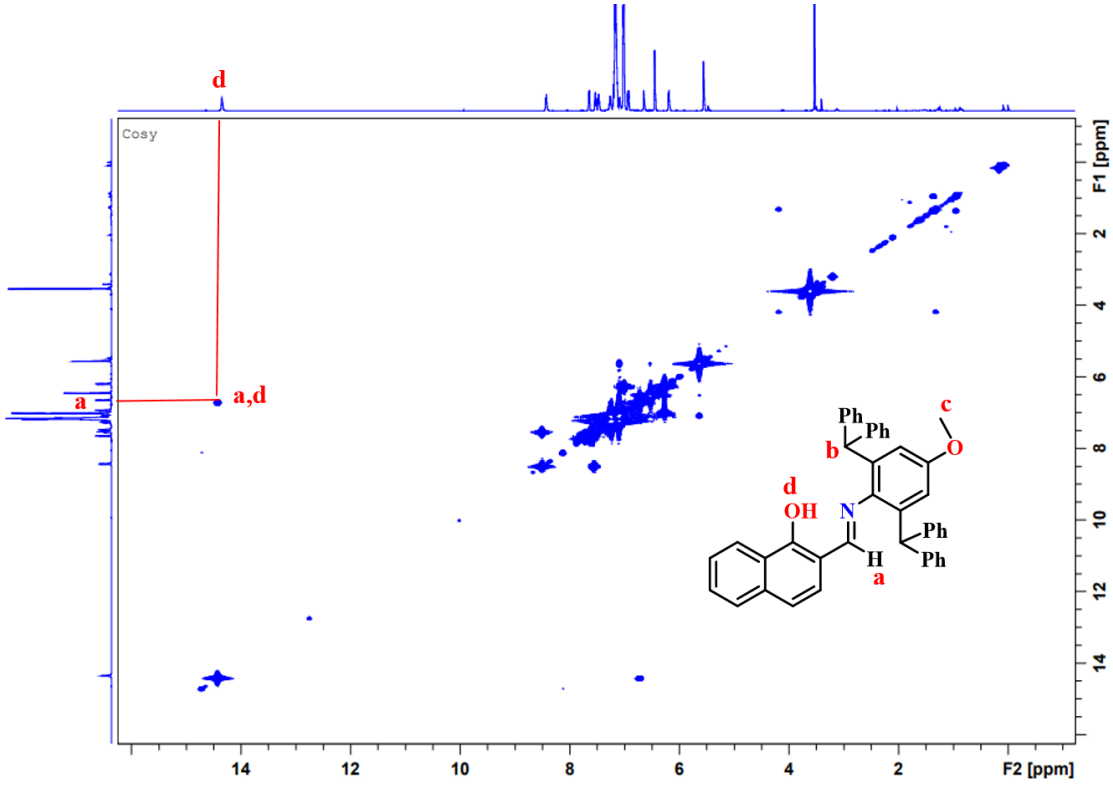

Figure S2.5: ^{1}H-^{1}H COSY NMR spectrum of **2L1** in $CDCl_3$ (500 MHz, 298 K).

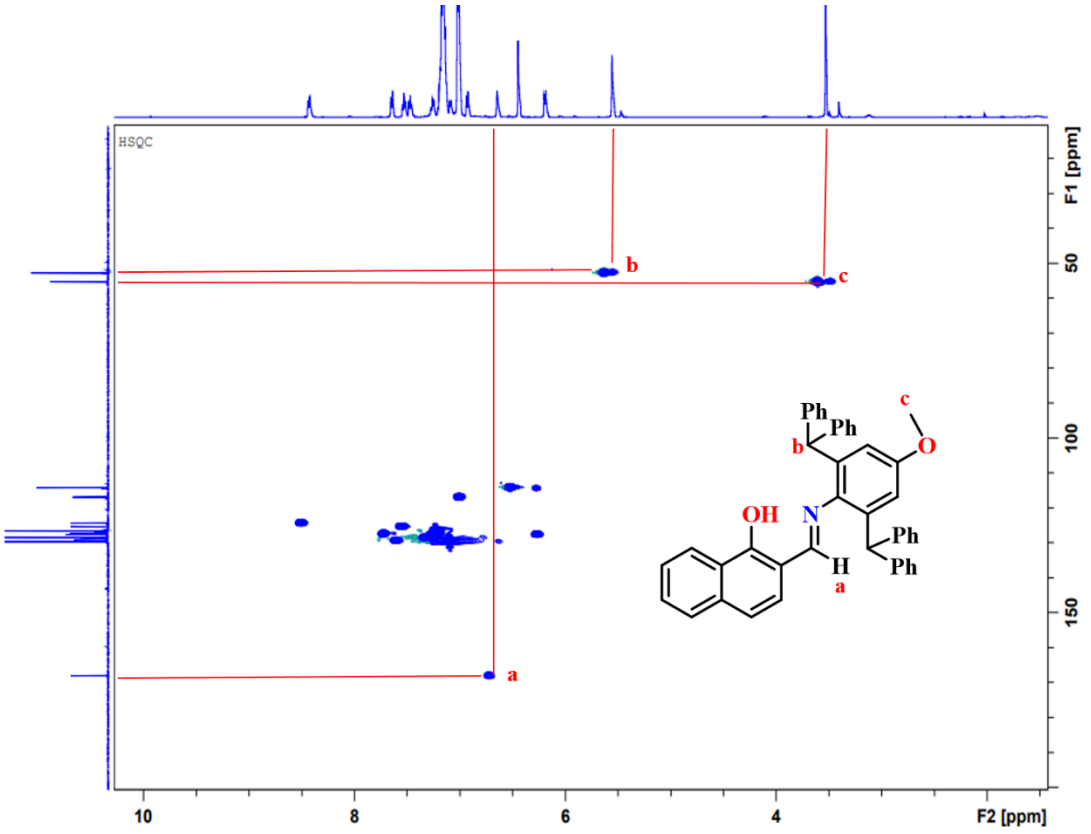

Figure S2.6: ^{1}H-^{13}C HSQC NMR spectrum of the **2L1** in $CDCl_3$ (500 MHz, 298 K).

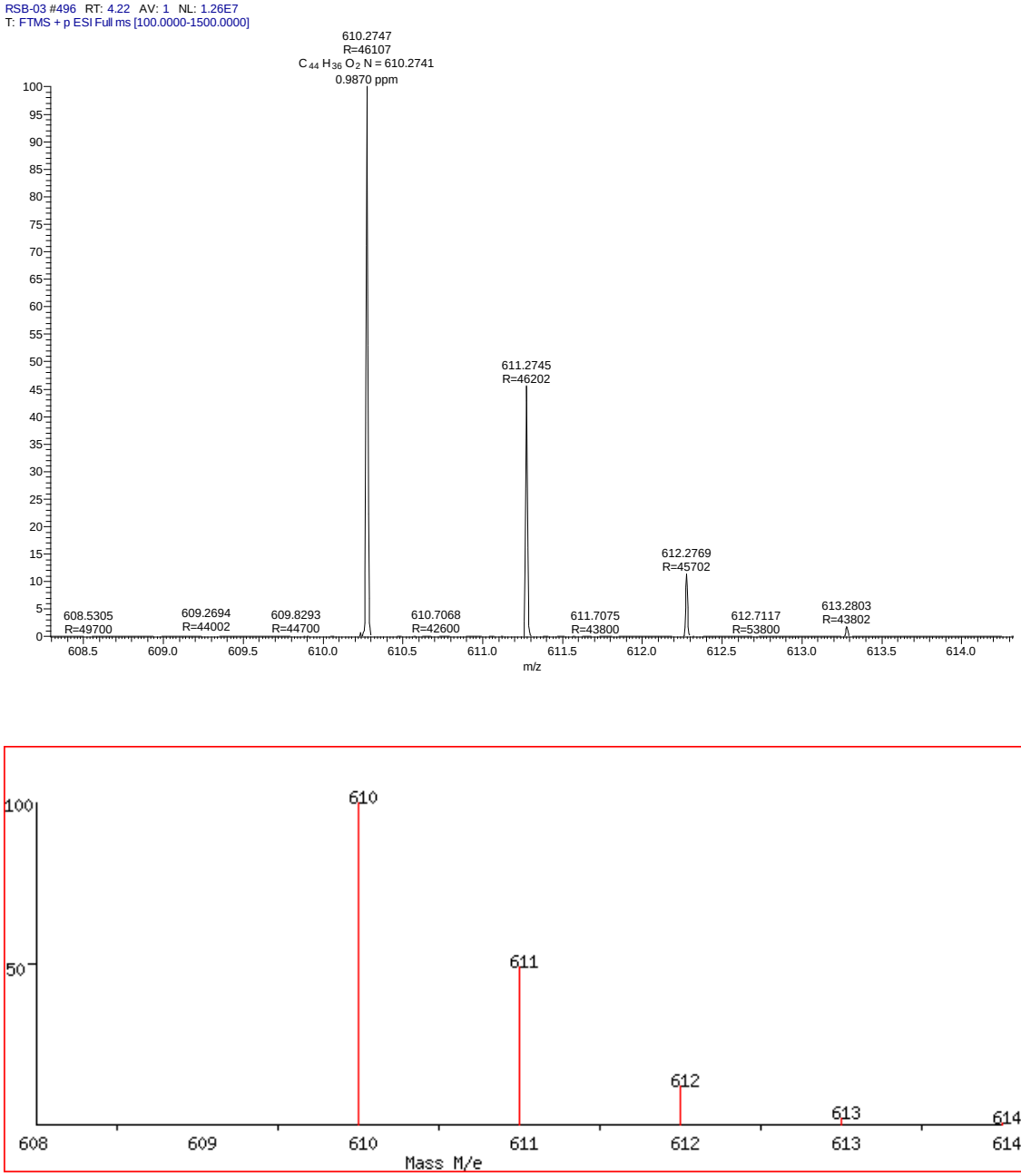

Figure S2.7: ESI MS data of 2L1; observed (top), simulated (bottom).

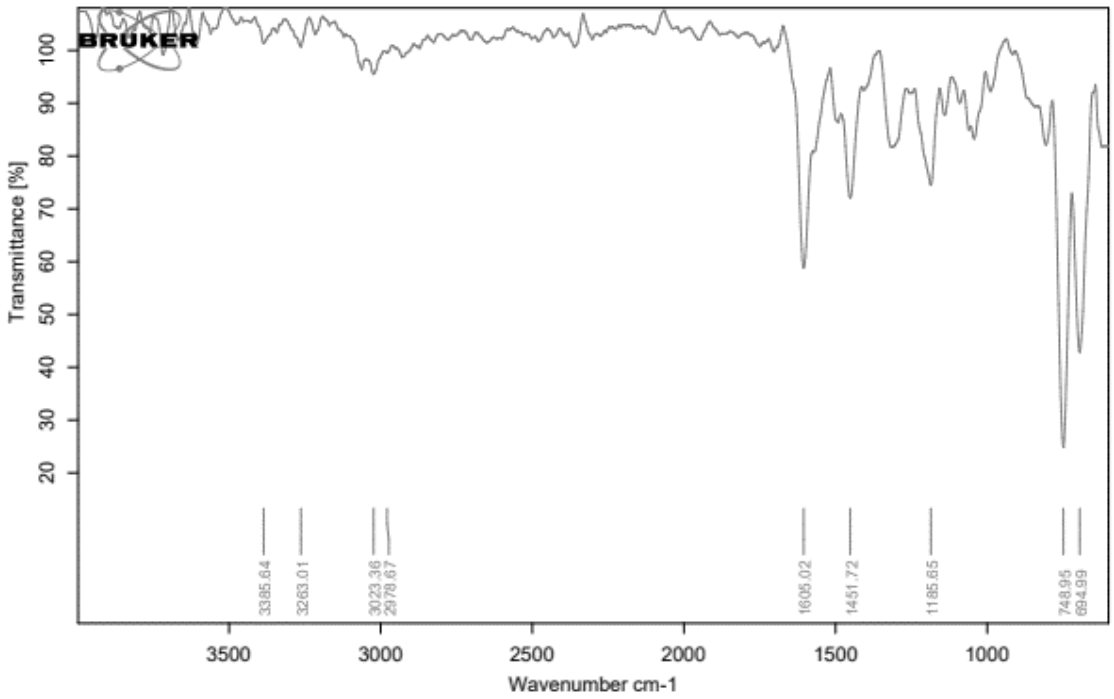

Figure S2.8: IR spectrum collected for ligand **2L1**.

2.5.2.3 Synthesis of 2-(((2,6-diisopropylphenyl)imino) methyl) naphthalen-1-ol (2L2): In an oven-dried Schlenk flask 1-hydroxy 2-naphthaldehyde (1 g, 0.0058 mol) was added along with 30 mL toluene. 2,6-diisopropyl amine (1.02 gm, 0.0058mol) was added to the above solution along with the catalytic amount of PTSA (10 mg, 0.058 mmol). The resultant reaction mixture was refluxed for 6 hours at 110 °C. The reaction mixture was cooled to room temperature, and volatiles were evaporated. The obtained crude product was purified using column chromatography (1 % ethyl acetate and 99% Petroleum ether) which produced a yellowish-color compound (872 mg, 50.57%).

^{1}H NMR (400 MHz ,$CDCl_3$) δ = 14.61 (m, 1 H), 8.49 (d, *J* = 8.0 Hz, 1 H), 8.16 (d, *J* = 2.6 Hz, 1 H), 7.72 (d, *J* = 8.1 Hz, 1 H), 7.58 (t, *J* = 7.4 Hz, 1 H), 7.54 - 7.47 (m, 1 H), 7.25 - 7.15 (m, 5 H), 3.10 (td, *J* = 6.8, 13.7 Hz, 2 H), 1.20 (d, *J* = 6.9 Hz, 12 H). **^{13}C NMR (100 MHz, $CDCl_3$)** δ = 167.2, 165.0, 142.9, 140.9, 136.8, 129.8, 127.6, 127.6, 127.2, 126.6, 125.7, 124.6, 123.7, 117.5, 111.0, 28.5, 23.8. **ESI-MS** (positive mode)**:** m/z = 332.20 Da $[M+H]^+$ (observed); 332.20 $[M+H]^+$ Da (calculated). IR (cm^{-1}) 1604.

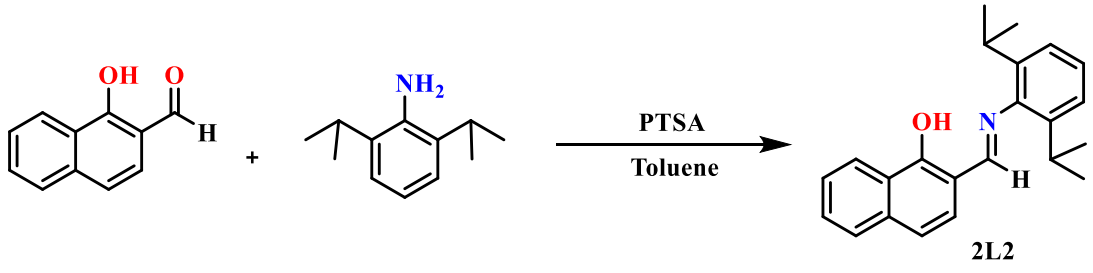

Scheme S2.3: Synthesis of **2L2**.

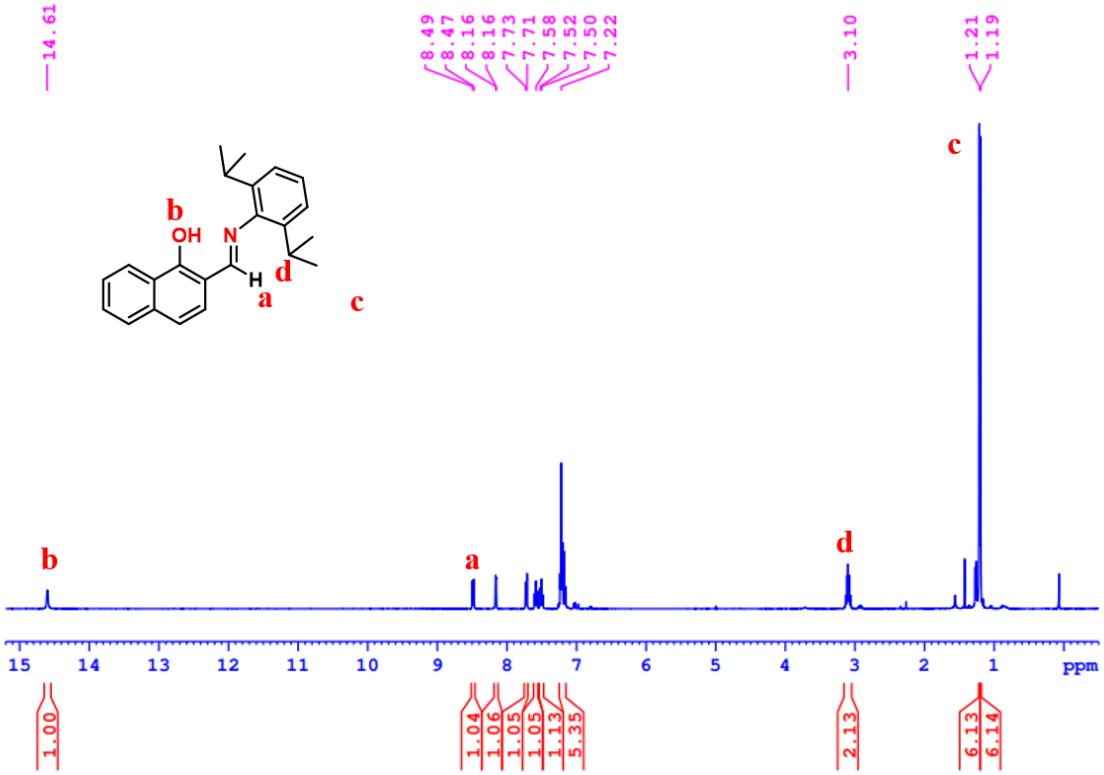

Figure S2.9: ^{1}H NMR spectrum of the **2L2** in $CDCl_3$ (400 MHz, 298 K).

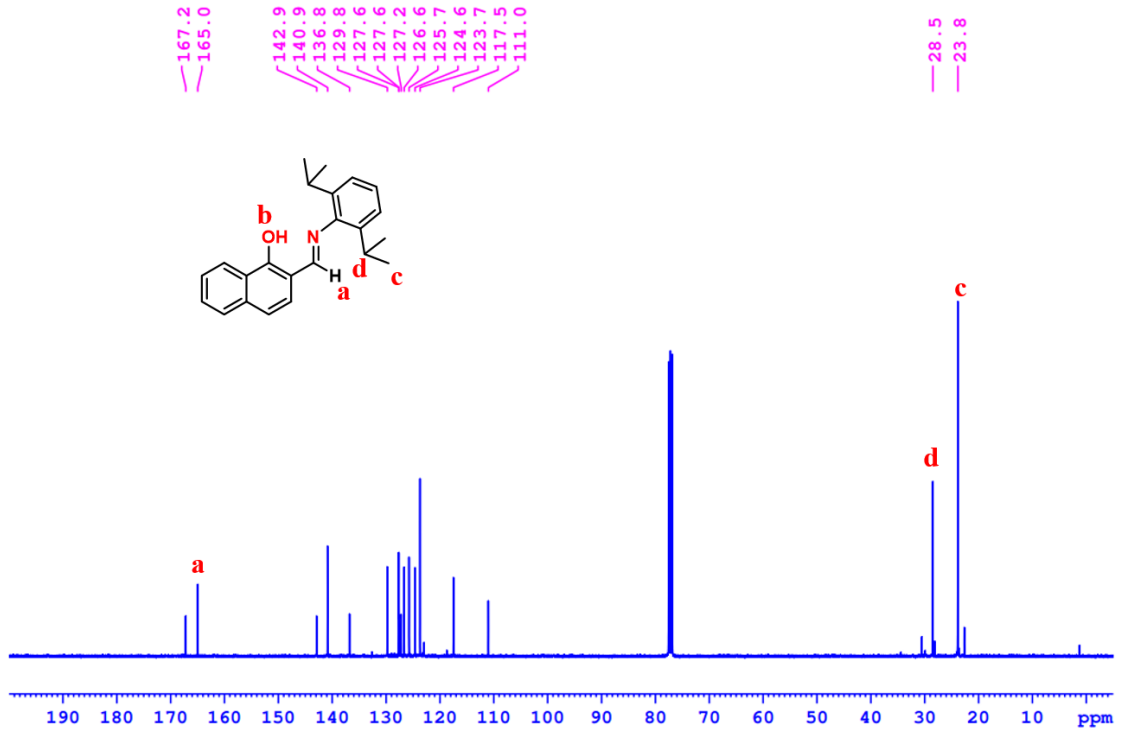

Figure S2.10: ^{13}C NMR spectrum of the **2L2** in $CDCl_3$ (100 MHz, 298 K).

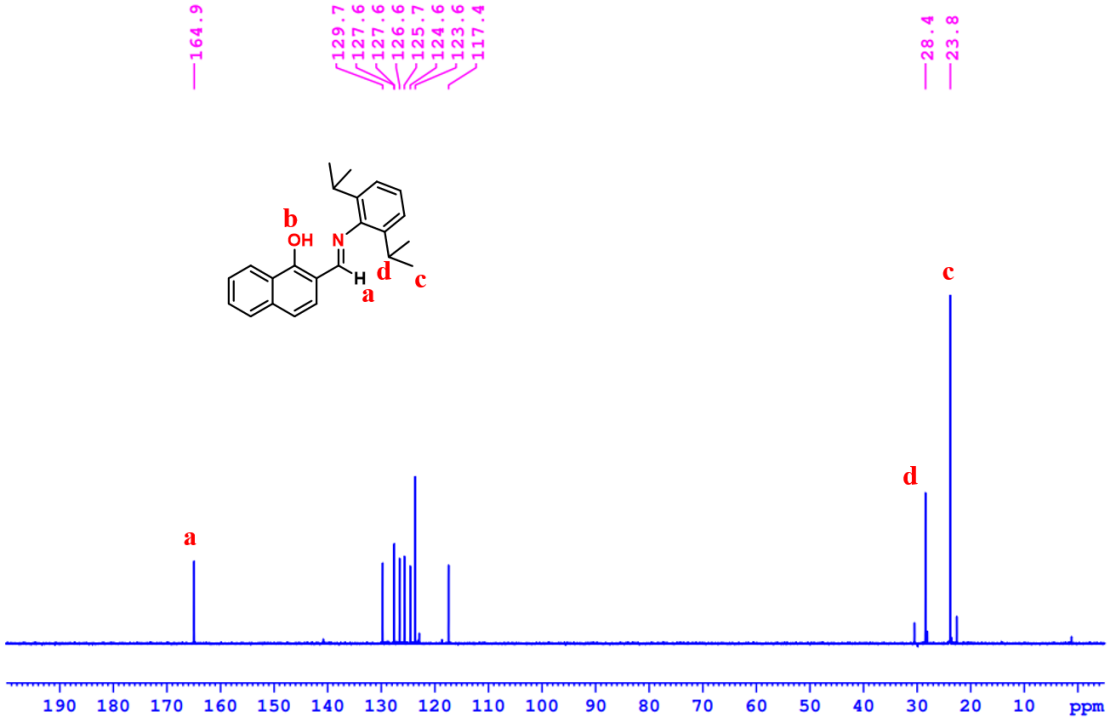

Figure S2.11: ^{13}C DEPT NMR spectrum of the **2L2** in $CDCl_3$ (100 MHz, 298 K).

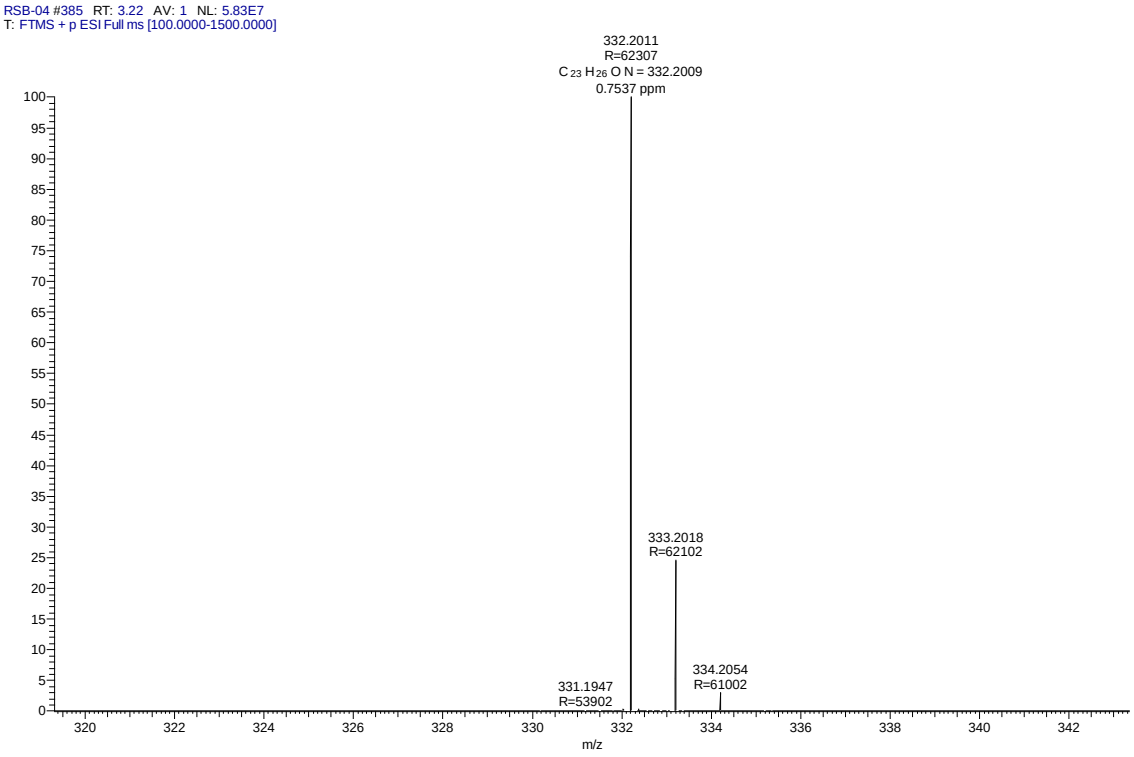

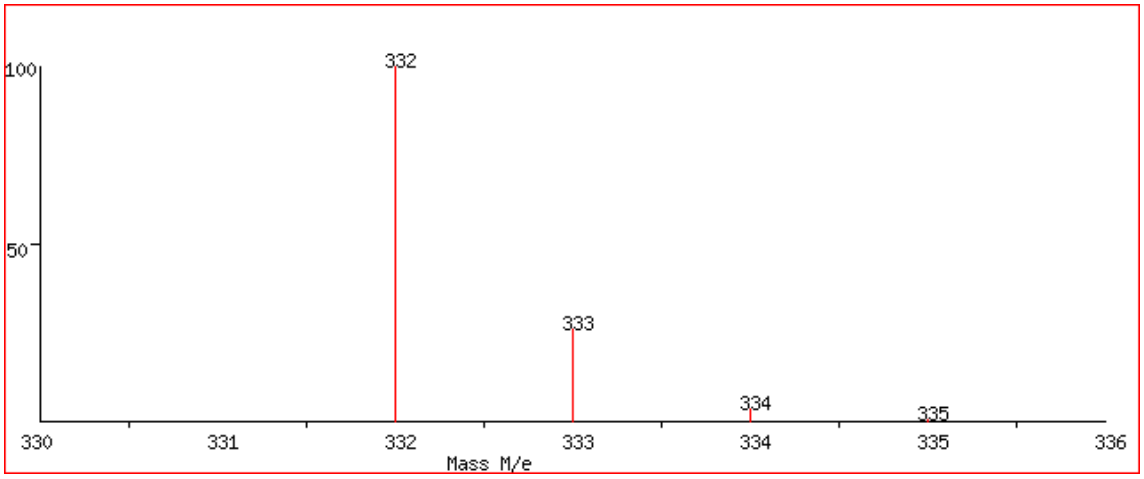

Figure S2.12: ESI-MS data of **2L2**; observed mass (top), simulated pattern (bottom).

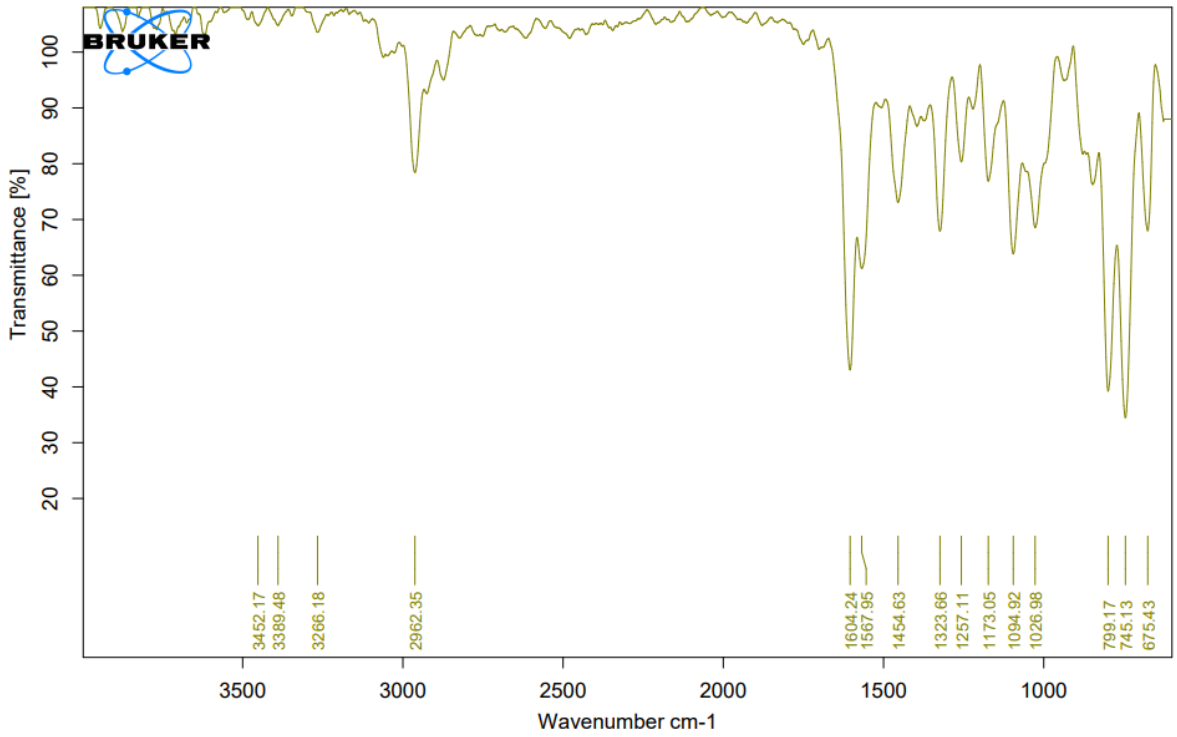

Figure S2.13: IR spectrum of the ligand **2L2**.

2.5.3. Synthesis of Pd-complex:

2.5.3.1. Synthesis of 2Pd1:

In an oven-dried Schlenk flask, ligand **2L1** (200 mg, 0.328 mmol) and [Pd(TMEDA)Me_2] (82.74 mg, 0.328 mmol) were dissolved in 5 mL pyridine. The resulting reaction mixture was stirred at room temperature for 2 hours. The pyridine was evaporated to dryness. Next, the second batch of pyridine (5 mL) was added to the above residue, and the content was stirred for another 1 hour. Pyridine was evaporated to dryness. The above step was performed again, and finally, the resultant residue was dried under a high vacuum to pull out excess pyridine.

The thus obtained crude product was washed with hexane (5 mL × 2), and dried to produce pure yellow-colored Pd-complex **2Pd1** (183 mg, 68.9%).

^{1}H NMR (400 MHz,$CDCl_3$) δ = 9.04 (dd, *J* = 1.5, 6.4 Hz, 2 H), 8.35 (d, *J* = 8.2 Hz, 1 H), 7.92 (s, 1 H), 7.57 - 7.50 (m, 3 H), 7.48 (s, 1 H), 7.33 - 7.27 (m, 5 H), 7.25 - 7.19 (m, 6 H), 7.09 - 7.01 (m, 10 H), 6.51 (s, 2 H), 6.45 (d, *J* = 8.5 Hz, 1 H), 6.29 (s, 2 H), 5.94 (s, 1 H), 5.51 (d, *J* = 8.9 Hz, 1 H), 3.61 (s, 3 H), 0.44 (s, 3 H). **^{13}C NMR** (125 MHz, $CDCl_3$) δ= 167.8, 166.8, 156.5, 152.8, 143.8, 143.8, 142.7, 139.7, 138.0, 137.6, 132.1, 130.1, 129.9, 129.7, 128.5, 128.3, 128.3, 127.1, 126.4, 125.7, 124.9, 123.8, 113.8, 112.4, 111.7, 55.2, 52.3, 1.9. **ESI-MS:** m/z = 809.20 $[M+H]^+$ (observed); 809.23 (calculated). **IR** (cm^{-1}): 1589.

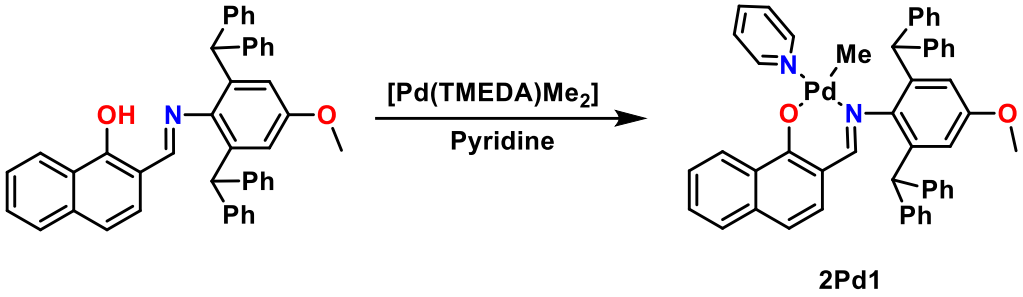

2Pd1

Scheme S2.4: Synthesis of **2Pd1.**

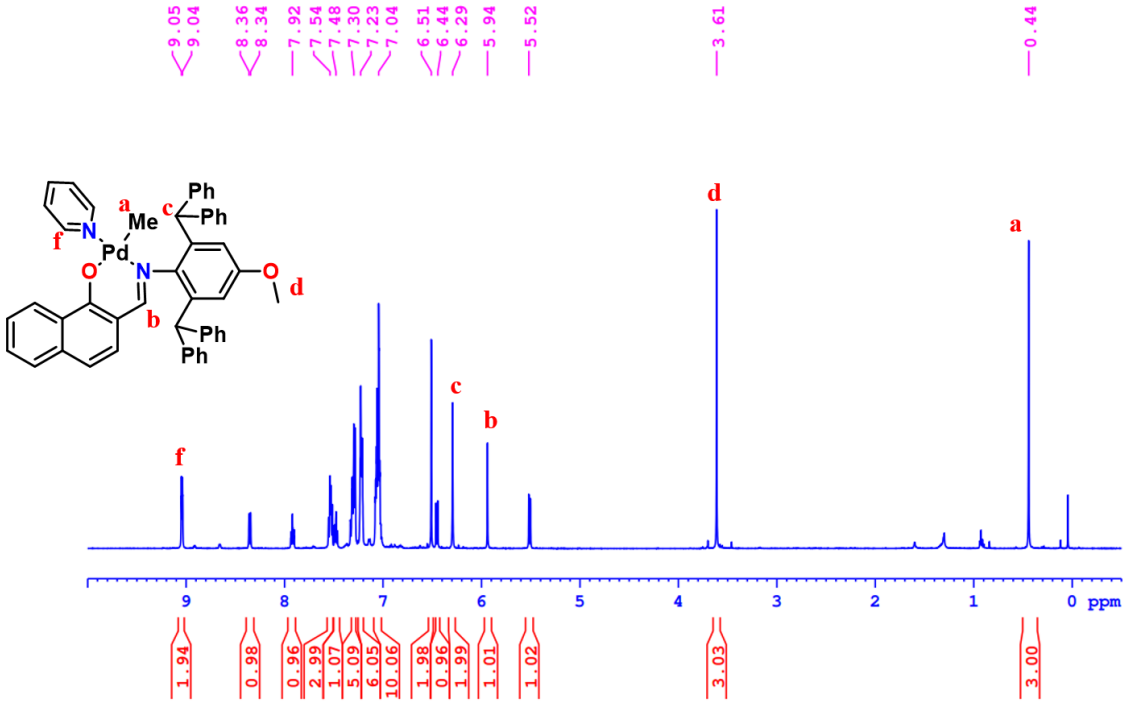

Figure S2.14: ^{1}H NMR spectrum of the **2Pd1** in $CDCl_3$ (400 MHz, 298 K).

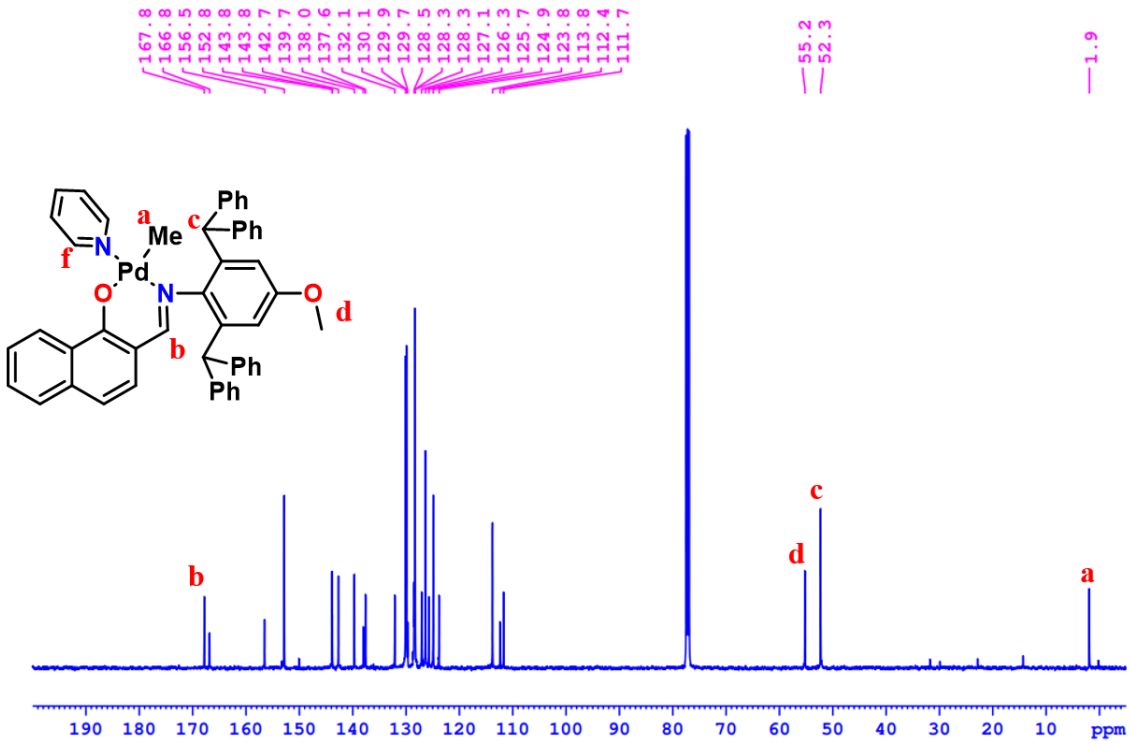

Figure S2.15: ^{13}C NMR spectrum of the **2Pd1** in $CDCl_3$ (100 MHz, 298 K).

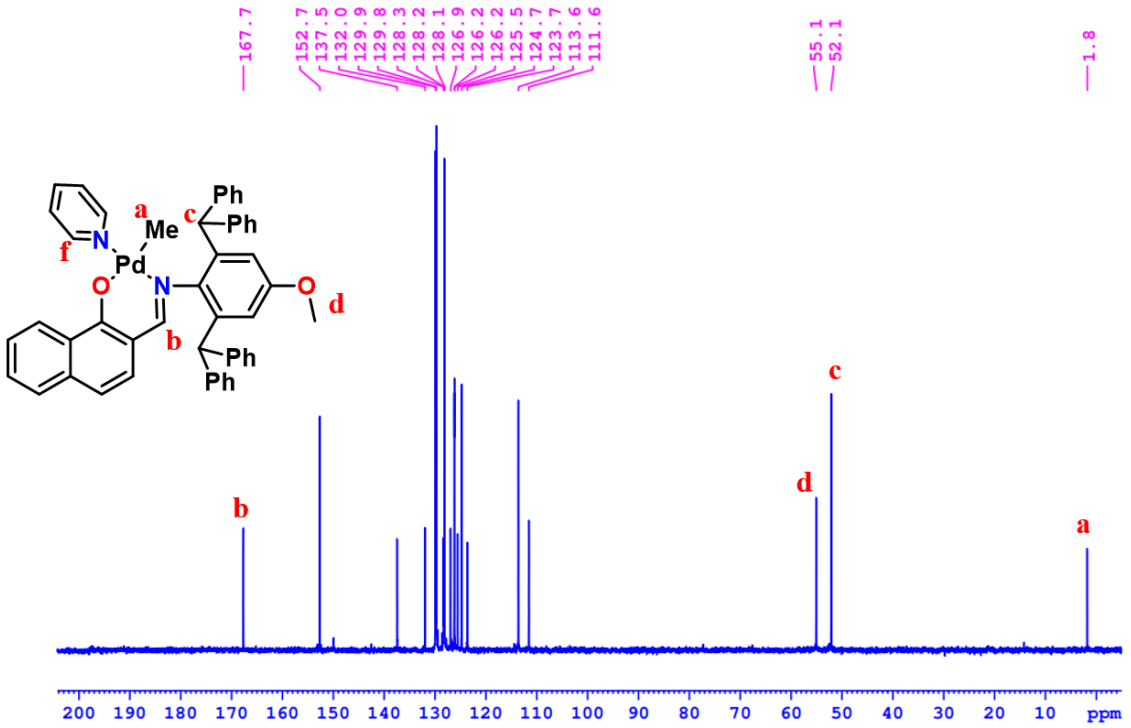

Figure S2.16: ^{13}C DEPT NMR spectrum of the **2Pd1** in $CDCl_3$ (100 MHz, 298 K).

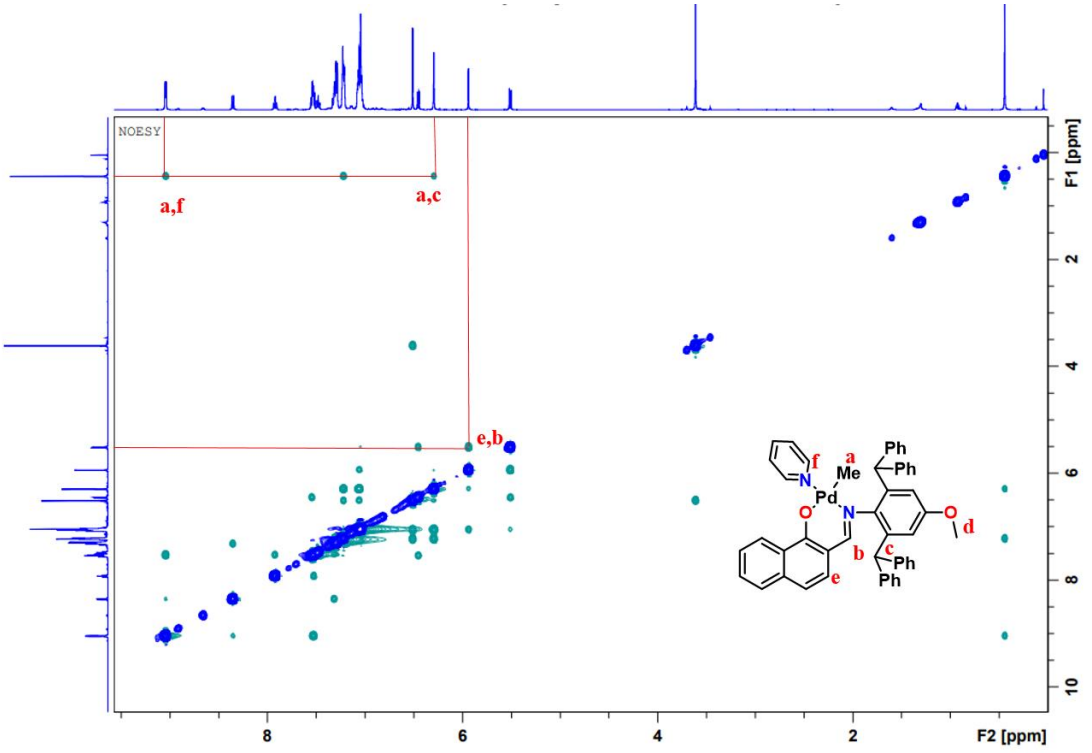

Figure S2.17: ^{1}H-^{1}H NOESY NMR spectrum of the **2Pd1** in $CDCl_3$ (400 MHz, 298 K).

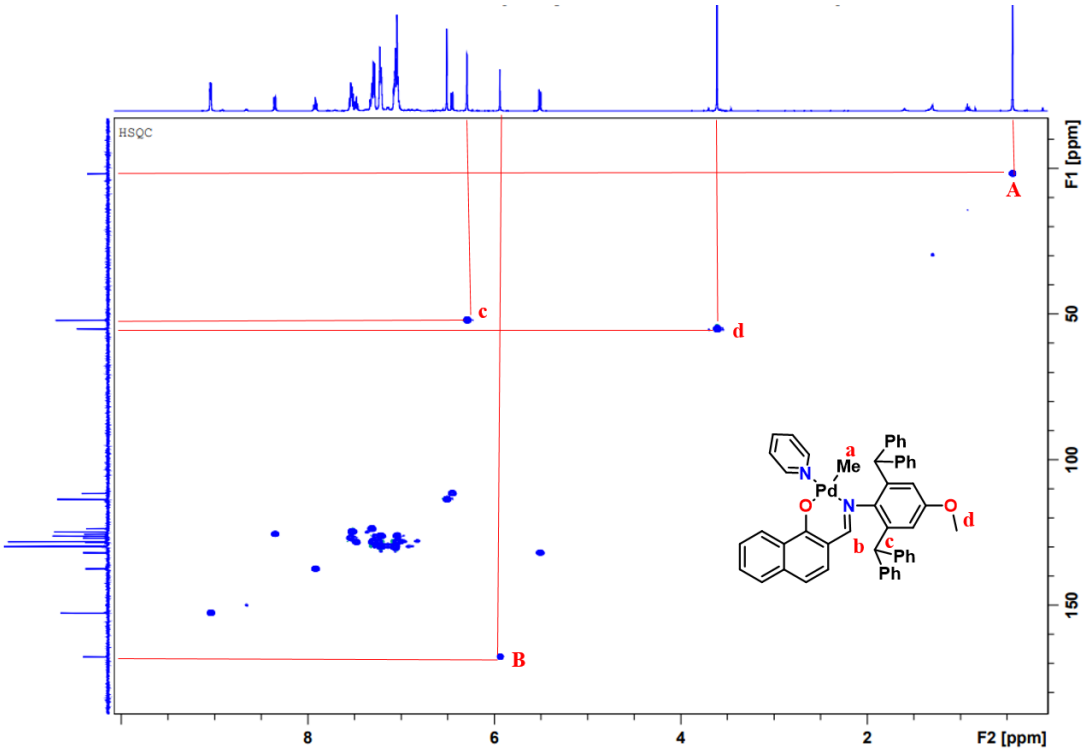

Figure S2.18: ^{1}H-^{13}C HSQC NMR spectrum of the **2Pd1** in $CDCl_3$ (400 MHz, 298 K).

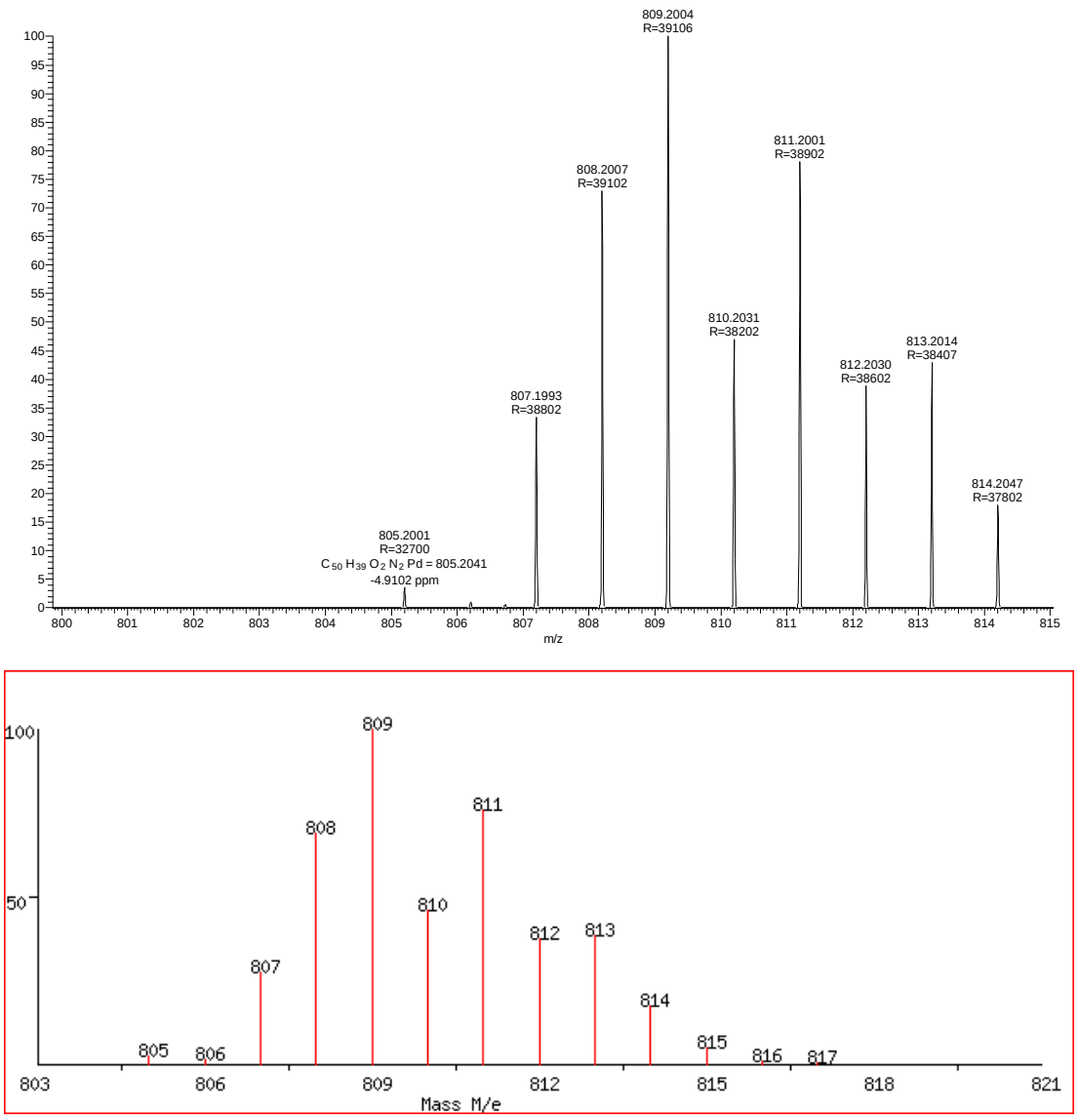

Figure S2.19: ESI MS data for **2Pd1**; observed (top), simulated (bottom).

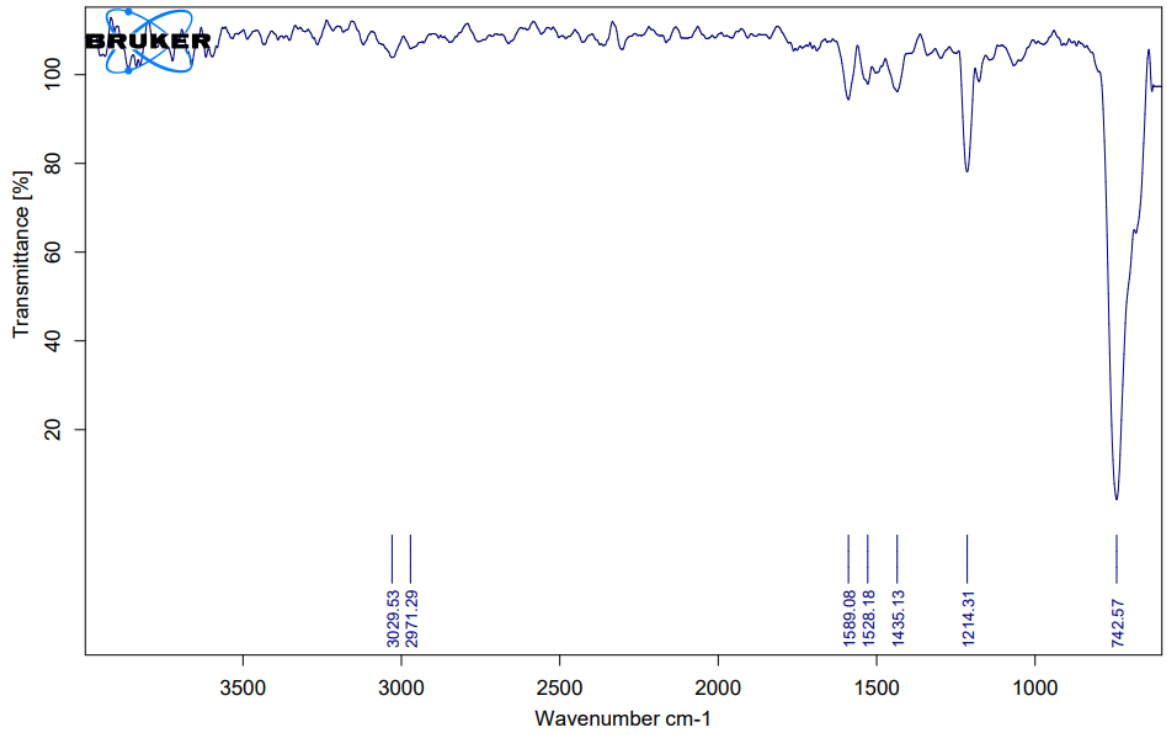

Figure S2.20: IR data of **2Pd1**.

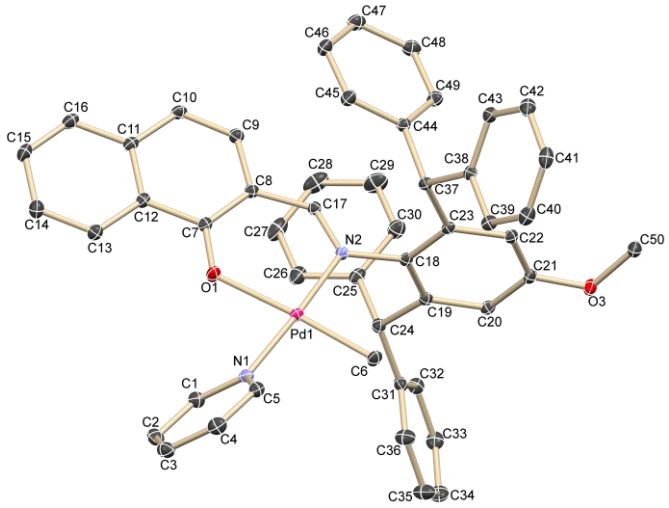

Figure S2.21: Molecular structure of **2Pd1**.

Chart S2.1: Crystal data and structure refinement for **2Pd1** (CCDC 2225185).

Cell:	a=12.6742(3)	b=20.3077(6)	c=15.1446(4)
	alpha=90	beta=94.370(1)	gamma=90
Temperature:	100 K		

	Calculated	Reported
Volume	3886.64(18)	3886.64(18)
Space group	P 21/n	P 21/n
Hall group	-P 2yn	-P 2yn
Moiety formula	C50 H42 N2 O2 Pd	C50 H42 N2 O2 Pd
Sum formula	C50 H42 N2 O2 Pd	C50 H42 N2 O2 Pd
Mr	809.26	809.25
Dx,g cm-3	1.383	1.383
Z	4	4
Mu (mm-1)	0.521	0.521
F000	1672.0	1672.0
F000'	1668.59	
h,k,lmax	17,27,20	17,27,20
Nref	10095	9902
Tmin,Tmax	0.877,0.910	0.682,0.746
Tmin'	0.808	

Correction method= # Reported T Limits: Tmin=0.682 Tmax=0.746
AbsCorr = MULTI-SCAN

Data completeness= 0.981 Theta(max)= 28.747

R(reflections)= 0.0322(8728) wR2(reflections)= 0.0808(9902)

S = 1.046 Npar= 498

2.5.3.2. Synthesis of 2Pd2:

In the Schlenk flask, ligand **2L2** (150 mg, 0.452 mmol) and [Pd(TMEDA)Me_2] (114.07 mg, 0.452 mmol) was dissolved in 5 mL pyridine. The resulting reaction mixture was stirred at room temperature for 2 hours. The pyridine was evaporated to dryness, again 5 mL pyridine was added and stirred for another 1 hour. Pyridine was evaporated to dryness. The above step was performed once again, and finally, the resultant residue was dried under a high vacuum to remove unreacted pyridine. The thus obtained crude product was washed with hexane (5 mL × 2), and dried to produce pure green colored Pd-complex **2Pd2** (214 mg, 89.1%).

^{1}H NMR (500 MHz , $CDCl_3$) δ = 8.91-8.89 (m, 2 H), 8.35-8.33 (m, 1 H), 7.84 (tt, *J* = 1.6, 7.7 Hz, 1 H), 7.75 (s, 1 H), 7.61 - 7.58 (m, 1 H), 7.48 (dt, *J* = 1.4, 7.4 Hz, 1 H), 7.44 - 7.40 (m, 2 H), 7.33 - 7.28 (m, 1 H), 7.24 - 7.17 (m, 3 H), 7.09 - 7.04 (m, 1 H), 6.84 (d, *J* = 8.5 Hz, 1 H), 3.68 - 3.54 (m, 2 H), 1.32 (d, *J* = 6.7 Hz, 6 H), 1.11 (d, *J* = 7.0 Hz, 6 H), 0.02 (s, 3 H). **^{13}C NMR (125 MHz, $CDCl_3$)** δ = 167.7, 164.8, 152.7, 149.0, 141.6, 138.0, 137.6, 131.7, 130.2,

128.9, 127.3, 126.4, 125.8, 124.8, 124.3, 123.4, 113.1, 112.3, 27.9, 25.0, 22.9, 0.7. **ESI-MS m/z** = 531.16 $(M+H)^+$ observed; 531.16 $(M+H)^+$ calculated. **IR** (cm^{-1}) 1586.

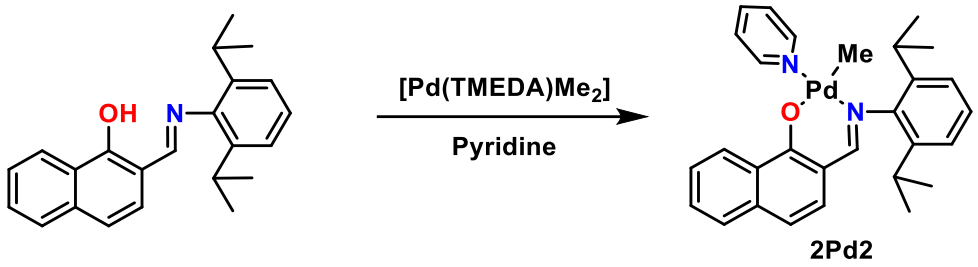

Scheme S2.5: Synthesis of **2Pd2.**

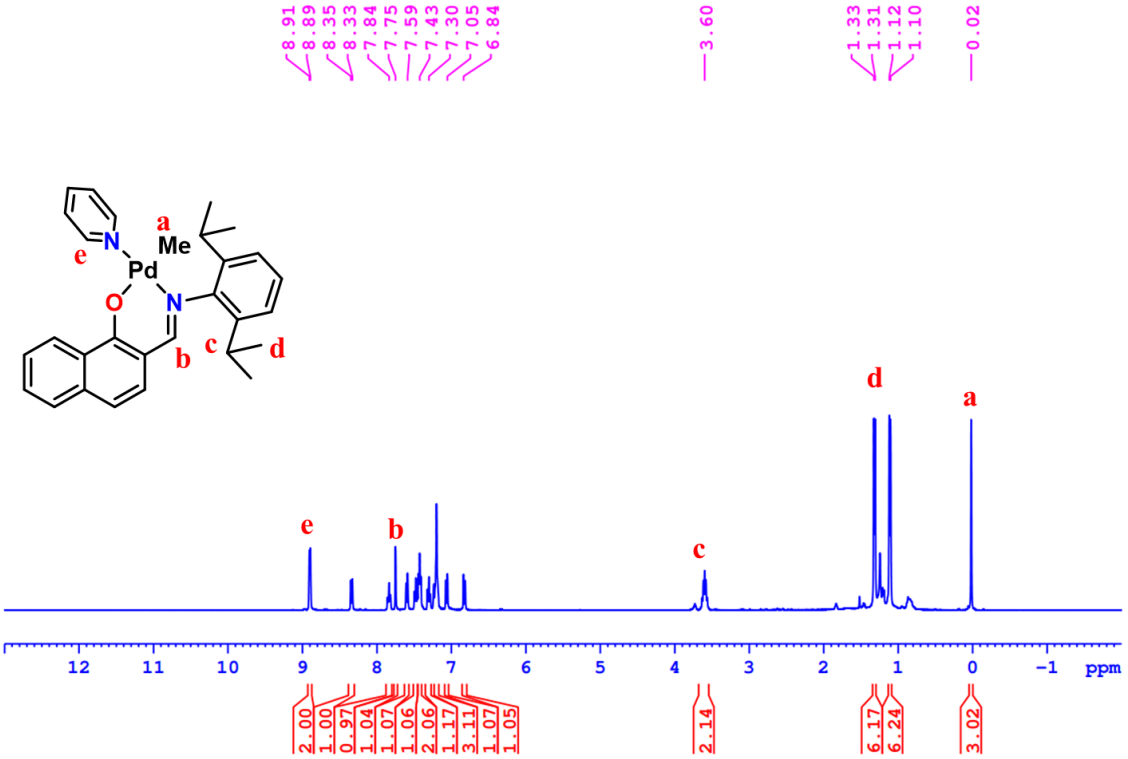

Figure S2.22: ^1H NMR spectrum of the **2Pd2** in $CDCl_3$ (500 MHz, 298 K).

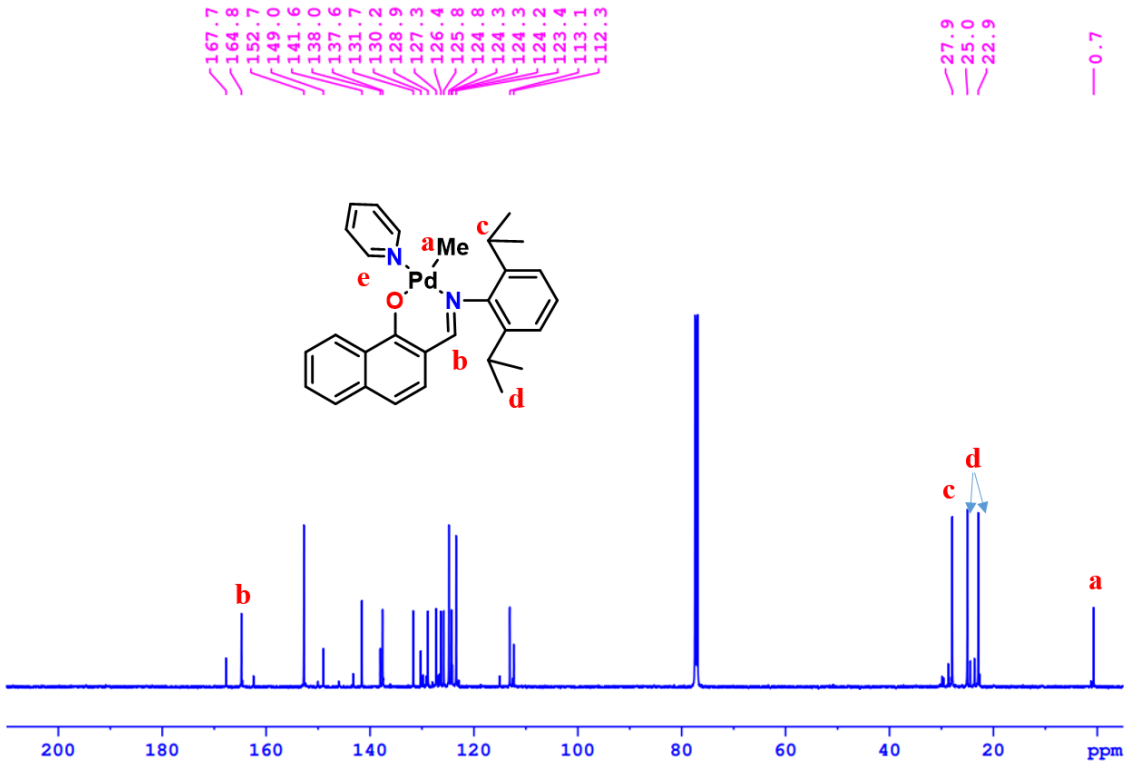

Figure S2.23: ^{13}C NMR spectrum of the **2Pd2** in $CDCl_3$ (100 MHz, 298 K).

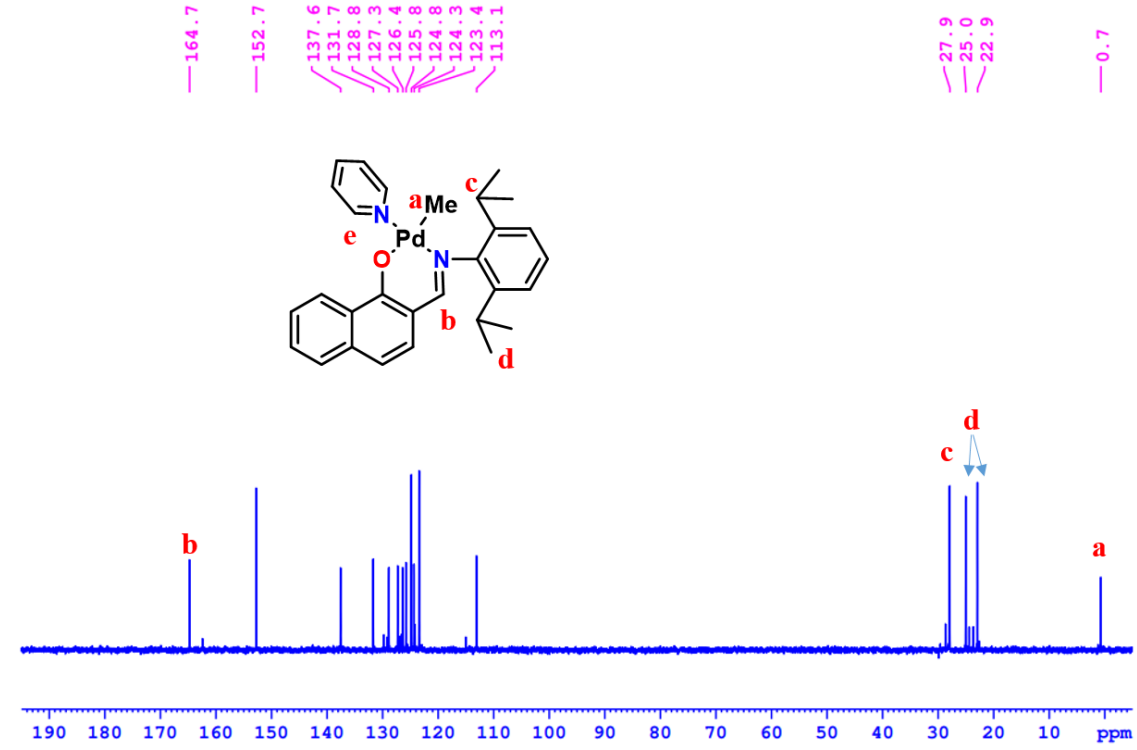

Figure S2.24: ^{13}C DEPT NMR spectrum of the **2Pd2** in $CDCl_3$ (100 MHz, 298 K).

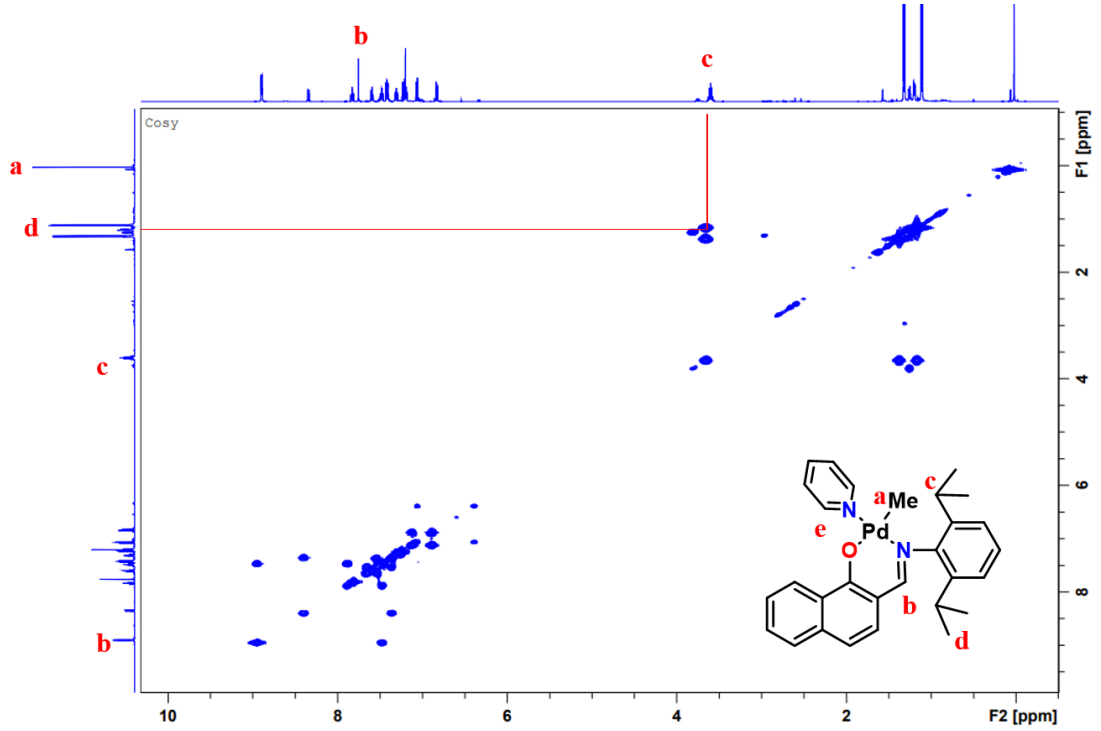

Figure S2.25: ^{1}H-^{1}H COSY NMR spectrum of the **2Pd2** in $CDCl_3$ (500 MHz, 298 K).

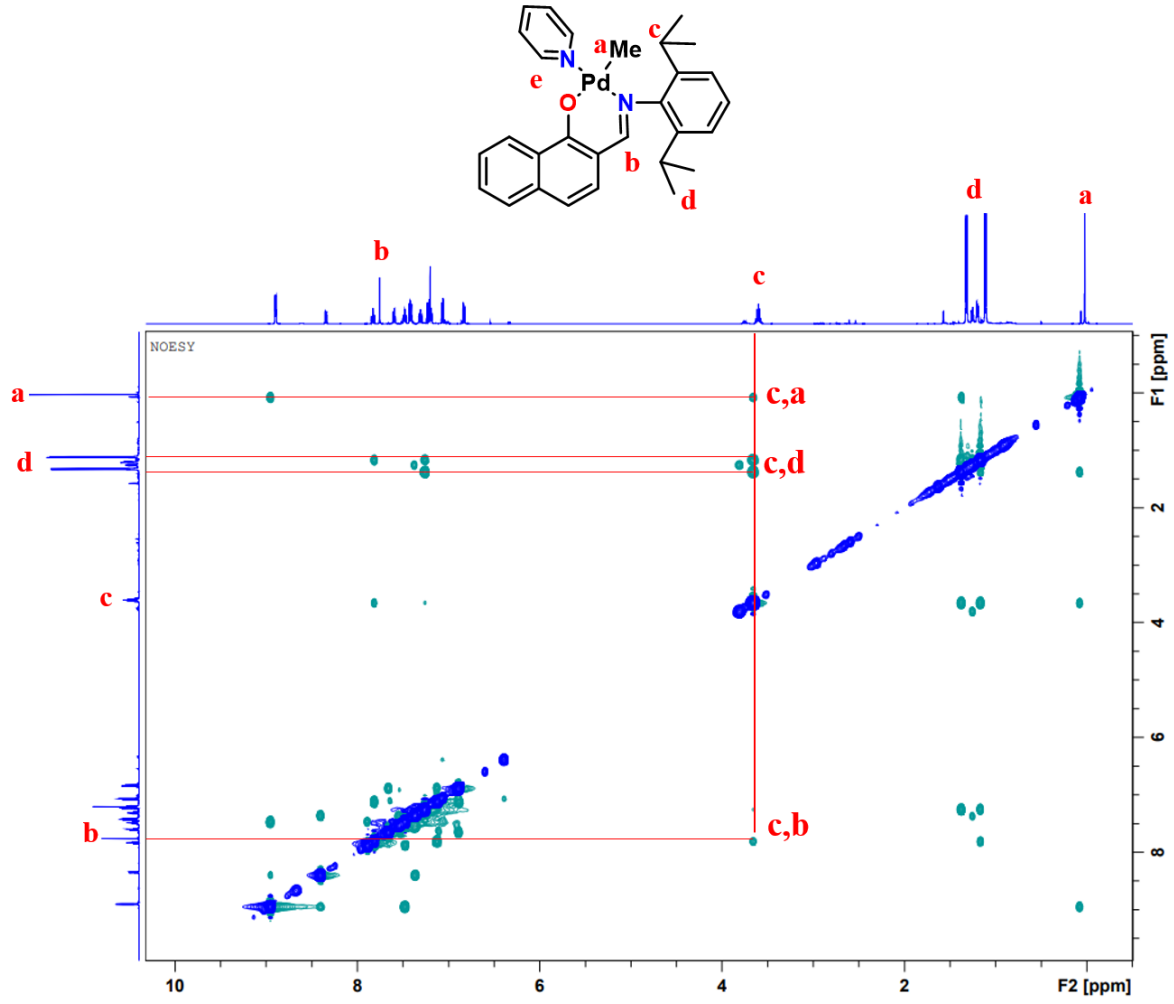

Figure S2.26: ^{1}H-^{1}H NOESY NMR spectrum of the **2Pd2** in $CDCl_3$ (500 MHz, 298 K).

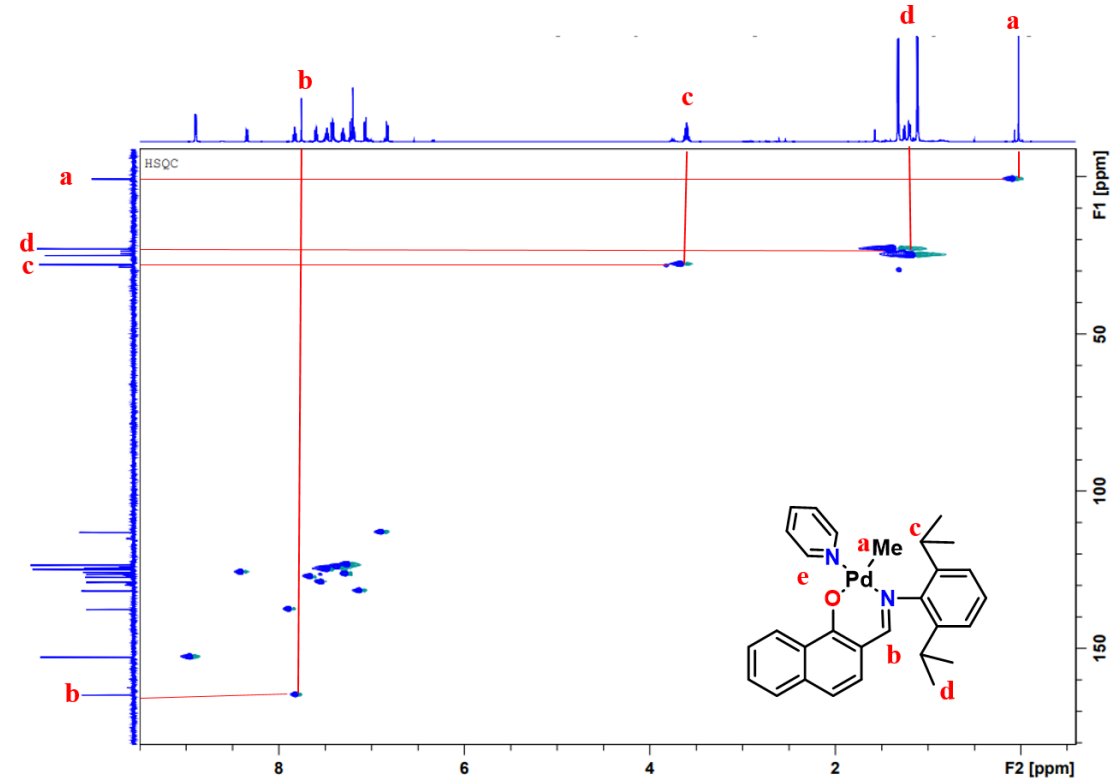

Figure S2.27: ^{1}H-^{13}C HSQC NMR spectrum of the **2Pd2** in $CDCl_3$ (500 MHz, 298 K).

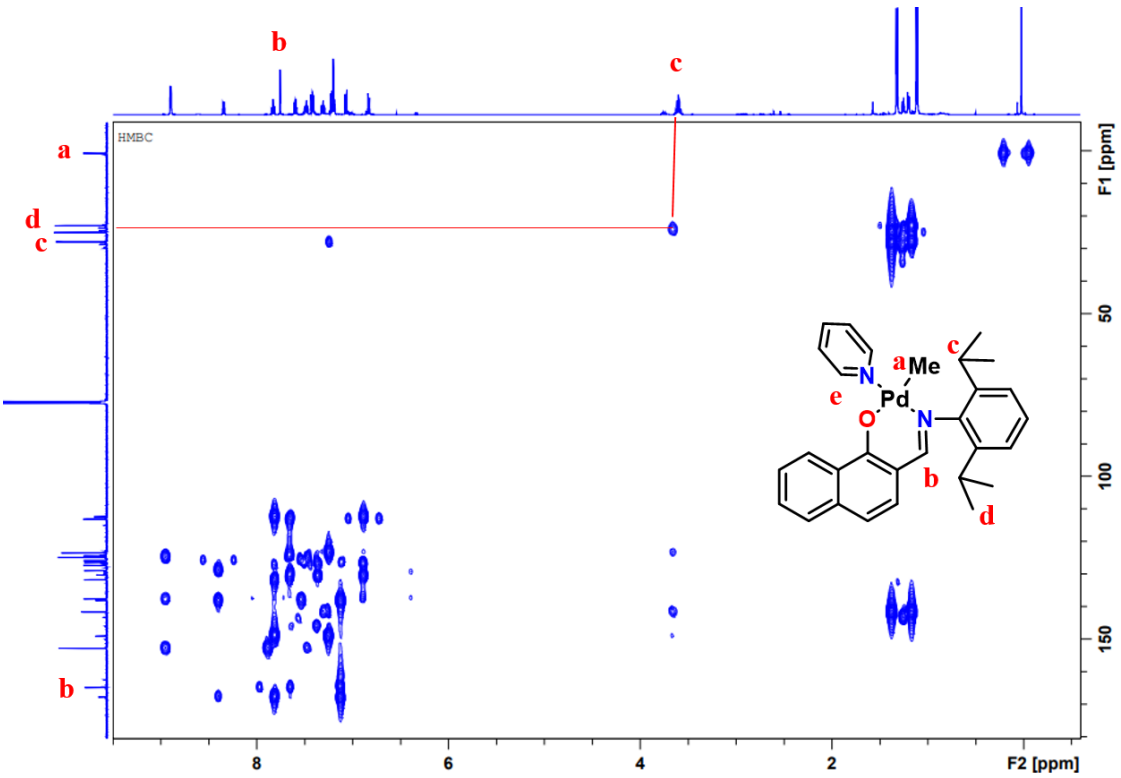

Figure S2.28: ^{1}H-^{13}C HMBC NMR spectrum of the **2Pd2** in $CDCl_3$ (500 MHz, 298 K).

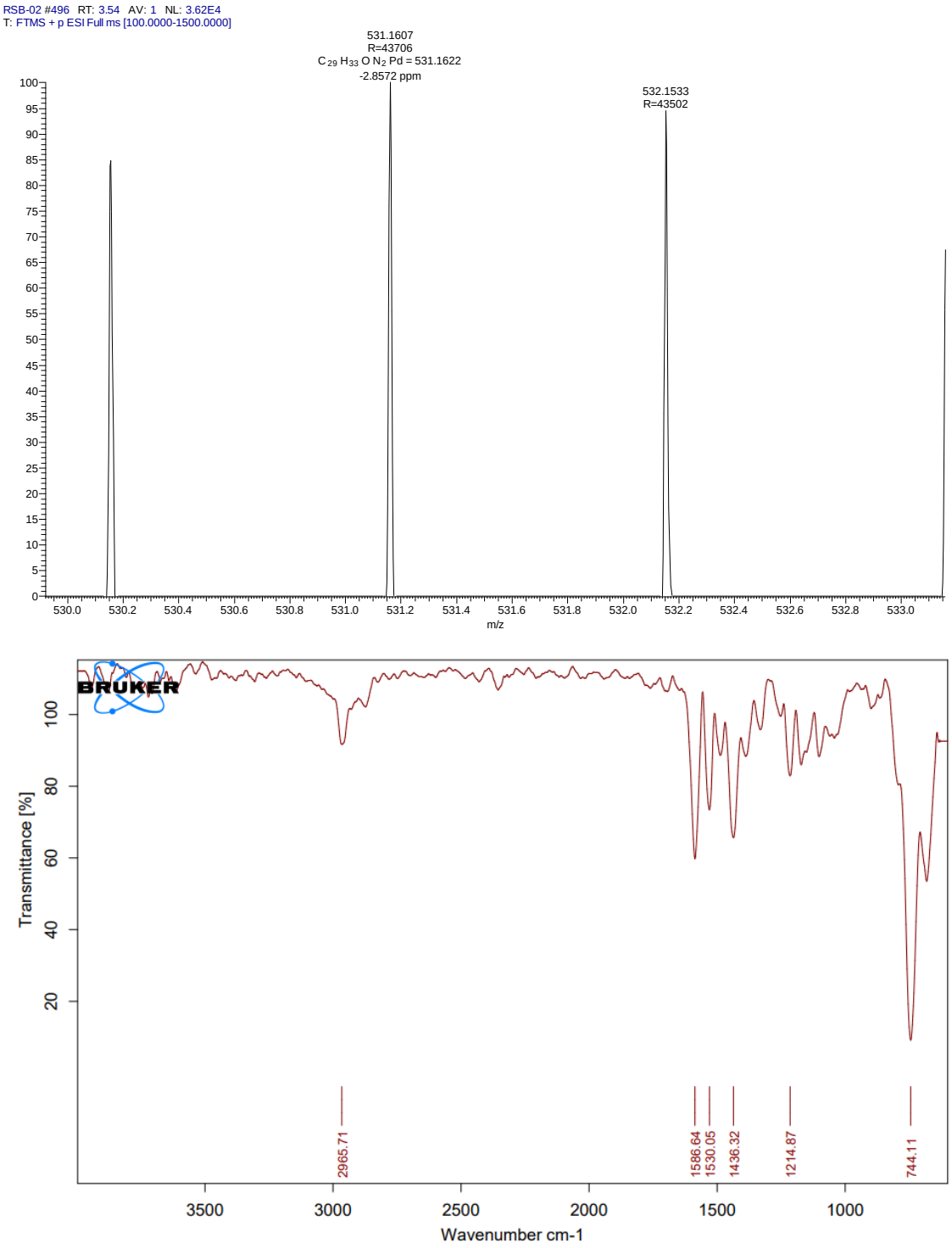

Figure S2.29: ESI-MS spectrum (top) and IR spectrum (bottom) of **2Pd2**.

2.5.4. Ethylene oligomerization:

The oligomerization reaction was carried out in a 250 mL stainless steel high-pressure Büchi (GlasUster cyclone 075) reactor equipped with a heating/cooling jacket and mechanical stirrer.

Prior to the experiment, the reactor was fully dried by heating it in vacuum at 90 °C for 1 hour, followed by cooling it to room temperature and filling it with argon. The reactor was maintained at the desired reaction temperature, and was purged with ethylene gas. To this, 100 mL of dried and freshly distilled solvent (toluene or other solvents) was added under positive ethylene pressure. Subsequently, the solvent was stirred under ethylene pressure for 30 minutes to dissolve ethylene. Suitable amount of catalyst was injected into the reactor using the syringe under positive ethylene pressure. Next, the reactor was pressurized to desired ethylene pressure with rapid stirring, and desired ethylene pressure was maintained throughout the reaction. After the completion of polymerization, excess ethylene was vented, and the solvent was evaporated under a high vacuum to yield highly viscous semi-solid ethylene oligomers. The yield is determined after subtracting the initial weight of the catalyst, and the resultant oligomers were characterized by various methods. Table 2.1 summarizes the most important runs using **2Pd1** and **2Pd2**.

2.5.4.1. Analysis of distribution of different branches by ^{13}C NMR:

Entry (Table 2.1)	Total branches[a]	Methyl (%)[b]	Ethyl (%)[b]	Propyl (%)[b]	Long chain branching (%)[c]	*Sec*-Butyl (%)[b]
Entry 8	78	51.3	19.9	15.7	9.1	3.9
Entry 9	90	37.42	25.4	21.5	8.7	7.0

[a]Branches per 1000 carbons calculated from ^{1}H NMR. [b]Calculated by the relative intensities of the methyl resonances $1B_1$, $1B_2$, $1B_3$, and sec-Bu. [c]LCB = butyl and longer branches, calculated by the relative intensity of the methine resonance.

2.5.4.2. GC-MS analysis of low boiling ethylene oligomer:

Ethylene oligomerization reaction was performed at optimized reaction conditions (80 °C, 5 bar, 90 minutes, and 100 mL of Toluene solvent). To check the presence of low boiling compound after completion of ethylene polymerization reaction we cooled the reactor to 0 °C and excess ethylene was vented. The reactor was maintained at 0 °C and the sample was taken and immediately performed GC-MS analysis of the oligomerization reaction mixture.

Method: Headspace GC-MS analysis was performed on an Agilent 7890B GC system equipped with Agilent HP-5 column. Inlet temperature was maintained at 250 °C, column flow = 3 ml/min. split ratio 75:1. Detector temperature was maintained at 300 °C. Temperature program: starting at 40 °C with hold time of 5 mins. Ramp 1: @ 10 °C to 320 °C.

GC chromatogram of ethylene oligomeric reaction mixture

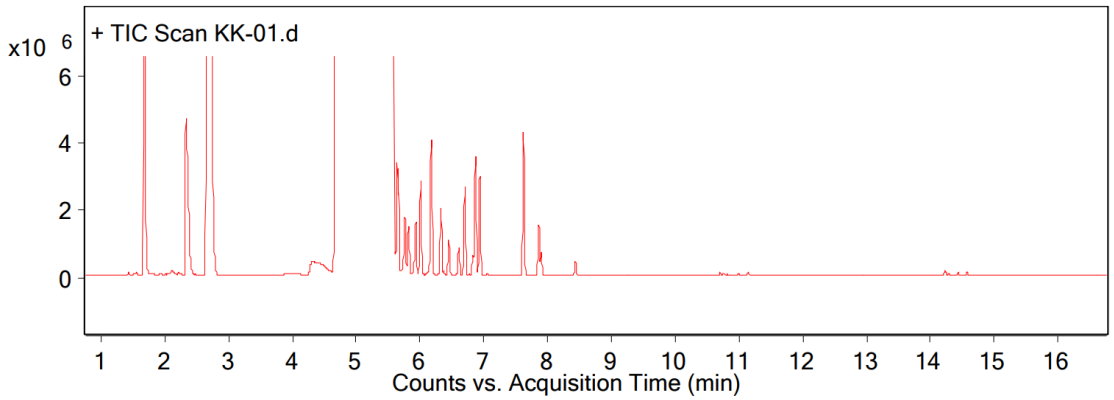

C7 Compound with olefin (Mass- 98.10) [5.9 minute].

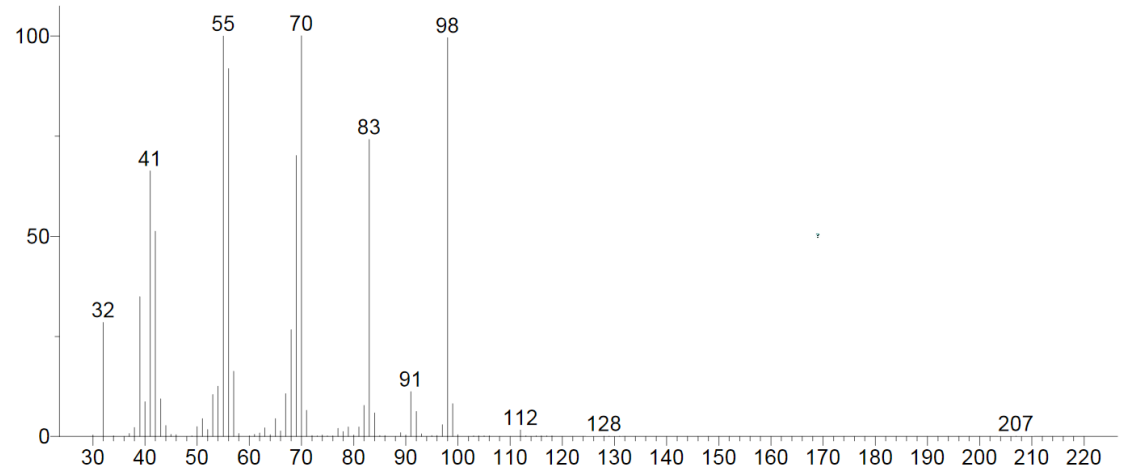

C8 Compound with olefin (Mass- 112.12) [5.7, 5.8, 6.0, 6.1, 6.3, 6.8, 6.9 minute]

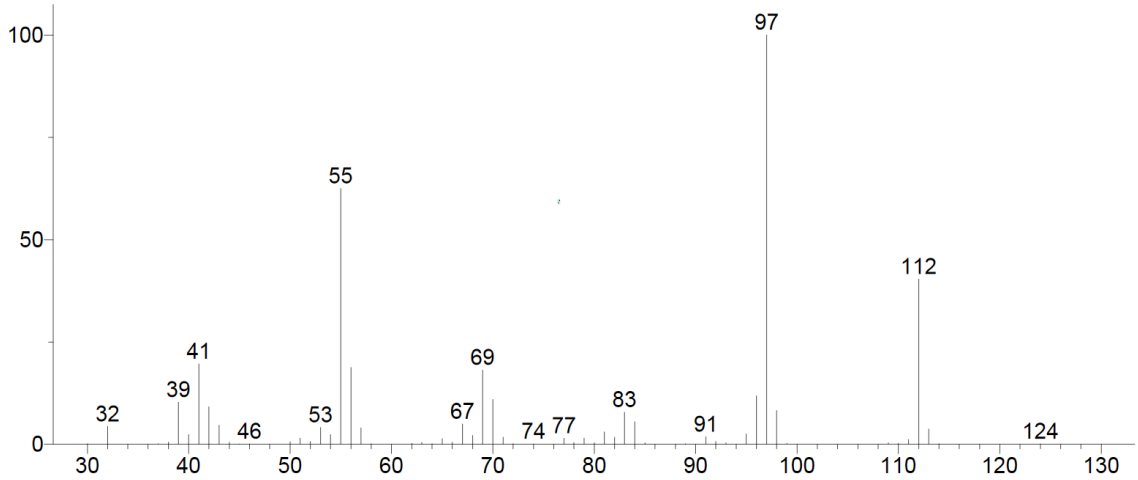

Figure S2.30: GC-MS chromatogram of ethylene oligomer.

2.5.4.3. M_n and $N_{branch/1000\text{-}C}$ calculation:

Calculation of M_n and $N_{Branches/1000C}$ from ^1H is well established in literature. Literature reported method was adopted and the number of branches per 1000 C-atoms is calculated as under.[75]

H_1 (vinylidene end group); H_2 (1,2-disubstituted olefin); H_3 (trisubstituted olefin); H_4 (α-olefin); H_5 (alkyl methyl, alk-CH3); H_6 (allylic methyl); H_7 (alkyl methylene and methine, alk-CH and alk-CH_2); H_8 (allylic methylene or methine).

In our case, more than <98% of polymeric chain ends were found to be of H_2 and H_4 type. Therefore, we modified the literature reported formula as under.

$V = H_2+(2/3)H_4$

$A = H_5+H_6+H_7+H_8-H_2-(1/3)H_4$

$N_{av} = (2/V) \times (A) +2$

$M_n = N_{av} \times 14.01$

N_{br} is number of methyl branches per 1000 C atoms.

$Y = (H_5+H_6)/3 \times (2/V)$

$X = [H_2+(H_4/3)] \times (2/V)$

$N_{br} = (1000/N_{av}) \times (Y-X)$

For Table 2.1, entry 3,

$V = H_2+(2/3)H_4$

$V = 6.27 + (0.66 \times 3.17) = 8.38$

$A = H_5+H_6+H_7+H_8-H_2-(1/3)H_4$

$A = (603.02-6.27-1.05)/2$

$A = 297.85$

$N_{av} = (2/V) \times (A) +2$

$N_{av} = (2/8.38) \times 297.85 + 2$

$N_{av} = 73.08$

$M_n = N_{av} \times 14.01$

$M_n = 73.08 \times 14.01 = 1023 \sim$**1000**

$Y = (H_5+H_6)/3 \times (2/V)$

$Y = (78.18+9.08)/3 \times (2/8.38)$

$Y = 29.08 \times 0.238 = 6.94$

$X = [H_2+(H_4/3)] \times (2/V)$

$X = [6.27+(3.17/3)] \times (2/8.38)$

$X = 7.32 \times 0.238 = 1.74$

$N_{br} = (1000/N_{av}) \times (Y-X)$

$N_{br} = (1000/73.08) \times (6.94-1.74)$

$N_{br} = 13.68 \times 5.2 = 71.13 \sim \mathbf{71}$

2.5.4.4. Reactivity of 2Pd1 with ethylene:

2Pd1 (3 mg, 3.7 mol) was dissolved in benzene-d6 (0.25mL) in a high-pressure NMR tube in a glove box, and the ^{1}H NMR spectrum was recorded (figure S2.30 top.). The NMR tube was then connected to the vacuum line, and the argon gas was evacuated from inside the NMR tube. The NMR tube was instantly charged with 4 bar of ethylene gas, and a proton NMR was recorded after 20 minutes, 4 and 24 hours. As depicted in figure S2.30, the initial Pd-Me resonance at 1.00 ppm slowly disappears, with the concomitant appearance of methylene (-CH_2-) resonance at 1.47 ppm. These mechanistic investigations suggest that the ethylene inserts in a Pd-Me bond and 2Pd1 is capable of ethylene insertion and oligomerization or polymerization, even at room temperature.

Stacked high-pressure ^{1}H NMR spectra of **2Pd1** in the presence of 4 bar ethylene at 0 and 20 minutes, 4 and 24 hours (at room temperature) was presented in figure 2.3.

2.5.5. Ethylene Oligomer Characterization:

2.5.5.1. NMR Data:

The assignment of peaks of ethylene oligomer in ^{1}H and ^{13}C NMR was performed using a literature method.[76]

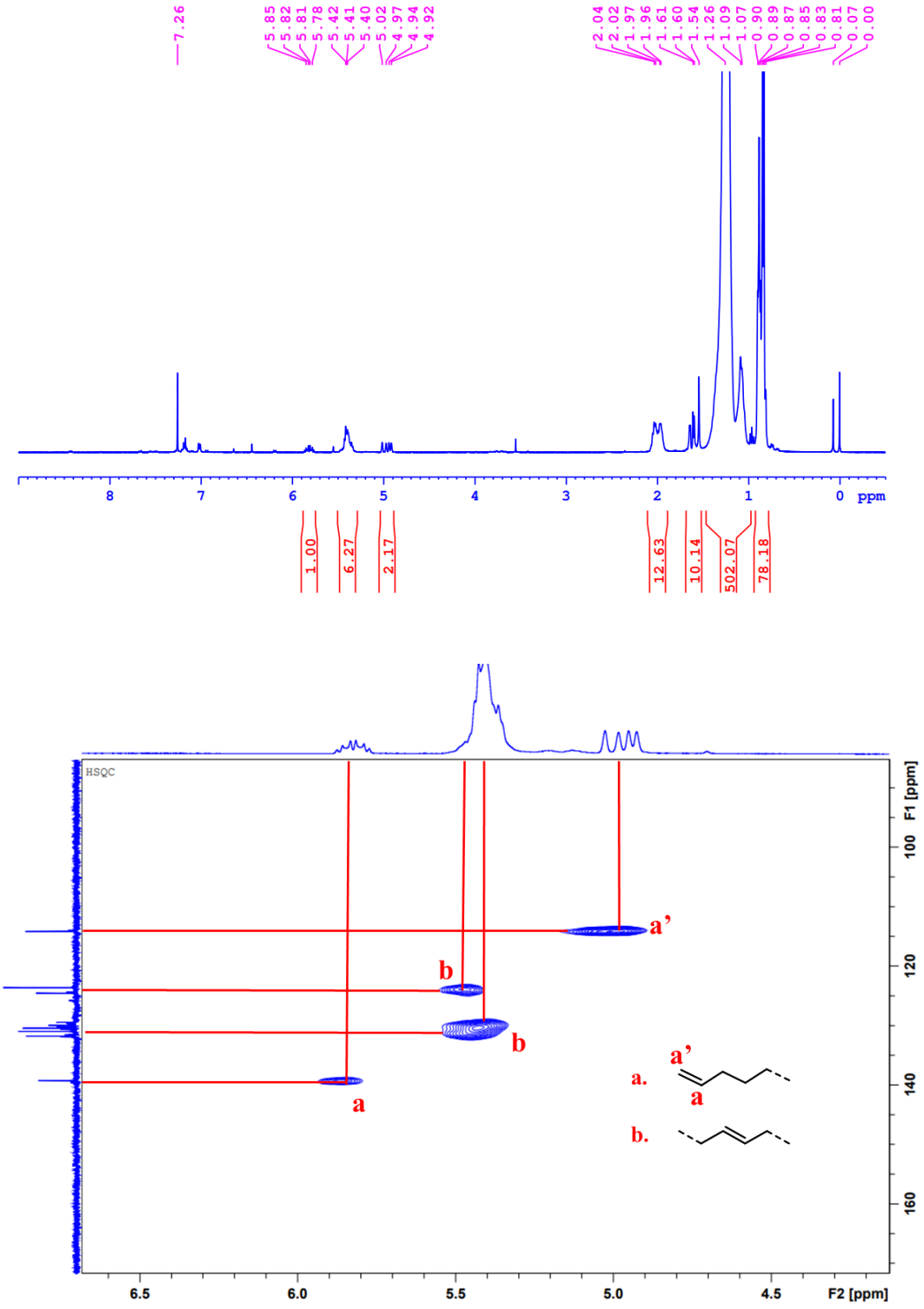

Figure S2.31: ^{1}H NMR spectra of oligomer in $CDCl_3$ (top), HSQC spectra of the oligomer in $CDCl_3$ (bottom) (Table 2.1, entry 3, 298 K).

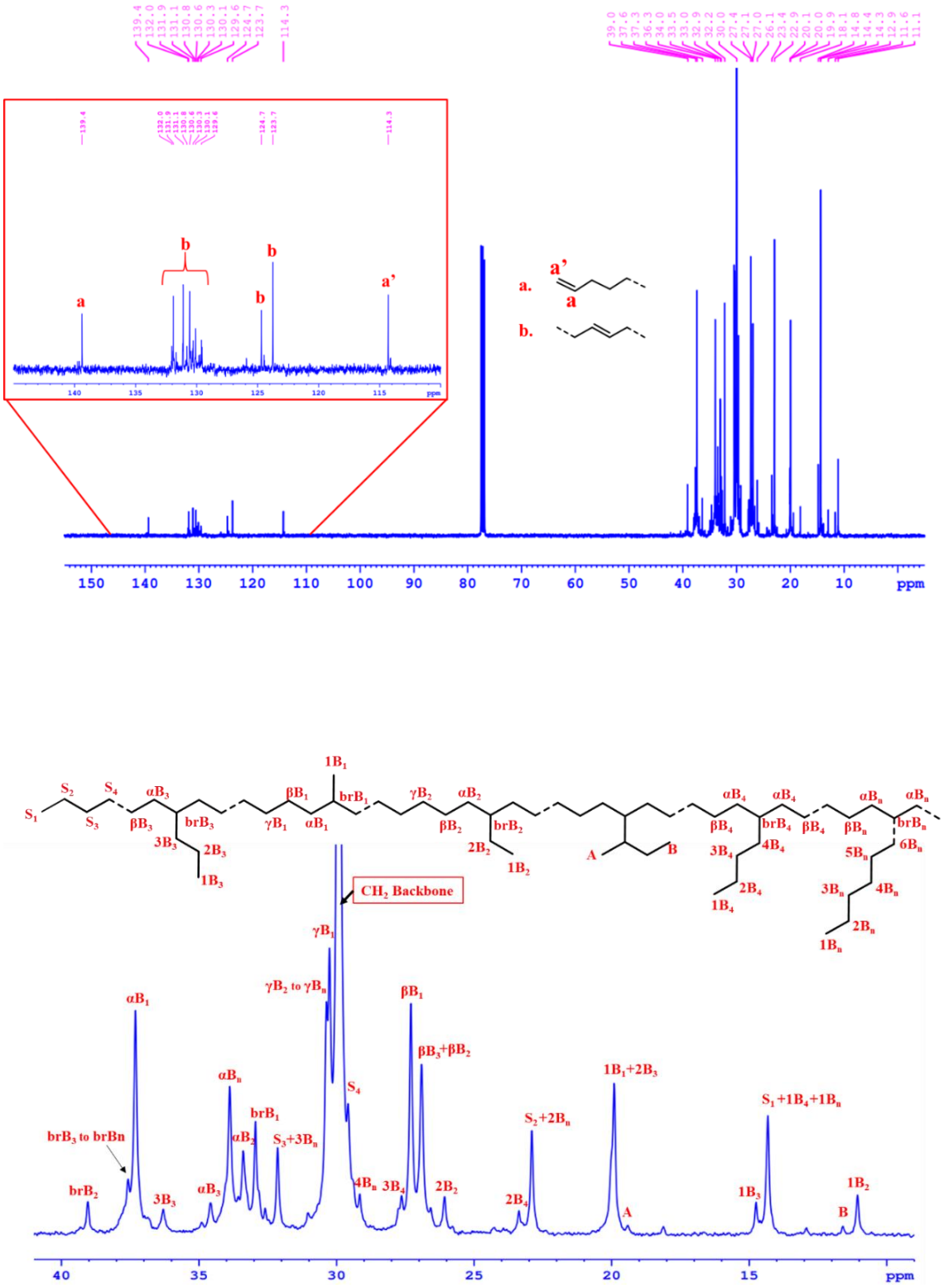

Figure S2.32: ^{13}C NMR spectra of the oligomer in $CDCl_3$ (top), expanded view (bottom) (Table 2.1, entry 3, 298 K)

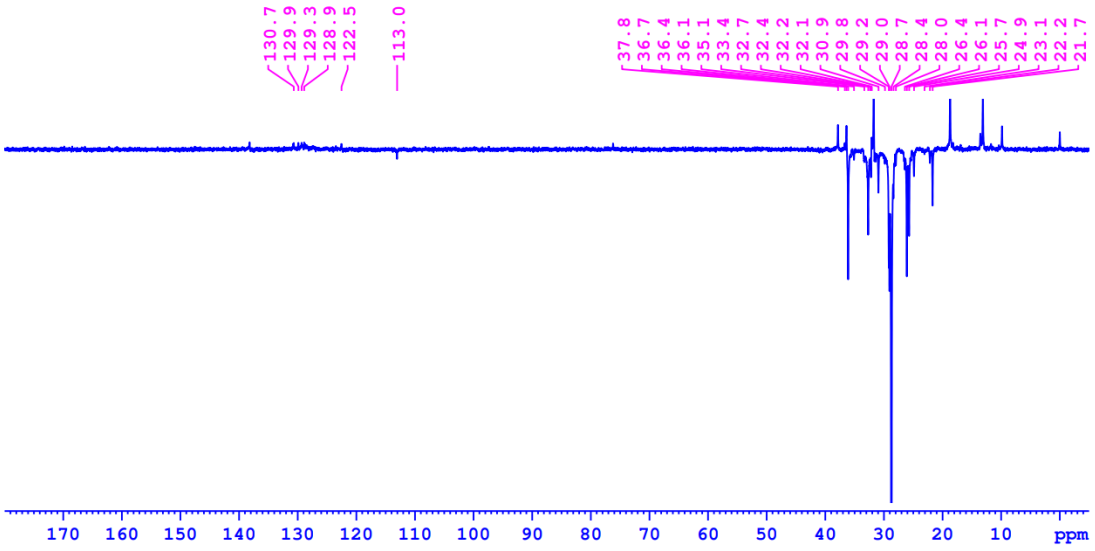

Figure S2.33: ^{13}C DEPT NMR spectrum of the oligomer in $CDCl_3$ (Table 2.1, entry 3, 298 K).

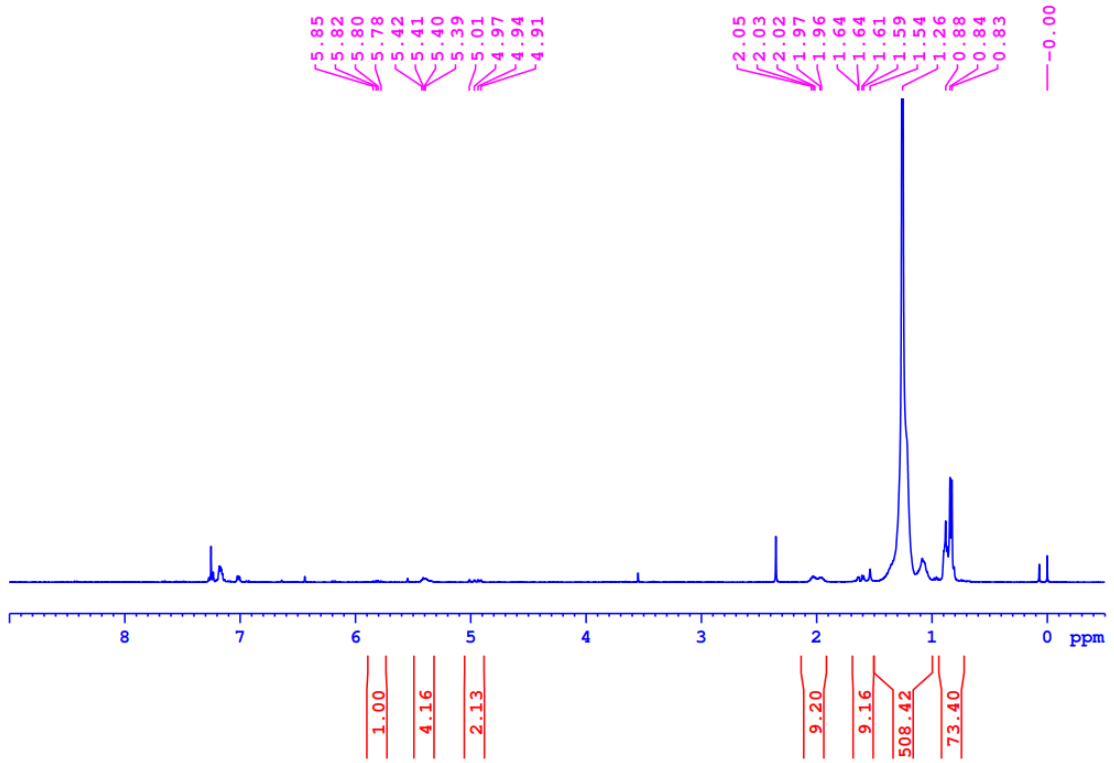

Figure S2.34: ^{1}H NMR spectrum of the oligomer in $CDCl_3$ (Table 2.1, entry 1, 298 K).

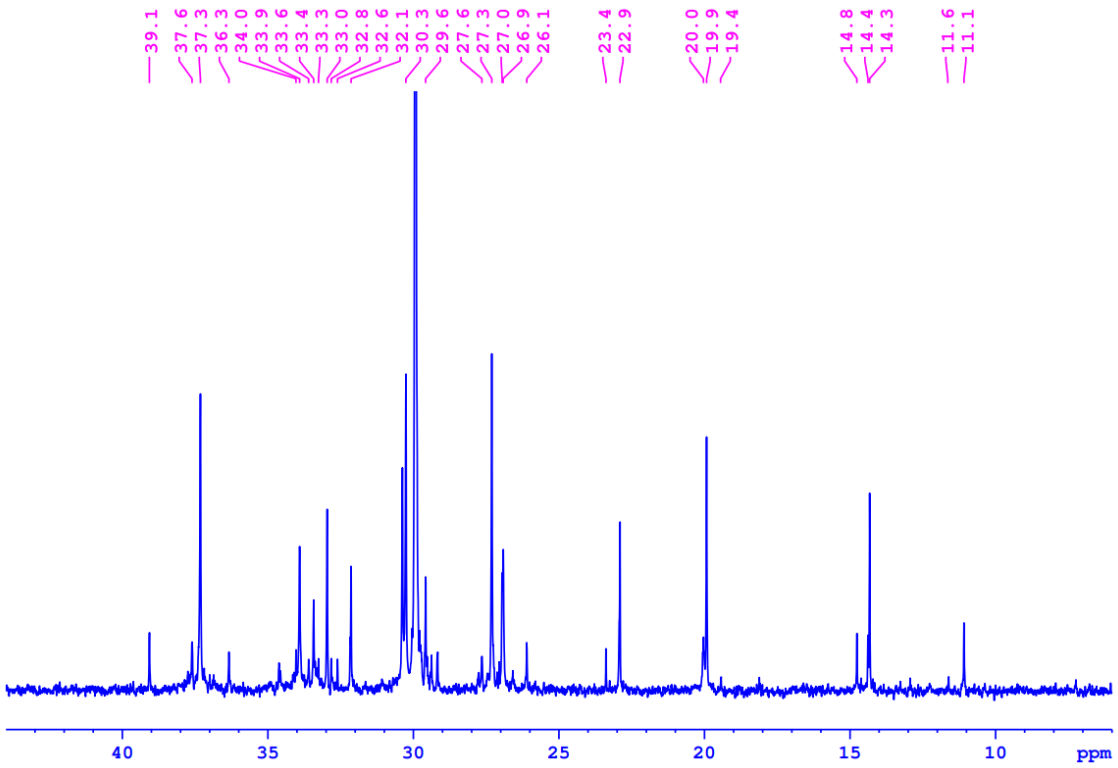

Figure S2.35: ^{13}C NMR spectrum of the oligomer in $CDCl_3$ (Table 2.1, entry 1, 298 K).

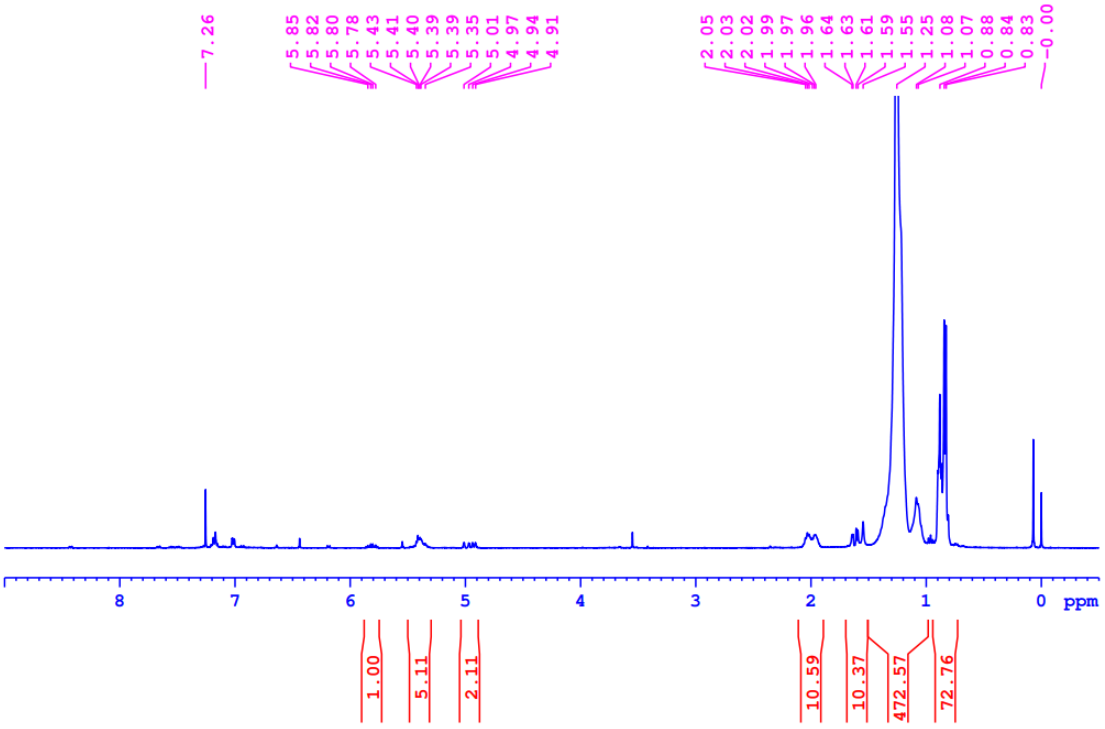

Figure S2.36: ^{1}H NMR spectrum of the oligomer in $CDCl_3$ (Table 2.1, entry 2, 298 K).

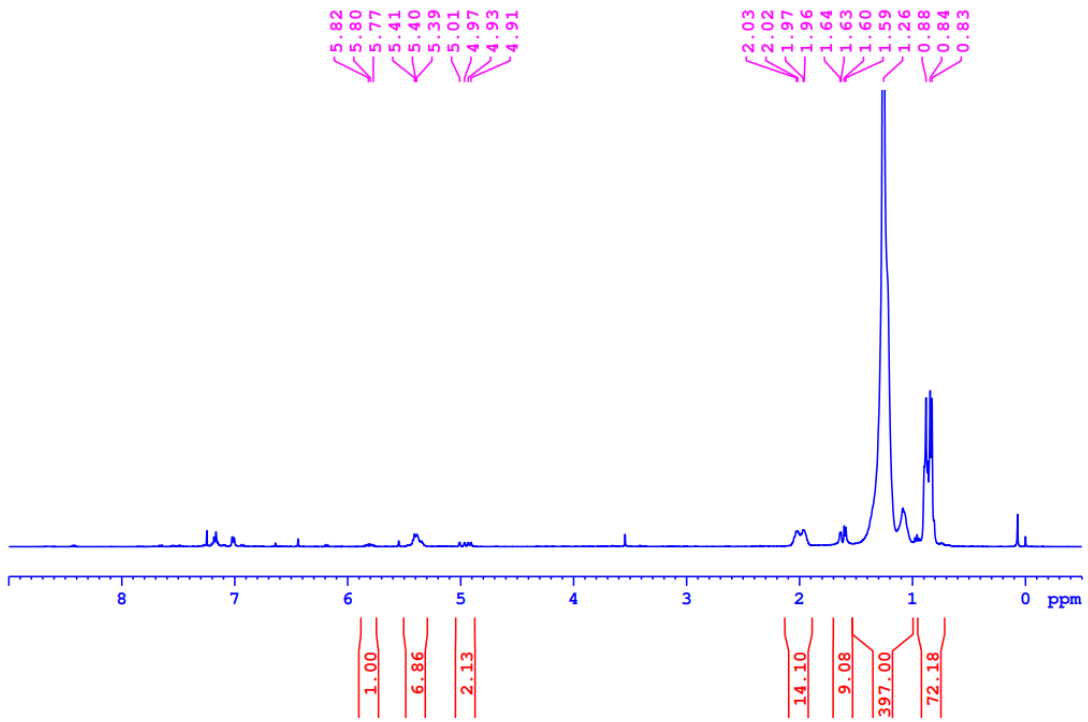

Figure S2.37: ^{1}H NMR spectrum of the oligomer in $CDCl_3$ (Table 2.1, entry 4, 298 K).

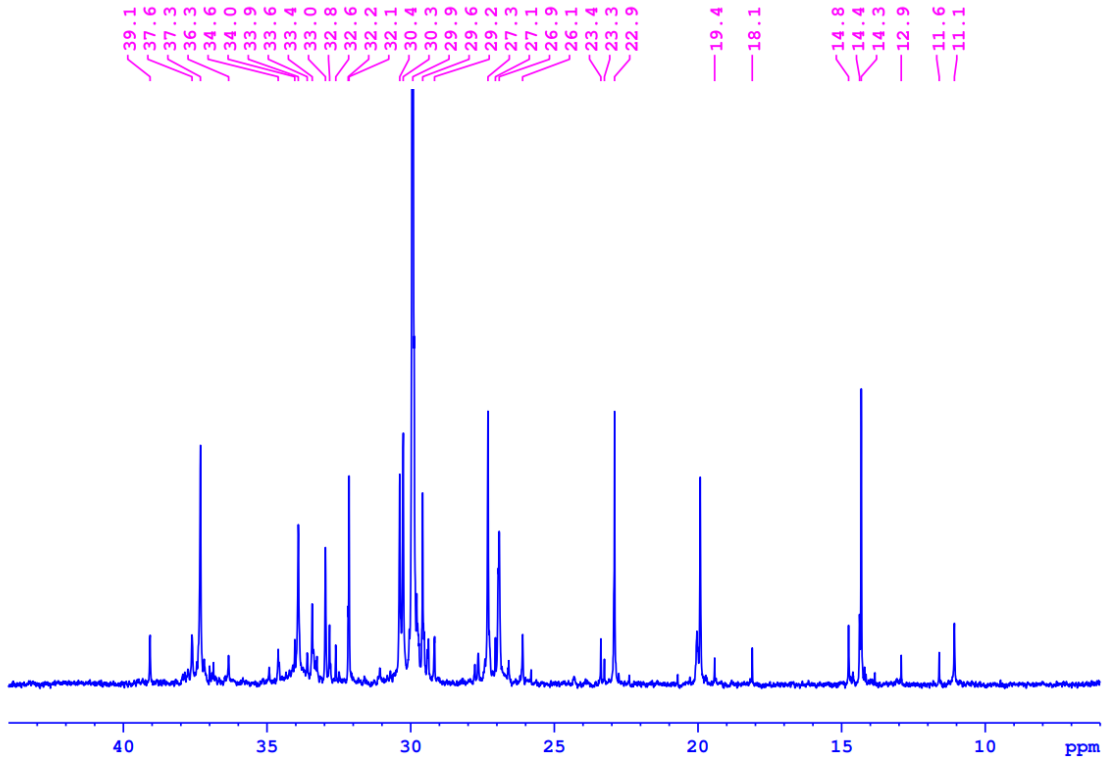

Figure S2.38: ^{13}C NMR spectrum of the oligomer in $CDCl_3$ (Table 2.1, entry 4, 298 K).

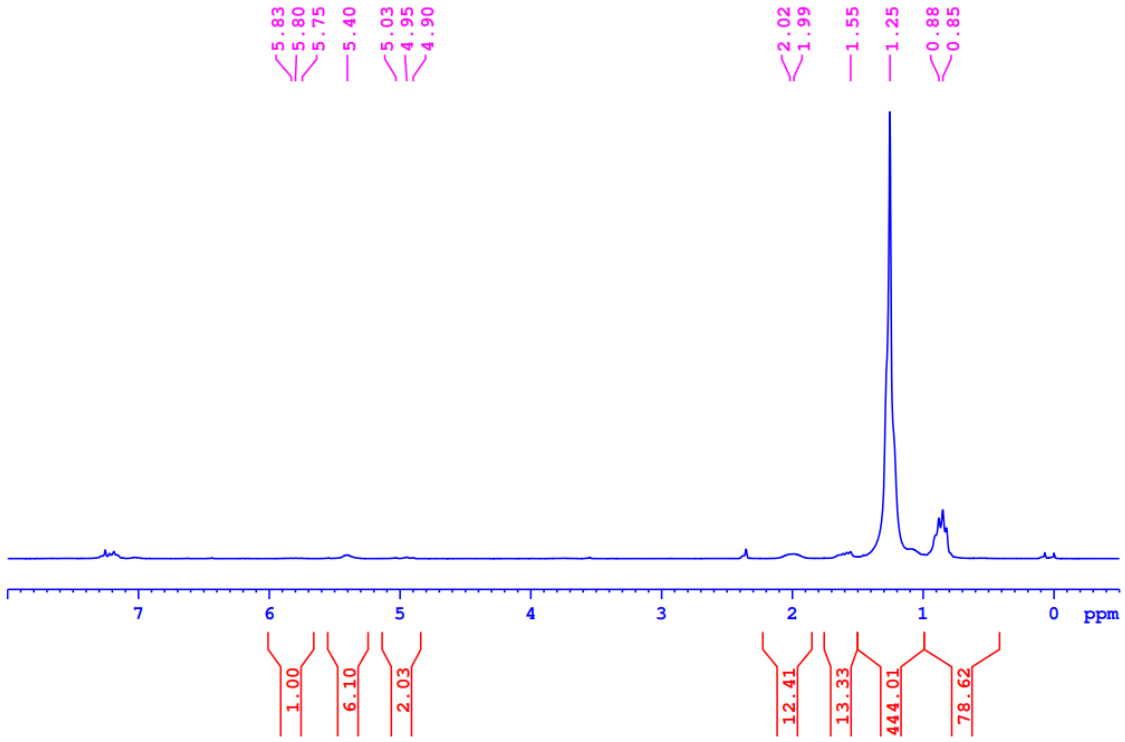

Figure S2.39: ^{1}H NMR spectrum of the oligomer in $CDCl_3$ (Table 2.1, entry 5, 298 K).

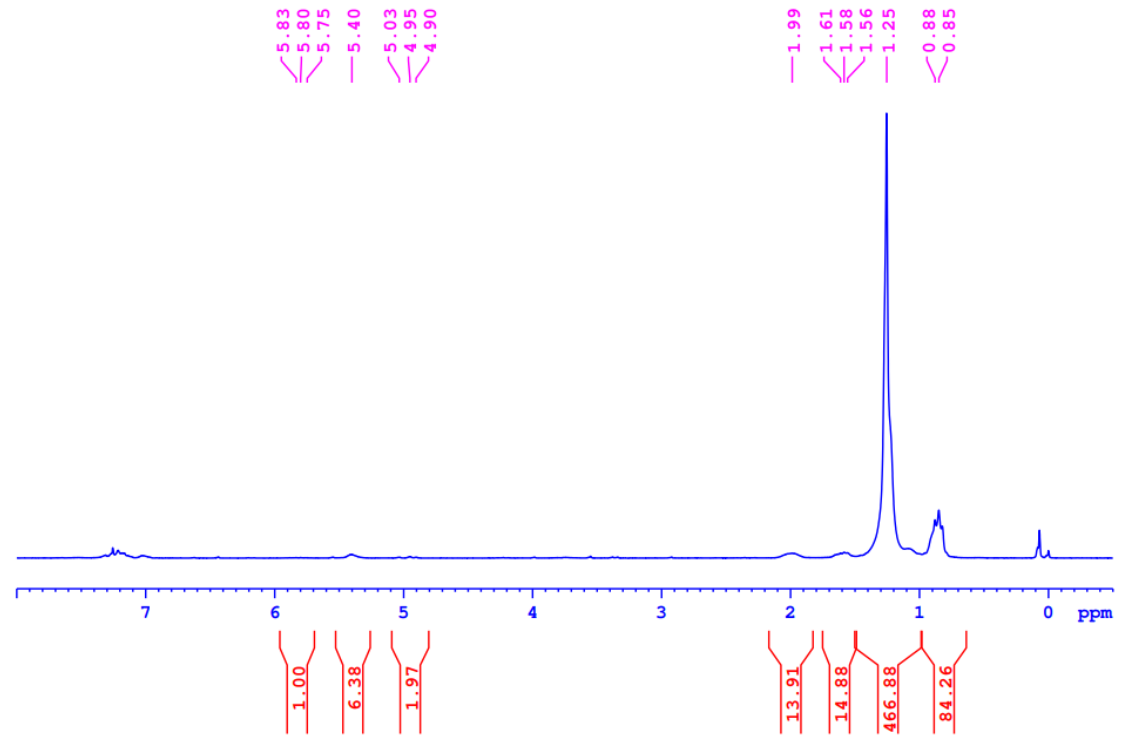

Figure S2.40: ^{1}H NMR spectrum of the oligomer in $CDCl_3$ (Table 2.1, entry 6, 298 K).

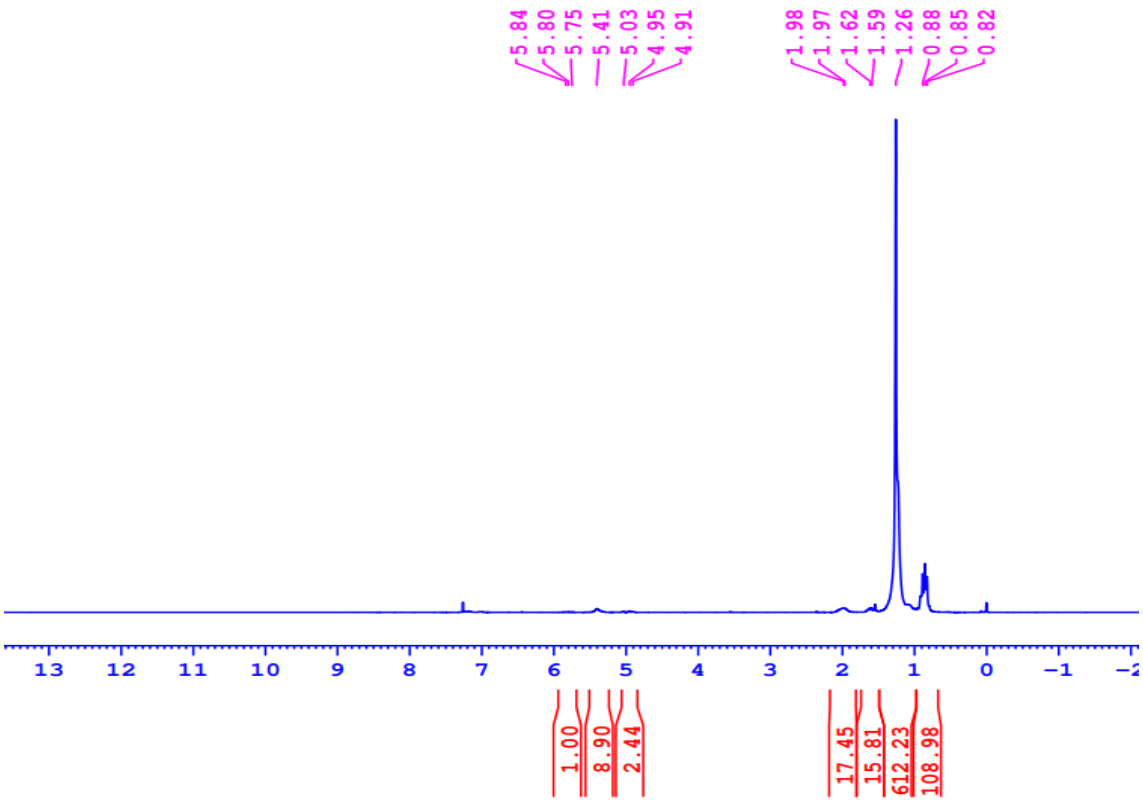

Figure S2.41: ^{1}H NMR spectrum of the oligomer in $CDCl_3$ (Table 2.1, entry 7, 298 K).

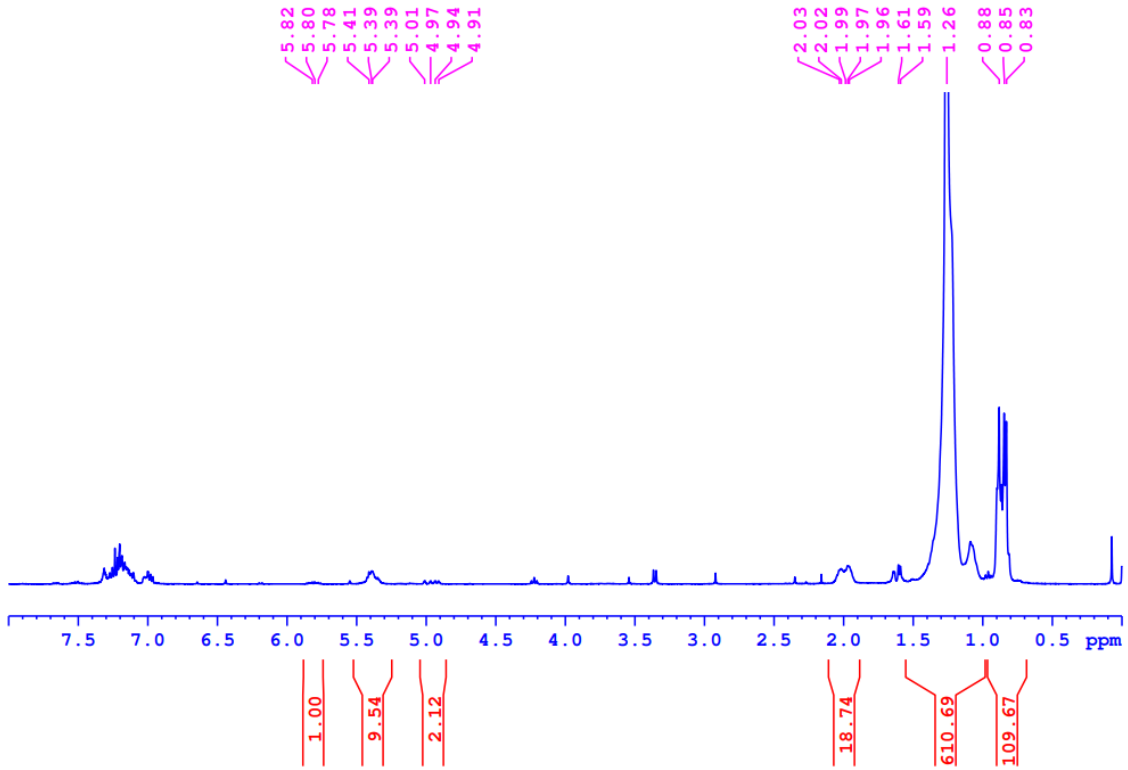

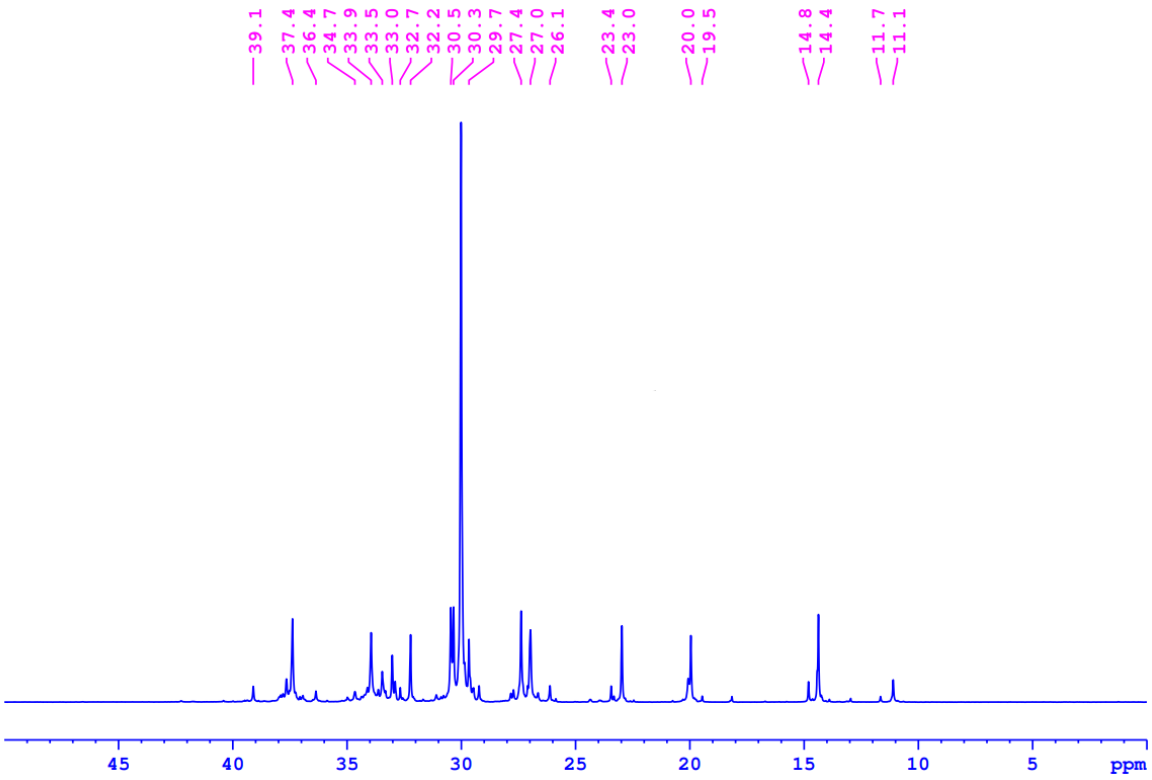

Figure S2.42: ^{1}H NMR and ^{13}C (quantitative) spectrum of the oligomer in $CDCl_3$ (Table 2.1, entry 8, 298 K).

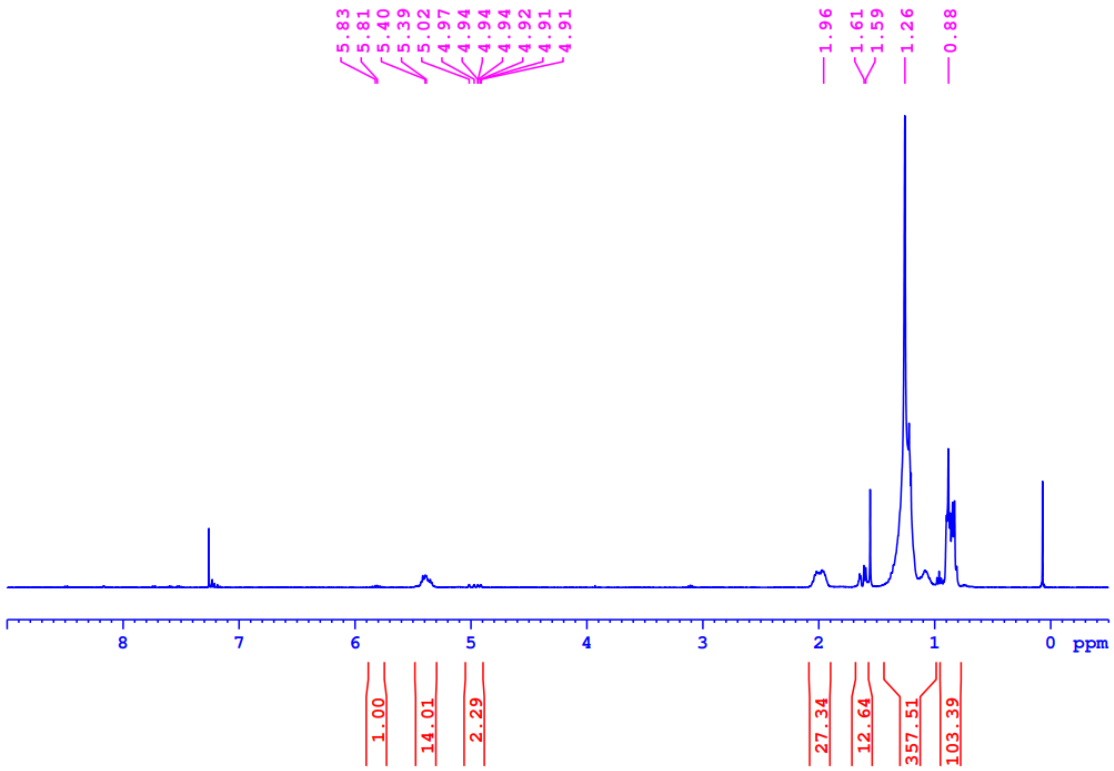

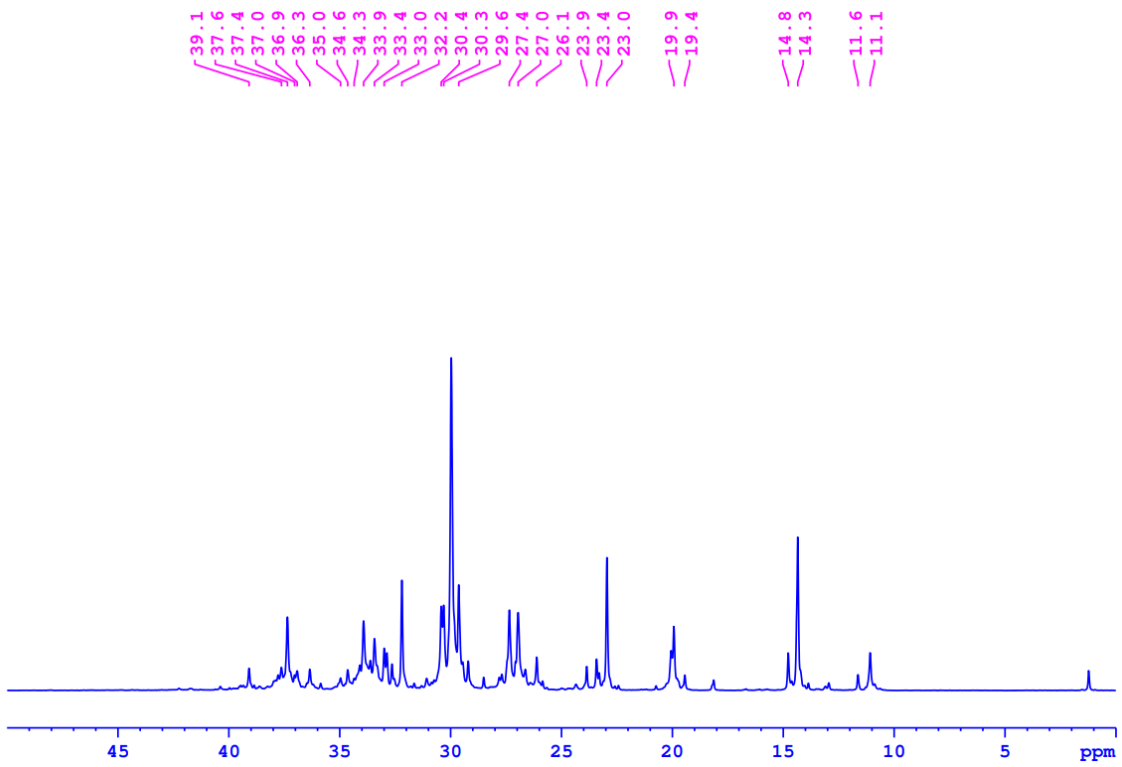

Figure S2.43: ^{1}H and ^{13}C (quantitative) NMR spectrum of the oligomer in $CDCl_3$ (Table 2.1, entry 9, 298 K).

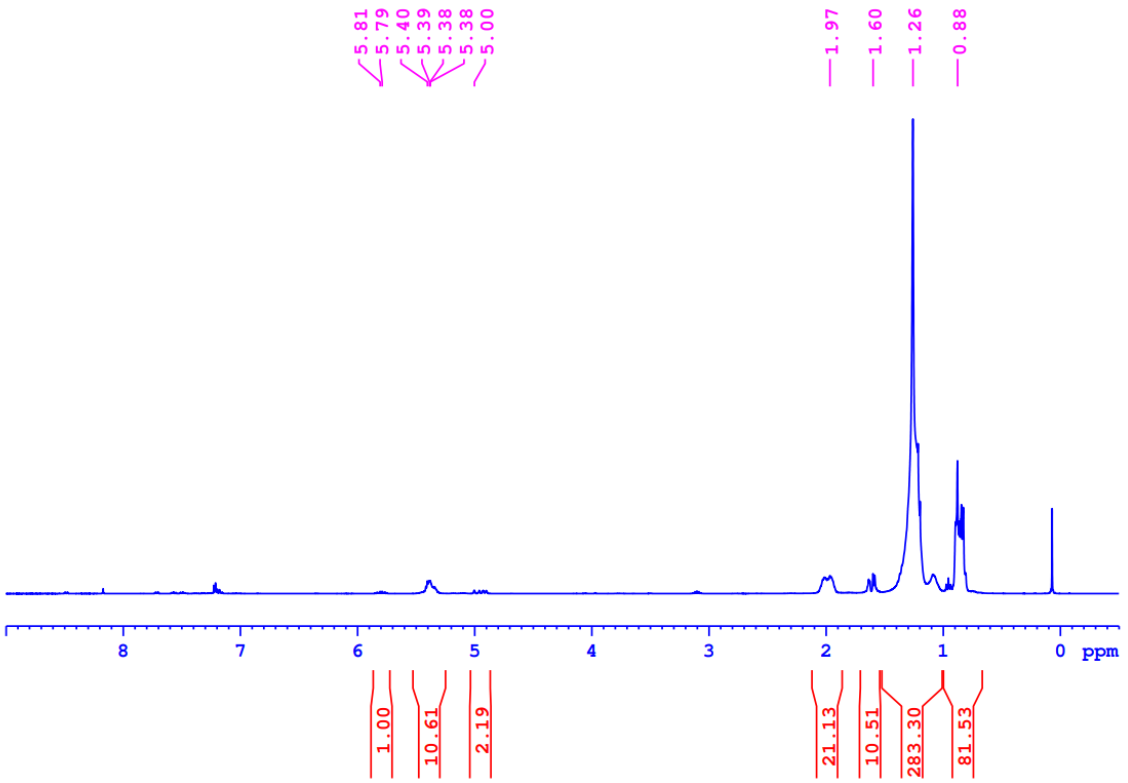

Figure S2.44: ^{1}H NMR spectrum of the oligomer in $CDCl_3$ (Table 2.1, entry 10, 298 K).

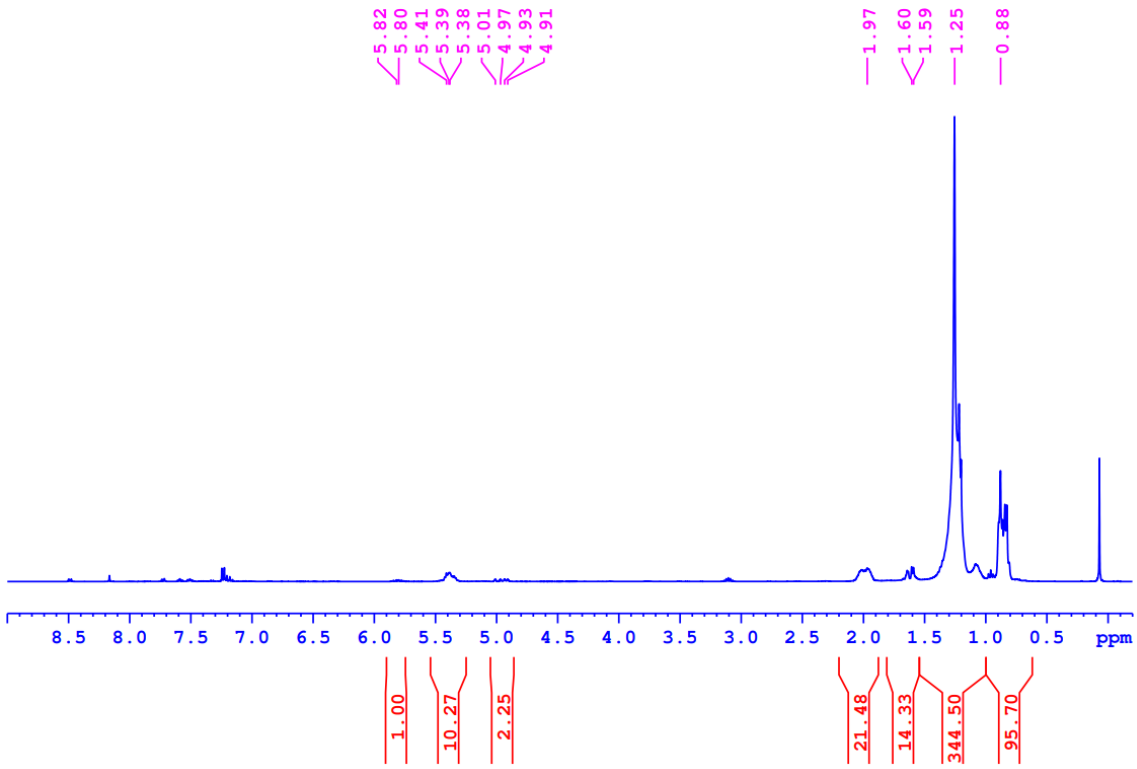

Figure S2.45: ^{1}H NMR spectrum of the oligomer in $CDCl_3$ (Table 2.1, entry 11, 298 K).

2.5.5.2. GPC data:

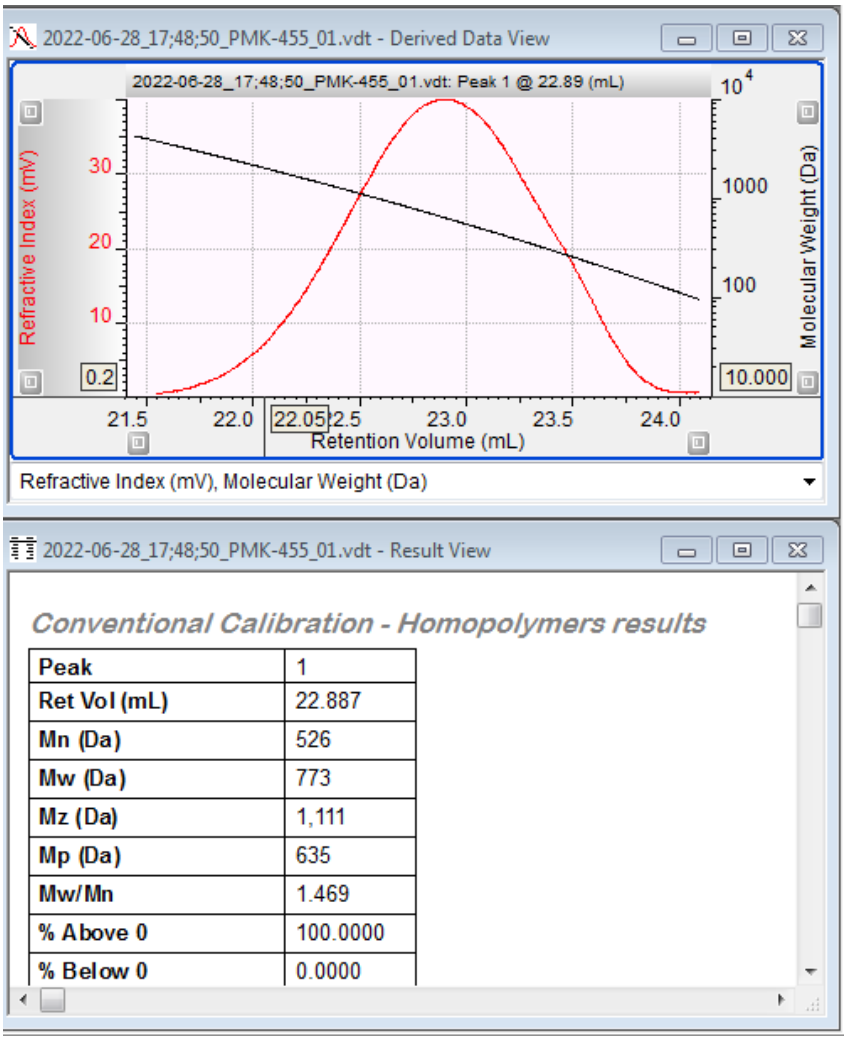

Peak	1
Ret Vol (mL)	22.887
Mn (Da)	526
Mw (Da)	773
Mz (Da)	1,111
Mp (Da)	635
Mw/Mn	1.469
% Above 0	100.0000
% Below 0	0.0000

Figure S2.46: Molecular weight (by GPC) of oligomer in THF (Table 2.1, entry 3).

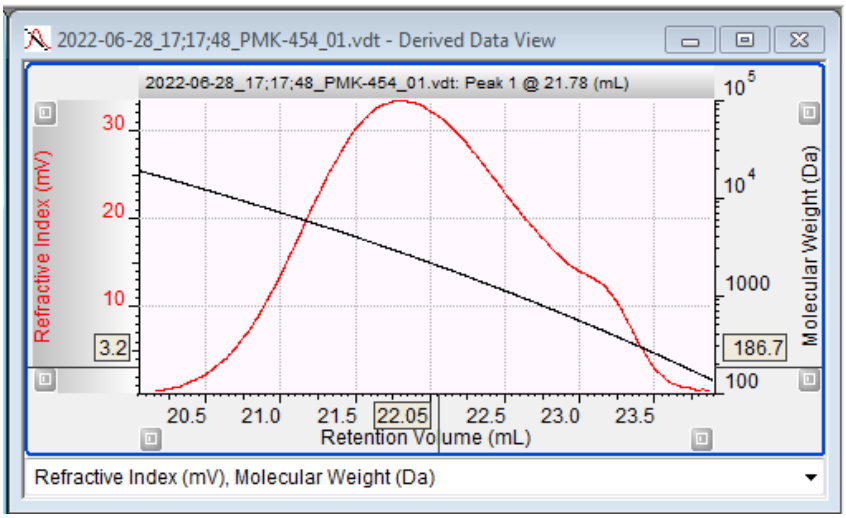

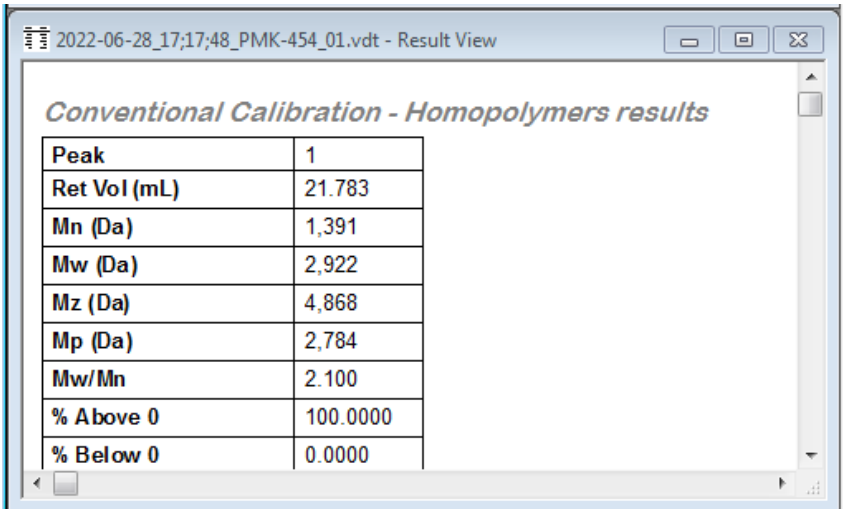

Peak	1
Ret Vol (mL)	21.783
Mn (Da)	1,391
Mw (Da)	2,922
Mz (Da)	4,868
Mp (Da)	2,784
Mw/Mn	2.100
% Above 0	100.0000
% Below 0	0.0000

Figure S2.47: Molecular weight (by GPC) of oligomer in THF (Table 2.1, entry 4).

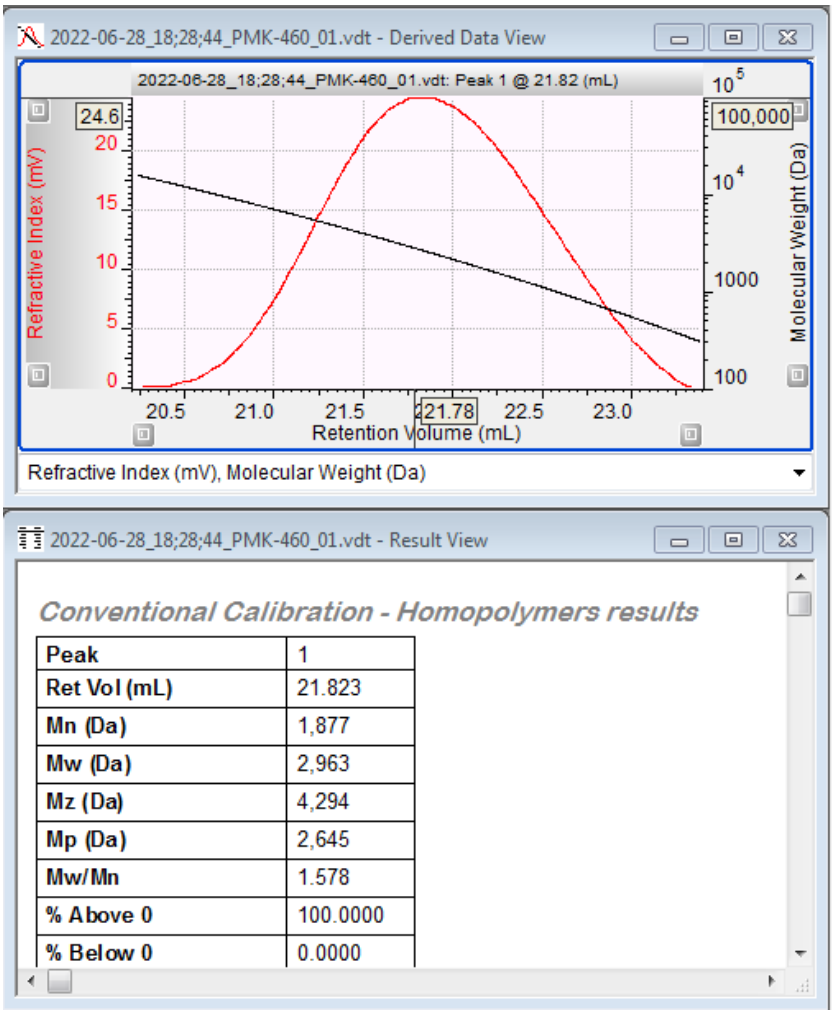

Peak	1
Ret Vol (mL)	21.823
Mn (Da)	1,877
Mw (Da)	2,963
Mz (Da)	4,294
Mp (Da)	2,645
Mw/Mn	1.578
% Above 0	100.0000
% Below 0	0.0000

Figure S2.48: Molecular weight (by GPC) of oligomer in THF (Table 2.1, entry 8).

2.5.5.3. GC-MS data:

When the polymerization reaction was performed in toluene, the friedel craft alkylation was observed in the literature.[77-79] To rule out that possibility we performed the GC-MS analysis for the oligomeric sample (Table 2.1 entries 6 and 8.). No Friedel craft alkylation products were discovered in the GC-MS analysis, and when we compared our data to those in the published literature, we found no such compounds.

a. GC-MS graph (Table 2.1 entry 6):

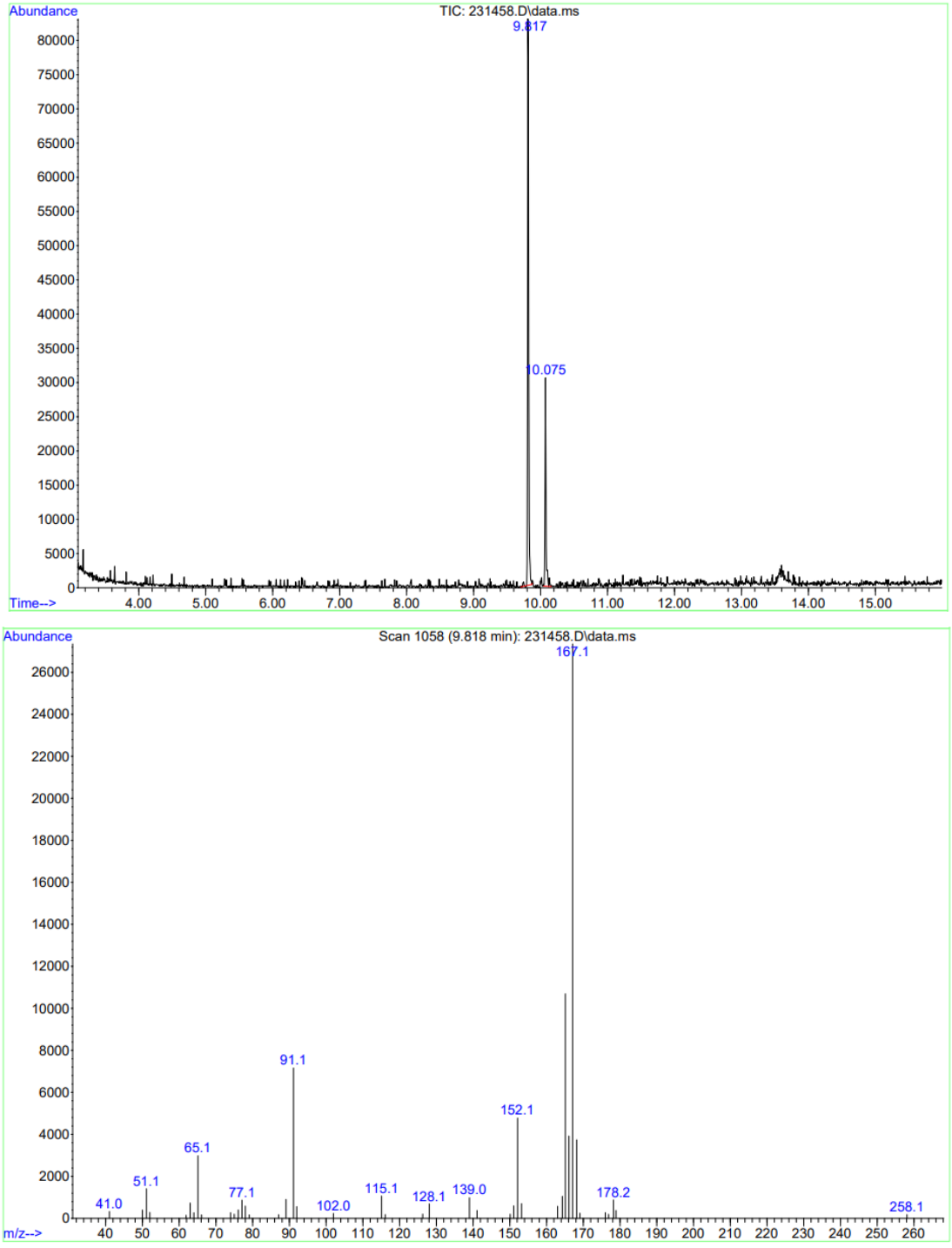

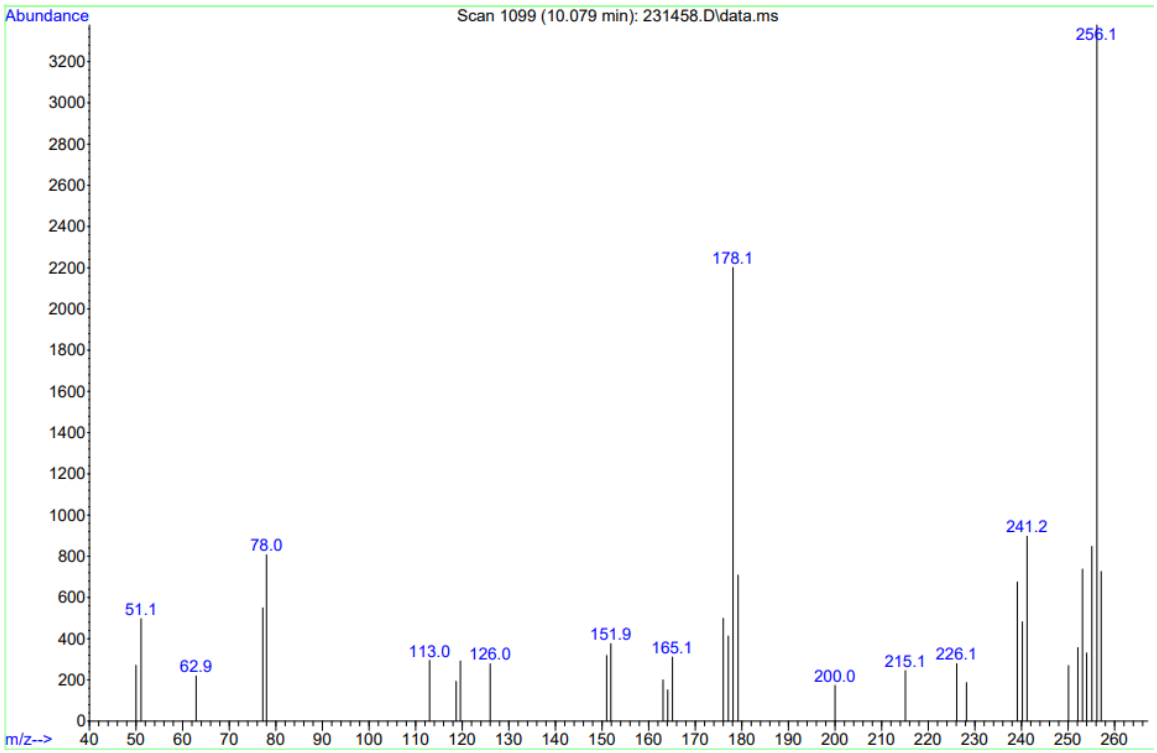

b. GC-MS graph (Table 2.1 entry 8):

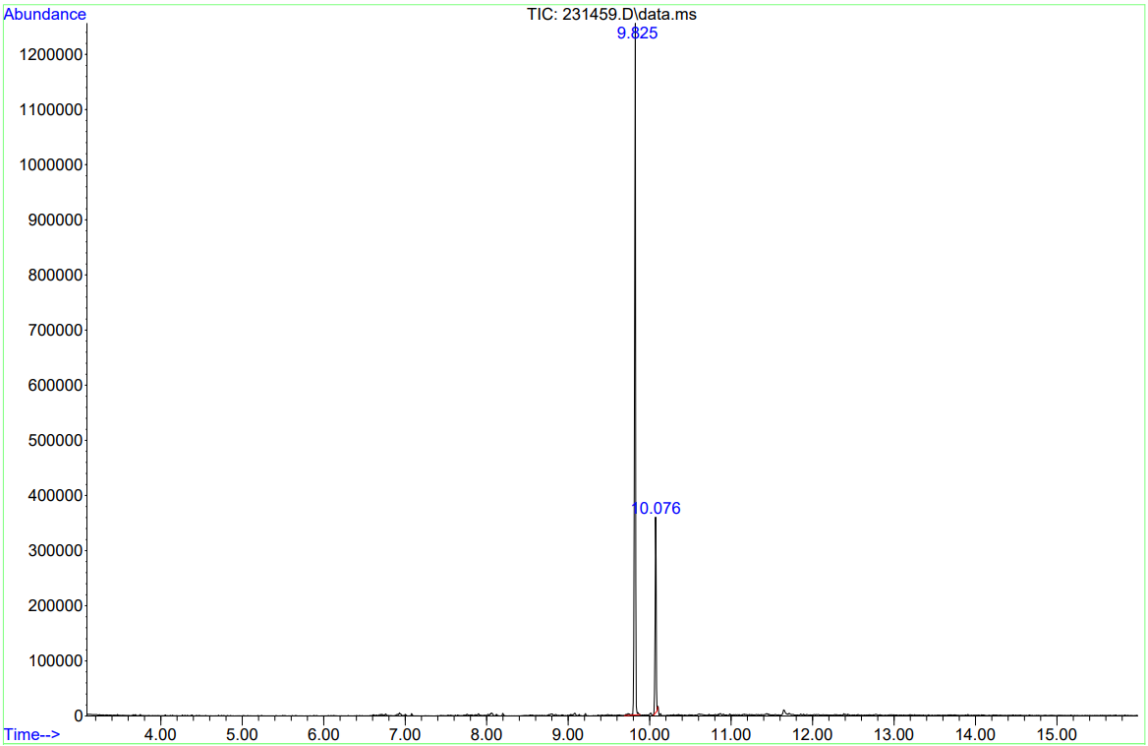

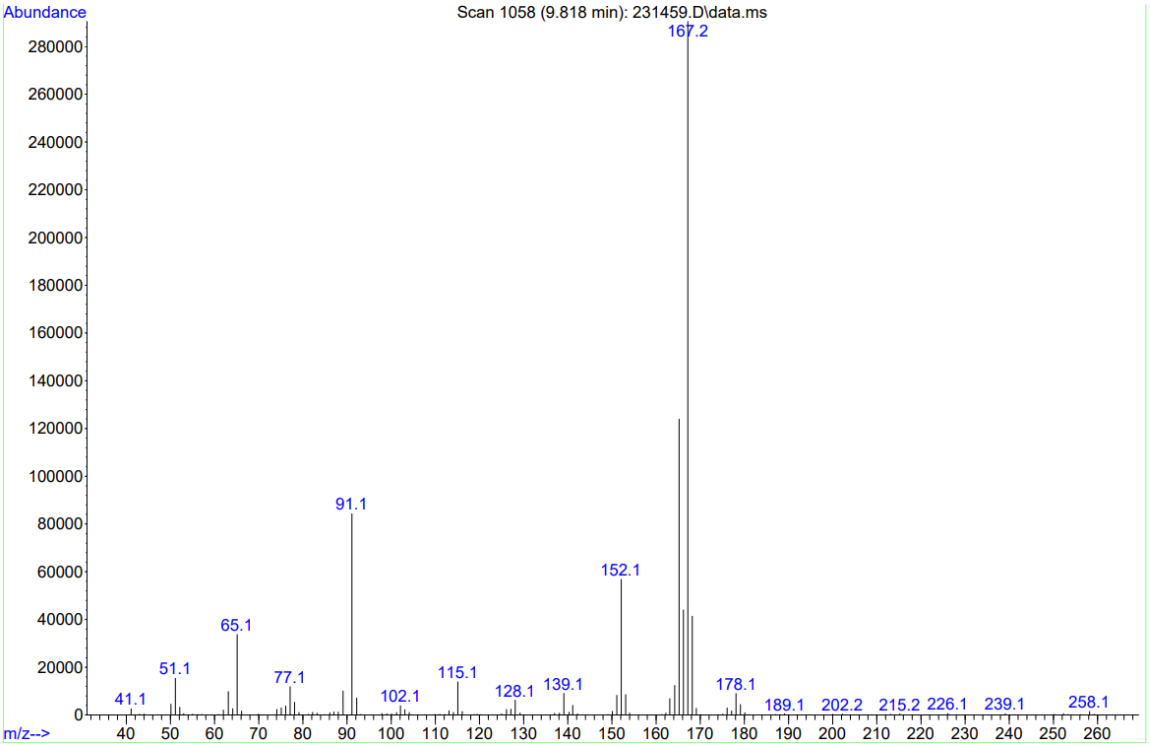
Abundance
Scan 1058 (9.818 min): 231459.D\data.ms
167.2
91.1
152.1
65.1
51.1
77.1
115.1
128.1
139.1
178.1
41.1
102.1
189.1
202.2
215.2
226.1
239.1
258.1
m/z-->

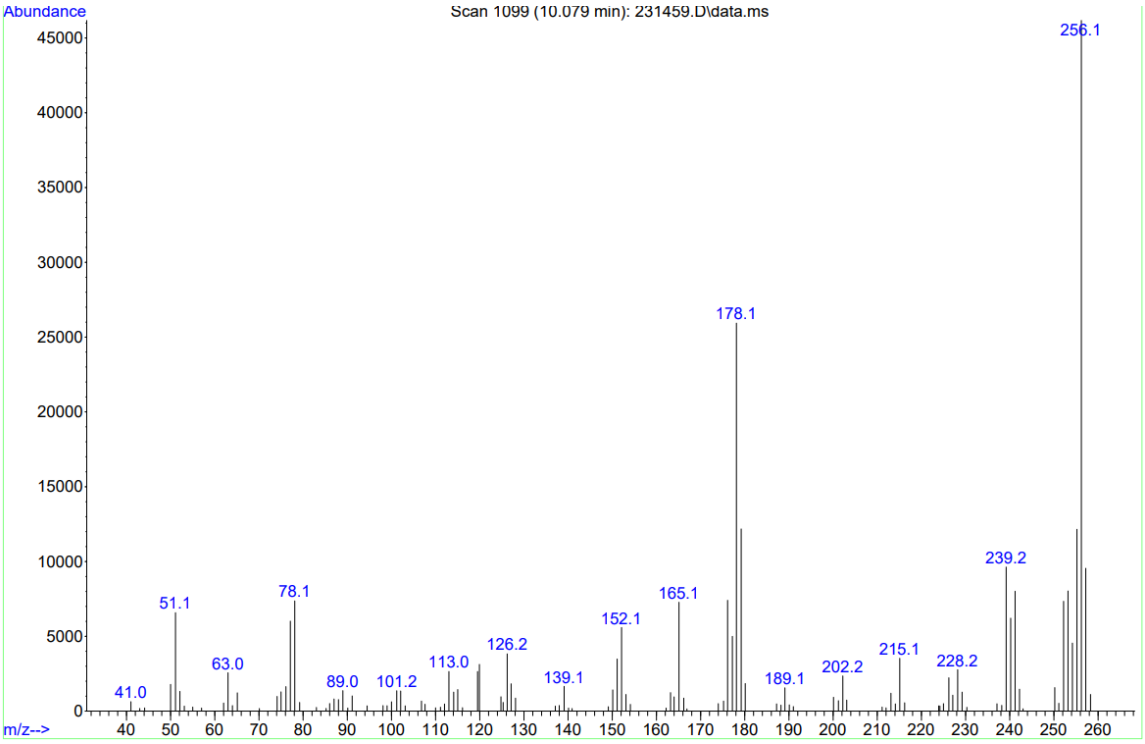
Abundance
Scan 1099 (10.079 min): 231459.D\data.ms
256.1
178.1
239.2
51.1
78.1
165.1
152.1
126.2
63.0
113.0
215.1
228.2
41.0
89.0
101.2
139.1
189.1
202.2
m/z-->

2.5.6. Effect of polar solvents:

2.5.6.1. Ethylene oligomerization in polar solvent:

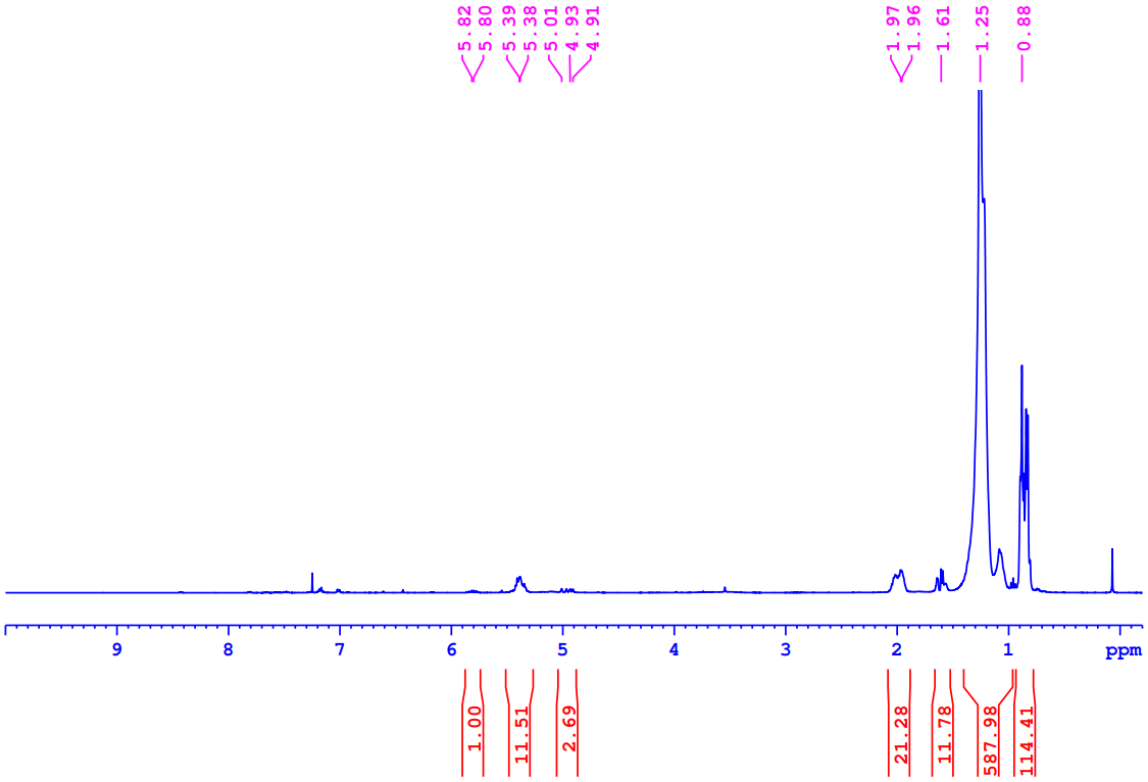

Figure S2.49: ^{1}H NMR spectrum of the oligomer in $CDCl_3$ (Table 2.2, Entry 1, 298 K) (DME).

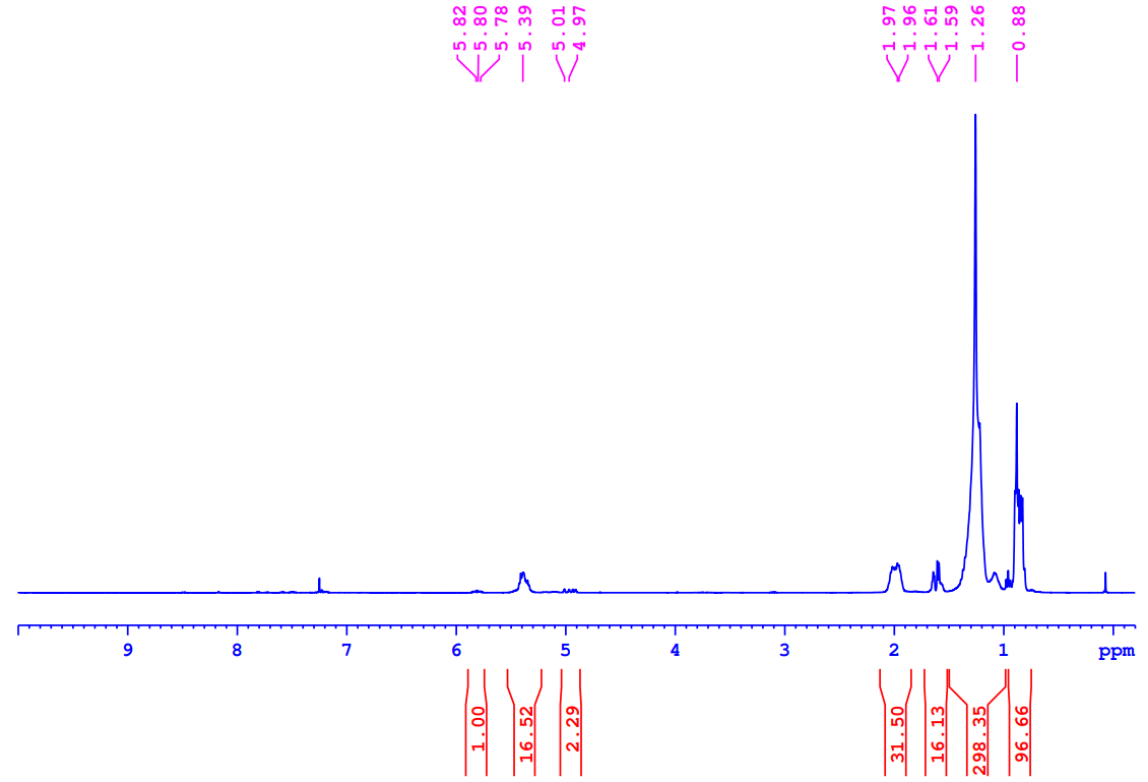

Figure S2.50: ^{1}H NMR spectrum of the oligomer in $CDCl_3$ (Table 2.2, Entry 2, 298 K) (DME).

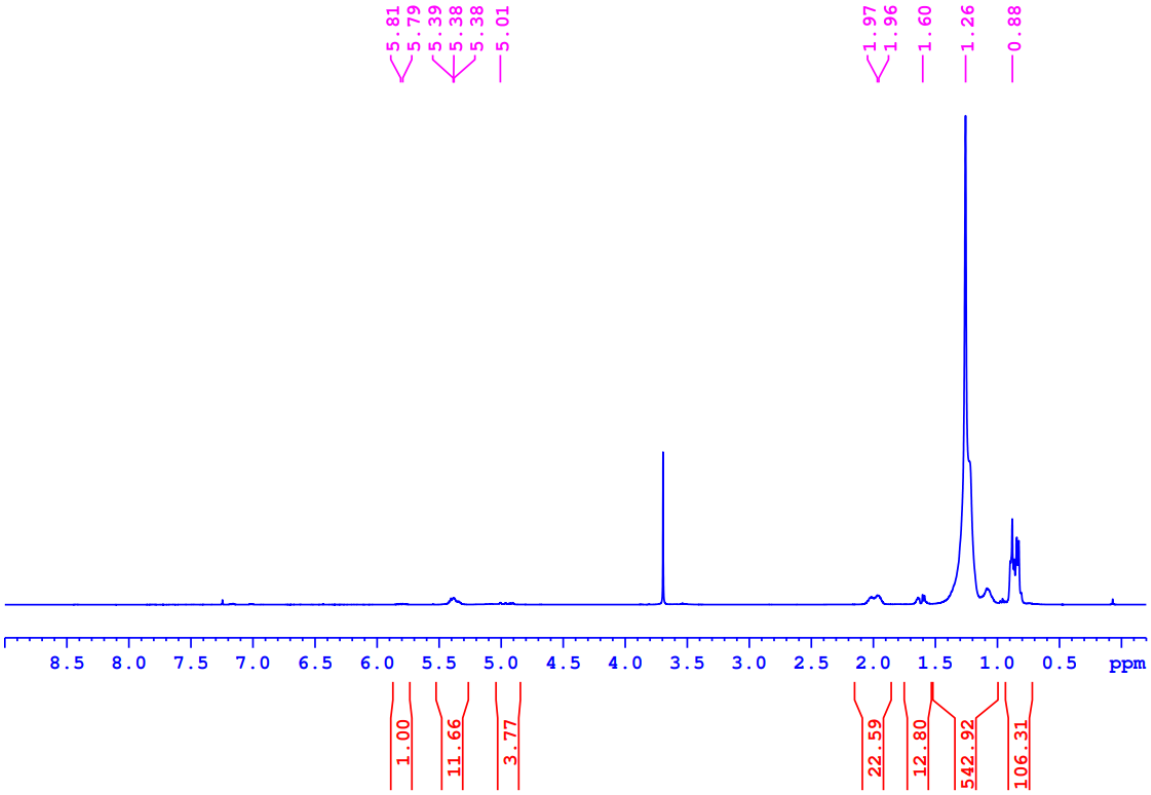

Figure S2.51: ^{1}H NMR spectrum of the oligomer in $CDCl_3$ (Table 2.2, Entry 3, 298 K) (1,4 dioxane).

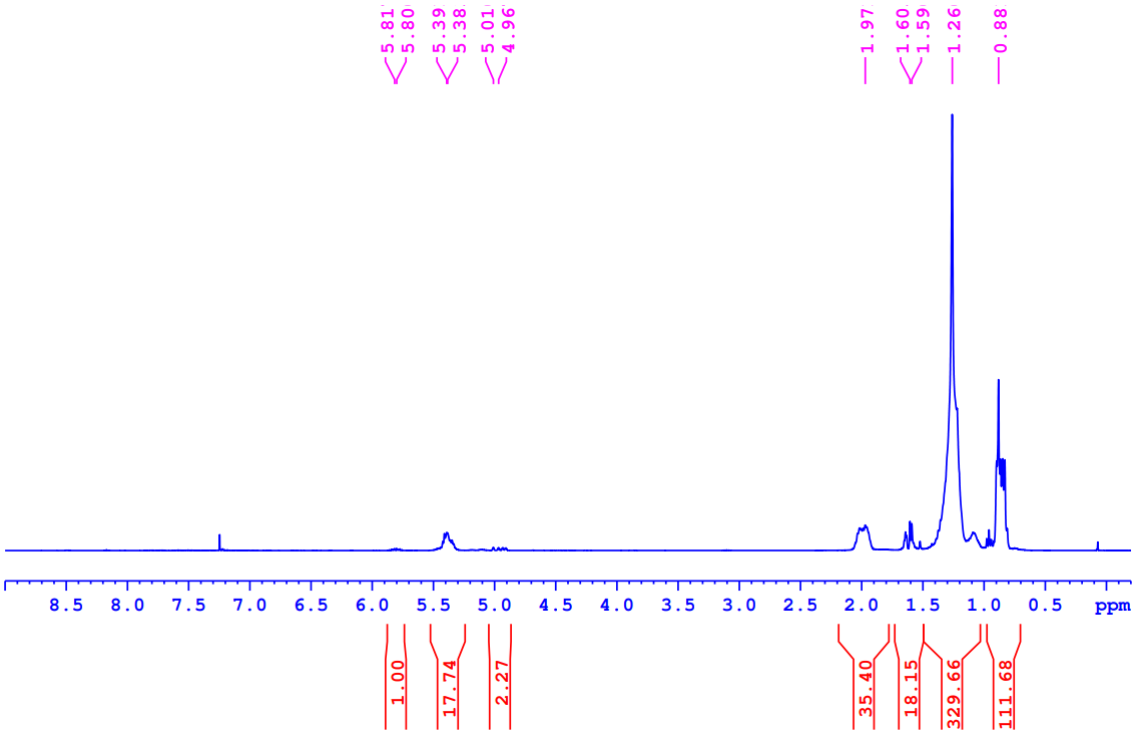

Figure S2.52: ^{1}H NMR spectrum of the oligomer in $CDCl_3$ (Table 2.2, Entry 4, 298 K) (1,4 dioxane).

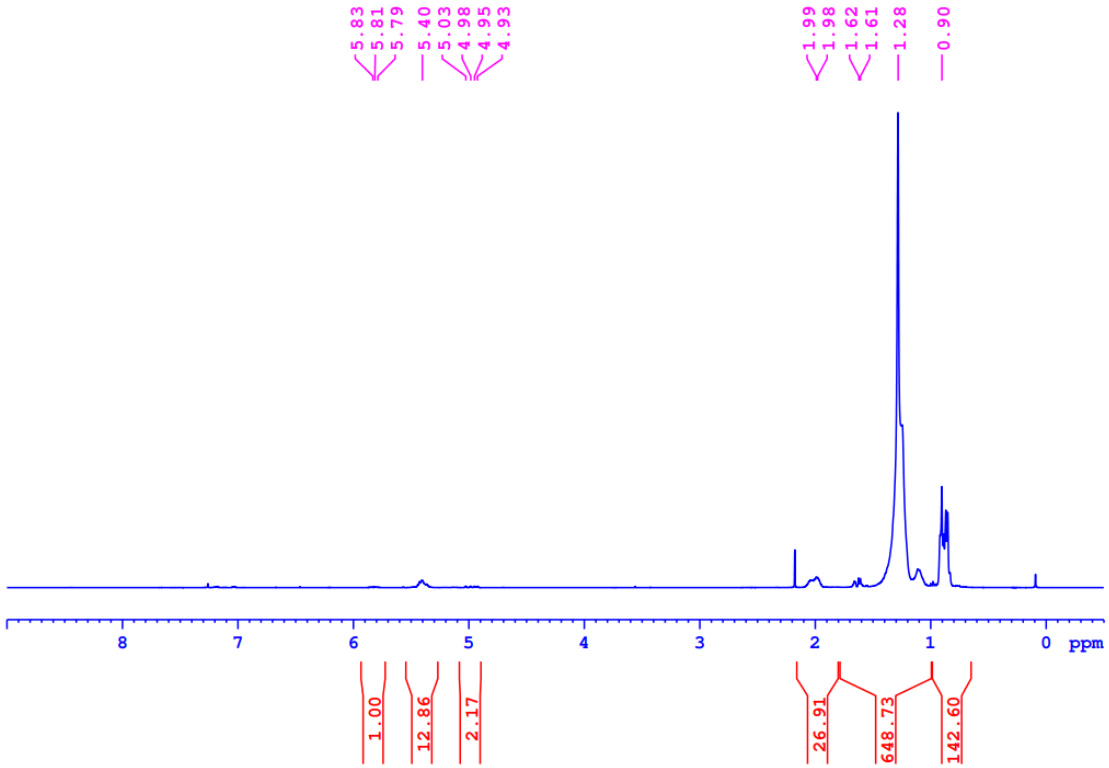

Figure S2.53: ^{1}H NMR spectrum of the oligomer in $CDCl_3$ (Table 2.2, Entry 5, 298 K) (Diethyl Ether)

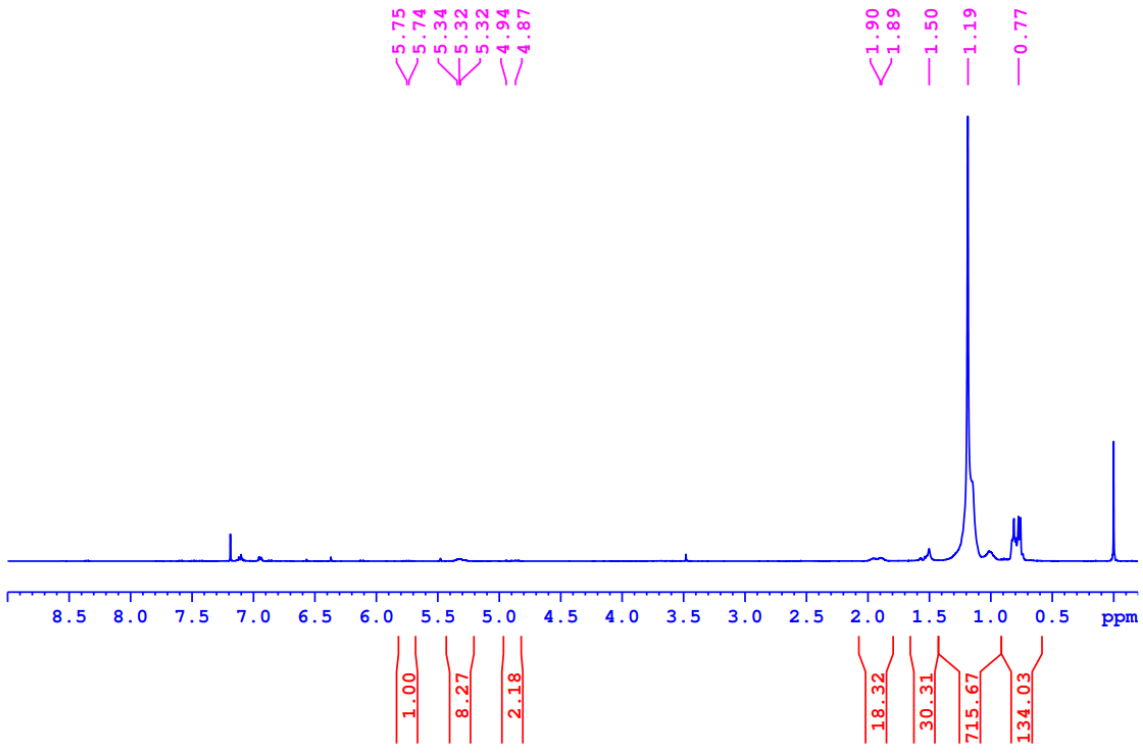

Figure S2.54: ^{1}H NMR spectrum of the oligomer in $CDCl_3$ (Table 2.2, Entry 6, 298 K) (DCM)

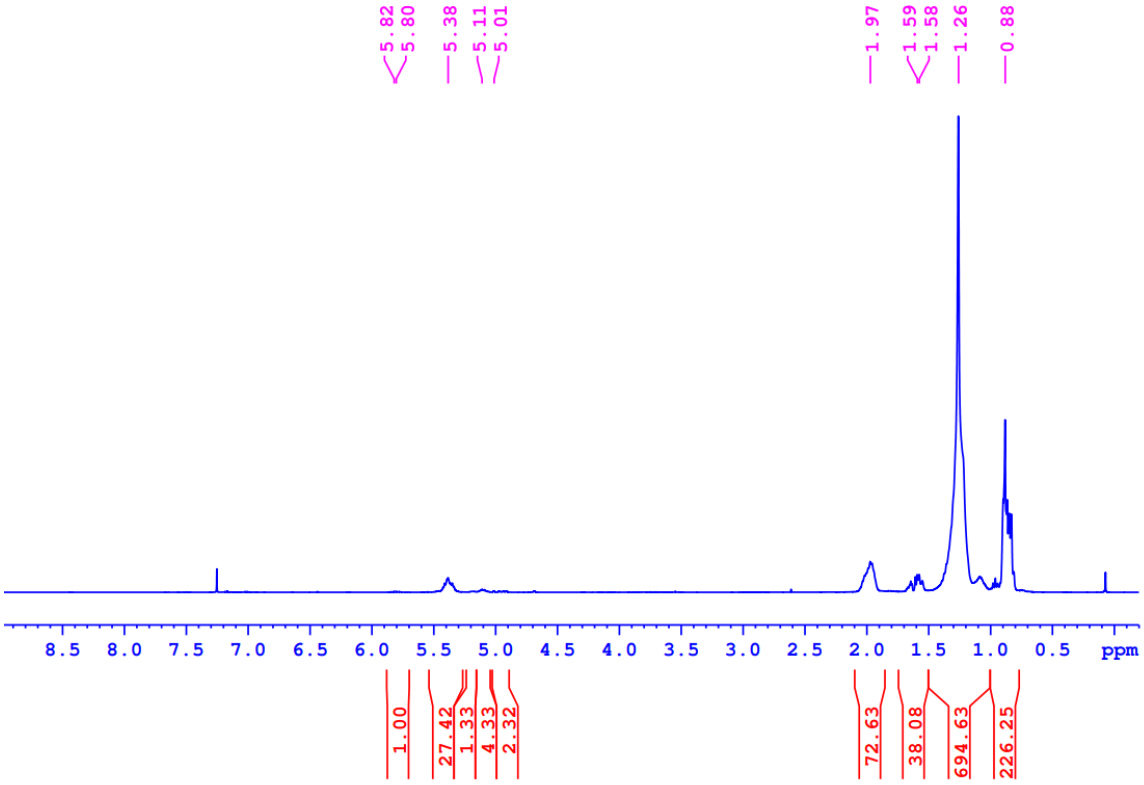

Figure S2.55: ^{1}H NMR spectrum of the oligomer in $CDCl_3$ (Table 2.2, Entry 7, 298 K) (Acetonitrile).

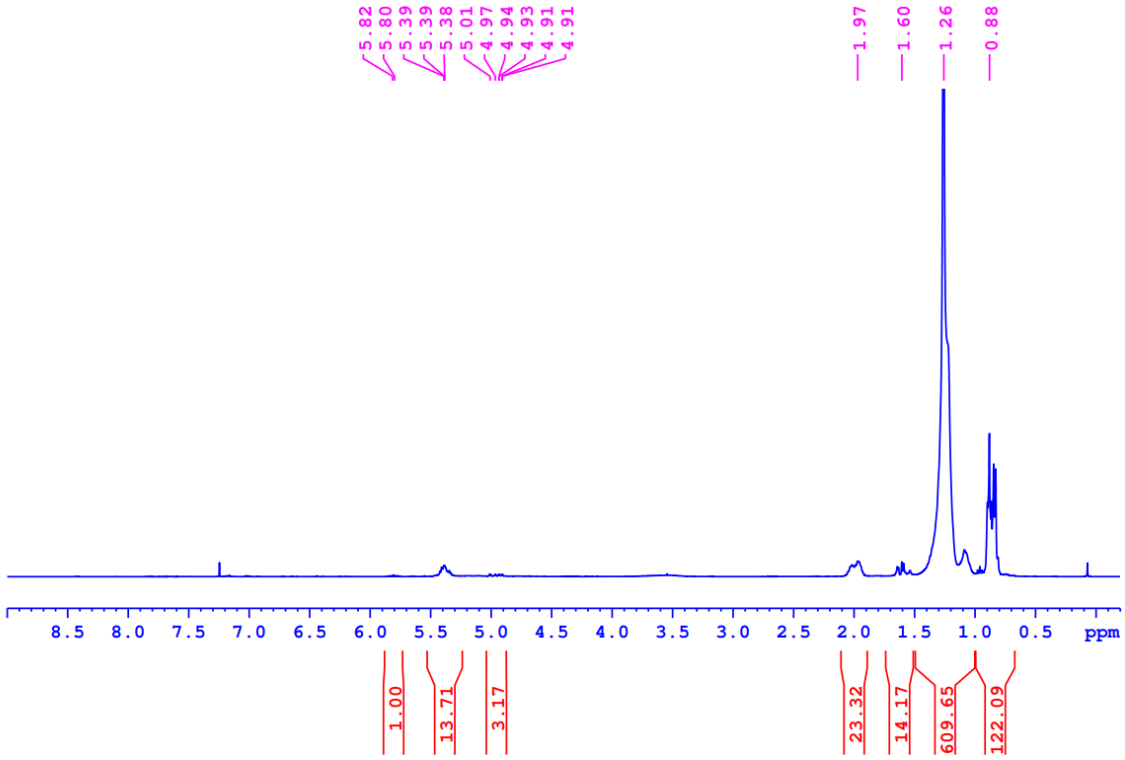

Figure S2.56: ^{1}H NMR spectrum of the oligomer in $CDCl_3$ (Table 2.2, entry 8, 298 K) (THF).

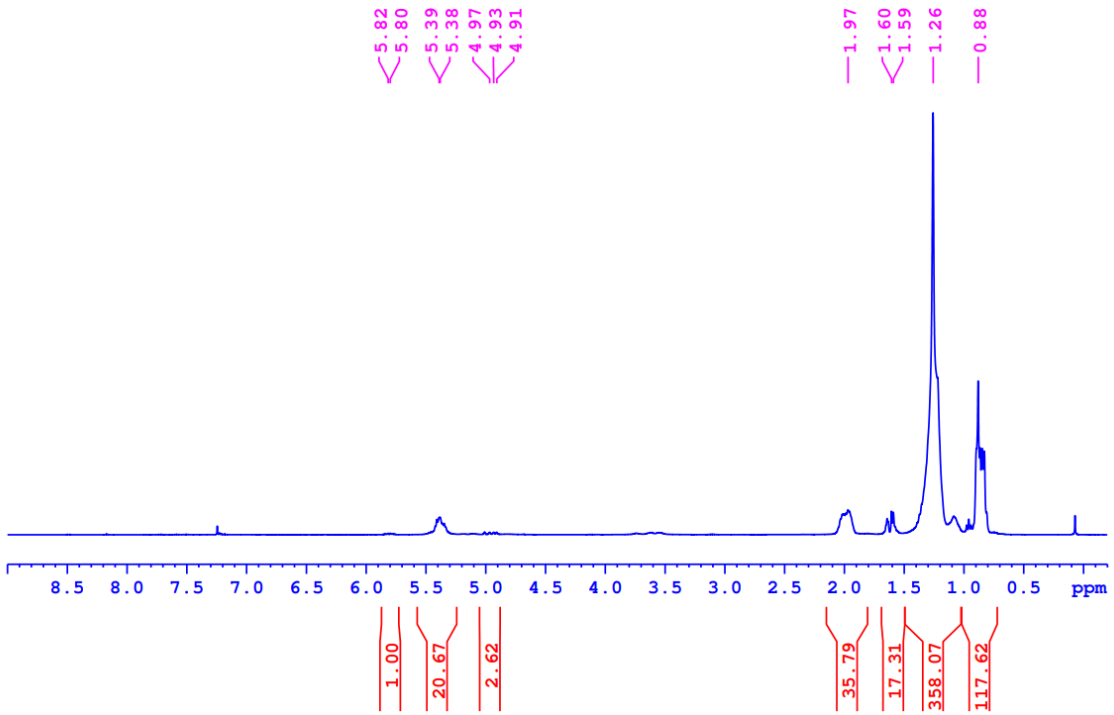

Figure S2.57: ^{1}H NMR spectrum of the oligomer in $CDCl_3$ (Table 2.2, Entry 9, 298 K) (THF).

2.5.6.2. Understanding the role of polar solvent:

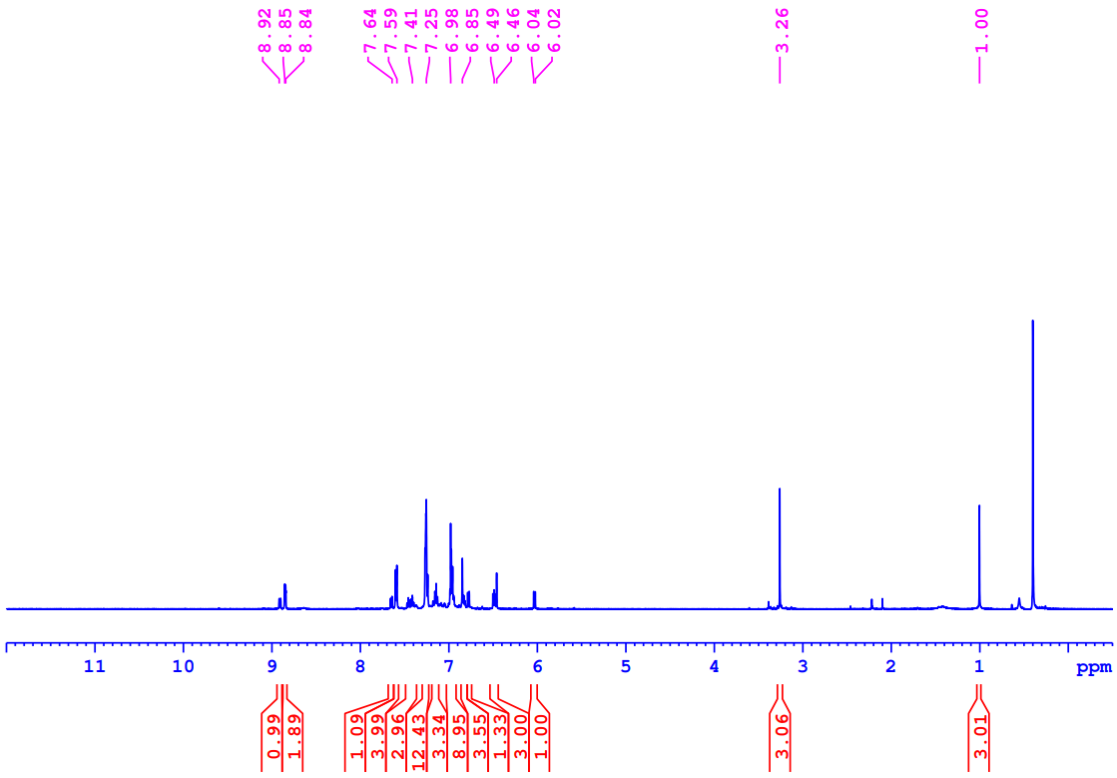

Figure S2.58: ^{1}H NMR spectrum of the 2Pd1 in C_6D_6 (298 K).

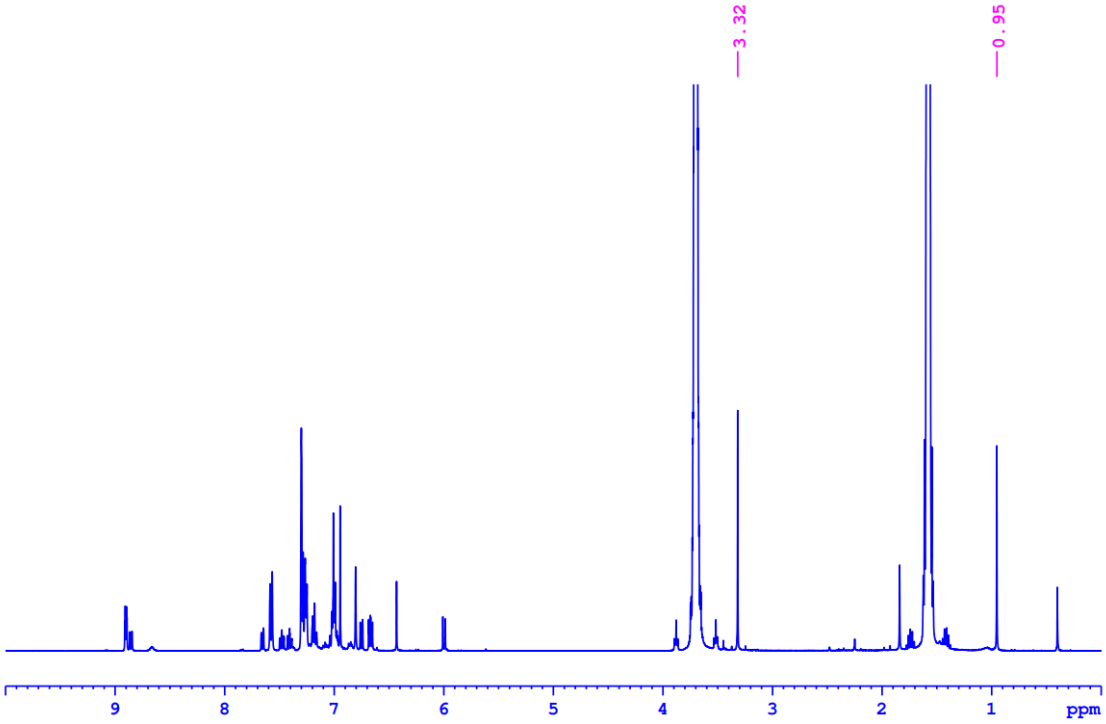

Figure S2.59: ^{1}H NMR spectrum of 2Pd1 + 50 eq. of THF in C_6D_6 (298 K).

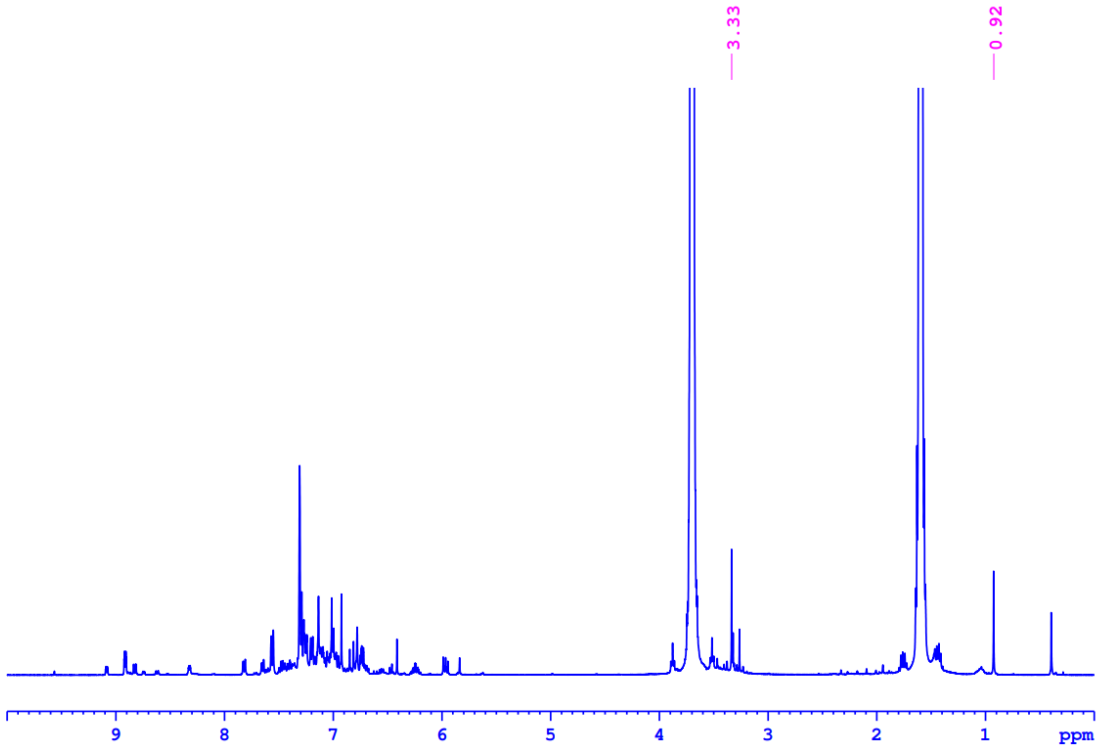

Figure S2.60: ^{1}H NMR spectrum of the 2Pd1 + 2 eq $B(C_6F_5)_3$ + 50 eq. of THF in C_6D_6 (298 K).

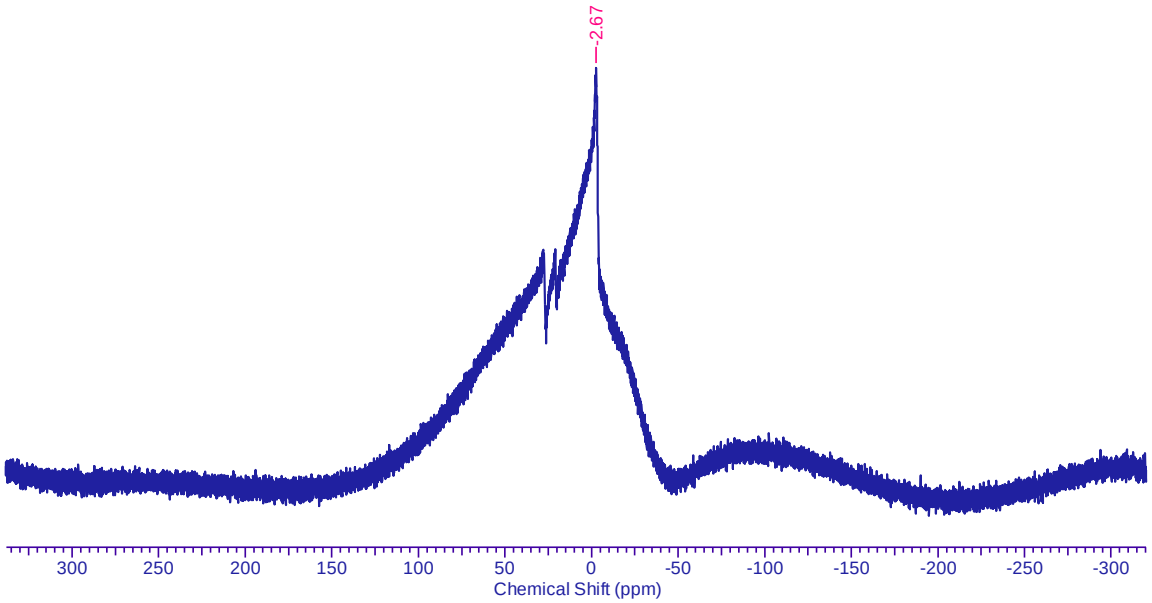

Figure S2.61: ^{11}B NMR spectrum of the 2Pd1 + 2 eq $B(C_6F_5)_3$ + 50 eq. of THF in C_6D_6 (298 K).

2.5.6.3. In-situ Pd.THF complex synthesis and its usage in ethylene oligomerization study:

Route I: In an oven-dried Schlenk flask, ligand **2L1** (24.85 mg, 0.040 mmol) and [Pd(TMEDA)Me_2] (10.28 mg, 0.040 mmol) were dissolved in 5 mL THF. The resulting reaction mixture was stirred at room temperature for 1 hour. The THF was evaporated to dryness. Next, the second batch of THF (5 mL) was added to the above residue, and the content was stirred for another 3 hours. This reaction content was directly transferred to the polymerization reactor and polymerization was performed (Time 90 min., Temperature-80 °C, pressure 5 bar, solvent-THF). After completion of reaction solvent was evaporated which produced 2.155g of ethylene oligomer.

Route II: In an oven-dried Schlenk flask, ligand **2L1** (24.85 mg, 0.040 mmol) and NaH (1mg, 0.040 mmol) were dissolved in 2 mL THF and stirred for 3 hours at 25 °C. In another round bottom flask [Pd(COD)MeCl] (10.81 mg, 0.040 mmol) was dissolved in 2 mLTHF and transfered to the sodium salt of ligand. The reaction content was further stirred for 3 hours at room temperature and solvent was evaporated to the dryness, and again 2 mL of THF was added and further stirred for 1 hour. This reaction content was directly added to the polymerization reactor and polymerization was performed (Time 90 min., Temperature-80 °C,

pressure 5 bar, solvent-THF). After completion of reaction solvent was evaporated which produced 2.42 g of ethylene oligomer.

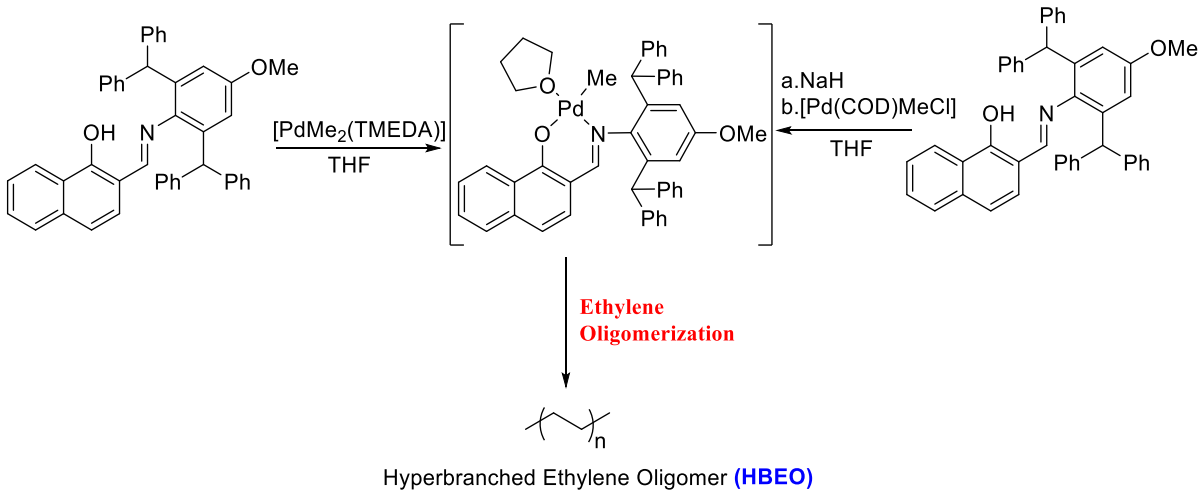

2.5.7. Functionalization of ethylene oligomer:

2.5.7.1. Ozonolysis (F1):[65]

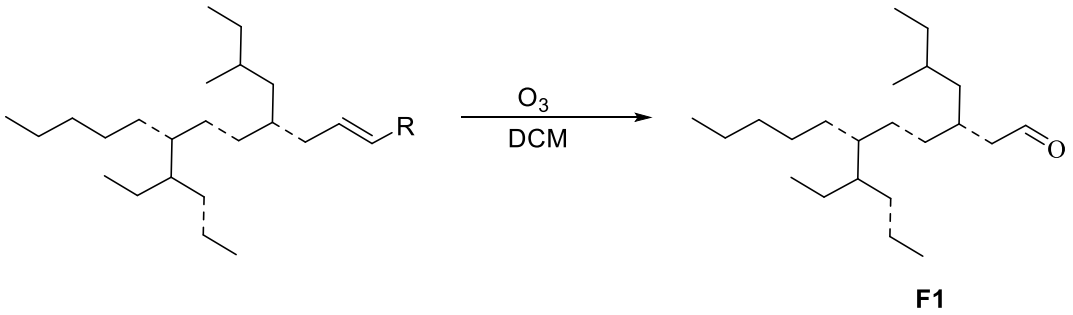

Scheme S2.6: Ozonolysis of ethylene oligomers.

In a round bottom flask, ethylene oligomer (250 mg) was dissolved in 30 mL DCM and cooled to -78 °C by using acetone and dry ice. Ozone gas was bubbled in the reaction mixture for 5 minutes; after that RB was purged with argon and dimethyl sulfide was added drop wise to the reaction mixture with vigorous stirring. Reaction mixture was allowed to warm to ambient temperature, and DCM was evaporated by using a high vacuum pump to yield chain-end functionalized ethylene oligomer (228 mg). A single peak at 9.76 ppm was observed for the terminal aldehyde.

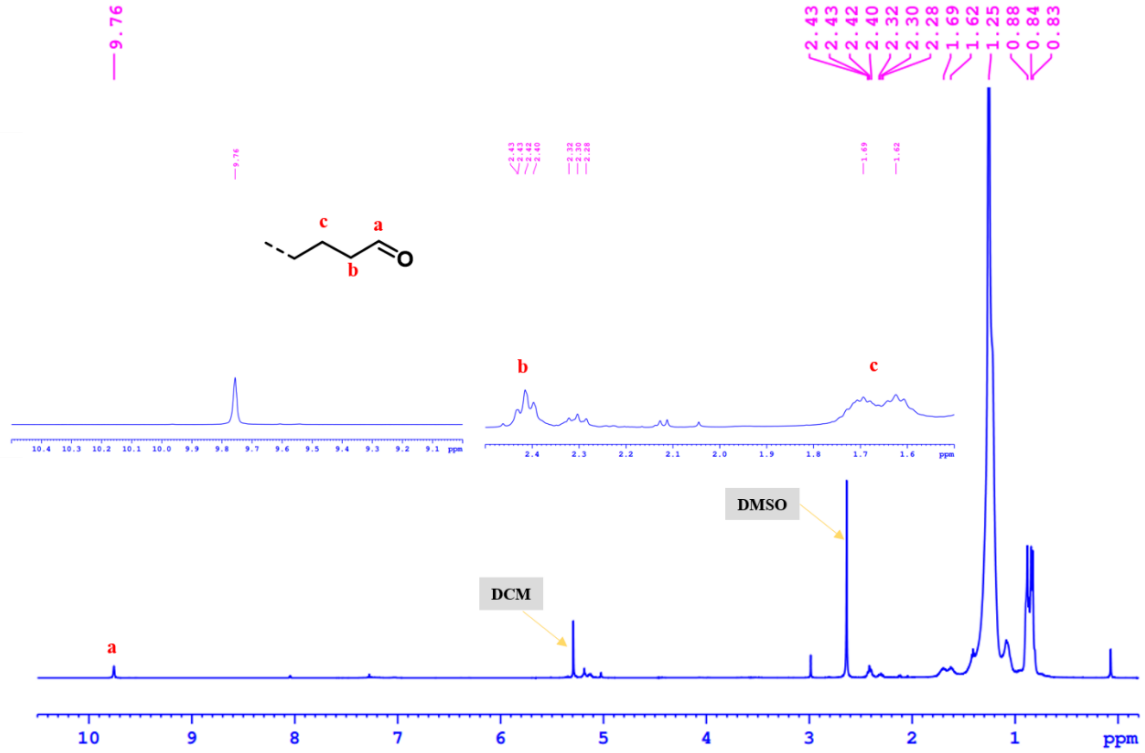

Figure S2.62: ^{1}H NMR specrum of the oligomer after ozonolysis (F1) in $CDCl_3$ (500 MHz, 298 K).

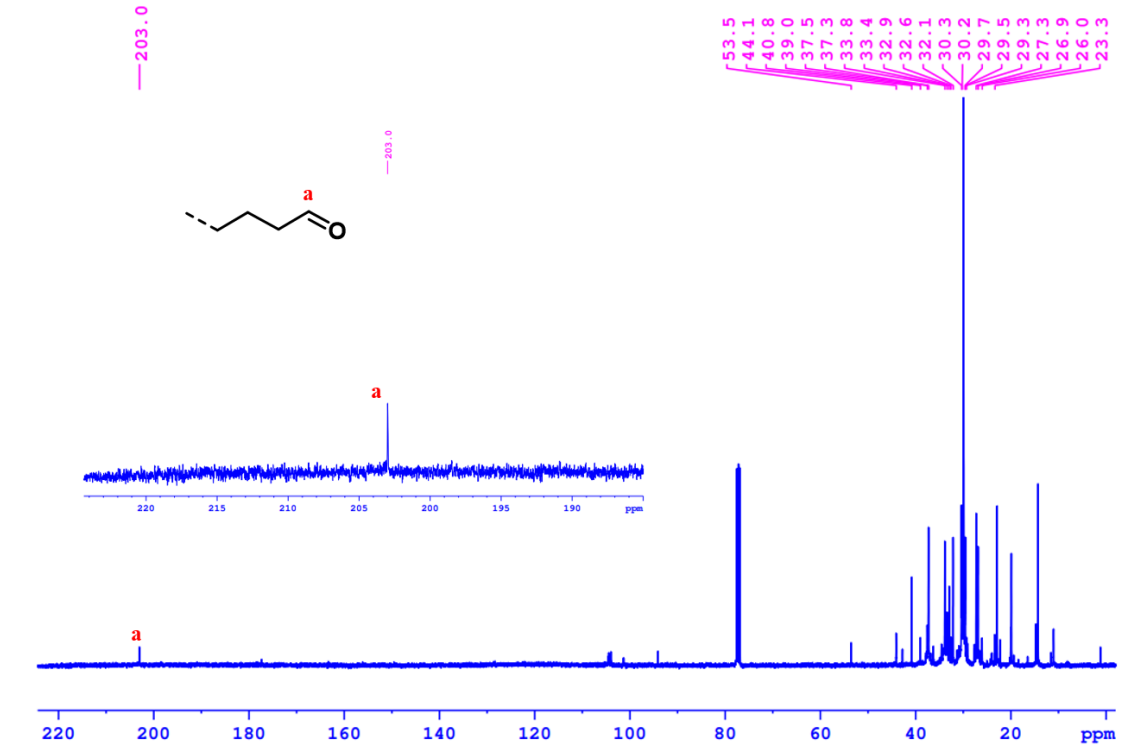

Figure S2.63: ^{13}C NMR spectrum of the oligomer after ozonolysis (F1) in $CDCl_3$ (125 MHz, 298 K).

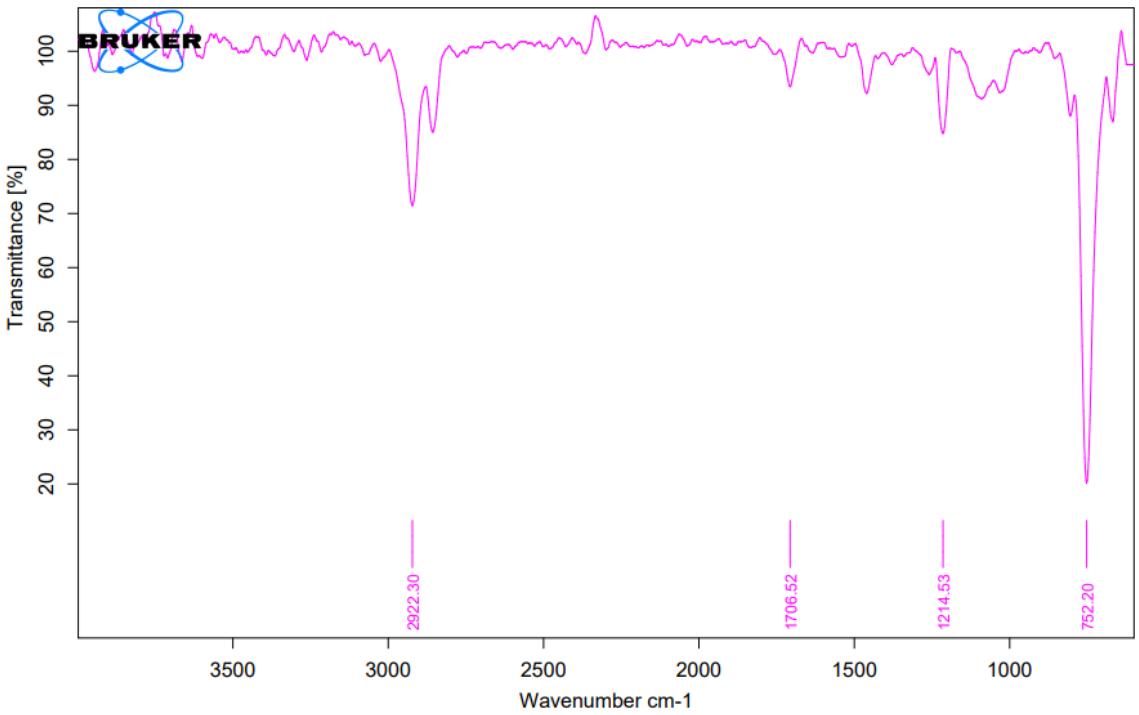

Figure S2.64: IR spectrum of oligomer after ozonolysis (F1).

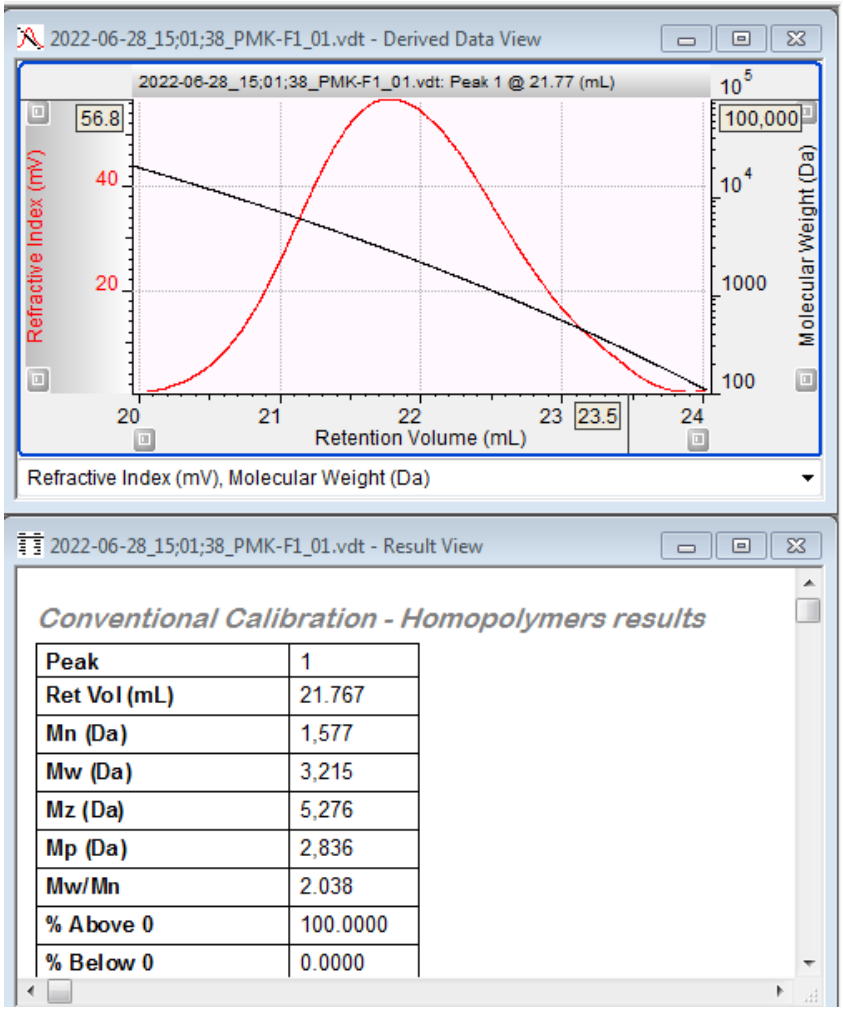

Peak	1
Ret Vol (mL)	21.767
Mn (Da)	1,577
Mw (Da)	3,215
Mz (Da)	5,276
Mp (Da)	2,836
Mw/Mn	2.038
% Above 0	100.0000
% Below 0	0.0000

Figure S2.65: GPC data of oligomer in THF after ozonolysis.

2.5.7.2. Hydroformylation (F2) [66]

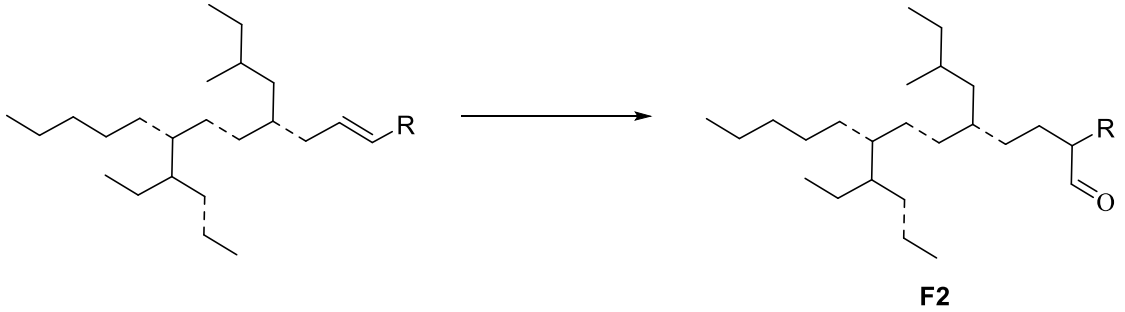

Scheme S2.7: Hydroformylation of ethylene oligomers.

Hydroformylation reaction was performed in a high-pressure Amar Equipment autoclave. Ethylene oligomer (1.19 g), $[Rh(acac)(CO)_2]$ (15 mg, 0.0581 mmol), and triphenylphosphine (30.4 mg, 0.116 mmol) were weighed in the vial, and 10 mL of toluene was added. The reaction vial was placed in the high-pressure autoclave, and the reactor was immediately pressurized with syngas (15 bar) after purging three times. Finally, the reactor was pressurized with 10 bar of syngas, and the temperature was raised to 100 °C for 18 hours with constant stirring. After completion of the reaction, the reactor was cooled to room temperature, and excess syngas was released. Toluene was evaporated, and the resultant crude product was submitted for NMR analysis. 10 mL hexane was added to the above crude reaction mixture, and the content was stirred for 5 minutes. The resultant solution was filtered, and the filtrate was evaporated. This process was repeated twice to obtain a highly viscous compound **F2** (1.2 gm).

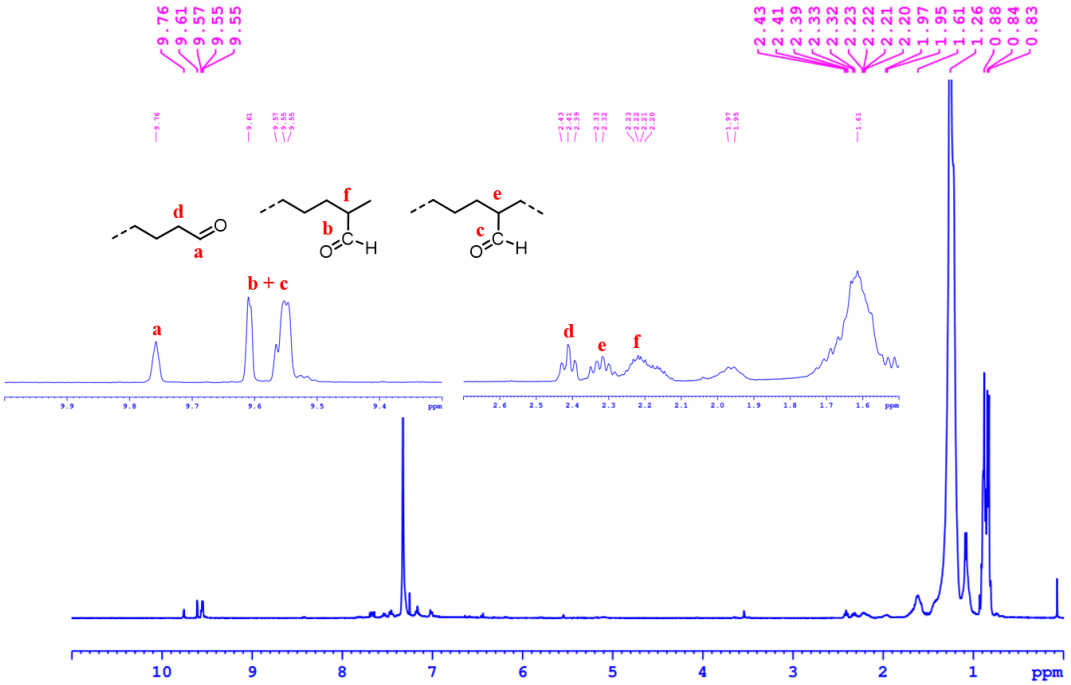

Figure S2.66A: ^1H NMR spectrum of the hydroformylated ethylene oligomer (F2) in $CDCl_3$ (500 MHz, 298 K).

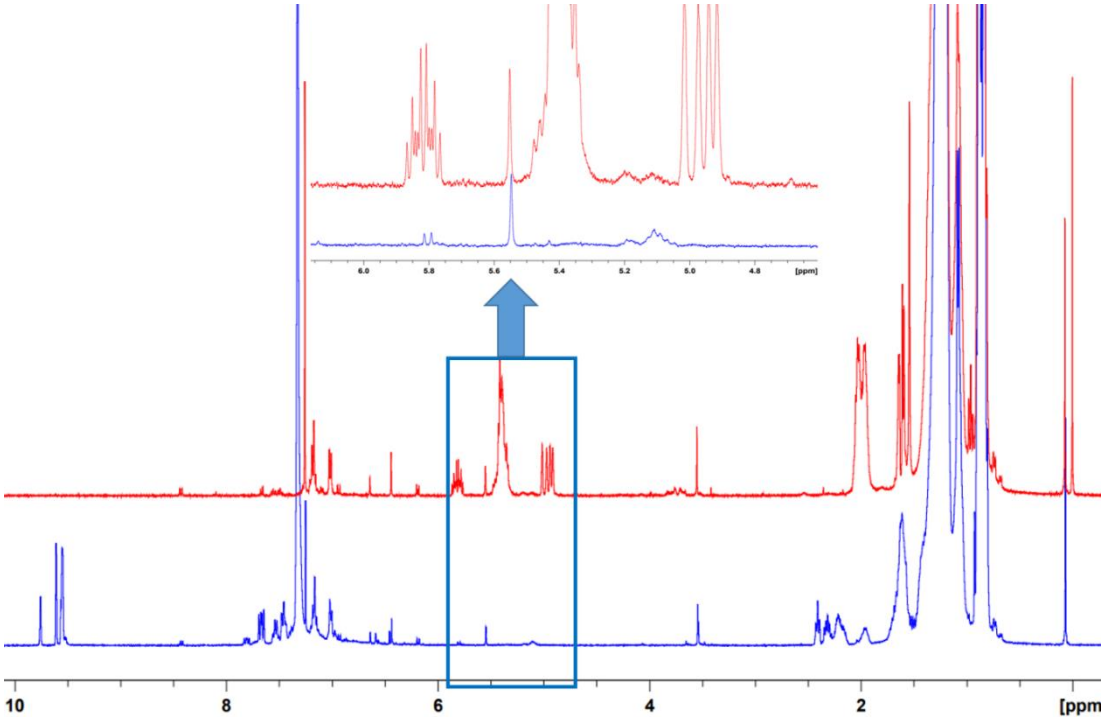

Figure S2.66B: Stacked ^{13}C NMR spectra of the olefinic product (top, red color line) and hydroformylated ethylene oligomer (bottom, blue color line) in $CDCl_3$ (125 MHz, 298 K). Expanded view in sets.

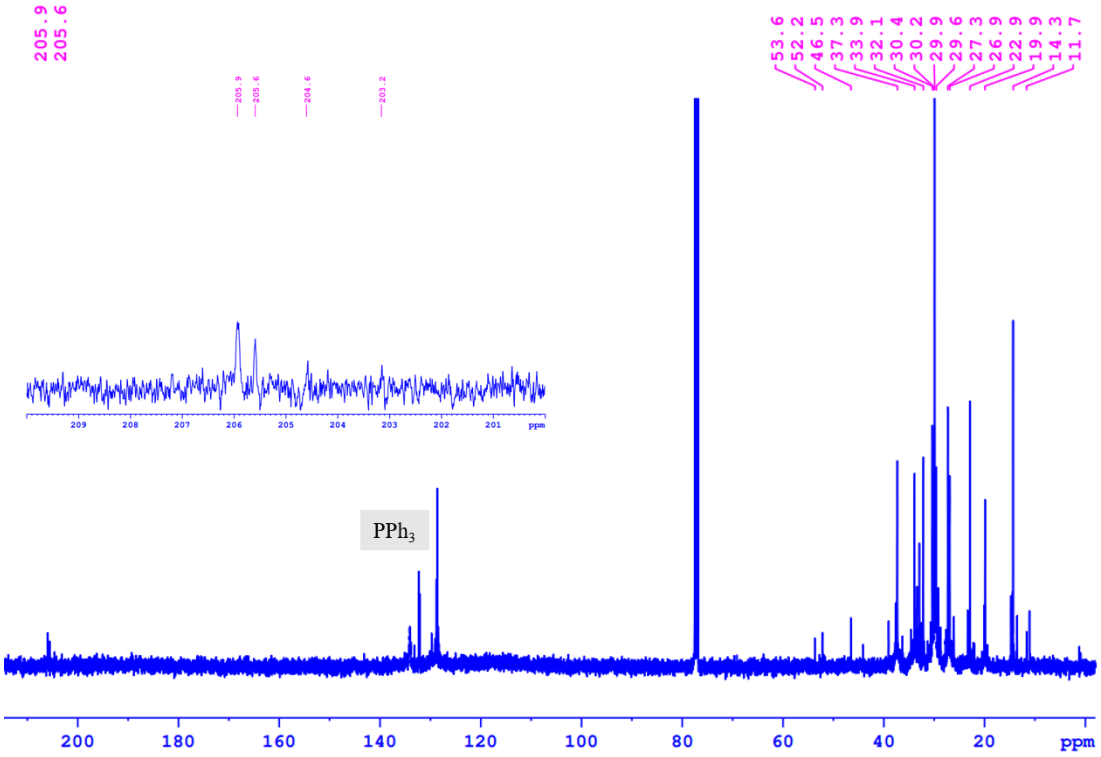

Figure S2.67: ^{13}C NMR spectrum of the hydroformylated ethylene oligomer (F2) in $CDCl_3$ (125 MHz, 298 K).

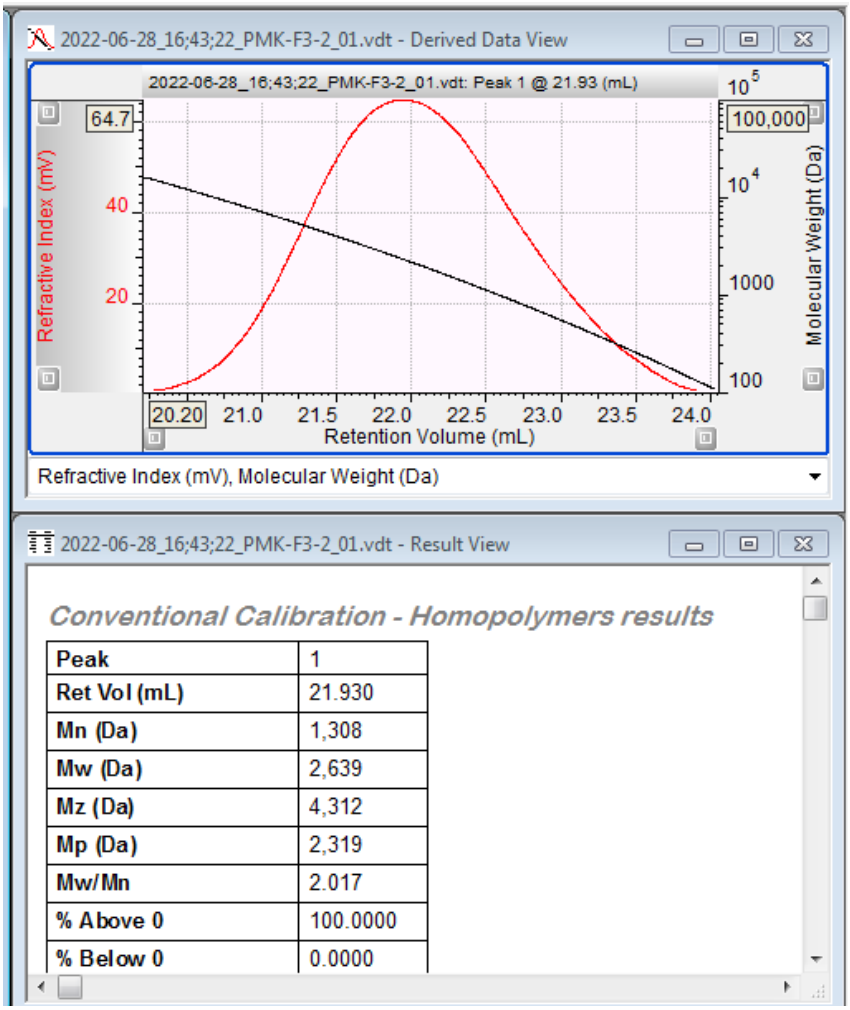

Peak	1
Ret Vol (mL)	21.930
Mn (Da)	1,308
Mw (Da)	2,639
Mz (Da)	4,312
Mp (Da)	2,319
Mw/Mn	2.017
% Above 0	100.0000
% Below 0	0.0000

Figure S2.68: GPC data of ethylene oligomer in THF after hydroformylation.

2.5.7.3. Epoxidation using mCPBA (F3):

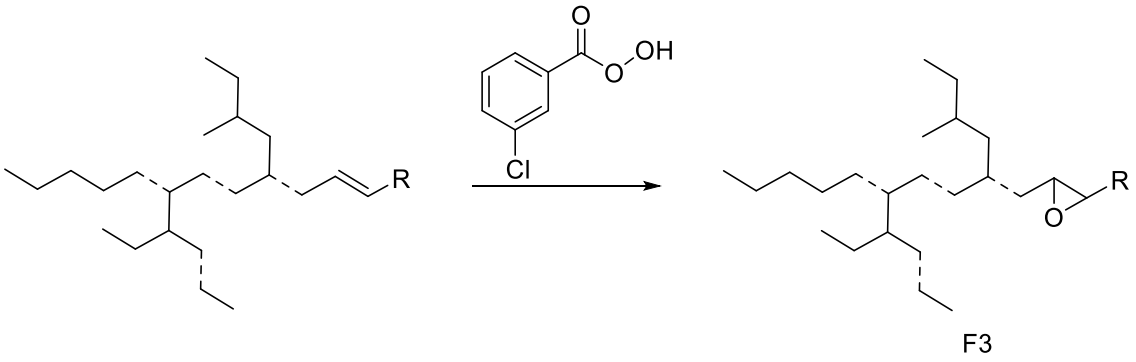

Scheme S2.8: Epoxidation of ethylene oligomers using mCPBA.

In a round bottom flask, 200 mg of ethylene oligomer was dissolved in 20 mL of dichloromethane. The reaction mixture was cooled to 0 °C, and mCPBA [50-55% (80 mg)] was added. Subsequently, the mixture was allowed to reach ambient temperature and was further stirred for 14 hours. A saturated sodium hydrogen carbonate solution was added to the reaction mixture and stirred for 10 minutes. The organic layer was washed three times with

$NaHCO_3$ and dried over Na_2SO_4. DCM was evaporated using a rota evaporator to obtain colorless oil (176 mg).

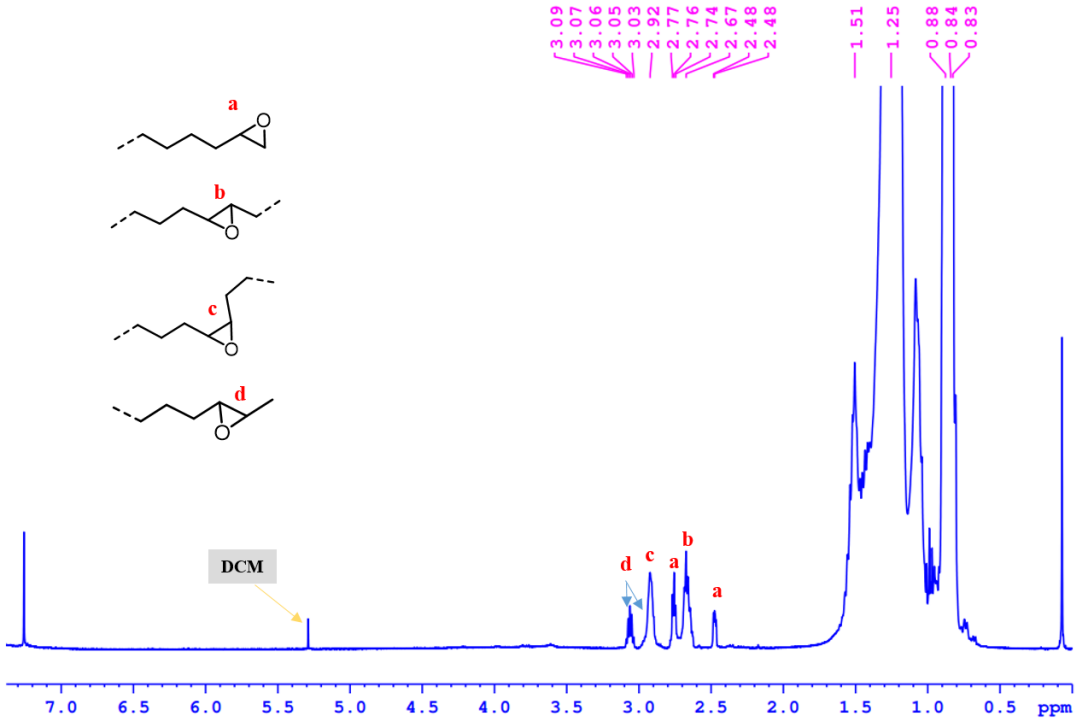

Figure S2.69: ^{1}H NMR spectrum of the epoxidation product (F3) of ethylene oligomer in $CDCl_3$ (500 MHz, 298 K).

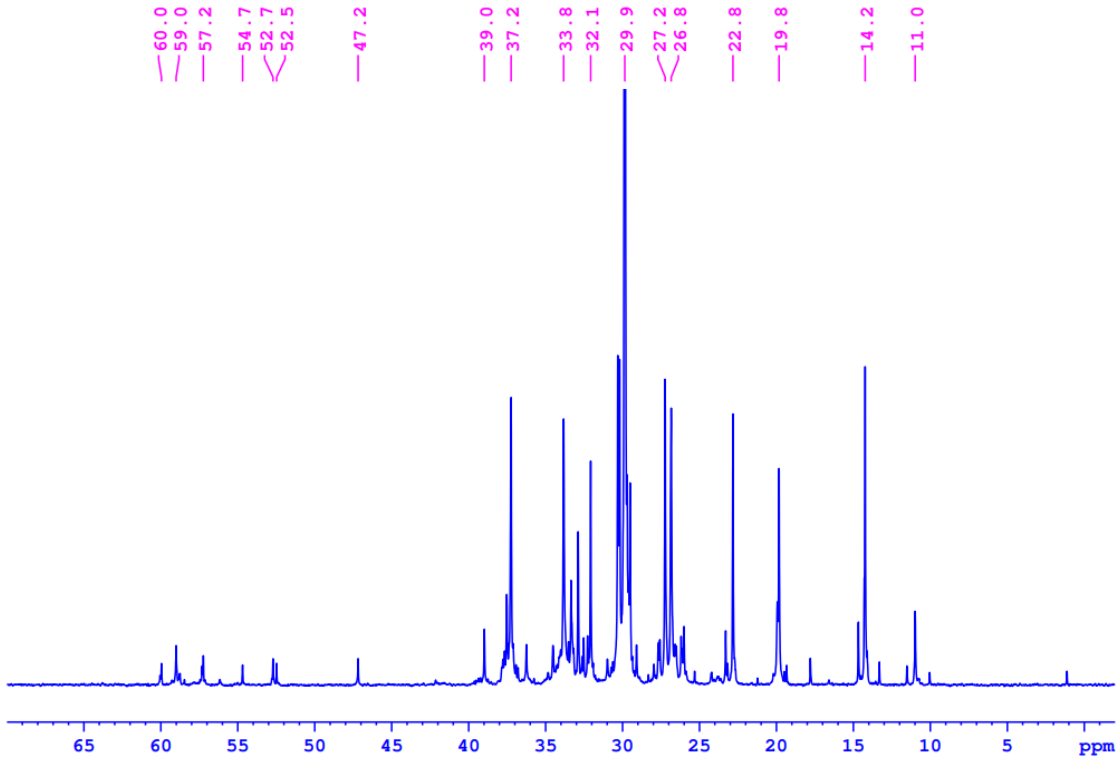

Figure S2.70: ^{13}C NMR spectrum of the epoxidation product (F3) of ethylene oligomer in $CDCl_3$ (125 MHz, 298 K).

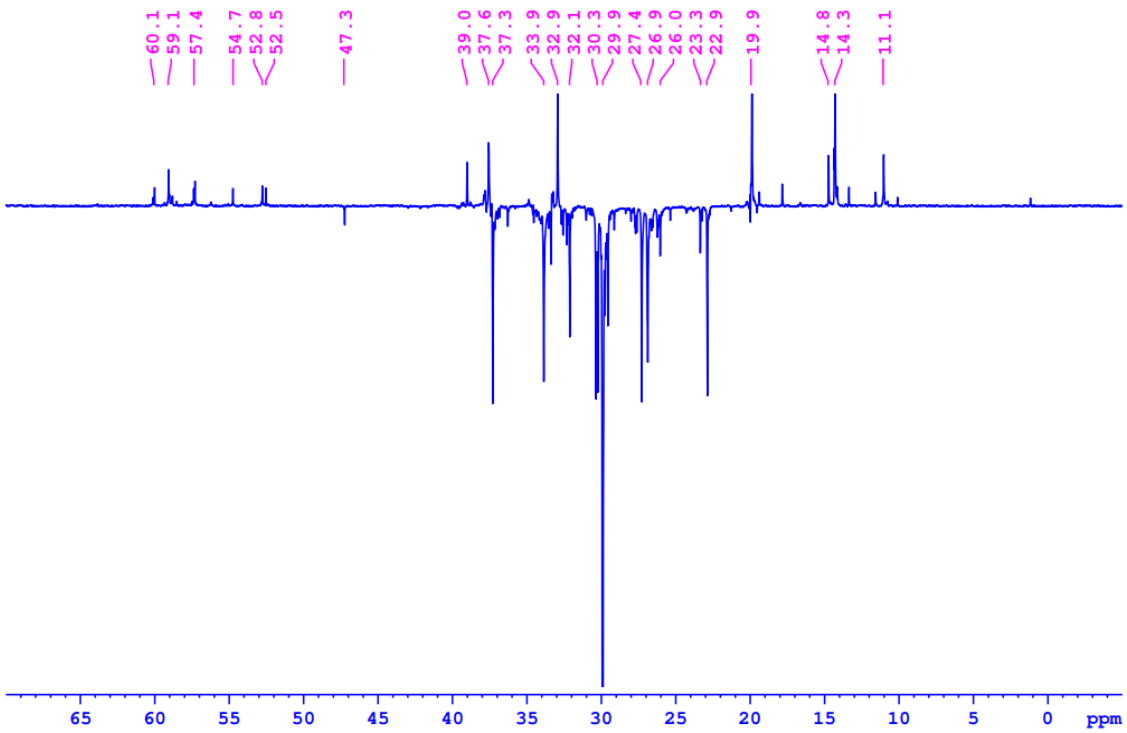

Figure S2.71: ^{13}C (DEPT) NMR spectrum of the epoxidation product (F3) of ethylene oligomer in $CDCl_3$ (125 MHz, 298 K).

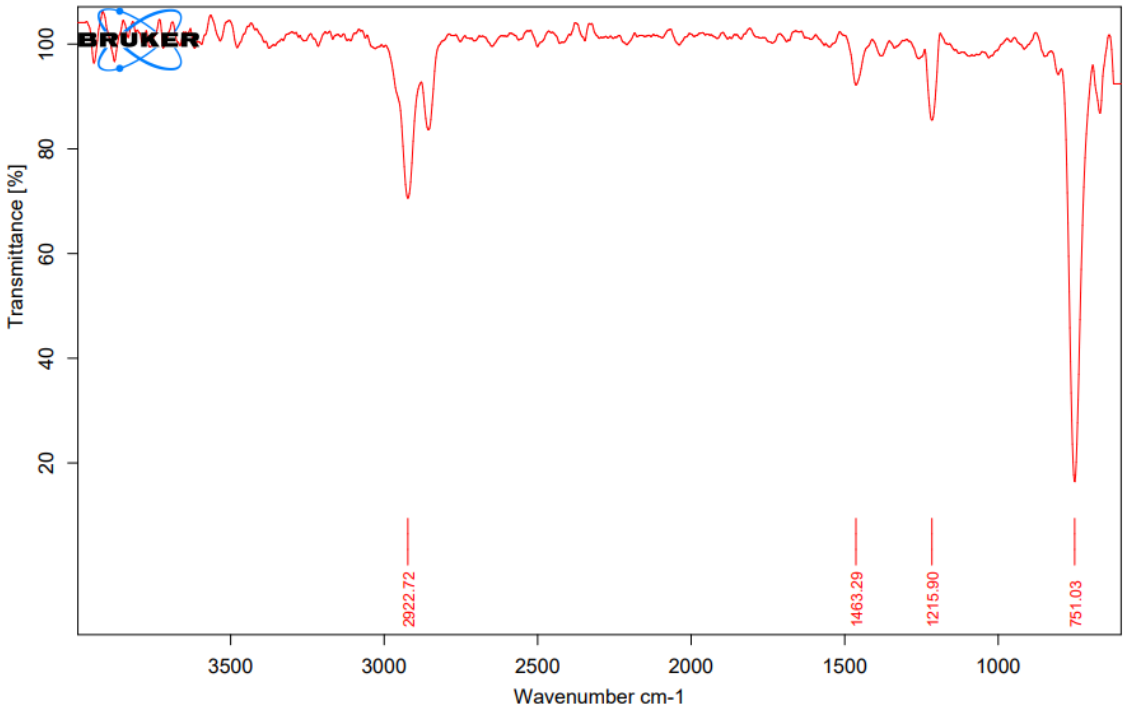

Figure S2.72: IR spectrum of the epoxidation product of ethylene oligomer.

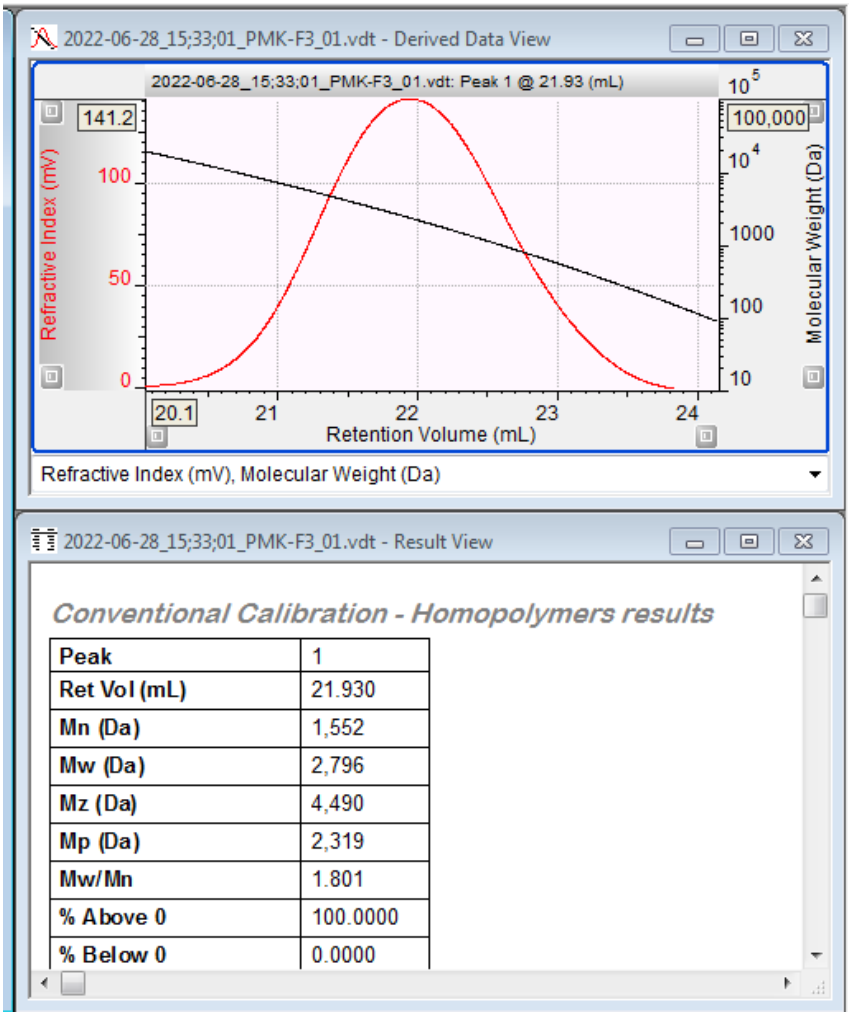

Peak	1
Ret Vol (mL)	21.930
Mn (Da)	1,552
Mw (Da)	2,796
Mz (Da)	4,490
Mp (Da)	2,319
Mw/Mn	1.801
% Above 0	100.0000
% Below 0	0.0000

Figure S2.73: Molecular weight (by GPC) of ethylene oligomer in THF after epoxidation.

2.5.7.4. Synthesis of hydroxy functionalized oligomers (F4):

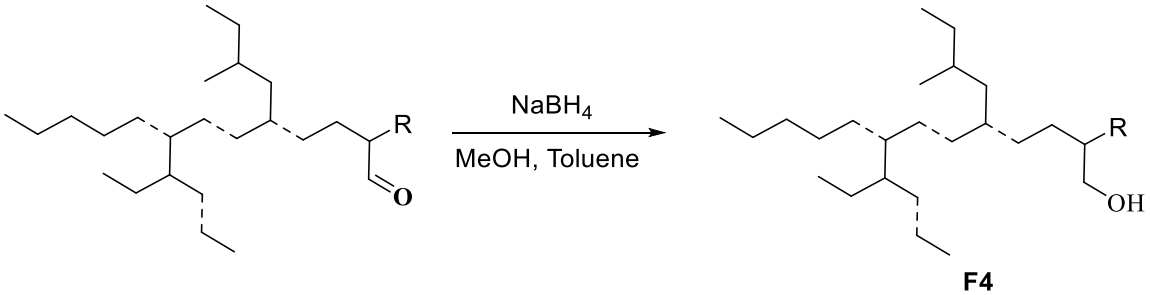

F4

Scheme S2.9: Synthesis of hydroxy functionalized ethylene oligomers.

The hydroformylation product (1.2 g) obtained from the above (F2 from hydroformylation) reaction mixture was directly used in this step. Methanol (1:1) was added to the toluene solution

of functional ethylene oligomer **F2,** and the mixture was cooled to 0 °C. Next, sodium borohydride ($NaBH_4$) (110 mg) was added with vigorous stirring and was allowed to warm to room temperature. It was further stirred for 14 hours at room temperature. The solvent was evaporated, and 10 mL hexane was added; the resultant mixture was stirred for 5 minutes. The hexane layer was decanted in another round bottom flask, and hexane was evaporated to produce **F4** (1.048 gm). The formation of hydroxyl functionalized ethylene oligomer was confirmed by ^{1}H NMR spectroscopy. It was found that the aldehyde peaks diminished, and new peaks appeared in the region of 3.6 ppm.

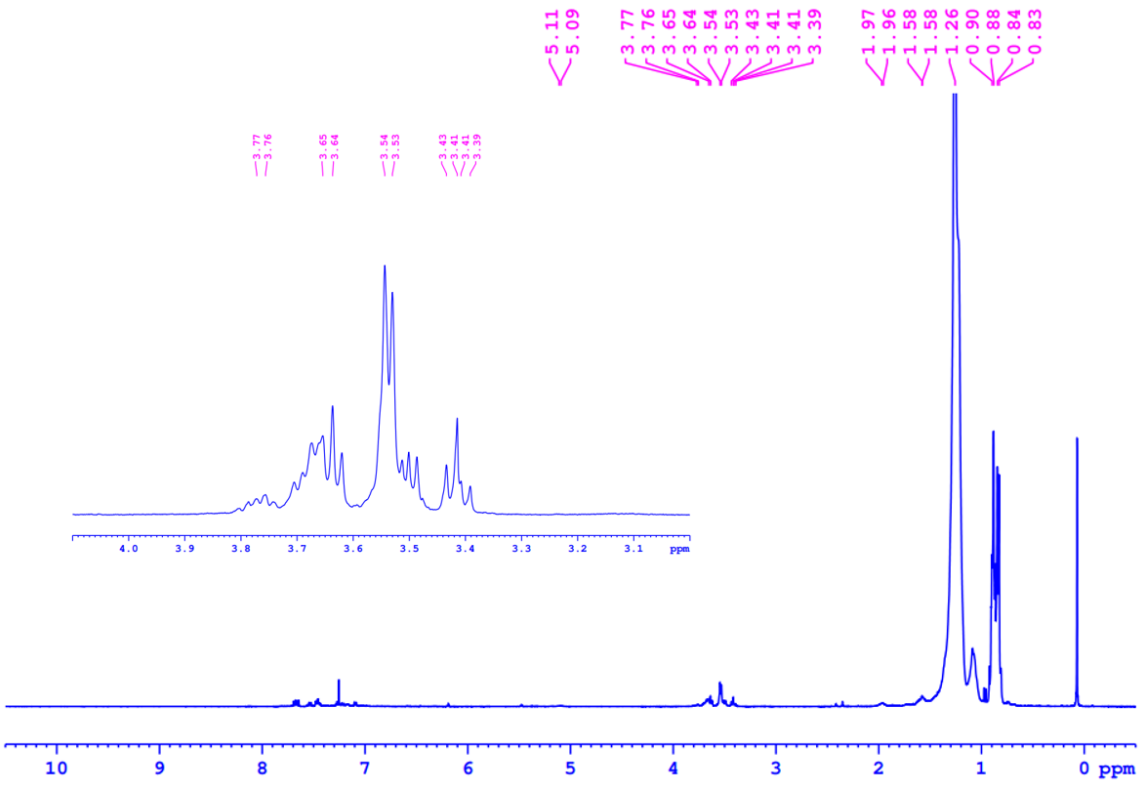

Figure S2.74: ^{1}H NMR spectrum of the hydroxyl functionalized ethylene oligomer (**F4**) in $CDCl_3$ (400 MHz, 298 K).

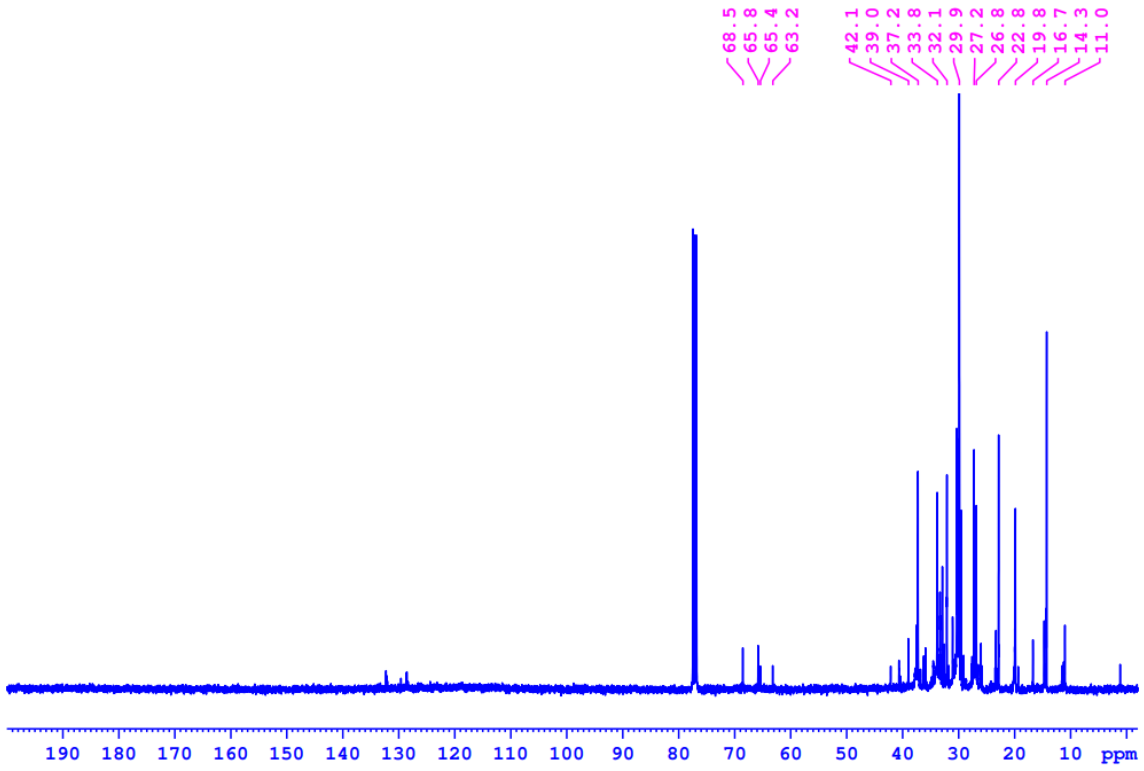

Figure S2.75: ^{13}C NMR spectrum of the hydroxyl functionalized (F4) ethylene oligomer in $CDCl_3$ (100 MHz, 298 K).

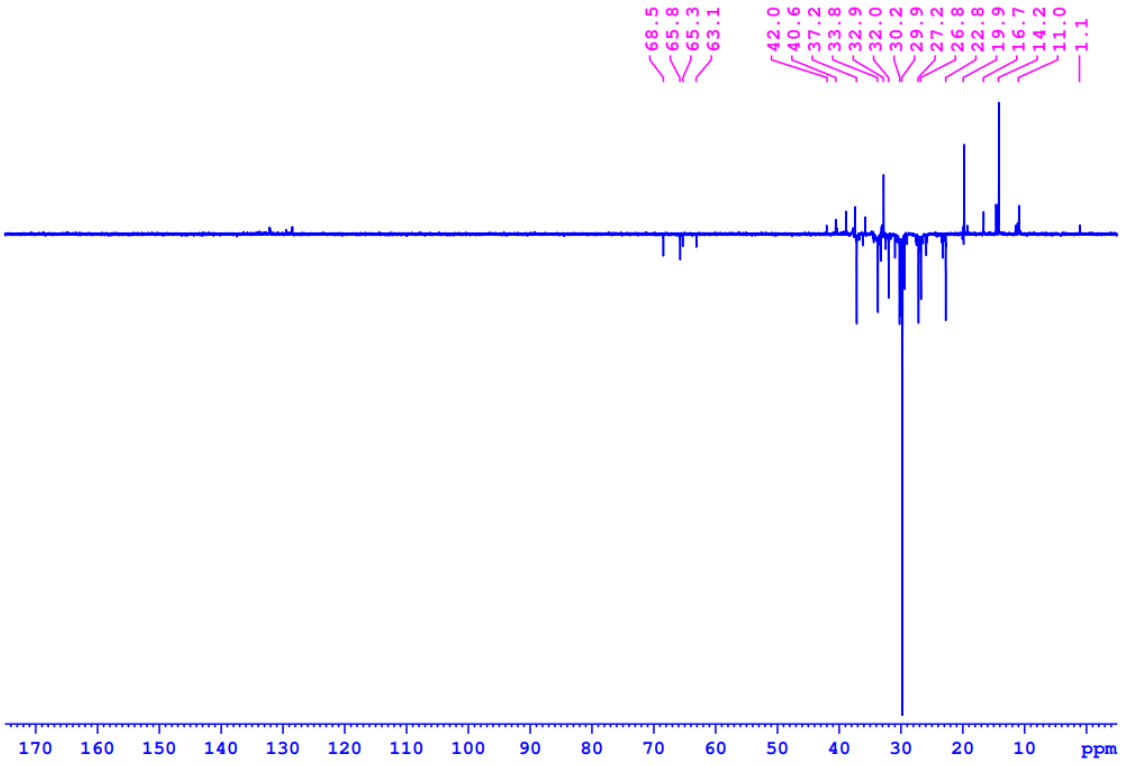

Figure S2.76: ^{13}C (DEPT) NMR spectrum of the hydroxyl functionalized (F4) ethylene oligomer in $CDCl_3$ (100 MHz, 298 K).

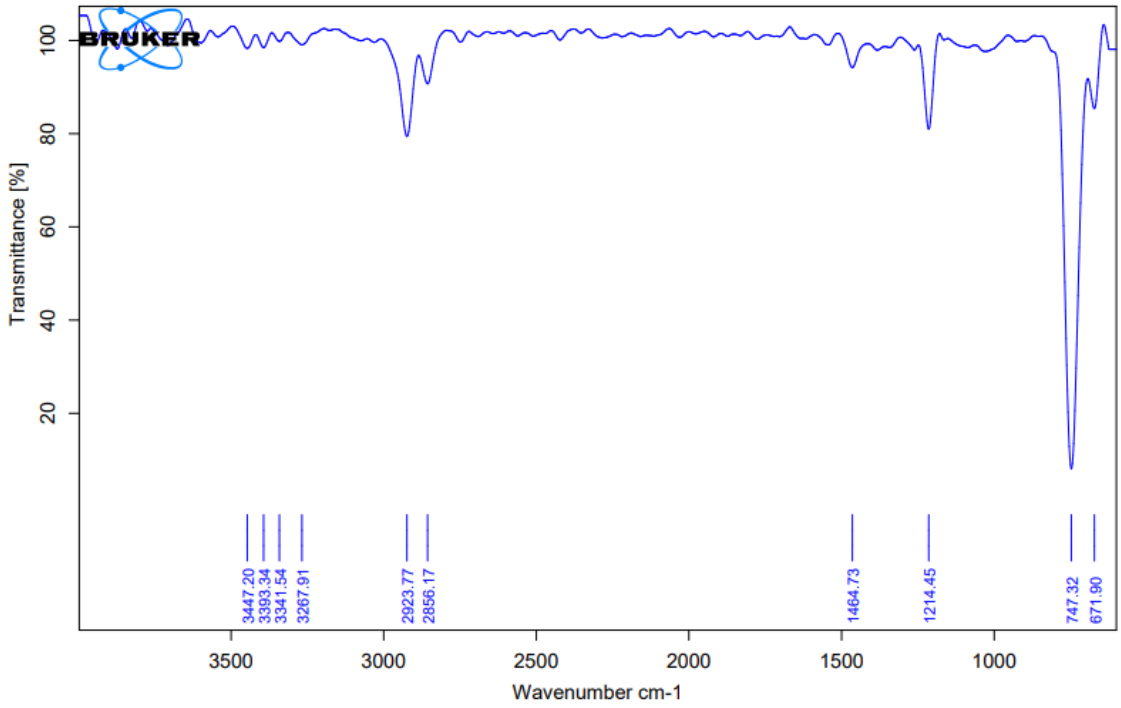

Figure S2.77: IR data of the hydroxyl functionalized (F4) ethylene oligomer.

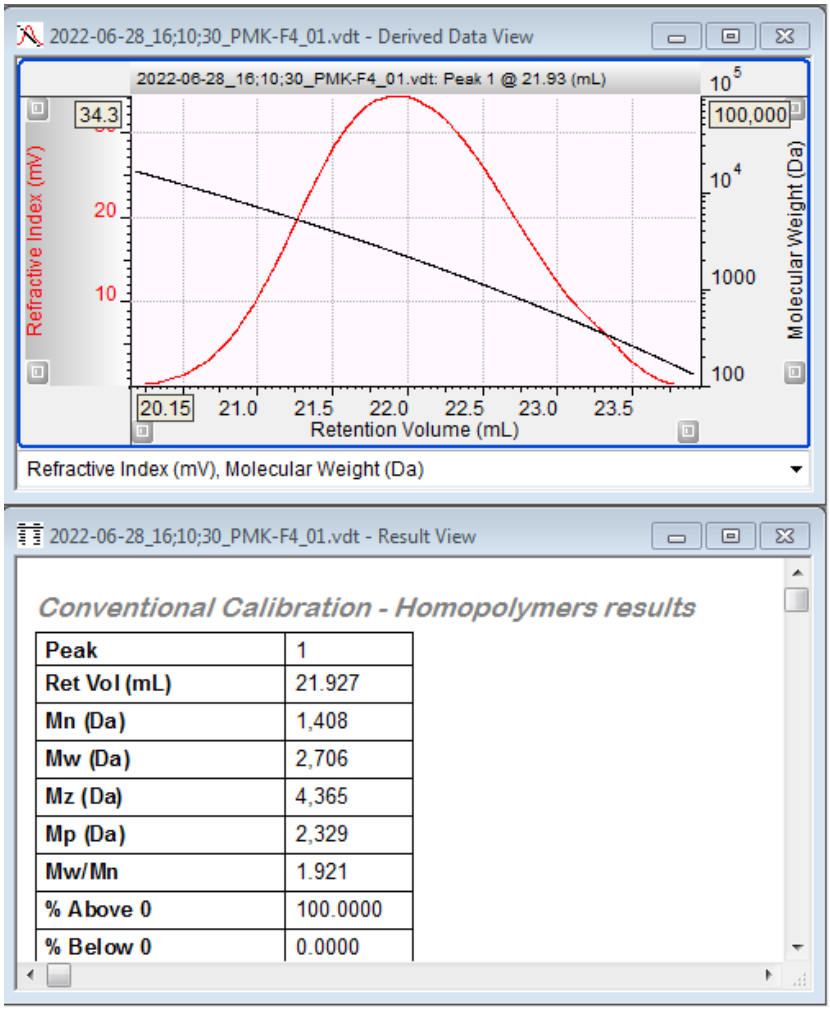

Peak	1
Ret Vol (mL)	21.927
Mn (Da)	1,408
Mw (Da)	2,706
Mz (Da)	4,365
Mp (Da)	2,329
Mw/Mn	1.921
% Above 0	100.0000
% Below 0	0.0000

Figure S2.78: Molecular weight (by GPC) data of oligomer in THF.

Table 2.3. Post functionalized ethylene oligomer, M_n, M_w and PDI as determined by GPC.

Sr. No.	Reaction	M_n	M_w	PDI
1.	Ozonolysis (F1)	1600	3200	2.038
2.	Hydroformylation (F2)	1300	2650	2.017
3.	Epoxidation (F3)	1550	2800	1.801
4.	Hydroxy functionalized (F4)	1400	2700	1.921

2.6. References:

1. Chikkali, S. H. (Eds.) In Metal Catalyzed Polymeriation: Fundamentals to Applications; CRC Press, Taylor and Francis Group: USA, 2017.
2. Stuerzel, M.; Mihan, S.; Muelhaupt, R. From Multisite Polymerization Catalysis to Sustainable Materials and All Polyolefin-composites. *Chem. Rev*. **2016**, *116*, 1398-1433.
3. Patel, K.; Chikkali, S. H.; Sivaram, S. Ultrahigh molecular weight polyethylene: Catalysis, structure, properties, processing and applications. *Prog. Polym. Sci*. **2020**, *109*, 101290/1-30.
4. Chen, C. Designing catalysts for olefin polymerization: Beyond electronic and steric tunning. *Nat. Rev. Chem*. **2018,** *2*, 6-14.
5. Boor, Jr., J. In Ziegler-Natta Catalysts and Polymerization; Academic Press: New York, 1979.
6. Shamiri, A.; Chakrabarti, M. H.; Jahan, S.; Hussain, M. A.; Kaminsky, W.; Aravind, P. V.; Yehye, W. A. The influence of Ziegler-Natta and metallocene catalysts on polyolefin structure, properties, and processing ability. *Materials* **2014**, *7*, 5069-5108.
7. Zanchin, G.; Leone, G. Polyolefin thermoplastic elastomers from polymerization catalysis: Advantages, pitfalls and future challenges. *Prog. Polym. Sci.* **2021**, *113*, 101342.
8. Tan, C.; Chen, C. Emerging Palladium and Nickel Catalysts for Copolymerization of Olefins with Polar Monomers. *Angew. Chem. Int. Ed.* **2019**, *58*, 7192−7200.
9. Franssen, N. M. G.; Reek, J. N. H.; de Bruin, B. Synthesis of Functional 'Polyolefins': State of the Art and Remaining Challenges. *Chem. Soc. Rev.* **2013**, 42, 5809−5832.
10. Birajdar, R. S.; Chikkali, S. H. Insertion copolymerization of functional olefins: Quo Vadis?. *Eur. Polym. J*. **2021**, *143*, 110183.

11. Nakamura, A.; Ito, S.; Nozaki, K. Coordination− insertion copolymerization of fundamental polar monomers. *Chem. Rev.* **2009**, *109*, 5215-5244.
12. Ziegler, K.; Gellert, H. G.; Zosel, K.; Holzkamp, E.; Schneider, J.; Söll, M.; Kroll, W. R. Metallorganische Verbindungen, XXXIV Reaktionen der Aluminium Kohlenstoff-Bindung mit Olefinen. *Justus Liebigs Ann. Chem*. **1960**, *629*, 121-166.
13. Noweck, K.; Grafahrend, W. Fatty Alcohols. In *Ullmann's Encyclopedia of Indisutrial Chemistry*; Wiley-VCH: Weinheim, Germany, 2006.
14. Wang, Z. Ziegler Alcohol Synthesis (Ziegler Higher Alcohol Synthesis, Alfol Process, Ziegler-Alfol Process, Ziegler-Alfol Synthesis), In *Comprehensive Organic Name Reactions and Reagents*; John Wiley & Sons, Inc. 2010.
15. Keim, W. Oligomerization of Ethylene to α-Olefins: Discovery and Development of the Shell Higher Olefin Process (SHOP) *Angew. Chem. Int. Ed.* **2013,** *52*, 12492−12496.
16. Kuhn, P.; Semeril, D.; Matt, D.; Chetcuti, M. J.; Lutz, P. Structure–reactivity relationships in SHOP-type complexes: tunable catalysts for the oligomerisation and polymerisation of ethylene. *Dalton Trans.* **2007**, 515−528.
17. Gibson, V. C.; Spitzmesser, S. K. Advances in non-metallocene olefin polymerization catalysis. *Chem. Rev.* **2003**, *103*, 283−316.
18. Mu, H.; Pan, L.; Song, D.; Li, Y. Neutral nickel catalysts for olefin homo-and copolymerization: relationships between catalyst structures and catalytic properties. *Chem. Rev*. **2015**, *115*, 12091−12137.
19. Olivier-Bourbigou, H.; Breuil, P. A. R.; Magna, L.; Michel, T.; Espada Pastor, M. F.; Delcroix, D. Nickel catalyzed olefin oligomerization and dimerization. *Chem. Rev.* **2020**, *120*(15), 7919-7983.
20. Wiedemann, T.; Voit, G.; Tchernook, A.; Roesle, P.; GöttkerSchnetmann, I.; Mecking, S. Monofunctional Hyperbranched Ethylene Oligomers. *J. Am. Chem. Soc.* **2014**, *136*, 2078−2085.
21. Johnson, L. K.; Killian, C. M.; Brookhart, M. New Pd (II)-and Ni (II)-based catalysts for polymerization of ethylene and alpha.-olefins. *J. Am. Chem. Soc.* **1995**, *117*, 6414−6415.
22. Johnson, L. K.; Mecking, S.; Brookhart, M. Copolymerization of ethylene and propylene with functionalized vinyl monomers by palladium (II) catalysts. *J. Am. Chem. Soc.* **1996**, *118*, 267−268.

23. Rose, J. M.; Cherian, A. E.; Coates, G. W. Living polymerization of α-olefins with an α-Diimine Ni (II) catalyst: Formation of well-defined ethylene− propylene copolymers through controlled chain-walking. *J. Am. Chem. Soc.* **2006**, *128*, 4186-4187.
24. Yan, D.; Gao, C.; Frey, H. (Eds). Hyperbranched Polymers Wiley: Hoboken, 2011.
25. Voit, B. I.; Lederer, A. Hyperbranched and Highly Branched Polymer Architectures-Synthetic Strategies and Major Characterization Aspects. *Chem. Rev.* **2009**, *109*, 5924−5973.
26. Calderon, M.; Quadir, M. A.; Sharma, S. K.; Haag, R. Dendritic polyglycerols for biomedical applications. *Adv. Mater.* **2010**, *22*, 190−218.
27. Gates, D. P.; Svejda, S. A.; Oñ ate, E.; Killian, C. M.; Johnson, L. K.; White, P. S.; Brookhart, M. Synthesis of branched polyethylene using (α-diimine) nickel (II) catalysts: influence of temperature, ethylene pressure, and ligand structure on polymer properties. *Macromolecules* **2000**, *33*, 2320-2334.
28. Wu, R.; Wu, W. K.; Stieglitz, L.; Gaan, S.; Rieger, B.; Heuberger, M. Recent advances on α-diimine Ni and Pd complexes for catalyzed ethylene (Co) polymerization: A comprehensive review. *Coord. Chem. Rev.* **2023**, *474*, 214844.
29. Zhang, Y.; Zhang, Y.; Jian, Z. A comprehensive picture on chain walking olefin polymerization. *Polymer* **2023**, *265*, 125578.
30. Qasim, M.; Bashir, M. S.; Iqbal, S.; Mahmood, Q. Recent advancements in α-diimine-nickel and-palladium catalysts for ethylene polymerization. *Eur. Polym. J.* **2021**, *160*, 110783.
31. Deng, L.; Woo, T. K.; Cavallo, L.; Margl, P. M.; Ziegler, T. The role of bulky substituents in Brookhart-type Ni (II) diimine catalyzed olefin polymerization: a combined density functional theory and molecular mechanics study. *J. Am. Chem. Soc.* **1997**, *119*, 6177-6186.
32. Xiang, P.; Ye, Z.; Subramanian, R. Synthesis and characterization of low-and medium-molecular-weight hyperbranched polyethylenes by chain walking ethylene polymerization with Pd–diimine catalysts. *Polymer* **2011**, *52*, 5027-5039.
33. Fujita, T.; Tohi, Y.; Mitani, M.; Matsui, S.; Saito, J.; Nitabaru, M.; Sugi, M.; Makio, H.; Tsutsui, T. Olefin polymerization catalysts, transition metal compounds, processes for olefin polymerization, and Alpha-olefin/conjugated diene copolymers EP-0874005, 1997.

34. Johnson, L. K.; Bennett, A. M.; Ittel, S. D.; Wang, L.; Parthasarathy, A.; Hauptman, E.; Simpson, R. D.; Feldman, J.; Coughlin, E. B. Polymerization of olefin. WO Patent 1998030609A1, 1998.
35. Bansleben, D. A.; Friedriich, S. K.; Younkin, T. D.; Grubbs, R. H.; Wang, C.; Li, R. T. Catalyst compositions and processes for olefin polymers and copolymers WO Patent 1998042664A1, 1998.
36. Wang, C.; Friedrich, S.; Younkin, T. R.; Li, R. T.; Grubbs, R. H.; Bansleben, D. A.; Day, M. W. Neutral nickel (II)-based catalysts for ethylene polymerization. *Organometallics* **1998**, *17*, 3149-3151.
37. Makio, H.; Terao, H.; Iwashita, A.; Fujita, T. FI Catalysts for olefin polymerization- A comprehensive treatment. *Chem. Rev.* **2011**, *111*, 2363-2449.
38. Baier, M. C.; Zuideveld, M. A.; Mecking, S. Post-metallocenes in the Industrial Production of Polyolefins. *Angew. Chem. Int. Ed.* **2014**, *53*, 9722−9744.
39. Zhang, Y.; Zhang, Y.; Hu, X.; Wang, C.; Jian Z. Advances on Controlled Chain Walking and Wupression of Chain Transfer in Catalytic Olefin Polymerization. *ACS Catal.* **2022**, *12*, 14304-14320.
40. See SI for details. Synthesis of 1-naphthols is reported in the following paper and reference therein. Compound 1 was synthesized based on the clues presented in this paper. Cai, L.; Zhu, X.; Chen, J.; Lin, A.; Yao, H. Rh(III)-Catalyzed C–H activation/annulation of salicylaldehydes with sulfoxonium ylides for the synthesis of chromones. *Org. Chem. Front.* **2019**, *6*, 3688-3692.
41. Meiries, S.; Speck, K.; Cordes, D. B.; Slawin, A. M. Z.; Nolan, S. P. [Pd(IPr*OMe)(acac)Cl]: Tuning the N-Heterocyclic Carbene in Catalytic C–N Bond Formation. *Organometallics* **2013**, *32*, 330-339.
42. Kang, M.; Sen, A. Neutral N-O Chelated Palladum (II) Complexes: Synthesis, Characterization and Reactivity. *Organometallics* **2005**, *24*, 3508-3515.
43. Chen, Y.; Mandal, S.; Sen, A. Synthesis of (N− O)-ligated palladium (II) complexes and their use in ethene homopolymerization and norbornene copolymerizations. *Organometallics* **2010**, *29*, 3160-3168.
44. Pong, F. Y.; Mandal, S.; Sen, A. Steric and Electronic Effects in Ethene/Norbornene Copolymerization by Neutral Salicylaldiminato-Ligated Palladium (II) Catalysts. *Organometallics* **2014**, *33*, 7044-7051.

45. Meinhard, D.; Wegner, M.; Kipiani, G.; Hearley, A.; Reuter, P.; Fischer, S.; Marti, O.; Rieger, B. New Nickel (II) Diimine Complexes and the Control of Polyethylene Microstructure by Catalyst Design. *J. Am. Chem. Soc.* **2007**, *129*, 9182-9191.
46. Guo, L.; Dai, S.; Sui, X.; Chen, C. Palladium and Nickel Catalyzed Chain Walking Olefin Polymerization and Copolymerization. *ACS Catal*. **2016**, *6*, 428-441.
47. D'Auria, I.; Maggio, M.; Guerra, G.; Pellecchia, C. Efficient Modulation of Polyethylene Microstructure by Proper Activation of (α-Diimine) Ni (II) Catalysts: Synthesis of well performing polyethylene elastomers. *Macromolecules* **2017**, *50*, 6586-6594.
48. Guan, Z.; Cotts, P. M.; McCord, E. F.; McLain, S. J. Chain Walking: A New Strategy to Control Polymer Topology. *Science* **1999**, *283*, 2059-2062.
49. Falivene, L.; Wiedemann, T.; Göttker-Schnetmann, I.; Caporaso, L.; Cavallo, L.; Mecking, S. Control of Chain Walking by Weak Neighboring Group Interactions in Unsymmetrical Catalysts. *J. Am. Chem. Soc*. **2018**, *140*, 1305-1312.
50. Fan, H.; Chang, G.; Bi, H.; Gui, X.; Wang, H.; Xu, G.; Dai, S. Facile Synthesis of Hyperbranched Ethylene Oligomers and Ethylene/Methyl Acrylate Co-oligomers with Different Microscopic Chain Architectures. *ACS Polym. Au*. **2022**, *2*, 88-96.
51. Chen, J.; Gao, Y.; Marks, T. J. Early Transition Metal Catalysis for Olefin-Polar Monomer Copolymerization. *Angew. Chem. Int. Ed.* **2020**, *59*, 14726-14735.
52. Younkin, T. R.; Connor, E. F.; Henderson, J. I.; Friedrich, S. K.; Grubbs, R. H.; Bansleben, D. A. Neutral, Single-component Nickel (II) Polyolefin Catalysts that Tolerate Heteroatoms. *Science* **2000**, *287*, 460−462.
53. Hicks, F. A.; Jenkins, J. C.; Brookhart, M. Synthesis and Ethylene Polymerization Activity of a Series of 2-Anilinotroponebased Neutral Nickel(II) Catalysts. *Organometallics* **2003**, *22*, 3533− 3545.
54. Friedberger, T.; Wucher, P.; Mecking, S. Mechanistic Insights into Polar Monomer Insertion Polymerization from Acrylamides. *J. Am. Chem. Soc.* **2012**, *134*, 1010−1018.
55. Zhang, Y.; Mu, H.; Pan, L.; Wang, X.; Li, Y. Robust Bulky [P,O] Neutral Nickel Catalysts for Copolymerization of Ethylene with Polar Vinyl Monomers. *ACS Catal.* **2018**, *8*, 5963−5976.
56. Jones, G. R.; Basbug Alhan, H. E.; Karas, L. J.; Wu, J. I.; Harth, E. Switching the Reactivity of Palladium Diimines with "Ancillary" Ligand to Select Between Olefin Polymerization, Branching Regulation, or Olefin Isomerization. *Angew. Chem. Int. Ed.* **2021**, *60*, 1635−1640.

57. Zhang, Y.; Jian, Z. Polar Additive Triggered Branching Switch and Block Polyolefin Topology in Living Ethylene Polymerization. *Macromolecules* **2021**, *54*, 3191−3196.
58. Gao, Y.; Chen, J.; Wang, Y.; Pickens, D. B.; Motta, A.; Wang, Q. J.; Chung, Y. W.; Lohr, T. L.; Marks, T. J. Highly branched polyethylene oligomers via group IV-catalysed polymerization in very nonpolar media. *Nat. Catal*. **2019**, *2*, 236-242.
59. Guironnet, D.; Rünzi, T.; Göttker-Schnetmann, I.; Mecking, S. Control of Molecular Weight in Ni(II)-Catalyzed Polymerization via the Reaction Medium. *Chem. Commun.* **2008**, 4965−4967.
60. Kenyon, P.; Wörner, M.; Mecking, S. Controlled Polymerization in Polar Solvents to Ultrahigh Molecular Weight Polyethylene. *J. Am. Chem. Soc.* **2018**, *140*, 6685−6689.
61. Wang, C.; Kang, X.; Mu, H.; Jian, Z. Positive Effect of Polar Solvents in Olefin Polymerization Catalysis. *Macromolecules* **2022**, *55*, 5441-5447.
62. Geier, S. J.; Gille, A. L.; Gilbert, T. M.; Stephan, D. W. From classical adducts to frustrated Lewis pairs: Steric effects in the interactions of pyridines and $B(C_6F_5)_3$. *Inorg. Chem.* **2009**, *48*, 10466-10474.
63. Hanley, P. S.; Hartwig, J. F. Intermolecular migratory insertion of unactivated olefins into palladium-nitrogen bonds. Steric and electronic effects on the rate of migratory insertion. *J. Am. Chem. Soc.* **2011**, *133*, 15661-15673.
64. Chen, Y.; Wang, L.; Yu, H.; Zhao, Y.; Sun, R.; Jing, G.; Huang, J.; Khalid, H.; Abbasi, N. M.; Akram, M. Synthesis and application of polyethylene-based functionalized hyberbranched polymers. *Prog. Polym. Sci.* **2015**, *45*, 23-43.
65. Mamane, V.; García, A. B.; Umarye, J. D.; Lessmann, T.; Sommer, S.; Waldmann, H. Stereoselective allylation of aldehydes on solid support and its application in biology-oriented synthesis (BIOS). *Tetrahedron* **2007** *63*, 5754-5767.
66. Dydio, P.; Detz, R. J.; Reek, J. N. Precise supramolecular control of selectivity in the Rh-catalyzed hydroformylation of terminal and internal alkenes. *J. Am. Chem. Soc.* **2013**, *135*, 10817-10828.
67. Nurttila, S. S.; Linnebank, P. R.; Krachko, T.; Reek, J. N. H. Supramolecular approaches to control activity and selectivity in hydroformylation catalysis. *ACS Catal*. **2018**, *8*, 3469-3488.
68. Pandey, S.; Chikkali, S. H. Highly regioselective isomerizing hydroformylation of long-chain internal olefins catalyzed by a rhodium bis(phosphite) complex. *ChemCatChem* **2015,** *7*, 3468-3471.

69. Pandey, S.; Shinde, D. R.; Chikkali, S. H. Isomerizing hydroformylation of cashew nut shell liquid. *ChemCatChem* **2017**, *9*, 3997-4004.
70. Kim, C.; Traylor, T. G.; Perrin, C. L. MCPBA epoxidation of alkenes: Reinvestigation of correlation between rate and ionization potential. *J. Am. Chem. Soc.* **1998**, *120*, 9513-9516 and the references therein.
71. Feng, J.; Zhang, G.; Maclnnis, K.; Li, Z.; Olah, A.; Baer, E. Effect of compatibilizer on morphology and properties of HDPE/Nylon 6 blends. *J. Polym. Sci. Part B: Polym. Phys.* **2019**, *57*, 281-290.
72. Tan, C.; Zou, C.; Chen, C. Material properties of functional polyethylenes from transition-metal-catalyzed ethylene-polar monomer copolymerization. *Macromolecules* **2022**, *55*, 1910-1922.
73. Na, Y.; Chen, C. Catechol-functionalized polyolefins. *Angew. Chem. Int. Ed.* **2020**, *59*, 7953-7959.
74. De Graaf, W.; Boersma, J.; Smeets, W. J.; Spek, A. L.; Van Koten, G. Dimethyl (N, N, N', N'-tetramethylethanediamine) palladium (II) and dimethyl [1, 2-bis (dimethylphosphino) ethane] palladium (II): syntheses, x-ray crystal structures, and thermolysis, oxidative-addition and ligand-exchange reactions. *Organometallics* **1989**, *8*, 2907-2917
75. Daugulis, O.; Brookhart, M. Polymerization of Ethylene with Cationic Palladium and Nickel Catalysts Containing Bulky Nonenolizable Imine− Phosphine Ligands. *Organometallics* **2002**, *21*(26), 5926-5934
76. Bézier, D.; Daugulis, O.; Brookhart, M. Oligomerization of ethylene using a diphosphine palladium catalyst. *Organometallics* **2017**, *36*(2), 443-447.
77. Budhai, A.; Omondi, B.; Ojwach, S. O.; Obuah, C.; Osei-Twum, E. Y.; Darkwa, J. Tandem ethylene oligomerisation and Friedel–Crafts alkylation of toluene catalysed by bis-(3, 5-dimethylpyrazol-1-ylmethyl) benzene nickel (II) complexes and ethylaluminium dichloride. *Catal. Sci. Technol*. **2013**, *3*, 3130.
78. Obuah, C.; Omondi, B.; Nozaki, K.; Darkwa, J. Solvent and co-catalyst dependent pyrazolylpyridinamine and pyrazolylpyrroleamine nickel (II) catalyzed oligomerization and polymerization of ethylene. *J. Mol. Catal. A Chem.* **2014** *382*, 31–40.
79. Dyer, P. W.; Fawcett, J.; Hanton, M. J. Rigid N-phosphino guanidine P, N ligands and their use in nickel-catalyzed ethylene oligomerization. *Organometallics* 2008, 27, 5082–5087.

Chapter 3

Regulating the Polyethylene Microstructure by Increasing Steric Crowding in Naphthoxy Imine Ligated Ni(II) Complexes

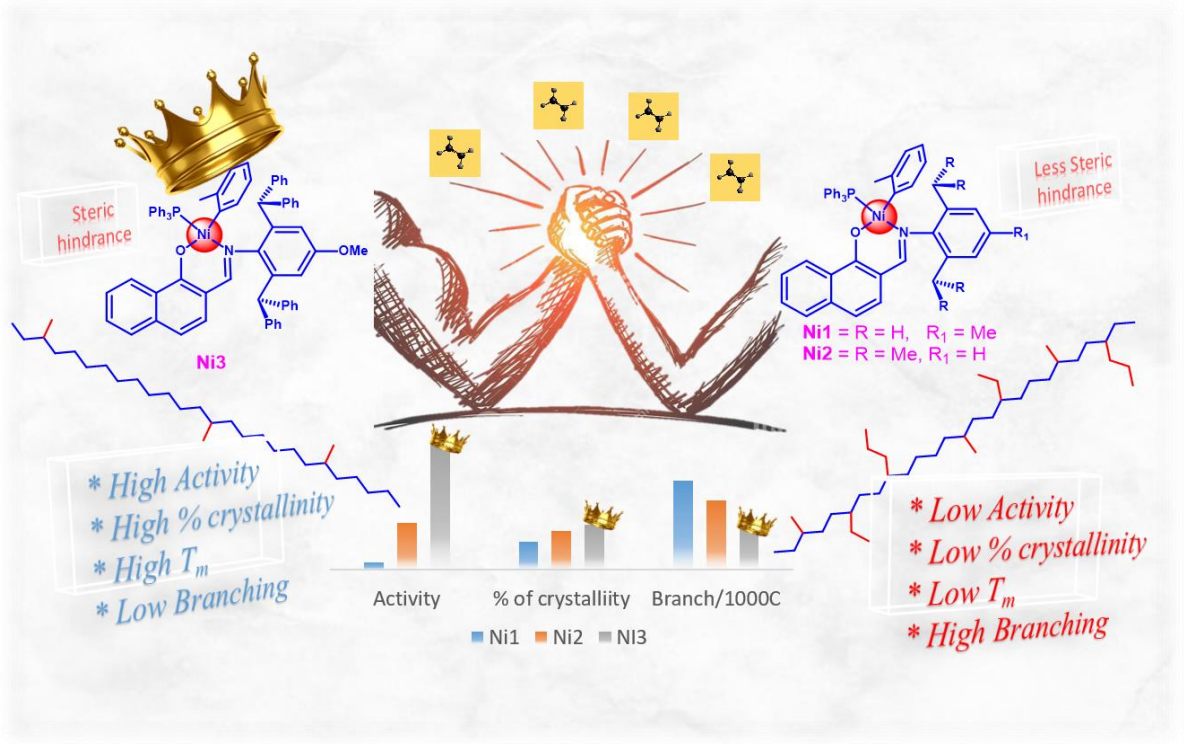

Birajdar, R. S.; Gonnade, R. G.; Chikkali, S. H. *Polym. Chem.* **2024**, *15*, 292-302.

3.1. Abstract:

Ligands play a prominent role in ethylene polymerization. However, it is a highly challenging task to regulate the branching through ligand modifications. Here we report the synthesis of systematically sterically tailored naphthoxy imine ligated nickel complexes (**Ni1**, **Ni2**, and **Ni3**), their performance in ethylene polymerization, and how the ligand steric controls branching in the resultant PE. **Ni1**-**Ni3** were prepared in one step with an excellent yield (73-93%). The identity of these complexes was unambiguously ascertained using ^{1}H, ^{13}C, 2D NMR spectroscopy, mass analysis, and single-crystal X-ray diffraction. The molecular structure revealed a cis arrangement of alkyl/aryl and donor group (C-Ni-D), which is necessary for initiating ethylene polymerization. Buried volume contours suggested **Ni3** to be sterically the most bulky among the three. When exposed to ethylene, the three nickel complexes **Ni1**, **Ni2,** and **Ni3** produced polyethylene with excellent activity. As predicted by buried volume calculations, the dibenzhydryl-substituted **Ni3** outperformed sterically less crowded **Ni1** and **Ni2**. Careful analysis of resultant PE disclosed that sterically less encumbered **Ni1** and **Ni2** produce PE with high branching (43-54 branches/1000-C atoms) density. While, the bulkiest **Ni3** revealed much lower branching (28 branches/1000-C atoms), a high TOF of 35400 mol of PE/mol of Ni h^{-1}, along with a high molecular weight of PE (61000 Da). The steric bulk in **Ni3**, most likely, reduces the chain-walking and thus lowers branching in resultant PE. As compared to the literature-reported analogs **2Pd1** catalyst, the **Ni3** catalyst discloses high TOF, high molecular weight, and less branched, linear polyethylene.

3.2. Introduction:

Polyolefins are the largest volume polymers produced in the world and nearly 180 million tons of polyolefin are manufactured annually.[1-4] Polyethylene (PE) and polypropylene (PP) are produced on an industrial scale using Ziegler-Natta-type catalysts, with few exceptions.[5] In the Ziegler-Natta type heterogeneous catalysts, Ti is the active metal, which is highly oxophilic in nature and gets easily poisoned even in the presence small amount of polar groups.[6,7] In order to address this challenge, researchers moved to late-transition metals, which are less oxophilic and show more tolerance to functional groups.[8] In 1995 Brookhart and coworkers demonstrated ethylene, α-olefin copolymerization catalyzed by Ni(II) and Pd(II) complexes bearing sterically hindered α-diimine ligands.[9,10] Also, the Pd(II) catalyst was able to incorporate polar comonomers into the polyethylene chain for the first time. The most distinctive property of these catalysts is the chain-walking process, which leads to the formation of highly branched

polyolefins. This seminal work opened doors to a flood of publications and several ligand and catalyst modifications have been reported to date.[11-19]

In these late-transition metal-catalysts, controlling the ratio of chain-walking/chain-transfer to chain propagation is crucial. This ratio determines the branching, crystallinity, and molecular weight of the resultant polyolefin.[13,20-24] The steric bulk of the ligand undisputedly plays a pivotal role in regulating chain walking and chain transfer with respect to chain propagation.[25-29] Furthermore, steric bulk has a significant influence on the thermal stability and polymerization activity of the catalyst.[16,30] Among several other sterically bulky groups, the dibenzhydryl moiety is commonly used to modify the α–diimine ligated Ni(II) or Pd(II) complexes.[16,31-39] The dibenzhydryl substituted catalysts are robust and yield high molecular weight PE with low branch density.[40] The thermal stability of the α–diimine-ligated catalysts and the molecular weight of the resulting PE are both significantly improved by the incorporation of the large dibenzhydryl moiety.[38,39,41] The α-diimine ligated Pd(II) complex containing dibenzhydryl group yields semicrystalline polymer, with significantly reduced branching.[39,41-46] In 2016 Chen and coworkers prepared a series of sterically tailored α–diimine ligated Pd(II) complexes and demonstrated that with an increase in steric, the molecular weight increases, activity increases, and branching reduces (see Figure 3.1).[26] Along the same line, Min Chen and coworkers demonstrated the influence of ligand steric bulk on catalytic activity, molecular weight, and polymer microstructure in ortho-dibenzhydryl or ortho-sec- phenyl substituted α-diimine nickel catalysts.[47] It was observed that dibenzhydryl substituted species gives higher activity [0.98–1.58) $*10^6$ g (mol Ni h)$^{-1}$], high polymer molecular weight [Mn: (8.0–13.1) * 10^5 g mol^{-1}] and low branch density (55-64/1000C) compared to the methyl-substituted nickel complexes [activity [0.63–0.44) $*10^6$ g (mol Ni h)$^{-1}$, molecular weight [Mn: (0.8–0.6) * 10^5 g mol^{-1}] and branch density (90-95/1000C). Along with steric, the ligand symmetry also plays an important role in controlling the polymer microstructure. Recently Dai and coworkers prepared dibenzobarrelenedione and dibenzhydrylanilines ligated α–diimine Ni(II) complex.[48] Complexes with a quasi-centrosymmetric structure produced semi-crystalline polyethylene with very high molecular weight and low branching densities (11-34/1000C). However, in plane-symmetric complex, having similar steric bulk, produced highly branched polymer (110-115/1000C) with no obvious melting point under identical polymerization conditions.

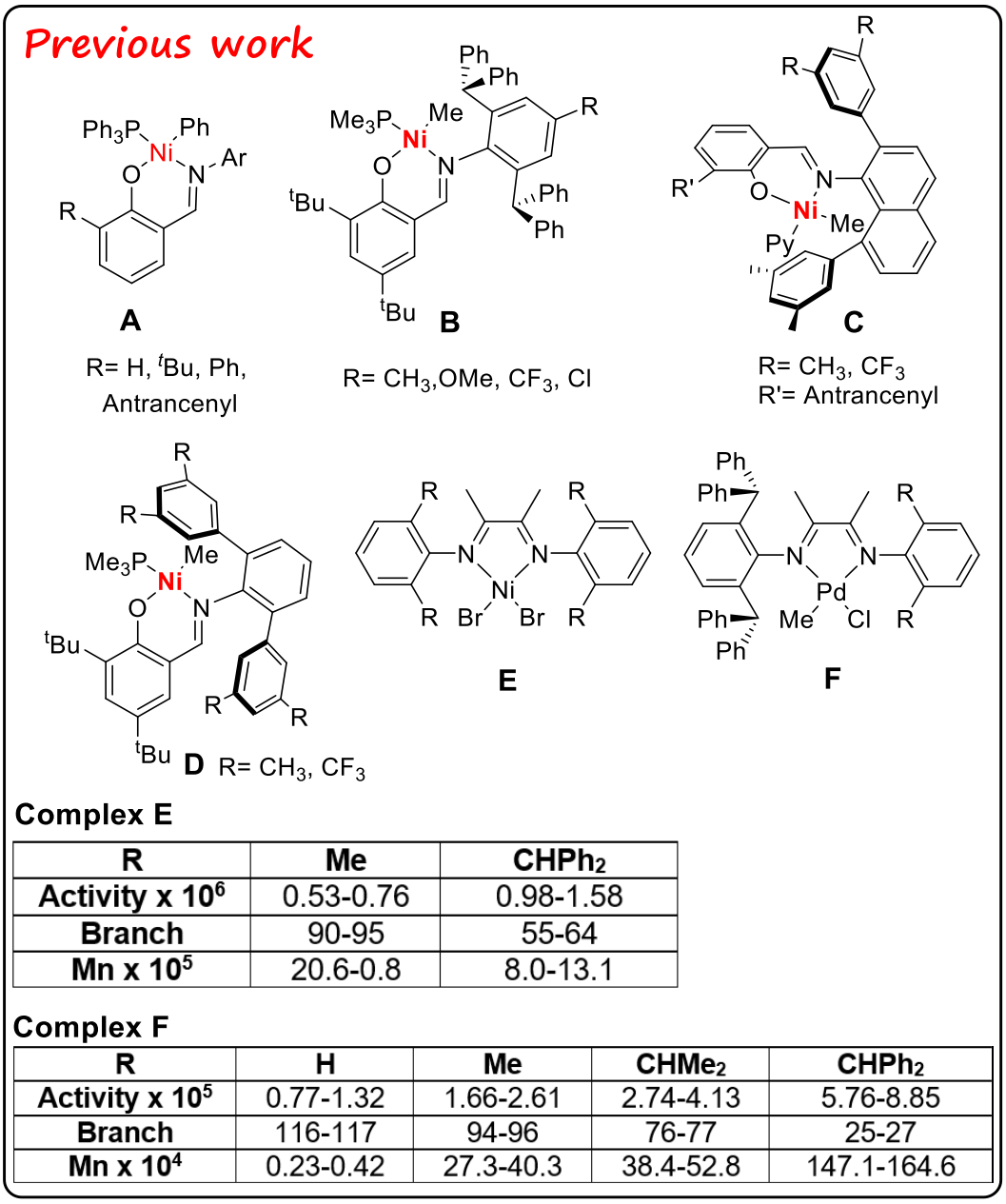

Complex E

R	Me	$CHPh_2$
Activity x 10^6	0.53-0.76	0.98-1.58
Branch	90-95	55-64
Mn x 10^5	20.6-0.8	8.0-13.1

Complex F

R	H	Me	$CHMe_2$	$CHPh_2$
Activity x 10^5	0.77-1.32	1.66-2.61	2.74-4.13	5.76-8.85
Branch	116-117	94-96	76-77	25-27
Mn x 10^4	0.23-0.42	27.3-40.3	38.4-52.8	147.1-164.6

Figure 3.1: Sterically demanding catalyst (representative) for ethylene polymerization (top).

Literature reports suggest that the bulkiness of N-aryl moiety (imine) and substituents on the ortho position to the O-donor group play a crucial role in phenoxy imine-ligated metal catalysts. These two groups help to build the molecular weight by retarding the chain transfer process, β-hydride elimination, and increase the polymerization activity by avoiding the formation of an inactive bis-ligated complex.[49-52] In 2014, Brookhart and coworkers produced branched ultrahigh-molecular-weight polyethylene using a sterically hindered 2,8-diaryl naphthyl substituted salicylaldimine ligated Ni(II) complex.[53] Along with steric bulk, the ligand electronic effect can considerably affect polymerization activity. Therefore, Marks and coworkers studied the effect of fluorine substituents in ethylene polymerization and found that

the CF_3-substituted catalyst shows higher stability and catalytic activity compared to the CH_3-substituted catalyst.[54] Furthermore, the resultant polymers revealed high molecular weight and low branch density (for CF_3: $M_w = 9.2 \times 10^4$, branching = 7/1000 C; for CH_3: $M_w = 1.4 \times 10^3$, branching = 88/1000 C). The authors proposed a weak interaction between the C-F of ligand and the C-H of the growing polymer chain, which suppresses the β-H elimination reaction. In 2022, Jian and coworkers reported sterically hindered sandwich-like neutral salicylaldiminato nickel catalyst having 8-aryl naphthyl and dibenzosuberyl groups as N-aryl moiety. This nickel catalyst yields linear UHMWPE at a high temperature of 90 °C.[55] Thus, the effect of steric bulk on ethylene polymerization has been investigated for mainly two types of ligand systems, namely, α–diamine (Figure 3.1, E-F) and phenoxy-imine (Figure 3.1, A-D). Such an in-depth understanding and analysis is missing for the naphthoxy-imine counterparts.

Here, we report the synthesis of three systematically sterically tuned naphthoxy-imine ligated Ni(II) complexes and examine their performance in ethylene polymerization. It turns out that sterically bulky, dibenzhydryl-substituted naphthoxy-imine ligated Ni-catalyst outperforms its less bulky counterpart catalysts. The dibenzhydryl substituted naphthoxy-imine ligated Ni-catalyst revealed the highest activity. The resultant polymer displayed high molecular weight, melting temperature, and lowest branching, among the polymers produced by the three catalysts.

3.3 Results and discussion:

3.3.1. Ligand synthesis:

Ligand **3L1** was prepared by treating 1-hydroxy 2-naphthaldehyde, with commercially available 2,4,6 trimethyl aniline in the presence of a catalytic amount of p-Toluenesulfonic acid (PTSA) (Scheme 3.1). After refluxing for 6 hours at 120 °C in toluene, ^{1}H NMR was recorded. The starting aldehyde peak slowly diminished with the consequent appearance of a new peak (imine proton) at 8.51 ppm (Figure S3.1), suggesting the completion of the reaction. The synthesized ligand was characterized using ^{1}H, ^{13}C, and ESI-MS analysis. The corresponding imine carbon was observed at 163.4 ppm (Figure S3.2) in a ^{13}C NMR spectroscopy. Sterically hindered ligands **2L1** and **2L2** were prepared in gram scale using our methodology reported earlier.[56]

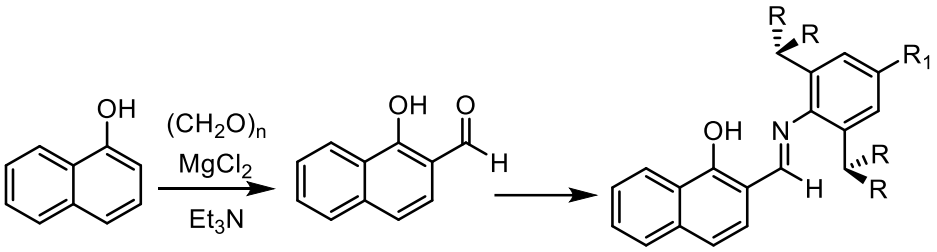

3L1 = R = H, R_1 = Me
2L2 = R = Me, R_1 = H
2L1 = R =Ph, R_1 =OMe

Scheme 3.1: Synthesis of ligands **3L1, 2L2**, and **2L1.**

3.3.2. Synthesis of Ni-complexes:

The ligands were deprotonated using an excess of sodium hydride in tetrahydrofuran as a solvent. The solvent was evaporated under high vacuum, and the resultant sodium salts of ligands can be directly used for complex synthesis. Sodium salts of ligands were treated with an appropriate amount (1 equiv.) of nickel precursor (*trans* [NiCl(*o*-Tol)(PPh_3)$_2$]) leading to the formation of complexes (**Ni1-Ni3**). The formation of the Ni-complex was monitored by ^{31}P NMR spectroscopy. The reduction in the ^{31}P peak intensity of the Ni-precursor and concomitant appearance of a new peak for the Ni-complex, along with de-coordinated triphenylphosphine (at around -6 ppm), suggested the formation of the desired Ni-complex. The identity of **Ni1-Ni3** was established using 1D, 2D NMR spectroscopy along with ESI-MS. The ^{31}P NMR spectrum of **Ni1** disclosed a singlet phosphorous peak at 25.19 ppm (Figure S3.5). The ^{1}H NMR spectrum revealed an imine proton at 7.85 ppm and corresponding imine carbon was observed at 164.8 ppm in ^{13}C NMR spectrum. The 2D (^{1}H- ^{1}H NOESY) NMR spectroscopy displayed a cross-peak of the imine proton to that of the methyl group on o-tolyl (substituent on the ligand).

The **Ni2** complex was thoroughly characterized using ^{31}P, ^{1}H, ^{13}C, and 2D NMR spectroscopy. A singlet phosphorous peak at 25.2 ppm (Figure S3.15) was observed. The ^{1}H NMR spectroscopy displayed imine proton at 7.92 ppm and imine carbon was observed at 165.2 ppm (Figure S3.16 & 17). Also, the ^{1}H- ^{1}H NOESY spectrum revealed that the diisopropylic CH shows a correlation with *o*-tolyl, confirming the complex formation.

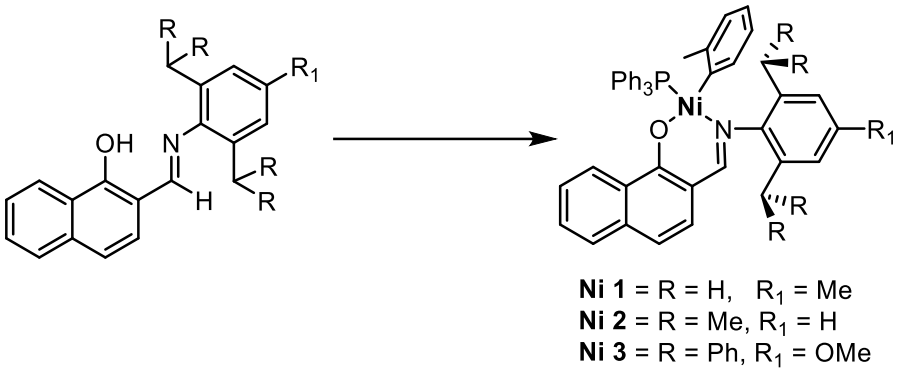

Scheme 3.2: Synthesis of Nickel complexes Ni1, Ni2, and Ni3.

The presence of **Ni3** complex was confirmed by 1-2D NMR spectroscopy. The ^{31}P NMR disclosed a singlet at 22.8 ppm (Figure S3.24). The ^{1}H NMR spectrum displayed a singlet at 3.07 ppm (Figure S3.25) that can be assigned to the methyl of the *o*-tolyl group. The imine proton was found to be shifted to a shielded region (as compared to 2L1) and appeared at 5.67 ppm (Figure S3.25). The presence of imine carbon was confirmed by ^{13}C NMR spectroscopy which appeared at 168.5 ppm (Figure S3.26). 2D NMR (^{1}H- ^{1}H NOESY) revealed a long-range correlation between the dibenzhydrylic CH and methyl of o-tolyl, confirming the formation of the **Ni3** complex.

The existence of **Ni1, Ni2,** and **Ni3** complexes was unambiguously ascertained using single-crystal X-ray diffraction. The molecular structures of **Ni1, Ni2,** and **Ni3** are shown in Figures 3.2, 3.3, and 3.4, respectively, along with selected bond distances and bond angles. Suitable crystals of **Ni1, Ni2,** and **Ni3** were obtained from dichloromethane and hexane solvent mixture at room temperature. The geometry around the nickel metal center was distorted square planar. In the **Ni1** complex, the *o*-tolyl group was placed *cis* to the imine nitrogen atom with a C1-Ni1-N1 bond angle of 91.55°. The triphenylphosphine was located *trans* to the imine nitrogen with an N1-Ni1-P1 bond angle of 176.42°. The oxygen atom and triphenylphosphine are *cis* to each other with O1-Ni1-P1 angle of 89.37° and *trans* to o-tolyl group with C1-Ni1-O1 angle of 176.33°. A nickel (**Ni1**) and imine (**N1**) bond distance of 1.92 Å suggests the coordination of imine nitrogen to nickel. While a shorter Ni-O bond distance of 1.89 Å suggests the formation of a covalent bond. These observed bond distances are similar to those reported in the literature.[57,58] The bond angle between C-Ni-P was found to be 87.05° suggesting the *cis* position of the PPh_3 and methyl group on nickel. The *cis* arrangement is crucial for initiating the ethylene polymerization.

The remaining nickel complexes, **Ni2** and **Ni3**, contain a common structural unit, i.e. the naphthoxy-imine ligated nickel complex in which the nickel is coordinated by four atoms and

assumes a distorted square planar geometry. As observed in **Ni1**, the oxygen atom forms a covalent bond and the imine nitrogen forms a coordinate bond with the central nickel atom. As compared to **Ni1**, the P-Ni bond distance in **Ni2** and **Ni3** was found to be slightly longer. This increase in P-Ni distance can be ascribed to increased steric in these complexes. Another noticeable difference is the N1-Ni-C1 bond angle. The N1-Ni-C1 bond angle of **Ni2** and **Ni3** is slightly larger than Ni1 complex. Furthermore, the C1-Ni-P1 angle in **Ni2** and **Ni3** was found to be *cis*-angle (<105°), suggesting that these catalysts will be able to initiate ethylene polymerization.[59]

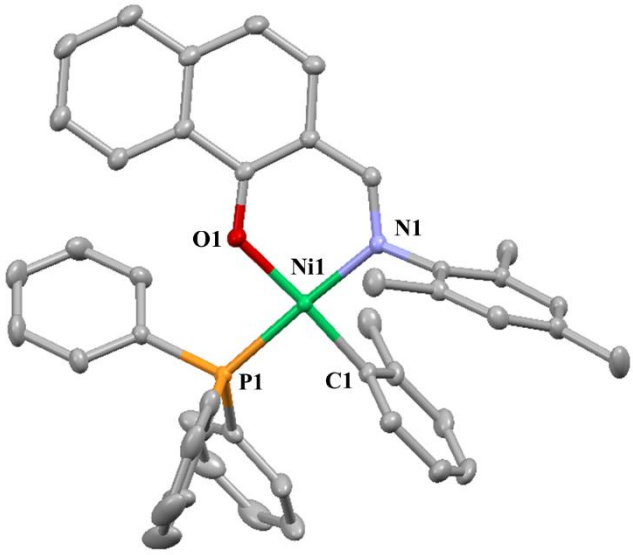

Figure 3.2: Molecular structure of **Ni1**. H-atoms have been omitted for clarity; thermal ellipsoids are drawn at the 50% probability level. Important bond distances and angles; Ni1-C1 1.89 Å, Ni1- O1 1.89 Å, Ni1-N1 1.92 Å, Ni1-P1 2.18 Å, C1-Ni1-P1 87.05°, O1-Ni1-P1 89.37°, N1-Ni1-P1 176.42°, C1-Ni1-N1 91.55°, O1-Ni1-N1 92.07°, C1-Ni1-O1 176.33°.

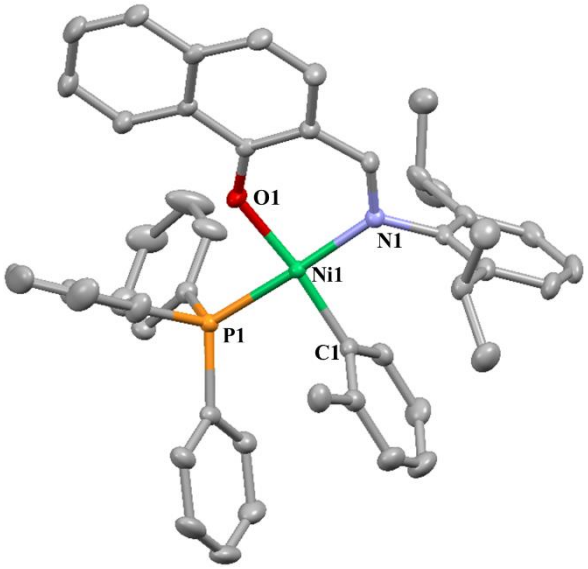

Figure 3.3: Molecular structure of **Ni2**. H-atoms have been omitted for clarity; thermal ellipsoids are drawn at the 50% probability level. Important bond distances and angles; Ni1-C1 1.89 Å, Ni1-O1 1.89 Å, Ni1-N1 1.93 Å, Ni1-P1 2.19 Å, C1-Ni1-P1 87.73°, O1-Ni1-P1 85.94°, N1-Ni1-P1 175.47°, C1-Ni1-N1 93.88°, O1-Ni1-N1 92.57°, C1-Ni1-O1 173.38°.

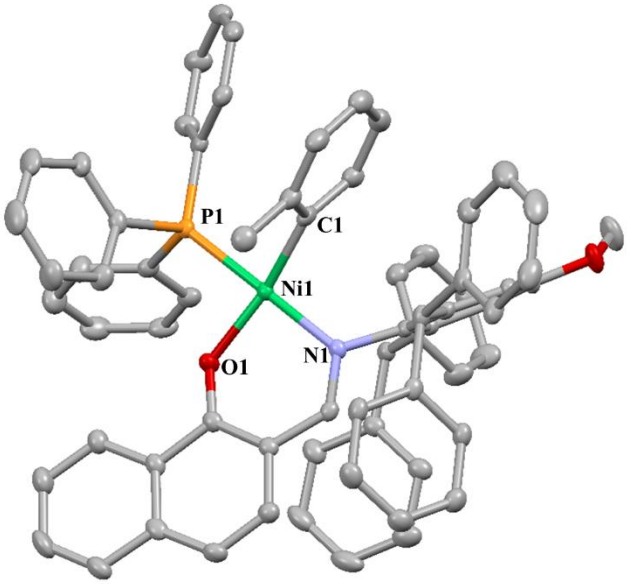

Figure 3.4: Molecular structure of **Ni3**. H-atoms have been omitted for clarity; thermal ellipsoids are drawn at the 50% probability level. Important bond distances and angles; Ni1-P1 2.19 Å, Ni1-O1 1.90 Å, Ni1-N1 1.92 Å, Ni1-C1 1.90 Å, P1-Ni1-O1 85.18°, P1-Ni1-N1 171.69°, P1-Ni1-C1 90.40°, O1- Ni1-N1 92.40°, O1- Ni1-C1 167.2°, N1-Ni1-C1 93.6°.

3.3.3. Insights on steric bulk:

As noted in scheme 3.2 and figures 3.2 to 3.4, the size of the imine-substituent increases from methyl to isopropyl to dibenzhydryl in **Ni1, Ni2, Ni3** respectively. In our attempts to quantify the steric bulk and to correlate the effect of steric bulk on polymerization activity, molecular weight, etc. we performed buried volume measurements using readily available Cavallo's SambVca 2.1 program (Figure 3.5).[60] The **Ni1** complex with simple methyl (Me) substituent displayed a buried volume of 47.5% (Vbur = 47.5 %), and **Ni2** with isopropyl substituent disclosed an almost similar buried volume of 47.3. While **Ni3** with the bulky dibenzhydryl substituent revealed a higher buried volume of 49.1%. Thus, the ligand covers more space around the nickel in **Ni3** and should provide higher steric bulk.[28]

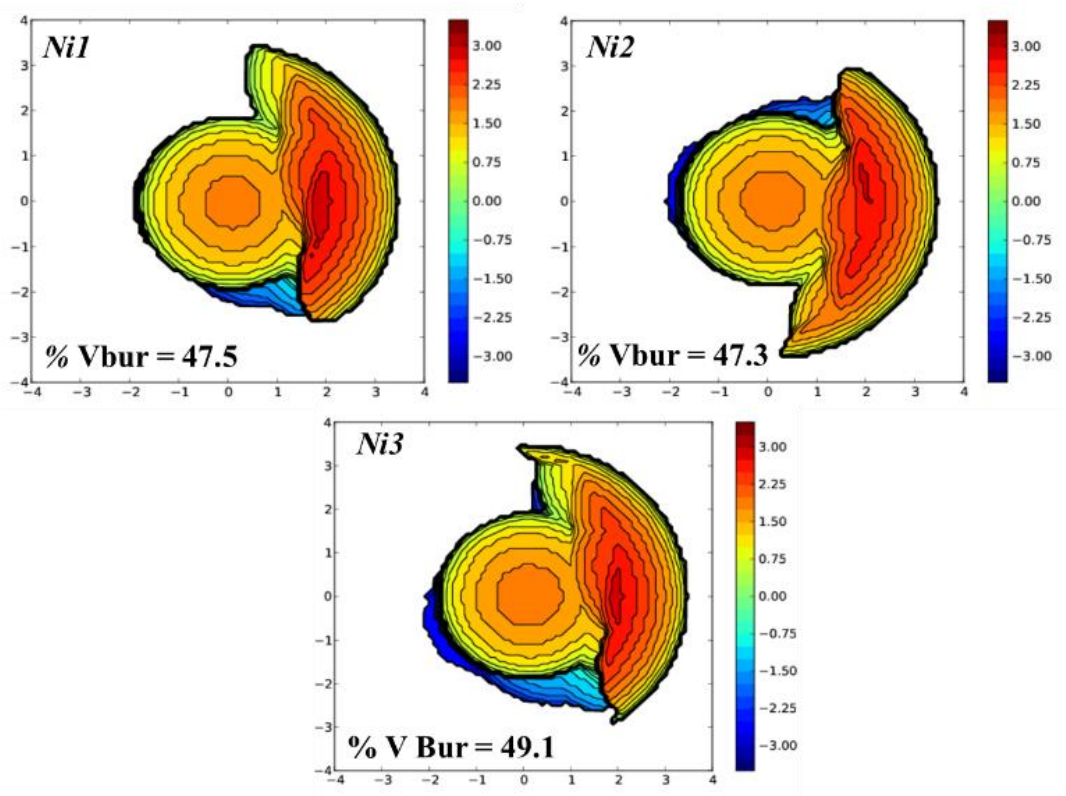

Figure 3.5: Topographic steric maps of nickel complexes **Ni1**, **Ni2**, and **Ni3**.

3.3.4. Ethylene polymerization:

After fully establishing the existence of **Ni1-Ni3** and their steric properties, we set out to examine their performance in ethylene polymerization. Ethylene polymerization study was carried out using **Ni1-Ni3** catalysts and $[Ni(COD)_2]$ or $B(C_6F_5)_3$ as co-catalysts (to scavenge phosphine). The ethylene polymerization was carried out in a Buchi high-pressure reactor using **Ni1** catalyst and $[Ni(COD)_2]$ as cocatalyst at 60 °C and 20 bar ethylene for 20 minutes (Table 3.1, Entry 1). After completion, excess ethylene was vented and the reaction mixture was poured into the acidic methanol to precipitate the polyethylene. Only 3 mg of polyethylene was observed under these conditions. Next, the polymerization temperature was increased to 70 °C and 80 °C to produce 28 mg and 204 mg of polyethylene respectively. With a further increase in temperature to 90 °C, polyethylene yield (124 mg) was found to reduce, due to the thermal decomposition of the catalyst.[61]

Subsequently, the **Ni2** catalyst was examined in ethylene polymerization. Under similar reaction conditions to that of **Ni1**, (20 bar ethylene pressure, 60 to 90 °C temperature and $[Ni(COD)_2]$ as cocatalyst to ensure a meaningful comparison), **Ni2** produced a little more (14 mg) amount of product (Table 3.1, entry 5). With an increase in polymerization temperature at constant ethylene feed, an increase in polyethylene yield was observed (Table 3.1, entries 6 and 7). The highest yield 2.42 g was observed at 90 °C with a TOF reaching 2.65×10^4 mol of

PE/mol of Ni h^{-1}. Next, the bulkier **Ni3** complex was tested in ethylene polymerization under similar reaction conditions. At a temperature of 60 °C and 20 bar ethylene pressure, the formation of 0.42 g of polyethylene was observed. An increase in temperature to 70 °C and 80 °C resulted in increased polyethylene production (1.74 g and 3.23 g, respectively). Further increasing the temperature to 90 °C led to reduced polyethylene yield (2.23 g; Table 3.1, entry 14). Thus, **Ni3** outperformed the other catalyst and 80 °C was found to be the most optimal polymerization temperature (Figure 3.6). At 80 °C the catalyst is thermally stable and displayed highest activity.

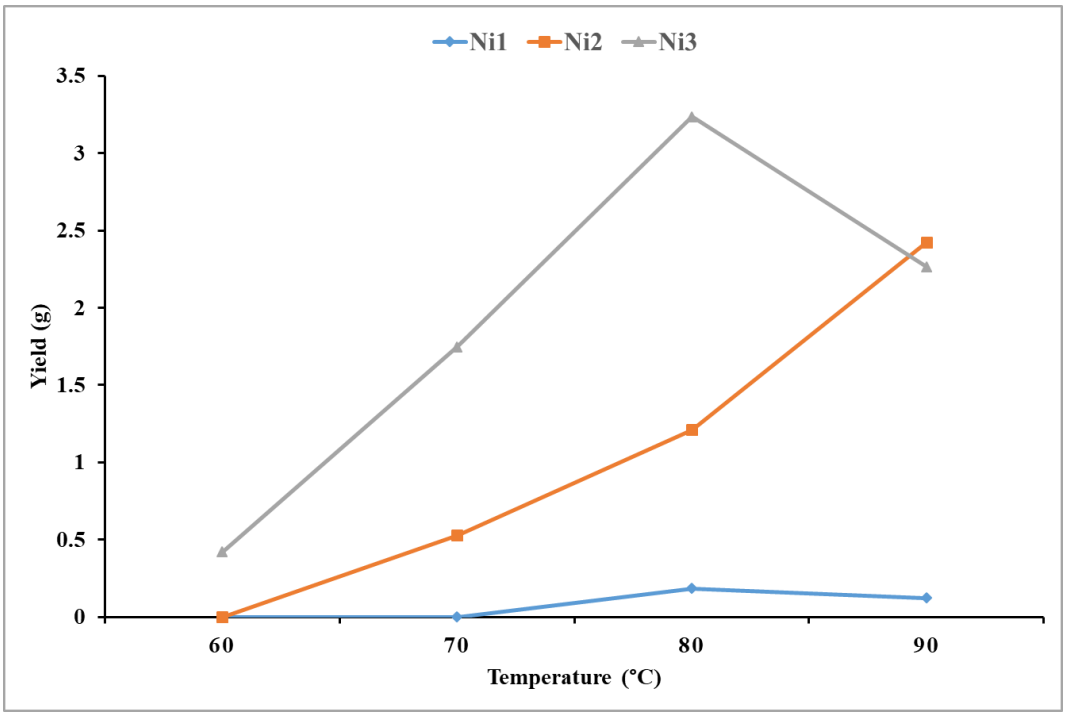

Figure 3.6: Plot of polyethylene yield versus polymerization temperature using catalysts **Ni1**, **Ni2**, and **Ni3**.

After identifying the best-performing catalyst and optimal temperature, we turned our attention towards ethylene pressure. The reaction was performed between 10-25 bar ethylene pressure and activity was recorded. It was found that with increasing ethylene pressure, the yield of the polyethylene increased up to 20 bar. With further higher ethylene pressure (25 bar), the yield of the polyethylene reduced (entry 15-17 versus entry 13). This could be because of the higher chain transfer to the monomer at higher ethylene pressure. The polymerization time was screened and the reaction was carried out for 10, 20, and 30 minutes (Table 3.1, entries 10-12). At 10 minutes, the TOF of the catalyst was 1.66×10^4 mol of PE/mol of Ni h^{-1} and at 20 minutes, an increase in TOF was observed (TOF = 1.95×10^4 mol of PE/mol of Ni h^{-1}). A longer polymerization time of 30 minutes led to a reduced TOF of 1.65×10^4 mol of PE/mol

of Ni h^{-1}. These observations suggest that, after 20 minutes of polymerization, the catalyst slowly deactivates. When the reaction was performed in the presence of $B(C_6F_5)_3$ as cocatalyst, TOF was almost comparable with $[Ni(COD)_2]$ co-catalyst (Table 3.1, entry 13 vs. entry 19).

3.3.5. Polyethylene analysis:

Polyethylene microstructure is a crucial parameter that differentiates one polyethylene from another, such as oligoethylenes or branched PE (HDPE, LLDPE, LDPE, etc.).[62] Therefore, the determination of polyethylene microstructure will allow us to gauge the potential of the PE. Thus, the PE produced under optimal conditions was dissolved in deuterated tetrachloroethane and a high-temperature NMR (80 °C) was recorded. The chain-end methyl group, as well as the methyl branch, appeared at 0.91 ppm in a ^{1}H NMR spectrum. The ^{1}H NMR peak at 1.33 ppm corresponds to the methylene ($-CH_2-$) group from the polymer backbone (Figure S3.35). The nickel catalyst **Ni1** produced a polyethylene with ~54 branches per 1000 carbon atoms. The **Ni2** complex equipped with diisopropyl substituent displayed ~43 branches per 1000 carbon atoms and the **Ni3** catalysts with sterically crowded dibenzhydryl substituent revealed only ~28 branches per 1000 C atoms (Figure 3.7). It was observed that with higher steric hindrance, the number of branches per 1000 carbon atoms was reduced. These observations suggest that the steric hindrance plays a crucial role and directly controls branching in polyethylene. These results are consistent with findings in the literature about the role of steric hindrance in controlling the branching of polyethylene.[12,13,15,26,27,40,47]

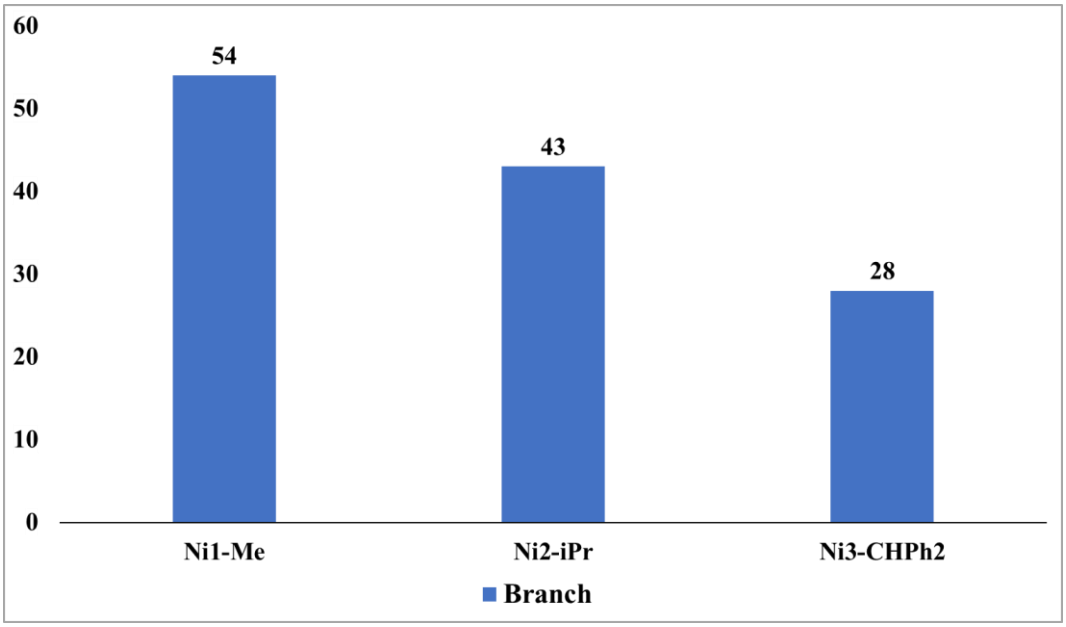

Figure 3.7: Comparison of branches (per 1000 carbon atoms) in polyethylene obtained using **Ni1, Ni2,** and **Ni3** (entry no. 3, 7 and 13)**.**

In our attempts to understand the type of branches (methyl, ethyl, propyl, isopropyl, etc.), the polyethylene produced by **Ni1**-**Ni3** was subjected to ^{13}C NMR analysis (Figure 3.8). The presence of methyl branch ($1B_1$) at 19.9 ppm, CH carbon (brB_1) at 32.9 ppm, and methylene group in the backbone (γB_1) at 29.7 ppm was identified based on the literature report.[63] As evident in Figure 3.8, the polyethylene produced by **Ni1** and **Ni2** displayed higher branching (like ethyl, propyl, and long chain branching). The type of branch [($1B_2$), (brB_2), (βB_2), (αB_3), ($1B_n$), ($2B_n$), etc.] and their chemical shifts have been mapped based on the literature reports.[64] As evident in Figure 3.8, sterically less crowded **Ni1** and **Ni2** catalysts displayed methyl, ethyl, propyl, and long-chain branching. While, sterically more crowded dibenzhydryl substituted **Ni3** catalyst revealed the presence of only methyl branch, leading to the generation of linear polyethylene.

As polymerization temperature increases, resulting polymer melting temperature (T_m) decreases, causing reduction in % crystallinity due to branched structures. These trends are consistent for all three nickel catalysts (Ni1-Ni3).

The effect of ethylene pressure on polyethylene characteristics was investigated at 10, 15, 20, and 25 bars at 80 °C. Although drawing a direct correlation between ethylene pressure to polyethylene melting temperature and % crystallinity may not be correct, following observation were made during our study. At a higher ethylene pressure of 25 bar, the melting temperature of the resultant PE was found to be 99.6 °C along with 36.5% of crystallinity. When the pressure was lowered to 20 bar, both, the T_m (96.3 °C) and % crystallinity (28.5%) reduced. The subsequent reduction in ethylene pressure to 15 and 10 bar further lowered the melting temperature and crystallinity. The molecular weight findings suggest that with decreasing ethylene pressure the rate of insertion decreases leading to the formation of low molecular weight polyethylene.

The molecular weight of the resultant PE was determined using high-temperature gel permeation chromatography (HT-GPC). It was observed that with increasing polymerization temperature, the number average molecular weight increases. For instance, at 70 °C, M_n was 39000 Da (Table 3.1, entry 10); at 80 °C, it increased to 61000 Da (Table 3.1, entry 13); and at 90 °C, it further increased to 70000 Da (Table 1, entry 14). Additionally, an increase in pressure led to higher molecular weights (Table 3.1, entry 14 versus 15). It was also observed that increase in ligand steric hindrance, (**Ni1**-**Ni3**) results in a higher molecular weight, as indicated by the data in Table 3.1 entries 3, 7, and 13. The powder diffraction data suggest that PE chains crystallize in orthorhombic structure. Also, it suggests that with increasing branch content, the

crystallinity reduces. In Ni1 case, 54 branches are present per 1000 C-atoms, and therefore, it displays low crystallinity (section 3.5.10).

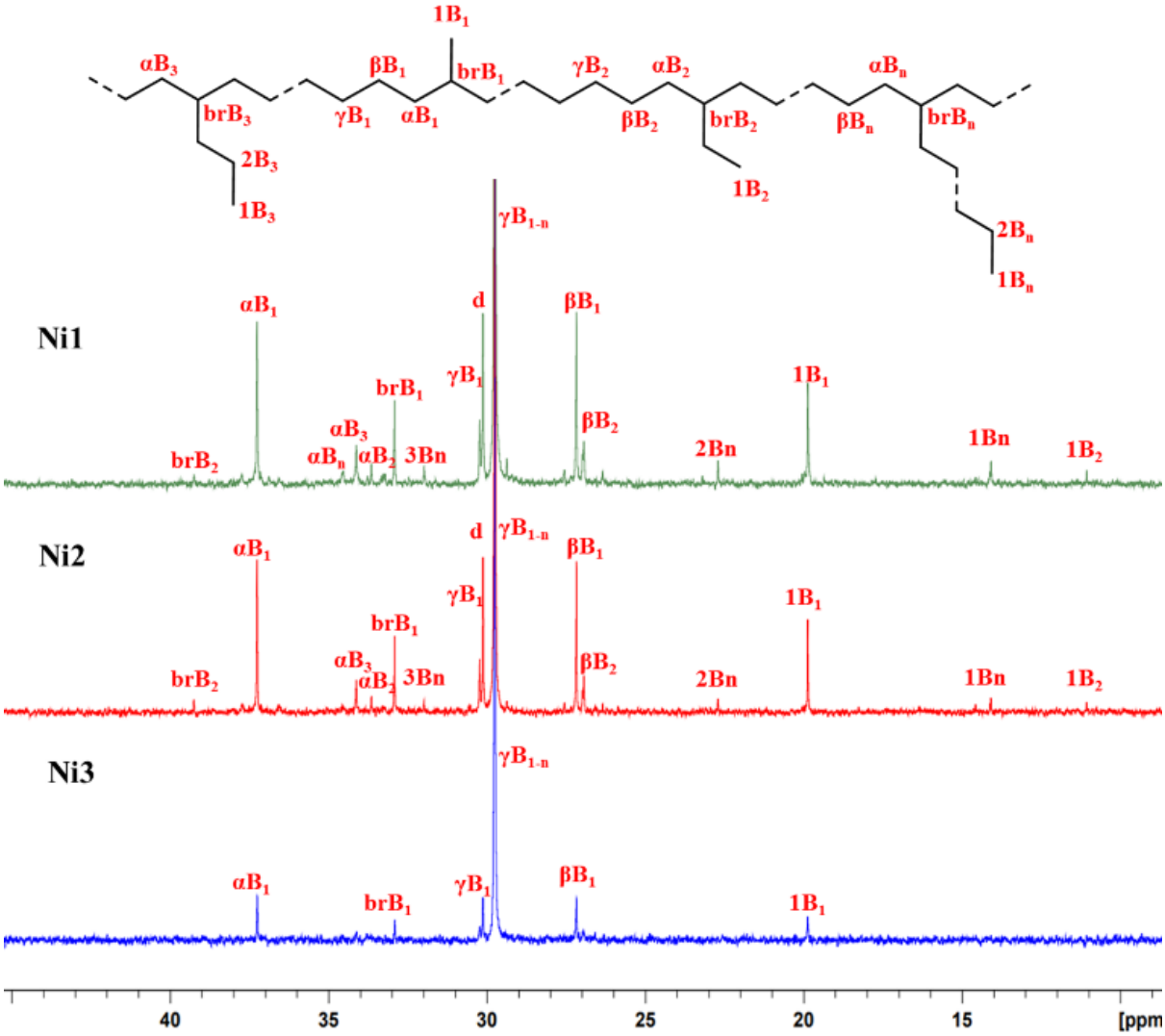

Figure 3.8: ^{13}C NMR spectra of polyethylene obtained from Ni1, Ni2 and Ni3 in $C_2D_2Cl_4$ at 80 °C (Entry no. 3, 7 and 13).

Table 3.1: Ethylene polymerization using nickel catalysts **Ni1-Ni3**.

Entry	Cat.	Temp. (°C)	Press. (bar)	Time (min.)	Yield (g)	TOF × 10^4	T_m	% of cryst.	M_n× 10^3	M_w× 10^3	PDI
1.	Ni1	60	20	20	0.003	-	97.5	16.8	-	-	-
2.	Ni1	70	20	20	0.026	0.028	94.4	27.8	-	-	-
3.	Ni1	80	20	20	0.185	0.204	83.1	11.7	3.9	7.9	2
4.	Ni1	90	20	20	0.124	0.135	75.93	12.8	-	-	-
5.	Ni2	60	20	20	0.014	0.015	107.0	49.0	-	-	-

6.	Ni2	70	20	20	0.528	0.578	101.7	32.3	-	-	-
7.	Ni2	80	20	20	1.210	1.325	94.6	24.9	6.6	13.2	2
8.	Ni2	90	20	20	2.423	2.65	80.5	10.4	-	-	-
9	Ni3	60	20	20	0.42	0.46	114.4	63.4	-	-	-
10	Ni3	70	20	20	1.748	1.95	106.3	55.1	39.0	100	2.5
11	Ni3	70	20	10	0.767	1.66	107.3	32.1	-	-	-
12	Ni3	70	20	30	2.265	1.65	107.6	47.7	-	-	-
13	Ni3	80	20	20	3.236	3.54	96.3	28.5	61.0	160	2.6
14	Ni3	90	20	20	2.235	2.4	81.4	11.5	70.0	113	1.6
15	Ni3	80	25	20	2.862	3.13	99.6	36.5	114	270	2.3
16	Ni3	80	15	20	3.186	3.49	89.1	23.5	-	-	-
17	Ni3	80	10	20	1.611	1.76	78.3	13.9	48.0	114	2.3
18[a]	Ni3	70	20	90	2.260	0.38	94.5	31.2	75.0	150	1.9
19[b]	Ni3	80	20	20	3.053	3.37	99.6	30.5	-	-	-
20[b]	2Pd 1	80	20	90	0.298	525	-	-	-	-	-

Reaction conditions: Toluene- 100 mL, Catalyst- 9.79 µmol., Co-catalyst [$Ni(COD)_2$] = 2 equivalent, Ethylene pressure- 10 to 25 bars, TOF in (mol of PE / mol of Ni h^{-1}), (-)- Not Determined. The reported yield is after re-precipitating the polyethylene in acidic methanol and drying in high vacuum for 4 hours. T_m and % of crystallinity was calculated from DSC. [% Crystallinity = ΔHm /ΔHm° (J/g) ×100]. Molecular weight, PDI was recorded using HT-GPC in TCB at 160 °C against polystyrene standards. a = catalyst-15 mg, Co-catalyst [$(C_6F_5)_3B$]- 2 equivalent, [b]Cocatalyst: [$(C_6F_5)_3B$] 1 equivalent, [c]Taken from the Ref. 56.

3.3.6. Comparison with corresponding Pd-catalysts:

To know where **Ni1**-**Ni3** catalysts stand in terms of activity, molecular weight, and branching, we compare the performance of these nickel catalysts with literature-reported corresponding palladium catalysts **2Pd1** (Figure 3.10).[56] Before we compare their performance in ethylene polymerization, it would be worth noting the structural similarities and differences between the two metal catalysts. Both the catalysts (**Ni3** and **2Pd1**) are ligated by the same ligand, i.e. 2L1. A single crystal X-ray diffraction data is depicted in Figure 3.9. The geometry around the Ni and Pd is distorted square-planar and bond distances (O-M and N-M) for **Ni3** were shorter than **2Pd1**.

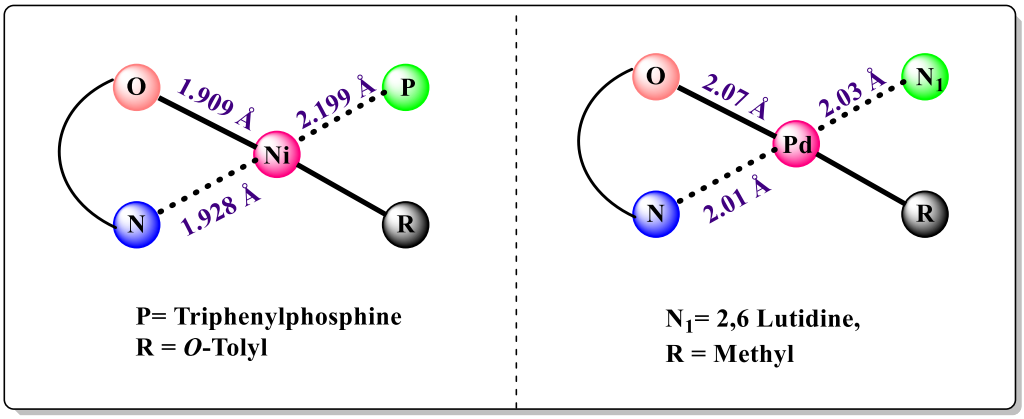

Figure 3.9: Comparative single crystal data (bond distance) for nickel (Ni3) and palladium (2Pd1) catalysts.

Ethylene (20 bar) polymerization using **2Pd1** catalyst at 80 °C produced low molecular weight (950 Da) viscous oily material, with a TOF value of 525 mol of PE / mol of Pd h^{-1} and shows 85 branches per 1000 carbon atoms. While, the nickel analog, nickel catalyst (**Ni3**) revealed a TOF of 35400 mol of PE/mol of Ni h^{-1}, along with the high molecular weight polymer (61000 Da) with much lower branching (28 branches per 1000 carbon atoms) (Figure 3.10).

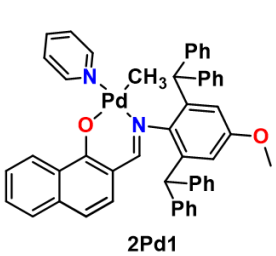

2Pd1

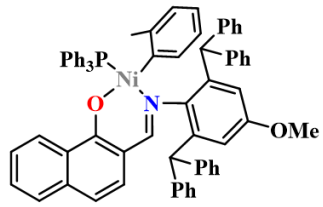

Ni3

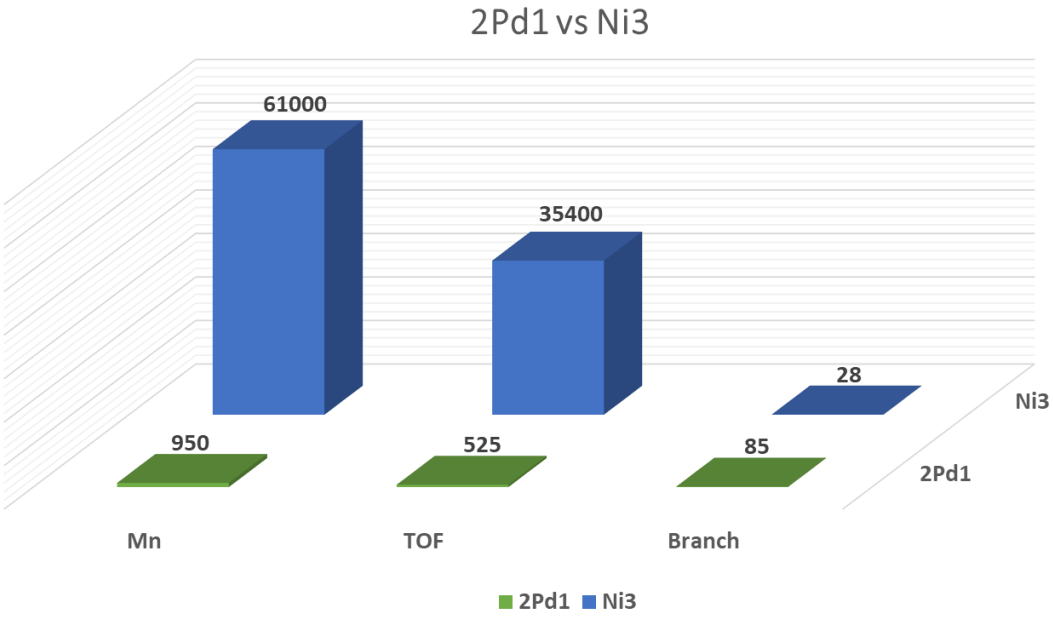

Figure 3.10: 2L1 ligated palladium catalyst (**2Pd1**) (top); comparison of TOF, molecular weight and branching between **Ni3** and **2Pd1** catalyzed ethylene polymerization (bottom).

The oligo/polyethylene produced by 2Pd1 displayed a hyperbranched microstructure with methyl, ethyl, propyl, and sec-butyl (that is branch on branch) branches (Figure 3.11). The palladium catalyst (**2Pd1**) shows extensive chain walking during the polymerization and yields hyperbranched polymer. In the literature, it was observed that Pd catalysts produce lower molecular weight polymers with a higher degree of branching.[62,65,66] However, the nickel catalyst (**Ni3**) revealed a higher rate of insertion than that of the chain walking and produced linear polyethylene with up to 63% crystallinity. A comparison of polyethylene produced by Ni3 and Pd1 is presented in Table 3.2.

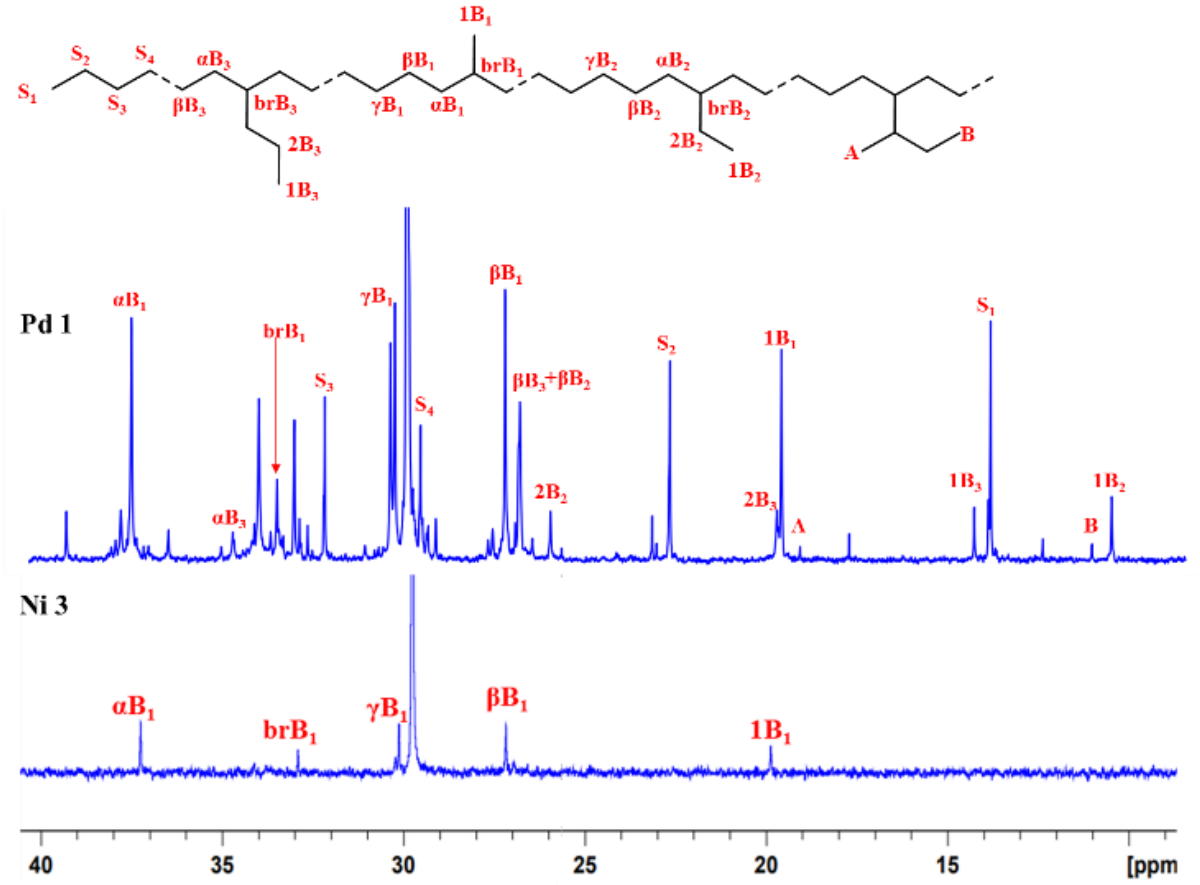

Figure 3.11: Comparative ^{13}C NMR spectra of polyethylene obtained using palladium (2Pd1) and nickel (Ni3) catalyst.

Table 3.2: A comparison of properties of polyethylene produced by Ni3 and 2Pd1 catalysts.

Entry no.[#]	Catalyst	T_m (°C)	% of Cryst.	Branch/ 1000C[a]	Methyl (%)[b]	Ethyl (%)[b]	Propyl (%)[b]	LCB (%)[c]	*Sec.*-Butyl (%)[b]
3.	Ni1	83.1	11.7	54	82.1	6.5	6.3	4.9	0
7.	Ni2	94.6	24.9	43	83.1	6.0	6.3	4.4	0
9.	Ni3	114.4	63.4	20	>99	0	0	0	0
13.	Ni3	96.3	28.5	28	>99	0	0	0	0
17.	Ni3	78.3	13.9	55	78.9	9.7	4.7	6.5	0
20[d]	2Pd1	-	-	85	46.3	14.8	14.0	21.7	3.2

#- entry numbers are based on the table 1, [a]Branches per 1000 carbons calculated from ^{1}H NMR. [b]Relative intensities of methyl (1B1, 1B2, 1B3), and *sec*-Bu resonances calculated using ^{13}C NMR [In ^{13}C NMR only methyl branch are observed for entry no. 9 and 13]. [c]LCB = butyl and longer branches. For Entry no. 3, 7 and 17 branch content were calculated by using a qualitative ^{13}C NMR, [d]Pd catalyst produced oily oligomeric compound which are viscous liquid at room temperature and therefore a quantitative ^{13}C was recorded.

3.4. Conclusions:

In summary, the synthesis of naphthoxy imine (NI) ligands 3**L1, 2L1** and 2**L2** with increasing steric bulk has been reported. The sodium salt of ligand (3**L1,** 2**L2** and **2L1**) was treated with [NiCl(*o*-Tol)(PPh_3)$_2$] to yield the corresponding nickel complexes **Ni1, Ni2,** and **Ni3** in excellent yield. The identity of the **Ni1**-**Ni3** has been unambiguously ascertained using 1-2D NMR, mass spectroscopy, and single-crystal X-ray diffraction. The molecular structure of **Ni1**-**Ni3** revealed that the central nickel atom assumes distorted square planar geometry. The alkyl/aryl group is situated *cis* to the donor atom, suggesting the potential of these complexes in ethylene polymerization. Indeed, the three nickel complexes (**Ni1**-**Ni3**) were found to be active in ethylene polymerization. The ligand steric was quantified using buried volume calculations and was found to affect the performance of the catalyst. When exposed to ethylene **Ni1**-**Ni3** produced polyethylene with variable degree of branching. Various polymerization parameters such as temperature, time and pressure were optimized. The optimal polymerization conditions were found to be 20 bar ethylene pressure, 80 °C temperature, and a polymerization time of 20 minutes. Under these optimal conditions, **Ni3** outperformed **Ni1** and **Ni2**. The sterically bulkiest catalyst **Ni3** (49% buried volume) disclosed higher activity and produced linear PE with high crystallinity. The microstructure analysis of the resultant polyethylene displayed a clear trend, i.e. with increasing steric around the metal, the activity increases,

molecular weight increases and the branching decreases. The most successful catalyst, **Ni3**, produced high molecular weight PE with only methyl branches and displayed the highest activity. These observations suggest that higher steric hindrance suppresses β-hydride elimination, increases the rate of propagation, and reduces chain-walking.

A comparison between **Ni3** and its palladium analogous revealed that the **Ni3** catalyst outperforms **2Pd1** in terms of activity, molecular weight, and branching.

3.5. Experimental section:

3.5.1. Methods and materials:

Unless noted otherwise, all manipulations were carried out under an inert atmosphere using standard Schlenk line techniques or M-Braun glove box. Toluene, diethyl ether, 1,4 dioxane, and THF were distilled from sodium/benzophenone under an argon atmosphere. Acetonitrile, methylene chloride, and pyridine were distilled on calcium-hydride. Ethylene was supplied by Praxiar India Ltd., India. 1-Naphthol, and diisopropyl aniline were supplied by Loba Chemie and were used as received. 2, 4, 6 trimethyl aniline, $B(C_6F_5)_3$, and $[Ni(COD)_2]$ were supplied by Sigma Aldrich and were used as received. Sodium borohydride was supplied by Avara Chemicals and was used as received. P-Anisidine and paraformaldehyde were supplied by Alfa aeser and were used as received. $[NiCl(o\text{-Tol})(PPh_3)_2]$,[67] 1-hydroxy 2-napthaldehyde,[68] aniline derivative[69] were synthesized following known procedures. The insertion polymerization was run in a Büchi glasuster cyclone 075 high-pressure reactor equipped with an overhead mechanical stirrer, heating/cooling jacket, and pressure regulators.

Solution NMR spectra were recorded on Bruker Avance 200, 400 and 500 MHz instruments. Chemical shifts are referenced to external reference TMS (^1H and ^{13}C). Coupling constants are given as absolute values. Multiplicities are given as follows s: singlet, d: doublet, t: triplet, m: multiplet. High-temperature NMR (HT-NMR) of the polymers was recorded in $C_2D_2Cl_4$ solvent at 80 °C. Chemical shifts are referenced to external reference TMS (^1H and ^{13}C). Mass spectra were recorded on Thermo Scientific Q-Exactive mass spectrometer, the column specification is Hypersil gold C18 column 150 × 4.6 mm diameter 8 µm particle size mobile phase used is 90 % methanol + 10 % water + 0.1 % formic acid. Differential scanning calorimeter (DSC) was carried out on DSC Q-10 equipment from TA instruments with a heating and cooling rate of 10 K min^{-1}, unless mentioned otherwise. High-temperature Gel Permeation Chromatography (HT-GPC) of the PE was recorded in 1,2,4- trichlorobenzene at 160 °C on a Viscotek GPC (HT-GPC module 350A) instrument equipped with a triple detector system. The columns were calibrated with linear polystyrene standards and the reported

molecular weights are with respect to polystyrene standards. The molecular weight measurement for entries 3 and 7 were performed on GPC – IR5 + Visco + LS (GPC-IR-I Polymer Char) at a flow rate of 1 ml/ min on a column 3 × PL gel Olexis Mix-Bed columns (13 microns), 300 × 7.5mm + guard column. Weight-average molecular weight (Mw), number average molecular weight (Mn) and polydispersity index (PDI) of the synthesized PE were recorded using HT-GPC.

3.5.2. Synthesis of Ligand 3L1:

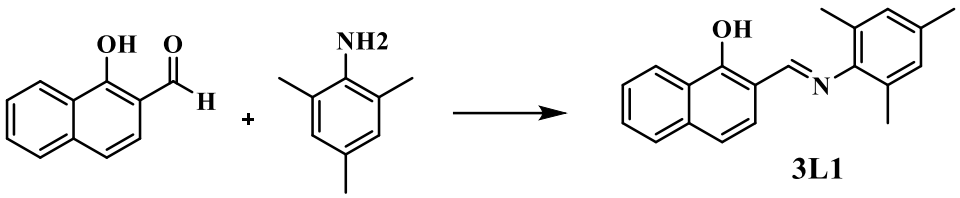

Scheme S3.1: Synthesis of naphthoxy imine ligand **3L1**.

In an oven-dried round bottom flask, 1-hydroxy 2-naphthaldehyde (0.010 mol, 1.8 g) and 2,4,6 trimethyl aniline (0.011mol, 1.55 g) were dissolved in 25 mL toluene. A catalytic amount of PTSA (5 mg) was added to the above solution and the resultant reaction mixture was refluxed for 6 hours. The color of the reaction mixture changed to yellowish; the reaction was monitored by TLC analysis. After completion of the reaction solvent was evaporated by using a rotatory evaporator and ligand was purified by silica gel column chromatography using pet ether (98%) and ethyl acetate (2%) as eluent (Yield: 2.9 g, < 99%).

^{1}H NMR (500 MHz, $CDCl_3$) δ = 14.66 (br. s., 1 H), 8.51 (d, *J* = 8.1 Hz, 1 H), 8.12 (br. s., 1 H), 7.70 (d, *J* = 8.0 Hz, 1 H), 7.59 (t, *J* = 7.4 Hz, 1 H), 7.55 - 7.46 (m, 1 H), 7.15 (d, *J* = 8.8 Hz, 1 H), 7.08 (d, *J* = 8.8 Hz, 1 H), 6.97 (s, 2 H), 2.33 (s, 3 H), 2.30 (s, 6 H). **^{13}C NMR (125 MHz, $CDCl_3$):** δ = 170.1, 163.4, 140.8, 136.9, 135.7, 130.2, 129.8, 129.4, 127.9, 127.6, 127.4, 125.4, 124.8, 116.7, 110.5, 20.9, 18.6. **ESI-MS** (positive mode): m/z = 290.1551 Da $[M+H]^+$ (observed); 290.1545 $[M+H]^+$ (calculated).

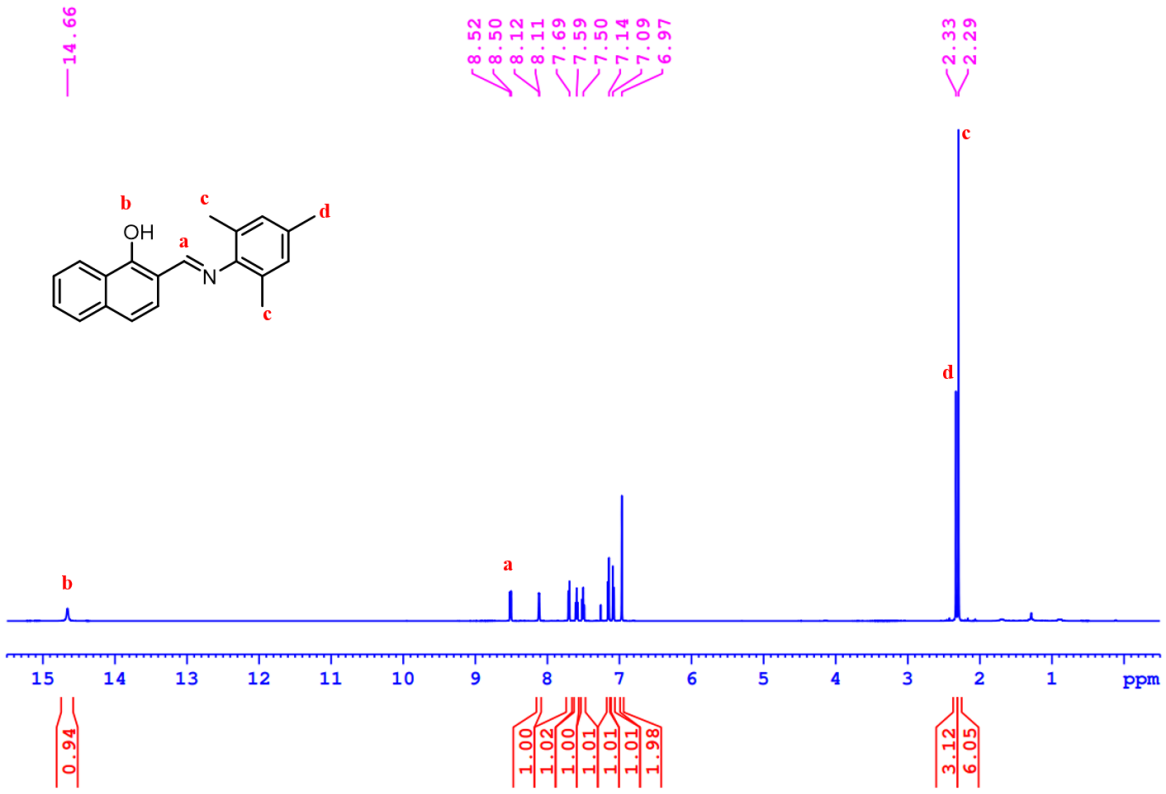

Figure S3.1: ^{1}H NMR spectrum of ligand 3L1 in $CDCl_3$.

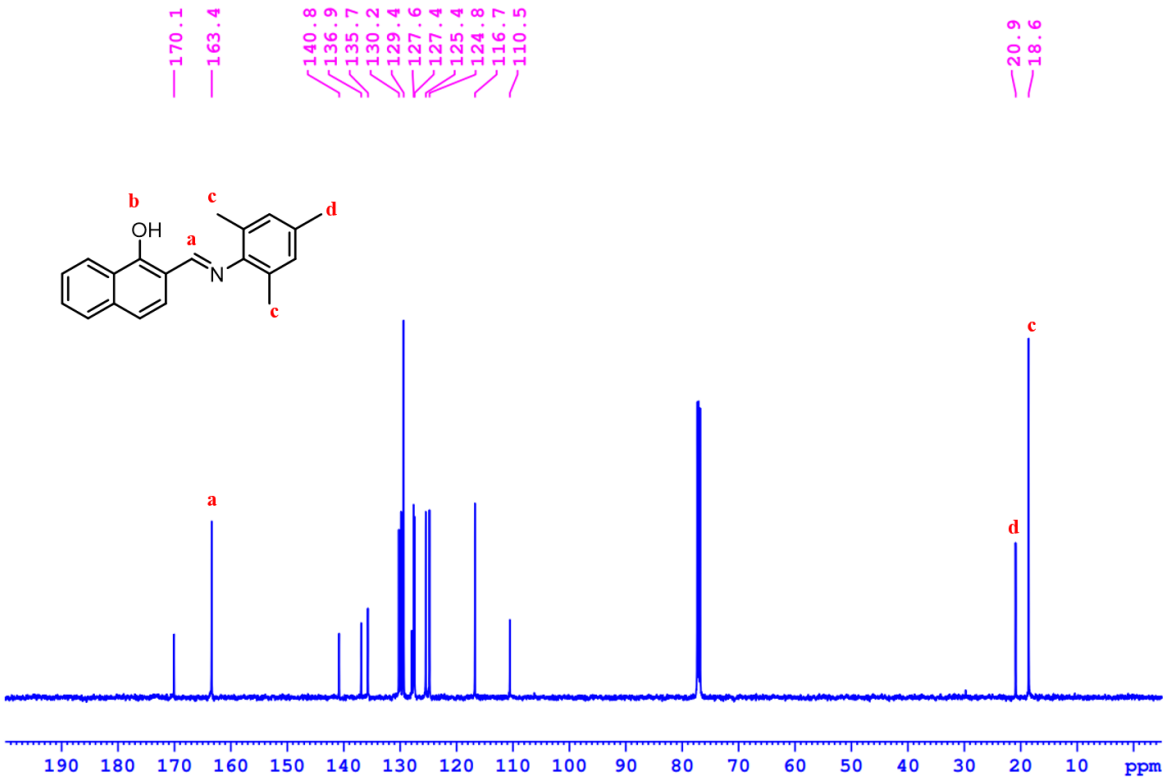

Figure S3.2: ^{13}C NMR spectrum of ligand 3L1 in $CDCl_3$.

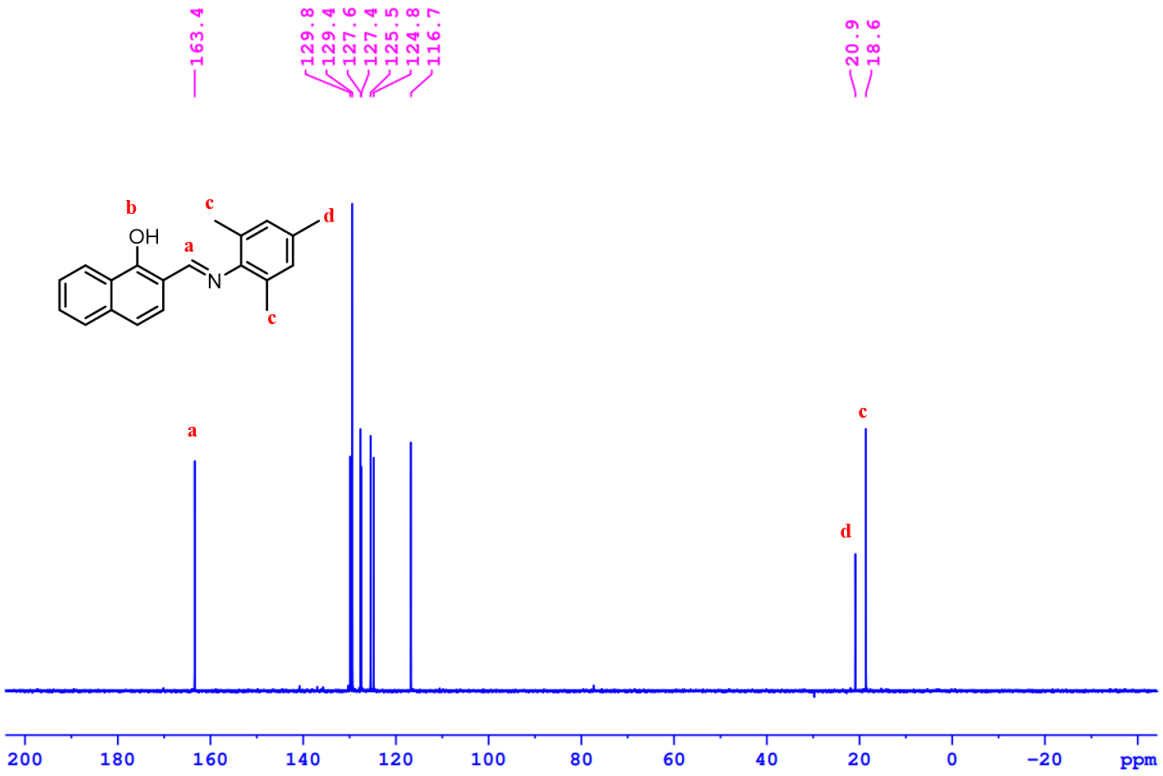

Figure S3.3: ^{13}C DEPT NMR spectrum of ligand 3L1 in $CDCl_3$.

Figure S3.4: ESI-MS data of ligand 3L1.

3.5.3. Synthesis of Ni(II) complex:

3.5.3.1. Synthesis of Ni1 complex:

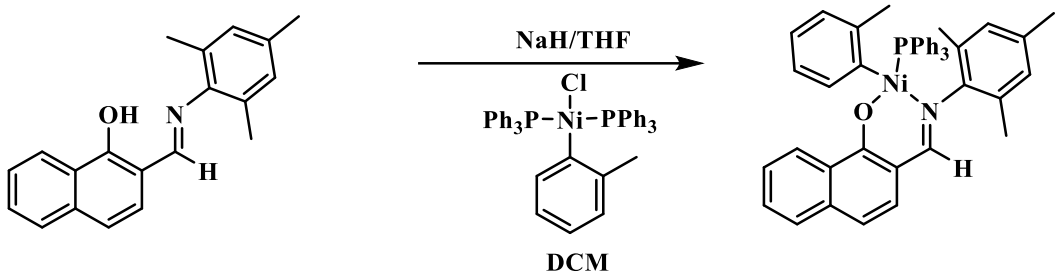

Scheme S3.2: Synthesis of Ni1 complex.

In an oven-dried Schlenk flask, NaH (13.6 mg, 0.566 mmol) and ligand L1 (81.5 mg, 0.281 mmol) were taken. The flask was cooled to 0 °C and 5 mL THF was added. The reaction mixture was stirred at 0 °C for 2 hours after that solvent was evaporated. The obtained compound was dissolved in 5 mL DCM and transferred dropwise to another flask that contained [NiCl(*o*-Tol)(PPh_3)$_2$] (200 mg, 0.281 mmol) precursor at 0 °C. The mixture was stirred at the same temperature for 2 hours and DCM was evaporated. The resultant complex was purified by recrystallization in DCM and Hexane at 0 °C (Yield-184 mg, 93%).

^{1}H NMR (500 MHz, $CDCl_3$): δ = 7.85 (d, *J* = 8.5 Hz, 1 H), 7.55 - 7.43 (m, 7 H), 7.37 - 7.29 (m, 5 H), 7.23 - 7.19 (m, 5 H), 7.07 (d, *J* = 8.2 Hz, 1 H), 6.85 (d, *J* = 8.2 Hz, 1 H), 6.73 (t, *J* = 6.7 Hz, 1 H), 6.64 (d, *J* = 7.0 Hz, 1 H), 6.56 (br. s., 1 H), 6.50 (d, *J* = 7.6 Hz, 1 H), 6.39 (br. s., 1 H), 6.31 - 6.21 (m, 1 H), 6.01 (d, *J* = 6.7 Hz, 1 H), 5.99 - 5.92 (m, 1 H), 2.62 (br. s., 3 H), 2.48 (br. s., 3 H), 2.07 (br. s., 3 H), 2.02 (br. s., 3 H). **^{13}C NMR (125 MHz, $CDCl_3$):** δ = 164.9, 164.8, 150.2, 143.2, 137.5, 137.1, 134.6, 134.5, 133.9, 133.8, 131.4, 131.0, 130.9, 129.9, 129.9, 129.7, 129.7, 128.8, 128.6, 128.6, 128.3, 128.1, 127.9, 127.9, 127.6, 126.7, 126.2, 126.0, 123.8, 121.8, 121.7, 113.6, 112.8, 26.4, 20.7, 19.7, 18.6. **^{31}P NMR (500 MHz, $CDCl_3$):** δ 25.19. **ESI-MS** (positive mode): $C_{45}H_{40}NNaNiOP$ m/z = 722.15 Da $[M+Na]^+$ (observed); 722.20 $[M+Na]^+$ (calculated).

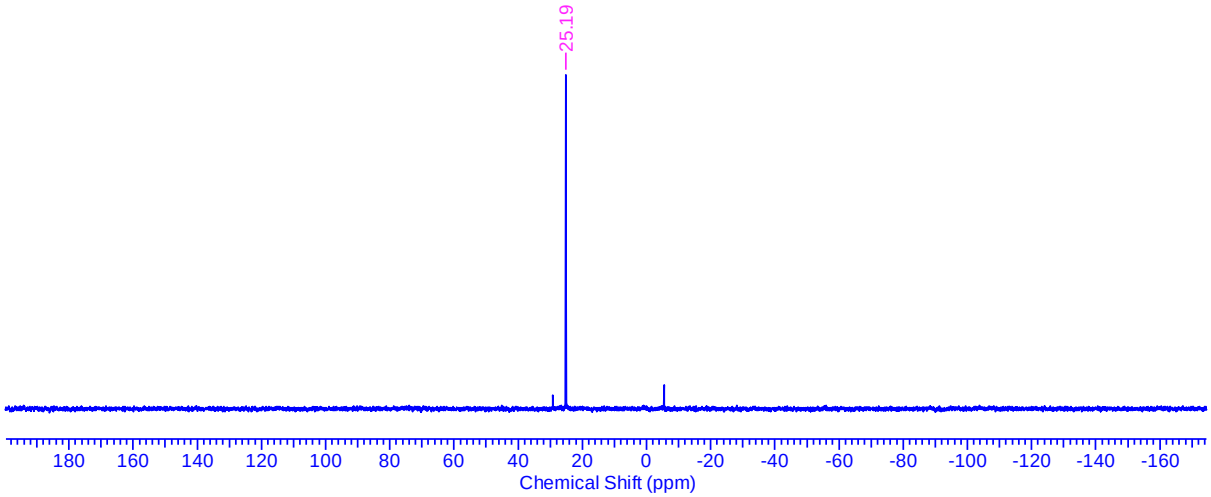

Figure S3.5: ^{31}P NMR spectrum of **Ni1** complex in $CDCl_3$.

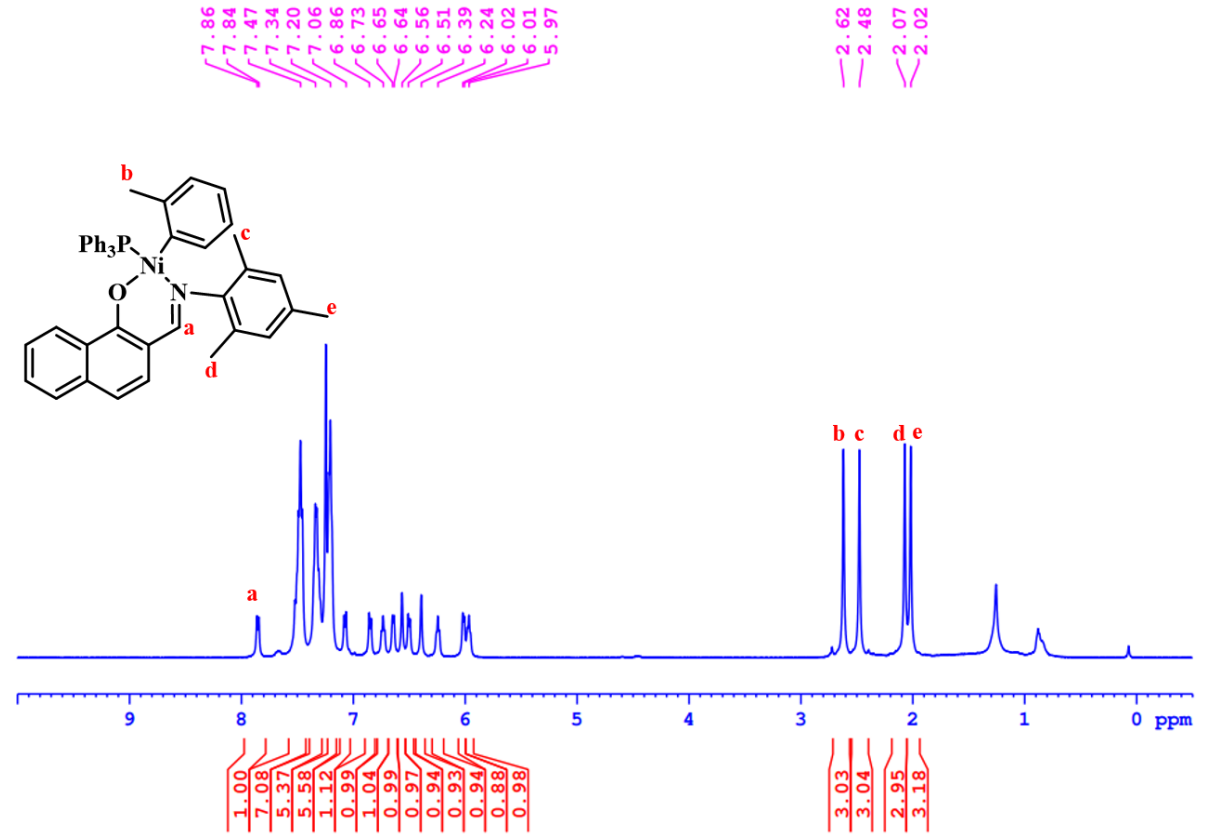

Figure S3.6: ^{1}H NMR spectrum of **Ni1** complex in $CDCl_3$.

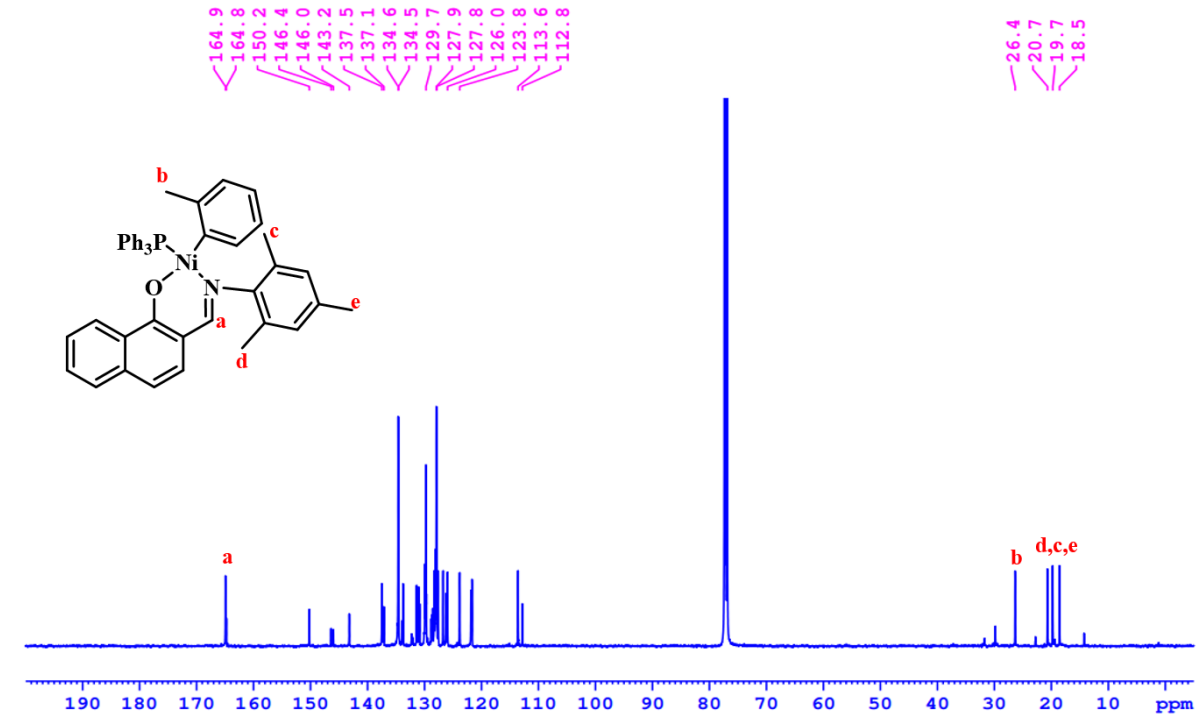

Figure S3.7: ^{13}C NMR spectrum of **Ni1** complex in $CDCl_3$.

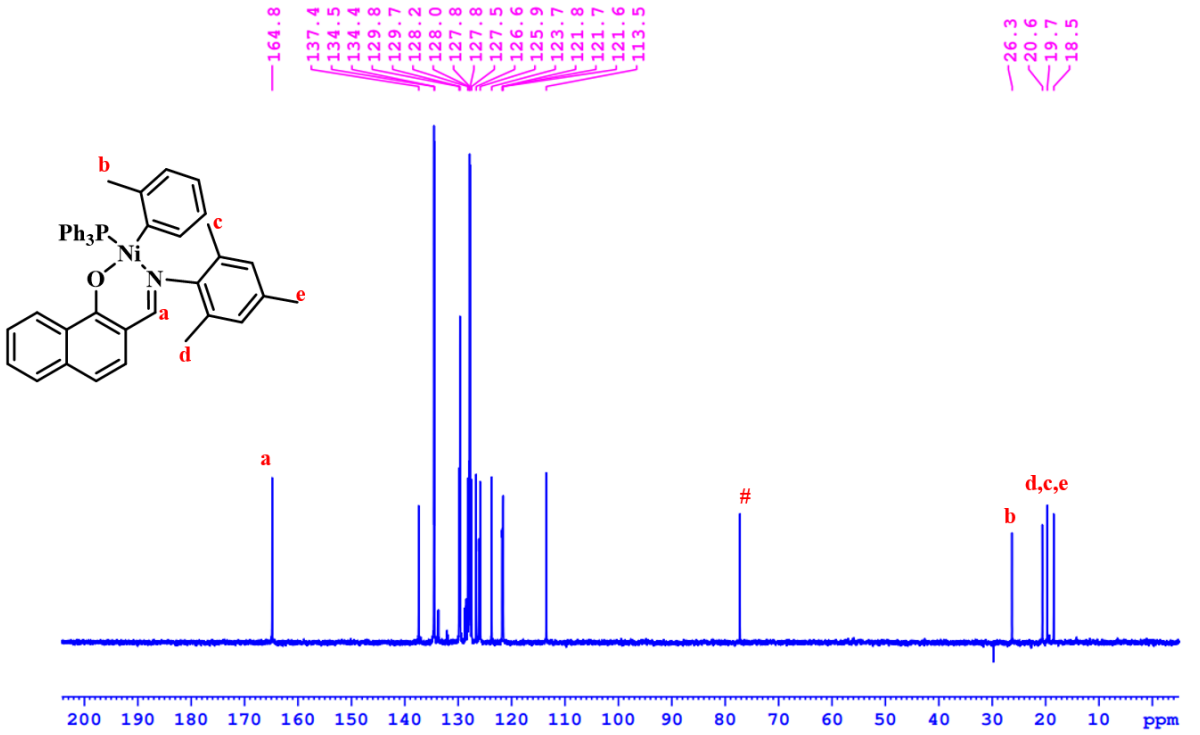

Figure S3.8: ^{13}C DEPT NMR spectrum of **Ni1** complex in $CDCl_3$.

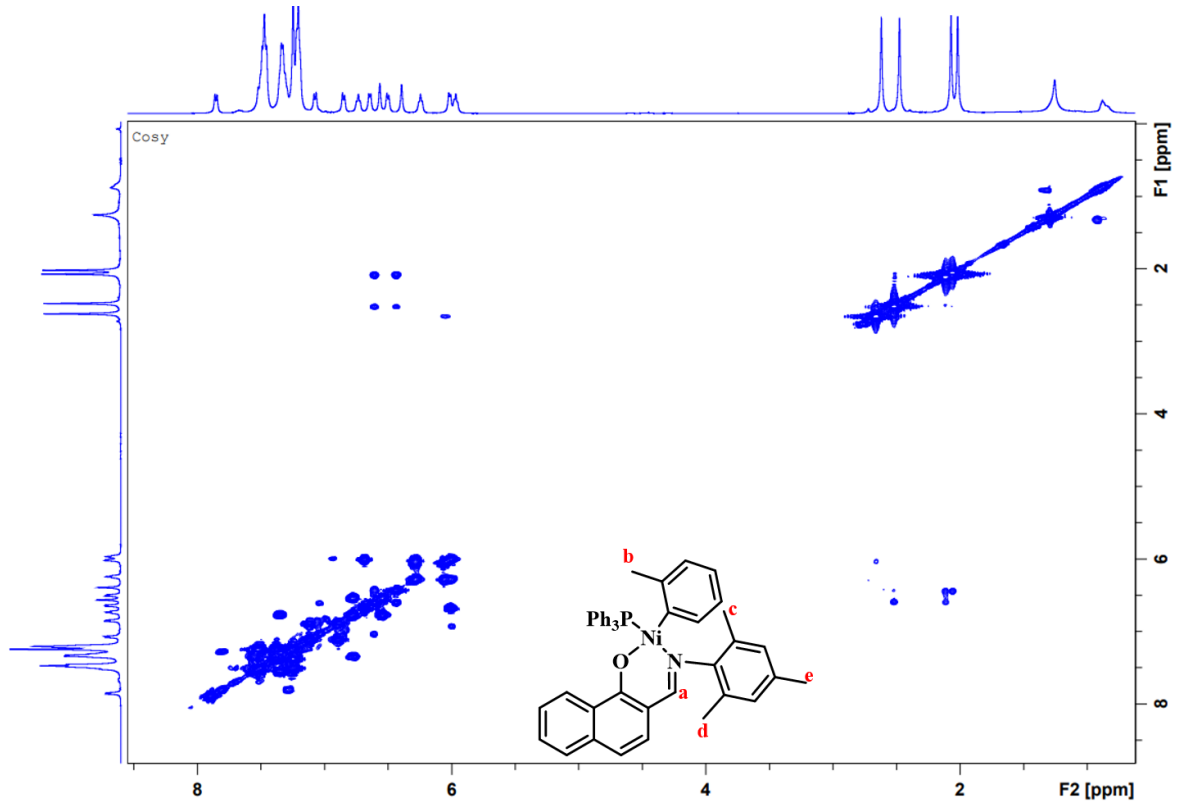

Figure S3.9: COSY NMR spectrum of **Ni1** complex in $CDCl_3$.

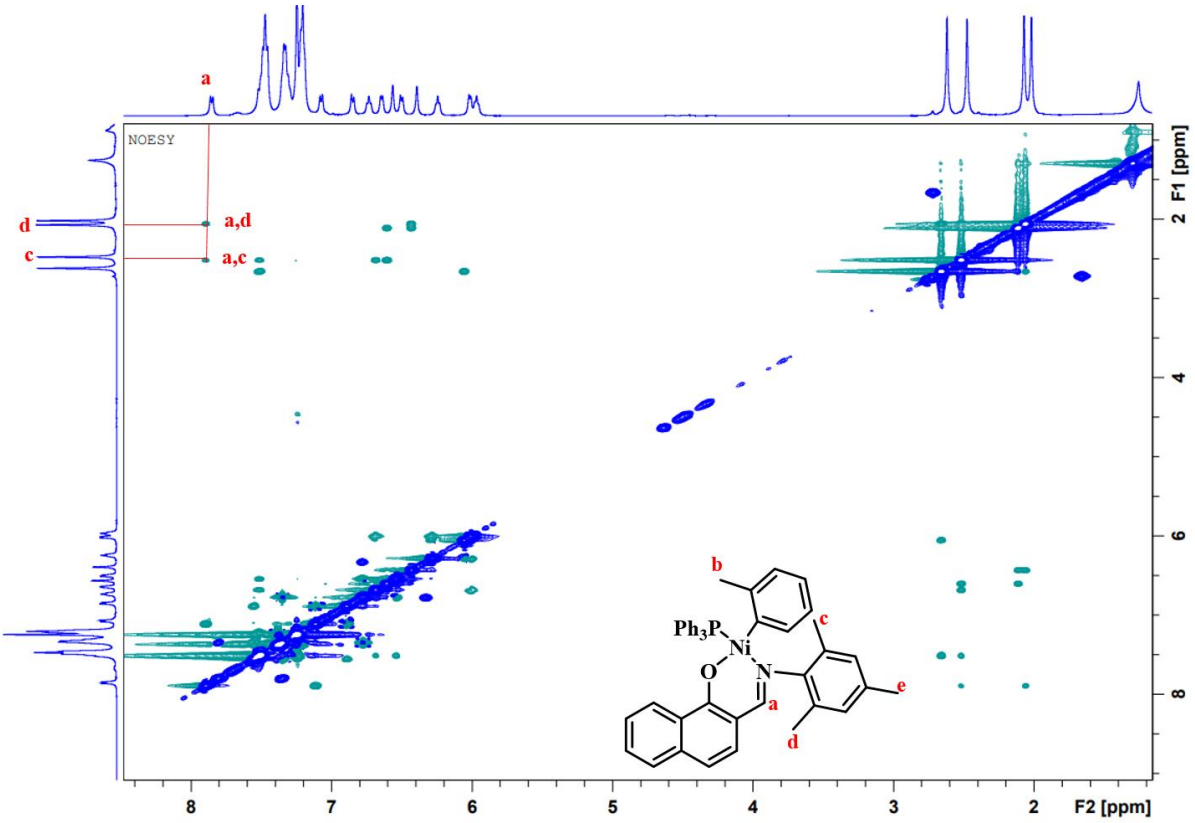

Figure S3.10: NOESY NMR spectrum of **Ni1** complex in $CDCl_3$.

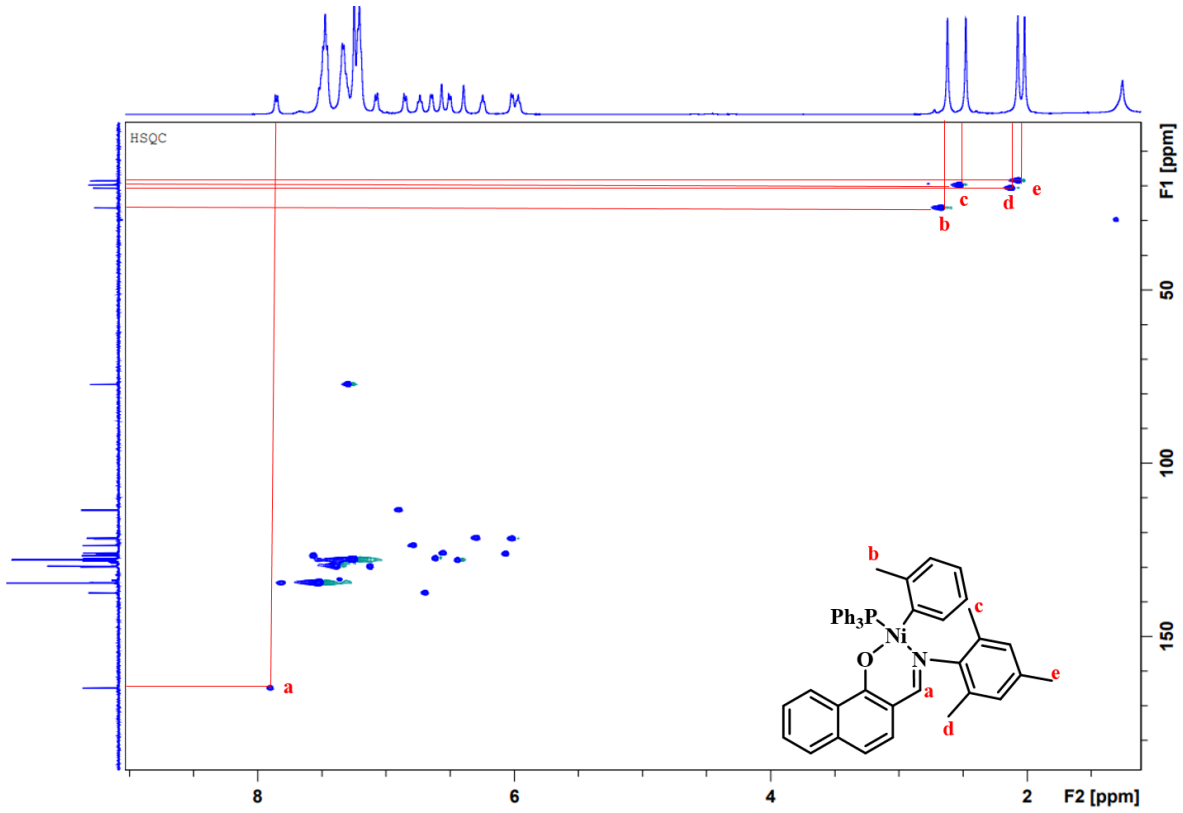

Figure S3.11: HSQC NMR spectrum of **Ni1** complex in $CDCl_3$.

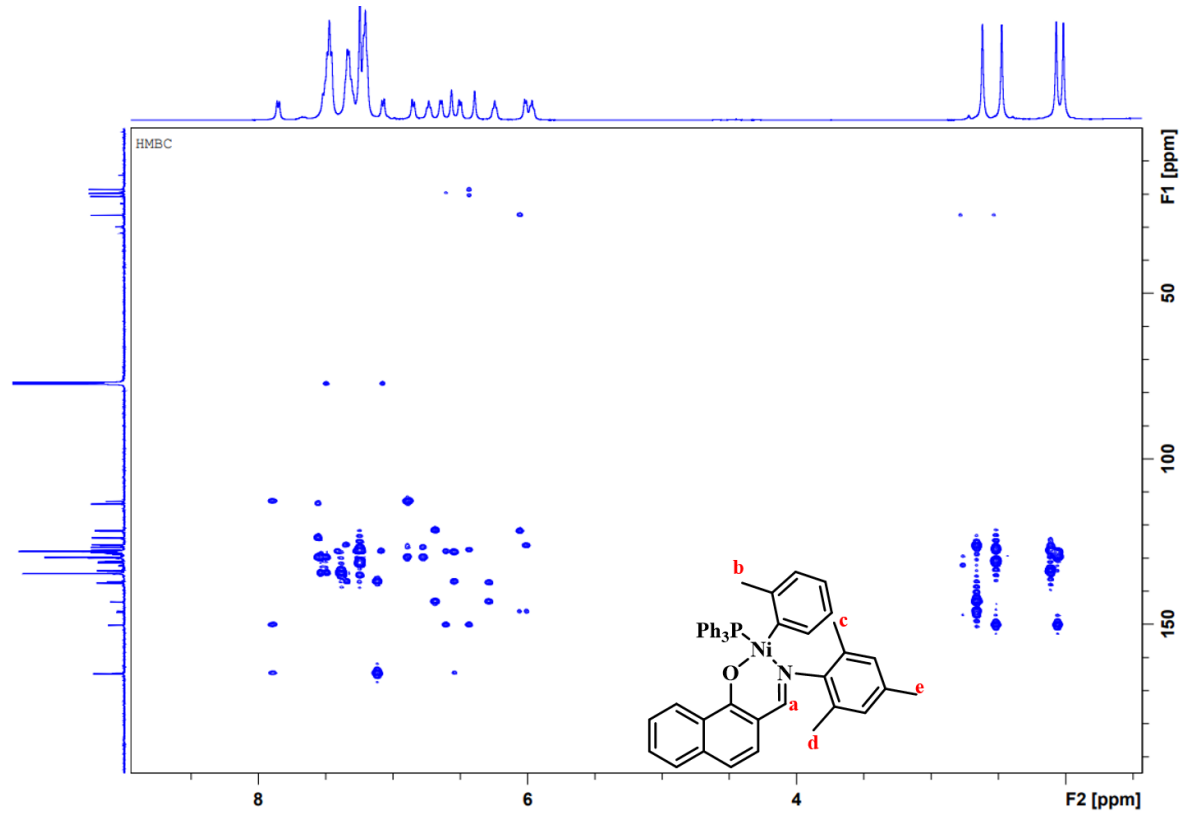

Figure S3.12: HMBC NMR spectrum of **Ni1** complex in $CDCl_3$.

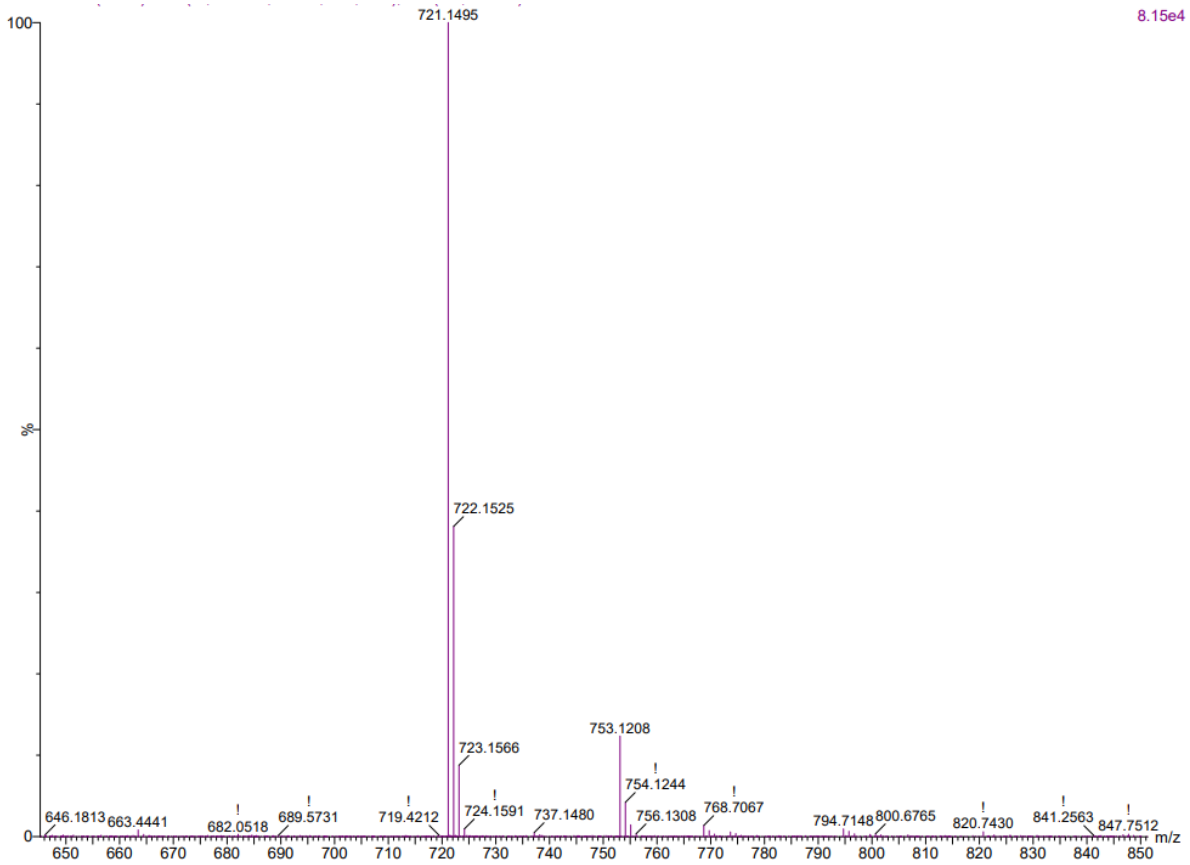

Figure S3.13: ESI-MS data of **Ni1**.

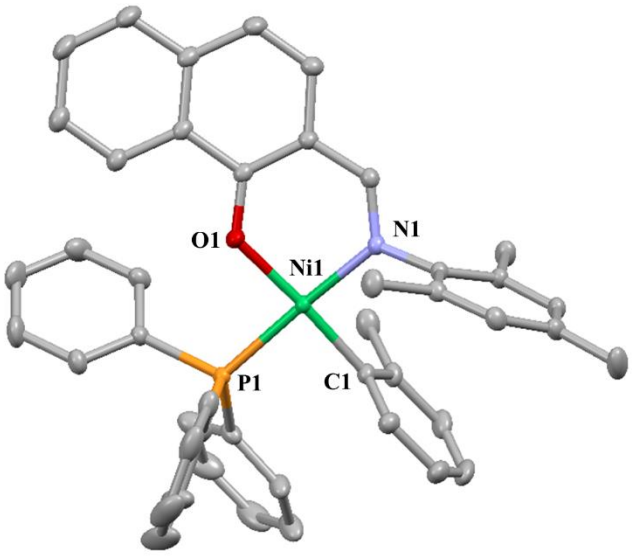

Figure S3.14: Molecular structure of **Ni1** complex.

Chart S3.1: Crystal data and structure refinement for Ni1.

```
Bond precision:   C-C = 0.0020 A          Wavelength=0.71073

Cell:           a=9.3181(12)       b=10.1498(12)     c=19.648(2)
                alpha=103.844(4)   beta=97.992(5)    gamma=92.327(4)
Temperature:    100 K

                 Calculated                  Reported
Volume           1781.5(4)                   1781.5(4)
Space group      P -1                        P -1
Hall group       -P 1                        -P 1
Moiety formula   C45 H40 N Ni O P            C45 H40 N Ni O P
Sum formula      C45 H40 N Ni O P            C45 H40 N Ni O P
Mr               700.44                      700.46
Dx,g cm-3        1.306                       1.306
Z                2                           2
Mu (mm-1)        0.626                       0.626
F000             736.0                       736.0
F000'            737.10
h,k,lmax         15,16,31                    15,16,31
Nref             15984                       14862
Tmin,Tmax        0.854,0.905                 0.660,0.747
Tmin'            0.788

Correction method= # Reported T Limits: Tmin=0.660 Tmax=0.747
AbsCorr = MULTI-SCAN

Data completeness= 0.930           Theta(max)= 35.265

R(reflections)= 0.0385( 11880)                wR2(reflections)=
                                              0.0979( 14862)
S = 1.039                  Npar= 446
```

3.5.3.2. Synthesis of Ni2 complex:

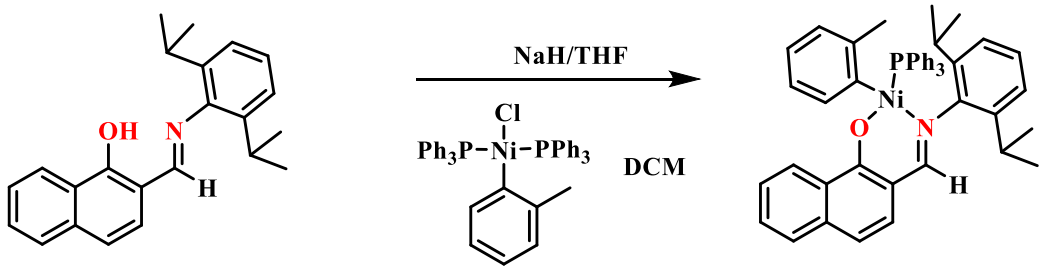

Scheme S3.3: Synthesis of **Ni2** complex.

In an oven-dried Schlenk flask, NaH (5.0 mg, 0.21 mmol) and ligand **L2** (35 mg, 0.10 mmol) were taken. The flask was cooled to 0 °C and 5 mL THF was added to that. The reaction mixture

was stirred at 0 °C for 2 hours, after that solvent was evaporated. The resultant compound was dissolved in 5 mL DCM and was dropwise transferred to another flask that contained [NiCl(*o*-Tol)(PPh_3)$_2$] (74.8 mg, 0.10 mmol) precursor at 0 °C. The mixture was stirred at the same temperature for 2 hours and DCM was evaporated. The complex was purified by recrystallization in DCM and hexane at 0 °C (Yield- 54 mg, 73%).

^{1}H NMR (500 MHz, $CDCl_3$): δ 7.92 (d, *J* = 8.5 Hz, 1 H), 7.50 (d, *J* = 8.5 Hz, 5 H), 7.35 - 7.30 (m, 7 H), 7.23 - 7.19 (m, 5 H), 7.08 - 7.02 (m, *J* = 8.5 Hz, 1 H), 7.00 - 6.96 (m, *J* = 7.6 Hz, 1 H), 6.90 (t, *J* = 7.8 Hz, 1 H), 6.87 - 6.82 (m, *J* = 8.5 Hz, 1 H), 6.73 (t, *J* = 7.5 Hz, 1 H), 6.67 - 6.62 (m, *J* = 7.3 Hz, 1 H), 6.47 (d, *J* = 7.9 Hz, 1 H), 6.42 - 6.36 (m, *J* = 7.3 Hz, 1 H), 6.22 - 6.13 (m, 1 H), 6.08 - 6.01 (m, *J* = 7.0 Hz, 1 H), 5.90 (t, *J* = 7.3 Hz, 1 H), 4.60 (td, *J* = 6.7, 13.4 Hz, 1 H), 3.01 (td, *J* = 6.6, 13.4 Hz, 1 H), 2.82 (s, 3 H), 1.51 (d, *J* = 6.7 Hz, 3 H), 1.03 (d, *J* = 6.7 Hz, 6 H), 0.80 (d, *J* = 6.7 Hz, 3 H). **^{13}C NMR (125 MHz, $CDCl_3$):** δ = 165.2, 164.8, 150.2, 145.7, 145.3, 142.6, 141.7, 140.4, 138.0, 137.1, 134.5, 134.4, 133.8, 133.7, 131.3, 130.9, 129.8, 129.7, 129.6, 128.7, 128.5, 128.5, 128.2, 127.9, 127.8, 126.8, 126.6, 125.9, 125.3, 123.7, 122.7, 122.0, 121.5, 113.7, 112.0, 29.1, 27.6, 26.0, 25.8, 22.7, 22.0. **^{31}P NMR (500 MHz, $CDCl_3$):** δ 25.2.

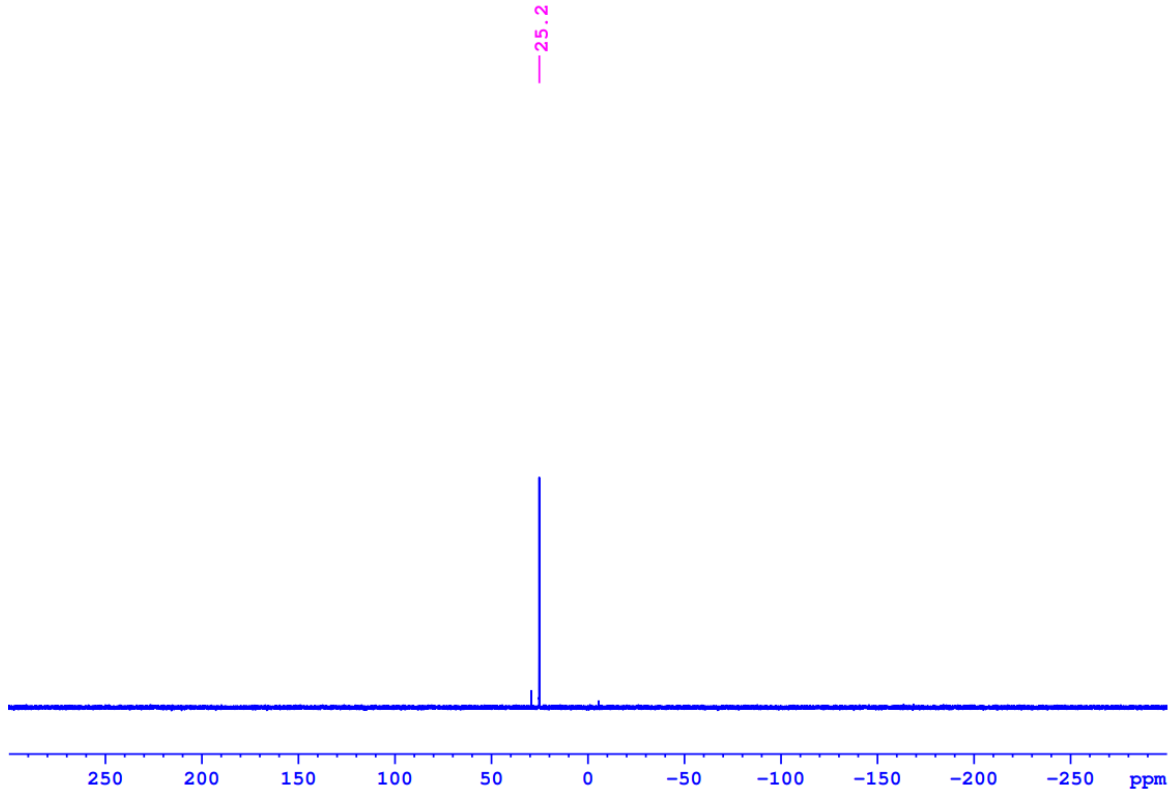

Figure S3.15: ^{31}P NMR spectrum of **Ni2** complex in $CDCl_3$.

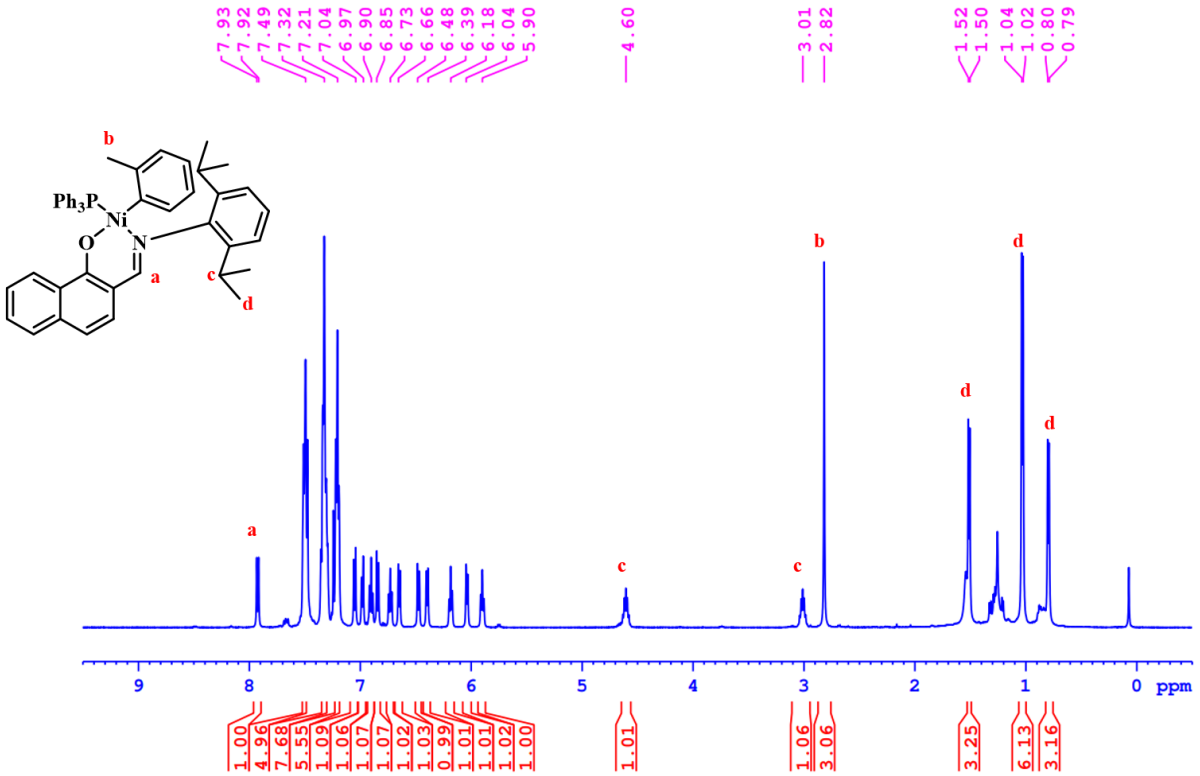

Figure S3.16: ^{1}H NMR spectrum of **Ni2** complex in $CDCl_3$.

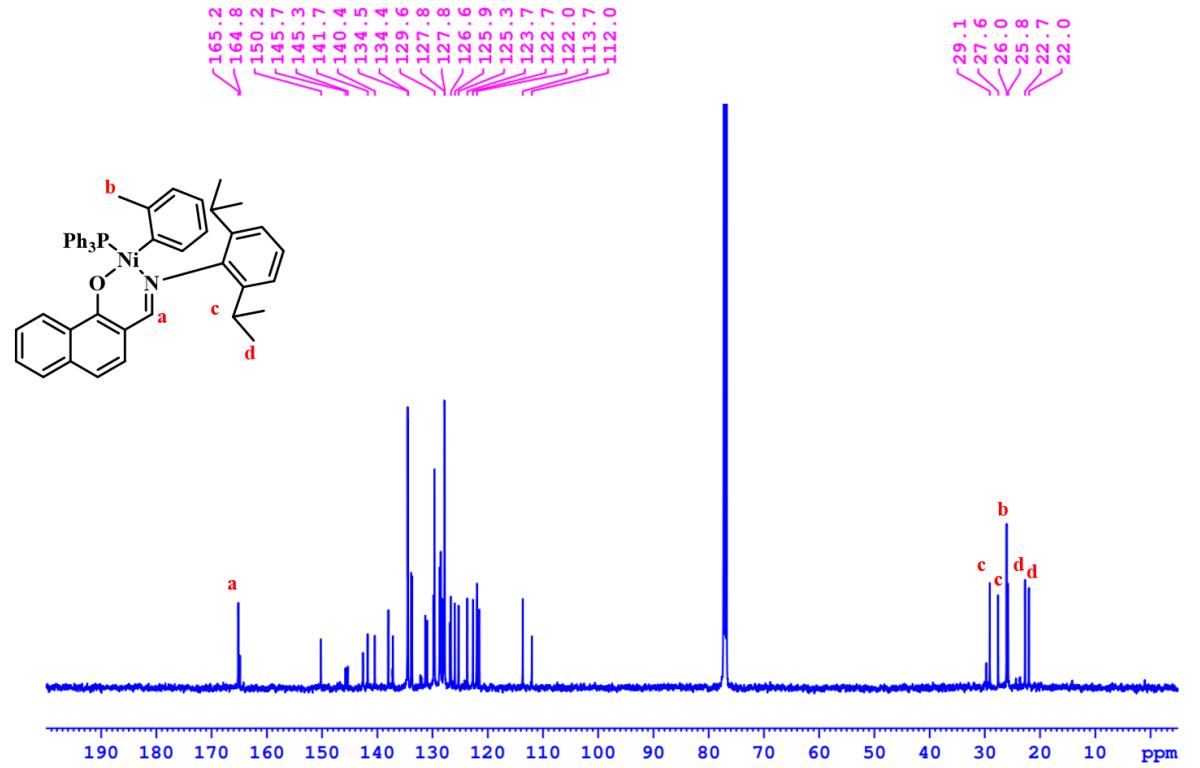

Figure S3.17: ^{13}C NMR spectrum of **Ni2** complex in $CDCl_3$.

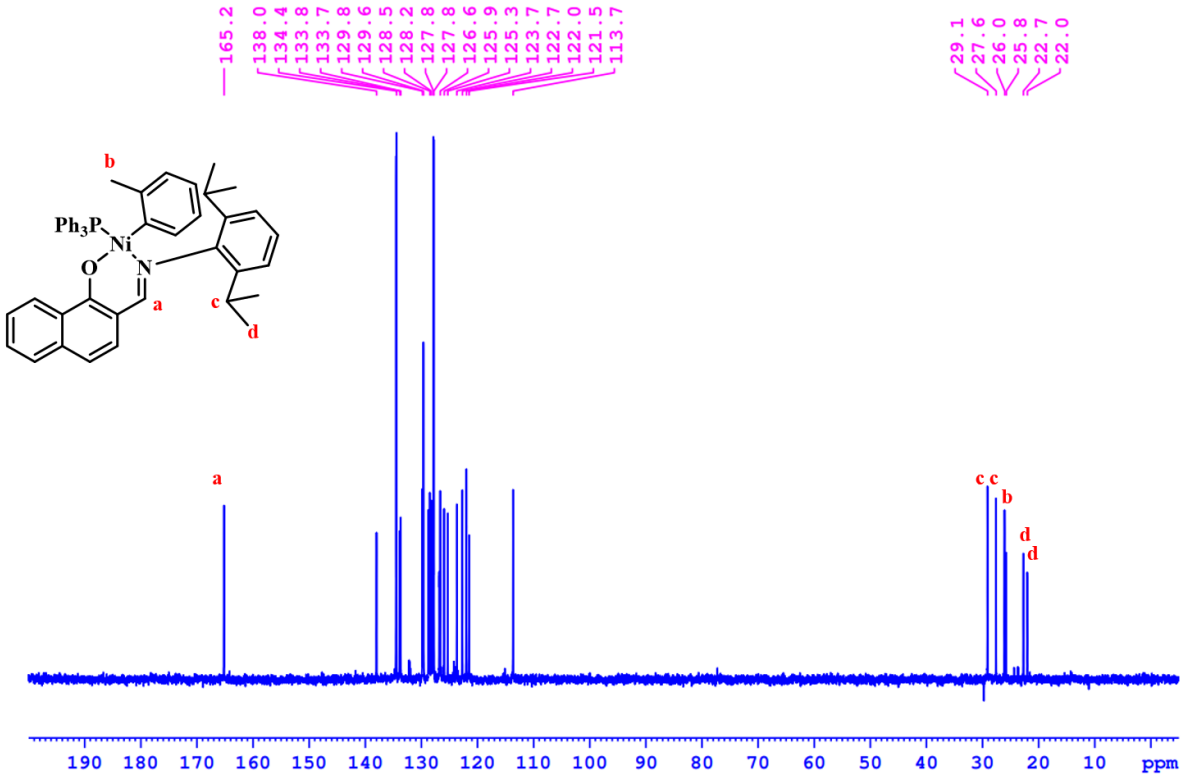

Figure S3.18: ^{13}C DEPT NMR spectrum of **Ni2** complex in $CDCl_3$.

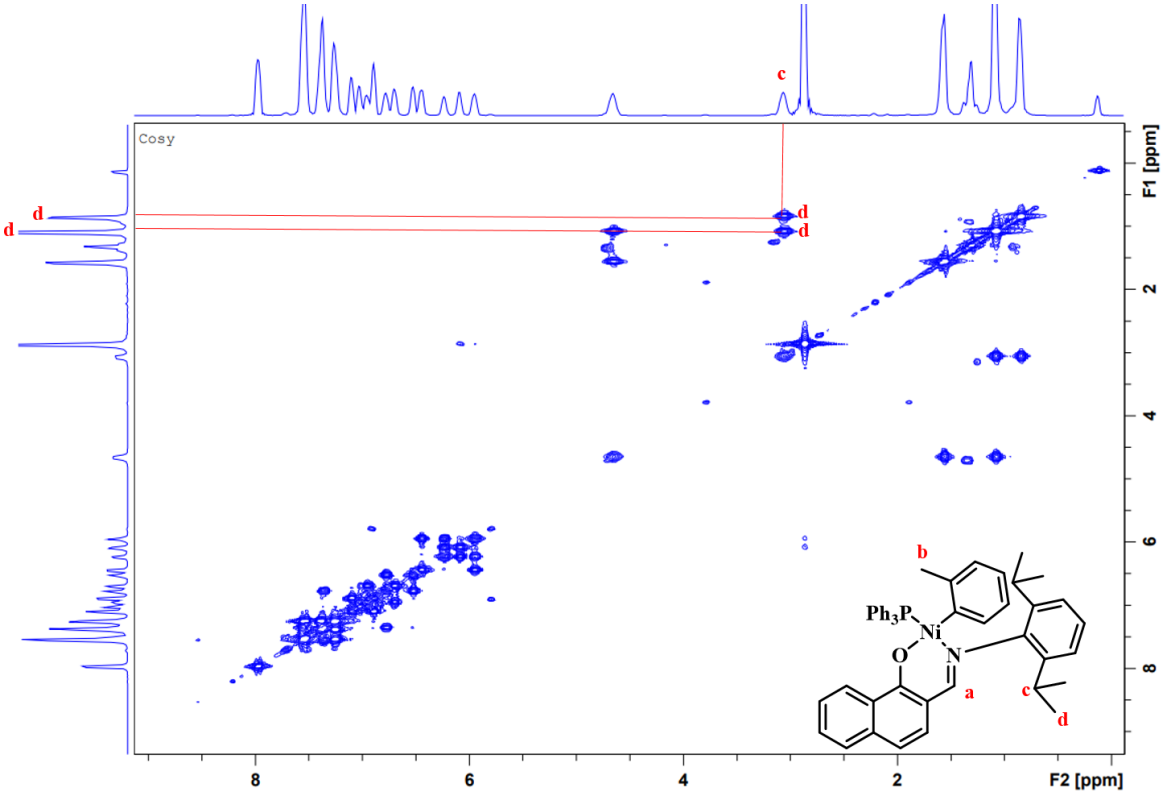

Figure S3.19: ^{1}H-^{1}H COSY NMR spectrum of **Ni2** complex in $CDCl_3$.

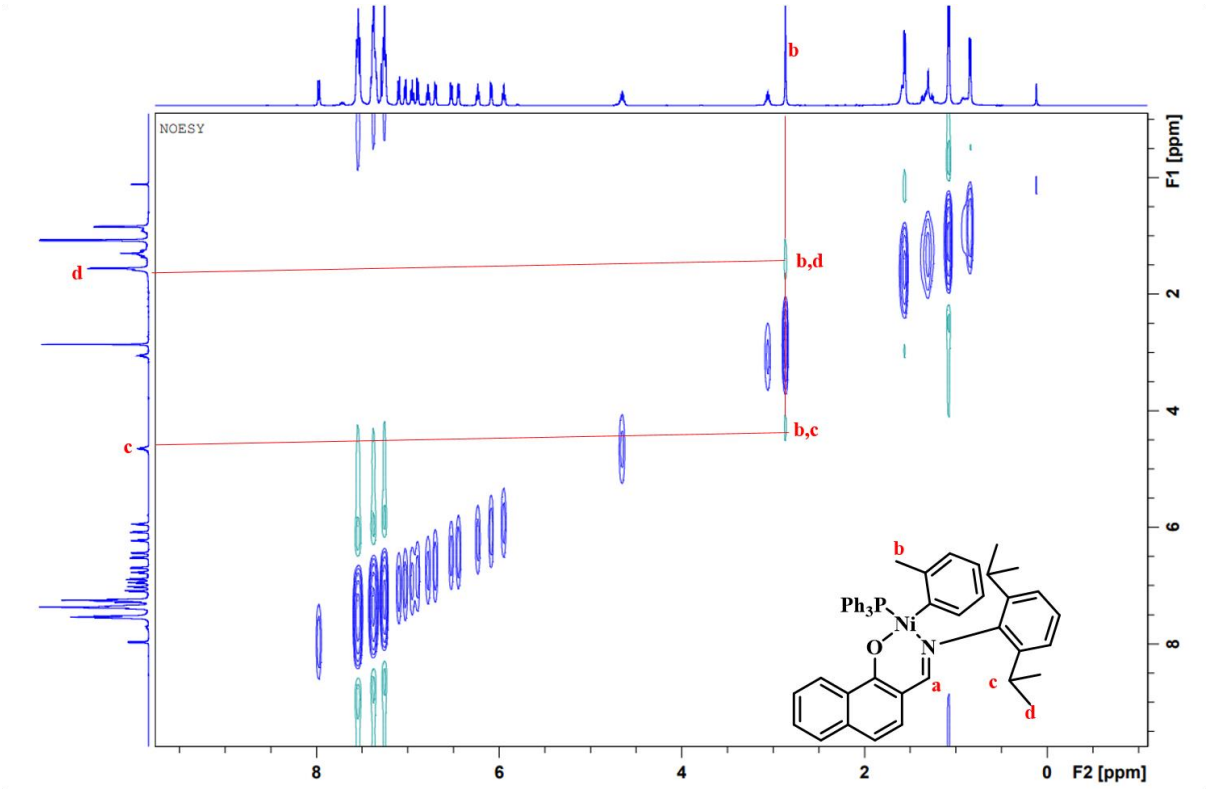

Figure S3.20: ^{1}H-^{1}H NOESY NMR spectrum of **Ni2** complex in $CDCl_3$.

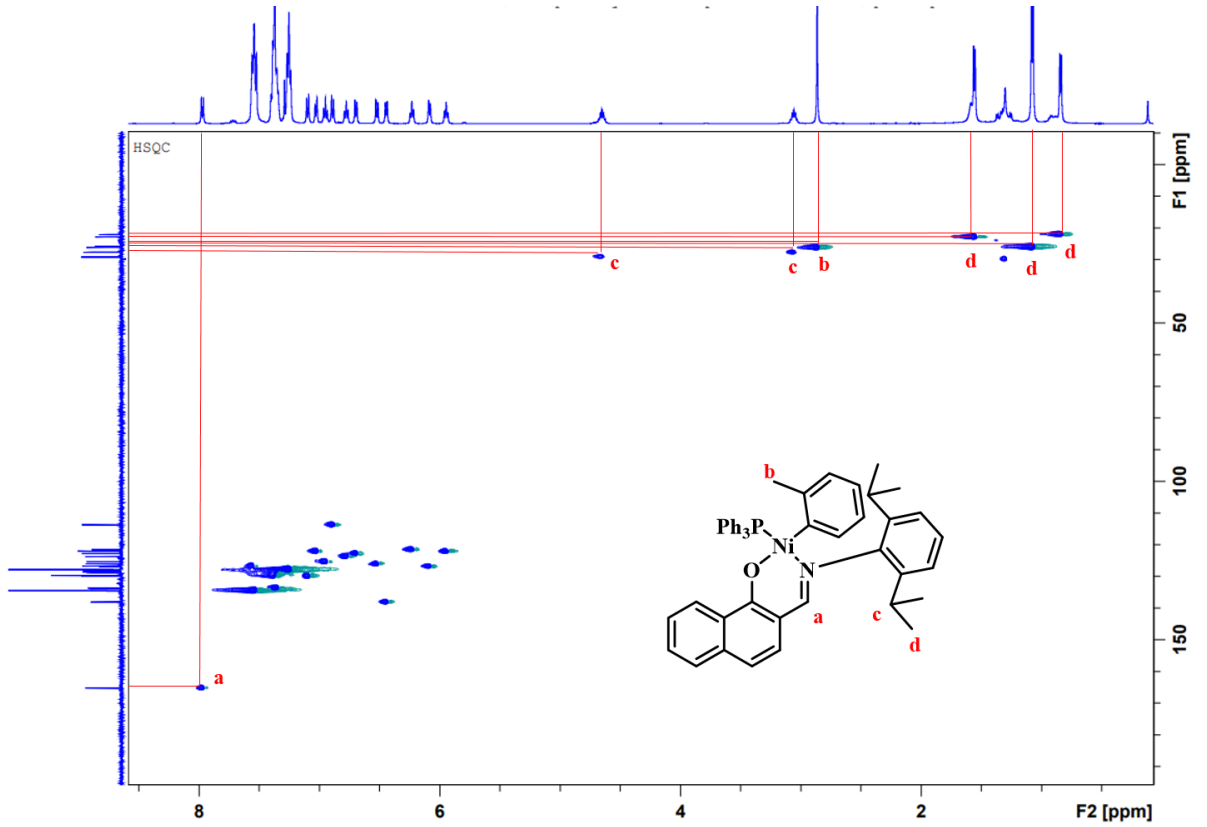

Figure S3.21: HSQC NMR spectrum of **Ni2** complex in $CDCl_3$.

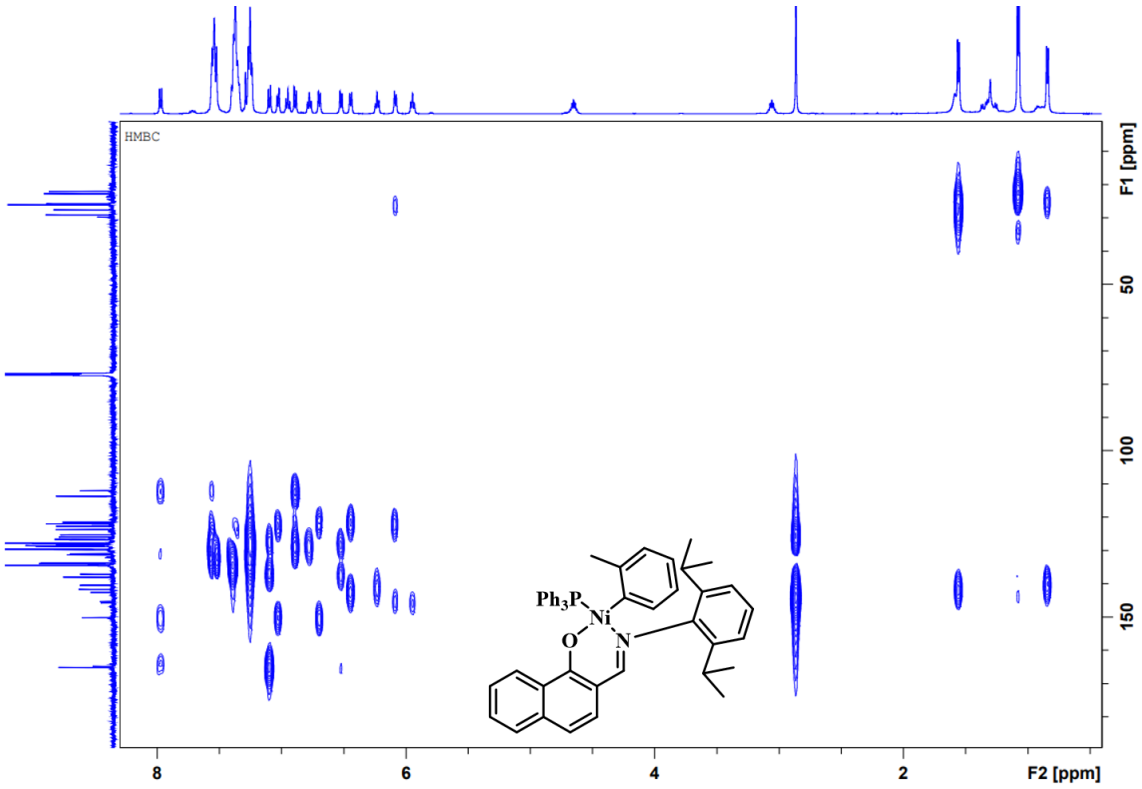

Figure S3.22: HMBC NMR spectrum of **Ni2** complex in $CDCl_3$.

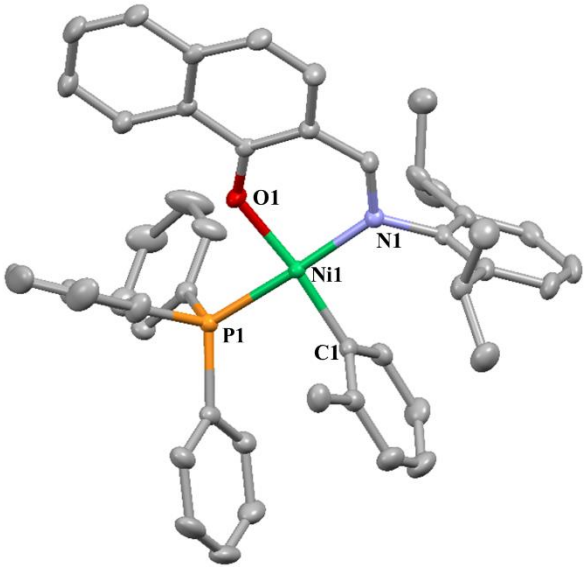

Figure S3.23: Molecular structure of **Ni2** complex.

Chart S3.2: Crystal data and structure refinement for Ni2.

```
Bond precision:   C-C = 0.0034 A          Wavelength=0.71073

Cell:           a=11.4531(19)      b=13.695(2)       c=14.417(3)
                alpha=77.010(6)    beta=66.853(5)    gamma=71.002(5)
Temperature:    100 K

                Calculated                  Reported
Volume          1953.8(6)                   1953.8(6)
Space group     P -1                        P -1
Hall group      -P 1                        -P 1
Moiety formula  C48 H46 N Ni O P            C48 H46 N Ni O P
Sum formula     C48 H46 N Ni O P            C48 H46 N Ni O P
Mr              742.52                      742.54
Dx,g cm-3       1.262                       1.262
Z               2                           2
Mu (mm-1)       0.575                       0.575
F000            784.0                       784.0
F000'           785.12
h,k,lmax        15,18,19                    15,18,19
Nref            9873                        9766
Tmin,Tmax       0.865,0.928                 0.684,0.746
Tmin'           0.827

Correction method= # Reported T Limits: Tmin=0.684 Tmax=0.746
AbsCorr = MULTI-SCAN

Data completeness= 0.989            Theta(max)= 28.442

R(reflections)= 0.0509( 7919)                wR2(reflections)=
                                             0.0893( 9766)
S = 1.068                  Npar= 504
```

3.5.3.3. Synthesis of Ni3 complex:

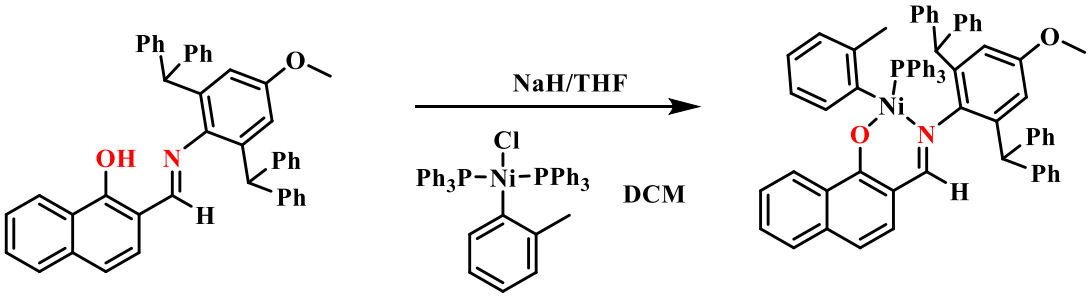

Scheme S3.4: Synthesis of **Ni3** complex.

In an oven-dried Schlenk flask, NaH (33.8 mg, 1.40 mmol) and ligand **L3** (429 mg, 0.704 mmol) were taken. The flask was cooled to 0 °C and 25 mL THF was added to that. The

reaction mixture was stirred at 0 °C for 1 hour, after that the solvent was evaporated. The resultant compound was dissolved in 20 mL DCM and was dropwise transferred to another flask that contained [NiCl(*o*-Tol)(PPh_3)$_2$] (500 mg, 0.704 mmol) precursor in 5 mL of DCM at 0 °C. The reaction mixture was stirred at the same temperature for 1 hour and DCM was evaporated. The resultant residue was purified by column chromatography using Pet Ether (98%)/ Ethyl acetate (2%) (Yield-620 mg, 86%).

^{1}H NMR (500 MHz, $CDCl_3$): δ 7.66 (s, 1 H), 7.53 (t, *J* = 8.8 Hz, 6 H), 7.40 (d, *J* = 7.9 Hz, 1 H), 7.35 - 7.31 (m, 3 H), 7.26 (s, 3 H), 7.24 (d, *J* = 3.5 Hz, 3 H), 7.21 (d, *J* = 1.9 Hz, 2 H), 7.20 - 7.19 (m, 3 H), 7.19 - 7.17 (m, 4 H), 7.05 - 7.00 (m, 5 H), 6.75 (d, *J* = 7.3 Hz, 2 H), 6.72 - 6.62 (m, 3 H), 6.60 - 6.53 (m, 3 H), 6.49 (d, *J* = 2.8 Hz, 1 H), 6.43 (t, *J* = 7.3 Hz, 1 H), 6.38 (d, *J* = 8.5 Hz, 1 H), 6.24 - 6.17 (m, 3 H), 6.11 (t, *J* = 7.1 Hz, 1 H), 5.97 (d, *J* = 2.8 Hz, 1 H), 5.67 (d, *J* = 8.8 Hz, 1 H), 5.28 (d, *J* = 8.8 Hz, 1 H), 5.20 (s, 1 H), 3.43 (s, 3 H), 3.07 (s, 3 H). **^{13}C NMR (125 MHz, $CDCl_3$):** δ = 168.5, 163.5, 155.8, 144.9, 143.7, 143.4, 143.3, 143.1, 139.7, 138.7, 138.6, 137.1, 134.4, 134.3, 131.3, 130.9, 130.5, 130.3, 130.2, 129.9, 129.6, 129.2, 128.5, 128.3, 128.0, 127.9, 127.7, 127.7, 127.4, 127.2, 126.4, 126.3, 126.2, 125.9, 125.8, 125.7, 123.3, 123.1, 121.8, 113.5, 113.3, 112.4, 112.1, 55.1, 53.5, 51.9, 26.5. **^{31}P NMR (500 MHz, $CDCl_3$):** δ = 22.8.

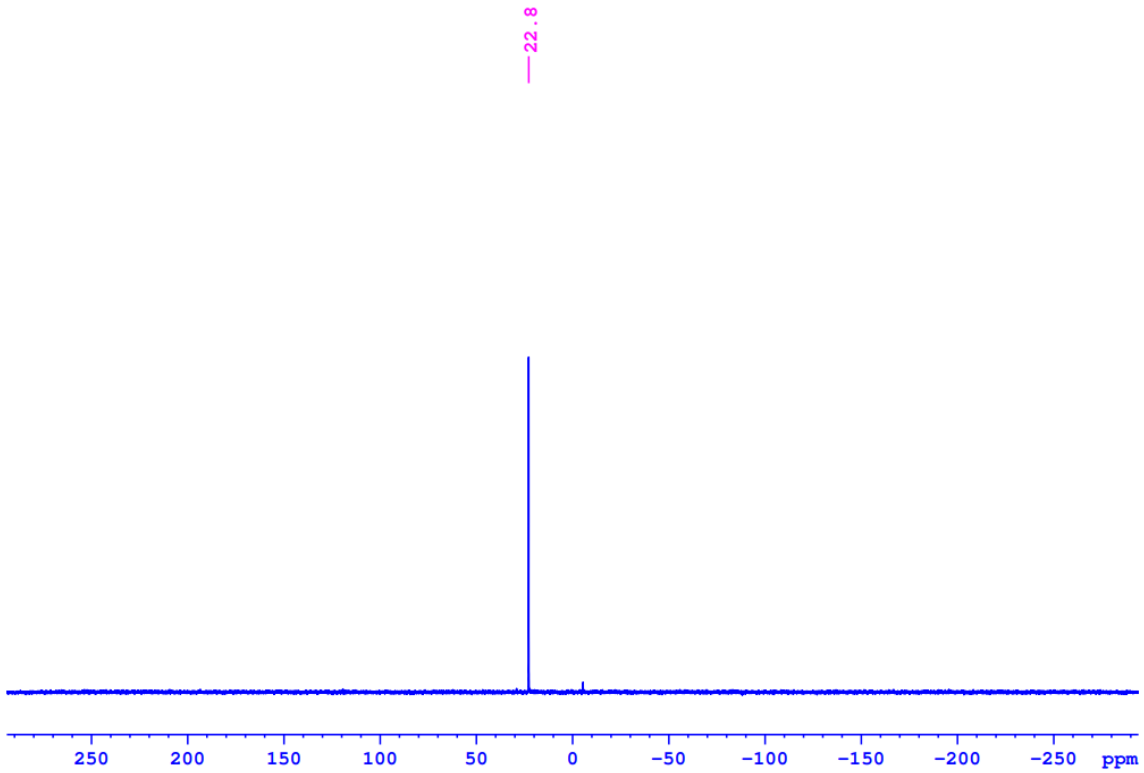

Figure S3.24: ^{31}P NMR spectrum of **Ni3** complex in $CDCl_3$.

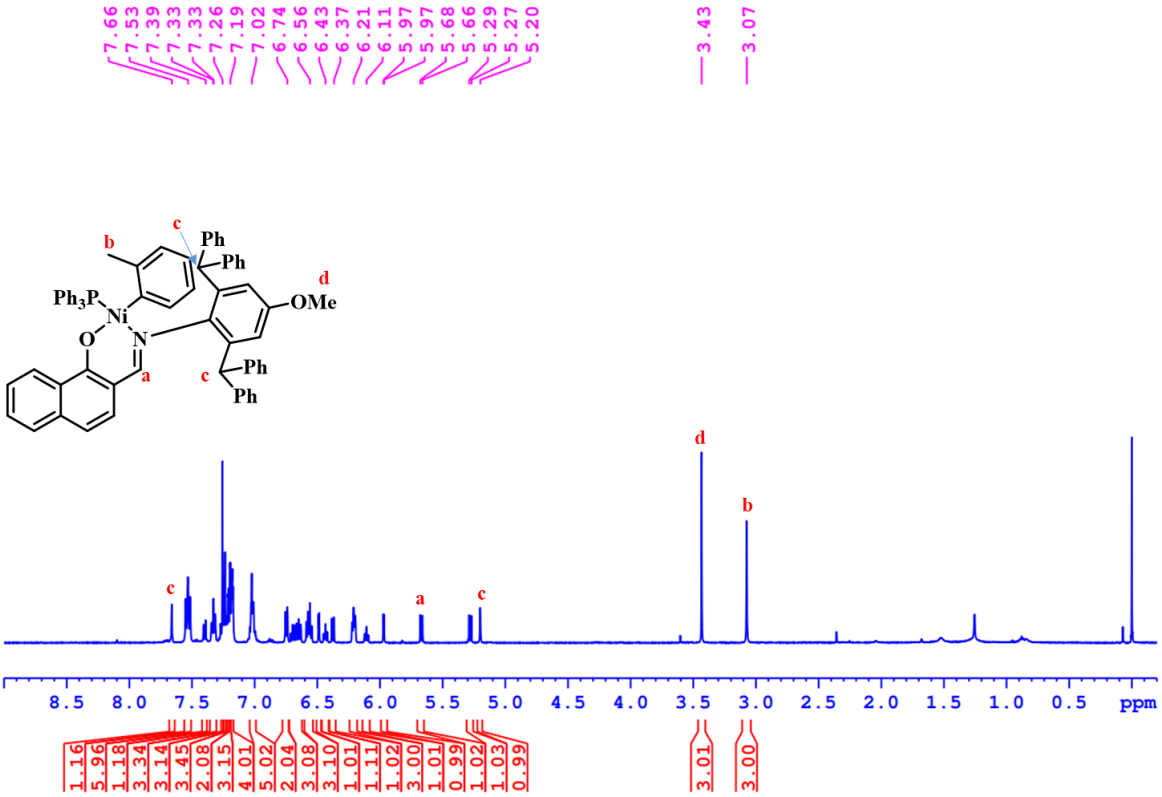

Figure S3.25: ^{1}H NMR spectrum of **Ni3** complex in $CDCl_3$.

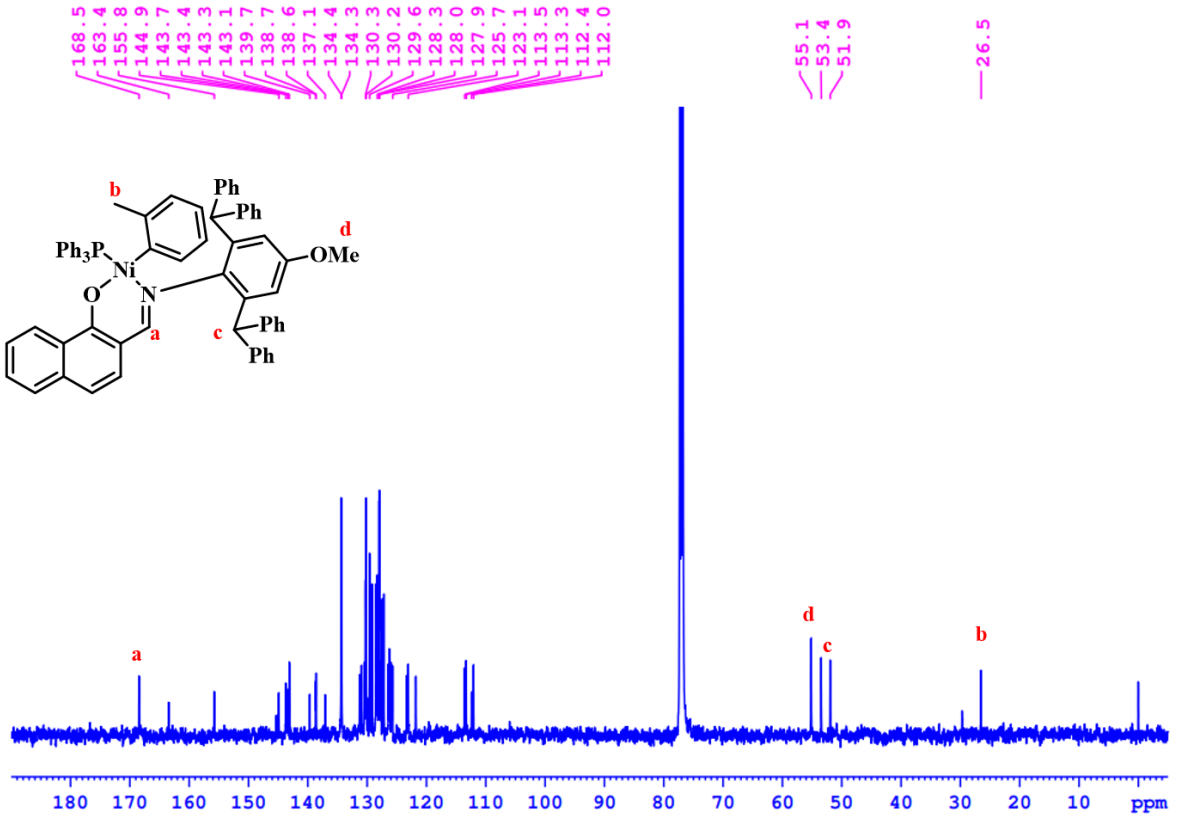

Figure S3.26: ^{13}C NMR spectrum of **Ni3** complex in $CDCl_3$.

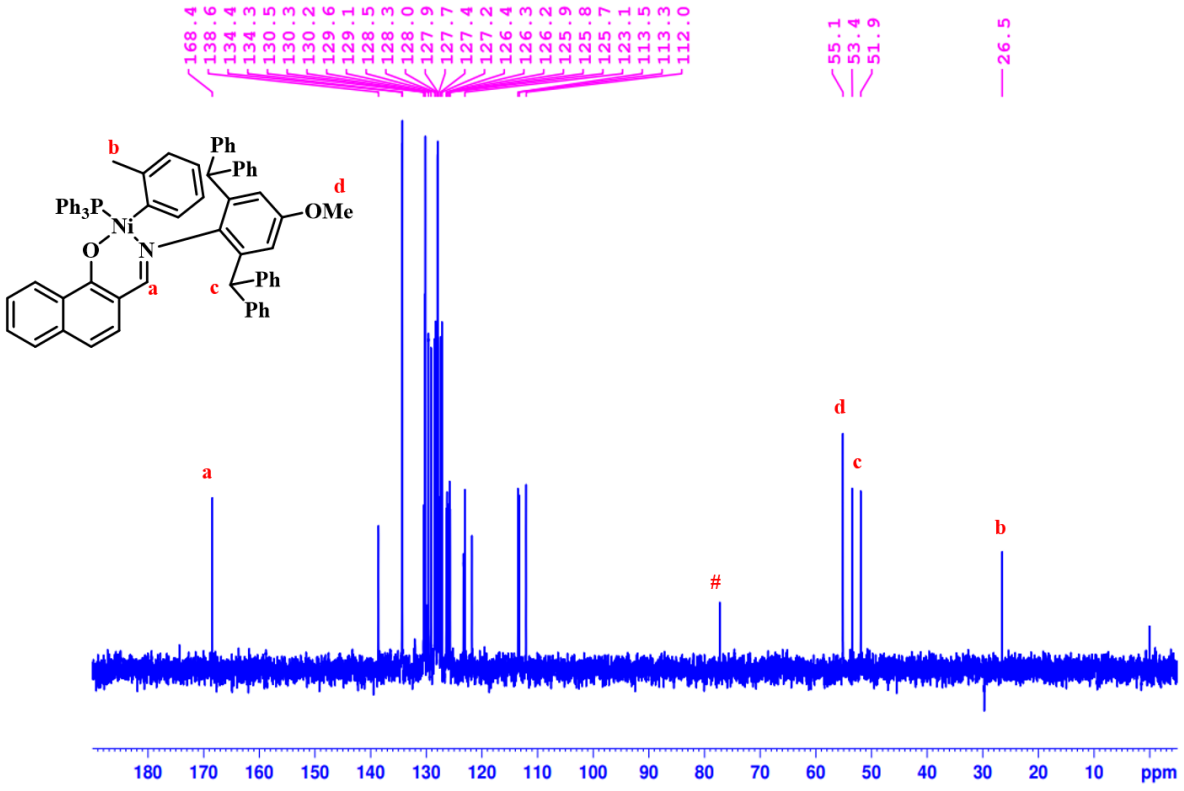

Figure S3.27: ^{13}C DEPT NMR spectrum of **Ni3** complex in $CDCl_3$.

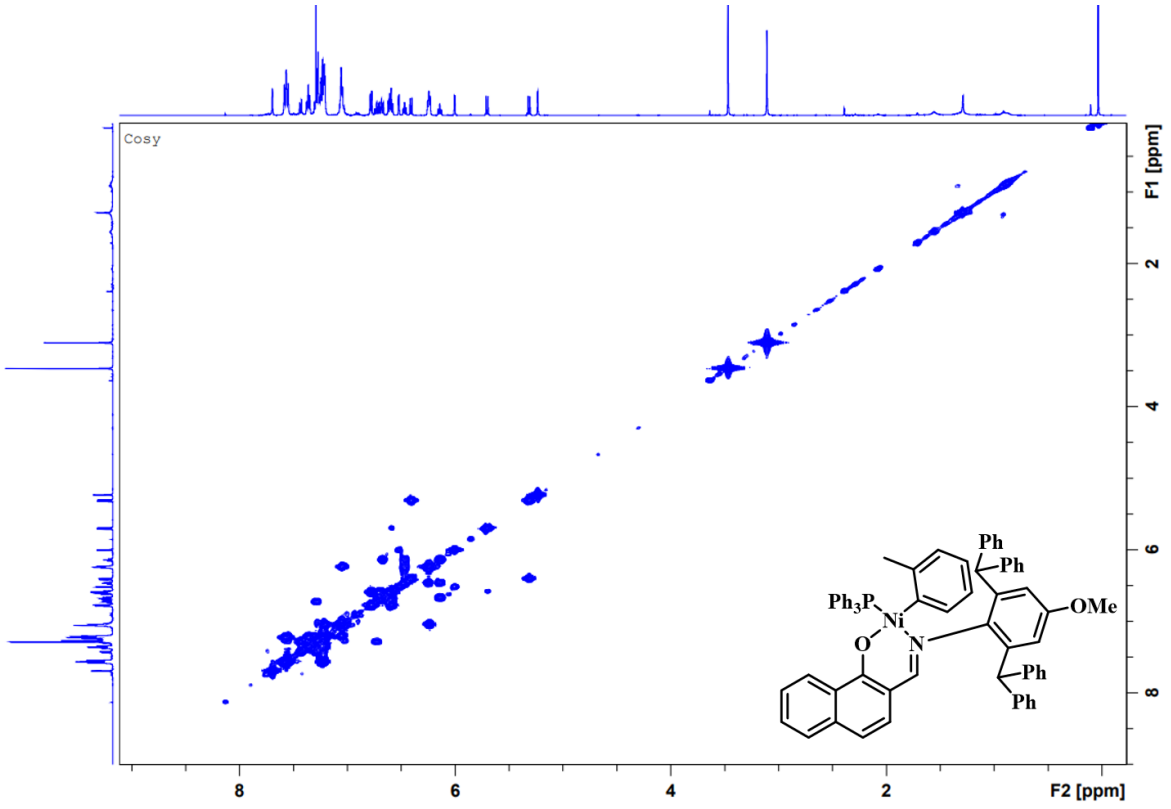

Figure S3.28: ^{1}H-^{1}H COSY NMR spectrum of **Ni3** complex in $CDCl_3$.

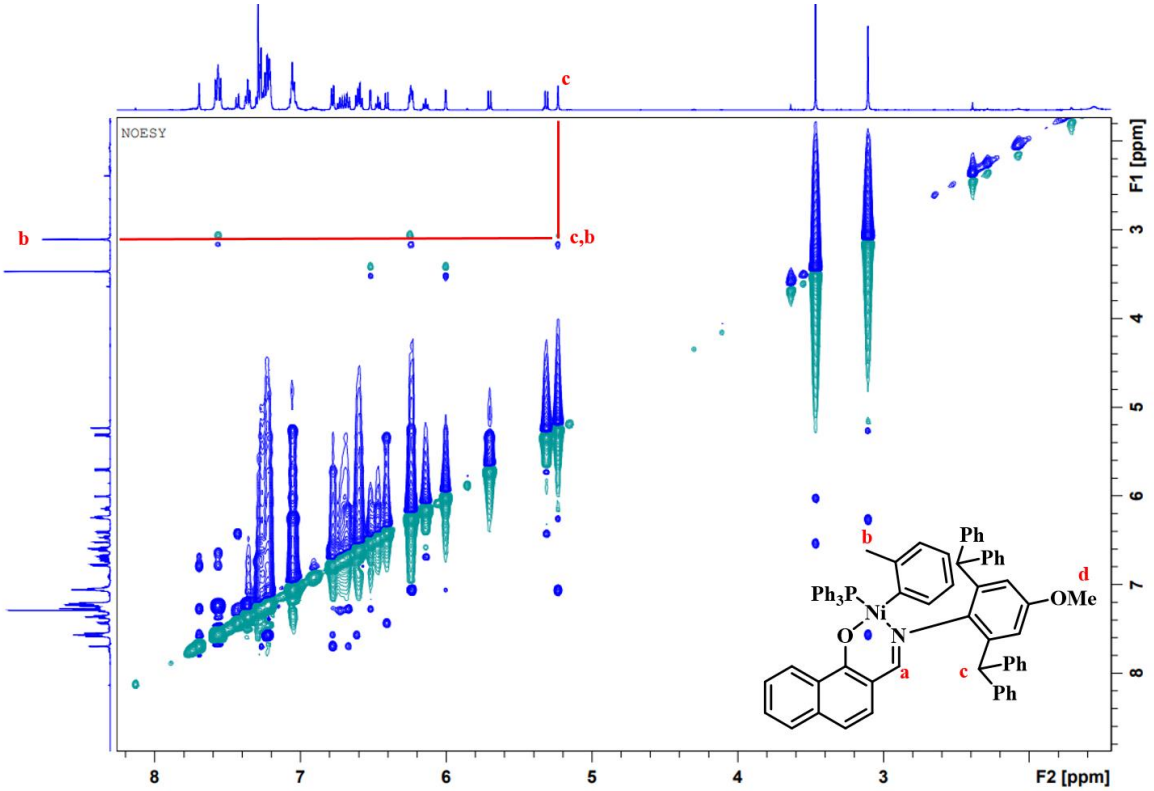

Figure S3.29: NOESY NMR of **Ni3** complex in $CDCl_3$.

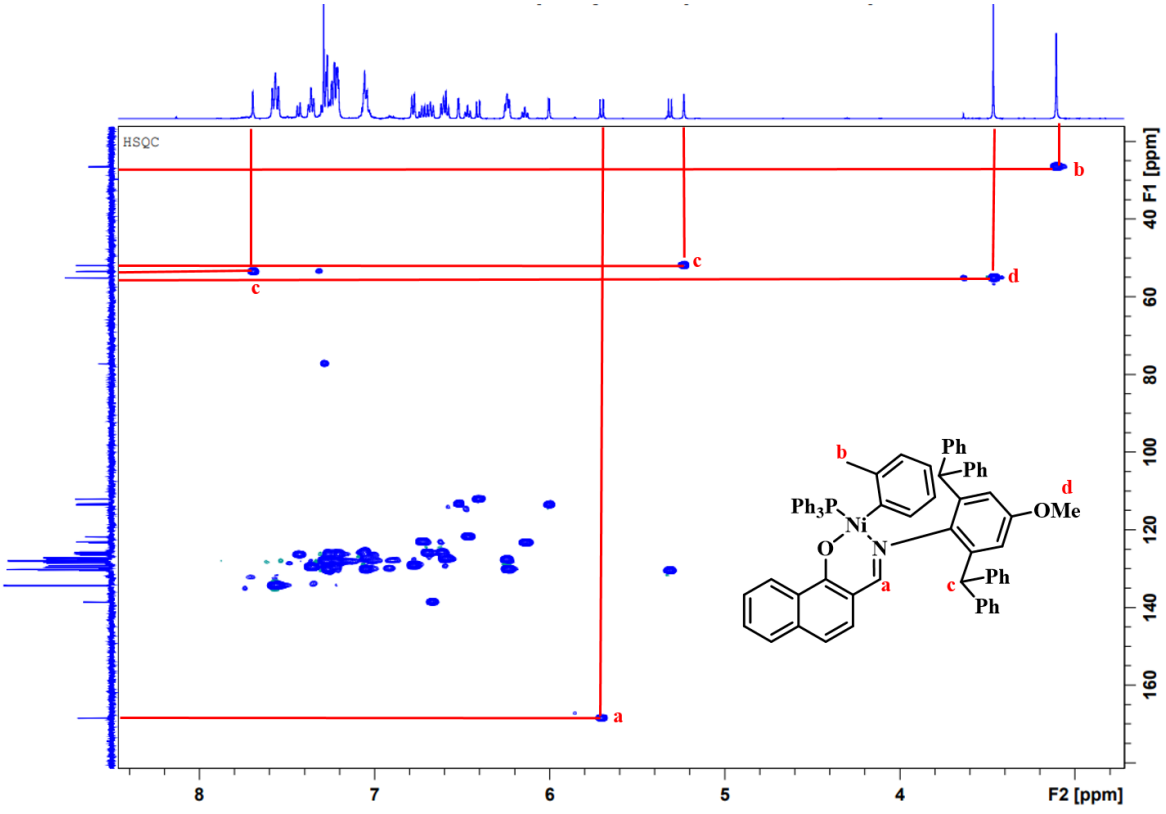

Figure S3.30: HSQC NMR spectrum of **Ni3** complex in $CDCl_3$.

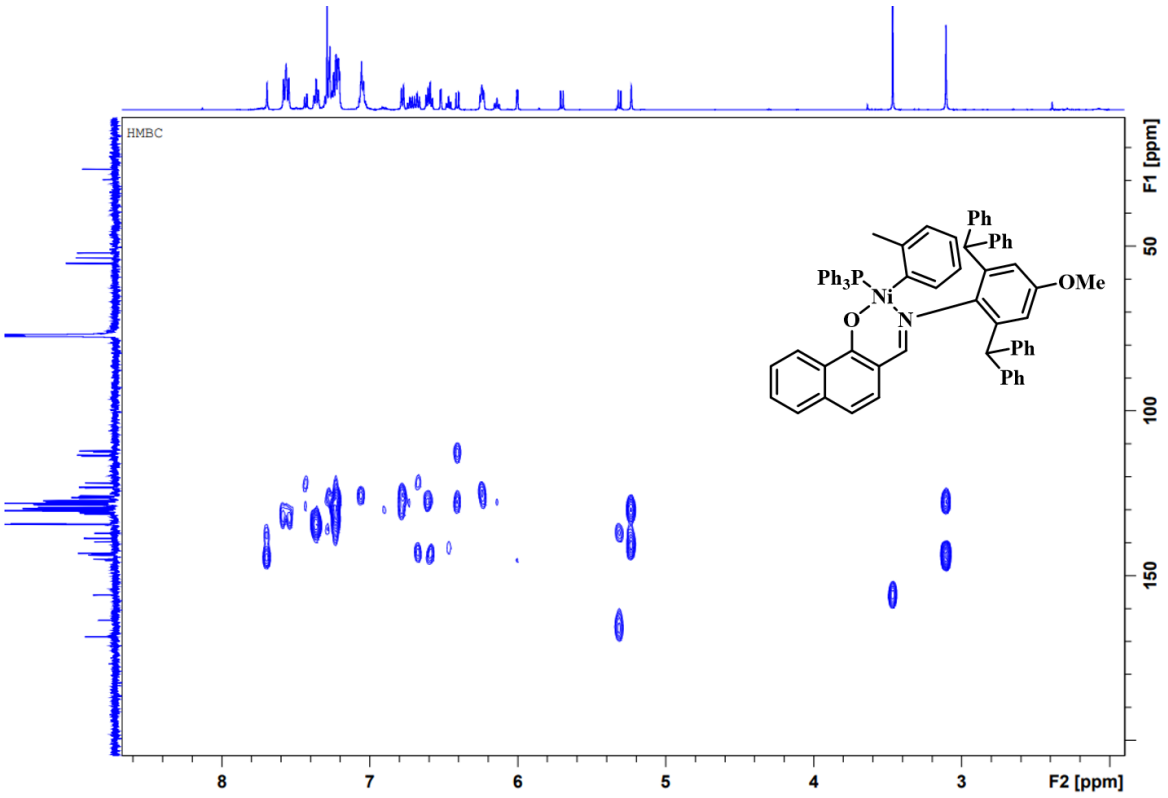

Figure S3.31: HMBC NMR spectrum of **Ni3** complex in $CDCl_3$.

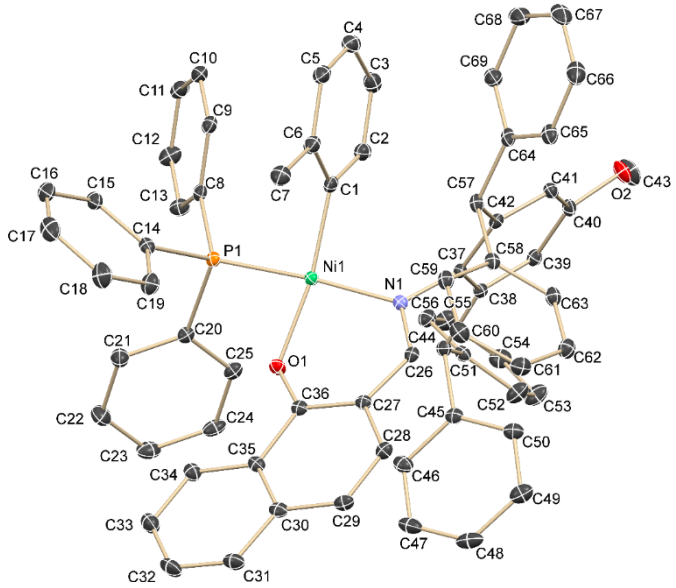

Figure S3.32: Molecular structure of **Ni3** complex.

Chart S3.3: Crystal data and structure refinement parameters for Ni3.

```
Bond precision:   C-C = 0.0044 A          Wavelength=0.71073

Cell:          a=10.6428(18)      b=16.779(2)       c=18.282(3)
               alpha=109.298(5)   beta=101.650(6)   gamma=92.667(6)
Temperature:   100 K

                Calculated                  Reported
Volume          2995.1(8)                   2995.1(8)
Space group     P -1                        P -1
Hall group      -P 1                        -P 1
Moiety formula  2(C69 H56 N Ni O2 P),       C69 H56 N Ni O2 P, 0.75(C10
                1.5(C10 H22)                H22)
Sum formula     C153 H145 N2 Ni2 O4 P2      C76.50 H72.50 N Ni O2 P
Mr              2255.03                     1127.53
Dx,g cm-3       1.250                       1.250
Z               1                           2
Mu (mm-1)       0.400                       0.400
F000            1195.0                      1195.0
F000'           1196.28
h,k,lmax        13,20,22                    13,20,22
Nref            11750                       11445
Tmin,Tmax       0.887,0.908                 0.454,0.495
Tmin'           0.887

Correction method= # Reported T Limits: Tmin=0.454 Tmax=0.495
AbsCorr = MULTI-SCAN

Data completeness= 0.974          Theta(max)= 25.999

R(reflections)= 0.0545( 9561)                wR2(reflections)=
                                             0.1531( 11445)
S = 1.053                 Npar= 706
```

Table S3.1: Nickel complexes and their CCDC number.

Complex	CCDC No.
Ni1	2285806
Ni2	2285654
Ni3	2225186

3.5.4. Percent buried volume data:

Percent buried volume data (%Vbur) were generated by SambVca 2.1 web application.[60]

More details for %Vbur calculation and steric maps are as under:

1) The nickel atom (Ni) defines the center of the xyz coordinate system.

2) Ni(PPh_3)(*o*-Tolyl) fragment was excluded.

3) Bondi radii was scaled by 1.17.

4) Mesh spacing for numerical integration was 0.10.

5) Sphere radius was set to 3.5 Å.

6) H atoms were excluded.

For all compounds positive x-plane was defined as imine nitrogen and negative z plane was defined as the oxygen of the naphthoxy ligand.

3.5.5. Ethylene polymerization:

The polymerization reaction was performed in a Buchi high-pressure metal reactor, which was connected to ethylene gas line. Initially, the reactor was dried at 90 °C under vacuum for 1 hour. The reactor temperature was maintained at the desired polymerization temperature and the reactor was purged with ethylene gas. To that, 100 mL of anhydrous toluene was added under positive ethylene gas flow. Further, toluene was stirred under the ethylene pressure for 30 minutes to dissolve ethylene in toluene. Excess ethylene was vented and the desired amount of catalyst and cocatalyst was injected into the reactor using the syringe. The reactor was pressurized with rapid stirring and the desired pressure was maintained throughout the polymerization. After the completion of polymerization, excess ethylene was vented and polymerization was quenched by adding acidic methanol. The polymer was filtered by using Whatman filter paper, polymer was dried under a high vacuum to yield polyethylene. Table S2 summarizes important runs using Ni-catalyst.

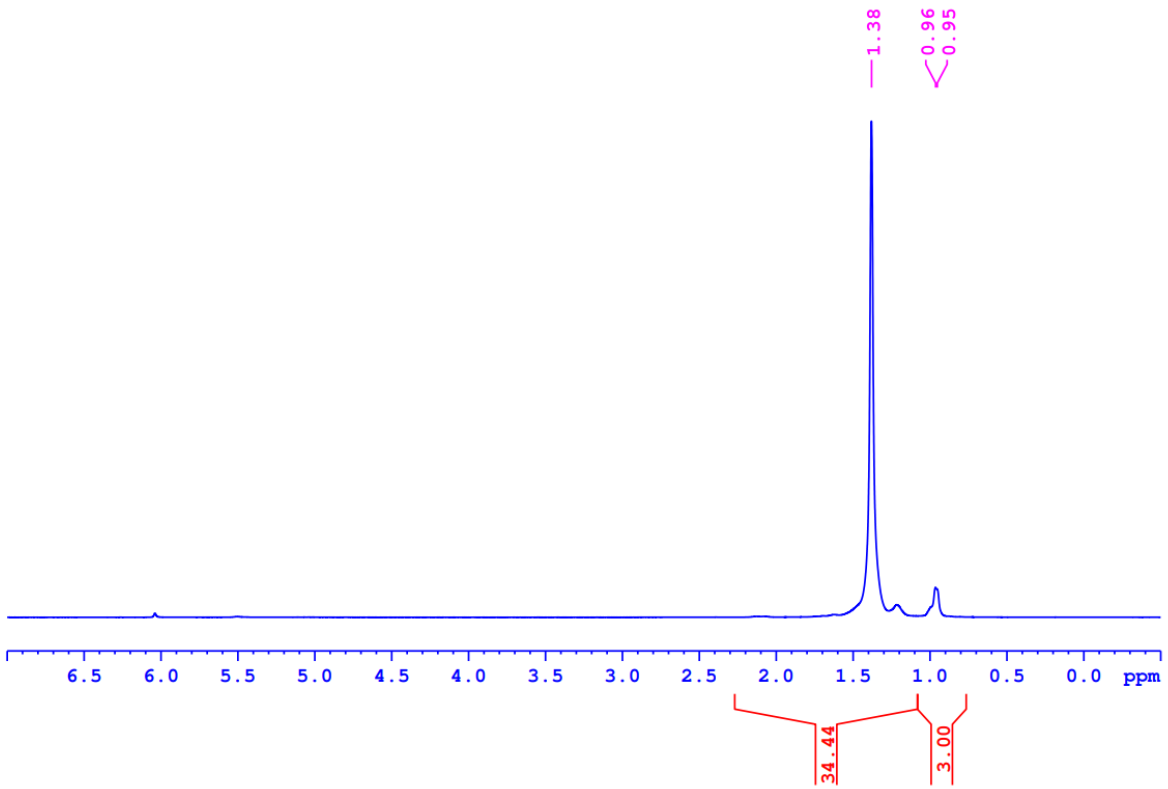

Figure S3.33: ^{1}H NMR spectrum of polyethylene in $C_2D_2Cl_4$ at 80 °C (Table3.1, entry no. 3).

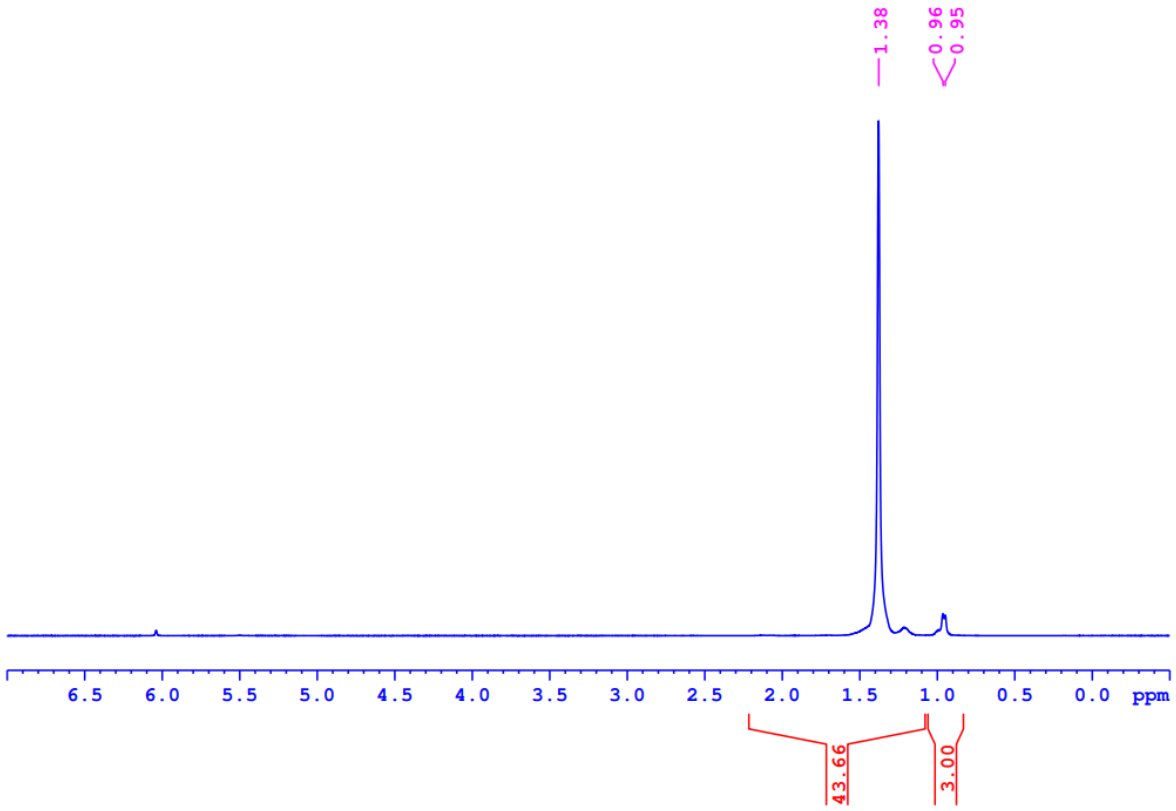

Figure S3.34: ^{1}H NMR spectrum of polyethylene in $C_2D_2Cl_4$ at 80 °C (Table3.1, entry no.7).

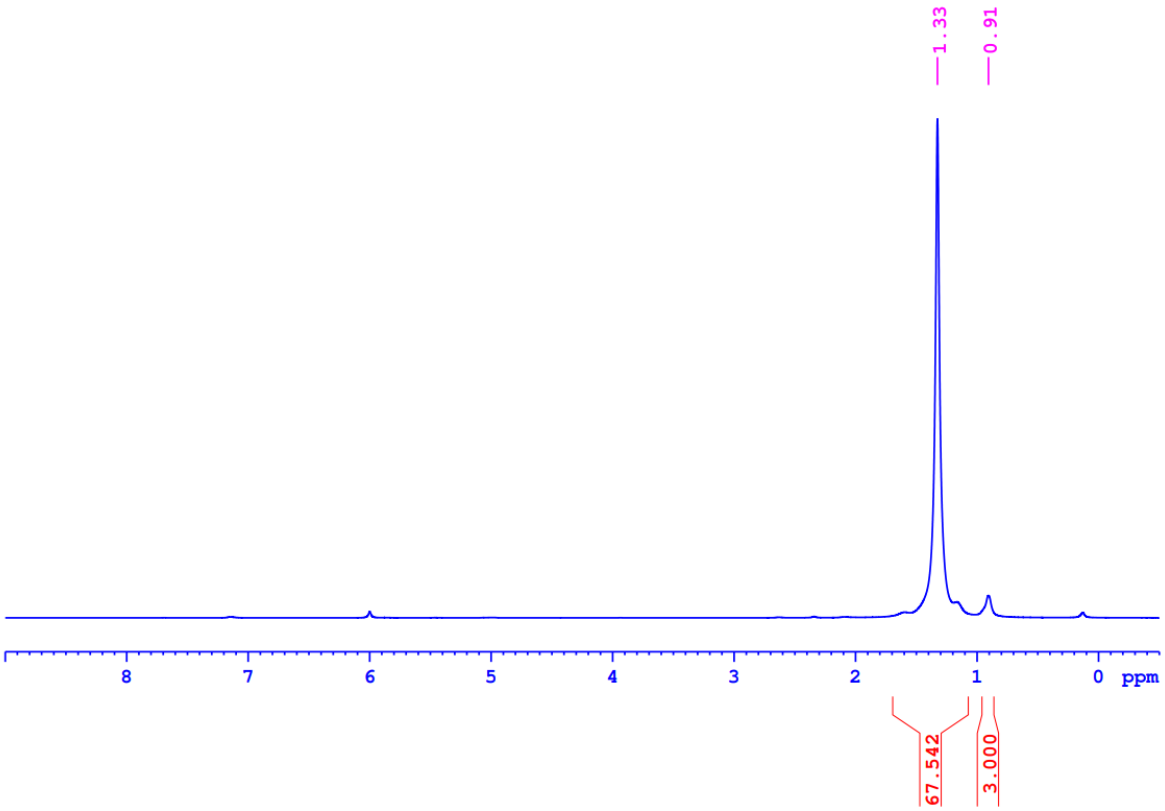

Figure S3.35: ^{1}H NMR spectrum of polyethylene in $C_2D_2Cl_4$ at 80 °C (Table3.1, entry no. 13).

3.5.5.1. Calculation of Me groups/1000C:[70]

Me groups/1000C = (2 * I_{Me} / 3 * I_{tot}) * 1000 …(*for figure S3.35, Table3.1, Entry 13*)

= (2 * 3 / 3 * 70.5) *1000

= 28.3 ~ **28**

3.5.5.2. Determination of percentage crystallinity:

%Crystallinity: The crystallinity of the resultant polyethylene was calculated from the melting enthalpy measured by DSC and relative to the theoretical value 293 J/g for 100% crystalline polyethylene (Table S3.2).

The term ΔHm° is a reference value and represents the heat of melting, if the polymer were 100% crystalline. This reference heat of melting has been established for each of the commonly used polymers and some of these are listed below.

Table S3.2. Melting enthalpy for 100% crystalline polymers.

Polymer	ΔHm° (J/g)
Nylon 6	230.1
PET	140
Nylon 6, 6	255.8
Polypropylene	207.1
Polyethylene	293

The DSC software directly provides melting enthalpy values to make the assessment of the percent crystallinity more convenient and easier. Crystallinity for one of the polyethylene samples is determined using the following method.

% Crystallinity = ΔHm /ΔHm° (J/g) ×100

Therefore, ΔHm = 49.32 J/g …(*Table 3.1, for entry 1.*)

ΔHm° = 293 J/g

% Crystallinity = 49.32 /293 ×100 = **16.8%**

3.5.6. DSC data:

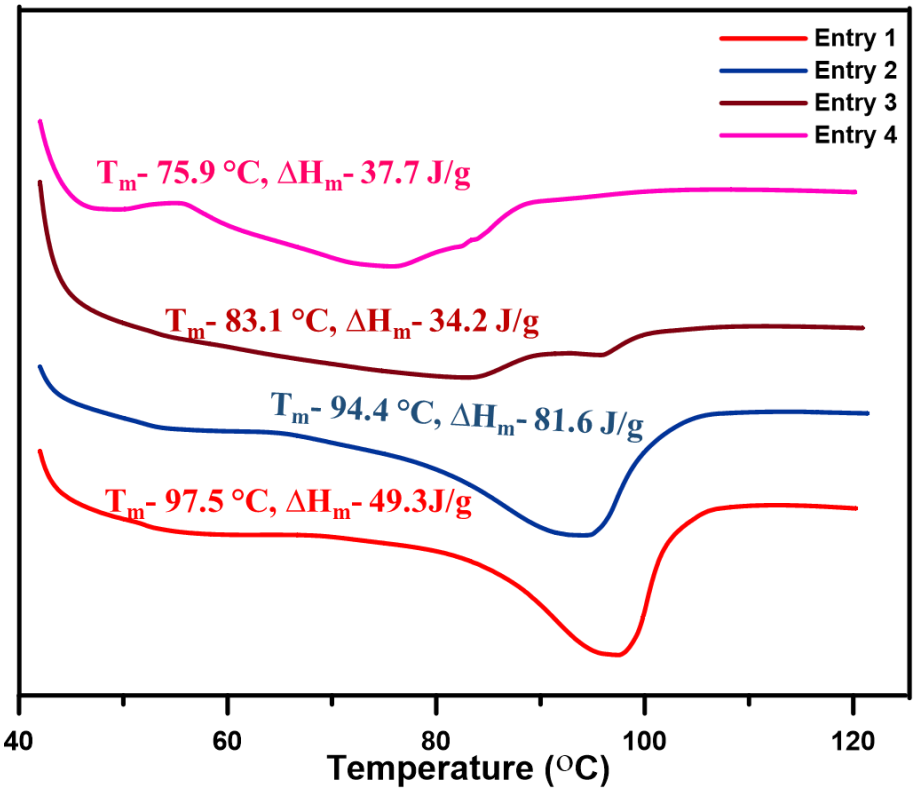

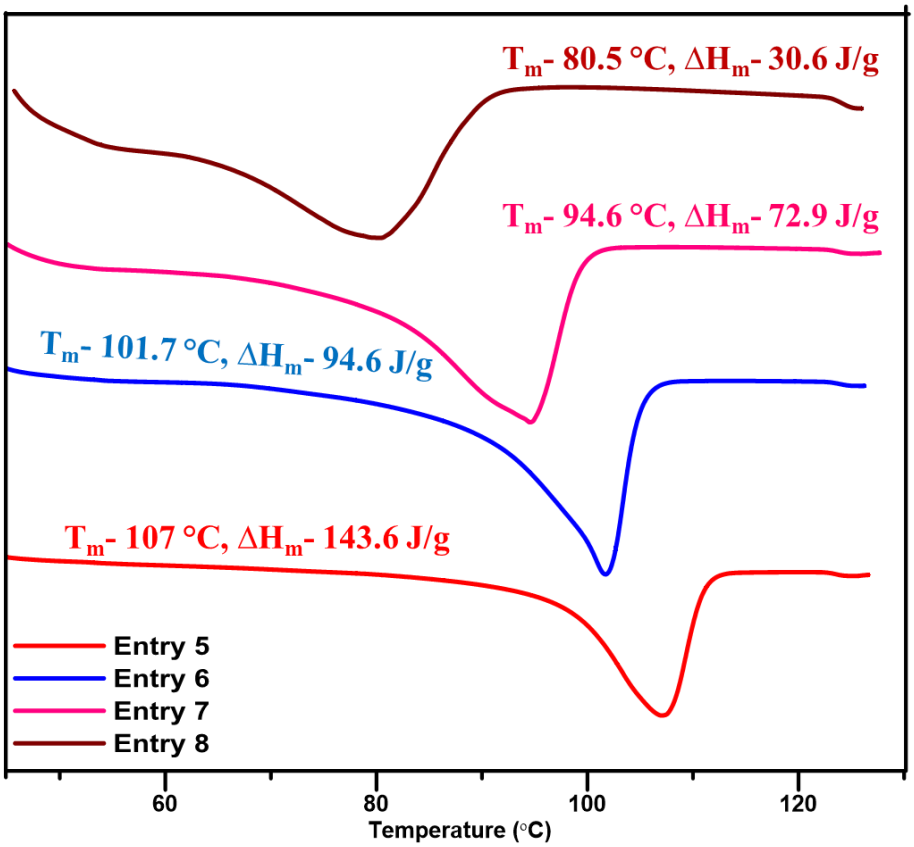
T_m- 80.5 °C, ΔH_m- 30.6 J/g
T_m- 94.6 °C, ΔH_m- 72.9 J/g
T_m- 101.7 °C, ΔH_m- 94.6 J/g
T_m- 107 °C, ΔH_m- 143.6 J/g
Entry 5
Entry 6
Entry 7
Entry 8
60
80
100
120
Temperature (°C)

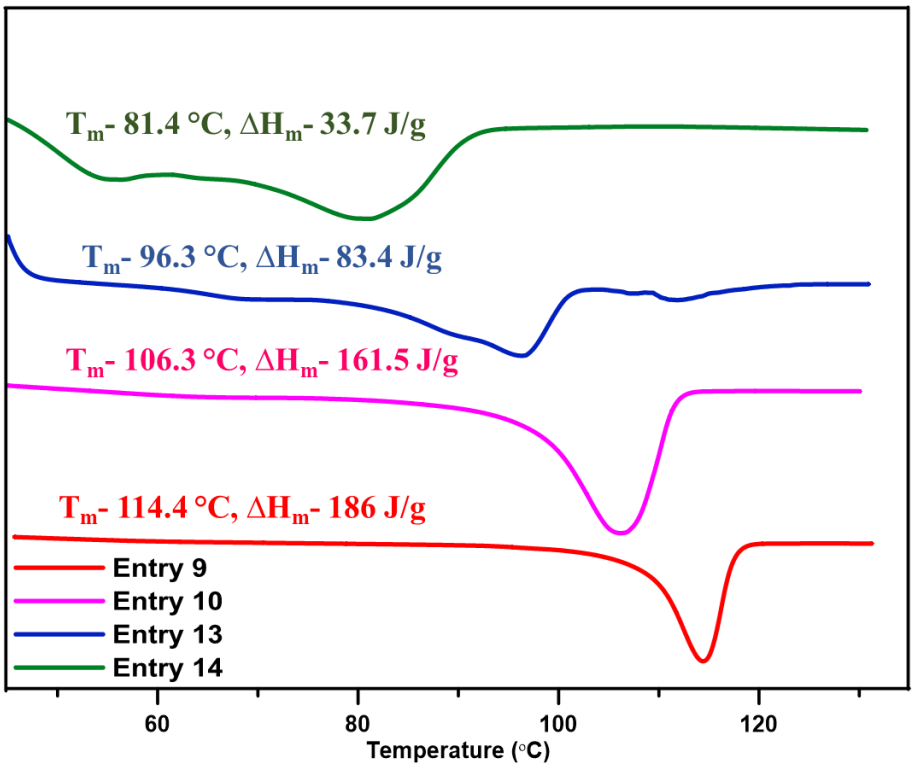
T_m- 81.4 °C, ΔH_m- 33.7 J/g
T_m- 96.3 °C, ΔH_m- 83.4 J/g
T_m- 106.3 °C, ΔH_m- 161.5 J/g
T_m- 114.4 °C, ΔH_m- 186 J/g
Entry 9
Entry 10
Entry 13
Entry 14
60
80
100
120
Temperature (°C)

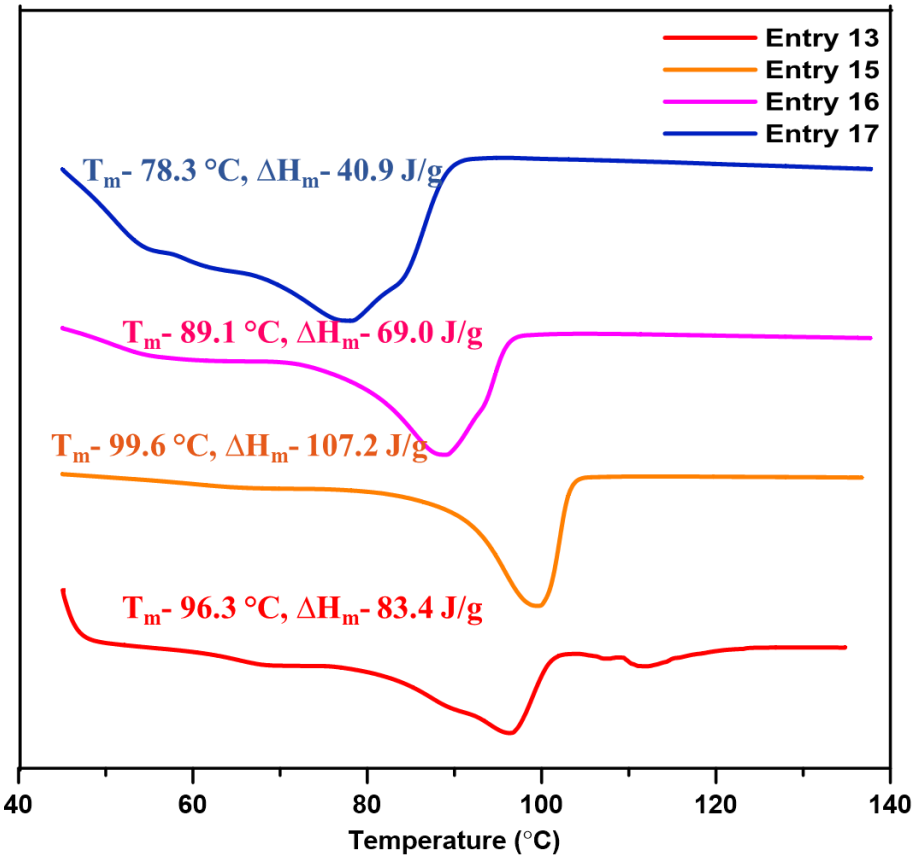

Figure S3.36: DSC thermogram of polyethylene for Table 3.1.

3.5.7. HT-GPC chromatogram :

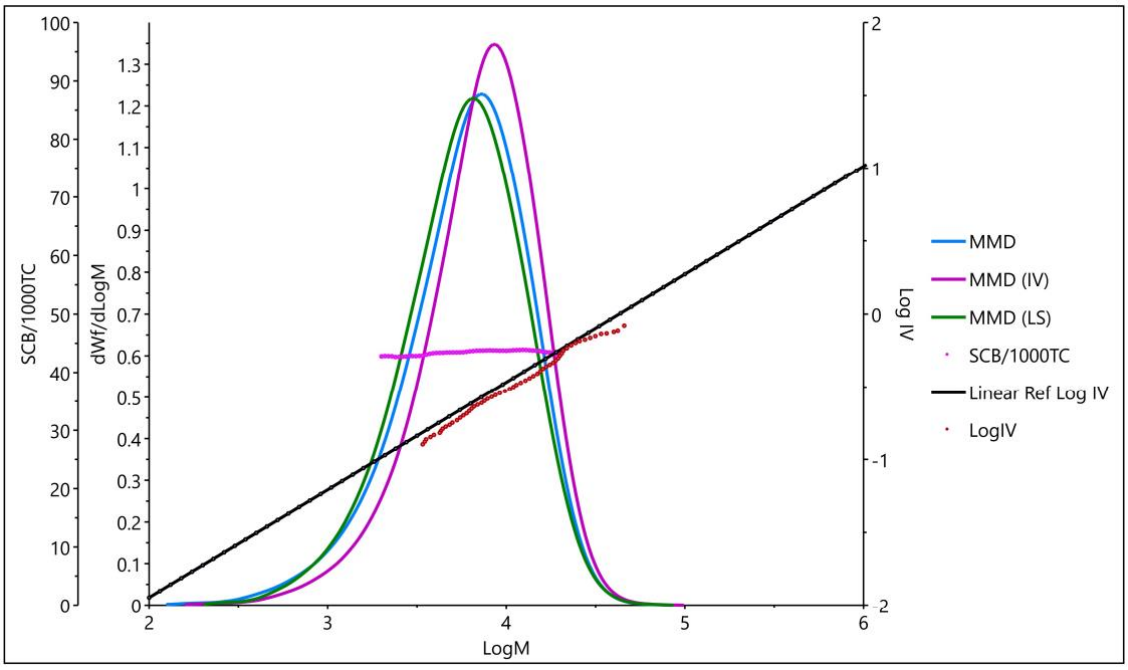

Results (Conventional)

Mw	7900	g/mol
Mn	3900	g/mol
Mw / Mn	2.0	
Mz	12400	g/mol
Mp	7300	g/mol
Mv	7300	g/mol
IVmwd	0.28	dL/g
Bulk CH3 / 1000C	51.4	
Bulk SCB / 1000C	44.5	

Figure S3.37: HT-GPC chromatogram of polyethylene for Table 3.1, entry 3.

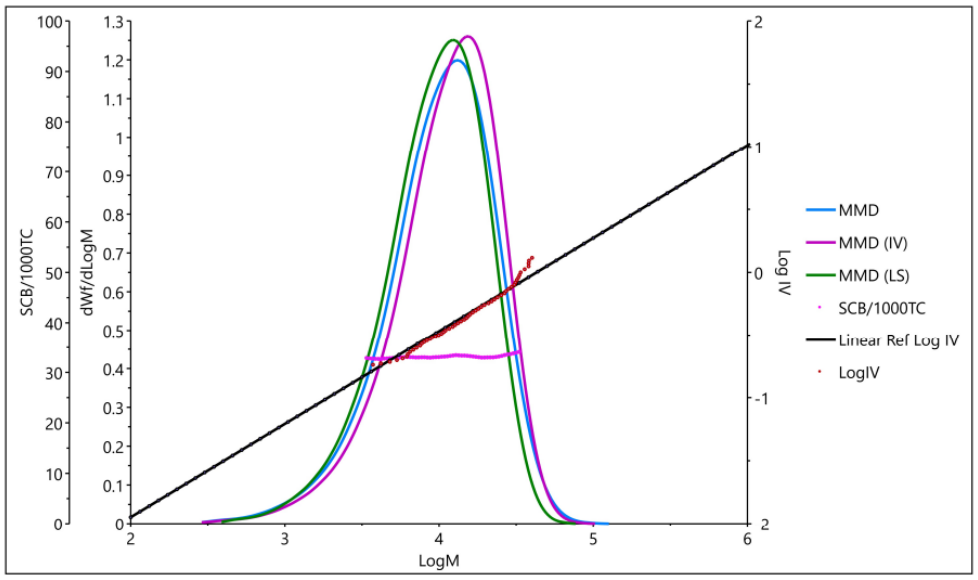

Results (Conventional)

Mw	13200	g/mol
Mn	6600	g/mol
Mw / Mn	2.0	
Mz	20600	g/mol
Mp	13100	g/mol
Mv	12300	g/mol
IVmwd	0.41	dL/g
Bulk CH3 / 1000C	38.6	
Bulk SCB / 1000C	34.5	

Figure S3.38: HT-GPC chromatogram of polyethylene for Table 3.1, entry 7.

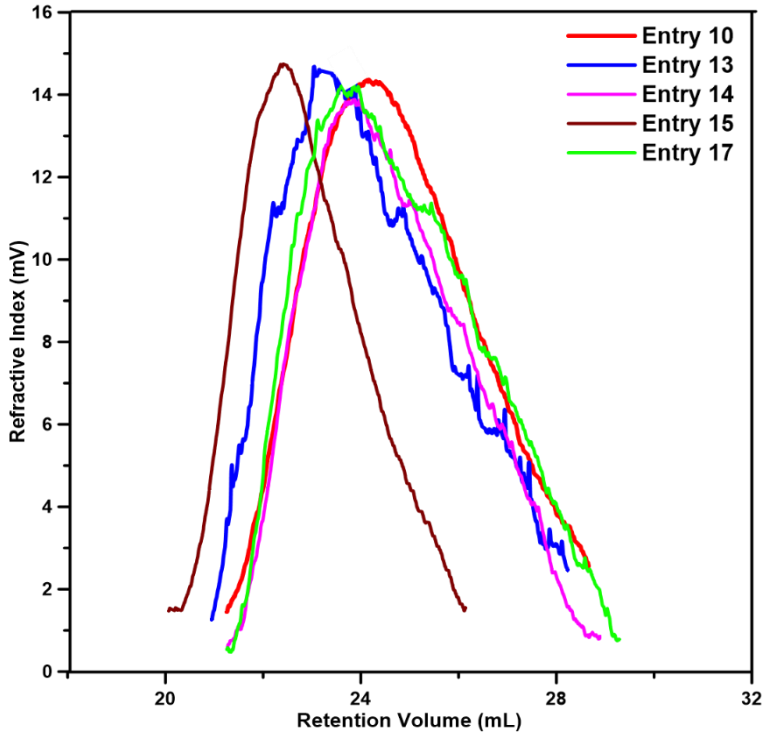

Figure S3.39: HT-GPC chromatogram of polyethylene for Table 3.1.

3.5.8. ^{13}C NMR data:

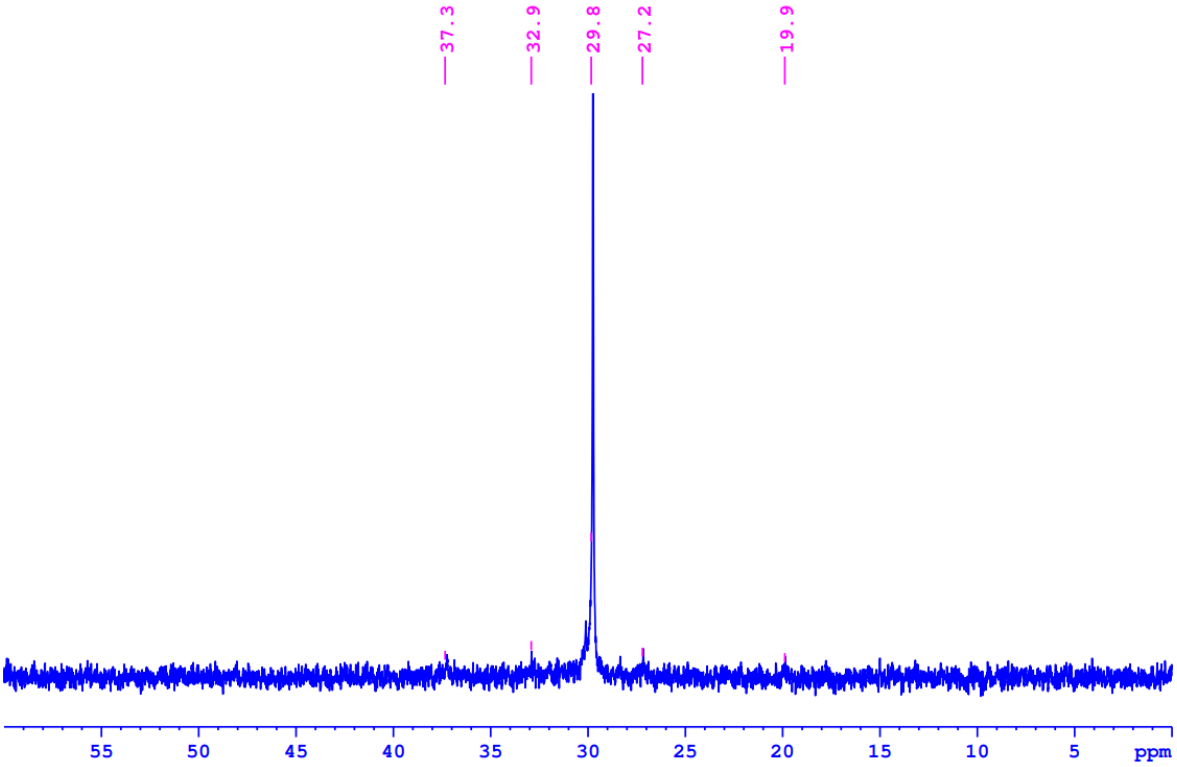

Figure S3.40: ^{13}C NMR spectrum of polyethylene in $C_2D_2Cl_4$ at 80 °C (Table 3.1, entry no. 9).

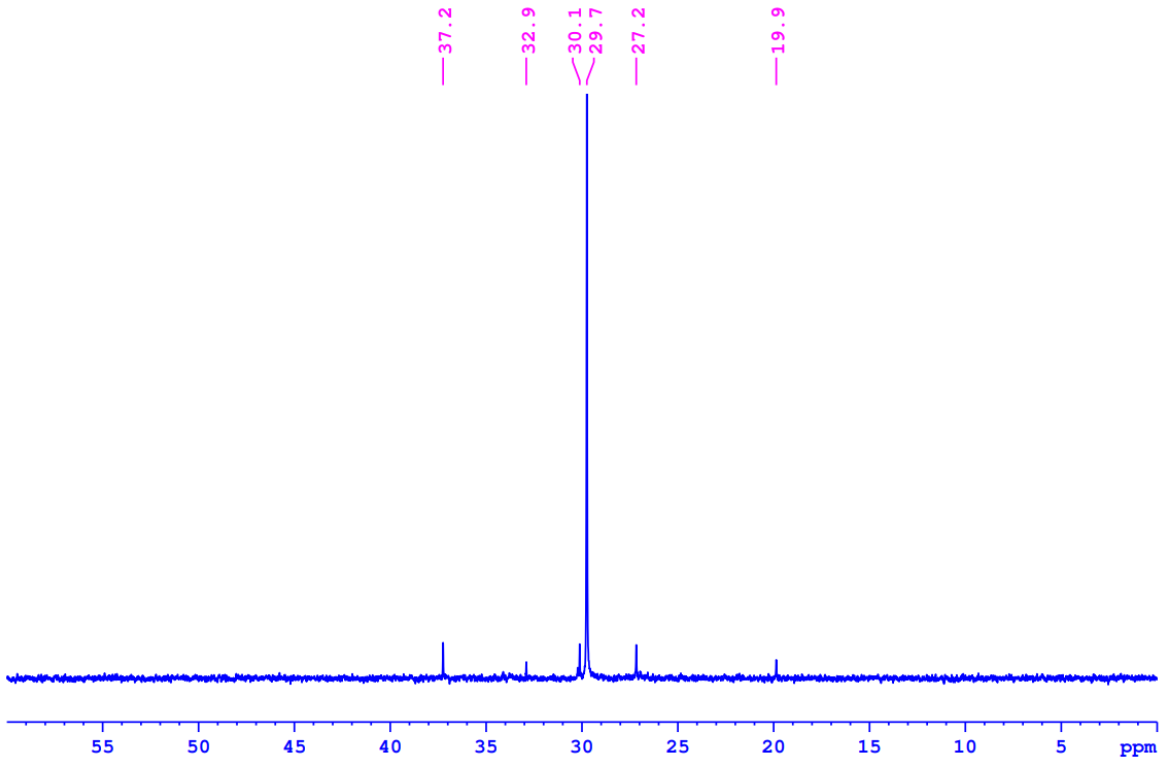

Figure S3.41: ^{13}C NMR spectrum of polyethylene in $C_2D_2Cl_4$ at 80 °C (Table 3.1, entry no. 13).

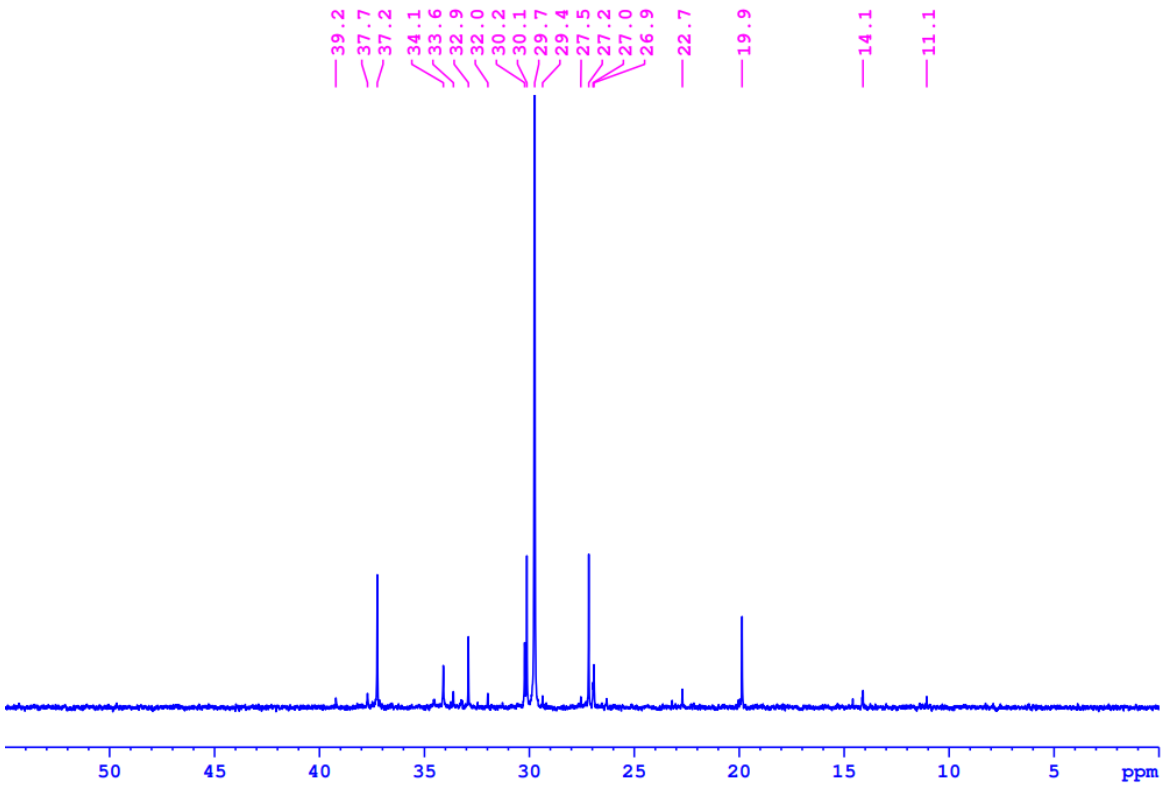

Figure S3.42: ^{13}C NMR spectrum of polyethylene in $C_2D_2Cl_4$ at 80 °C (Table 3.1, entry no. 17).

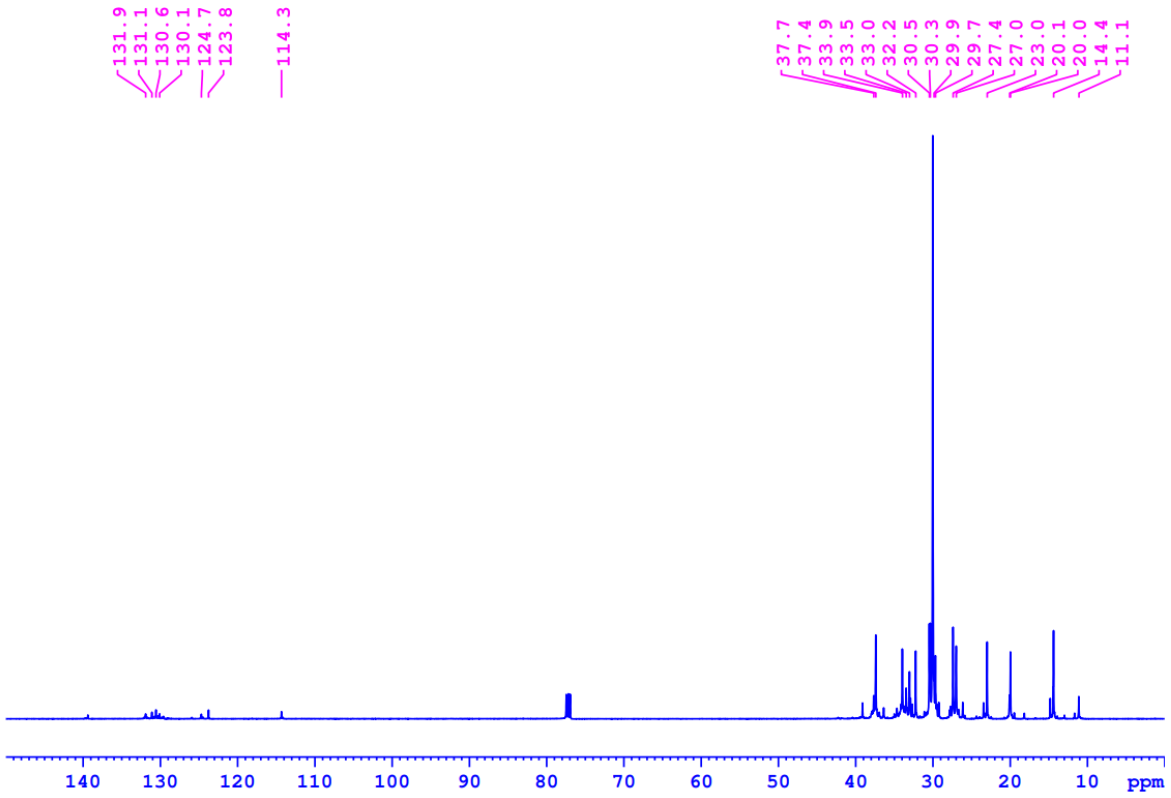

Figure S3.43: Quantitative ^{13}C NMR of ethylene oligomer in $CDCl_3$ obtained from Pd catalyst.

3.5.9. Melting temperature versus branching/1000C:

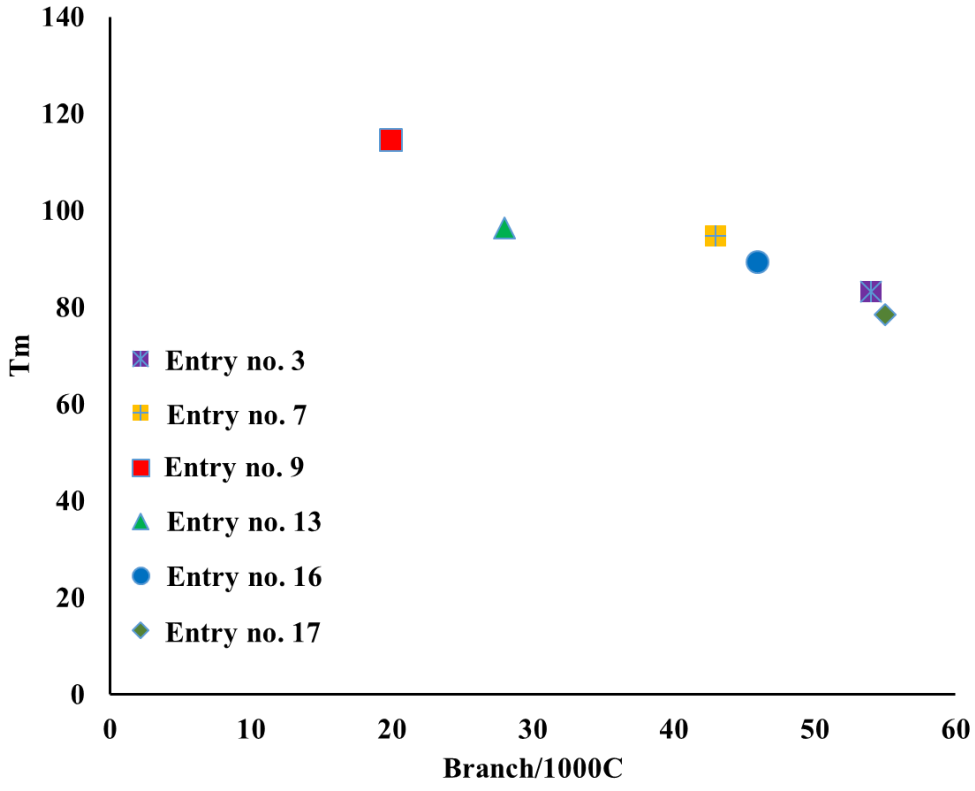

Figure S3.44: Plot of melting temperature versus branching.

Table S3.3. Determination of number of branches per 1000 carbon atoms.

Entry No.[a]	Branch/1000C[b]	T_m
3	54	83.1
7	43	94.6
9	20	114.4
13	28	96.3
16	46	89.1
17	55	78.3

[a]entry numbers are based on the table 1, [b]Branches per 1000 carbons calculated by ^{1}H NMR.

3.5.10. WAXS data:

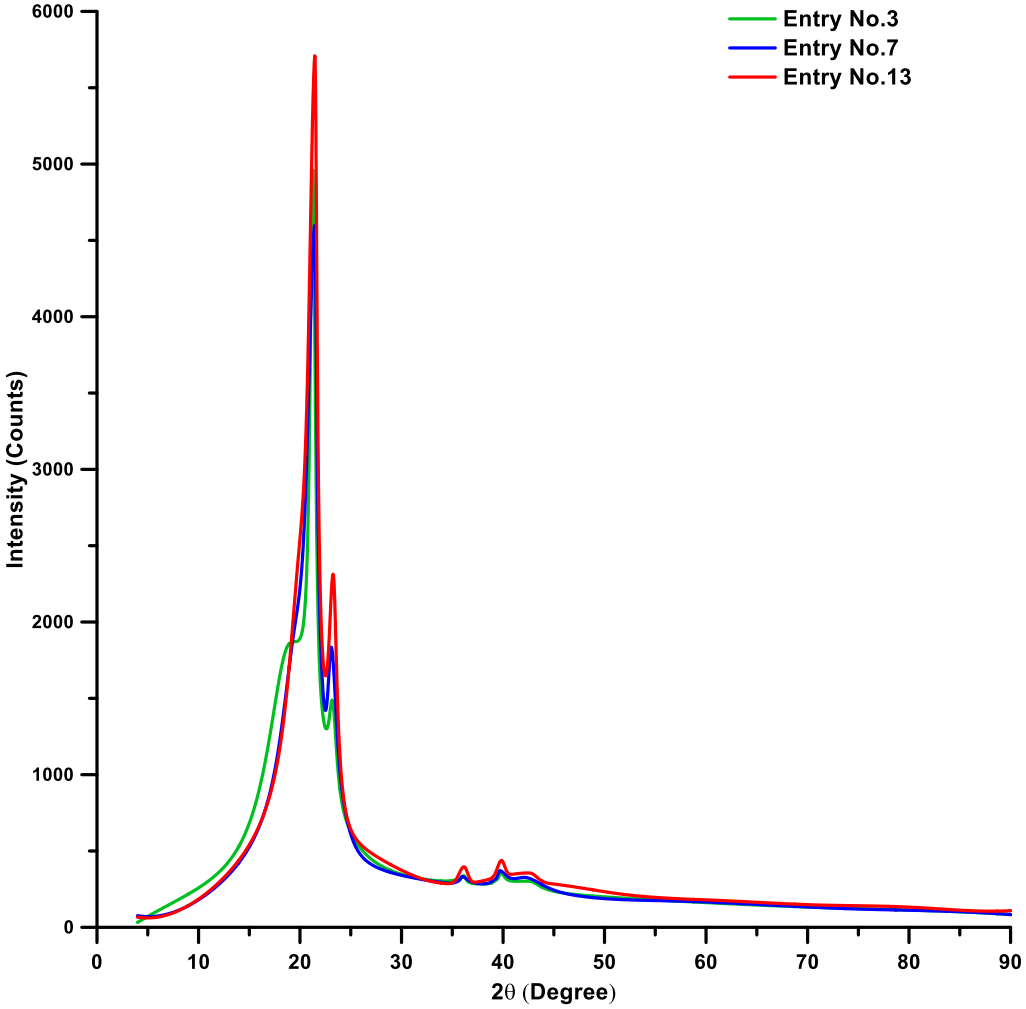

Figure S3.45: WAXS graph of polyethylene for Table 3.1.

The % of crystallinity of the samples were calculated by X- ray graph by using an following formula.

Crystallinity (%) = Area of crystalline peaks/ (Area of crystalline + Area of amorphous peaks) x 100

Ni1= 10262.13/32341.27

Ni2= 16908.01/31782.14

Ni3= 18998.96/35773.57

Sr. No	Cat. Used for PE synthesis	Entry No.	Branch/1000C	Crystallinity (%) by X-ray
1	Ni1	Entry no. 3	54	31.7
2	Ni2	Entry no. 7	43	53.1
3	Ni3	Entry no. 13	28	53.1

3.6. References:

1. S. H. Chikkali, In Metal Catalyzed Polymerization: Fundamentals to Applications, CRC Press, Taylor and Francis Group: USA, 2017.
2. Chen, C. Designing catalysts for olefin polymerization: Beyond electronic and steric tunning. *Nat. Rev. Chem.* **2018,** *2*, 6-14.
3. Stuerzel, M.; Mihan, S.; Muelhaupt, R. From Multisite Polymerization Catalysis to Sustainable Materials and All Polyolefin-composites. *Chem. Rev*. **2016**, *116*, 1398-1433.
4. Patel, K.; Chikkali, S. H.; Sivaram, S. Ultrahigh molecular weight polyethylene: Catalysis, structure, properties, processing and applications. *Prog. Polym. Sci*. **2020**, *109*, 101290/1-30.
5. Jr., J. Boor, In Ziegler-Natta Catalysts and Polymerization, Academic Press, New York, (1979).
6. Chikkali, S. H. Ziegler–Natta polymerization and the remaining challenges. *Resonance* **2017**, *22*, 1039-1060.
7. Claverie, J. P.; Schaper, F. Ziegler-Natta catalysis: 50 years after the Nobel Prize. *MRS Bulletin* **2013**, *38*, 213-218.
8. Sauter, D. W.; Taoufik, M.; Boisson, C. Polyolefins, a success story. *Polymers* **2017**, *9*, 185.

9. Johnson, L. K.; Killian C. M.; Brookhart, M. New Pd (II)-and Ni (II)-based catalysts for polymerization of ethylene and. alpha-olefins. *J. Am. Chem. Soc.* **1995**, *117*, 6414-6415.
10. Killian, C. M.; Tempel, D. J.; Johnson L. K.; Brookhart, M. Living polymerization of α-olefins using NiII− α-diimine catalysts. Synthesis of new block polymers based on α-olefins. *J. Am. Chem. Soc.* **1996**, *118*, 11664-11665.
11. Birajdar, R. S.; Chikkali, S. H. Insertion copolymerization of functional olefins: Quo Vadis?. *Eur. Polym. J.* **2021**, *143*, 110183.
12. Mahmood, Q.; Li, X.; Qin, L.; Wang, L.; Sun, W. H. Structural evolution of iminopyridine support for nickel/palladium catalysts in ethylene (oligo) polymerization. *Dalton Trans.* **2022**, *51*, 14375 – 14407.
13. Wang, Z.; Liu, Q.; Solan, G. A.; Sun, W. H. Recent advances in Ni-mediated ethylene chain growth: Nimine-donor ligand effects on catalytic activity, thermal stability and oligo-/polymer structure. *Coord. Chem. Rev.* **2017**, *350*, 68-83.
14. Zhang, Y.; Zhang, Y.; Hu, X.; Wang, C.; Jian, Z. Advances on controlled chain walking and suppression of chain transfer in catalytic olefin polymerization. *ACS Catal.* 2022, **12**, 14304–14320.
15. Qasim, M.; Bashir, M. S.; Iqbal, S.; Mahmood, Q. Recent advancements in α-diimine-nickel and-palladium catalysts for ethylene polymerization. *Eur. Polym. J.* **2021**, *160*, 110783.
16. Wang, Y.; Gao, R.; Gou, Q.; Lai, J.; Zhang, R.; Li, X.; Guo, Z Developments in late transition metal catalysts with high thermal stability for ethylene polymerization: A crucial aspect from laboratory to industrialization. *Eur. Polym. J.* **2022**, 111693.
17. Zhou, G.; Cui, L.; Mu, H.; Jian, Z. Custom-made polar monomers utilized in nickel and palladium promoted olefin copolymerization. *Polym. Chem.* **2021**, *12*, 3878-3892.
18. Mu, H.; Zhou, G.; Hu, X.; Jian, Z. Recent advances in nickel mediated copolymerization of olefin with polar monomers. *Coord. Chem. Rev.* **2021**, *435*, 213802.
19. Wu, R.; Wu, W. K.; Stieglitz, L.; Gaan, S.; Rieger, B.; Heuberger, M. Recent advances on α-diimine Ni and Pd complexes for catalyzed ethylene (Co) polymerization: A comprehensive review. *Coord. Chem. Rev.* **2023** *474*, 214844.

20. Mu, H.; Pan, L.; Song, D.; Li, Y. Neutral Nickel Catalysts for Olefin Homo and Copolymerization: Relationships between Catalyst Structures and Catalytic Properties. *Chem. Rev.* **2015**, *115*, 12091− 12137.
21. Advances on Controlled Chain Walking and Suppression of Chain Transfer in Catalytic Olefin Polymerization. *ACS Catal.* **2022,** *12*, 14304−14320.
22. Guan, Z.; Cotts, P. M.; McCord, E. F.; McLain, S. J. Chain walking: a new strategy to control polymer topology. *Science*, **1999**, *283*(5410), 2059-2062.
23. So, L. C.; Faucher, S.; Zhu, S. Synthesis of low molecular weight polyethylenes and polyethylene mimics with controlled chain structures. *Prog. Polym. Sci.* **2014**, *39*, 1196-1234.
24. Nele, M.; Soares, J. B.; Pinto, J. C. Evolution of Molecular Weight and Long Chain Branch Distributions in Olefin–Diene Copolymerization. *Macromol. Theory Simul.* **2003**, *12*, 582-592.
25. Gates, D. P.; Svejda, S. A.; Oñate, E.; Killian, C. M.; Johnson, L. K.; White, P. S.; Brookhart, M. Synthesis of Branched Polyethylene Using (α-Diimine) Nickel(II) Catalysts: Influence of Temperature, Ethylene Pressure, and Ligand Structure on Polymer Properties. *Macromolecules* **2000**, *33*, 2320−2334.
26. Dai, S.; Zhou, S.; Zhang, W.; Chen, C. Systematic Investigations of Ligand Steric Effects on α-Diimine Palladium Catalyzed Olefin Polymerization and Copolymerization. *Macromolecules* **2016**, *49*, 8855−8862.
27. Gong, Y.; Li, S.; Gong, Q.; Zhang, S.; Liu, B.; Dai, S. Systematic Investigations of Ligand Steric Effects on α-diimine Nickel Catalyzed Olefin Polymerization and Copolymerization. *Organometallics* **2019**, *38*, 2919−2926.
28. Ota, Y.; Ito, S.; Kuroda, J.; Okumura, Y.; Nozaki, K. Quantification of the Steric Influence of Alkylphosphine-Sulfonate Ligands on Polymerization, Leading to High-Molecular-Weight Copolymers of Ethylene and Polar Monomers. *J. Am. Chem. Soc.* **2014**, *136*, 11898−11901.
29. Piche, L.; Daigle, J. C.; Poli, R.; Claverie, J. P. Investigation of Steric and Electronic Factors of (Arylsulfonyl) phosphane-Palladium Catalysts in Ethene Polymerization. *Eur. J. Inorg. Chem.* **2010**, 4595–4601.
30. de Oliveira, O. B.; Brandao, S. T.; de Freitas, A. J. D.; da Silva, E. P.; Meneghetti, S. M. P.; Meneghetti, M. R. High-temperature and high-pressure ethylene polymerization using a cationic activated metallocene catalytic system. *Polym. Int.* **2008**, *57***,** 1012-1016.

31. Yue, E. L.; Xing, Q. F.; Zhang, L. P.; Shi, Q. S.; Cao, X. P.; Wang, L.; Redshaw, C.; Sun, W. H. Synthesis and characterization of 2-(2-benzhydrylnaphthyliminomethyl) pyridylnickel halides: formation of branched polyethylene. *Dalton Trans.* **2014**, *43*, 3339-3346.
32. Yue, E. L.; Zhang, L. P.; Xing, Q. F.; Cao, X. P.; Hao, X.; Redshaw C.; Sun, W. H. 2-(1-(2-Benzhydrylnaphthylimino) ethyl) pyridylnickel halides: synthesis, characterization, and ethylene polymerization behavior. *Dalton Trans*. **2014**, *43*, 423-431.
33. Kong, S. L.; Guo, C. Y. ;. Yang, W. H ; Wang, L.; Sun, W. H.; Glaser, R. 2, 6-Dibenzhydryl-N-(2-phenyliminoacenaphthylenylidene)-4-chloro-aniline nickel dihalides: Synthesis, characterization and ethylene polymerization for polyethylenes with high molecular weights. *J. Organomet. Chem.* **2013**, *725*, 37-45.
34. Song, K. F.; Yang, W. H.; Li, B. X.; Liu, Q. B.; Redshaw, C.; Li, Y. S.; Sun, W. H. Nickel (ii) complexes bearing 4, 5-bis (arylimino) pyrenylidenes: synthesis, characterization, and ethylene polymerization behaviour. *Dalton Trans.* **2013**, *42*, 9166-9175.
35. Kong, S. L.; Song, K. F.; Liang, T. L.; Guo, C. Y.; Sun, W. H.; Redshaw, C. Methylene-bridged bimetallic α-diimino nickel (II) complexes: synthesis and high efficiency in ethylene polymerization. *Dalton Trans*. **2013**, *42*, 9176-9187.
36. Lai, J. J.; Hou, X. H.; Liu, Y. W.; Redshaw, C.; Sun, W. H. 2-[1-(2, 6-Dibenzhydryl-4-methylphenylimino) ethyl]-6-[1-(arylimino) ethyl] pyridylnickel (II) halides: Synthesis, characterization and ethylene oligomerization behavior. *J. Organomet. Chem.* **2012**, *702*, 52-58.
37. Zhou, Z. H.; Hao, X.; Redshaw, C.; Chen, L. Q.; Sun, W. H. Nickel bis {4, 6-dibenzhydryl-2-[(arylimino) methyl] phenoxylate} complexes: Synthesis, structures, and catalytic behaviour towards ethylene and norbornene. *Catal. Sci. Technol.* **2012**, *2*, 1340-1345.
38. Rhinehart, J. L.; Brown, L. A.; Long, B. K. A robust Ni (II) α-diimine catalyst for high temperature ethylene polymerization. *J. Am. Chem. Soc.* **2013**, *135*, 16316-16319.
39. Dai, S.; Sui, X.; Chen, C. Highly Robust Palladium (II) αDiimine Catalysts for Slow-Chain-Walking Polymerization of Ethylene and Copolymerization with Methyl Acrylate. *Angew. Chem. Int. Ed.* **2015**, *54*, 9948−9953.

40. Hu, X.; Dai, S.; Chen, C. Ethylene polymerization by salicylaldimine nickel (II) complexes containing a dibenzhydryl moiety. *Dalton Trans.* **2016**, *45*, 1496-1503.
41. Dai, S.; Chen, C. Direct Synthesis of Functionalized High Molecular-Weight Polyethylene by Copolymerization of Ethylene with Polar Monomers. *Angew. Chem. Int. Ed.* **2016**, *55*, 13281− 13285.
42. Lu, W.; Fan, W.; Dai, S. A Rigid−Flexible Double-Layer Steric Strategy Promoting Ethylene Polymerization and Copolymerization in Alkane Solvents. *Inorg. Chem. Front.* **2022**, *10*, 108−117.
43. Guo, L.; Hu, X.; Lu, W.; Xu, D.; Liu, Q.; Dai, S. Investigations of Ligand Backbone Effects on Bulky Diarylmethyl-based Nickel(II) and Palladium(II) Catalyzed Ethylene Polymerization and Copolymerization. *J. Organomet. Chem.* **2021**, *952*, 122046.
44. Gong, Y.; Li, S.; Tan, C.; Kong, W.; Xu, G.; Zhang, S.; Liu, B.; Dai, S. π−π Interaction Effect in Insertion Polymerization with αDiimine Palladium Systems. *J. Catal.* **2019,** *378*, 184−191.
45. Dau, H.; Keyes, A.; Basbug Alhan, H. E.; Ordonez, E.; Tsogtgerel, E.; Gies, A. P.; Auyeung, E.; Zhou, Z.; Maity, A.; Das, A.; Powers, D. C.; Beezer, D. B.; Harth, E. Dual Polymerization Pathway for Polyolefin-Polar Block Copolymer Synthesis via MILRad: Mechanism and Scope. *J. Am. Chem. Soc.* **2020**, *142*, 21469−21483.
46. Keyes, A.; Dau, H.; Matyjaszewski, K.; Harth, E. Tandem Living Insertion and Controlled Radical Polymerization for Polyolefin−Polyvinyl Block Copolymers. *Angew. Chem., Int. Ed.* **2022,** *134*, No. e202112742.
47. Sun, J.; Wang, F.; Li, W.; Chen, M. Ligand steric effects on α-diimine nickel catalyzed ethylene and 1-hexene polymerization. *RSC Adv.* **2017**, *7*, 55051-55059.
48. Lu, Z.; Xu, X.; Luo, Y.; He, S.; Fan, W.; Dai, S. Unexpected Effect of Catalyst's Structural Symmetry on the Branching Microstructure of Polyethylene in Late Transition Metal Polymerization Catalysis. *ACS Catal.* **2023**, *13*, 725−734.
49. Younkin, T. R.; Connor, E. F.; Henderson, J. I.; Friedrich, S. K.; Grubbs, R. H.; Bansleben, D. A. Neutral, single-component nickel (II) polyolefin catalysts that tolerate heteroatoms. *Science* **2000**, *287*, 460-462.
50. Wang, C.; Friedrich, S.; Younkin, T. R.; Li, R. T.; Grubbs, R. H.; Bansleben, D. A.; Day, M. W. Neutral nickel (II)-based catalysts for ethylene polymerization. *Organometallics* **1998**, *17*, 3149-3951.

51. Waltman, A. W.; Younkin, T. R.; Grubbs, R. H. Insights into the deactivation of neutral nickel ethylene polymerization catalysts in the presence of functionalized olefins. *Organometallics* **2004**, *23*, 5121-5123.
52. Berkefeld, A.; Mecking, S. Deactivation pathways of neutral Ni (II) polymerization catalysts. *J. Am. Chem. Soc.* **2009**, *131*, 1565-1574.
53. Chen, Z.; Mesgar, M.; White, P. S.; Daugulis, O.; Brookhart, M. Synthesis of branched ultrahigh-molecular-weight polyethylene using highly active neutral, single-component Ni (II) catalysts. *ACS Catal.* **2015**, *5*, 631-636.
54. Weberski Jr, M. P.; Chen, C.; Delferro, M.; Zuccaccia, C.; Macchioni, A.; Marks, T. J. Suppression of β-hydride chain transfer in nickel (II)-catalyzed ethylene polymerization via weak fluorocarbon ligand–product interactions. *Organometallics* **2012**, *31*, 3773-3789.
55. Wang, C.; Kang, X.; Mu, H.; Jian, Z. Positive Effect of Polar Solvents in Olefin Polymerization Catalysis. *Macromolecules* **2022**, *55*(13), 5441-5447.
56. Birajdar, R. S.; Gonnade, R. G.; Pol, H. V.; Basava Prabhu, M.; Rokade, D.; Nandimath, S.; Chikkali, S. H. Palladium-catalyzed polar solvent empowered synthesis of hyperbranched ethylene oligomer and their applications. *Polym. Chem.* **2023**, 14, 3239-3251.
57. Schiebel, E.; Santacroce, S.; Falivene, L.; Goettker-Schnetmann, I.; Caporaso, L.; Mecking, S. Tailored Strength Neighboring Group Interactions Switch Polymerization to Dimerization Catalysis. *ACS Catal.* **2019**, *9*, 3888-3894.
58. Deshmukh, S. S.; Gaikwad, S. R.; Gonnade, R.; Pandole, S. P.; Chikkali, S. H. Pd-Imincarboxylate complexes and Their Behavior in Ethylene Polymerization. *Chem. Asian. J.* **2020**, *15*, 398-405.
59. For cis-angle, see: Gaikwad, S. R.; Deshmukh, S. S.; Gonnade, R. G.; Rajamohanan, P. R.; Chikkali, S. H. Insertion copolymerization of difunctional polar vinyl monomers with ethylene. *ACS Macro Lett.* **2014**, *4*, 933-937.
60. Falivene, L.; Cao, Z.; Petta, A.; Serra, L.; Poater, A.; Oliva, R; Scarano, V.; Cavallo, L. Towards the online computer-aided design of catalytic pockets. *Nat. Chem.* **2019**, *11*, 872-879.
61. Song, D. P.; Wang, Y. X.; Mu, H. L.; Li, B. X.; Li, Y. S. Observations and mechanistic insights on unusual stability of neutral nickel complexes with a sterically crowded metal center. *Organometallics* **2011**, *30*(5), 925-934.

62. For oligoethylenes see: Mote, N. R.; Gaikwad, S. R.; Khopade, K. V.; Gonnade, R. G.; Chikkali, S. H. Controlled di-lithiation enabled synthesis of phosphine-sulfonamide ligands and implications in ethylene oligomerization. *Dalton Trans*. **2021**, *50*, 3717-3723.
63. Guan, Z. Control of polymer topology by chain-walking catalysts. *Chem. Eur. J.* **2002**, *8*, 3086-3092.
64. Wiedmann, T.; Voit, G.; Tchernook, A.; Roesle, P.; Goettker-Schnetmann, I.; Mecking, S. Monofunctional hyperbranched ethylene oligomers. *J. Am. Chem. Soc.* **2014**, *136*, 2078-2085.
65. H.Fan, G. Chang, H. Bi, X. Gui, H. Wang, G. Xu, and S. Dai, *ACS Polymers Au*, 2021, **2**, 88-96.
66. L. Guo, W. Liu, K. Li, M. Sun, W. Sun, L. Zhao, G. Jiang, H. Peng, Z. Liu, and S. Dai, *Eur. Polym. J.*, 2019, **115**, 185-192.
67. Standley, E. A.; Smith, S. J.; Müller, P.; Jamison, T. F. A broadly applicable strategy for entry into homogeneous nickel (0) catalysts from air-stable nickel (II) complexes. *Organometallics* **2014**, *33*, 2012-2018.
68. Cai, L.; Zhu, X.; Chen, J.; Lin, A.; Yao, H. Rh(III)-Catalyzed C–H activation/annulation of salicylaldehydes with sulfoxonium ylides for the synthesis of chromones. *Org. Chem. Front.* **2019**, *6*, 3688-3692.
69. Meiries, S.; Speck, K.; Cordes, D. B.; Slawin, A. M. Z.; Nolan, S. P. [Pd(IPr*OMe)(acac)Cl]: Tuning the N-Heterocyclic Carbene in Catalytic C–N Bond Formation. *Organometallics* **2013**, *32*, 330-339.
70. Xia J.; Zhang Y.; Kou S.; Jian Z. A concerted double-layer steric strategy enables an ultra-highly active nickel catalyst to access ultrahigh molecular weight polyethylenes. *J.Cat.***2020**, *390*, 30-36.

Chapter 4

Synthesis of Imine-Phenoxy Ligated Palladium Complexes for Norbornene Homopolymerization

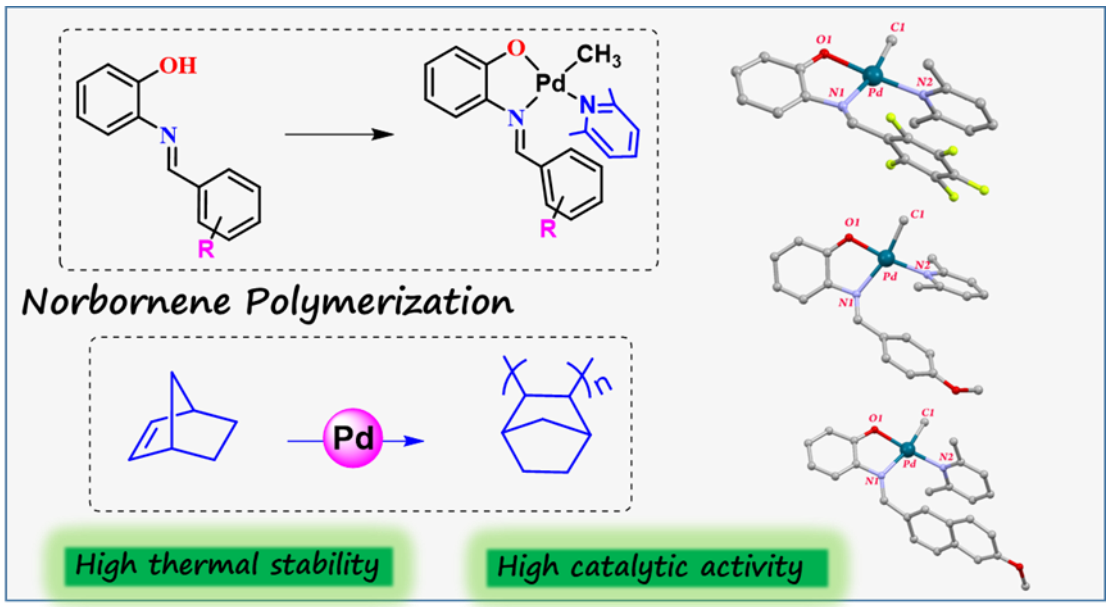

4.1. Abstract:

Ligands play a crucial role in olefin polymerization and control molecular weight, crystallinity, and stereo-regularity. We report a single step synthesis of imine-phenoxy ligands in excellent yield (81-93%). A condensation of 2-aminophenol and different electronically tuned aniline derivatives produced electronically tuned imine phenoxy ligands (4L1-4L4). The identity of the ligands was unambiguously ascertained using a combination of spectroscopic and analytical methods. These ligands were treated with [Pd(COD)MeCl] in presence of 2,6-lutidine, resulting in the formation of discrete mononuclear palladium complexes 4Pd1-4Pd4 with excellent yields. 1-2D NMR, mass analysis, and single-crystal X-ray diffraction confirmed the identity of the palladium complexes. The single crystal X-ray diffraction analysis revealed a distorted square planar geometry around palladium in 4Pd1, 4Pd2 and 4Pd4 complexes. A crucial cis arrangement of the methyl group on palladium and 2,6-lutidine,was observed, which is essential for insertion polymerization of olefins. Proton NMR analysis suggest, 4Pd1 catalyst is deshielded, suggesting electronically deficient palladium metal compared to other complexes and also 4Pd1 catalyst shows the highest percent of buried volume (%Vbur =44.9). When exposed to norbornene, 4Pd1-Pd4 were found to be active and produced poly(norbornene) (PNB). Boron and aluminium based cocatalysts were screened and MMAO was found to outperform others with a high catalytic activity (upto 63.2×10^5 g of PNB (mol. of Pd)$^{-1}$ h^{-1}) in norbornene homopolymerization.

4.2. Introduction:

Metal-catalyzed olefin polymerization is known for decades and polyolefins, the largest volume polymers, are industrially produced using Ziegler-Natta, metallocene catalysts. Norbornene (NB) is a type of cycloolefin that can be polymerized using the three different methods: cationic or radical polymerization; ring-opening metathesis polymerization; and vinyl-addition polymerization.[1] Vinyl addition norbornene polymer (PNB) stands as a notable class of specialty polymers renowned for its remarkable optical and mechanical properties, including a high glass transition temperature, exceptional optical transparency, and low dielectric constant, rendering it highly attractive for a diverse range of industrial applications.[2-5] Metal complexes have been successfully used as pre-catalysts for vinyl polymerization of NB, and can be divided into early transition metal catalysts and late transition catalysts. Early transition metal catalysts, especially metallocene,[6] Ziegler–Natta catalysts,[7] zirconium catalysts, could produce crystalline polymers with extremely high glass-transition temperatures.

Similar to homopolymerization copolymerization of ethylene and norbornene (E-NB) has been a subject of considerable research aimed at improving the solubility and processability of resulting polymers. Initially explored by Kaminsky et al., who utilized zirconocene catalysts, this method has since sparked investigations into various catalysts based on both early and late transition metals.[8,9] While early transition metal catalysts have traditionally been employed for E-NB copolymerization, they are unsuitable for norbornene homopolymerization due to the low solubility and high melting temperatures of resulting polymers, which leads to difficulties in processsibility.[9] Conversely, late transition metal catalysts have garnered significant interest due to their low oxophilicity, offering the potential to incorporate polar monomers during olefin polymerization.[10-12] In 1995, Brookhart et al. reported cationic Ni(II) and Pd(II) complexes with bulky α-diimine ligands, enabling the production of branched polyethylene and copolymerization of ethylene with polar monomers. Since then, late transition-metal catalysts have been extensively studied. Towards the end of the 20th century, Grubbs et al. introduced neutral Ni(II) complexes with salicylaldimine ligands, demonstrating high catalytic activity in olefin polymerization without a cocatalyst. These unique characteristics have spurred interest in developing novel neutral Pd(II) and Ni(II) catalysts for olefin (co)polymerization.

In olefin polymerization as ligand plays an prominent role to control an molecular weight, crystallinity and sterioregularity. Recent studies have emphasized on the bidentate ligand with late transition metal catalyst. In the combination with bidendate ligand with nickel complex like bis(imino)pyridine Ni(II) catalysts,[13] α-diimine Ni(II) catalysts,[14-17] salicylaldimine Ni(II) catalysts,[18] phosphine-sulfonate Ni(II) catalysts,[19] β-enaminoketonato Ni(II) catalysts,[20] aryloxide-NHC Ni(II) catalysts,[21,22] and (anilino)anthraquinone Ni(II) catalysts[23] are widely studied in the copolymerization of norbornene with ethylene, α-olefins, and polar monomers. While, palladium catalysts have been widely studied and used in the homopolymerization of NB.[24-37]

In 1966, simple palladium chloride, without ligand, was used as catalyst for norbornene polymerization and moderate to high catalytic activity was observed.[38] Recently, research efforts have focused on developing highly active palladium catalysts with various ligands for the vinyl polymerization of norbornene (Figure 4.1, C1-C6).[24-37] Among these ligands, [N,N] bidentate ligands such as α-diimine, β-diimine, pyrrolide-imine, pyridine-imine, anilido-imine, and amidinate have been extensively studied.[39-55] In a similar vein, Hu et al. reported binuclear (N-O) neutral nickel and palladium complexes for norbornene homopolymerization.[56]

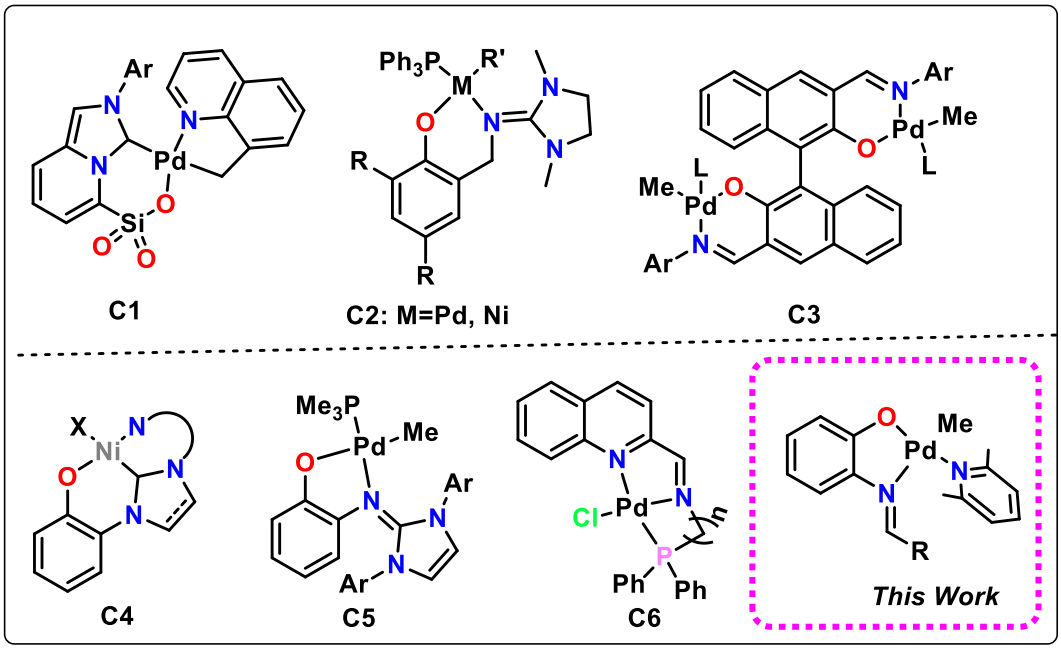

Figure 4.1: Selected examples of previously reported catalysts for norbornene polymerization.

As evident from C1-C6, electronic and steric effect of the ligands plays an important role in olefin polymerization and control the molecular weight and activity. The electronic and steric effect of ligands on ethylene polymerization is widely studied but to our knowledge, such as effect on the norbornene polymerization remains unexplored. As a result, there is an need to synthesize an electronically tuned ligand, corresponding palladium catalysts and study the effect of those on the catalytic activity with and without aluminium cocatalysts.

Here in, we report a single step synthesis of imine-phenoxy ligands (4L1-4L4) and corresponding 5-membered palladium complexes (4Pd1-4Pd4). The ligands and palladium complexes have been characterized using spectroscopic and analytical tools, including single crystal X-ray diffraction. The performance of 4Pd1-4Pd4 in norbornene homopolymerization has been examined.

4.3. Results and discussion:

4.3.1. Ligand synthesis:

As depicted in Scheme 4.1, the ligands 4L1-4L4 were synthesized via a condensation reaction between 2-aminophenol and electronically tuned aldehyde derivatives. 2-aminophenol was initially dissolved in ethanol and 2,3,4,5,6-pentafluorobenzaldehyde was then added dropwise, resulting in the rapid formation of a solid precipitate of the imine ligand 2-(((perfluorophenyl)methylene)amino)phenol(4L1). The reaction mixture was subsequently stirred for 10 minutes at room temperature to ensure complete reaction. The ethanol layer was decanted into another round-bottom flask, and the obtained solid was washed with cold hexane

to yield pure red-colored ligand in excellent yield (93.5%) . The identity of the obtained ligand was confirmed using ^{1}H, ^{13}C, and DEPT NMR spectroscopy. The proton NMR spectrum displayed a sharp singlet at 8.75 ppm (Figure S4.1), corresponding to the imine proton. The presence of the imine carbon was further confirmed by ^{13}C and DEPT NMR spectroscopy, with the imine carbon resonating at 152.5 ppm (Figure S4.2).

Similarly, ligands 4L2 and 4L3 were synthesized by treating aldehyde derivatives containing electron-donating groups (4-methoxybenzaldehyde, 2,4,6-trimethoxybenzaldehyde) with 2-aminophenol in ethanol, resulting in excellent yields (88 and 90%, respectively). Ligand L4 was synthesized by treating the sterically hindered rigid 6-methoxy-2-naphthaldehyde with 2-aminophenol in ethanol, with 81% yield. The structures of ligands 4L2, 4L3, and 4L4 were confirmed using NMR spectroscopy. The corresponding imine proton peaks are observed in ^{1}H and ^{13}C NMR. Additionally, mass spectrometry analysis of ligand 4L4 revealed a molecular ion peak at m/z = 278.11 Da $[M + H]^{+}$, further confirming the identity (Figure S4.12).

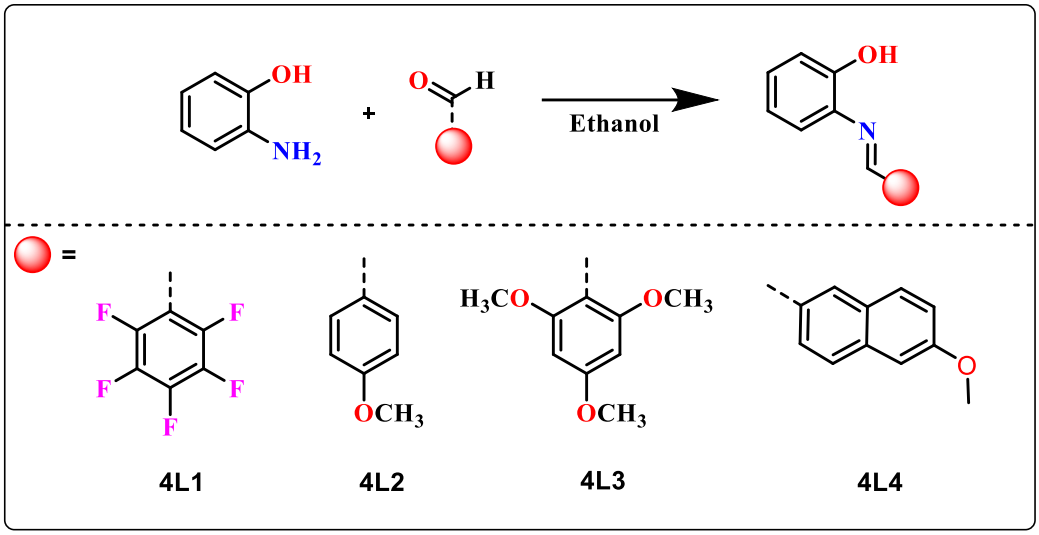

Scheme 4.1: synthesis of Ligand (4**L1-4L4**).

4.3.2. Synthesis of complex:

Initially, ligand 4L1 was subjected for deprotonation reaction using sodium hydride in THF for 3 hours. Subsequently, the above sodium salt of the ligand was added to the [Pd(COD)MeCl] in THF, followed by the addition of 2,6-lutidine. After 1 hour, the solvent was evaporated, and ^{1}H NMR was recorded. Surprisingly, no Pd-Me peak or 2,6-lutidine peaks were observed in the crude reaction mixture. But, signals corresponding to imine protons were detected at 8.67 ppm (Figure S4.28), along with peaks in the aromatic region. Based on the NMR data and

comparison with previous literature,[57-58] it was confirmed that the species [1,4] oxazepines (Scheme 4.2, P1) was formed under these conditions.

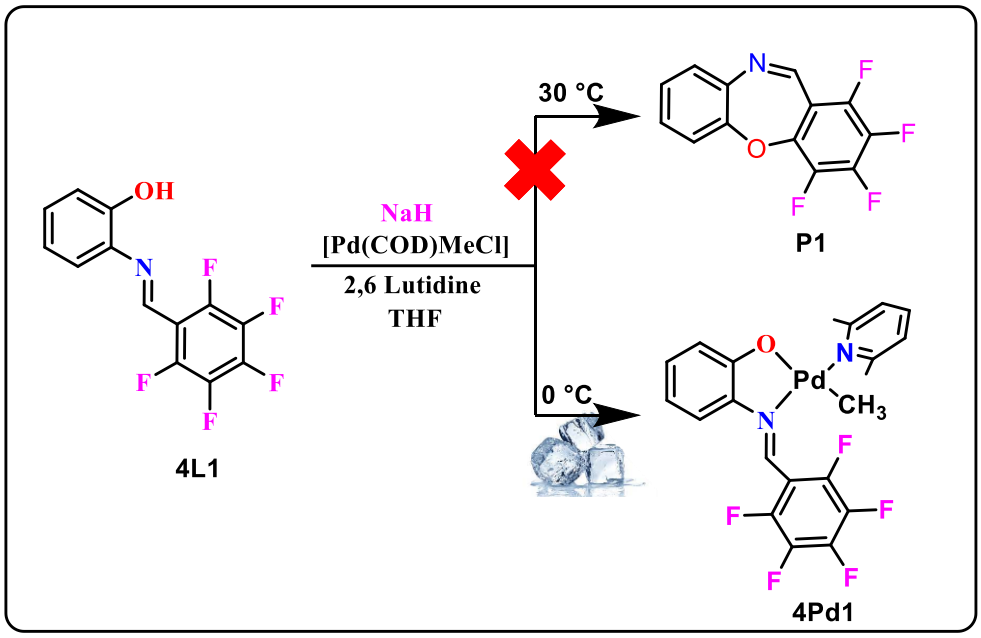

Scheme 4.2: Synthetic route for synthesis of [1,4] Oxazepines **(P1)** and palladium(4Pd1) complex.

Literature reports suggest that reaction temperature plays a crucial role for formation of [1,4] Oxazepines.[57,58] Therefore, we performed the same reaction as above but at 0 °C. Interestingly, this modification led to the selective formation of the 4Pd1 complex, with no detectable presence of the anticipated [1,4] oxazepines (P1) compound. The obtained 4Pd1 complex was thoroughly characterized using 1D and 2D NMR spectroscopy. ^{1}H NMR disclosed the Pd-Me species in the shielded region at 0.69 ppm (Figure S4.14), with its corresponding Pd-carbon observed at -4.9 ppm. Additionally, peaks representing 2,6-lutidine were observed in the aromatic region, alongside the lutidine methyl peak at 3.07 ppm and its corresponding carbon at 28.1 ppm. The imine proton was detected at 8.50 ppm. Further insights were gained through 2D NMR (^{1}H-^{1}H NOESY), revealing cross peaks between the Pd-Me and 2,6-lutidine methyl protons. This observation suggests that these two groups are associated within the same metal centre.

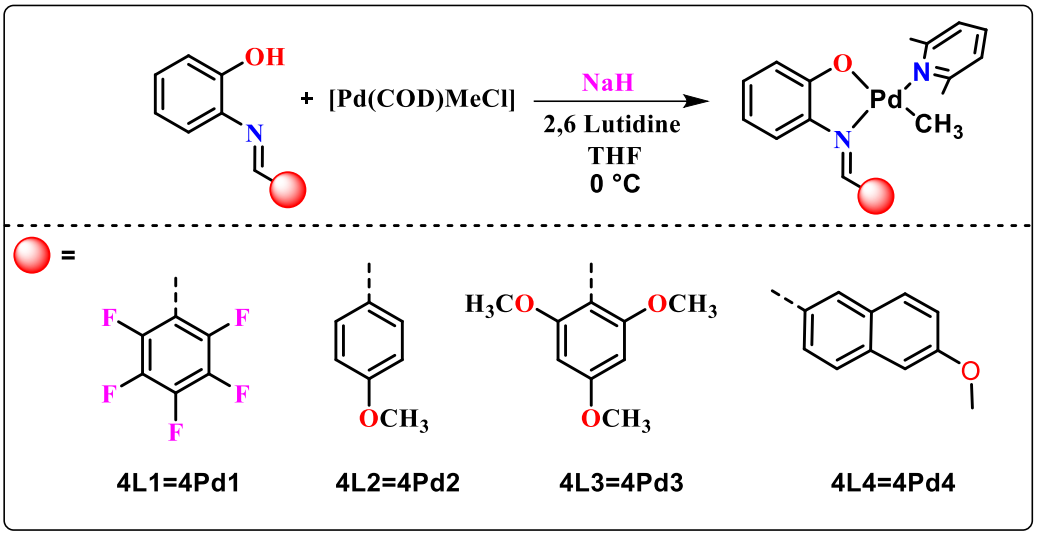

Scheme 4.3: Synthesis of palladium complex (4Pd1-4Pd4).

All complexes were obtained in good to excellent yields and their existence was confirmed via 1-2D NMR spectroscopy as well as mass spectrometry. In the ^{1}H NMR spectra of the 4Pd1-4Pd4 complexes, the Pd-Me peaks were consistently observed in the shielded region, ranging from 0.49 to 0.69 ppm.

The identification of 4Pd1, 4Pd2, and 4Pd4 complexes was conclusively confirmed through single-crystal X-ray diffraction analysis. Figure 4.2, 4.3, and 4.4 illustrate the molecular structures of 4Pd1, 4Pd2, and 4Pd4, respectively, while Table 2.1 presents selected bond distances and angles. Crystals suitable for analysis were obtained from a solvent mixture of dichloromethane and hexane at ambient temperature. The geometry around the palladium metal centre exhibited a distorted square planar configuration.

In the complex 4Pd1, the methyl group was positioned *cis* to the 2,6-lutidine nitrogen atom, forming a C1–Pd–N2 bond angle of 87.8(5)°. The 2,6-lutidine ligand was located *cis* to the imine nitrogen, resulting in an N1–Pd–N2 bond angle of 104.7(7)°. Additionally, the oxygen atom and methyl group were *cis* to each other, with an O1–Pd–C1 angle of 88.3(4)°, and *trans* to the 2,6-lutidine group, with an O1–Pd–N2 angle of 176.0(5)°. The bond distances between palladium (Pd1) and imine (N1), and 2,6-lutidine were found to be 2.17(1) Å and 2.14(1) Å, respectively, suggesting coordination of both nitrogen atoms to the central palladium. Shorter bond distances of Pd–O and Pd-C1 (methyl) at 2.10(8) Å and 1.99(1) Å, respectively, indicates the formation of covalent bonds. The observed C1–Pd–N2 bond angle of 87.8(5)° supported the *cis* position of the 2,6-lutidine and methyl groups on palladium, which is crucial for initiating insertion polymerization.

The 4Pd2 and 4Pd4 complexes share a common structural motif, the imine-naphthoxy ligated palladium complex, wherein palladium is coordinated by four atoms, adopting a distorted square planar geometry. Similar to 4Pd1, both 4Pd2 and 4Pd4 exhibited covalent bonds between the oxygen and methyl atoms, and coordinate bonds with the imine nitrogen of the ligand and 2,6-lutidine with the central palladium atom. Furthermore, the C1–Pd–N2 angle in 4Pd2 and 4Pd4 was found to be *cis* (<105°), indicating their potential as catalyst in insertion polymerization.

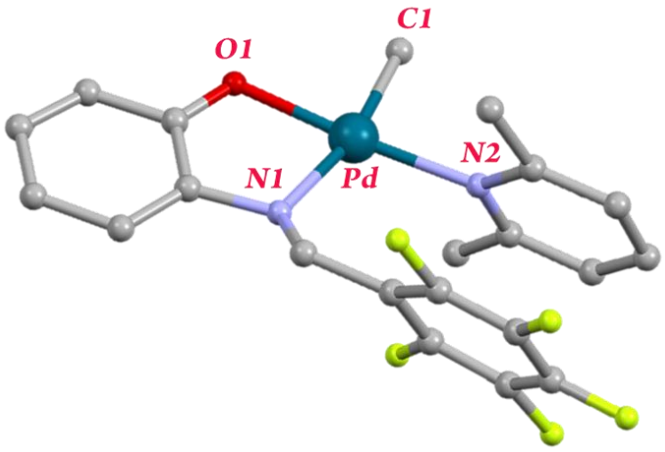

Figure 4.2: Molecular structure of **4Pd1**. H-atoms have been omitted for clarity; thermal ellipsoids are drawn at the 50% probability level.

Table 4.1: Selected Bond Lengths (Å) and Angles (deg) for Pd(II) Complexes.

Sr. No.		4Pd1	4Pd2	4Pd4
1.	Pd-C1	1.99(1)	2.03(1)	2.02(1)
2.	Pd-O1	2.10(8)	2.01 (9)	2.01(1)
3.	Pd-N1	2.17(1)	2.19(2)	2.18(2)
4.	Pd-N2	2.14(1)	2.02(2)	2.08(2)
5.	O1-Pd-N1	79.2(6)	81.4(6)	80.2(7
6.	O1-Pd-N2	176.0(5)	169.9(5)	174.9(7)
7.	O1-Pd-C1	88.3(4)	86.5(5)	87.2(5)
8.	N1-Pd-N2	104.7(7)	105.6(7)	104.8(8)
9.	N1-Pd-C1	166.8(6)	163.9(6)	167.0(7)
10.	N2-Pd-C1	87.8(5)	87.8(6)	87.8(7)

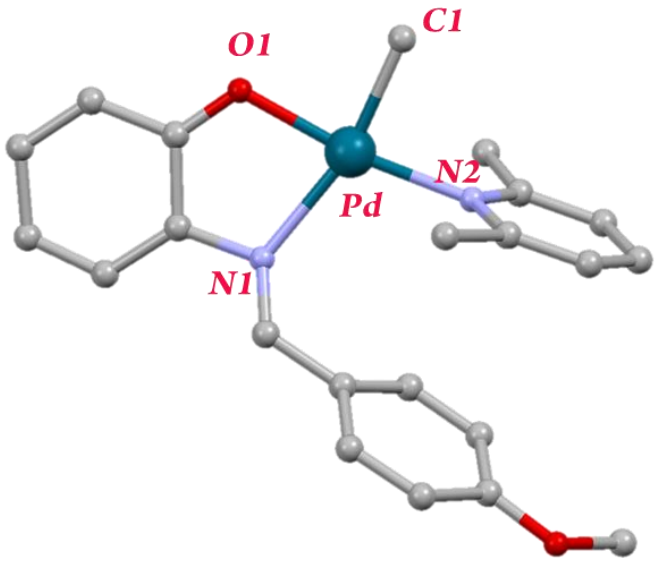

Figure 4.3: Molecular structure of **4Pd2**. H-atoms have been omitted for clarity; thermal ellipsoids are drawn at the 50% probability level.

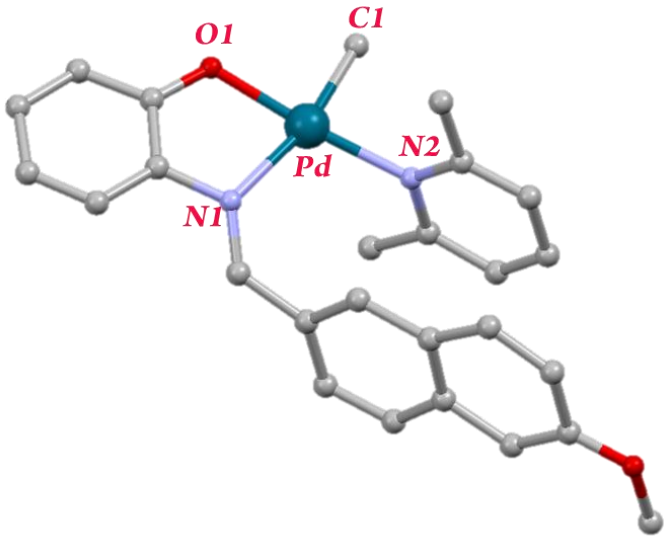

Figure 4.4: Molecular structure of **4Pd4**. H-atoms have been omitted for clarity; thermal ellipsoids are drawn at the 50% probability level.

4.3.3. Influence of steric and electronic parameters:

Using both NMR and crystallographic data, we investigated the electronic effects of various ligands on the palladium centre. To identify the effect, we focused on methyl group covalently bonded to palladium, and we recorded the proton NMR spectra for all complexes. The ^{1}H NMR spectra and crystallographic data for the palladium methyl species are summarized in Table 4.2, and the corresponding NMR spectra for 4Pd1-4Pd4 complexes are presented in the figure 4.5.

Analysis of the NMR spectra revealed that ligands with 2,3,4,5,6-pentafluoro substituents (4Pd1) exhibited deshielded methyl peaks at 0.69 ppm, while the corresponding Pd-C bond length was smaller (1.99(1) Å). In contrast, the 4Pd2 complex, featuring a methoxy group, displayed a shielded methyl peak at 0.64 ppm compared to the fluorine-substituted metal complex, with a higher bond length (2.03(1) Å). These findings suggest that pentafluoro substituents makes palladium more electron-deficient, resulting in a stronger Pd-methyl bond as evidenced by the decrease in bond length and the deshielded nature of the proton.

Further analysis indicated that the ligand with 2,4,6 trimethoxy substitution (4Pd3) led to highly shielded methyl peaks (0.49 ppm), while 4Pd4 exhibited a deshielded region (0.62 ppm) due to the presence of electron-donating groups located farther from the metal centre. Corresponding changes in bond length were observed in the crystal data. The presence of electron-donating groups weakened the palladium methyl bond, leading to an increase in the metal-methyl distance observed in the crystallographic data and a shift towards shielded regions in the proton spectra. This suggests that an increase in the number of methoxy groups weakens the palladium methyl bond.

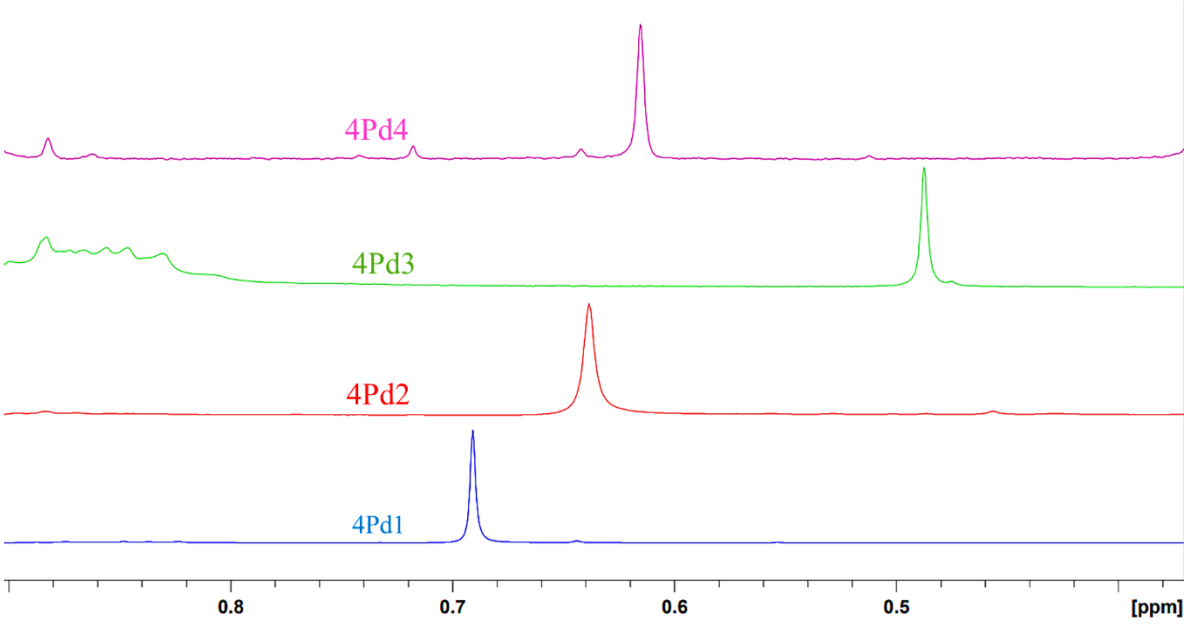

Figure 4.5: Pd-Me peaks in palladium catalyst (**4Pd1-4Pd4**).

Table 4.2: Bond Lengths (Å) and δ values for Pd-Me bond in 4Pd1-4Pd4.

Sr. No.	Catalyst	Pd-Me (ppm)	Pd-Me bond length (Å)
1.	4Pd1	0.69	1.99(1)
2.	4Pd2	0.64	2.03(1)
3.	4Pd3	0.49	-

4.	4Pd4	0.62	2.02(1)

To assess the quantification of ligand steric effects around the palladium metal center, we calculated the % Vbur for complexes 4Pd1, 4Pd2, and 4Pd4 using the SambVCA 2.1 web application (Figure 4.6).[59] The % Vbur calculation revealed that the pentafluoro-ligated metal center in 4Pd1 exhibited 44.9% steric crowding around the metal center. Conversely, 4Pd2 and 4Pd4 displayed % Vbur values of 43.0% and 43.6%, respectively. The higher steric crowding observed in 4Pd1 can be attributed to the presence of fluorine atoms. In 4Pd2, the presence of a methoxy group in the para position led to a decrease in the % Vbur compared to 4Pd1. On the other hand, 4Pd4 exhibited higher steric effects compared to 4Pd2 due to the presence of a naphthyl group, which contributed to greater steric crowding around the metal centre.

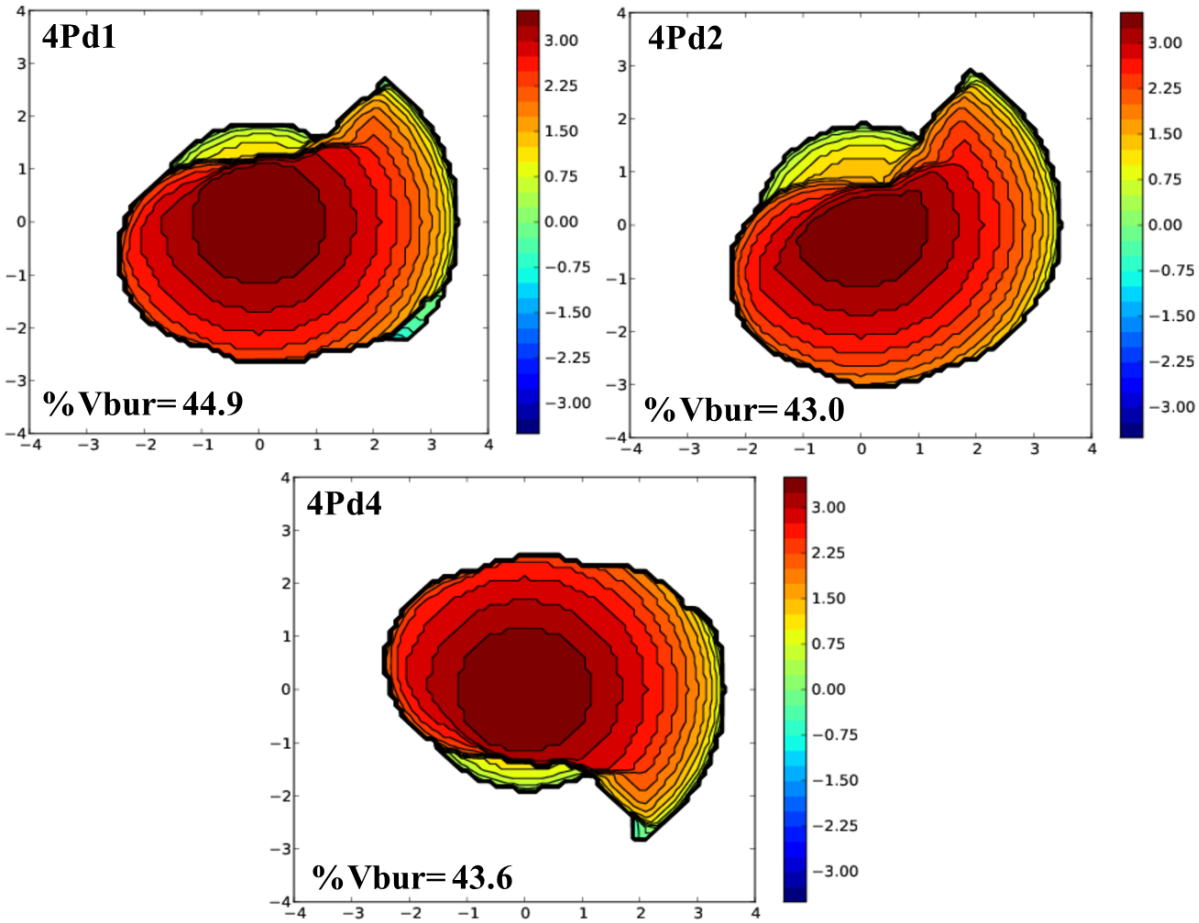

Figure 4.6: % Vbur data for Palladium catalyst (**4Pd1, 4Pd2** and **4Pd4**).

4.3.4. Norbornene polymerization:

4.3.4.1. NMR tube experiment:

Before initiating norbornene polymerization, it was important to assess the reactivity of the palladium catalyst toward norbornene. The preliminary experiment was conducted in a NMR tube. The 4Pd1 was dissolved in $CDCl_3$, and the ^1H NMR spectrum was recorded. Subsequently, the NMR tube was charged with 5 equivalents of norbornene along with 2 equivalent of $B(C_6F_5)_3$ and a proton NMR was recorded after 60 minutes. Additionally, the NMR spectrum of norbornene was recorded separately in $CDCl_3$. As illustrated in figure 4.7, the initial Pd–Me resonance at 0.69 ppm (figure 4.7 a) and the olefinic peak of the norbornene (figure 4.7 b) diminished (figure 4.7 c), accompanied by the emergence of polynorbornene broad peaks at 0.9-2.5 ppm. These mechanistic investigations indicate that norbornene inserts into a Pd–Me bond, and 4Pd1 is capable of norbornene insertion polymerization, producing polynorbornene.

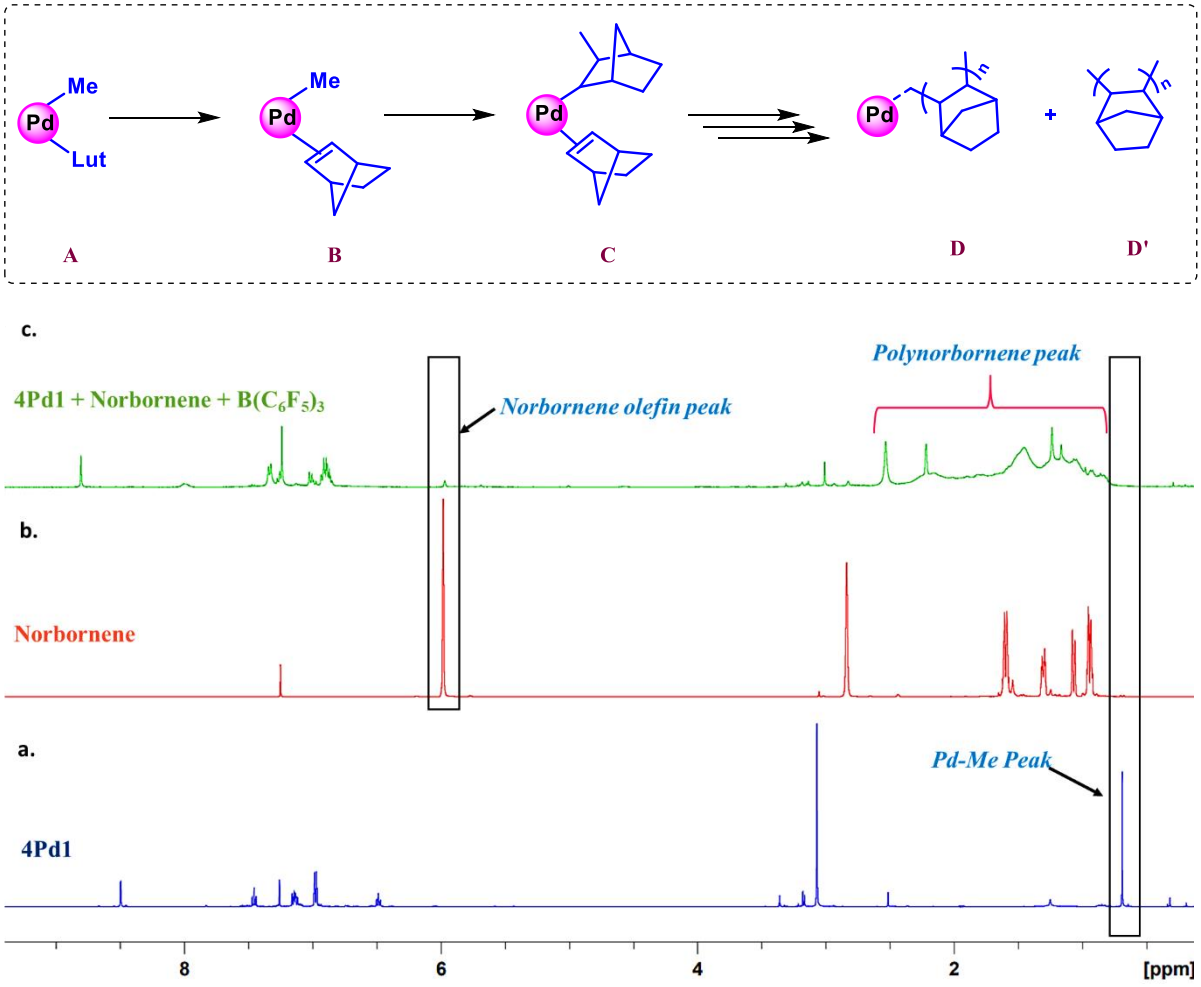

Figure 4.7: Stacked ^1H NMR spectra of i) 4Pd1(bottom), ii) Norbornene (center), iii) insertion product after norbornene insertion polymerization (top).

4.3.4.2. Gram scale norbornene homopolymerization:

Initially, norbornene polymerization was conducted without a cocatalyst at room temperature and elevated temperatures. However, only trace amounts of poly(norbornene) PNB was detected, indicating very low catalytic activity. To enhance the reactivity of the metal catalyst by decoordinating the 2,6-lutidine (a donor solvent) from the palladium complex, pentafluoroborane (PFB) was employed as a cocatalyst. Despite the inclusion of PFB, only trace amounts of PNB was obtained.

We sought to address this challenge by employing $[Ph_3C]^+[B(C_6F_5)_4]^-$ as a cocatalyst. In our experiments, we conducted norbornene polymerization with reduced cocatalyst loading (25 equivalents) (Table 4.3, entry 5). Remarkably, using 4Pd1 with 25 equivalents of cocatalyst resulted in significant PNB formation with high catalytic activity (2.86 x 10^5 g of PNB (mol. of Pd)$^{-1}$ h^{-1}) (Table 4.3, entry 5). Similarly, 4Pd2 exhibited comparable catalytic activity (2.97 x 10^5 g of PNB (mol. of Pd) $^{-1}$ h^{-1}) (Table 4.3, entry 6). Moreover, 4Pd3 and 4Pd4 catalysts also demonstrated high catalytic activity, yielding PNB as the product.

Literature reports on the mechanism of vinyl polymerization of norbornene catalyzed by palladium catalysts often highlight the crucial role of aluminum cocatalysts, such as MAO (Methyl aluminoxane), MMAO (Modified methyl aluminoxane), Et_2AlCl, and $EtAlCl_2$. These aluminum-based cocatalysts are typically essential as scavengers of donor groups, facilitating the creation of active palladium centers.[60] Therefore, higher Lewis acidity of MAO, MMAO, and $EtAlCl_2$ results in faster chain initiation and exhibit higher activity than that of the Pd/PFB catalytic system.

In our experiments, we delved deeper into the behavior of the selected 4Pd1 complex upon activation with aluminum compounds (MMAO) (Table 4.3). At a Pd/MMAO ratio of 1500, only trace amounts of polynorbornene was observed. However, upon increasing the cocatalyst loading to 3500, a notable improvement was observed (Table 4.3, entry 10). Specifically, 92 mg of PNB was produced with a catalytic activity of 5.7 x 10^5 g of PNB (mol. of Pd)$^{-1}$ h^{-1}. The MMAO/Pd systems yielded insoluble PNB with remarkably high catalytic activity, reaching upto 63.2 × 10^5 g of PNB (mol. of Pd)$^{-1}$ h^{-1} and >99% PNB formation. Notably, to achieve the high catalytic activity, a high (5500equivalent) MMAO/Pd ratio was necessary.

Table 4.3: Norbornene homopolymerization with 4Pd1-4Pd4 catalyst.

Entry	Catalyst	Co-catalyst	Pd/ Cocatalyst	Temp. (°C)	Time (min.)	Yield (mg)	Conv. (%)	Activity
1.	4Pd1	-	-	30	10	Trace	-	-
2.	4Pd1	$B(C_6F_5)_3$	20	30	5	trace	-	-
3.	4Pd1	$B(C_6F_5)_3$	50	90	120	30	3.0	0.078
4.	4Pd2	$B(C_6F_5)_3$	50	90	120	22	2.2	0.058
5.	4Pd1	$[Ph_3C]^+[B(C_6F_5)_4]^-$	25	80	60	545	54.5	2.86
6.	4Pd2	$[Ph_3C]^+[B(C_6F_5)_4]^-$	25	80	60	565	56.5	2.97
7.	4Pd3	$[Ph_3C]^+[B(C_6F_5)_4]^-$	25	80	60	462	46.2	2.43
8.	4Pd4	$[Ph_3C]^+[B(C_6F_5)_4]^-$	25	80	60	496	49.6	2.61
9.	4Pd1	MMAO	1500	30	5	Trace	-	-
10.	4Pd1	MMAO	3500	30	5	92	9.2	5.7
11.	4Pd1	MMAO	5500	30	5	998	>99	63.2
12.	4Pd1	MMAO	4500	90	10	908	90.8	28.7
13.	-	MMAO	5500	30	5	0	0	0

Reaction Condition: Norbornene 1 gm, Catalyst 4Pd1- 4Pd4 =1.9 µmol., Solvent toluene (10mL), Conversion are calculated PNB precipitation in methanol after the completion of reaction and dried under vacuum for 4 hours, Activity in unit of 10^5 g of PNB (mol. of Pd)$^{-1}$ h^{-1}, MMAO 7wt% aluminum in toluene.

However, the poly(norbornene) (PNB) produced by these palladium complexes is insoluble in common solvents such as chloroform, chlorobenzene, toluene, DMF, THF, and DMSO. As a result, it is challenging to determine the molecular weights of the polynorbornene. To verify the existence of PNB, we recorded the solid-state ^{13}C CP-MAS NMR spectrum. As depicted in Figure 4.8, the CP-MAS spectrum revealed peaks in the aliphatic region between 29-57 ppm. This ^{13}C CP-MAS NMR data correlates well with reported ^{13}C NMR resonances for PNB.[29] Notably, the absence of olefinic resonances in the polynorbornenes formed by vinyl addition polymers suggests high stereoregularity, which contributes to their insolubility.

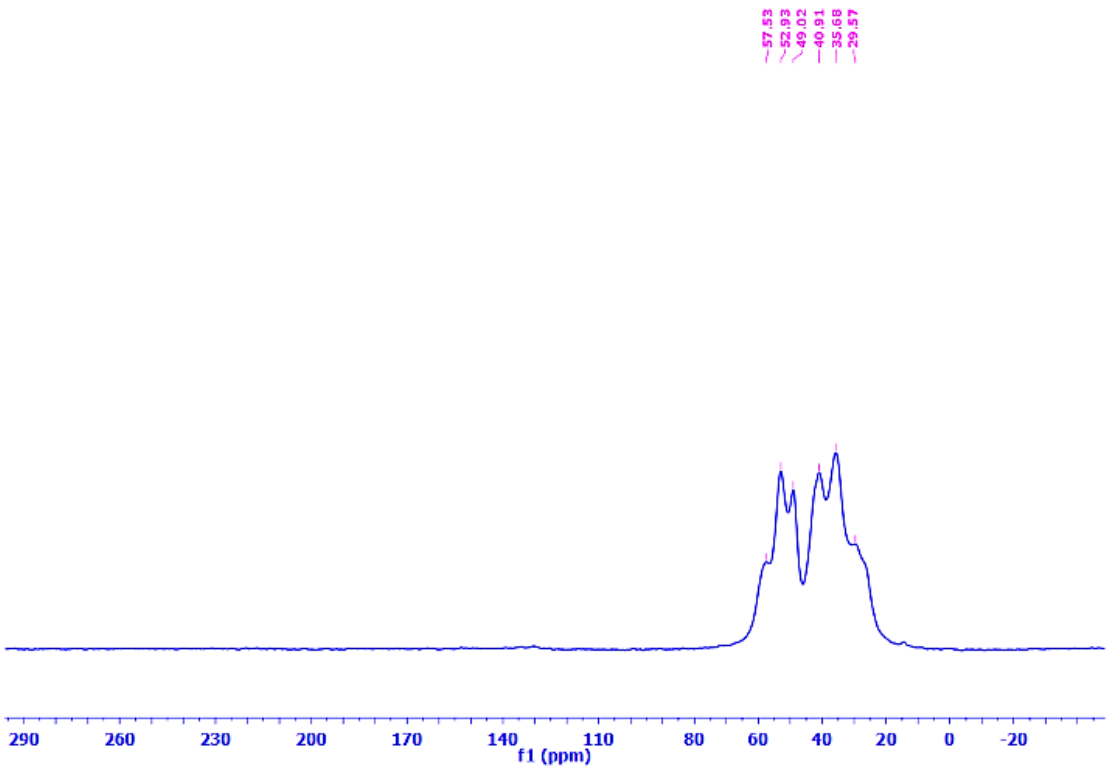

Figure 4.8: ^{13}C CP-MAS NMR spectrum of polynorbornene.

4.4. Conclusions:

In summary, the synthesis of imine phenoxy ligands via condensation reactions between 2-aminophenol and electronically tuned aniline derivatives has been successfully achieved. These ligands 4L1-4L4 react with [Pd(COD)MeCl] and 2,6-lutidine, leading to the formation of 4Pd1-4Pd4 complexes in a single step with high yields (72-93%). The identity of palladium complexes 4Pd1-4Pd4 has been unambiguously ascertained using spectroscopic and analytical methods, including single crystal X-ray diffraction. Molecular structure of 4Pd1, 4Pd2 and 4Pd4 disclosed cis configuration between the methyl group of palladium and 2,6-lutidine, a crucial feature necessary for insertion polymerization.

Moreover, proton NMR analysis of 4Pd1 has indicated deshielding, implying an electronically deficient palladium metal in comparison to other complexes. Norbornene polymerization with $[Ph_3C]^+[B(C_6F_5)_4]^-$ as cocatalyst yields a PNB with high catalytic activity (upto 2.97×10^5 g of PNB (mol. of Pd)$^{-1}$) even with low cocatalyst concentration. Furthermore, these complexes, when employed in conjunction with MMAO as the cocatalyst, exhibited remarkable catalytic activity (upto 63.2×10^5 g of PNB (mol. of Pd)$^{-1}$ h^{-1}), achieving over 99% conversion in norbornene homopolymerization reactions.

4.5. Experimental section:

4.5.1. Methods and materials:

Unless noted otherwise, all manipulations were carried out under an inert atmosphere using standard Schlenk line techniques or M-Braun glove box. Toluene was distilled from sodium and THF from sodium/benzophenone under argon atmosphere. methylene chloride was distilled on calcium-hydride. Norbornene, MMAO, $B(C_6F_5)_3$, 2,3,4,5,6 Pentafluorobenzaldehyde, 6 methoxy-2-naphthaldehyde, 2,4,6-trimethoxy benzaldehyde were obtained from sigma aldrich and were used as received. 2-amino phenol and P-anisaldehyde were received from the spectrochem and used as received. $[Ph_3C]^+[B(C_6F_5)_4]^-$ was obtained from BLD pharm and was used as received

Solution NMR spectra were recorded on a Bruker Avance 200, 400 and 500 MHz instruments. Chemical shifts are referenced to external reference TMS (^1H and ^{13}C). Coupling constants are given as absolute values. Multiplicities are given as follows s: singlet, d: doublet, t: triplet, m: multiplet. Mass spectra were recorded on Thermo scientific Q-Exactive mass spectrometer, the column specification is Hypersil gold C18 column 150 x 4.6 mm diameter 8 µm particle size mobile phase used is 90 % methanol + 10 % water + 0.1 % formic acid..

4.5.2. Synthesis of ligand:

4.5.2.1. Synthesis of 2-(((perfluorophenyl)methylene)amino)phenol (4L1):

In 100 mL round bottom flask 2-amino phenol (0.5 g, 4.58 mmol) was dissolved in 15 mL of ethanol. 2,3,4,5,6-pentafluoro benzaldehyde (0.89 g, 4.58 mmol) was added dropwise to the above reaction mixture, reaction mixture readily turns into solid precipitation of imine. Further reaction mixture was stirred for 10 minutes at room temperature (30 °C). Ethanol layer was decanted to the another round bottom flask, obtained solid was washed with cold ethanol and hexane yielding a red coloured pure ligand (1.23 g, 93.5%).

^{1}H NMR (500MHz ,DMSO-d$_6$) δ = 8.75 (s, 1 H), 7.47 - 7.27 (m, 3 H), 7.24 (d, *J* = 7.6 Hz, 1 H).

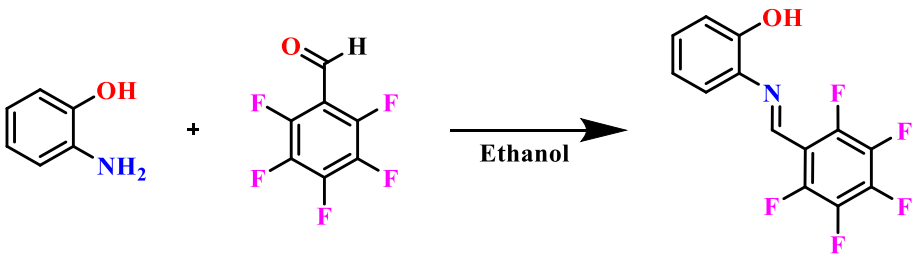

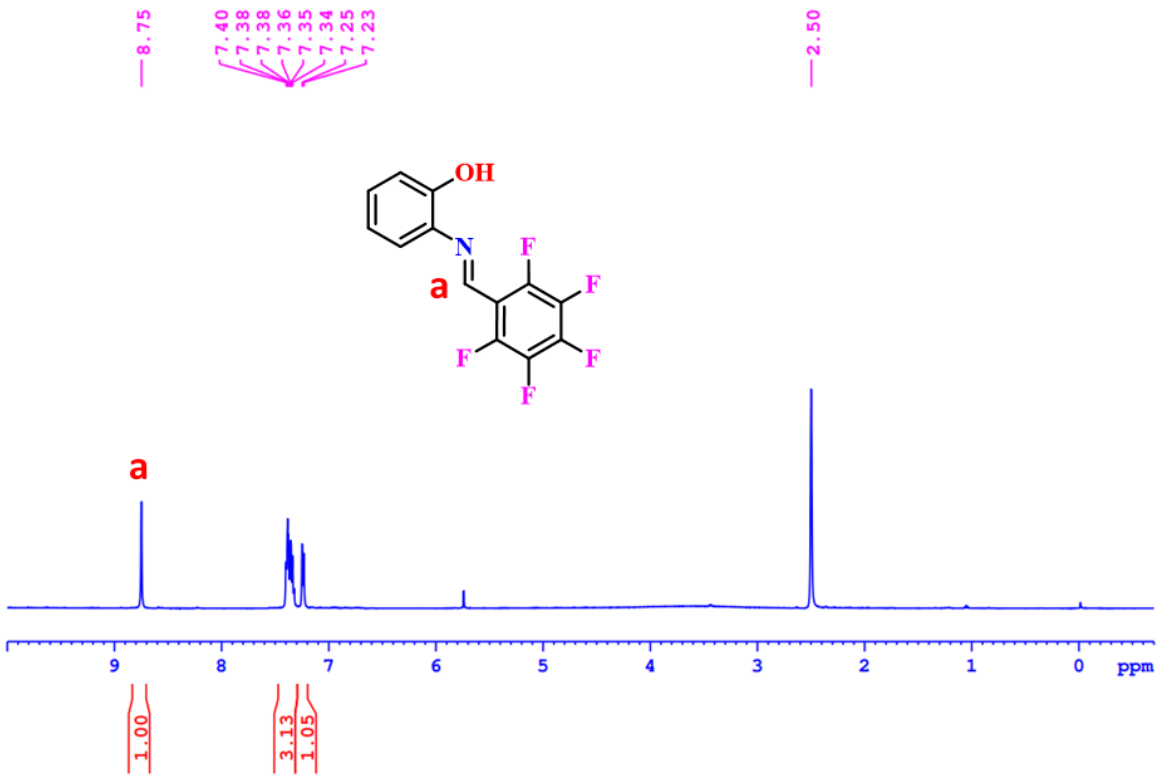

Figure S4.1: ^{1}H NMR of the **4L1** in DMSO-d_6.

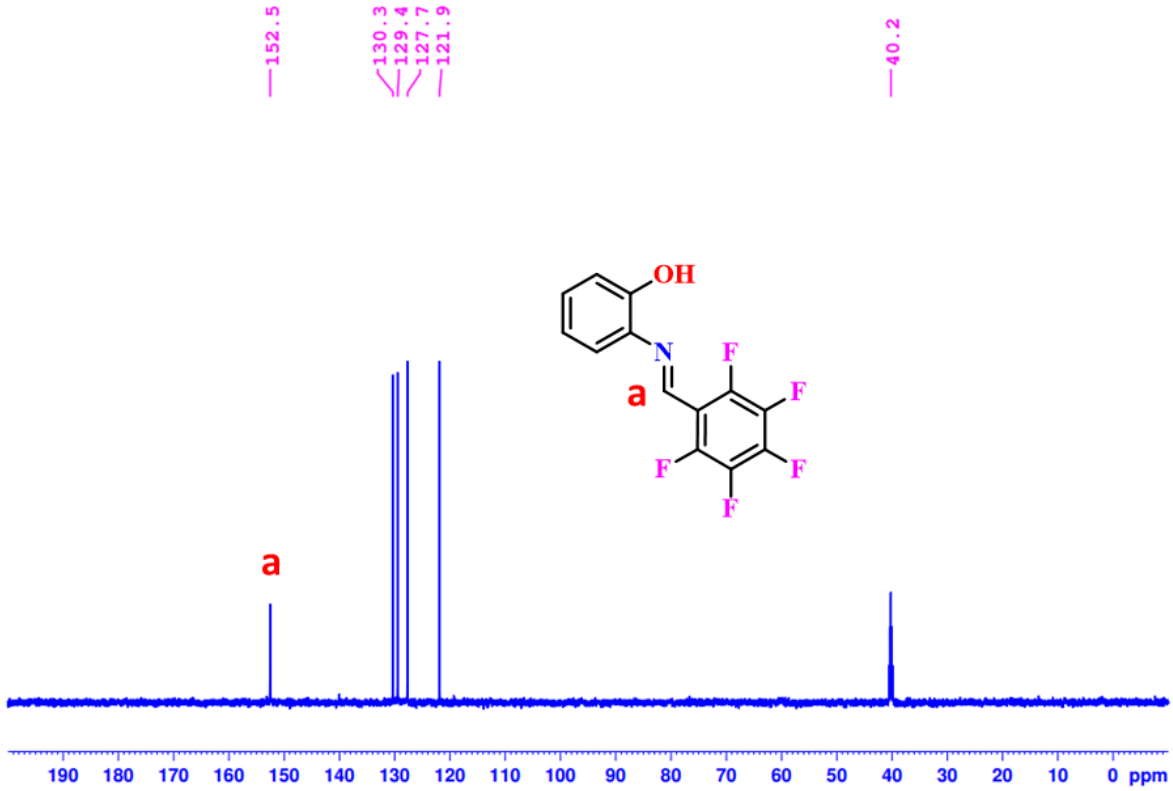

Figure S4.2: ^{13}C DEPT NMR of the **4L1** in DMSO-d_6.

4.5.2.2. Synthesis of 2-((4-methoxybenzylidene)amino)phenol (4L2):

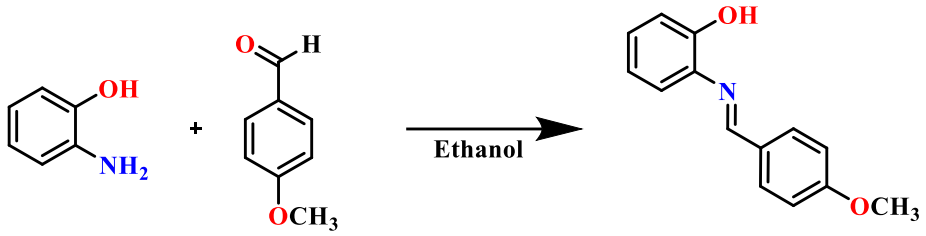

In 100 mL round bottom flask 2-amino phenol (0.5 g, 4.58 mmol) was dissolved in 15 mL of ethanol. P-anisaldehyde (0.62 g, 4.58 mmol) was added dropwise to the above reaction mixture, reaction mixture readily turns into solid precipitate of imine. Further reaction mixture was stirred for 10 minutes at room temperature (30 °C). Ethanol layer was decanted to the another round bottom flask, obtained solid was washed with cold ethanol and hexane to yield red coloured pure ligand L2 (0.92 g, 88%).

^{1}H NMR (400MHz , $CDCl_3$) δ= 8.58 (s, 1 H), 7.86 - 7.80 (m, 2 H), 7.24 (dd, *J* = 1.3, 8.0 Hz, 1 H), 7.19 - 7.12 (m, 1 H), 7.02 - 6.94 (m, 3 H), 6.89 (dd, *J* = 1.3, 7.6 Hz, 1 H), 3.85 (s, 3 H**);** **^{13}C NMR (100MHz , $CDCl_3$)** δ = 162.6, 156.6, 152.1, 135.9, 130.6, 128.9, 128.3, 120.1, 115.8, 114.8, 114.3, 55.5.

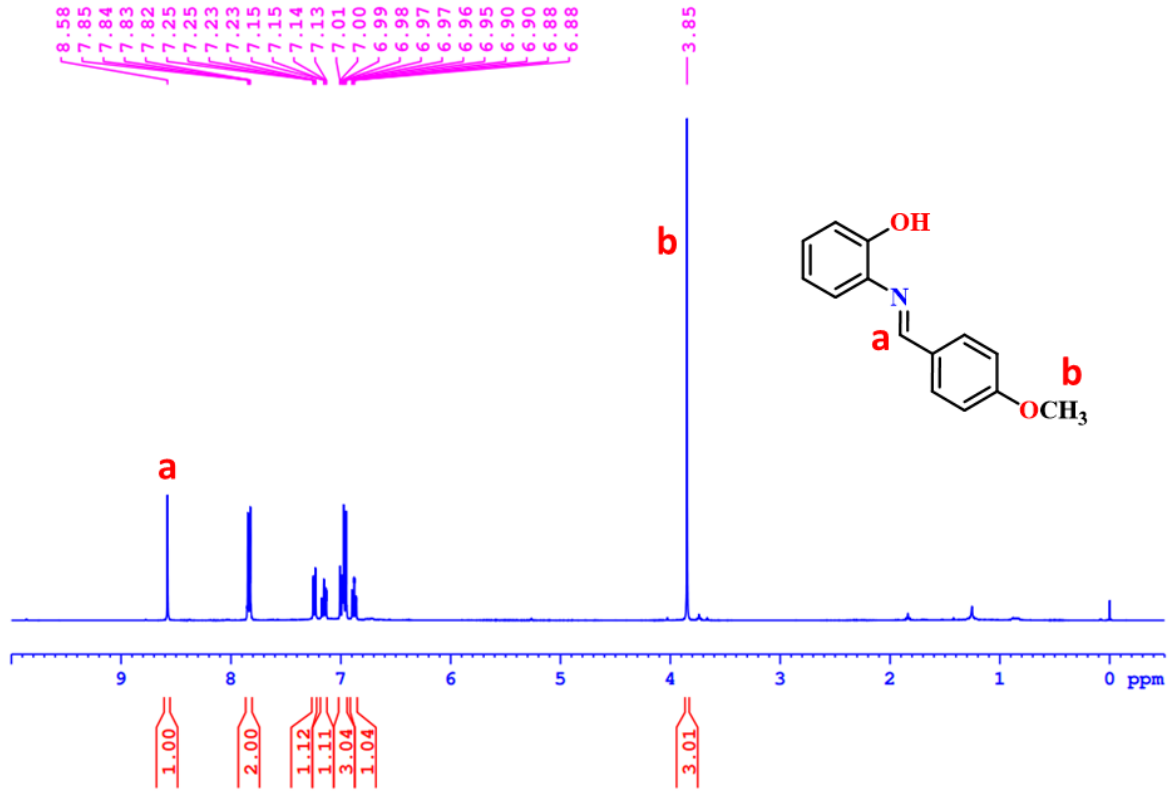

Figure S4.3: ^{1}H NMR of the **4L2** in $CDCl_3$.

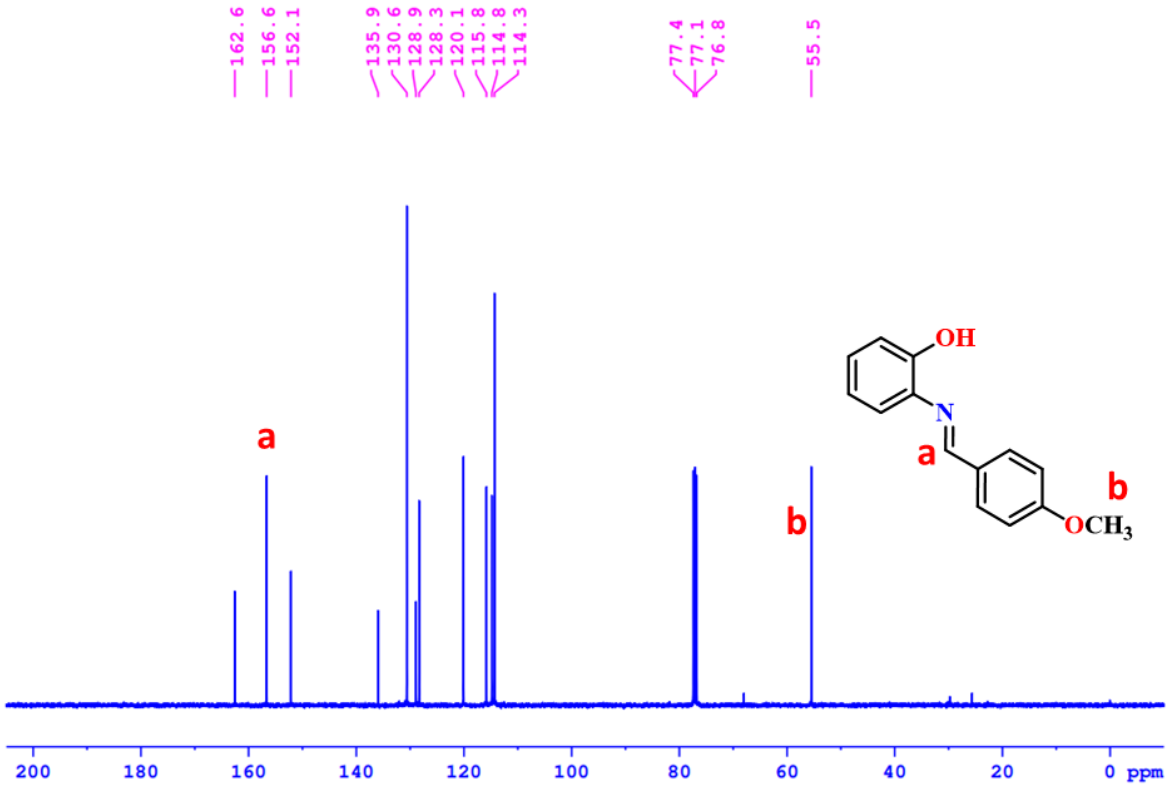

Figure S4.4: ^{13}C NMR of the **4L2** in $CDCl_3$.

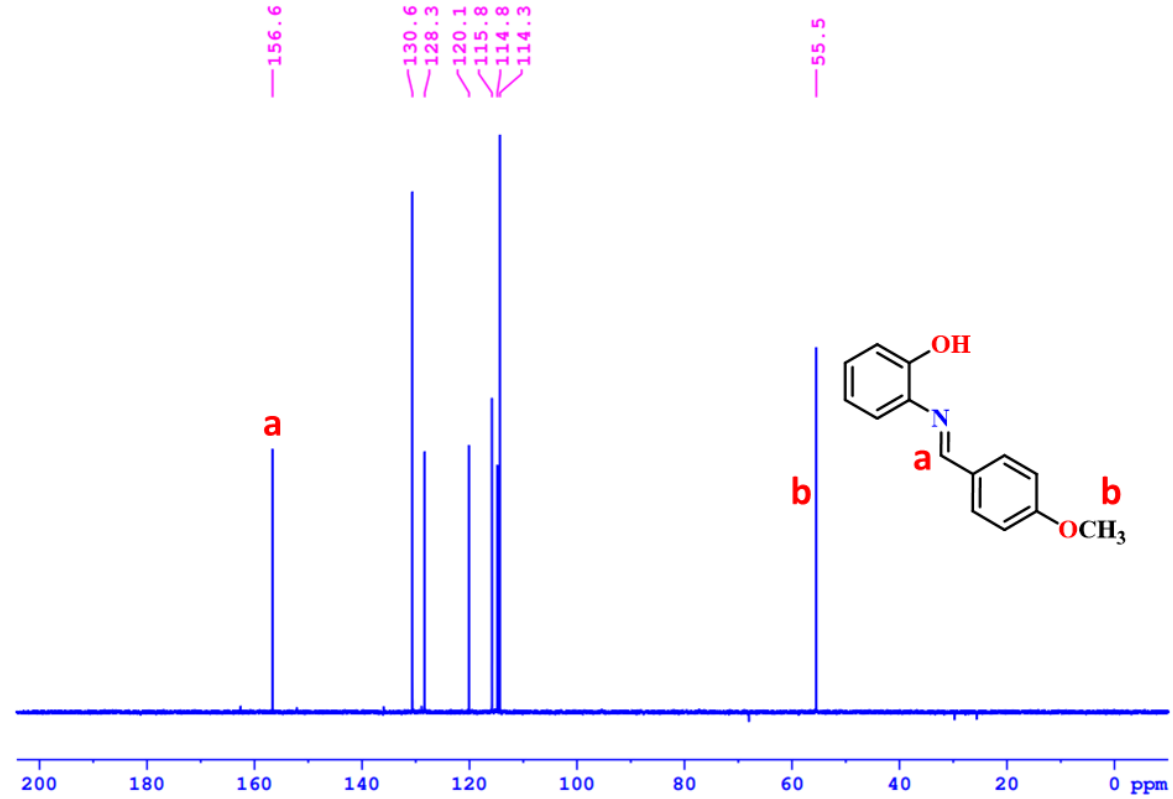

Figure S4.5: ^{13}C DEPT NMR of the **4L2** in $CDCl_3$.

4.5.2.3. Synthesis of 2-((2,4,6-trimethoxybenzylidene)amino)phenol (4L3):

In 100 mL round bottom flask 2-amino phenol (0.5 g, 4.58 mmol) was dissolved in 10 mL of ethanol. 2,4,6-trimethoxybenzaldehyde (0.89 g, 4.58 mmol) was added dropwise to the above reaction mixture, reaction mixture readily turns into solid precipitate of imine. Further, reaction mixture was stirred for 10 minutes at room temperature (30 °C). Ethanol layer was decanted to the another round bottom flask, obtained solid was washed with cold ethanol and hexane yielding red coloured pure ligand L3 (1.18 g, 90%).

^{1}H NMR (400MHz, $CDCl_3$) δ = 9.02 (s, 1 H), 7.29 - 7.23 (m, 1 H), 6.97 (d, *J* = 1.1 Hz, 1 H), 6.85 (d, *J* = 1.0 Hz, 1 H), 6.13 (s, 2 H), 3.88 (s, 6 H), 3.85 (s, 3 H). **^{13}C NMR (100MHz, $CDCl_3$)** δ = 163.7, 162.0, 152.3, 152.2, 137.7, 127.4, 119.5, 115.3, 114.1, 106.9, 90.6, 55.9, 55.3.

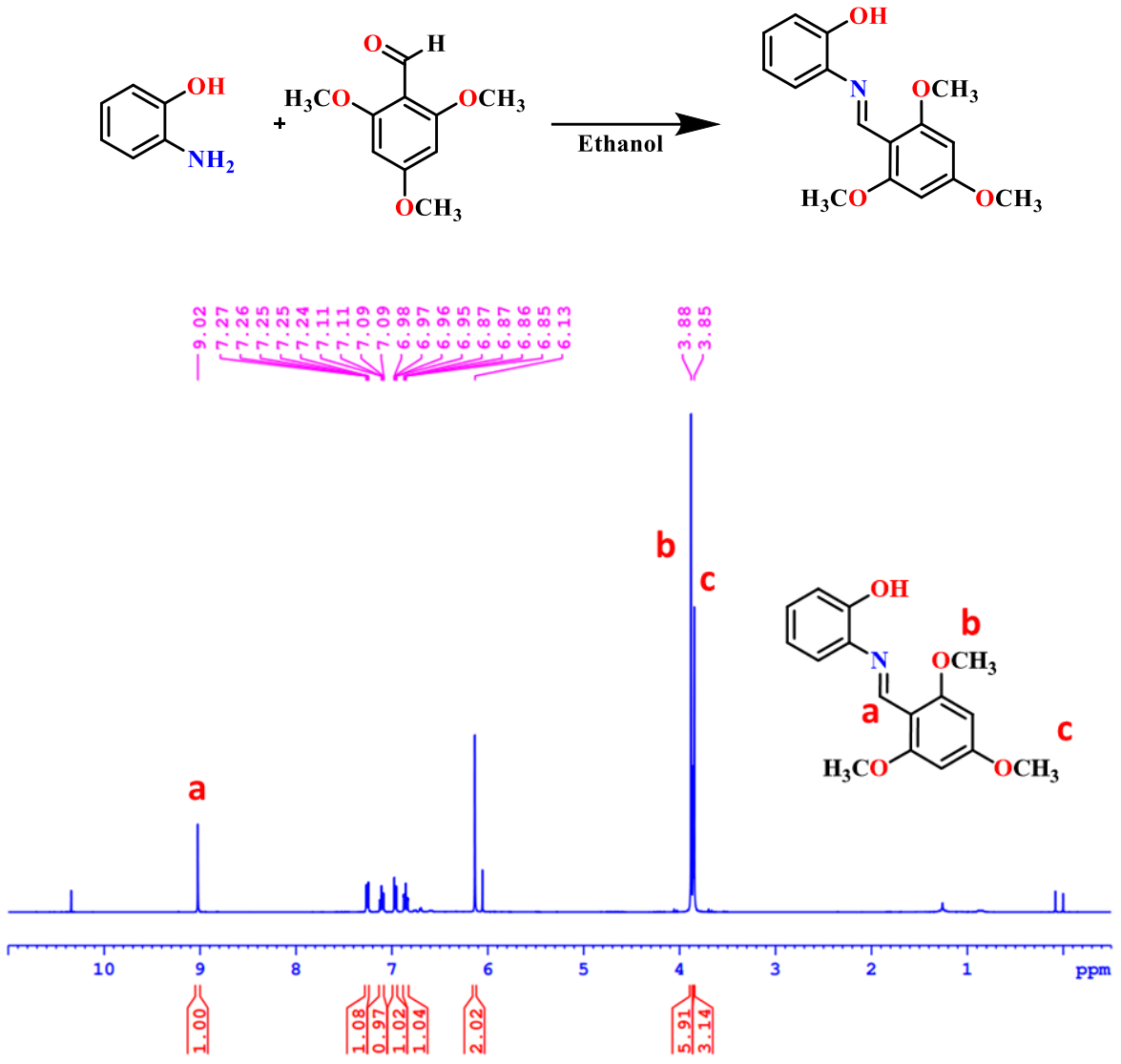

Figure S4.6: ^{1}H NMR of the **4L3** in $CDCl_3$

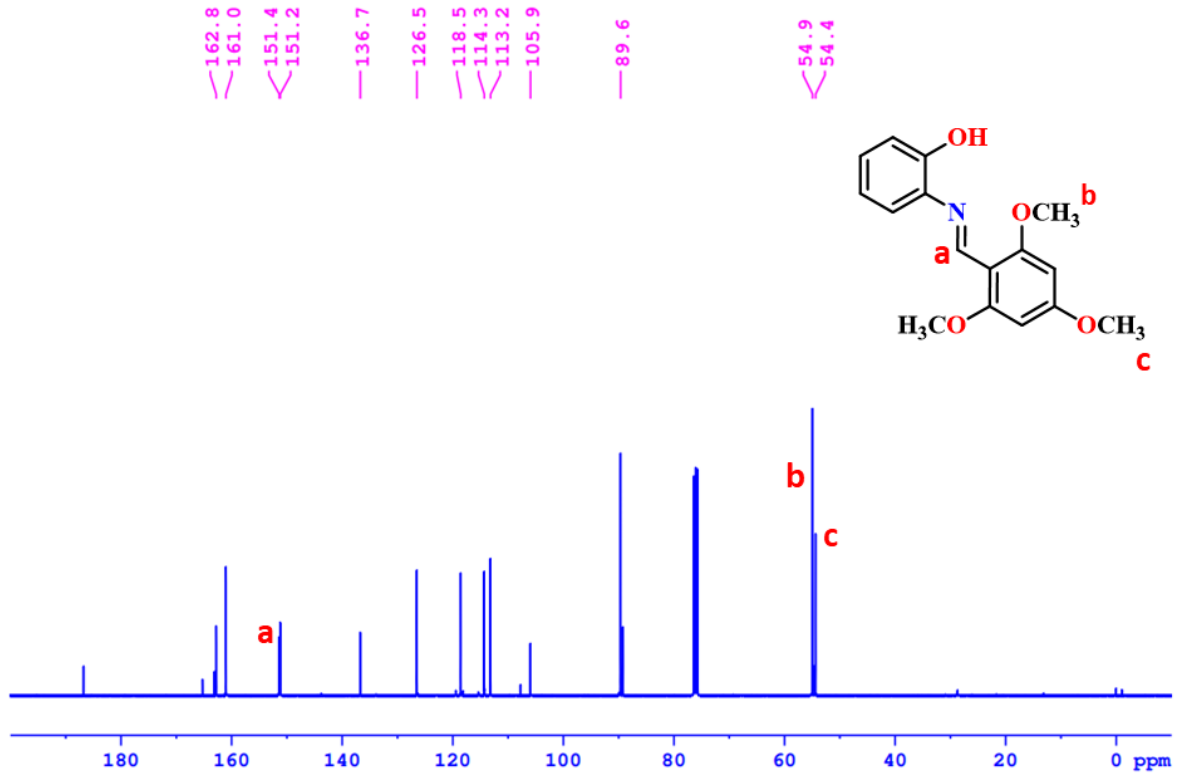

Figure S4.7: ^{13}C NMR of the **4L3** in $CDCl_3$.

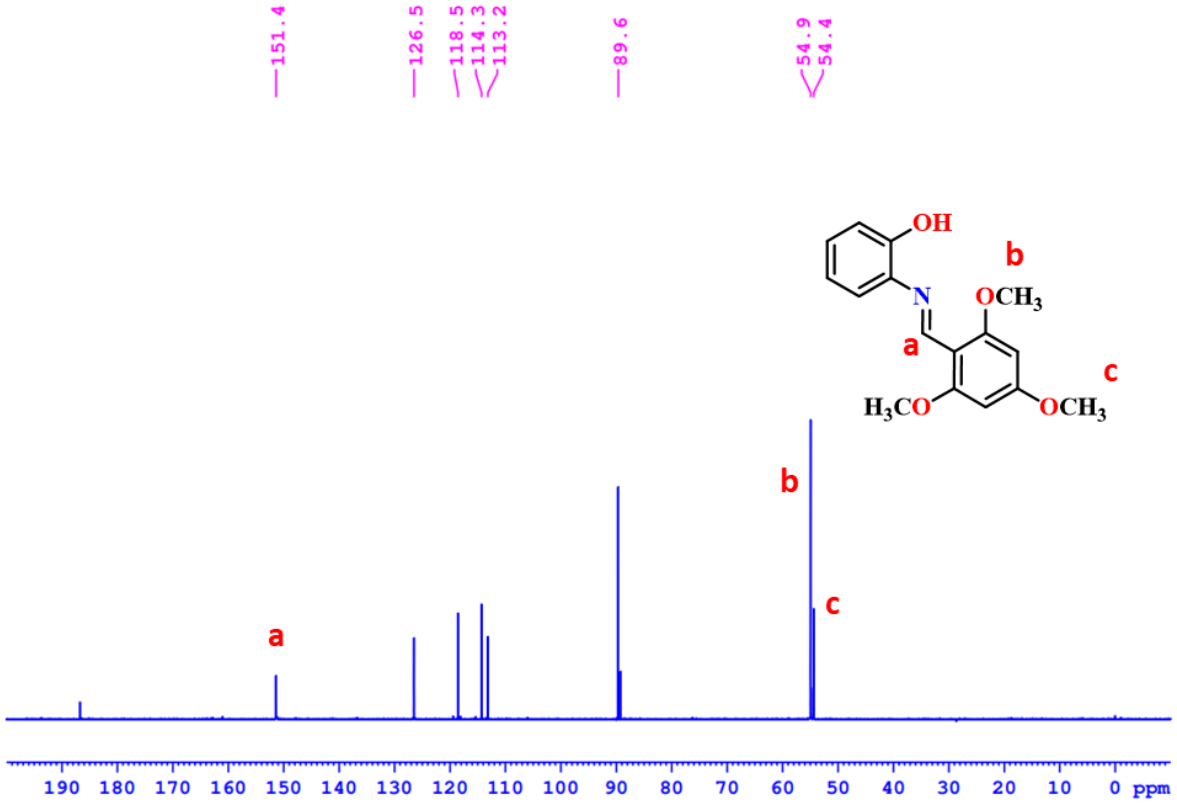

Figure S4.8: ^{13}C DEPT NMR of the **4L3** in $CDCl_3$.

4.5.2.4. Synthesis of 2-(((6-methoxynaphthalen-2-yl) methylene)amino) phenol (L4):

In 100 mL round bottom flask 2-amino phenol (146 mg, 1.34 mmol) was dissolved in 5 mL of ethanol. 6 methoxy 2-naphthaldehyde (250 mg, 1.34 mmol) was added dropwise to the above reaction mixture, reaction mixture readily turns into solid precipitate of imine. Further, reaction mixture was stirred for 10 minutes at room temperature (30 °C). Ethanol layer was decanted to the another round bottom flask, obtained solid was washed with cold ethanol and hexane, yielding red coloured pure ligand (302 mg, 81.2%).

^{1}H NMR (400MHz , $CDCl_3$) δ= 8.78 (s, 1 H), 8.11 (s, 2 H), 7.80 (t, *J* = 9.9 Hz, 2 H), 7.33 (dd, *J* = 1.4, 8.0 Hz, 1 H), 7.23 - 7.15 (m, 3 H), 7.06 - 7.01 (m, 1 H), 6.92 (t, *J* = 7.7 Hz, 1 H), 3.94 (s, 3 H) **^{13}C NMR (100MHz, $CDCl_3$)** δ = 159.4, 157.3, 152.4, 136.8, 135.9, 131.7, 131.6, 130.5, 128.7, 128.5, 127.7, 124.3, 120.2, 119.6, 115.9, 115.0, 106.3, 55.5. . **ESI-MS** (positive mode): m/z = 278.11 Da $[M + H]^+$ (observed); 278.11 $[M + H]^+$ Da (calculated).

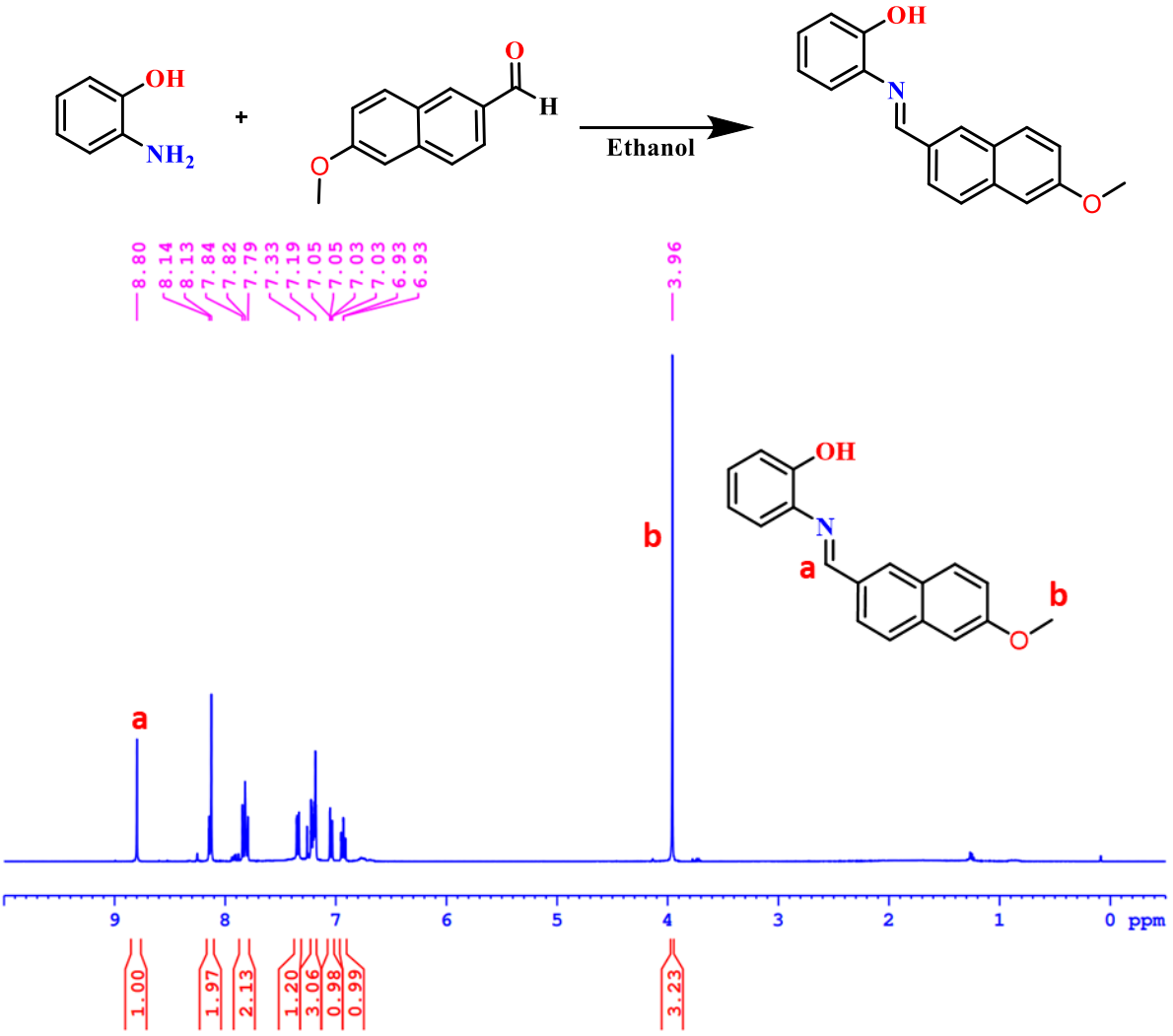

Figure S4.9: ^{1}H NMR of the **4L4** in $CDCl_3$.

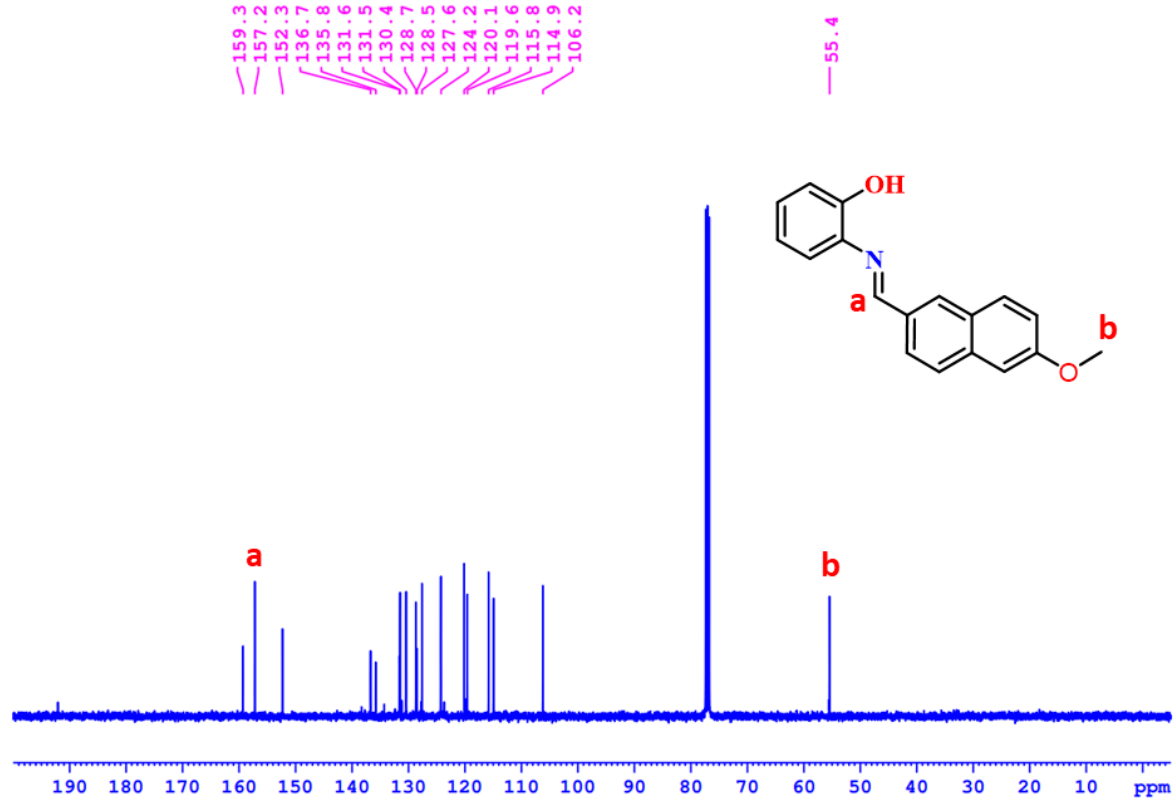

Figure S4.10: ^{13}C NMR of the **4L4** in $CDCl_3$.

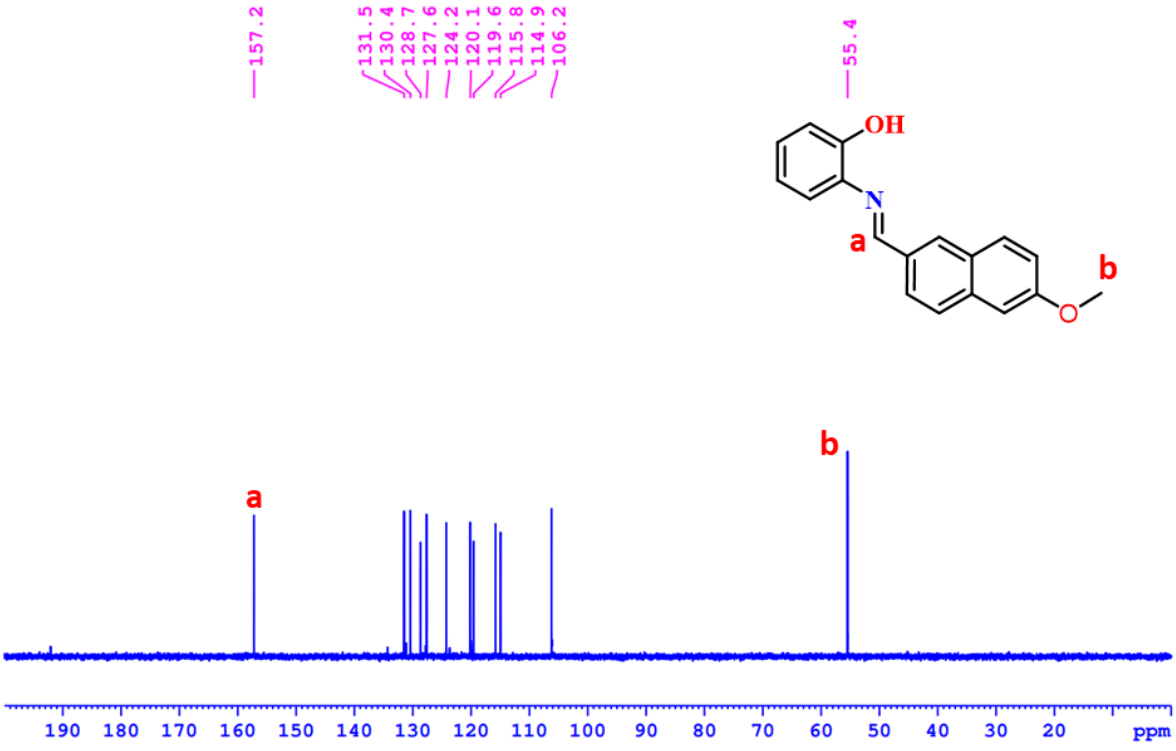

Figure S4.11: ^{13}C DEPT NMR of the **4L4** in $CDCl_3$.

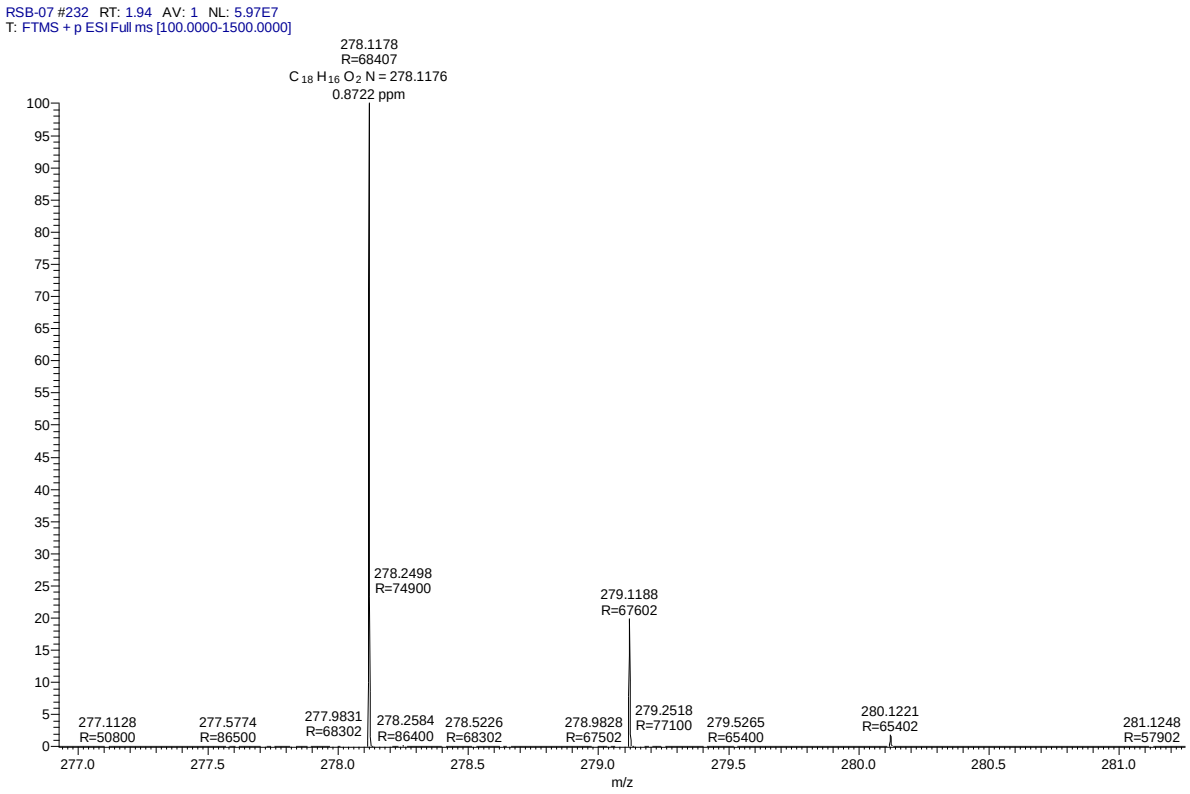

Figure S4.12: ESI-MS data of the **4L4** in $CDCl_3$.

4.5.3. Synthesis of Pd complexes:

4.5.3.1. Synthesis of 4Pd1:

In an oven-dried Schlenk flask sodium hydride (50.1 mg, 2.09 mmol) was dissolved in anhydrous THF (25 mL). In another Schlenk flask, ligand (300 mg, 1.04 mmol) was dissolved in THF, ligand solution was added dropwise to the NaH with vigorous stirring at room temperature. The reaction mixture was stirred for 3 hours at room temperature. Solvent was evaporated and washed with hexane and dried under vaccum for 2 hours.

In another Schlenk flask [Pd(COD)MeCl] (85.7 mg, 0.32 mmol) was dissolved 5 mL of THF. In another Schlenk flask sodium salt of ligand (100 mg, 0.32 mmol) was dissolved in THF solution and was dropped into the [Pd(COD)MeCl] at 0 °C. After 10 minutes, 2,6-lutidine was added, and the reaction mixture was stirred at 0 °C for 4 hours. A high vacuum was used to evaporate the solvent, and the complex was extracted in DCM. The resulting complex was washed with hexane to produce a pure product. Yield 156 mg, 93%.

^{1}H NMR (400MHz, $CDCl_3$) δ= 8.50 (s, 1 H), 7.46 (t, *J* = 7.7 Hz, 1 H), 7.13 (s, 1 H), 7.16 (s, 1 H), 6.98 (d, *J* = 7.6 Hz, 3 H), 6.49 (t, *J* = 7.0 Hz, 1 H), 3.07 (s, 6 H), 0.69 (s, 3 H). **^{13}C NMR (100MHz, $CDCl_3$)** δ = 169.9, 160.7, 140.3, 138.4, 137.1, 132.0, 122.0, 121.6, 117.6, 114.5, 28.1, -4.9.

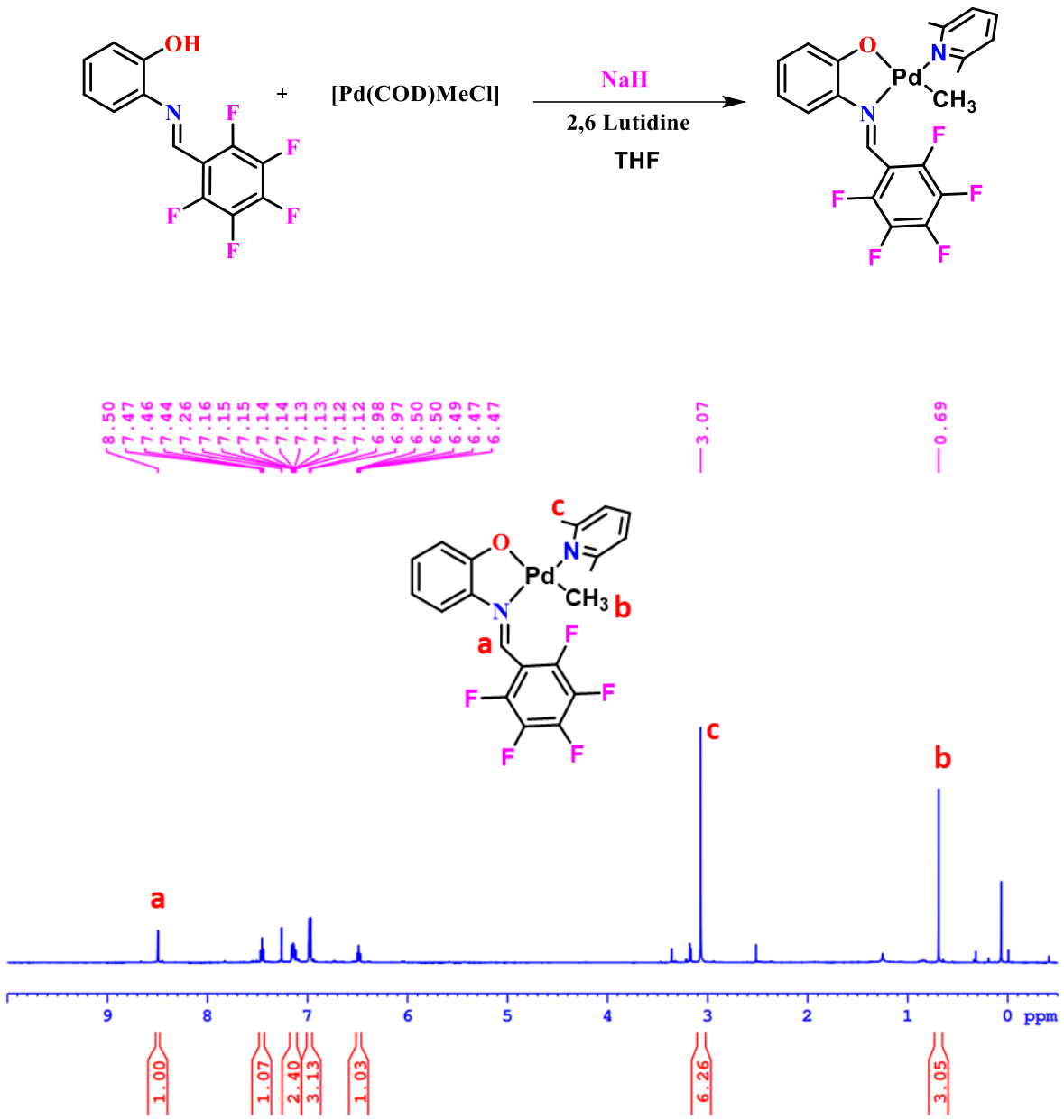

Figure S4.13: ^{1}H NMR of the **4Pd2** in $CDCl_3$.

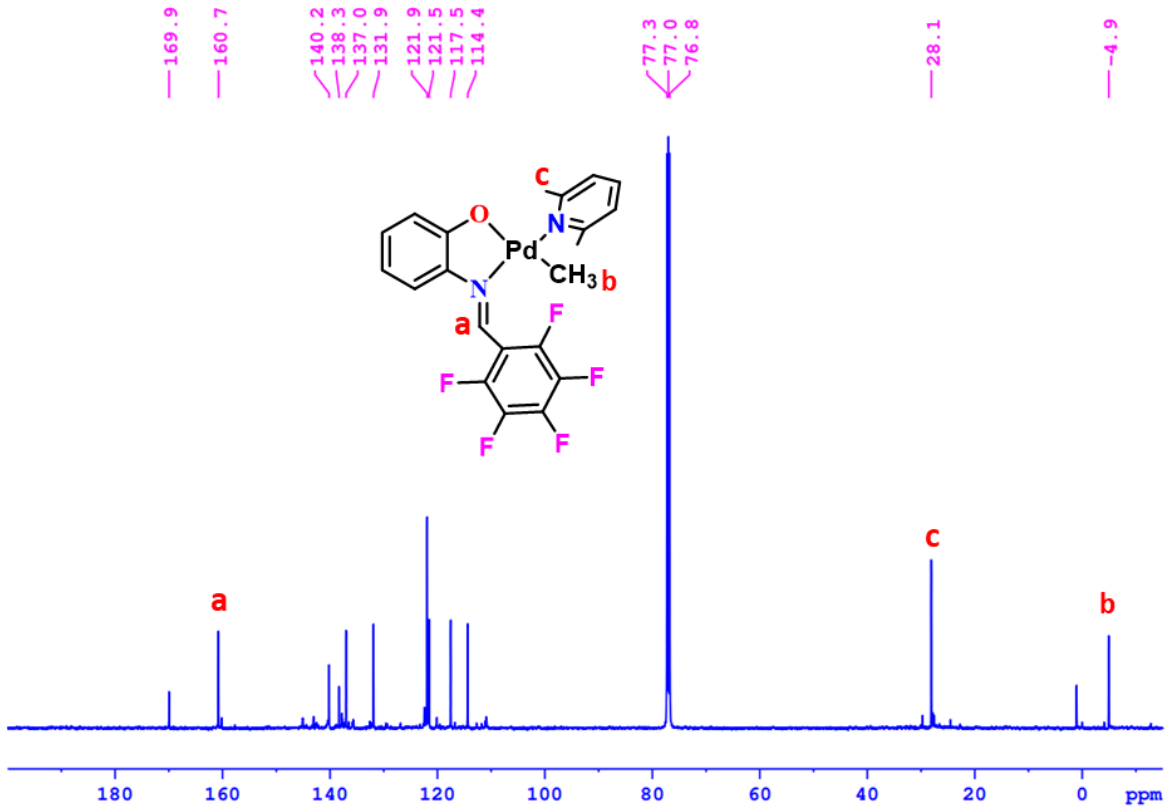

Figure S4.14: ^{13}C NMR of the **4Pd1** in $CDCl_3$.

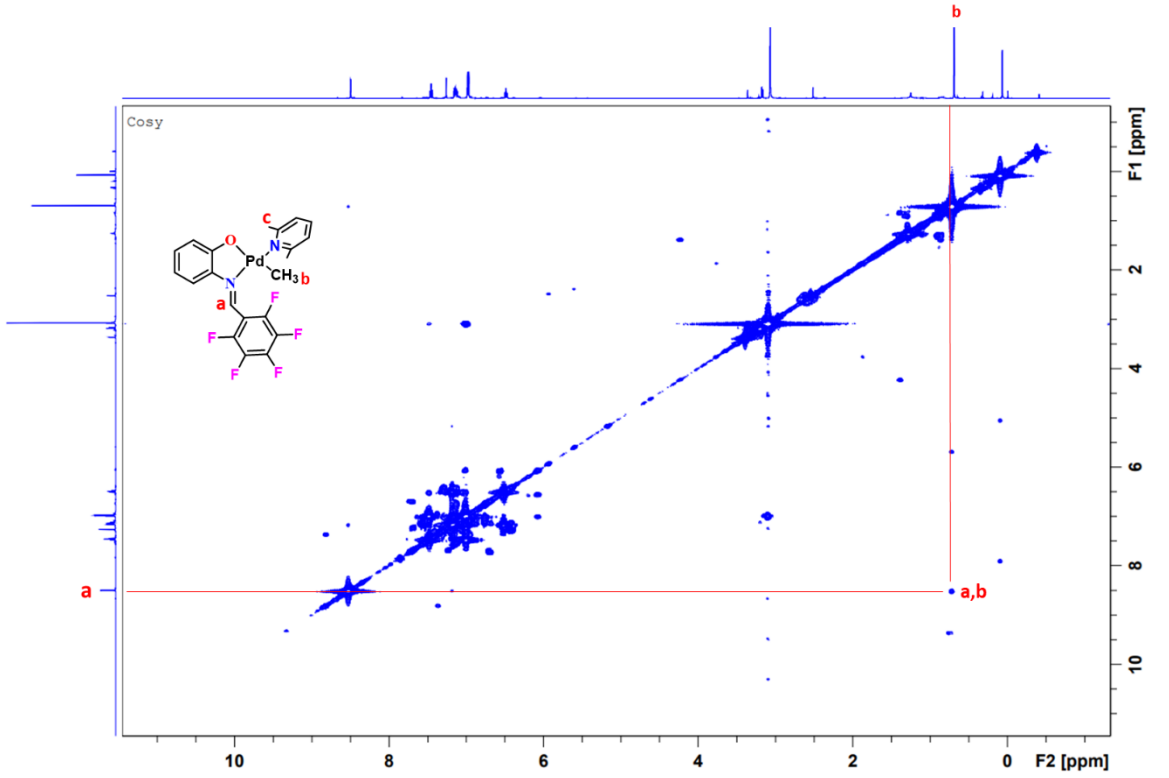

Figure S4.15: ^{1}H-^{1}H COSY NMR of the **4Pd1** in $CDCl_3$.

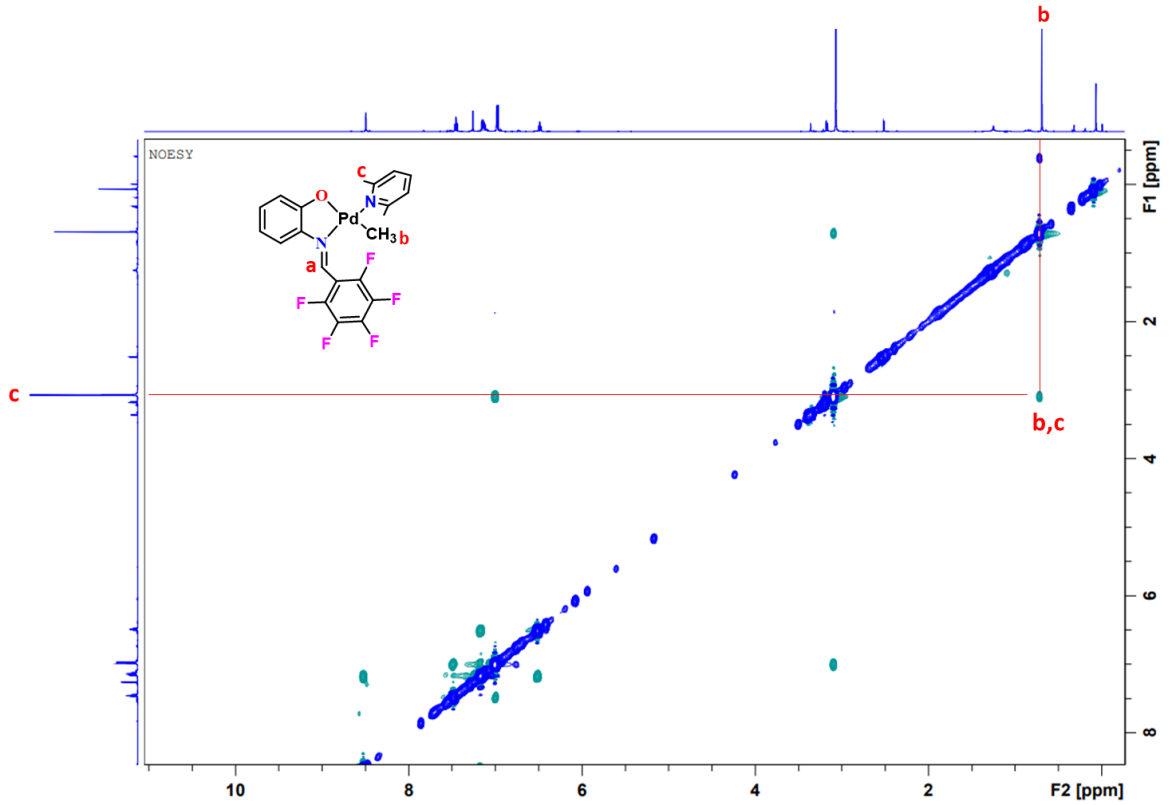

Figure S4.16: ^{1}H-^{1}H NOESY NMR of the **4Pd1** in $CDCl_3$.

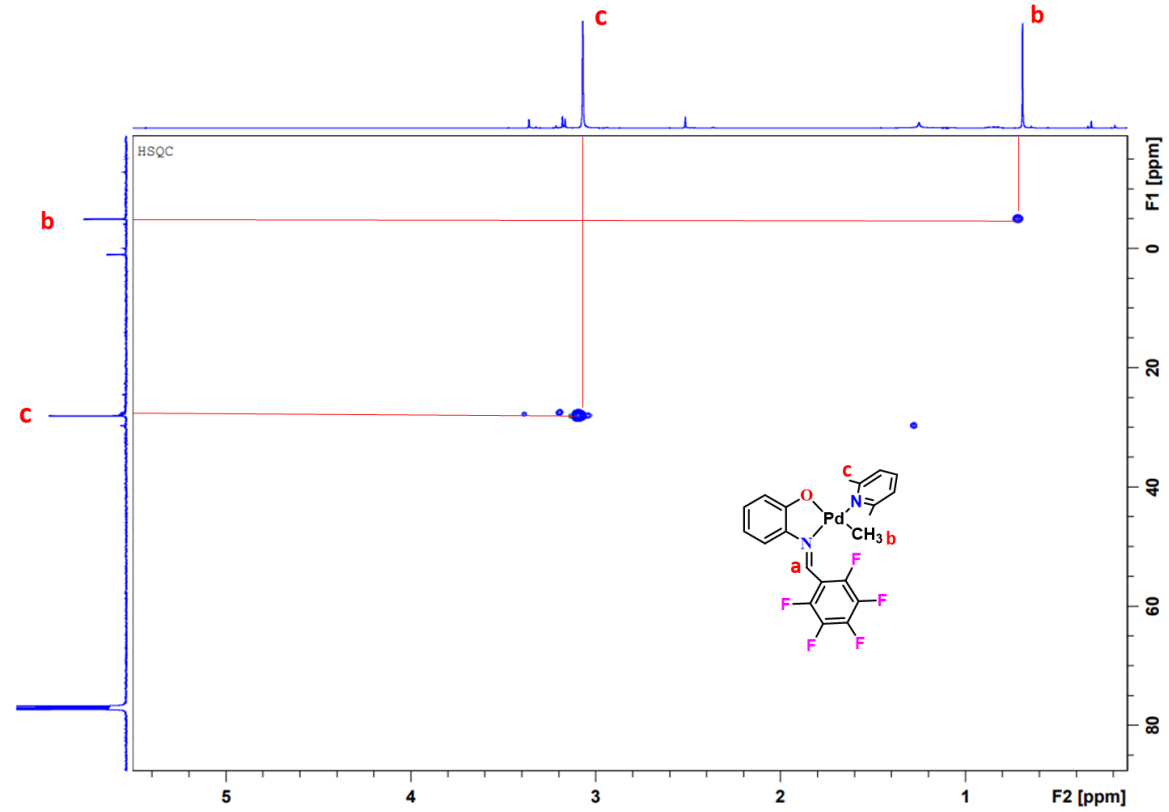

Figure S4.17: ^{1}H-^{13}C HSQC NMR of the **4Pd1** in $CDCl_3$.

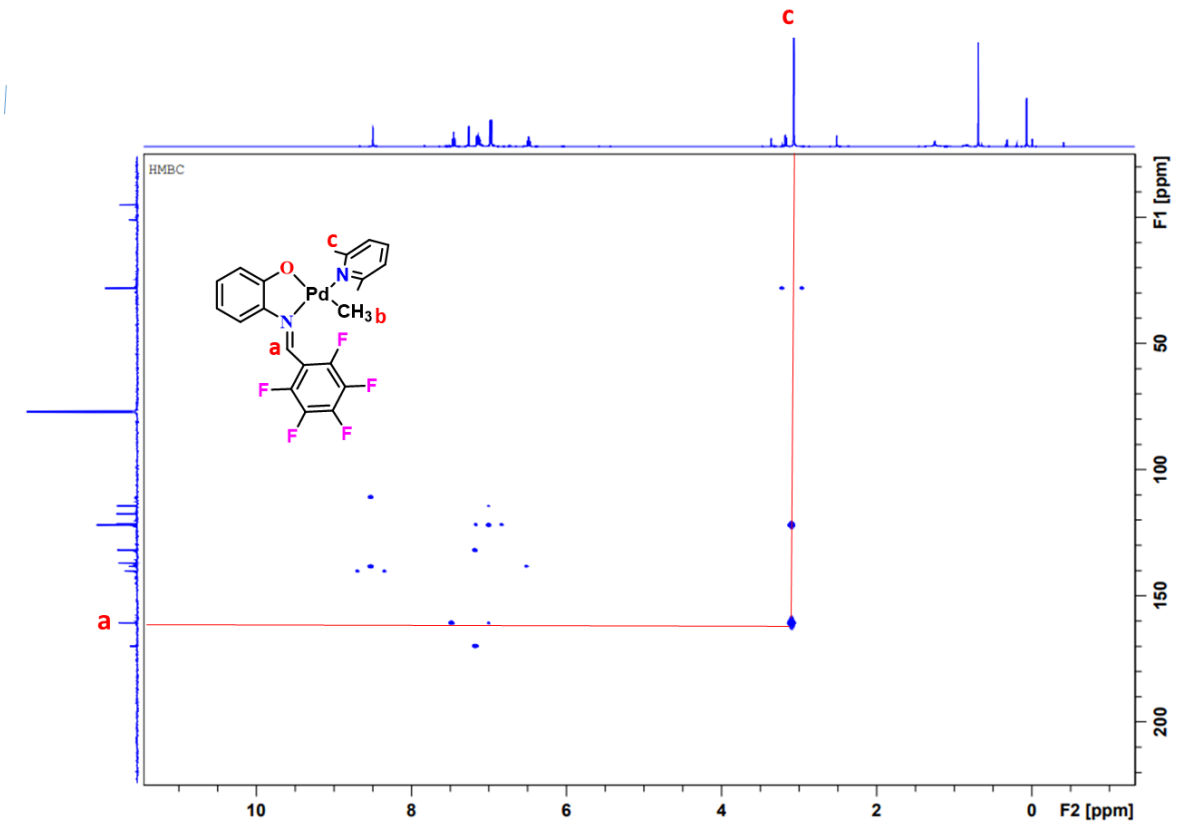

Figure S4.18: ^{1}H-^{13}C HMBC NMR of the **4Pd1** in $CDCl_3$.

4.5.3.2. Synthesis of 4Pd2:

In an oven-dried Schlenk flask, sodium hydride (9.0 mg, 0.377 mmol) was dissolved in anhydrous THF. In another Schlenk flask, ligand (46.8 mg, 0.188 mmol) was dissolved in THF (5 mL), ligand solution was added dropwise to the NaH with vigorous stirring at room temperature. The reaction mixture was stirred for 3 hours at room temperature. In another Schlenk flask [Pd(COD)MeCl] (50 mg, 0.188 mmol) was dissolved THF (5 mL). The ligand solution was dropped into the [Pd(COD)MeCl] at 0 °C. After 10 minutes, 2,6-lutidine (100 mg, 0.94 mmol) was added, and the reaction was stirred at 0 °C for 15 minutes and ice bath was removed. Further reaction content was stirred at room temperature at 30 °C for 3 hours. A high vacuum was used to evaporate the solvent, and the complex was extracted in DCM. The resulting complex was washed with hexane to produce a pure product. [62 mg, 72% yield].

^{1}H NMR (400 MHz , $CDCl_3$) δ = 8.75 (s, 1 H), 7.35 (t, *J* = 7.8 Hz, 1 H), 7.08 (d, *J* = 8.4 Hz, 2 H), 7.02 - 6.93 (m, 3 H), 6.86 (d, *J* = 7.6 Hz, 2 H), 6.46 (t, *J* = 7.2 Hz, 1 H), 6.34 (d, *J* = 8.8 Hz, 2 H), 3.68 (s, 3 H), 3.01 (s, 6 H), 0.64 (s, 3 H).

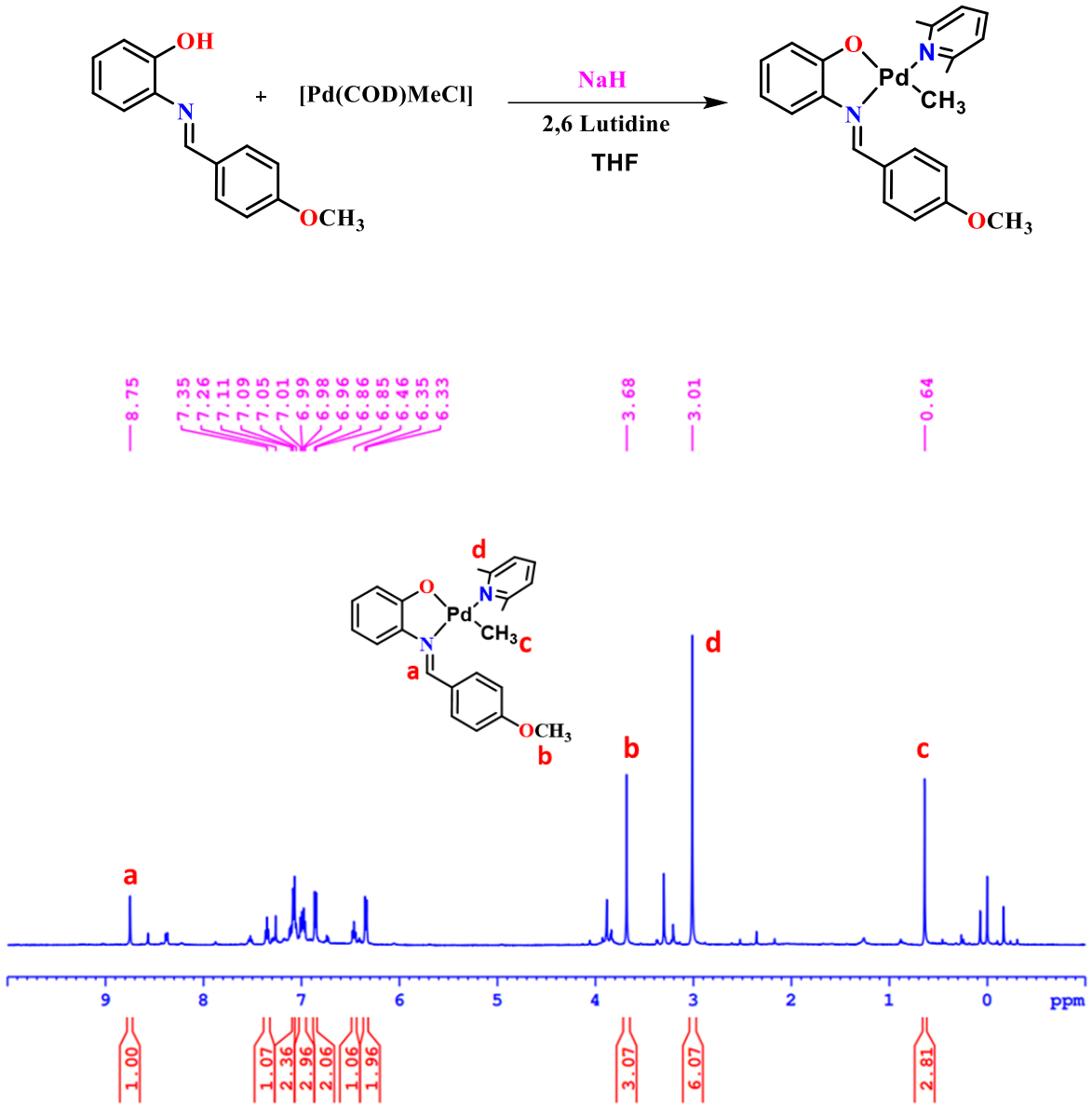

Figure S4.19: ^{1}H NMR of the **4Pd2** in $CDCl_3$.

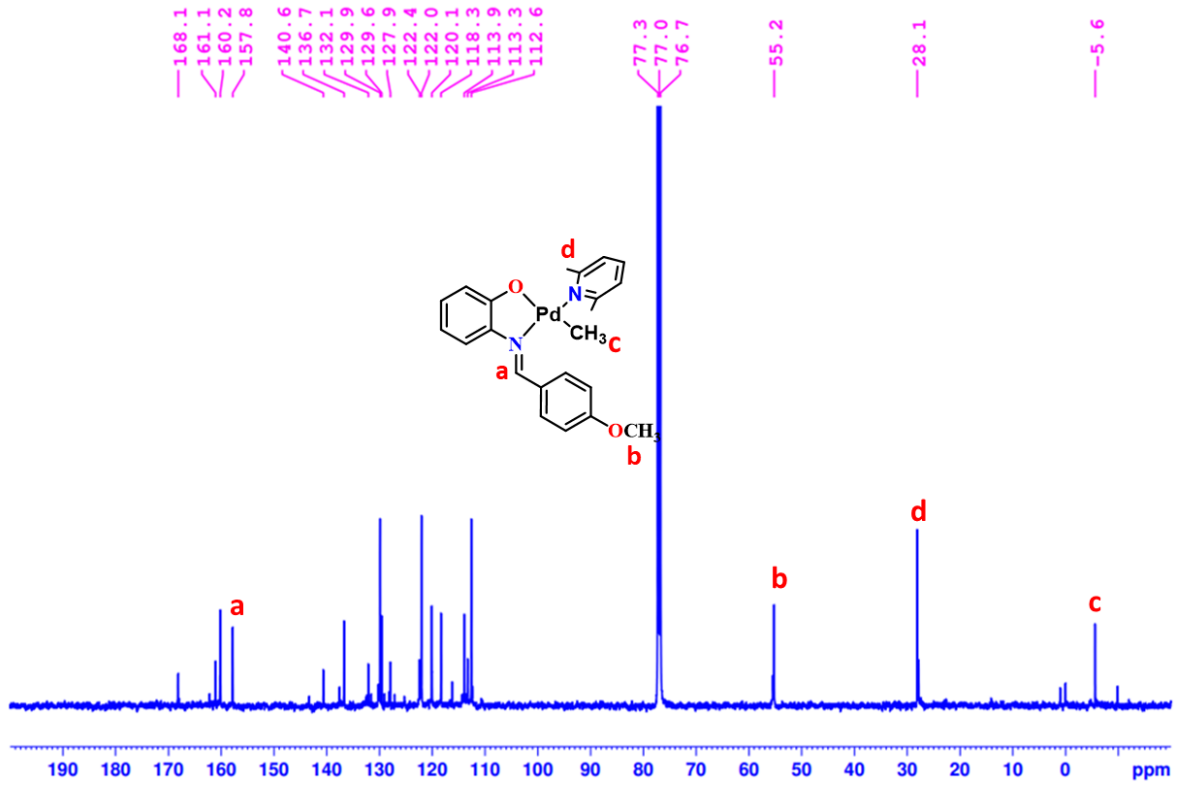

Figure S4.20: ^{13}C NMR of the **4Pd2** in $CDCl_3$.

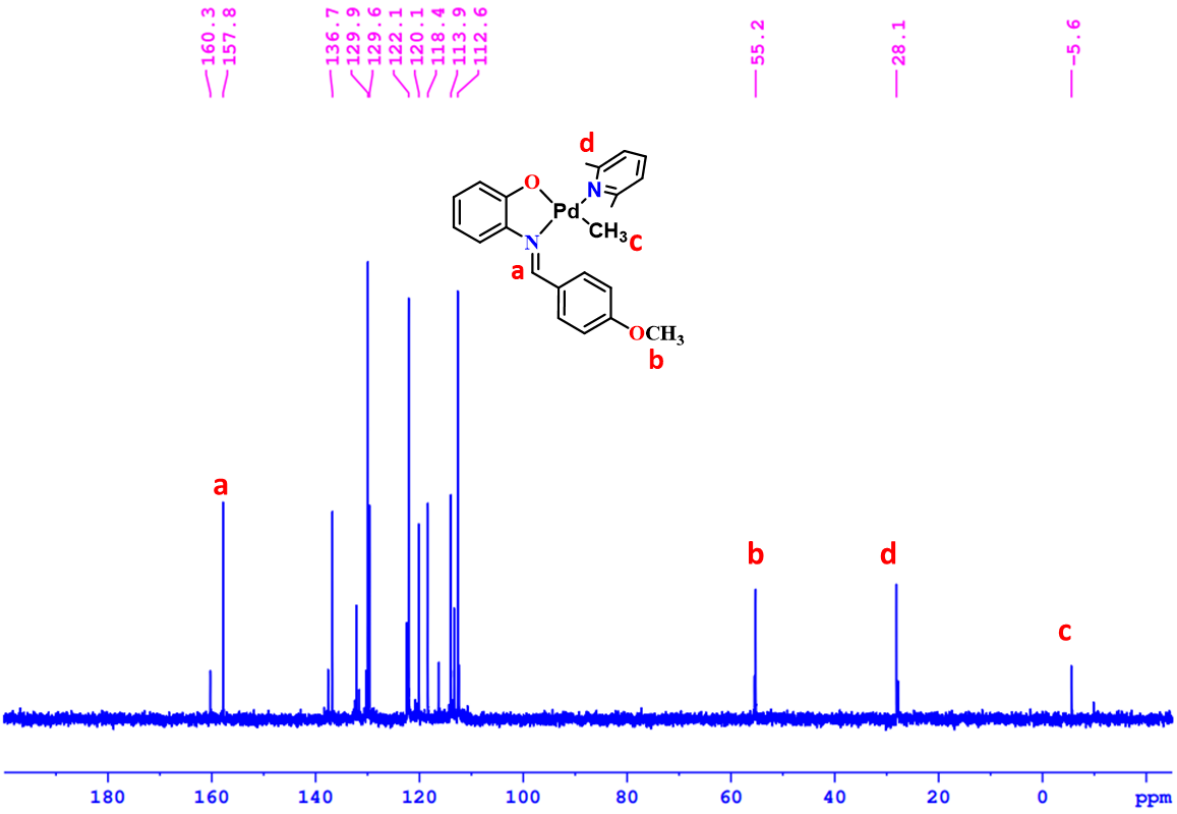

Figure S4.21: ^{13}C DEPT NMR of the **4Pd2** in $CDCl_3$.

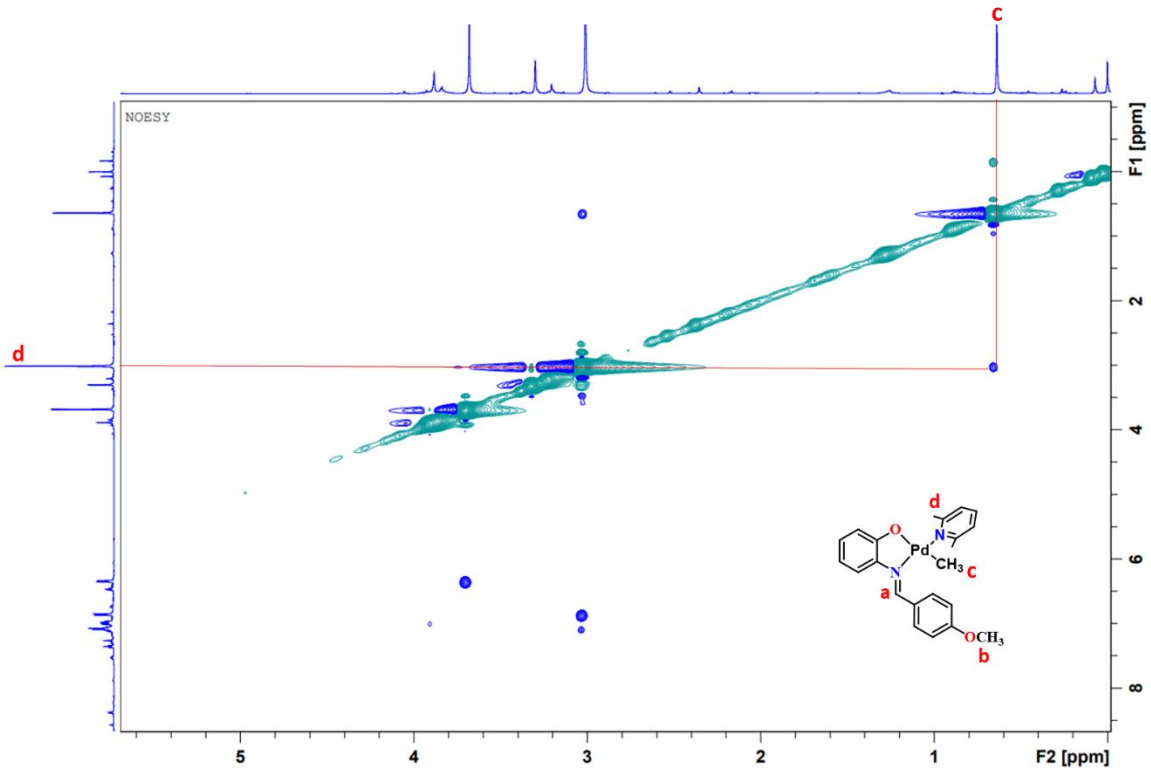

Figure S4.22: ^{1}H-^{1}H NOESY NMR of the **4Pd2** in $CDCl_3$.

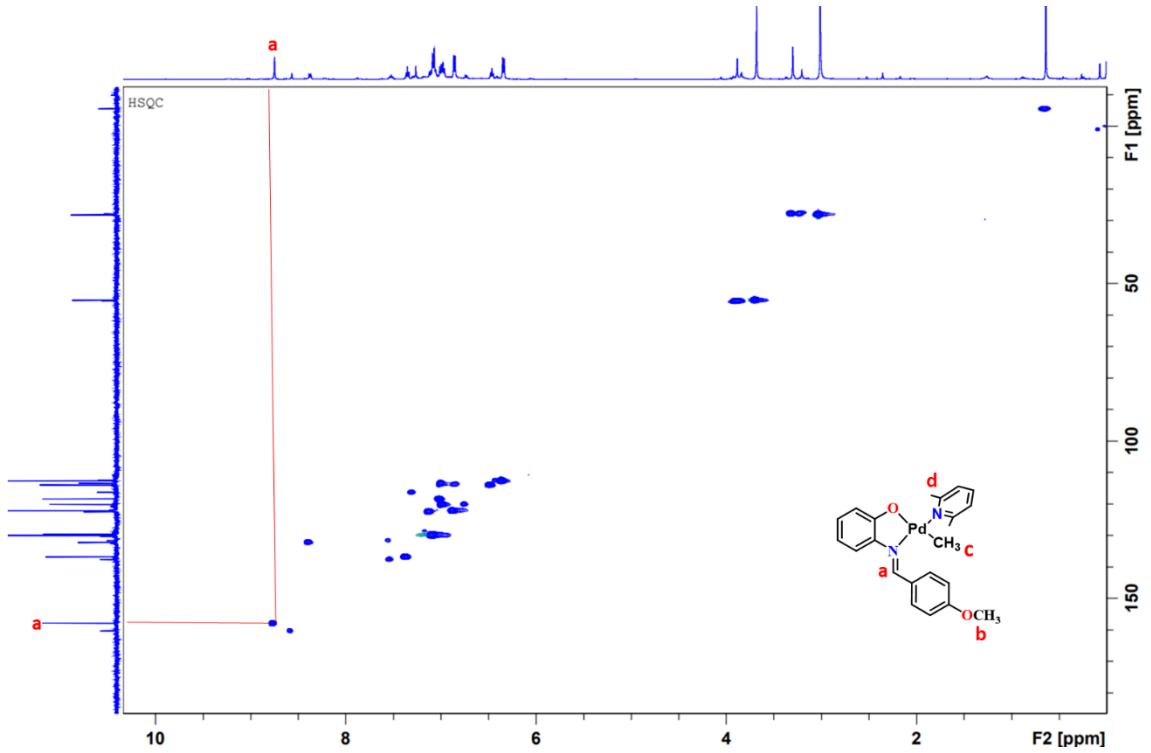

Figure S4.23: ^{1}H-^{13}C HSQC NMR of the **4Pd2** in $CDCl_3$.

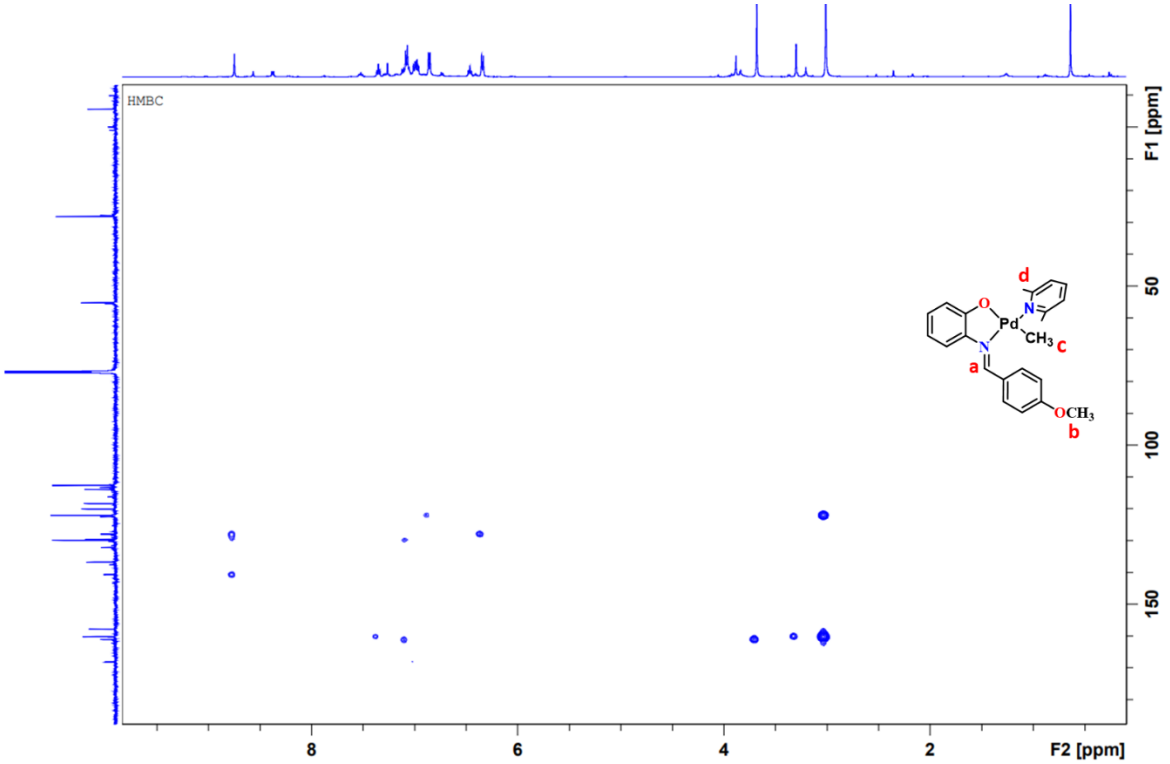

Figure S4.24: ^{1}H-^{13}C HMBC NMR of the **4Pd2** in $CDCl_3$.

4.5.3.3. Synthesis of 4Pd3:

In an oven-dried Schlenk flask, sodium hydride (83. mg, 0.34 mmol) was dissolved in anhydrous THF (10 mL). In another Schlenk flask, ligand L3 (50 mg, 0.17 mmol) was dissolved in THF (5 mL), ligand solution was added dropwise to the NaH with vigorous stirring at room temperature. The reaction mixture was stirred for 3 hours at room temperature. In another Schlenk flask [Pd(COD)MeCl] (46.1mg, 0.17 mmol) was dissolved THF (5 mL). The ligand solution was dropped into the [Pd(COD)MeCl] at 0 °C. After 10 minutes, 2,6-lutidine (93.2 mg, 0.87 mmol) was added, and the reaction stirred at 0 °C for 15 minutes and ice bath was removed. Further, the reaction content was stirred at room temperature at 30 °C for 3 hours. A high vacuum was used to evaporate the solvent, and the complex was extracted in DCM. The resulting complex was washed with hexane to produce a pure product Pd3 in excellent yield (71 mg, 79 %).

^{1}H NMR (400MHz , $CDCl_3$) δ= 8.50 (s, 1 H), 7.08 - 7.05 (m, 2 H), 6.77 (d, J = 7.6 Hz, 2 H), 6.46 (t, J = 7.5 Hz, 1 H), 6.06 (s, 2H), 5.57 (s, 2 H), 3.81 (s, 3 H), 3.63 (s, 6 H), 3.00 (s, 6 H), 0.49 (s, 3 H).

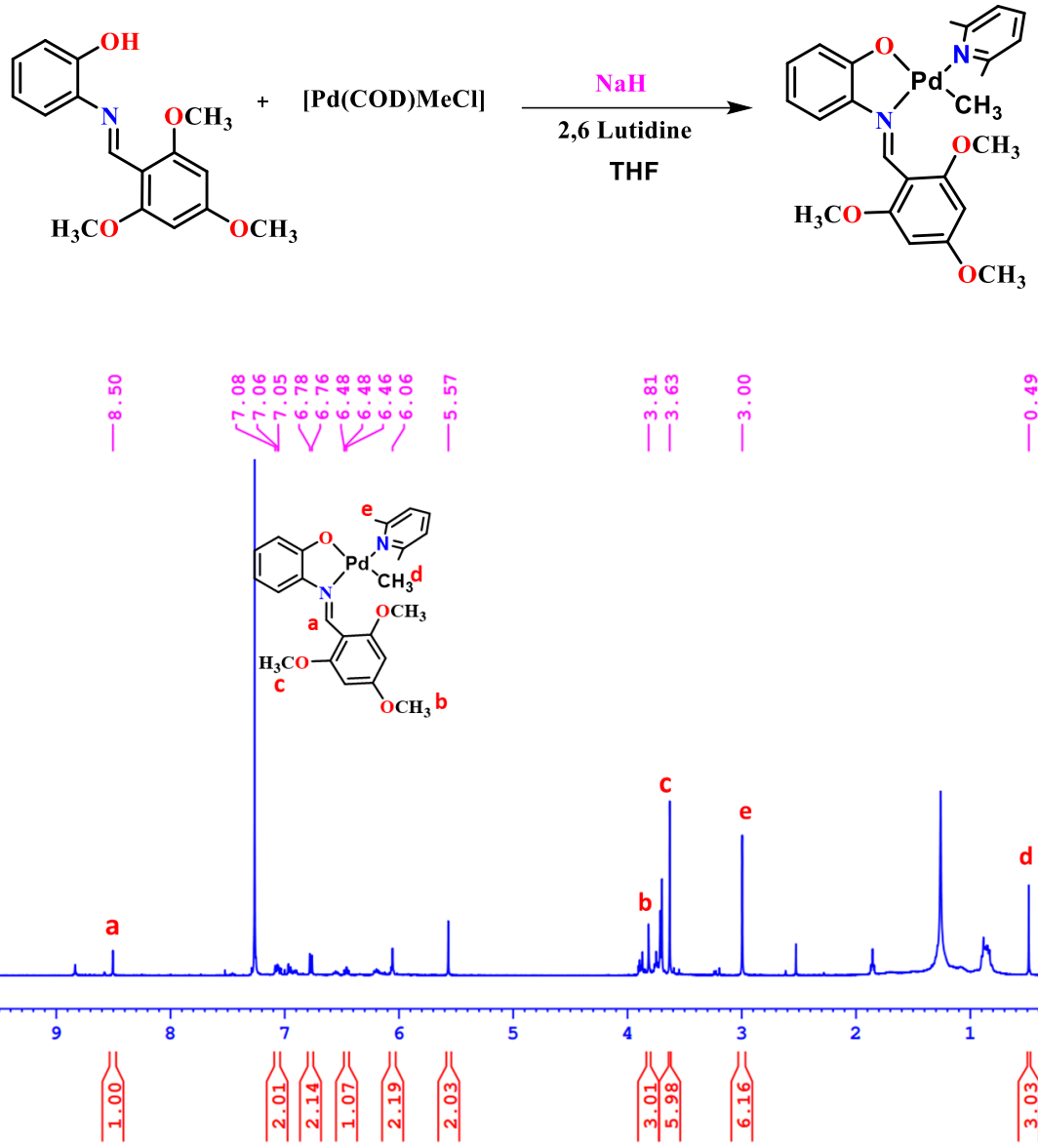

Figure S4.25: ^{1}H NMR of the **4Pd3** in $CDCl_3$.

4.5.3.4. Synthesis of 4Pd4:

In an oven-dried Schlenk flask, sodium hydride (17.3 mg, 0.72 mmol) was dissolved in anhydrous THF (mL). In another Schlenk flask, ligand 4L4 (100 mg, 0.36 mmol) was dissolved in THF (mL), ligand solution was added dropwise to the NaH with vigorous stirring at room temperature. The reaction mixture was stirred for 3 hours at room temperature. In another Schlenk flask, [Pd(COD)MeCl] (94.43 g, 0.36 mmol) was dissolved THF (mL). The ligand solution was dropped into the [Pd(COD)MeCl] at 0 °C. After 10 minutes, 2,6-lutidine was added, and the reaction mixture was stirred at 0 °C for 4 hours. A high vacuum was used to evaporate the solvent, and the complex was extracted in DCM. The resulting complex was washed with hexane to produce a pure product in an excellent yield (165 mg, 90 %).

^{1}H NMR (400MHz , $CDCl_3$) δ= 8.96 (s, 1 H), 7.53 (s, 1 H), 7.45 (d, J = 9.0 Hz, 1 H), 7.22 (s, 2 H), 7.14 - 7.06 (m, 4 H), 7.01 (s, 1 H), 6.89 (s, 1 H), 6.87 - 6.82 (m, 1 H), 6.49 (d, J = 7.6 Hz, 2 H), 3.92 (s, 3 H), 3.00 (s, 6 H), 0.62 (s, 3 H). **ESI-MS** (positive mode): m/z = 505.10 Da [M + H]$^+$ (observed); 505.11 [M + H]$^+$ Da (calculated).

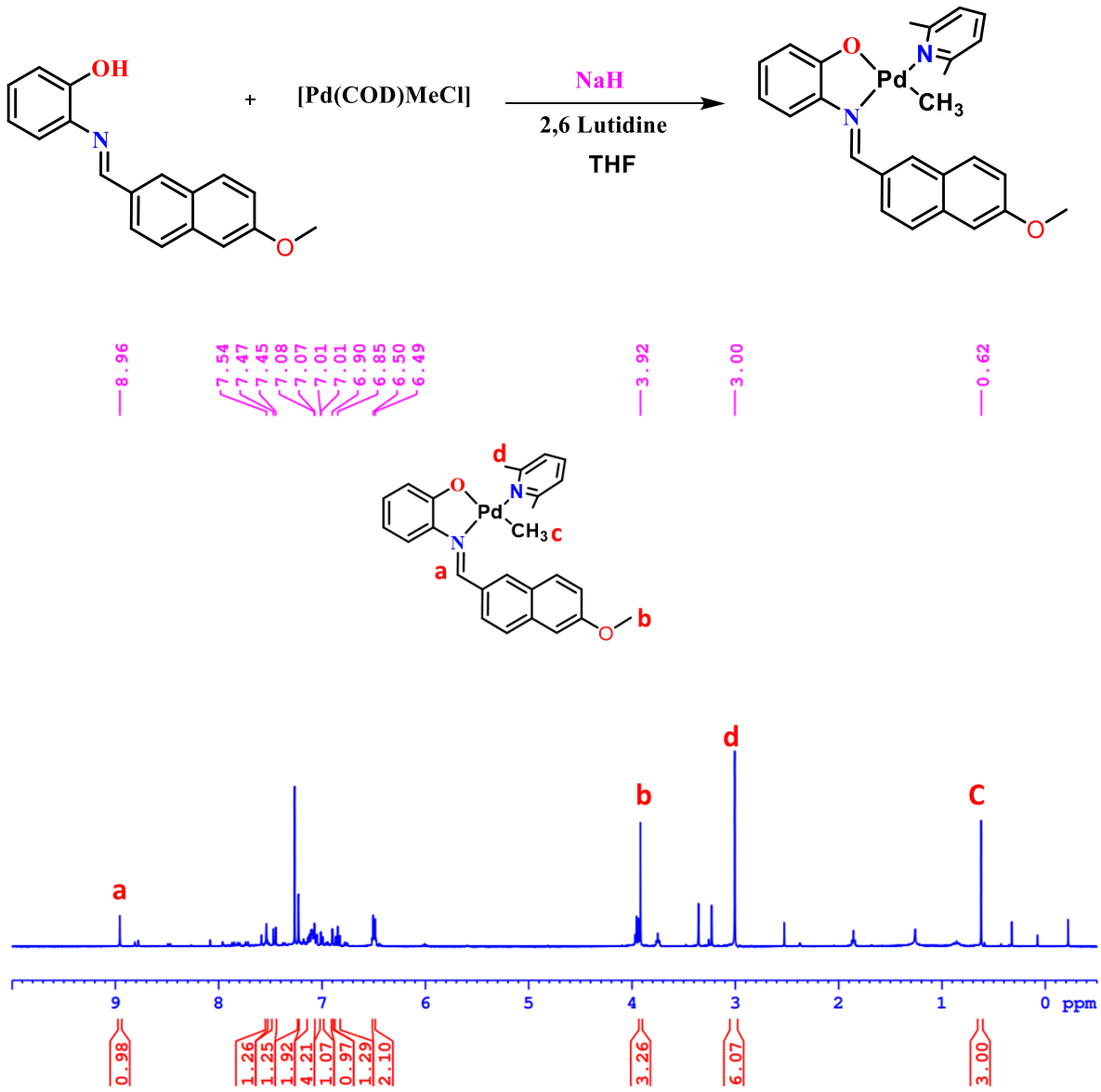

Figure S4.26: ^{1}H NMR of the **4Pd4** in $CDCl_3$. (400 MHZ)

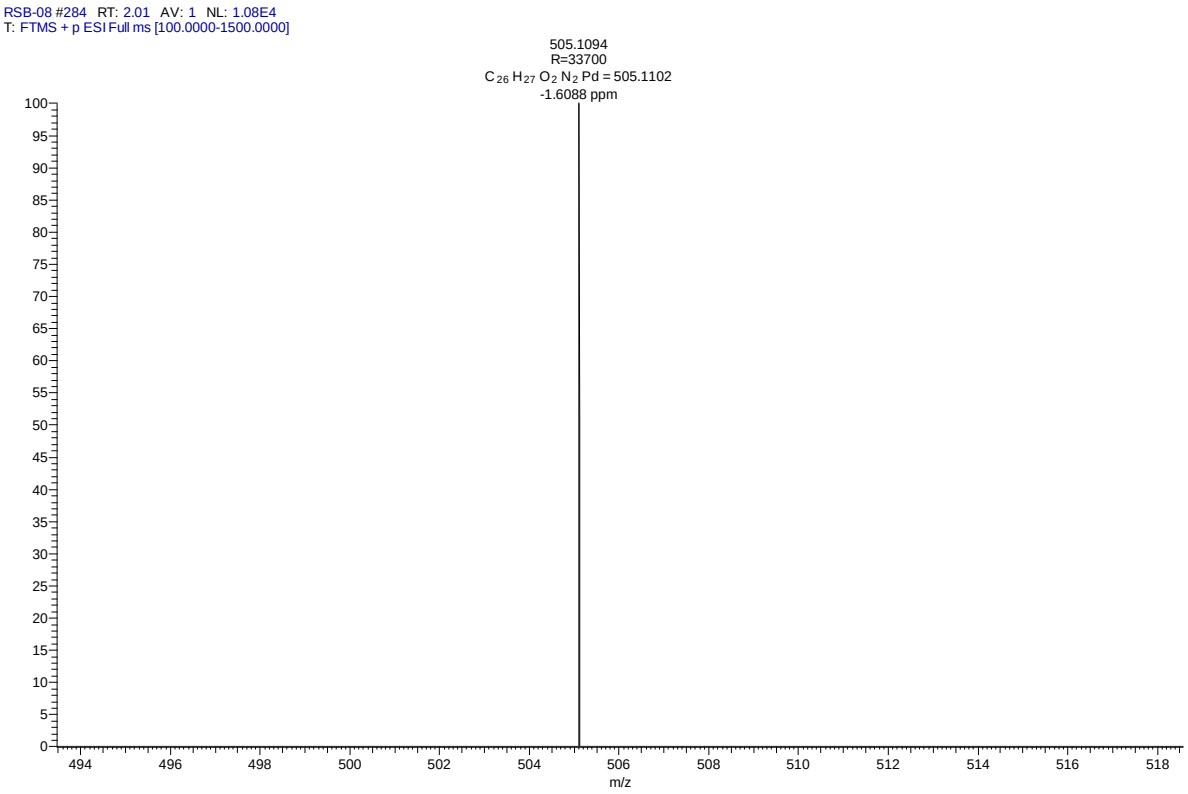

Figure S4.27: ESI-MS data of the **4Pd4**.

4.5.3.5. ^{1}H NMR of [1,4] oxazepines (P1):

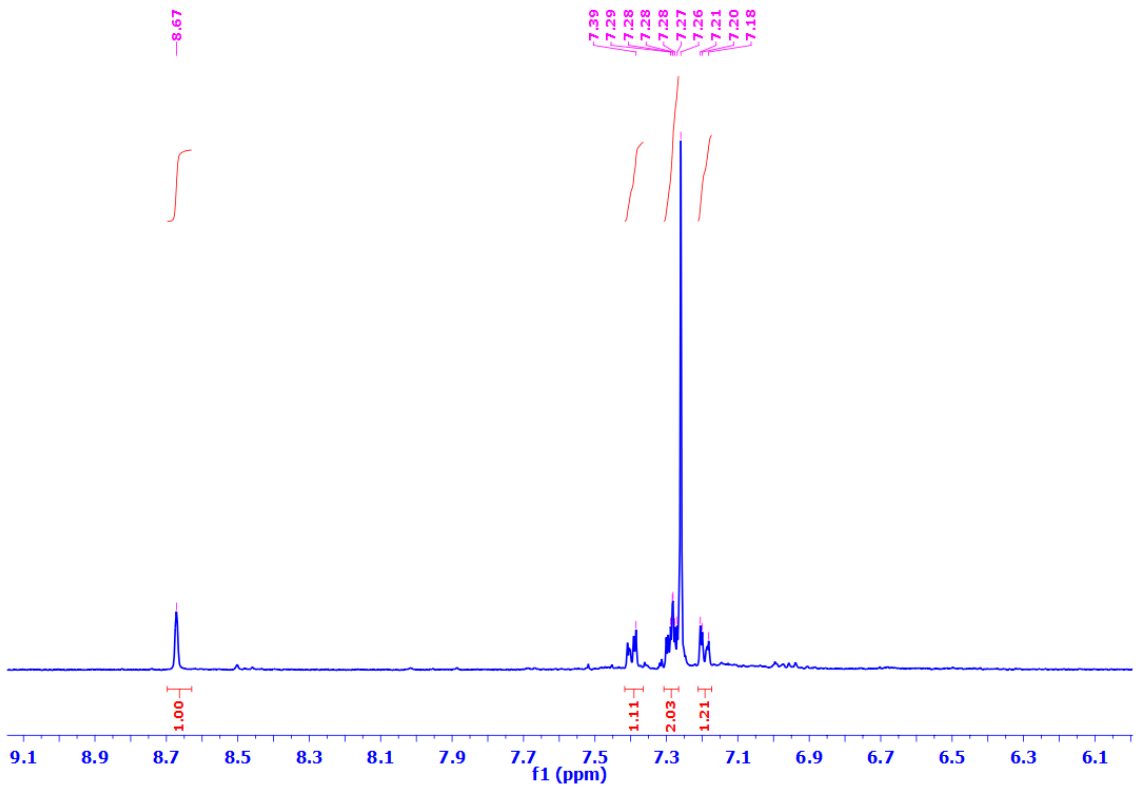

Figure S4.28. ^{1}H NMR of the **P1** in $CDCl_3$.

4.5.4. General procedure for norbornene homopolymerization:

Norbornene polymerization was performed in a 50 mL Schlenk tube equipped with a magnetic stirrer and carried out as follows. At first, the flask was charged with a calculated amount of catalyst, cocatalyst and toluene under nitrogen. After that norbornene was introduces to the reaction content and immediately reaction mixture was kept at the desired preset temperature in oil bath for polymerization. After a desired time, the polymerization was terminated by pouring the reaction content to the methanol. The precipitated polymer was washed with methanol and dried at 40 °C in a vacuum to a constant weight. For all the polymerization procedures, the amount of toluene and norbornene is same.

4.6. References:

1. Blank, F.; Janiak, C. Metal catalysts for the vinyl/addition polymerization of norbornene. *Coord. Chem.Rev.* **2009**, *253*, 827-861.
2. Tritto, I.; Boggioni, L.; Ferro, D. R. Metallocene catalyzed ethene-and propene co-norbornene polymerization: Mechanisms from a detailed microstructural analysis. *Coord. Chem. Rev.* **2006**, *250*, 212-241.
3. Janiak, C.; Lassahn, P. G. Metal catalysts for the vinyl polymerization of norbornene. *J. Mol. Catal. A Chem.* **2001**, *166*, 193-209.
4. Buchmeiser, M. R. Homogeneous metathesis polymerization by well-defined group VI and group VIII transition-metal alkylidenes: Fundamentals and applications in the preparation of advanced materials. *Chem. Rev.* **2000**, *100*, 1565-1604.
5. Coates, G. W. Precise control of polyolefin stereochemistry using single-site metal catalysts. *Chem. Rev.* **2000**, *100*, 1223-1252.
6. Hasan, T.; Ikeda, T.; Shiono, T. Highly efficient Ti-based catalyst systems for vinyl addition polymerization of norbornene. *Macromolecules* **2004**, *37*, 7432-7436.
7. Ziegler, K.; Holzkamp, E.; Breil, H.; Martin, H. Das mülheimer normaldruck-polyäthylen-verfahren. *Angew. Chem.* **1955**, *67*, 541-547.
8. Kaminsky, W.; Bark, A.; Arndt, M. New polymers by homogenous zirconocene/aluminoxane catalysts. *Macromol. Symp*. **1991**, *47*, 83.
9. Kaminsky, W.; Arndt-Rosenau, M. in Metallocene-based Polyolefins, ed. J. Scheirs and W. Kaminsky, Wiley, Chichester, 2000, p. 91.
10. Nakamura, A.; Ito, S.; Nozaki, K. Coordination− insertion copolymerization of fundamental polar monomers. *Chem. Rev.* **2009**, *109*, 5215- 5244.

11. Makio, H.; Terao, H.; Iwashita A.; Fujita, T. FI Catalysts for olefin polymerization- A comprehensive treatment. *Chem. Rev.* **2011**, *111*, 2363.
12. Birajdar, R. S.; Chikkali, S. H. Insertion copolymerization of functional olefins: Quo Vadis?. *Eur. Polym. J.* **2021**, *143*, 110183.
13. Antonov, A. A.; Semikolenova, N. V.; Zakharov, V. A.; Zhang, W.; Wang, Y.; Sun, W. H.; Talsi, E. P.; Bryliakov, K. P. Vinyl polymerization of norbornene on nickel complexes with bis (imino) pyridine ligands containing electron-withdrawing groups. O*rganometallics* **2012**, *31*, 1143–1149.
14. Huo, P.; Li, J.; Liu, W.; Mei, G.; He, X. A highly active and thermally stable 6, 13-dihydro-6, 13-ethanopentacene-15, 16-diimine nickel (II) complex as catalyst for norbornene polymerization. *RSC Adv*. **2017**, *7*, 51858–51863.
15. Huo, P.; Liu, W.; He, X.; Wang, H.; Chen, Y. Nickel (II) complexes with three-dimensional geometry α-diimine ligands: synthesis and catalytic activity toward copolymerization of norbornene. *Organometallics* **2013**, *32*, 2291–2299.
16. He, X.; Deng, Y.; Jiang, X.; Wang, Z.; Yang, Y.; Han, Z.; Chen, D. Copolymerization of norbornene and butyl methacrylate at elevated temperatures by a single centre nickel catalyst bearing bulky bis (α-diimine) ligand with strong electron-withdrawing groups. *Polym. Chem.* **2017**, *8*, 2390–2396.
17. Huo, P.; Li, J.; Liu, W.; Mei, G.; He, X. A highly active and thermally stable 6, 13-dihydro-6, 13-ethanopentacene-15, 16-diimine nickel (II) complex as catalyst for norbornene polymerization. *RSC Adv*. **2017**, *7*, 51858–51863.
18. Makio, H.; Terao, H.; Iwashita, A.; Fujita, T. FI Catalysts for olefin polymerization A comprehensive treatment. *Chem. Rev.* **2011**, *111*, 2363–2449.
19. Chen, M.; Zou, W.; Cai, Z.; Chen, C. Norbornene homopolymerization and copolymerization with ethylene by phosphine-sulfonate nickel catalysts. *Polym. Chem.* **2015**, *6*, 2669–2676.
20. Wang, H. Y.; Zhang, J.; Meng, X.; Jin, G. X. Nickel (II) complexes with β-enaminoketonato chelate ligands: Synthesis, solid-structure characterization and reactivity toward the addition polymerization of norbornene. *J. Organomet. Chem*. **2006**, *691*, 1275–1281.
21. Kong, Y.; Cheng, M.; Ren, H.; Xu, S.; Song, H.; Yang, M.; Wang, B. Synthesis, structures, and norbornene polymerization behavior of bis (aryloxide-N-heterocyclic carbene) nickel complexes. *Organometallics* **2011**, *30*, 1677–1681.

22. Yang, D.; Dong, J.; Wang, B. Homo-and copolymerization of norbornene with tridentate nickel complexes bearing o-aryloxide-N-heterocyclic carbene ligands. *Dalton Trans.* **2018**, *47*, 180–189.
23. Cheng, H.; Cai, Z. (Anilino) anthraquinone Nickel-Catalyzed Random Copolymerization of Norbornene and Ethylene. *ChemCatChem* **2018**, *10*, 497–500.
24. Bermesheva, E. V.; Bermeshev, M. V. Single-Component Catalysts for the Vinyl-Addition Polymerization of Norbornene and its Derivatives. *ChemCatChem*, **2023**, *15*, e202300818.
25. Zhuang, R.; Liu, H.; Guo, J.; Dong, B.; Zhao, W.; Hu, Y.; Zhang, X. Highly active nickel (II) and palladium (II) complexes bearing N, N, P tridentate ligand for vinyl addition polymerization of norbornene. *Eur. Polym. J.* **2017**, *93*, 358–367.
26. Suslov, D. S.; Bykov, M. V.; Abramov, P. A.; Pakhomova, M. V.; Ushakov, I. A.; Voronov, V. K.; Tkach, V. S. Synthesis, characterization, and application for addition polymerization of norbornene of novel acetylacetonate bis (anilines) palladium (II) complexes. *Inorg. Chem. Commun.* **2016**, *66*, 1–4.
27. Li, M.; Song, H.; Wang, B. Synthesis, structures, and norbornene polymerization behavior of palladium methyl complexes bearing N-heterocyclic carbene-sulfonate ligands. *J. Organomet. Chem.* **2016**, *804*, 118–122.
28. Dang, L.; Song, H.; Wang, B. Synthesis, structures, and norbornene polymerization behavior of o-aryloxide-substituted NHC-ligated σ, π-cycloalkenyl palladium complexes. *Organometallics* **2014**, *33*, 6812–6818.
29. Deng, J.; Gao, H.; Zhu, F.; Wu, Q. Synthesis and structure of imine–N-heterocyclic carbene palladium complexes and their catalytic behavior in norbornene polymerization. *Organometallics* **2013**, *32*, 4507–4515.
30. Deng, J.; Gao, H.; Zhu, F.; Wu, Q. Synthesis and structure of imine–N-heterocyclic carbene palladium complexes and their catalytic behavior in norbornene polymerization. *Organometallics* **2013**, *32*, 4507–4515.
31. He, J.; Liu, Z.; Du, G.; Fu, Y.; Zhang, S.; Li, X. Chiral Palladium (II) and Nickel (II) complexes with C 2-symmetrical tridentate Bis (oxazoline) ligands: synthesis, characterization, and catalytic norbornene polymerization. *Organometallics* **2014**, *33*, 6103–6112.
32. Kong, Y.; Ren, H.; Xu, S.; Song, H.; Liu, B.; Wang, B. Synthesis, structures, and norbornene polymerization behavior of bis (aryloxide-N-heterocyclic carbene) palladium complexes. *Organometallics* **2009**, *28*, 5934–5940.

33. Yang, D.; Tang, Y.; Song, H.; Wang, B. Synthesis, structures, and norbornene polymerization behavior of palladium complexes bearing tridentate o-aryloxide-N-heterocyclic carbene ligands. *Organometallics* **2016**, *35*, 1392–1398.
34. Liang, H.; Liu, J.; Li, X.; Li, Y. Synthesis, structure and norbornene polymerization behavior of neutral palladium complexes. *Polyhedron* **2004**, *23*, 1619– 1627.
35. Zheng, T.; Liao, H.; Gao, J.; Zhong, L.; Gao, H.; Wu, Q. Synthesis and characterization of α-diamine palladium complexes and insight into hybridization effects of nitrogen donor atoms on norbornene (co) polymerizations. *Polym. Chem.* **2018**, *9*, 3088–3097.
36. Tian, J.; He, X.; Liu, J.; Deng, X.; Chen, D. Palladium (II) and copper (II) chloride complexes bearing bulky α-diimine ligands as catalysts for norbornene vinyl-addition (co) polymerization. *RSC Adv.* **2016**, *6*, 22908–22916.
37. Dang, L.; Guo, J.; Song, H.; Liu, B.; Wang, B. Synthesis, structures, and norbornene polymerization behavior of C (sp 3), N-chelated palladacycles bearing o-aryloxide-N-heterocyclic carbene ligands. *Dalton Trans*. **2014**, *43*, 17177–17183.
38. Schultz, R. G. The chemistry of palladium complexes. III. The polymerization of norbornene systems catalyzed by palladium chloride (1). *J. Polym. Sci., Part C: Polym. Lett.* **1966**, *4*, 541–546.
39. Shin, D. M.; Son, S. U.; Hong, B. K.; Chung, Y. K.; Chun, S. H. Preparation of palladium complexes of 1, 3-di (2-pyridyl) propane derivatives and their use in norbornene polymerization. *J. Mol. Catal. A: Chem.* **2004**, *210*, 35–46.
40. Cho, H. Y.; Hong, D. S.; Jeong, D. W.; Gong, Y. D.; Woo, S. I. High-Throughput Synthesis of New Ni (ii), Pd (ii), and Co (ii) Catalysts and Polymerization of Norbornene Utilizing the Self-Made Parallel Polymerization Reactor System. *Macromol. Rapid Commun*. **2004**, *25*, 302–306.
41. Liang, H.; Liu, J.; Li, X.; Li, Y. Synthesis, structure and norbornene polymerization behavior of neutral palladium complexes. *Polyhedron* **2004**, *23*, 1619– 1627.
42. Abu-Surrah, A. S.; Thewalt, U.; Rieger, B. Chiral palladium (II) complexes bearing tetradentate nitrogen ligands: synthesis, crystal structure and reactivity towards the polymerization of norbornene. *J. Organomet. Chem.* **1999**, *587*, 58–66.
43. Lozana, V.; Lassahn, P. G.; Zhang, C.; Wu, B.; Janiak, C.; Rheinwald, G.; Lang, H. Dinuclear nickel (II) and palladium (II) complexes in combination with different co-catalysts as highly active catalysts for the vinyl/addition polymerization of norbornene. *Z. Naturforsch., B: J. Chem. Sci.* **2003**, *58*, 1152–1164.

44. Blank, F.; Scherer, H.; Ruiz, J.; Rodríguez, V.; Janiak, C. Palladium (ii) complexes with pentafluorophenyl ligands: structures, C_6 F_5 fluxionality by 2D-NMR studies and pre-catalysts for the vinyl addition polymerization of norbornene. *Dalton Trans.* **2010**, *39*, 3609–3619.
45. Li, Y.; Jiang, L.; Wang, L.; Gao, H.; Zhu, F.; Wu, Q. Nickel (II) complexes supported by a fluorinated β-diketiminate backbone ligand: synthesis, catalytic activity toward norbornene polymerization, and the oxygenated species. *Appl. Organomet. Chem.* **2006**, *20*, 181–186.
46. Gao, H.; Guo, W.; Bao, F.; Gui, G.; Zhang, J.; Zhu, F.; Wu, Q. Synthesis, molecular structure, and solution-dependent behavior of nickel complexes chelating anilido−imine donors and their catalytic activity toward olefin polymerization. *Organometallics* **2004**, *23*, 6273–6280.
47. Gao, H.; Chen, Y.; Zhu, F.; Wu, Q. Copolymerization of norbornene and styrene catalyzed by a novel anilido–imino nickel complex/methylaluminoxane system. *J. Polym. Sci., Part A: Polym. Chem.* **2006**, *44*, 5237–5246.
48. Li, Y.; Wang, L.; Gao, H.; Zhu, F.; Wu, Q. Novel nickel (II) complexes chelating β-diketiminate ligands: synthesis and simultaneous polymerization and oligomerization of ethylene. *Appl. Organomet. Chem.* **2006**, *20*, 436–442.
49. Zhang, J.; Gao, H.; Ke, Z.; Bao, F.; Zhu, F.; Wu, Q. Investigation of 1-hexene isomerization and oligomerization catalyzed with β-diketiminato Ni (II) bromide complexes/methylaluminoxane system. *J. Mol. Catal. A: Chem.* **2005**, *231*, 27–34.
50. Zhang, J.; Ke, Z.; Bao, F.; Long, J.; Gao, H.; Zhu, F.; Wu, Q. Ethylene polymerization and oligomerization catalyzed by bulky β-diketiminato Ni (II) and β-diimine Ni (II) complexes/methylaluminoxane systems. *J. Mol. Catal. A: Chem.* **2006**, *249*, 31–39.
51. Gao, H.; Liu, Y.; Li, G.; Xiao, Z.; Liang, G.; Wu, Q. Catalytic synthesis of polyethylene-block-polynorbornene copolymers using a living polymerization nickel catalyst. *Polym. Chem.* **2014**, *5*, 6012–6018.
52. Long, J. M.; Gao, H. Y.; Liu, F. S.; Song, K. M.; Hu, H.; Zhang, L. Wu, Q. Nickel and palladium complexes bearing ortho-phenoxy modified anilido-imine ligands: Drastic steric effect on coordinated geometry, and catalytic property toward olefin polymerization. *Inorg. Chim. Acta* **2009**, *362*, 3035–3042.
53. Gao, H.; Pei, L.; Li, Y.; Zhang, J.; Wu, Q. Vinyl polymerization of norbornene with nickel catalysts bearing [N, N] six-membered chelate ring: Important influence of ligand structure on activity. *J. Mol. Catal. A: Chem.* **2008**, *280*, 81–86.

54. He, X.; Deng, Y.; Jiang, X.; Wang, Z.; Yang, Y.; Han, Z.; Chen, D. Copolymerization of norbornene and butyl methacrylate at elevated temperatures by a single centre nickel catalyst bearing bulky bis (α-diimine) ligand with strong electron-withdrawing groups. *Polym. Chem.* **2017**, *8*, 2390–2396.
55. Huo, P.; Liu, W.; He, X.; Wei, Z.; Chen, Y. Substituent effects and activation mechanism of norbornene polymerization catalyzed by three-dimensional geometry α-diimine palladium complexes. *Polym. Chem.* **2014**, *5*, 1210–1218.
56. Hu, T.; Li, Y. G.; Li, Y. S.; Hu, N. H. Novel highly active binuclear neutral nickel and palladium complexes as precatalysts for norbornene polymerization. *J. Mol. Cat. A: Chem.* **2006**, 253, 155–164.
57. Petrenko, N. I.; Kozlova, M. M.; Gerasimova, T. N. Synthesis of polyfluorodibenz [b, f][1, 4] oxazepines by cyclization of polyfluorinated o hydroxybenzylidenanilines. *J. fluo. Chem.* **1987**, *36*, 93-98.
58. Allaway, C. L.; Daly, M.; Nieuwenhuyzen, M.; Saunders, G. C. Synthesis of polyfluorodibenz [b, f][1, 4] oxazepines by the cyclization of 2-[(polyfluorobenzylidene) amino] phenols. *J. fluo. Chem.* **2002**, *115*, 91-99.
59. Falivene, L.; Cao, Z.; Petta, A.; Serra, L.; Poater, A.; Oliva, R; Scarano, V.; Cavallo, L. Towards the online computer-aided design of catalytic pockets. *Nat. Chem.* **2019**, *11*, 872-879.
60. Yang, D.; Tang, Y.; Song, H.; Wang, B. Synthesis, structures, and norbornene polymerization behavior of palladium complexes bearing tridentate o-aryloxide-N-heterocyclic carbene ligands. *Organometallics* **2016**, *35*, 1392–1398.

Chapter 5

Depolymerization and Repolymerization of Polyethylene-like Polymers

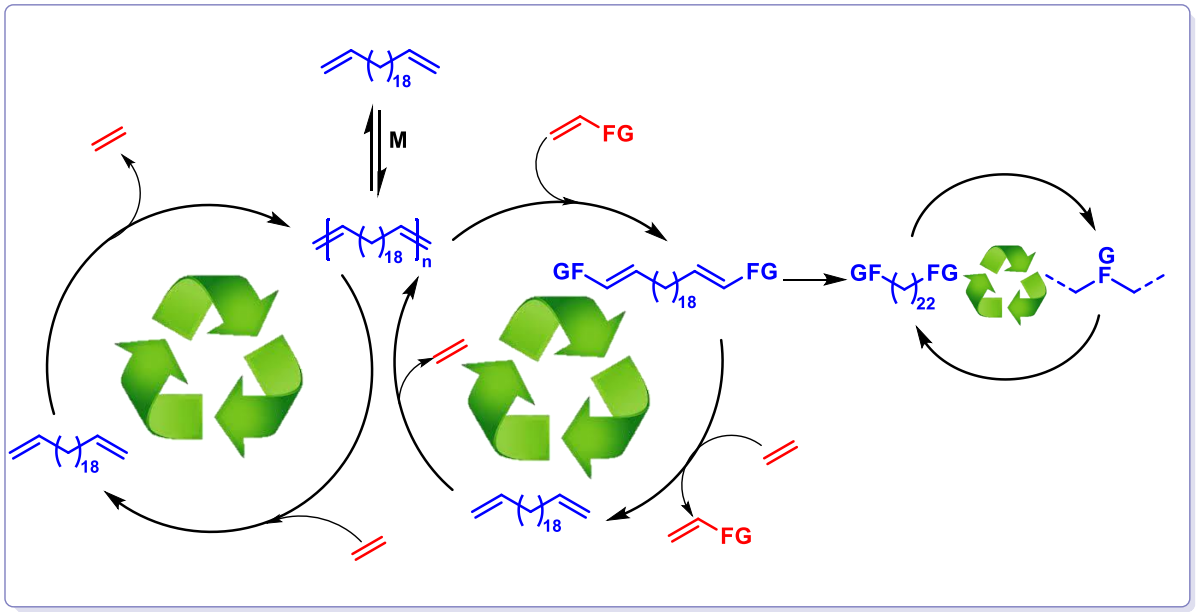

5.1. Abstract:

Polyolefins, a prominent class of synthetic polymers, have garnered widespread attention due to their exceptional versatility, durability, and affordability. The substantial utilization of polyolefins leads to significant amount of waste generation. To mitigate the plastic waste, it is crucial to synthesize chemically depolymerizable or recyclable polyolefins. Polyolefins featuring unsaturation in their backbone are particularly desirable for the production of chemically recyclable polymers. In this chapter we demonstrate a sustainable paradigm shift in polymer science, embodying the principles of a circular economy. This chapter outlines the synthesis of docosa-1,21-diene monomer with excellent yield (94%), which is subsequently polymerized into a polymer (P1) through ADMET polymerization. The resulting polymer (P1) displayed a molecular weight (M_w) of up to 17.6 kDa and PDI of 1.7. Analysis through DSC, TGA and WAXS shows data closely resembling to commercial polyethylene. Furthermore, in depolymerization experiments, exposure of the synthesized polymer (P1) to ethylene with HG-II catalyst effectively converts the polymer back into its original monomer (RM1), and oligomers. Obtained monomers and oligomers are repolymerized to its parent polymer (RP1) to achieve a closed loop system. The versatility of this methodology is demonstrated by the generation of a functionalized monomer through depolymerization of polymer (P1) with acrylates. The functionalized monomer takes center stage as it undergoes a transformative process, culminating in the synthesis of a polyester with polyethylene-like material (P2) with molecular weight (Mw) of 6.4kDa. In the spirit of a circular economy, the study focused on the depolymerization and subsequent repolymerization of the polyester, demonstrating a closed-loop system.

5.2. Introduction:

In the pursuit of sustainable and eco-friendly practices, the concept of circular economy of plastic has emerged as a challenger to the traditional linear models of resource consumption and waste generation.[1,2] At the forefront of this transformative approach lies the polyethylene lifecycle, a cornerstone in the global plastics industry. Polyethylene, one of the most ubiquitous and versatile polymers, has found its way into an array of applications, ranging from packaging materials to medical devices.[3] However, its persistent environmental footprint and the escalating plastic waste crisis demand innovative solutions to balance its indispensable utility with environmental stewardship.[4]

As polyethylene is one of the most commonly used plastics in the world. The disposal of polyethylene products has become a significant environmental concern.[5] When polyethylene

is discarded, it can end up in landfills, oceans, and other natural environments, where it can take hundreds of years to degrade. This can cause environmental pollution, harm wildlife, and have adverse effects on human health.[6] Therefore, there is a need for alternative solutions that can reduce the environmental impact of polyethylene. Recycling and depolymerization are essential strategies for managing polyolefin waste sustainably.[7] Recycling involves collecting and processing used polyolefin items, transforming them into new products, reducing resource consumption, and minimizing environmental impact. Depolymerization takes recycling a step further by breaking down polyolefins into their constituent monomers or oligomers, enabling the recovery of high-quality building blocks for new plastics. These processes collectively contribute to a circular economy, reducing plastic waste, conserving resources, and promoting a more environmentally responsible approach to plastic usage.

The depolymerization of polyolefins is very challenging and it is performed by thermal and catalytic processes. In catalytic process catalysts, are used to facilitate the breakdown of polyolefins into smaller molecules under controlled conditions. This method can enhance selectivity and efficiency in producing desired products. In 2016, Huang et al. reported the chemical recycling of PEs via a tandem cross alkane metathesis (CAM) method.[8] This process begins with Ir catalysed dehydrogenation of PE and short chain alkanes (using n-hexane as an example) in a closed reactor, yielding unsaturated PE and hexenes and Ir-H_2; the unsaturated PE and hexenes then undergo cross alkene metathesis, resulting in PE degradation. Hartwig and coworkers reported the synthesis of propylene by partial dehydrogenation of polyethylene followed by tandem isomerizing ethenolysis of the unsaturated polyethylene chain.[9] Dehydrogenation of high-density polyethylene was performed by iridium-pincer complex and by using an second-generation Hoveyda-Grubbs metathesis catalyst along with $[PdP(tBu)_3(\mu\text{-}Br)]_2$ as an isomerization catalyst they selectively degraded this unsaturated polymer to propylene in yields exceeding 80%. Coates and coworker reported degradation of HDPE via a tandem dehydrogenation/cross alkene metathesis/hydrogenation procedure to produce ester-terminated telechelic macromonomer for the manufacture of closed-loop chemically recyclable polymers.[10] The partly unsaturated HDPE was converted into telechelic macromonomers by cross-metathesis with 2-hydroxyethyl acrylate followed by hydrogenation. Further they used this hydrogenated macromonomer directly and repolymerized it through transesterification to the polymer.

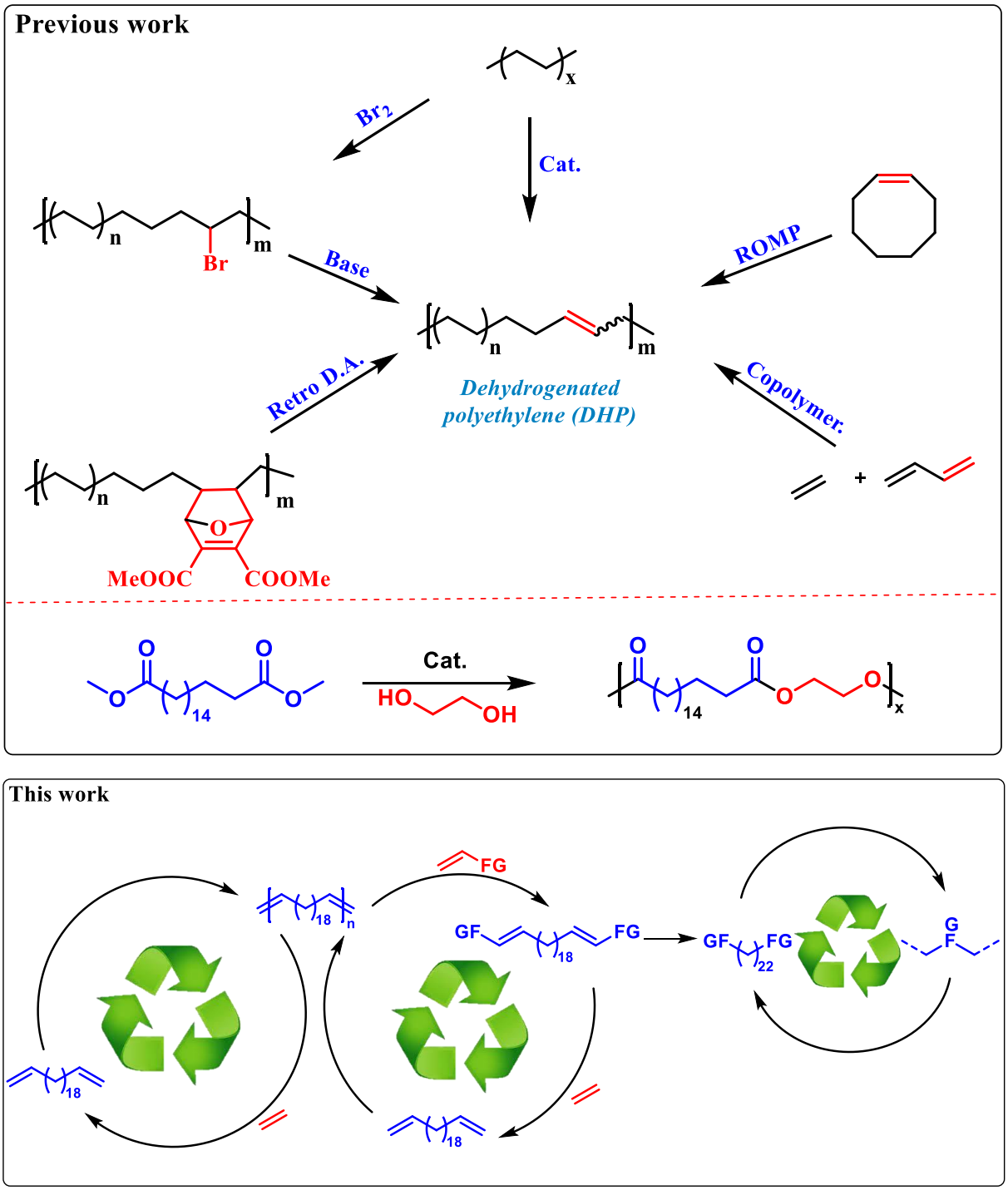

Figure 5.1: Previous efforts to generate unsaturated polyethylene (top), Current work (bottom).

Major depolymerization of polyethylene was performed by the dehydrogenation followed by the metathesis reaction. The introduction of double bond in the polyethylene is very challenging and researcher have achieved it through different routes. Incorporation of bromine in polymer using Br_2 in presence of light produced a brominated polyethylene. Dehydrobromination of brominated polyethylene produces the unsaturated polymer.[11] In 2023, Coates and co-worker prepared the masked unsaturated polymer through a copolymerization

of ethylene with dimethyl 7-oxa bicyclo-[2.2.1].[12] Through this they synthesized high-density polyethylene (HDPE) with 2.34 mol% of comonomer incorporation. By using retro Diels-Alder reaction the author unmasked the double bond in the polymer backbone. This unsaturated polymer was cross alkene metathesized with 2-hydroxyethylacrylate to produces telechelic macromonomer. Further hydrogenation and repolymerization via trans esterification produced the polymer. The direct unsaturation was achieved through an ROMP of cyclooctene or the copolymerization of ethylene with butadiene. But through this process the obtained polymer was found to have more olefin content.[13,14] The higher olefin content will compremizes the polymer properties which are different than the HDPE. To address this problem Mecking and co-worker developed polyester material from readily available and easily accesible biobased 1,18-octadecanedi-carboxylic acid and ethylene glycol. This material exhibit a polyethylene-like solid-state structure and also possesses similar tensile properties to high density polyethylene (HDPE).[15] In this polymer functional groups are situated after the long [$(CH_2)_{16}$] hydrophobic repeating units, and it behaves like polyethylene. Also they studied the biodegradation of this material and observed 95 % of degradation within 2 months.

This chapter delves into the intricate dynamics of polyethylene like polymer synthesis, its depolymerization, and repolymerization, with a dedicated focus on advancing circular economy principles. The interplay between these processes holds the key to reshaping the life cycle of polyethylene, offering a pathway towards sustainability and waste reduction.

5.3. Results and discussion:

5.3.1. Monomer synthesis:

Castor oil, derived from the seeds of the castor plant *Ricinus communis (Euphorbiaceae)*, is a non-edible oil found in tropical and subtropical regions.[16] Globally, approximately 1 million tons of castor seeds are produced annually, with India, China, and Brazil being the leading producers.[17,18] The fatty acid fraction in castor oil primarily consists of ricinoleic acid, constituting approximately 90%. Ricinoleic acid is a monounsaturated 18-carbon fatty acid characterized by a hydroxyl function at position 12, which is a notably unique structure for a naturally occurring fatty acid. When ricinoleic acid is heated at 300 °C under vacuum conditions, it yields undecylenic acid or 10-undecenoic acid.[19,20] In literature it was known that the reduction followed by the halogenation yields an 11-bromo-1-undecene in good yield.[21,22]

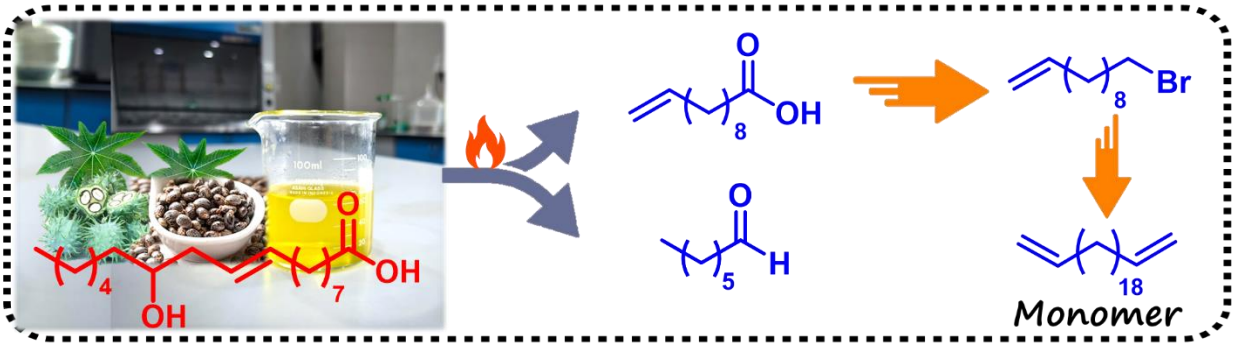

Scheme 5.1: Synthesis of Monomer.

11-bromo-1-undecene can be synthesized from a biobased caster oil source and the synthesis process is reported. In our study, since it is commercially available as a building block we purchased the chemical directly and utilized it for further reactions. To obtain the desired diene monomer, a homocoupling reaction of 11-bromo-1-undecene was performed. In this reaction, $NiCl_2•6H_2O$ is used as the catalyst in the presence of activated zinc, resulting in the production of a docosa-1,21-diene monomer with an excellent yield of up to 94%. This resulting monomer manifests as a colorless, oily compound, a characterization confirmed through NMR spectroscopy. In the ^1H NMR spectrum, distinct peaks corresponding to terminal olefins are evident at 5.74-5.83 and 4.94-5.02 ppm (Figure 5.14). While the ^{13}C NMR spectrum reveals olefin carbon peaks around 114 and 139 ppm (figure 5.15). In DSC analysis it was observed that the sharp melting peak was observed at 31.8 °C (Figure 5.17). Subsequently, the obtained monomer was subjected to direct ADMET polymerization.

5.3.2. Polymerization:

Docosa-1,21-diene monomer was directly subjected for the ADMET polymerization using an Grubbs-II metathesis catalyst. Initial experimentation at room temperature (30 °C) revealed a modest production of only 0.2% of internal olefins which is confirmed by ^1H NMR, indicating the need for high energy for effective polymerization. Substantially increase in the polymerization temperature to 50, 60 and 75 °C (Table 5.1, entry no. 3 to 9), resulted in to a higher molecular weight polymer. At 75 °C, an increase in molecular weight was observed over time, with the polymer reaching 3500 Da after 0.5 hours, 4300 Da after 1 hour, and a substantial 11000 Da after 3 hours (Table 5.1, entry no. 7, 8 and 9). These observations reaffirm that ADMET follows a step-growth mechanism.

To further explore the impact of temperature on polymerization, experiments were conducted at 80 °C (Table 5.1, entry no. 10 and 11). These higher temperatures facilitated the synthesis

of polymers with increased molecular weights, addressing the challenges posed by viscous and solid reaction masses at elevated molecular weights. Polymerization at 80 °C yielded polymers with molecular weights of up to 17600 Da, as determined using THF GPC at 60 °C. This systematic investigation provides valuable insights into optimizing the ADMET polymerization process for the synthesis of high molecular weight polymers.

In Differential Scanning Calorimetry (DSC) analysis of the polymer disclosed a melting temperature of 100.6 °C (Table 5.1, entry no. 11), that is close to the commercial polyethylene. Wide angle X-ray scattering (WAXS) diffractograms of the materials prepared are virtually identical to that of HDPE. We observed peaks at 2θ values of 21.4, 30, and 40°, corresponding to the orthorhombic crystalline form of PE. The DSC and WAXS confirms the presence olefin bond (after the every 18 carbon) does not affect the crystallization of polymer, long aliphitic chains are aligned to form a crystalline domains. DSC data disclosed 59% crystallinity. The thermogravametric analysis data also suggest similar thermal degradation as that to the HDPE.

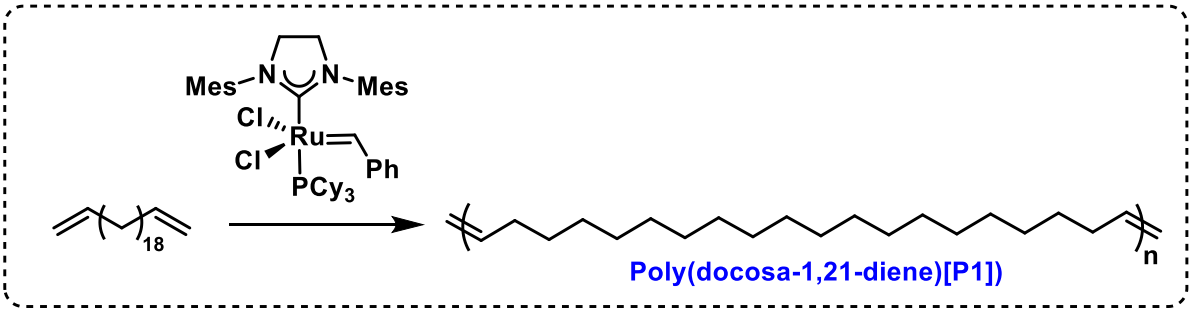

Scheme 5.2: ADMET polymerization of docosa-1,21-diene monomer.

Table 5.1: Polymerization of docosa-1,21-diene to poly(docosa-1,21-diene) (P1).[a]

Entry No.	Temperature (°C)	Time (h)	Internal Protons	M_n (NMR)	M_w (GPC)	PDI
1.	30	9	0.2	300	-	-
2.	40	8	3.27	700	-	-
3.	50	4	4.42	900	-	-
4.	50	6	9.24	1600	-	-
5.	60	0.5	3.52	800	-	-
6.	60	1	9.29	1600	-	-
7.	75	0.5	23.06	3500	-	-
8.	75	1	28.78	4300	-	-
9.	75	3	76.61	11000	-	-

10.	80	4	-	-	11500	1.3
11.[b]	80	24	-	-	17600	1.7

[a]**Reaction Condition**- Monomer 300 mg (0.98 mmol), Catalyst Grubbs-II (2.9 µmol.), M_w and PDI were recorded using GPC in THF at 60 °C against polystyrene standard, [b]Reaction were performed at 1 gm scale.

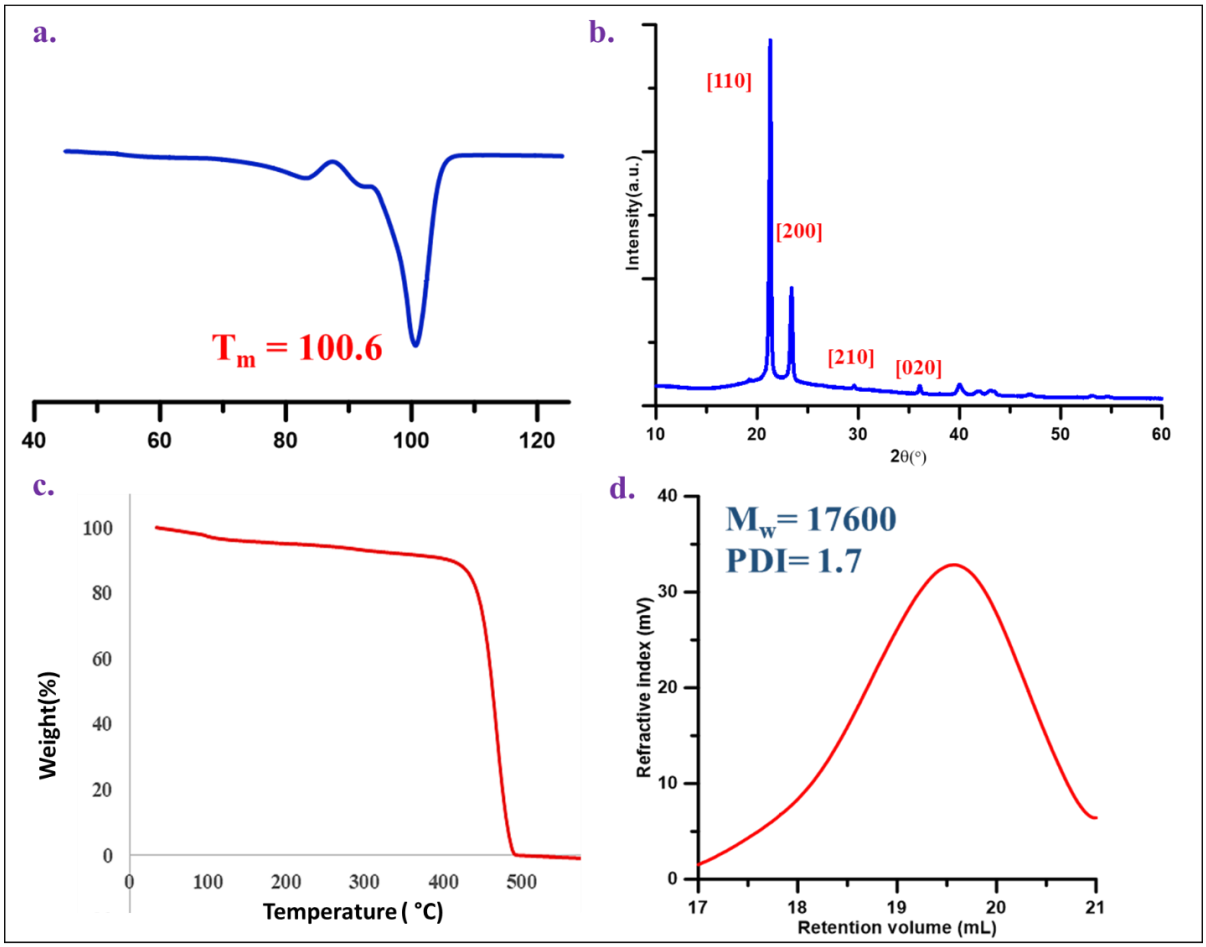

Figure 5.2: a) DSC thermogram of P1, b) WAXS diffractograms of P1, c) Thermogravimetric analysis (TGA) thermogram of P1, d) GPC data of P1.

5.3.3. Depolymerization with ethylene and its repolymerization:

To avoid the waste generation and to follow the principles of circular economy the depolymerization via cross alkene metathesis (CAM) with ethylene to obtain monomer (M1) and repolymerization of M1 to P1 is crucial (scheme 5.3).

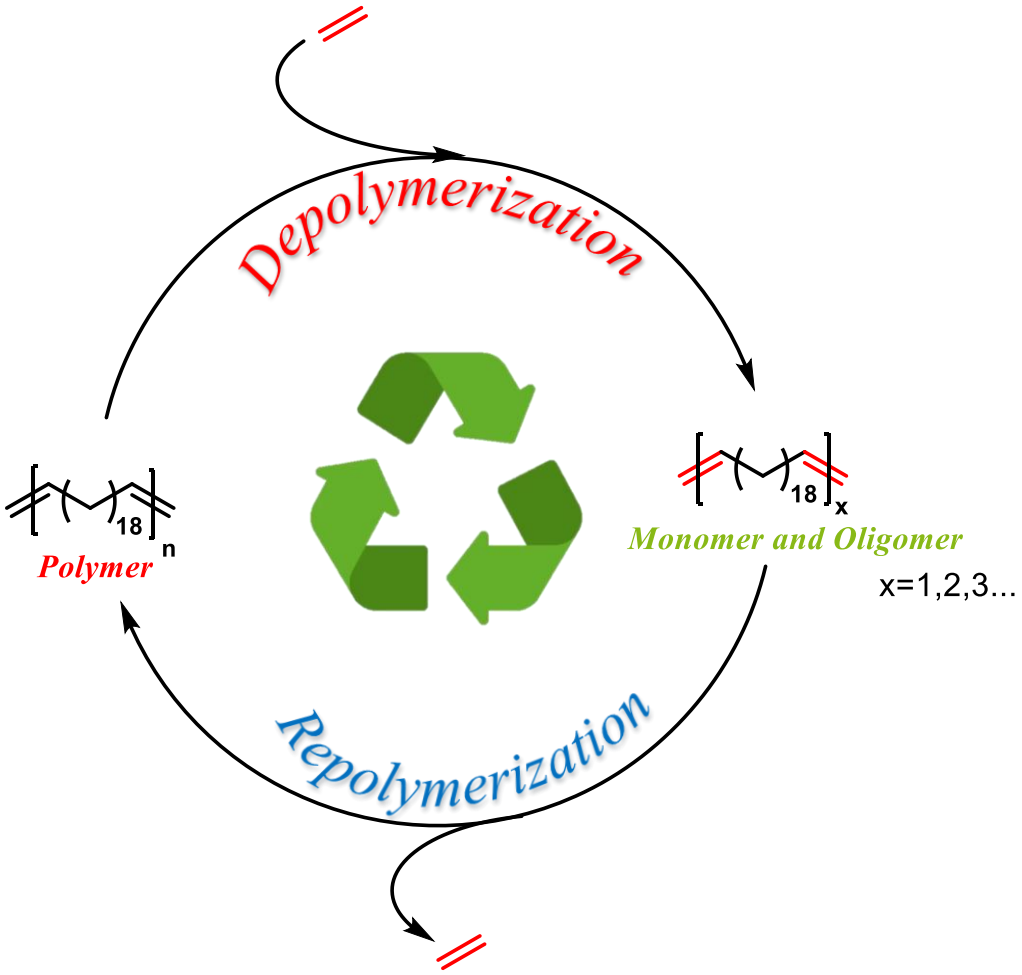

Scheme 5.3: Depolymerization of polymer (P1) to monomer/ oligomer and its repolymerization to polymer (RP1).

To achieve this, polymer (P1) was subjected to ethylene cross-metathesis using metathesis catalyst [Grubbs-I(G-I), Grubbs-II(G-II), Hoveyda Grubbbs-I (HG-I) and Hoveyda Grubbbs-II (HG-II)] and 25 bar of ethylene pressure. With Grubbs-I catalyst (5 wt %), 32% conversion was observed after 2 hours of cross alkene metathesis (Table 5.3, Entry 1). Under similar reaction condition, Grubbs-II catalyst produces 48 % of depolymerized products (Table 5.3, Entry 2). The Hoveyda Grubbs-I catalyst displayed enhanced depolymerized product (72%) compared to Grubbs catalyst (Table 5.3, Entry 3). Hoveyda Grubbs-II catalyst outperforms the above all catalysts with >99% conversion (Table 5.3, Entry 4). Also, to achieve an optimal reaction condition various reaction parameters like time, temperature and pressure were screened. Using a HG-II catalyst with 25 bar of ethylene pressure within a 30 minutes up to 88% conversion was observed (Table 5.3, Entry 9). With lowering the ethylene pressure, there was no significant change in depolymerization. At 15 bar of ethylene pressure 98% conversion was observed and at 5 bar 88% conversion was observed (Table 5.3, Entry 14 and 15).

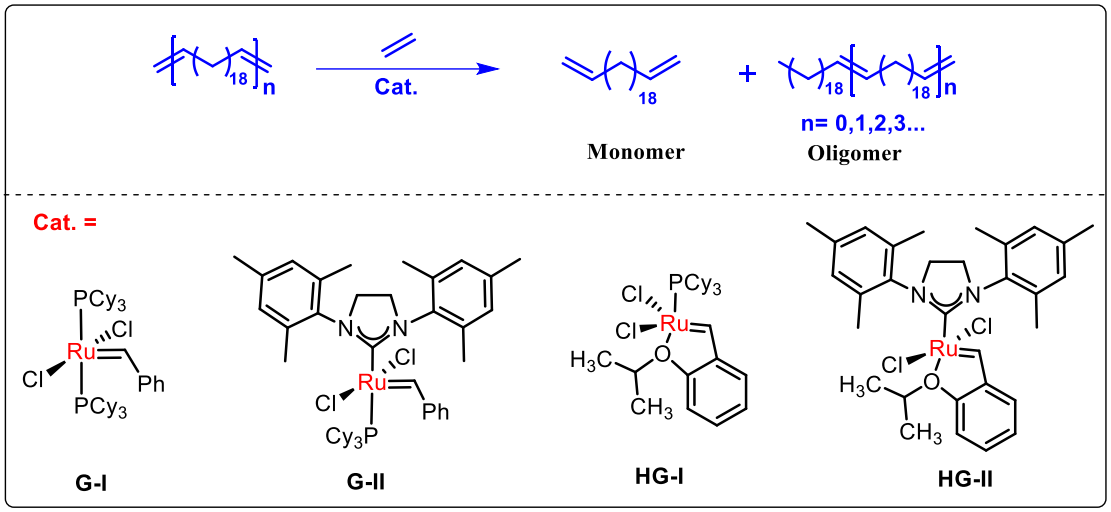

Scheme 5.4: Depolymerization of poly(docosa-1,21-diene) (P1) to monomer and oligomer.

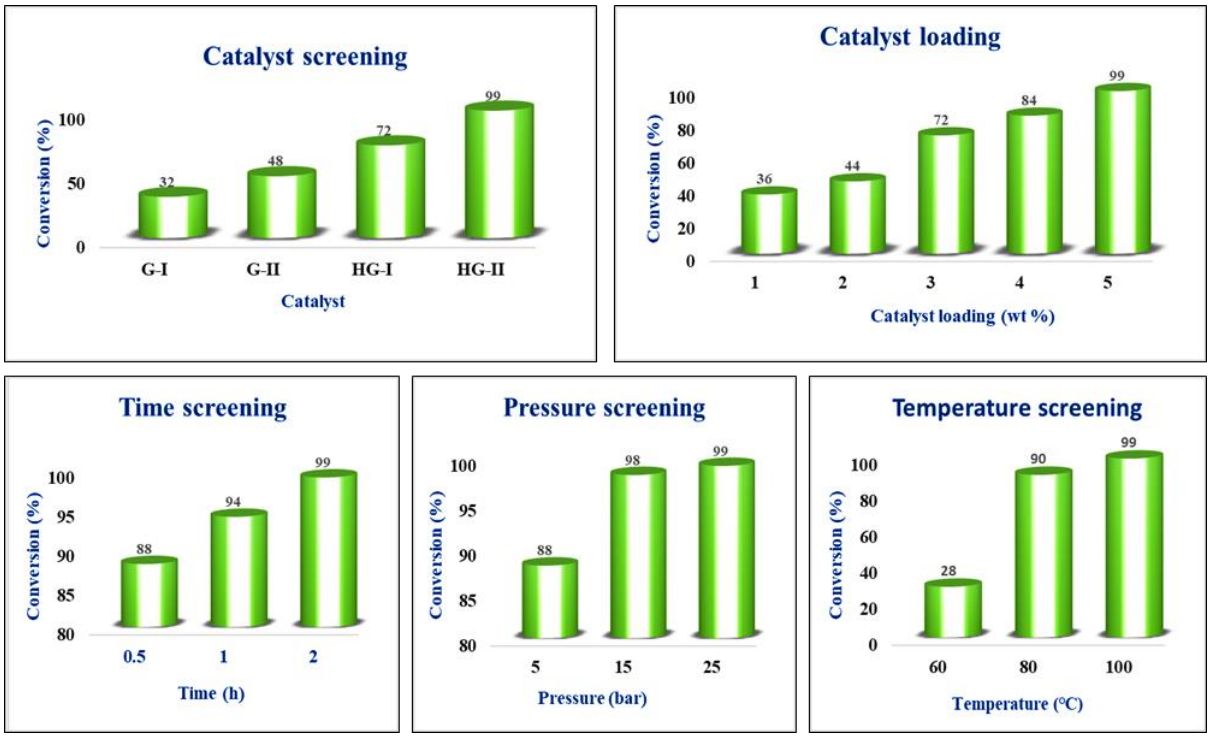

Figure 5.3: Depolymerization of poly(docosa-1,21-diene) (P1) at various reaction conditions.

After the completion of reaction, solvent was evaporated and obtained reaction content was analyzed using various spectroscopic and analytic methods. ^{1}H NMR of the crude reaction content suggest that terminal as well as internal olefin peaks are present in sample (figure 5.4 A). This observation suggest that obtained reaction content is low molecular weight. To confirm the presence of monomer in the reaction content, differential scanning calorimetry (DSC) and gas chromatographic analysis was performed. In GC analysis, the monomer peak was observed at a retention time of 24.3 min. The depolymerization reaction mixture was

injected to GC and exactly same peak was observed at same retention time suggesting that the monomer was formed (figure 5.4, B). DSC analysis of the depolymerized sample revealed a melting temperature of 32.3 °C, which is matches with the melting point of monomer. This observation suggest formation of monomer after depolymerization (figure 5.6, left). The molecular weights was determined for the entry no 4 (Table 5.3) in THF GPC. The initial polymer molecular weight was 17600 Da, after metathesis M_w dropped to 500 Da. These observations suggest the polymer (P1) breaks down to monomer (RM1) as well as low molecular weight oligomers. The low molecular weight oligomers may originate from repolymerization of monomer formed during the reaction as the catalyst is present inside reaction mixture. During the depolymerization, the cross alkene metathesis partner ethylene is gaseous compound which is present in the gas form, whereas soluble ethylene is only taking part for the depolymerization reaction.

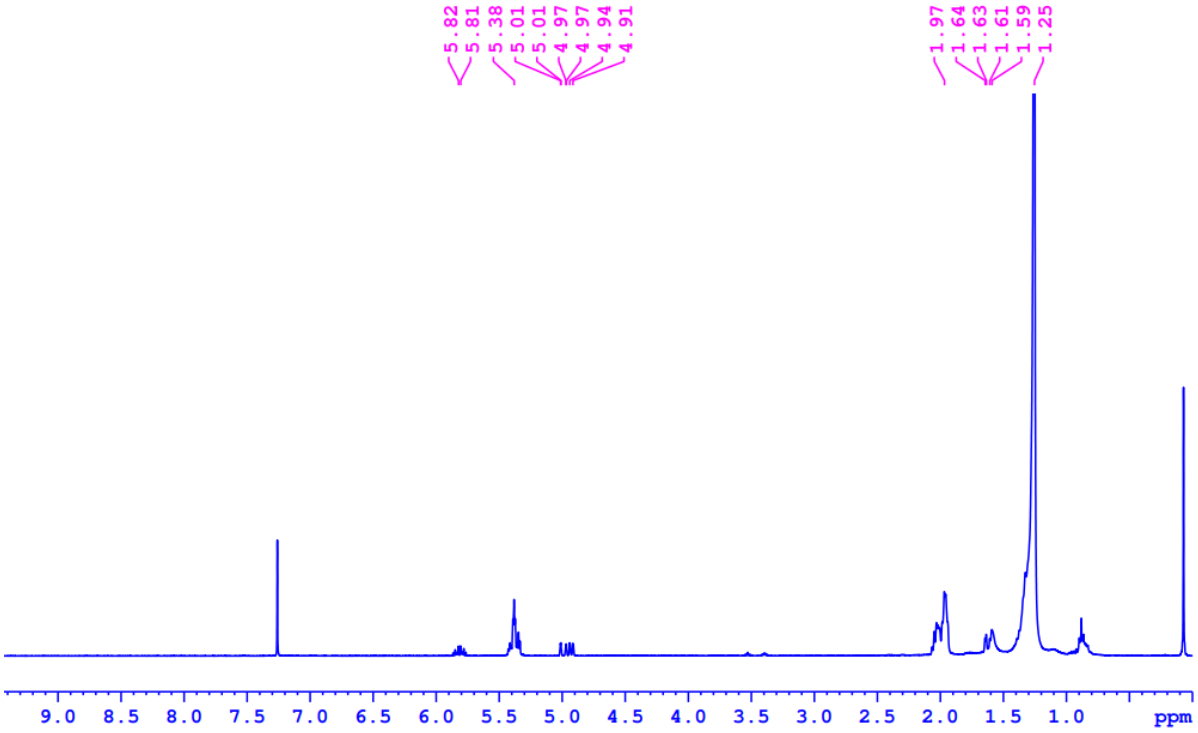

Figure 5.4 A: ^{1}H NMR of depolymerized product in $CDCl_3$.

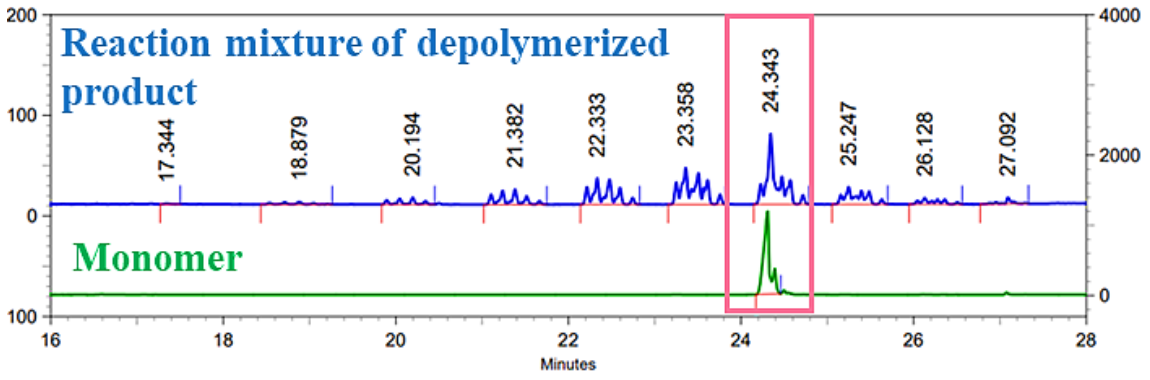

Figure 5.4 B: GC- Chromatogram for neat monomer (M1) and reaction mixture.

From the above technique we confirmed the presence of monomer as well as oligomer and the proton NMR disclosed the presence of terminal olefins. These terminal olefins can be potentially repolymerized via ADMET polymerization. We subjected the depolymerized material to repolymerization using Grubbs-II catalyst. The DSC analysis displayed a shift in melting temperature from 32 °C to a sharp melting peak at 88 °C (figure 5.6, Right). In ^{1}H NMR of the repolymerized material disclosed only internal olefins (figure 5.5). GPC data revealed an enhanced molecular weight (8.2 kDa) of the repolymerized material.

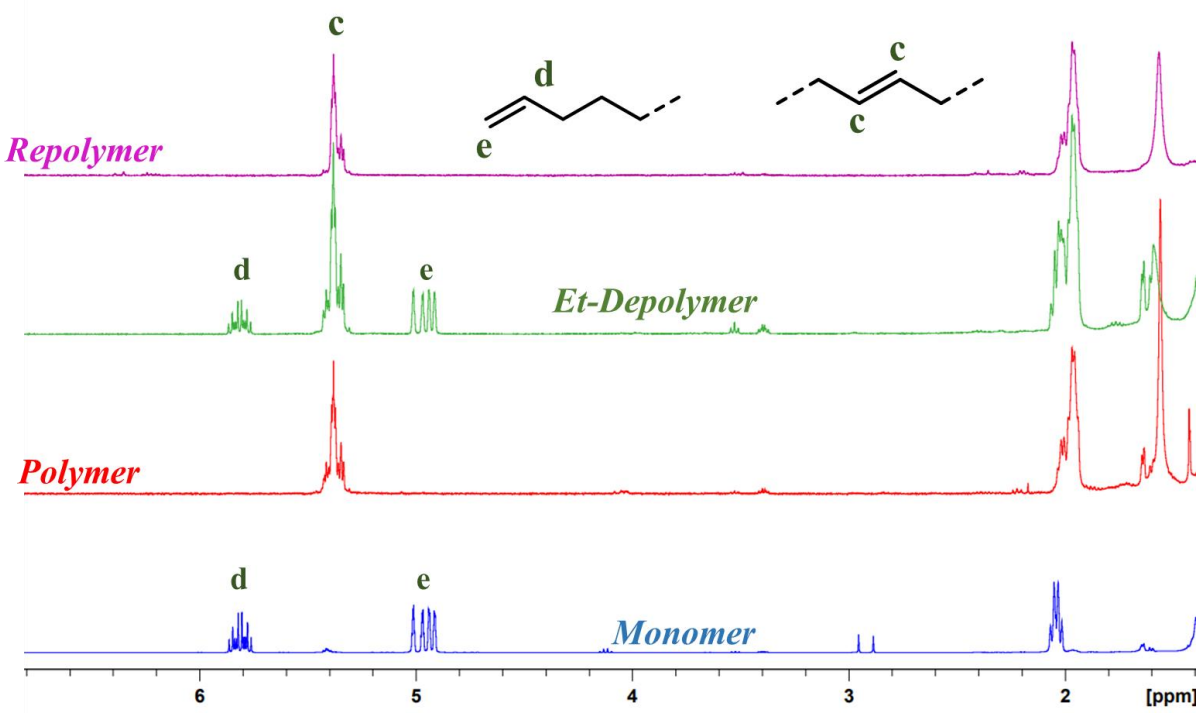

Figure 5.5: Stacked ^{1}H NMR of monomer, polymer, depolymerized, and repolymerized product in $CDCl_3$.

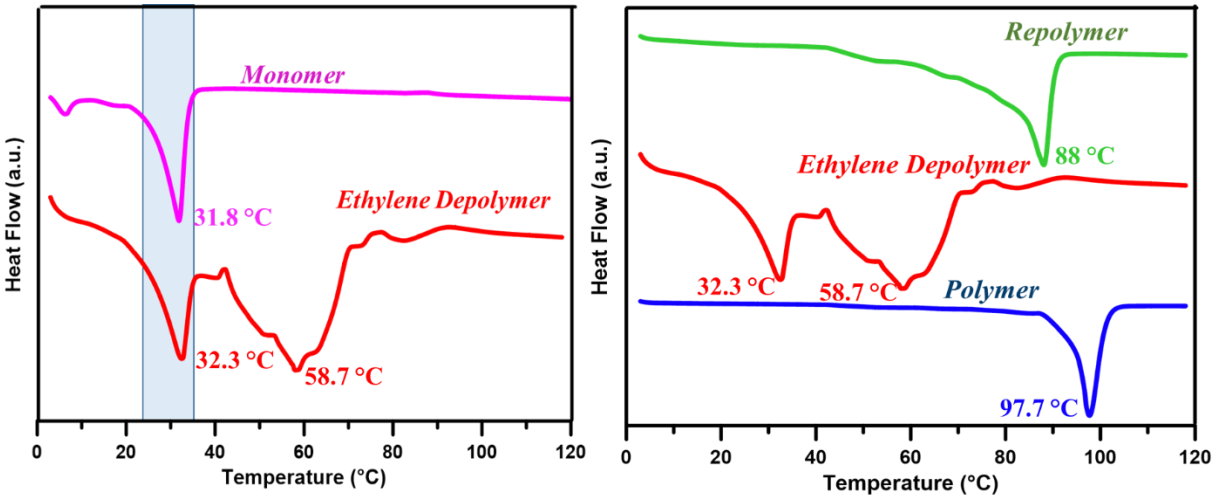

Figure 5.6: DSC thermogram of neat monomer and depolymerized product (left) and comparison of depolymerized polymer and repolymerized product (Right).

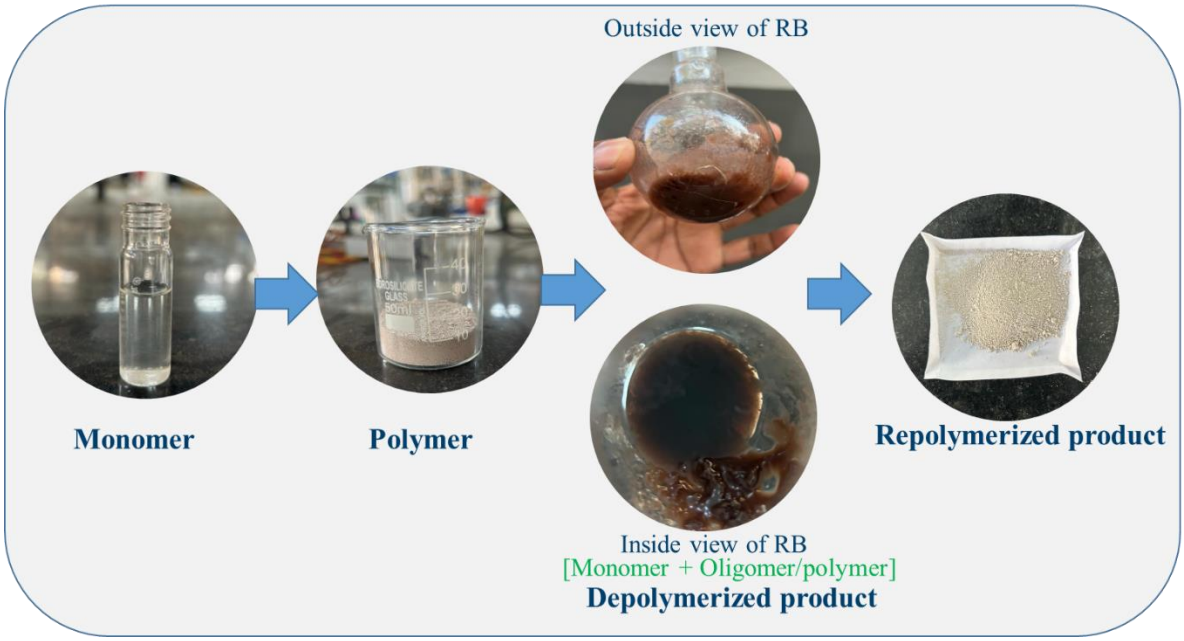

Figure 5.7: Images for the monomer, polymer, depolymer, and repolymerized products.

5.3.4. Controlled hydrogenation of polymer (P1):

The presence of crystalline domains in HDPE contribute to better mechanical properties such as tensile strength, which is valuable for various applications in daily life. Although the synthesized polymer (P1) is crystalline in nature, the percentage of crystallinity was relatively low (T_m- 86.2 °C and % of cryst. 39%) due to the presence of in chain double bonds (Table 5.1, entry no. 9). To enhance the crystallinity, the obtained polymer P1 (Table 5.1, entry no. 9), was subjected to controlled hydrogenation to reduce the olefin content. This process aims to increase the percentage of crystallinity and the melting temperature of the polymer, thereby achieving better mechanical properties.

Hydrogenation of P1 was performed using a [Rh(COD)$_2$OTf] catalyst and PPh_3 as ligand under H_2 pressure. Initially 1 mg of ligand and catalyst were added to P1 and mixture was subjected to hydrogenation with 5 bar of hydrogen pressure. The reaction was performed for a 0.5 hour and was quenched by the releasing the hydrogen pressure and pouring the reaction content in methanol to reprecipitate the polymer. The resultant polymer was dried under vacuum and DSC was recorded. DSC chromatogram of hydrogenated P1 revealed an enhanced melting temperature (95.2 °C) as well as % of crystallinity (46%) (Table 5.2, Entry no. 2). The above experiment suggest the hydrogenation was feasible and enhanced the crystallinity of the polymer. Further, under a similar reaction condition, the reaction time was varied (were 1 and 1.5 hour). From the DSC analysis, it was observed that with increase in time the melting temperature as well as % of crystallinity improved (Table 5.2, Entry no. 3 and 4). After 1 hour hydrogenation of polymer P1, it displayed a T_m of 113.4 °C and % of cryst. 55%. For 1.5 hour, it was increased to T_m- 118.9 °C and % of cryst. 68%. To check the complete hydrogenation of polymer, reactions were performed for 2 hour at 20 bar of hydrogen pressure along with lowering the metal to polymer ration (1 mg/30 mg) (Table 5.2, Entry no. 5). Melting temperature of this polymer was observed at T_m- 124 °C and % of cryst. 79%. To confirm this, the reaction are performed for 6 hours and with increased catalyst loading. In these cases, similar melting temperature and % of crystallinity was observed (Table 5.2, Entry no. 6 and 7).

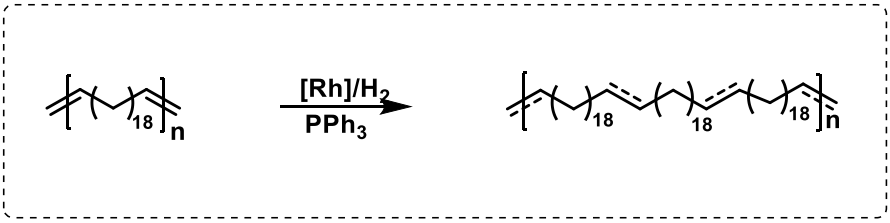

Scheme 5.5: Hydrogenation of poly(docosa-1,21-diene) (P1) [Rh] = [Rh(COD)OTf].

Table 5.2: Hydrogenation of poly(docosa-1,21-diene) (P1).

Entry No.	Cat. (mg)	Ligand (mg)	Polymer (mg)	Pressure (bar)	Time (h)	T_m (°C)	% Cryst.
1.	-	-	-	-	-	86.2	39
2.	1	1	50	5	0.5	95.2	46
3.	1	1	50	5	1	113.4	55
4.	1	1	50	5	1.5	118.9	68
5.	1	1	30	20	2	124	79
6.	1	1	30	20	6	124	82

7.	2	2	30	20	6	124.7	81

Reaction condition- Solvent- benzene (1 mL), Catalyst- [Rh(COD)OTf], Temperature- 70 °C, T_m and % of cryst. was recorded and calculated from DSC data.

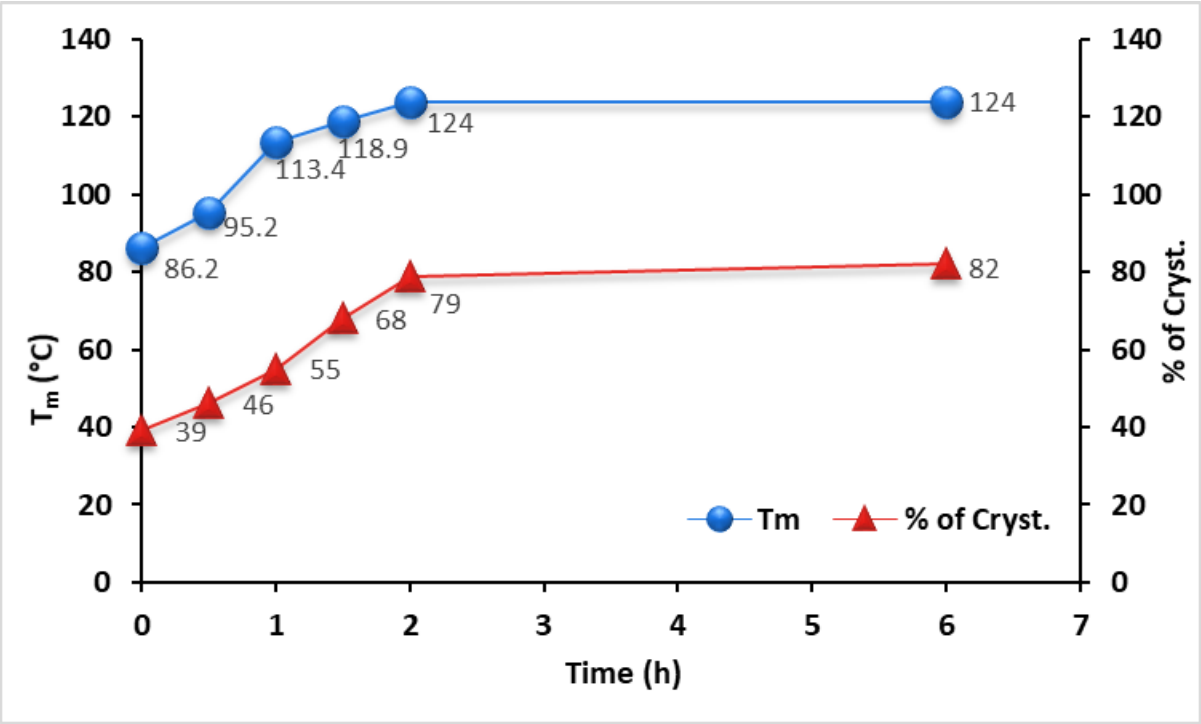

Figure 5.8: Correlation of melting temperature and % of crystallinity versus hydrogenation reaction performed over time in hours.

5.3.5. Depolymerization with acrylates:

In depolymerization reaction with ethylene, the cross alkene metathesis partner is gaseous ethylene which requires higher pressure, also the depolymerized content is participating in repolymerization to dimer and oligomer. To avoid this, use of liquid and readily available monomer is crucial to achieve a selective depolymerization to monomer. Methyl acrylate was chosen as cross alkene metathesis partner, as it is readily available and is easy to separate. The polymer (P1) was subjected to depolymerization with methyl acrylate and 2-hydroxy ethyl acrylate. The depolymerization reaction with acrylates were studied as it produces difunctionalized monomer. Polymer (P1) was treated with methyl acrylate in the presence of Grubbs-II catalyst for 2.5 hours. The reaction mixture was poured in methanol to remove the high molecular weight polymer and soluble parts (monomer and oligomer) were analyzed by NMR. The ^{1}H NMR disclosed selective depolymerization of P1 to difunctionalized monomer (M2). Further, this product was characterized by 1-2D NMR spectroscopy. The ^{1}H NMR

disclosed –OMe protons at 3.71 ppm, the α-β unsaturated protons appeared at 5.79 and 6.95 ppm (figure 5.9). Internal protons could not be observed in molecules that confirm the monomeric form with functional groups at both chain ends (Scheme 5.6).

To study the mechanism of the depolymerization and to check whether depolymerization follows random chain scissoring mechanism or it follows chain end scissoring mechanism, depolymerization of polymer P1 with methyl acrylate was performed over different time interval (2.5 hour, 5 hour and 14 hours). After 2.5 hour depolymerization the resultant residue was analyzed by DSC and disclosed two melting peaks, one 78.3 °C and 35.9 °C (Figure 5.10, Right). The 78.3 °C peak corresponds to the polymer and the 35.9 °C peak belongs to the difunctionalized monomer (M2). ^{1}H NMR of the crude reaction content was recorded in $CDCl_3$ at room temperature. The ^{1}H NMR tube displayed soluble part along with insoluble white solid at the bottom. Soluble part shows the selective formation of M2. Further depolymerization reaction was performed for 5 and 14 hours. The DSC chromatogram disclosed melting peak at 32.1 and 35.2 °C that can be assigned to difunctional monomer M2 and along with reduced melting point and broad melting peak for the polymer (P1). Using THF GPC molecular weights were determined, the depolymerization reaction with MA resulted into a M_w of 450 Da without any high molecular weight trace (Figure 5.11). The above experiment suggest that depolymerization follow the chain end scissoring mechanism where the functionalized monomer is forming initially, with decrease in melting peak of the polymer. It was also supported by the DSC (Figure 5.10).

Similar to the methyl acrylate (M2), 2-hydroxy ethyl acrylate (M3) was subjected to cross alkene metathesis reaction with P1. The ^{1}H NMR spectrum of the depolymerized residue disclosed presence of the α-β unsaturated protons at 6.83 ppm and 7.00 ppm along with $–OCH_2$ protons at 3.85 and 4.27 ppm (Figure 5.25). Internal olefins were also observed in the NMR, suggesting the presence of unreacted low molecular weight polymer. The free hydroxyl group in the 2-hydroxy ethyl acrylate reduces the catalytic activity in the depolymerization reaction. DSC analysis revealed a sharp melting peak around 37.3 and broad peak at 58, 65 and 83 °C. GPC data displayed low molecular weight compound M_w - 650 Da (Figure 5.11).

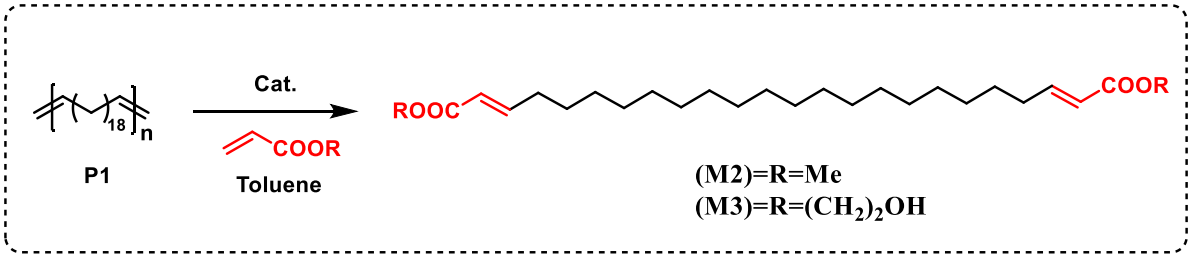

Scheme 5.6: Depolymerization of poly(docosa-1,21-diene) (P1) with acrylates.

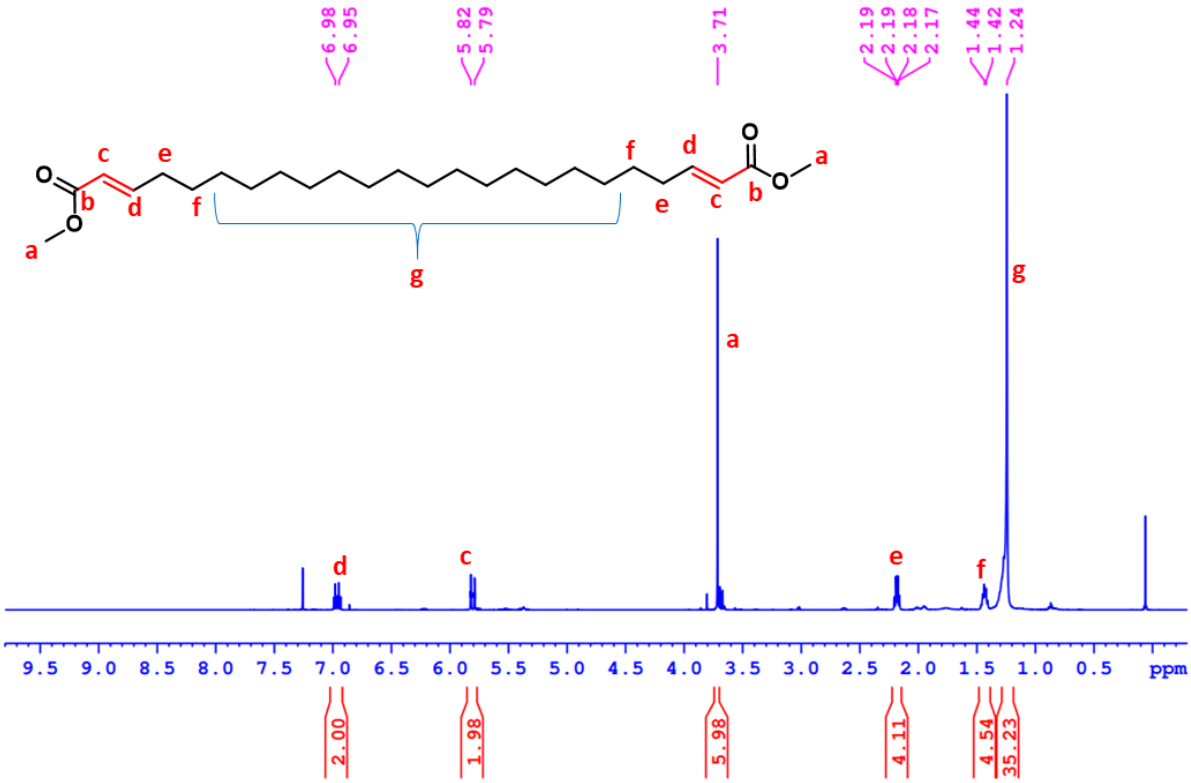

Figure 5.9: ^{1}H NMR of depolymerized product M2 with MA in $CDCl_3$.

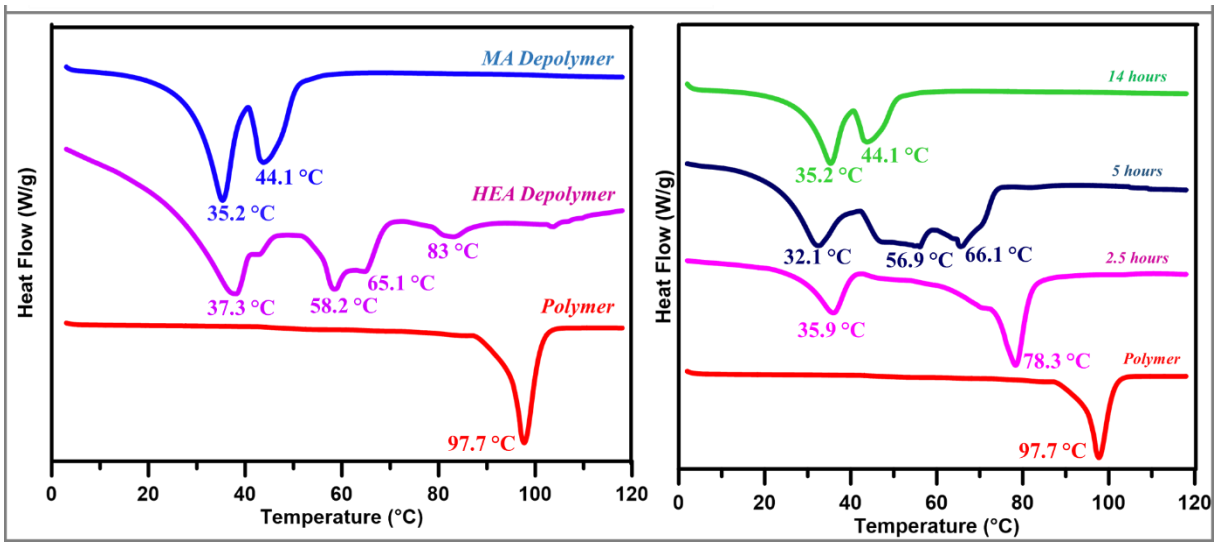

Figure 5.10: Comparison of DSC thermogram of depolymerization of polymer (P1) with MA

and HEA (left). Comparison of DSC thermogram of depolymerization of polymer (P1) with MA at different time intervals (2.5, 5, 14 hours) (right).

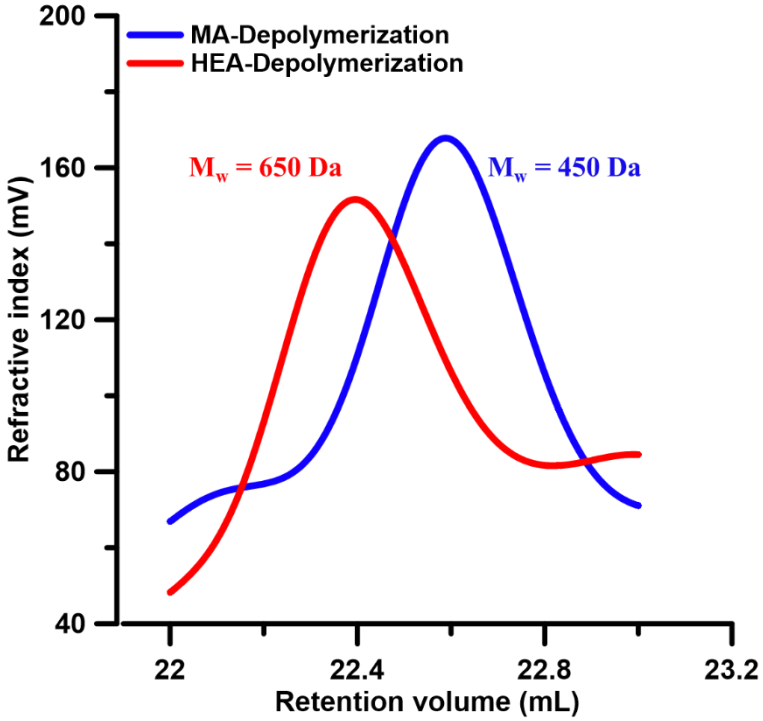

Figure 5.11: GPC data of depolymerized product with MA and HEA.

5.3.6. Repolymerization to polyester:

The α-β unsaturated difunctional monomer (M2) was subjected to hydrogenation using 10 bar hydrogen pressure, $[Rh(COD)_2OTf]$ as catalyst, ligand (PPh_3) in THF. After 1 hour, the reaction mixture was analyzed by NMR and it was observed that the α-β unsaturated protons absent (Figure 5.26 and 5.27). The above NMR data confirmed selective hydrogenation of α-β unsaturated double bond. This compound was subjected to repolymerization via condensation polymerization.

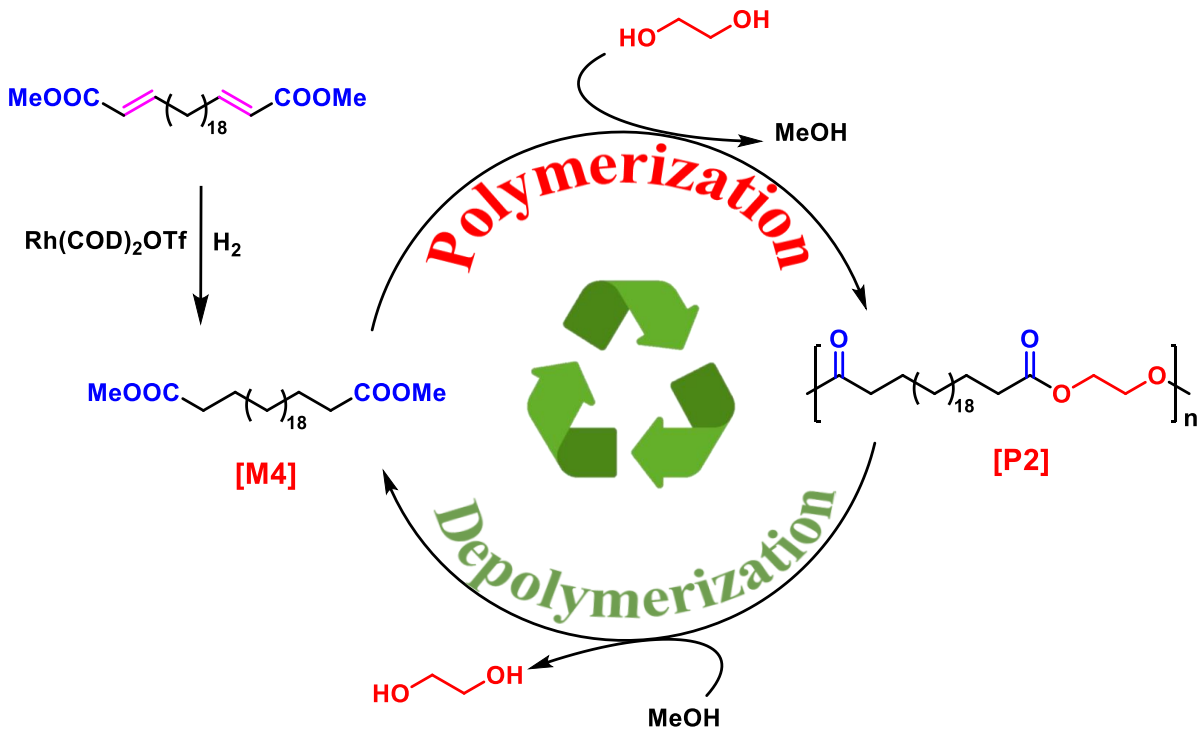

Scheme 5.7: Polymerization of monomer (M4) and depolymerization of polymer (P2).

Obtained ester functionalized monomer (M4) was subjected to repolymerization, yielding polyester (P2). Initially, repolymerization was investigated with diester (M4), ethylene glycol, and p-Toluenesulfonic acid (PTSA) as catalyst. The reactions was performed at high temperature (180 °C) and vacuum was applied throughout the reaction to remove methanol and excess of ethylene glycol. The resultant polymer P2 was characterized by ^{1}H NMR, DSC and GPC analysis. The proton NMR data suggest that 4.25 and 3.66 ppm peaks correspond to the ethylene glycol unit in the polymer (Figure 5.12). Peaks adjacent to carbonyl was observed at 2.32 ppm and backbone methylene protons were observed at 1.25 ppm. DSC analysis recealed a sharp melting temperature peak at 73.9 °C (Figure 5.13). While GPC analysis displayed weight average molecular weight of 6.4 kDa. Further, the polymerization reactions was performed with catalyst [Sn(Oct)$_2$] at 180 °C for 10 hours and 24 hours yielding polymer (P2). The depolymerization of polyesters with long aliphatic chains and ester functional groups has been reported in the literature.[10,12] These polymers can be chemically recycled using similar reaction conditions.

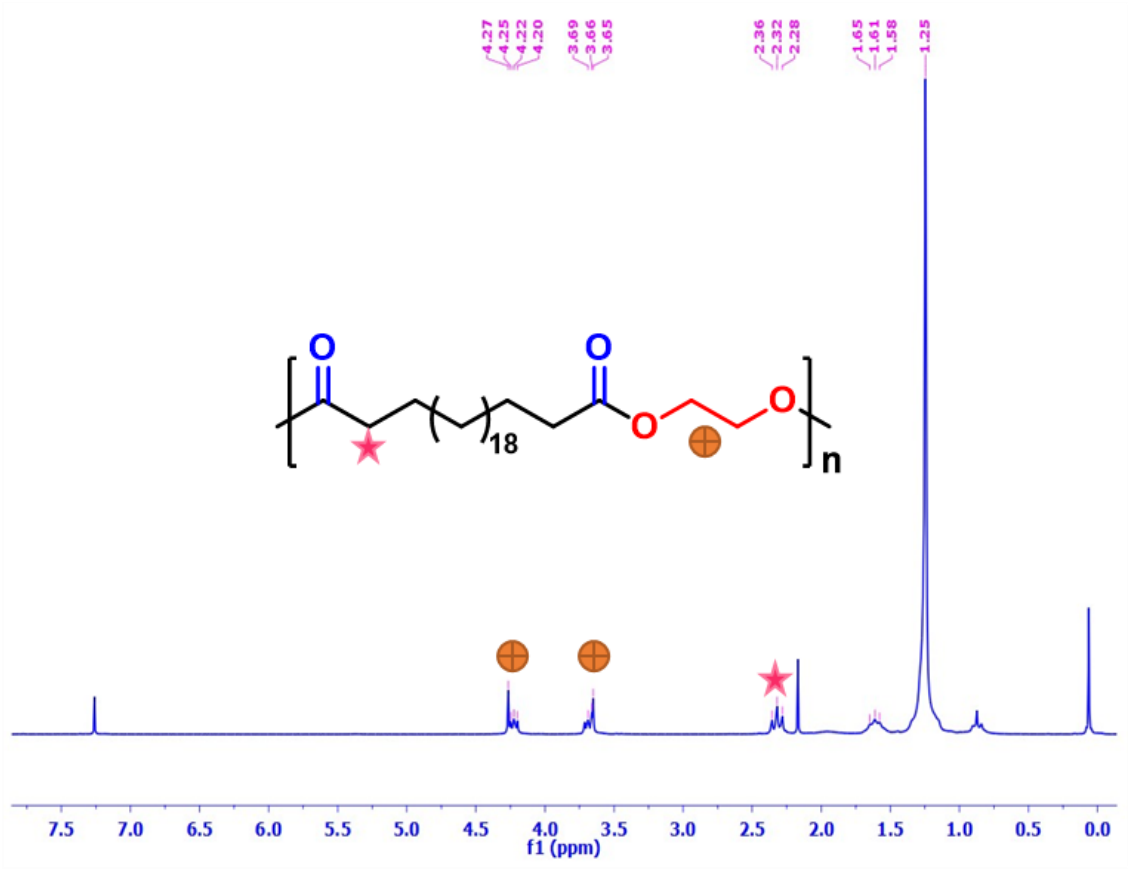

Figure 5.12: ^{1}H NMR of repolymerized polymer P2 obtained from M4 with ethylene glycol.

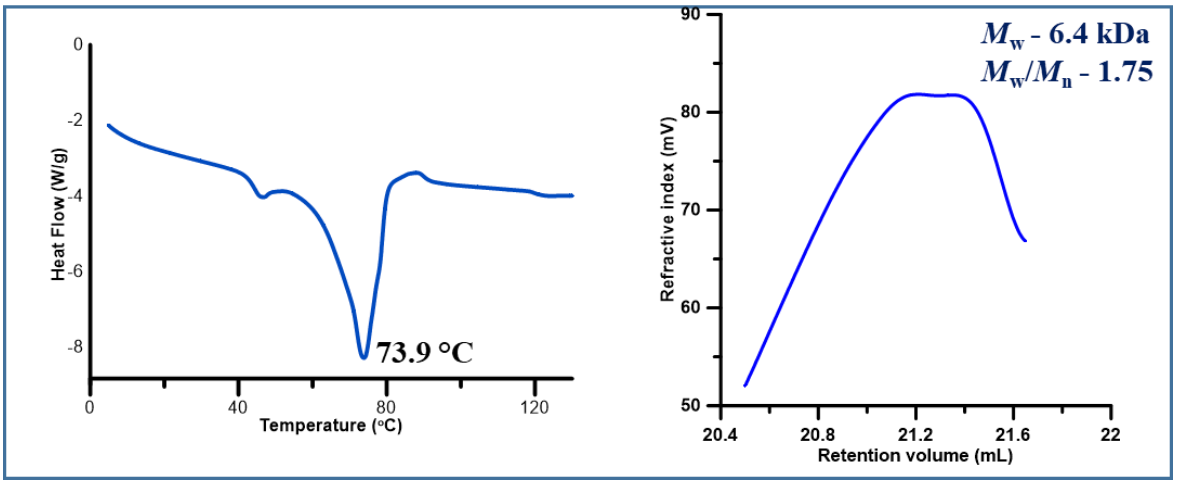

Figure 5.13: DSC thermogram of polymerized product (P2) (left). GPC data of polymer (P2) (Right).

5.4. Conclusions:

In summary, we have synthesized the docosa-1,21-diene monomer, which was subjected to ADMET polymerization. The resultant polymer shows high melting temperature (100 °C) and crystallized in orthorhombic form, similar to HDPE crystallization. The obtained polymers disclosed high molecular weight of 1.76 x 10^4 Da. To achieve an circular economy, obtained

polymers P1 was subjected to cross alkene metathesis using ethylene and resulted into a monomer, which was confirmed using an NMR, GC and DSC. The GPC data suggest that this material is very low molecular weight (500 Da). In addition, these monomers and oligomers were subjected for repolymerization, and we achieved repolymer (P1) with 8.2 x 10^3 Da molecular weight.

The polymer (P1) was subjected to cross alkene metathesis with acrylates, and selective formation of functional monomers/α-β unsaturated ester was observed. These compounds were subjected to hydrogenation followed by the condensation polymerization with diol to produce polyethylene like material having in chain ester functional groups. Ester functionalized polymers P2 was subjected to depolymerization, resulting into a starting functionalized monomer (M4).

5.5. Experimental section:

5.5.1 Methods and materials:

Unless noted otherwise, all manipulations were carried out under an inert atmosphere using standard Schlenk line techniques or M-Braun glove box. Toluene, diethyl ether, and THF were distilled from sodium/benzophenone under an argon atmosphere. Methylene chloride, and were distilled on calcium-hydride. Ethylene (3.5 grade) was supplied by greenoma industries, India. 11-bromo 1-undecene, terpyridine were supplied by BLD pharm and were used as received. Metathesis catalysts (Grubbs-I, Grubbs-II, Huveyda Grubbs-I, Huveyda Grubbs-II were supplied by Sigma Aldrich and were used as received. Methyl acrylate and 2 hydroxy ethyl acrylate were supplied by Alfa Aesar and were used as received. The ADMET polymerization was run in a Schlenk tube in heating oil bath and the Schlenk tube was connected to a high vacuum pump.

Solution NMR spectra were recorded on Bruker Avance 200, 400 and 500 MHz instruments. Chemical shifts are referenced to external reference TMS (^{1}H and ^{13}C). Coupling constants are given as absolute values. Multiplicities are given as follows s: singlet, d: doublet, t: triplet, m: multiplet. Size exclusion chromatography (SEC or GPC) was performed on Malvern instrument and THF as the eluent, separations were performed using serially connected size exclusion columns at 60 °C and at a flow rate of 1.0 mL/min, and molecular weights were determined from the calibration curve generated from narrow polystyrene standards. TGA was performed on diamond TG/DTA in argon atmosphere with a heating rate 10 °C min^{-1}. Differential Scanning Calorimetry (DSC) was carried out on DSC Q-10 equipment from TA

instruments with a heating and cooling rate of 10 °C min^{-1}, unless mentioned otherwise. PXRD was performed on Smartlab X-ray diffraction (XRD) (Rigaku).

Gas Chromatography (GC) analysis was performed on an Agilent 7890B GC system using HP-05 column (30 m × 320 μm × 0.25 μm), split ratio 75:1, column pressure 10 psi, injector temperature of 260 °C, detector temperature of 330 °C, argon carrier gas. Temperature program: Initial temperature 40 °C, hold for 5 min.; ramp 1: 10 °C/min. to 320 °C hold for 1 min. The instrument was set to an injection volume of 1 μL, an inlet split ratio of 10:1, and inlet and detector temperatures of 250 and 320 °C, respectively. UHP-grade argon was used as carrier gas with a flow rate of 30 mL/min. Response factors for all the necessary compounds with respect to standard n-decane were calculated from the average of three independent GC runs.

5.5.1.1. Synthesis of monomer (docosa-1,21-diene):

In an oven-dried Schlenk flask, 11-bromo-1-undecene (200 mg, 0.85 mmol), terpyridine (10 mg, 0.042 mmol), activated zinc (56 mg, 0.85 mmol), and $NiCl_2$•$6H_2O$ (10 mg, 0.042 mmol) were weighed and 4 mL of DMF was added to the flask. The resulting reaction mixture was stirred for 4 hours at room temperature (25 °C) in an argon atmosphere. During the reaction, the color of the reaction mixture turned light green. After completion, the reaction mixture was poured into ice-cold water, and 25 mL of ethyl acetate was added. Reaction mixture was filtered through whatman filter paper to remove insoluble zinc. The compound was then extracted from the aqueous phase with ethyl acetate (3 x 25 mL). The organic layer was dried over sodium sulfate, and the solvent was distilled using a rotary evaporator.

The obtained oily compound was stored at 20-25 °C. The monomer was solidified, and the remaining portion was decanted. To the solidified monomer, 2 mL of hexane was added and cooled to 0 °C. The hexane layer was decanted, yielding pure docosa-1,21-diene (122 mg, 94% yield).

^{1}H NMR (400 MHz, $CDCl_3$) δ = 5.86 - 5.73 (m, 2 H), 5.03 - 4.87 (m, 4 H), 2.03 (q, J = 6.9 Hz, 4 H) 1.25 (br. s., 32 H). **^{13}C NMR (100 MHz, $CDCl_3$)** δ = 139.2, 114.1, 33.9, 29.7, 29.7, 29.6, 29.2, 29.0.

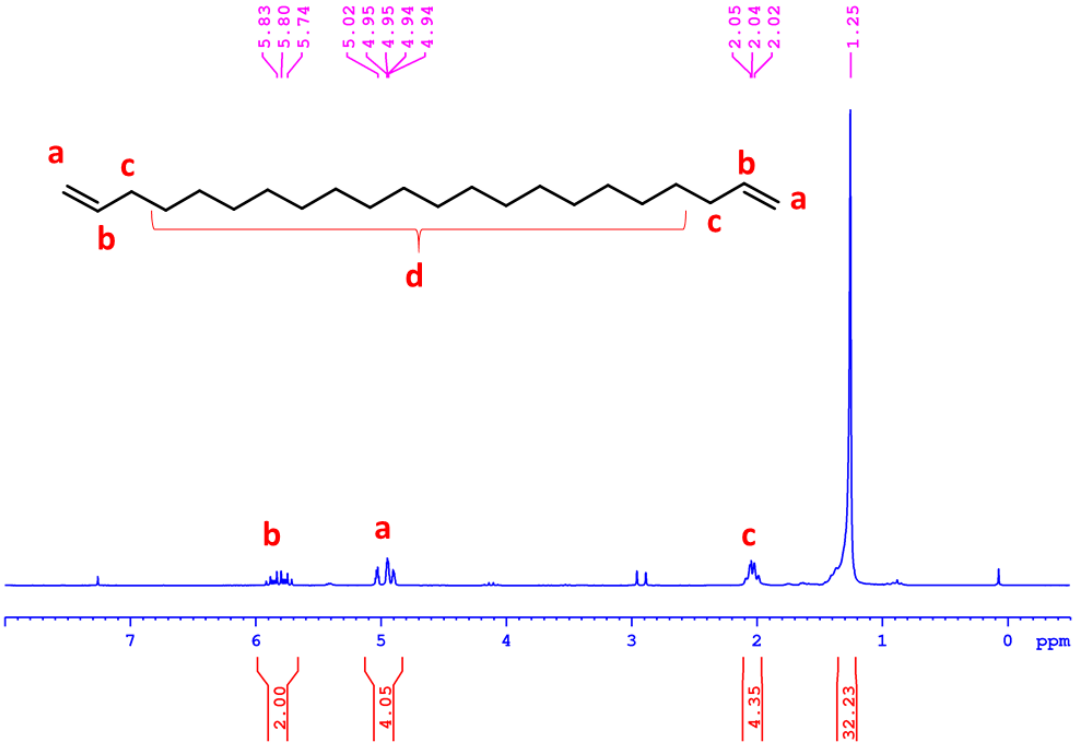

Figure 5.14: ^{1}H NMR of monomer (M1) in $CDCl_3$ (400 MHz).

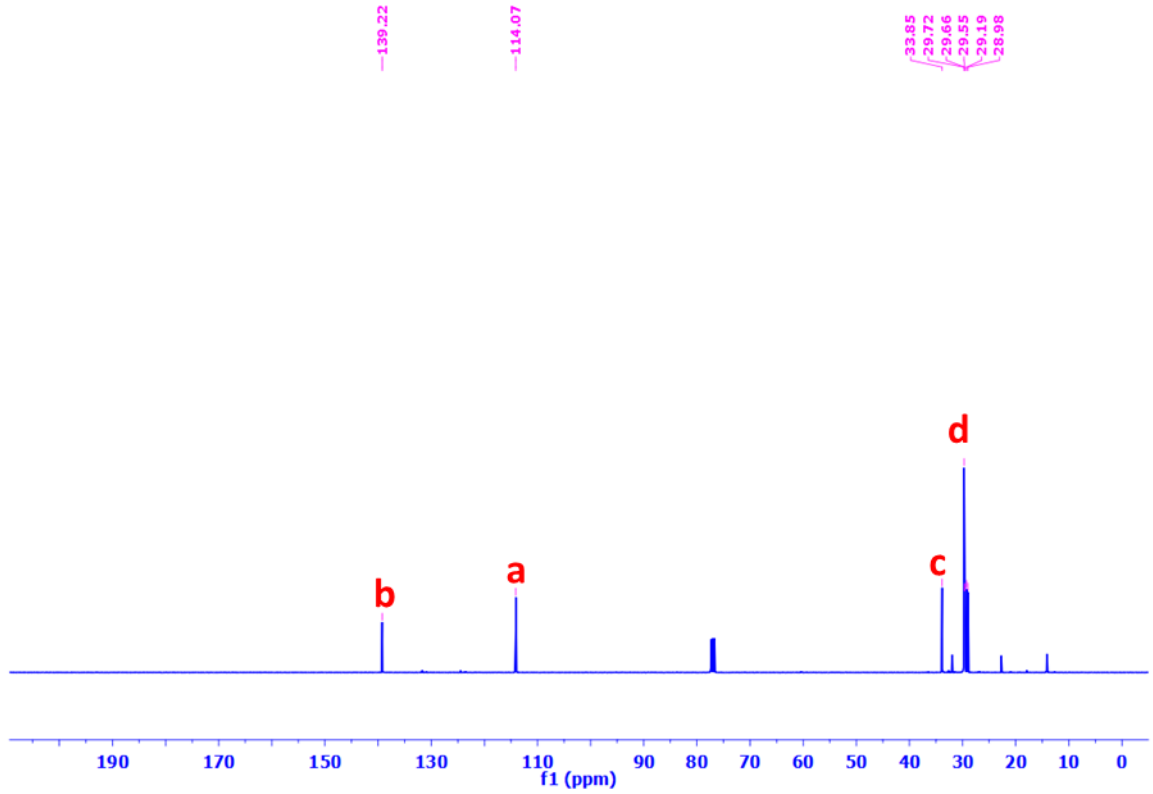

Figure 5.15: ^{13}C NMR of monomer (M1) in $CDCl_3$ (100 MHz).

Area % Report

Data File: D:\Result\2023\dec\rsb c22 mon.rslt\Agilent 7890.42 2023-12-21 13-12-33 (GMT +05-30).dat
Method: D:\Method\Cooling.met
Acquired: 12/21/2023 1:14:51 PM (GMT +05-30)
Printed: 1/18/2024 10:20:47 AM (GMT +05-30)

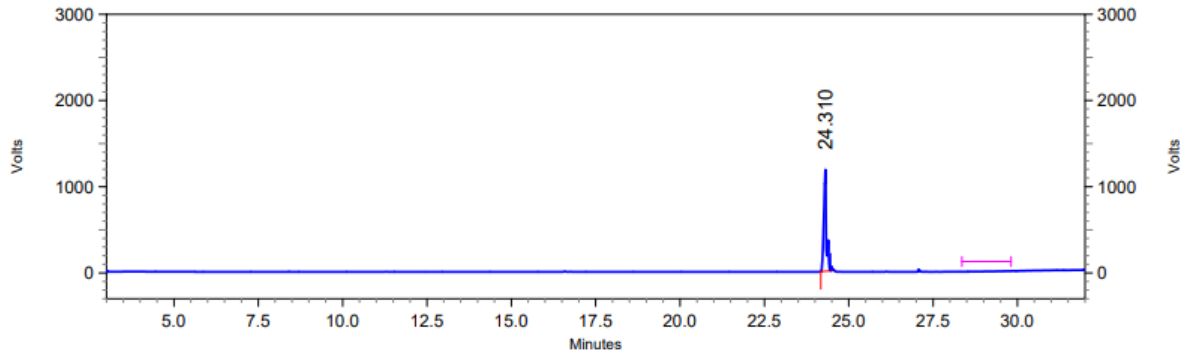

Front Signal Results

Retention Time	Area	Area %
24.310	45829413	100.00
Totals	45829413	100.00

Figure 5.16: GC data of monomer (M1).

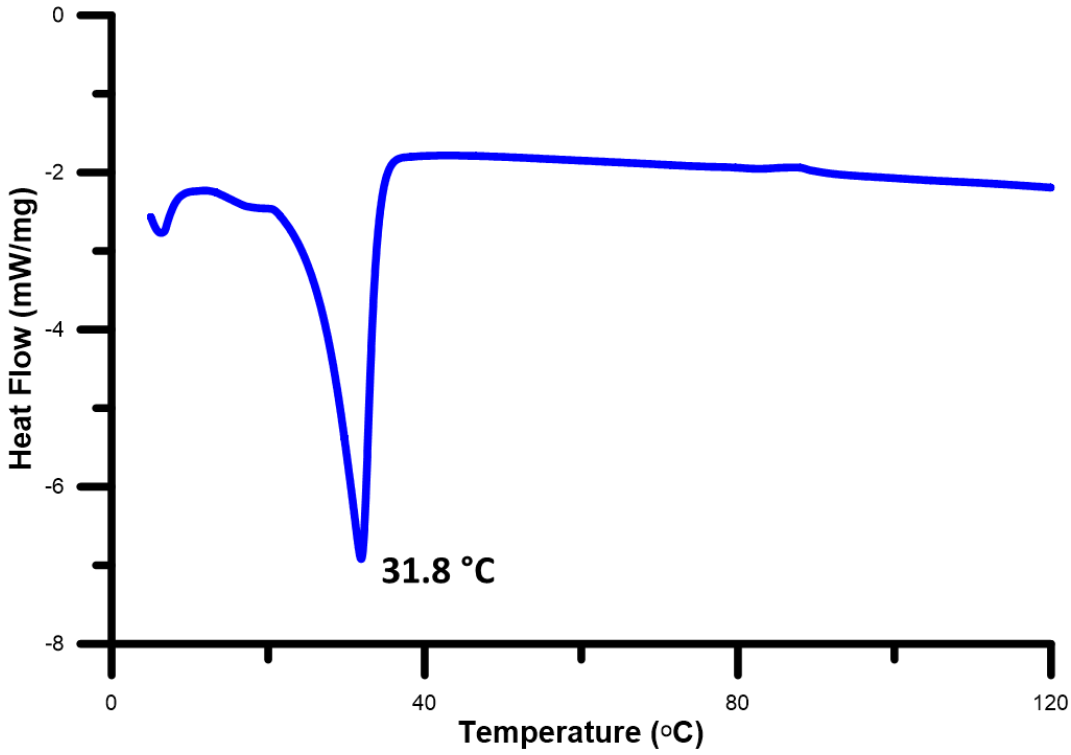

Figure 5.17: DSC data of monomer (M1).

5.5.2. General procedure for ADMET polymerization:

The polymerization reaction was conducted in a 50 mL Schlenk tube connected to a high vacuum line to strip-off the by-product ethylene gas. An oven-dried Schlenk tube with a magnetic stir bar was attached to the Schlenk line, and the Schlenk tube was cooled under vacuum. The desired amount of monomer was then added, followed by the addition of Grubbs-II catalyst. The Schlenk tube was placed in an oil bath preset to the desired temperature, and vacuum was immediately applied. The reaction proceeded for the desired time under vacuum. After completion of the reaction time, toluene was added to dissolve the polymer, and the reaction mixture was poured into methanol. The precipitated polymer was then filtered and dried under vacuum for 4 hours.

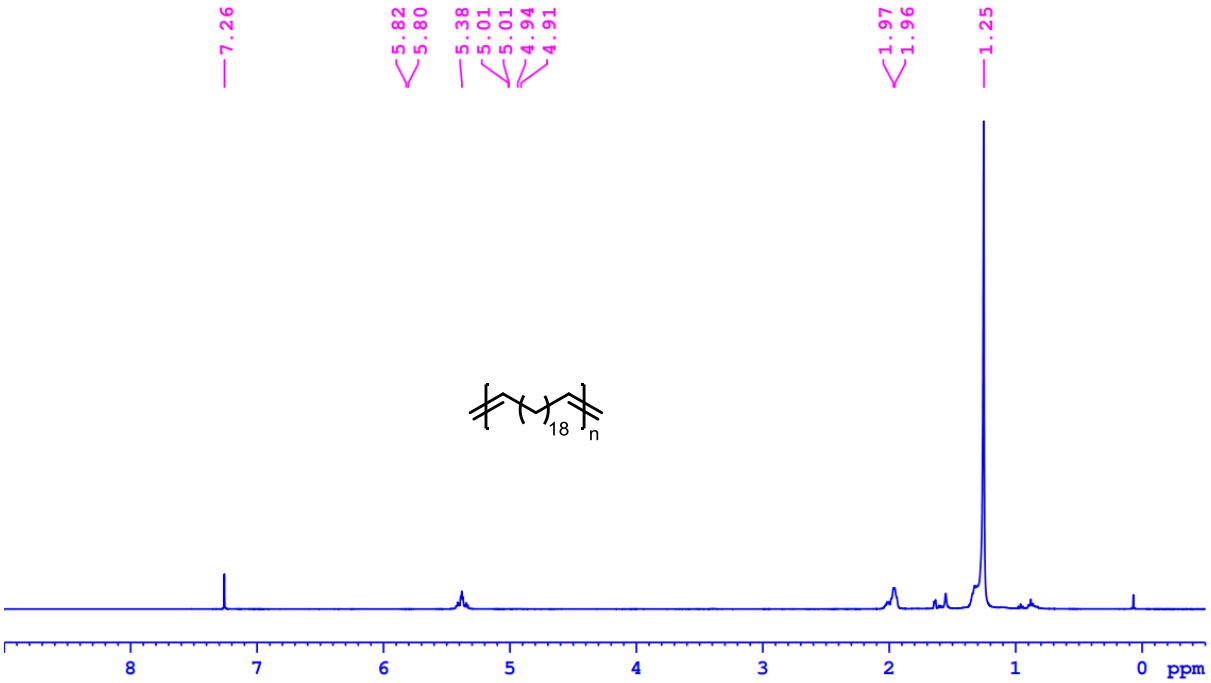

Figure 5.18: ^{1}H NMR of polymer (P1) in $CDCl_3$ (400 MHz).

5.5.3. General procedure for the depolymerization with ethylene:

A glass vial (5 mL) with magnetic needle was cooled under vacuum and transferred to a glove box. The vial was then charged with 50 mg of P1, and metathesis catalyst (1-5 wt %). The reaction vial was then closed using a screw cap, transferred to a large opening Schlenk-type container, and was then taken out from the glove box. 2 mL dry toluene was added to the vial in an inert atmosphere. After that the reaction vial was shifted to an autoclave and the autoclave was purged three times using ethylene gas (30 bars). Finally, the autoclave was pressurized to the desired ethylene gas pressure (5-25 bar) and temperature (60-100 °C) for the allotted time. After the desired time, the autoclave was cooled to room temperature (25 °C), excess pressure

was released and the autoclave was opened. The vials were taken out from the autoclave. The reaction mixture was poured in acetone to reprecipitate the unreacted polymer. Insoluble polymer was filtered and dried under high vacuum for 2 hours at 35 °C and weighed, to calculate the % of conversion.

Table 5.3: Depolymerization of polymer (P1) using ethylene.

Entry No.	Catalyst	Time (h)	Temp. (°C)	Ethylene Press. (bar)	Weight Loss (mg)	Recovered Polymer (mg)	% conversion
1.	G1(5Wt%)	2	100	25	16	34	32
2.	G2(5Wt%)	2	100	25	24	26	48
3.	HG1(5Wt%)	2	100	25	36	14	72
4.	HG2(5Wt%)	2	100	25	50	0	>99
5.	HG2(1Wt%)	2	100	25	18	32	36
6.	HG2(2Wt%)	2	100	25	22	28	44
7.	HG2(3Wt%)	2	100	25	36	14	72
8.	HG2(4Wt%)	2	100	25	42	8	84
9.	HG2(5Wt%)	0.5	100	25	44	6	88
10.	HG2(5Wt%)	1	100	25	47	3	94
11.	HG2(5Wt%)	2	60	25	14	36	28
12.	HG2(5Wt%)	2	80	25	45	5	90
14.	HG2(5Wt%)	2	100	5	44	6	88
15.	HG2(5Wt%)	2	100	15	49	1	98

Reaction Condition: 50 mg of polymer (P1), after the completion, reaction content was poured into methanol and the reprecipitated polymer was recovered [weight loss= Initial polymer weight - Recovered polymer], [% Convversion = (weight loss of polymer x 100) /Initial polymer weight]

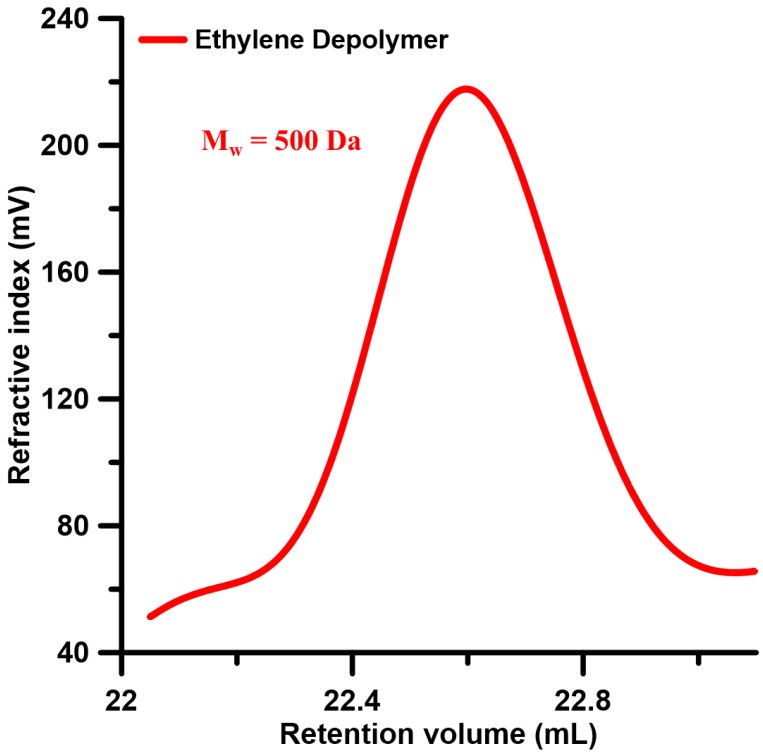

Figure 5.19: GPC chromatogram of depolymerized polymer.

5.5.4. General procedure for repolymerization to RP1:

The repolymerization reaction was conducted in a 50 mL Schlenk tube connected to a high vacuum line to remove ethylene gas. An oven-dried Schlenk tube with a magnetic stir bar was attached to the Schlenk line, and the Schlenk tube was cooled under vacuum. The desired amount of depolymerized product (100 mg) was then added, followed by the addition of Grubbs-II catalyst (2 mg). The Schlenk tube was placed in an oil bath preset to the desired temperature (90 °C), and vacuum was immediately applied. The reaction proceeded for the desired time (4hrs) under vacuum.

After completion of the reaction time, toluene was added to dissolve the polymer, and the reaction mixture was poured into methanol. The precipitated polymer was then filtered and dried under vacuum for 4 hours yielding an 84 mg of the polymer.

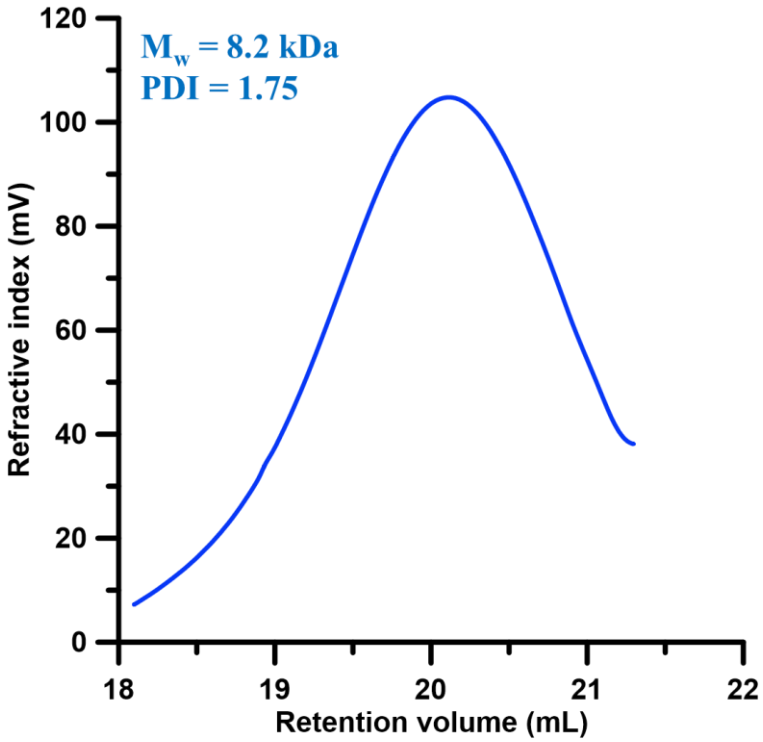

Figure 5.20: GPC chromatogram of repolymerized product.

5.5.5. Controlled hydrogenation of polymer (P1):

Hydrogenation of the polymer P1 was conducted in a high-pressure autoclave reactor. In an oven-dried 2.5 mL reaction vial with a magnetic stir bar, a desired amount of polymer (P1) was added. To that desired amount of catalyst [$Rh(COD)_2OTf$] and ligand PPh_3 were added to the vial in a glove box. Then, 1 mL of anhydrous benzene was added in an argon atmosphere.

The reaction vial was placed in a high-pressure autoclave reactor and immediately pressurized to 10 bar of H_2 pressure. The autoclave reactor was purged three times with 10 bar of pressure and finally maintained at 5 bar or desired reaction pressure of hydrogen. The pressurized reactor was then placed in a preheated oil bath (70 °C), and stirring of the reaction was started. The reaction proceeded for a desired time. After completion of the reaction, the pressure was released, and the benzene solution was poured into 10 mL of methanol solvent. The polymer precipitated and this polymer was filtered using a whatman filter paper. Obtained polymer was dried under high vacuum for 4 hours at 50 °C.

[Hydrogenation table and reaction condition is in table 5.2]

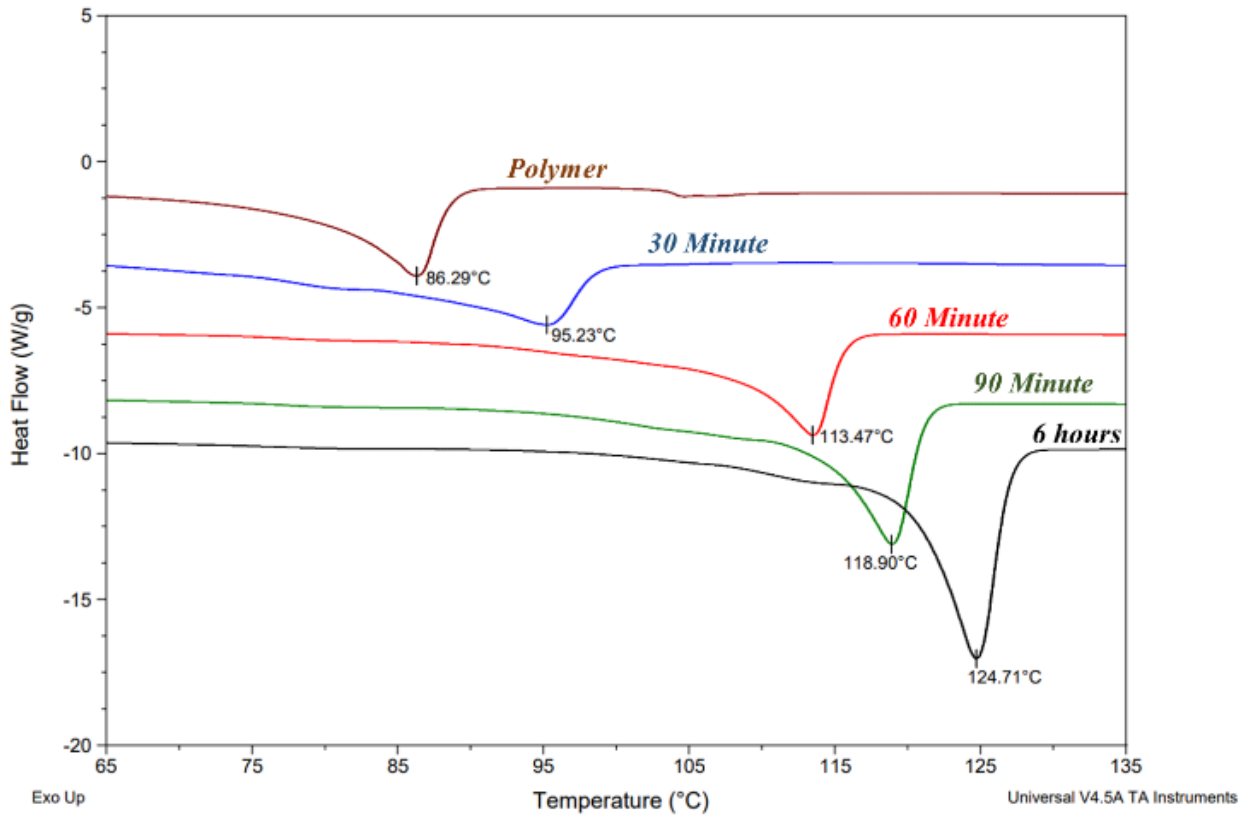

Figure 5.21: Comparison of DSC thermogram of hydrogenated of polymer (P1) at varied hydrogenation reaction time.

5.5.6. General procedure for the depolymerization with methyl acrylates to M2:

The depolymerization reaction was conducted in a 100 mL Schlenk flask connected to the condenser. An oven-dried Schlenk flask with a magnetic stir bar was attached to the Schlenk line, and the Schlenk flask was cooled under vacuum. The desired amount of polymer P1 (100 mg) was added, followed by the addition of Grubbs-II catalyst (2 mg, 0.002 mmol.) and toluene (2 mL) as solvent. To above reaction content excess of methyl acrylate (0.2 mL, 2.2 mmol) was added and immediately it was placed into an oil bath preset to the desired temperature (90 °C). The reaction proceeded for the desired time (14 hours).

After completion of the reaction time, the reaction mixture was poured into methanol. The methanol soluble part was separated, and solvent was removed on rotary evaporator, followed by the high vacuum yielding the difunctionalized monomer M2 (138 mg).

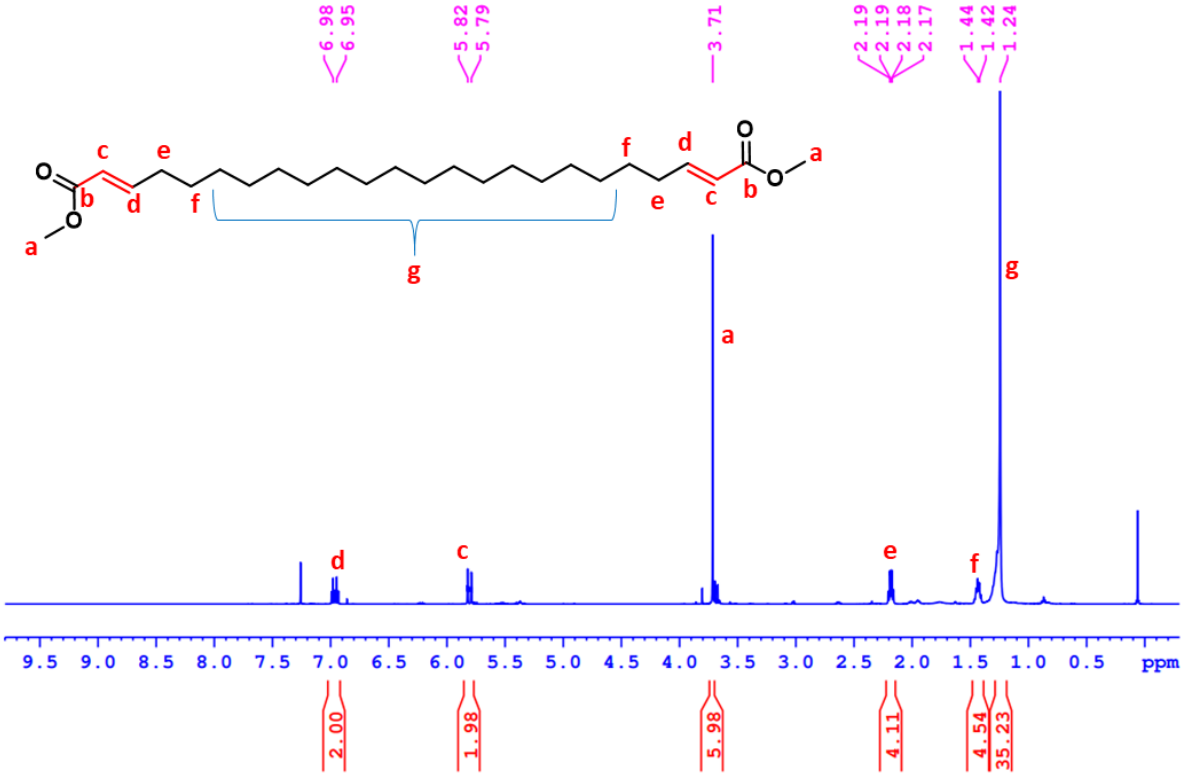

Figure 5.22: ^{1}H NMR of depolymerized product (M2) with MA in $CDCl_3$ (500 MHz).

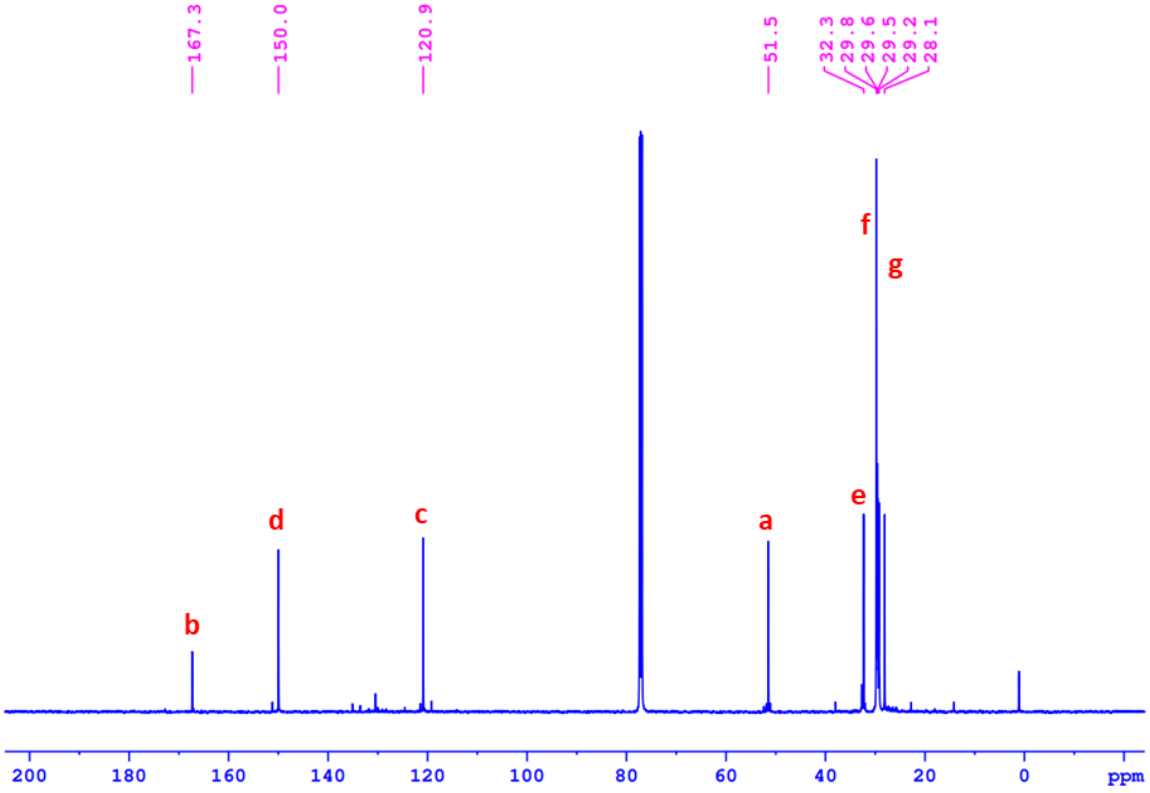

Figure 5.23: ^{13}C NMR of depolymerized product (M2) with MA in $CDCl_3$ (125 MHz).

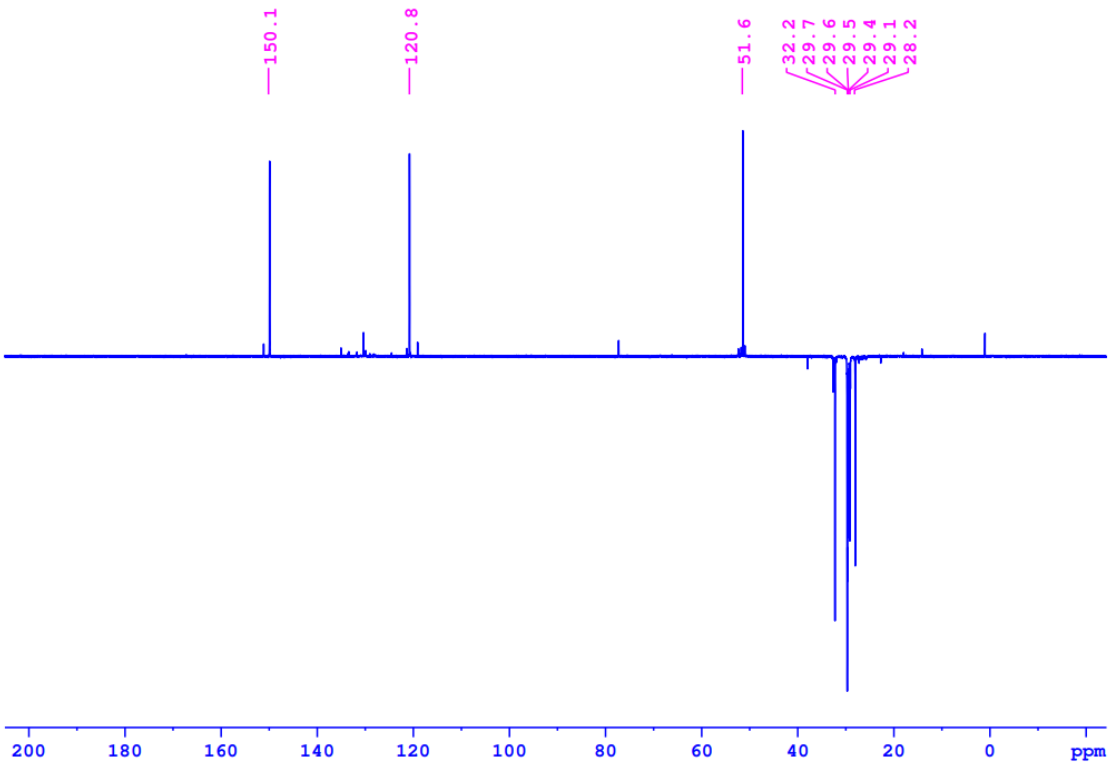

Figure 5.24: ^{13}C (DEPT) NMR of depolymerized product (M2) with MA in $CDCl_3$ (125 MHz).

5.5.7. General procedure for the depolymerization with 2-hydroxyethyl acrylate to M3:

The depolymerization reaction was conducted in a 100 mL Schlenk flask connected to the condenser. An oven-dried Schlenk flask with a magnetic stir bar was attached to the Schlenk line, and the Schlenk flask was cooled under vacuum. The desired amount of polymer (500 mg) was added, followed by the addition of Hoveyda-Grubbs-II catalyst (10 mg, 0.015 mmol.) and toluene (5 mL) as solvent. To above reaction content excess of 2-hydroxyethyl acrylate (0.5 mL, 4.35 mmol) was added and it was immidiatly placed into an oil bath preset to the desired temperature (85 °C). The reaction proceeded for the desired time (24 hours).

After completion of the reaction time, reaction mixture was evaporated on high vacuum pump and washed with diethyl ether and methanol (10 mL each) yields the difunctionalized monomer (yield- 493 mg).

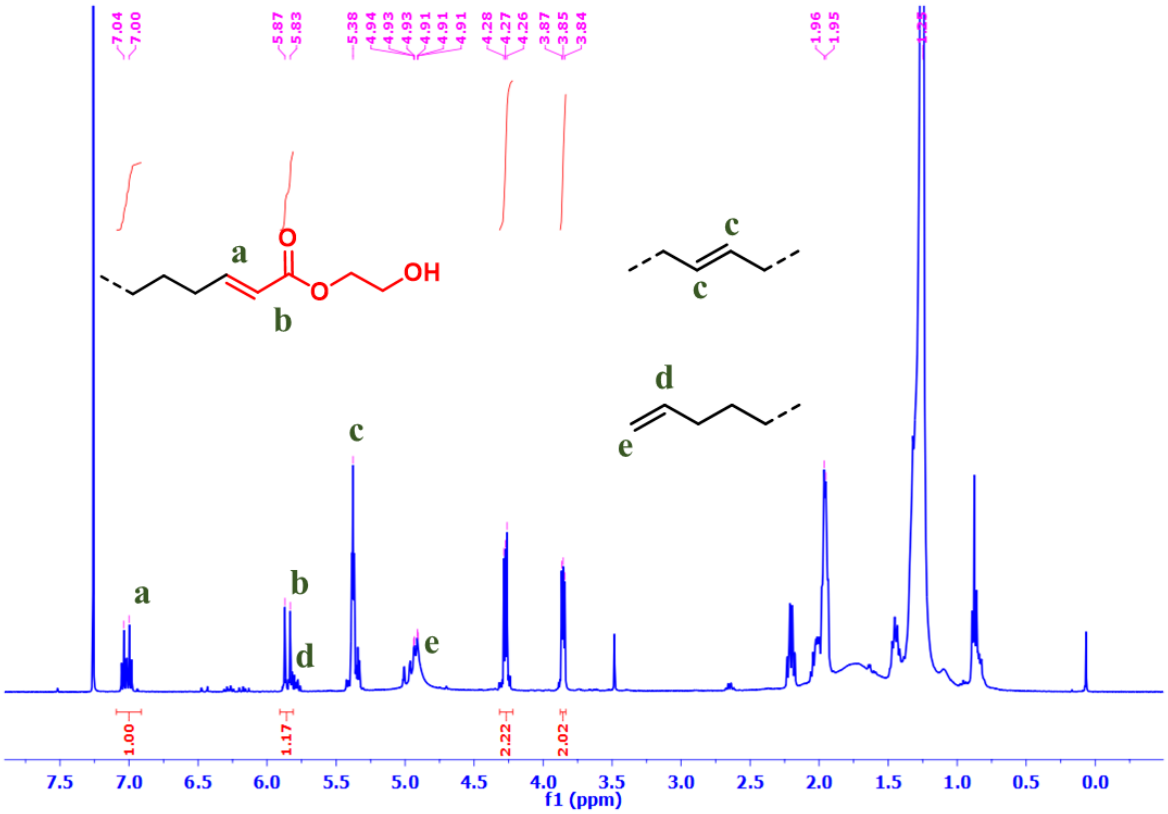

Figure 5.25: ^{1}H NMR of depolymerized product with HEA in $CDCl_3$ (400 MHz).

5.5.8. Hydrogenation of M2:

Selective hydrogenation of the olefin was conducted in a high-pressure autoclave reactor. In an oven-dried 50 mL conical flask with a magnetic stir bar, 1 gm of depolymerized product (M2) was weighed. Catalyst $[Rh(COD)_2OTf]$ (20 mg, 0.04 mmol.) and PPh_3 (20 mg, 0.076 mmol.) were added to the flask inside a glove box. Then, 20 mL of anhydrous THF was added in an argon atmosphere.

The conical flask was placed in a high-pressure autoclave reactor and immediately pressurized to 15 bar of H_2 pressure. The autoclave reactor was purged three times with 15 bar hydrogen pressure and finally maintained at 10 bar. The pressurized reactor was then placed in a preheated oil bath (65 °C), and stirring of the reaction was started. The reaction proceeded for one hour. After completion of the reaction, the pressure was released, and the THF solution was poured into 20 mL of methanol which was passed through a small bed of silica. The obtained filtrate was evaporated and dried under vacuum, yielding an oily compound (**M4**) (982 mg), which was then directly subjected to the repolymerization reaction.

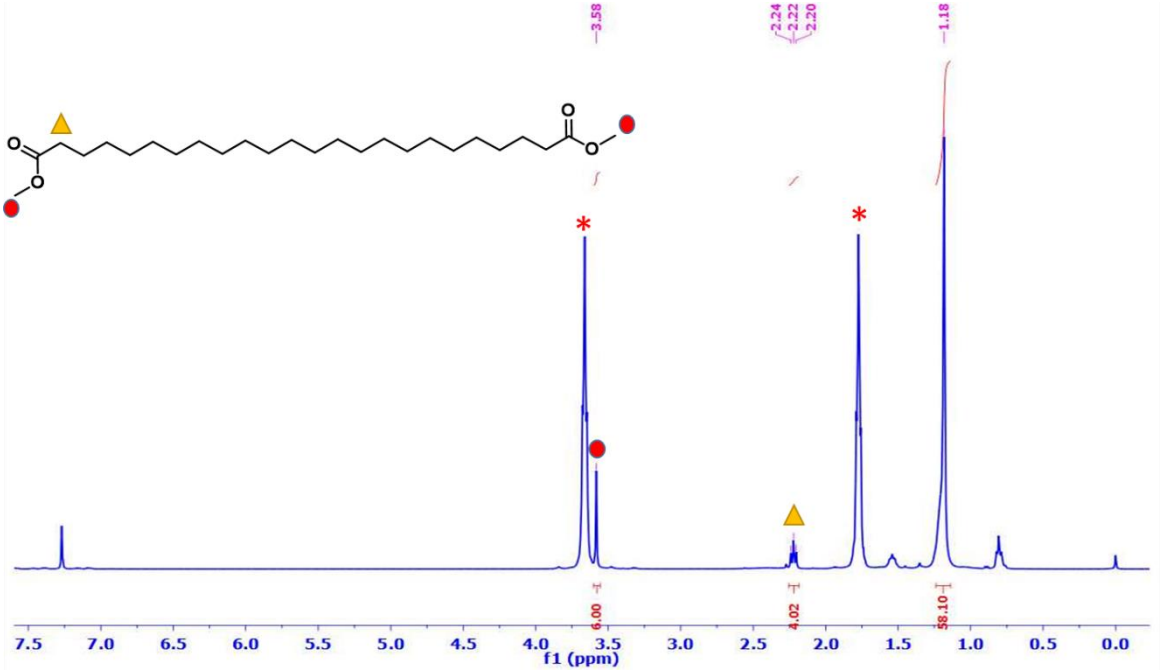

Figure 5.26: ^{1}H NMR of monomer (M4) (* - THF) in $CDCl_3$ (500 MHz).

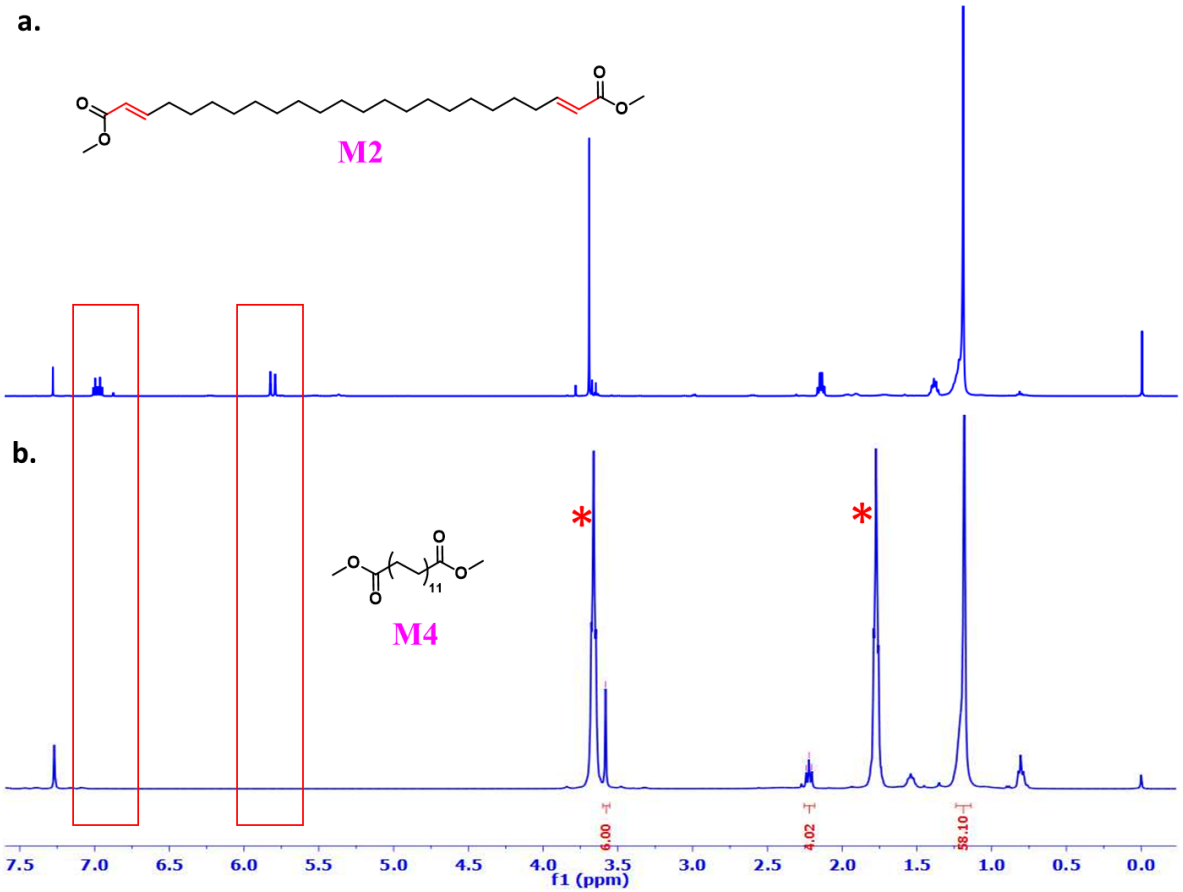

Figure 5.27: Comparison ^{1}H NMR of M2 vs M4 (before and after hydrogenation) (* - THF).

5.5.9. Repolymerization of M4 to polyester (P2):

The viscous oily compound M4 was directly utilized for the repolymerization reaction. The polymerization reaction was conducted in a 50 mL Schlenk tube connected to a high vacuum line to remove the by-product methanol after the condensation step. An oven-dried Schlenk flask with a magnetic stir bar was attached to the Schlenk line, and the Schlenk tube was cooled under vacuum. The desired amount of monomer M4 (300 mg, 0.703 mmol.) was then added, followed by the addition of desired amount of catalyst (shown in table 5.4) and ethylene glycol (shown in table 5.4). The Schlenk tube was placed in an oil bath preset to 150-160 °C and stirred in argon atmosphere for 1 hour. After that the temperature of the reaction mixture was increased to 180 °C, and vacuum was immediately applied. The reaction proceeded for the desired time under vacuum.

After completion of the reaction time, toluene was added to dissolve the polymer, and the reaction mixture was poured into methanol. The precipitated polymer was then filtered and dried under vacuum for 4 hours.

Table 5.4: Repolymerization to polymer (P2)[a].

Entry No.	Catalyst	Weight of Catalyst	Ethylene glycol	Time (h)	Yield (mg)	T_m (°C)	% Cryst.	M_w kDa	PDI
1.	PTSA	2 mg (0.012 mmol)	0.1 mL (1.78 mmol)	24	262	73.9	41.9	6.4	1.75
2.	$[Sn(Oct)_2]$	14.24 mg (0.035 mmol.)	0.08mL (1.43 mmol.)	10	142	80.8, 88.5	45.5	-	-
3.	$[Sn(Oct)_2]$	14.24 mg (0.035 mmol.)	0.08mL (1.43 mmol.)	24	162	86.1	45.9	-	-

[a]Reaction condition, Monomer M4 - 300 mg, Temperature- 180 °C, GPC was recorded on THF at 60 °C.

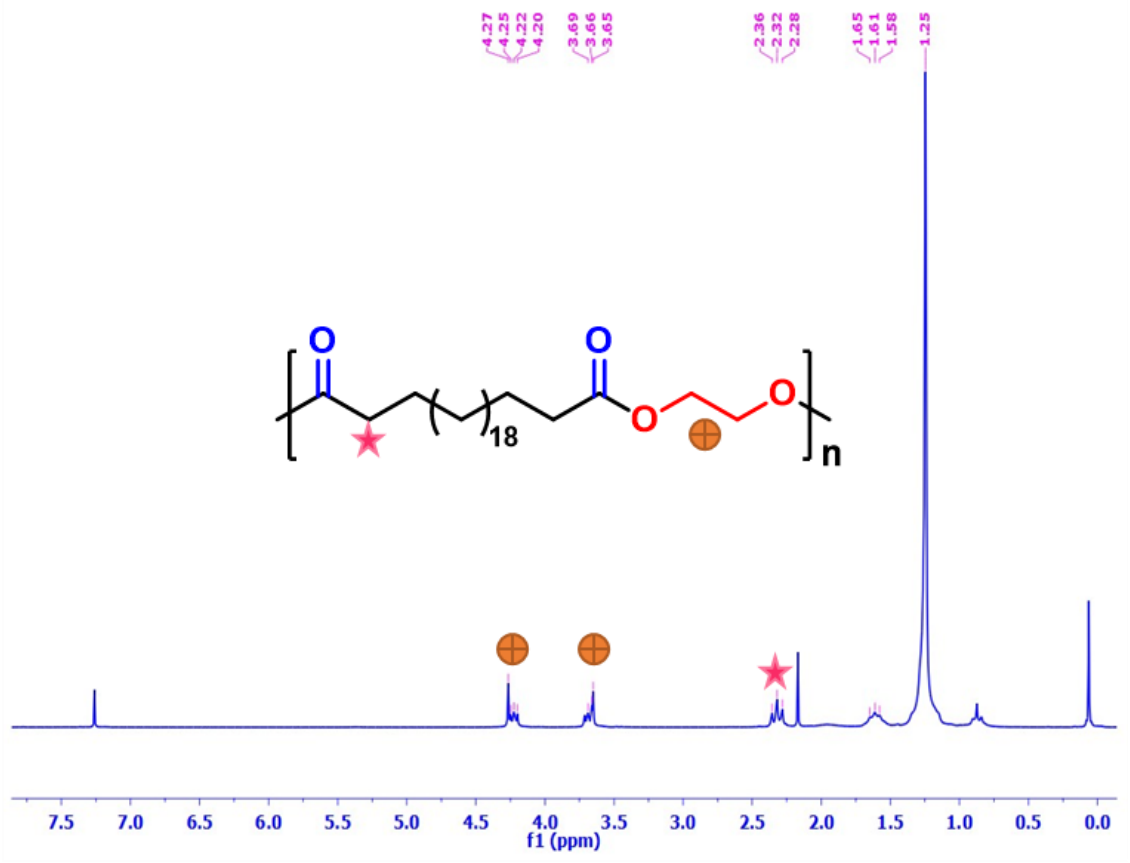

Figure 5.28: ^{1}H NMR of polymer (P2) in $CDCl_3$ (200 MHz) (Table 5.4, entry no. 1).

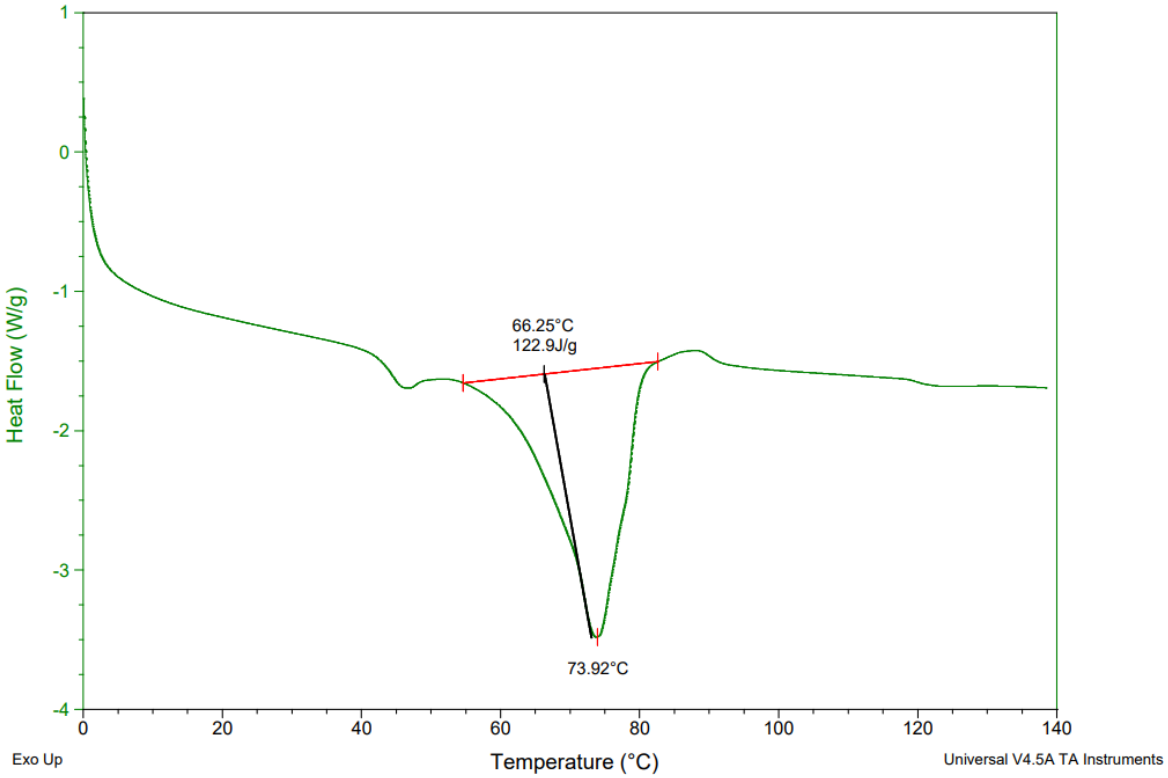

Figure 5.29: DSC thermogram of polyester P2 (Table 5.4, entry no. 1).

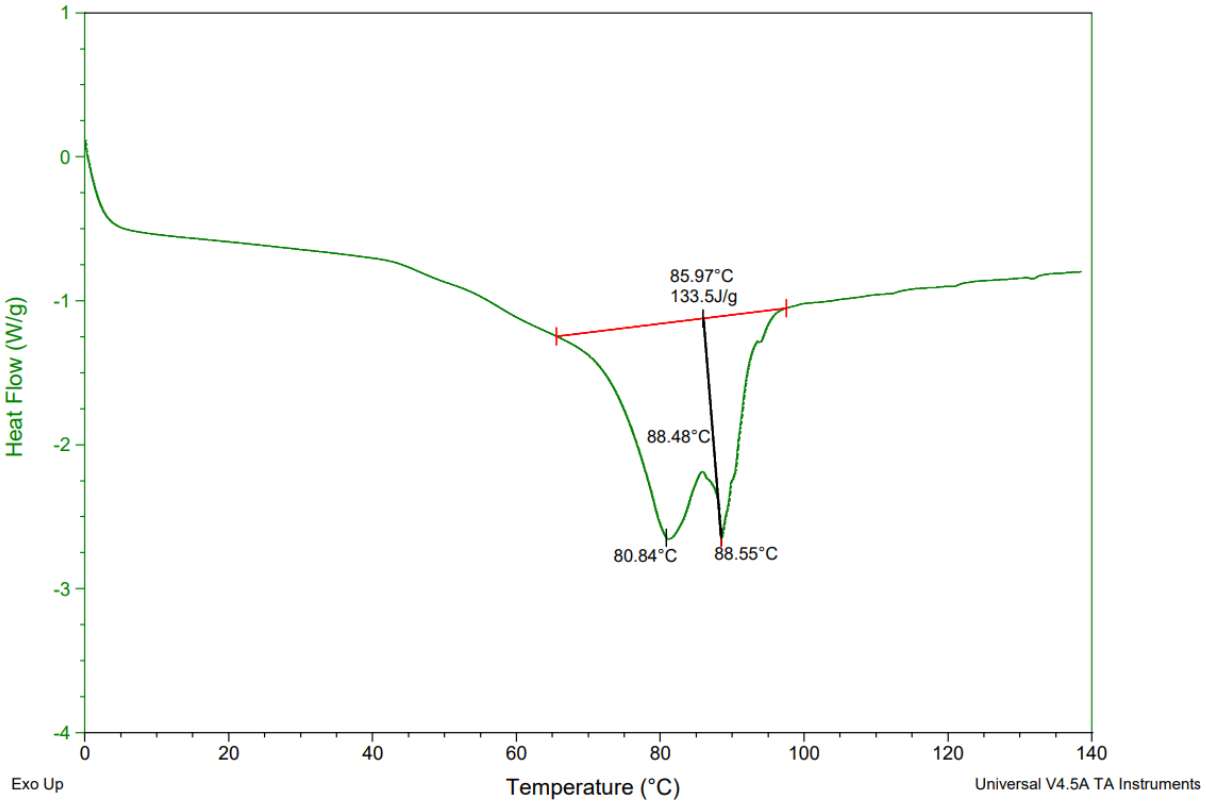

Figure 5.30: DSC thermogram of polyester P2 (Table 5.4, entry no. 2).

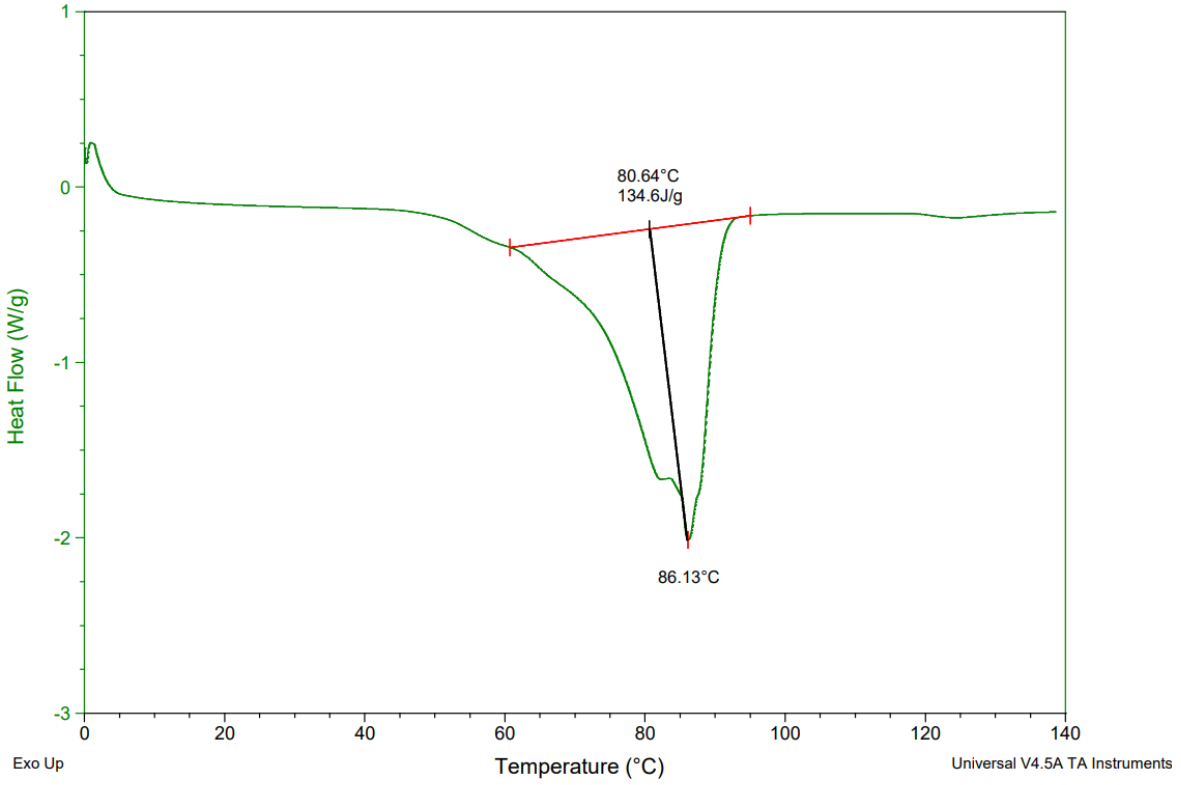

Figure 5.31: DSC thermogram of polyester P2 (Table 5.4, entry no. 3).

5.6. References:

1. Velenturf, A. P.; Purnell, P. Principles for a sustainable circular economy. *Sustain. Prod. Consum.* **2021**, *27*, 1437-1457.
2. Plastics- the facts. Plastics Europe. Onlineat https://plasticseurope.org/knowledge-hub/plastics-the-facts-2020/(accessed2023-10-28).
3. Peacock, A. (2000). Handbook of polyethylene: structures: properties, and applications. *CRC press.*
4. Evode, N.; Qamar, S. A.; Bilal, M.; Barceló, D.; Iqbal, H. M. Plastic waste and its management strategies for environmental sustainability. *CSCEE* **2021**, *4*, 100142.
5. Mihai, F. C.; Gündoğdu, S.; Markley, L. A.; Olivelli, A.; Khan, F. R.; Gwinnett, C.; Gutberlet, J.; Reyna-Bensusan, N.; Llanquileo-Melgarejo, P.; Meidiana, C.; Molinos-Senante, M. Plastic pollution, waste management issues, and circular economy opportunities in rural communities. *Sustainability* **2021**, *14*, 20.
6. Rustagi, N.; Pradhan, S. K.; Singh, R. Public health impact of plastics: An overview. *indian J. Occup. Environ. Med.* **2011**, *15*, 100-103.
7. Khopade, K. V.; Chikkali, S. H.; Barsu, N. Metal-catalyzed plastic depolymerization. *Cell Rep. Phys. Sci.* **2023**, *4*, 101341.
8. Jia, X.; Qin, C.; Friedberger, T.; Guan, Z.; Huang, Z. Efficient and selective degradation of polyethylenes into liquid fuels and waxes under mild conditions. *Sci. Adv.* **2016**, *2*, e1501591. *doi:10.1126/sciadv.1501591*.
9. Conk, R. J.; Hanna, S.; Shi, J. X.; Yang, J.; Ciccia, N. R.; Qi, L.; Bloomer, B. J.; Heuvel, S.; Wills, T.; Su, J.; Bell, A. T. Catalytic deconstruction of waste polyethylene with ethylene to form propylene. *Science* **2022**, *377*, 1561-1566.
10. Arroyave, A.; Cui, S.; Lopez, J. C.; Kocen, A. L.; LaPointe, A. M.; Delferro, M.; Coates, G. W. Catalytic chemical recycling of post-consumer polyethylene. *J. Am. Chem. Soc*. **2022**, *144*, 23280−23285
11. Zeng, M.; Lee, Y. H.; Strong, G.; LaPointe, A. M.; Kocen, A. L.; Qu, Z; Abu-Omar, M. M. Chemical upcycling of polyethylene to value-added α, ω-divinyl-functionalized oligomers. *ACS Sustain. Chem. Eng.* **2021**, *9*, 13926-13936.

12. Parke, S. M.; Lopez, J. C.; Cui, S.; LaPointe, A. M.; Coates, G. W. Polyethylene incorporating Diels–Alder comonomers: A "Trojan Horse" strategy for chemically recyclable polyolefins. *Angew. Chem. Int. Ed.* **2023**, *62*, e202301927.
13. Martinez, H.; Ren, N.; Matta, M. E.; Hillmyer, M. A. Ring-opening metathesis polymerization of 8-membered cyclic olefins. *Polym. Chem.* **2014**, *5*, 3507-3532.
14. Adnan Akram, M.; Liu, X.; Fu, Z.; Fan, Z. Ethylene-butadiene copolymerization and ethylene-1-hexene-butadiene terpolymerization with a $MgCl_2$-supported Ziegler-Natta catalyst: Polymer structure and active centers. *Chemistry Select* **2021**, *6*, 8288-8298.
15. Eck, M.; Schwab, S. T.; Nelson, T. F.; Wurst, K.; Iberl, S.; Schleheck, D.; Mecking, S. Biodegradable high-density polyethylene-like material. *Angew. Chem.* **2023** *135*, e202213438.
16. Mubofu, E. B. Castor oil as a potential renewable resource for the production of functional materials. *Sustain. Chem. Process.* **2016**, *4*, 1-12.
17. Chauke, N. P.; Mukaya, H. E.; Nkazi, D. B. Chemical modifications of castor oil: A review. *Sci. Prog.* **2019**, *102*, 199-217.
18. Ogunniyi, D. S. Castor oil: A vital industrial raw material. *Biores Technol.* **2006**, *97*, 1086–1091.
19. Van der Steen, M.; Stevens, C. V.; Eeckhout, Y.; De Buyck, L.; Ghelfi, F.; Roncaglia, F. Undecylenic acid: A valuable renewable building block on route to Tyromycin A derivatives. *Eur. J. Lipid Sci. Technol.* **2008**, *110*, 846–852.
20. Van der Steen, M.; Stevens, C. V. Undecylenic acid: a valuable and physiologically active renewable building block from castor oil. *ChemSusChem* **2009**, *2*, 692 – 713.
21. Van den Berg, O.; Dispinar, T.; Hommez, B.; Du Prez, F. E. Renewable sulfur-containing thermoplastics via AB-type thiol-ene polyaddition. *Eur. Polym. J.* **2013**, *49*, 804-812.
22. Kawafuchi, A.; Kutsumizu, S.; Kawase, Y.; Tokiwa, I.; Udagawa, T.; Miwa, Y. Molecular design of anti-spindle-like molecules by use of siloxanyl terminals for a thermotropic bicontinuous cubic phase. *Phys. Chem. Chem. Phys.* **2020**, *22*, 10132-10141.

Chapter 6

Summary and Outlook

6.1. Summary:

This Ph.D Thesis entitled as "**Transition Metal Catalyzed Polymerization of Olefins and Depolymerization of Polyolefins"** consists of six chapters. In chapter 1, we summarized the historical development and recent advancements in metal-catalyzed olefin polymerization and oligomerization. Historically, a major breakthrough occurred in the 1950s with the development of low-pressure metal-catalyzed olefin polymerization using a Ziegler catalyst. Even after 70 years of the first catalytic process, the field of polyolefin catalysis remains very active. It has greatly transformed over time, evolving from intrinsically multisite catalysts to new advanced single-site catalysts, leading to increasingly advanced materials year after year. In the last three decades, significant discoveries have been made regarding ligand modifications for metal-catalyzed olefin polymerization. This research has primarily focused on designing ligands and their metal catalysts for olefin homo- and copolymerization. There are only a handful of catalysts capable of performing ethylene-functional olefin copolymerization. A significant amount of research has also focused on understanding the steric and electronic effects of ligands on catalytic activity, molecular weight, crystallinity, and other properties.

Similar to polyethylene, its low molecular weight oligomers are important materials for various applications (lubricants, plasticizer, etc.). On an industrial scale, the synthesis of ethylene oligomers is performed using a SHOP catalyst. This catalyst exhibits higher β-hydride elimination, resulting in low molecular weight linear oligomers. Recent catalyst modifications have produced hyperbranched ethylene oligomers.[1,2] These modified catalysts behave similar to SHOP catalysts but also exhibit a chain walking leading to branched and hyperbranched ethylene oligomers.

As discussed earlier, synthesis of hyperbranched ethylene oligomer is very challenging and only a handful of catalysts can produce it with moderate to low catalytic activity. To achieve this, the catalyst must exhibit higher β-hydride elimination along with chain walking. In chapter 2, we addressed this challenge by synthesizing sterically tuned naphthoxy imine ligands (2L1 and 2L2). These naphthoxy imine ligands were treated with [Pd(TMEDA)Me_2] and 2,6-lutidine, resulting in the 2Pd1 and 2Pd2 catalysts with good to excellent yields. The obtained catalysts were characterized by spectroscopic and analytical methods. Crystals grown in DCM and hexane solvent mixture were analyzed, indicating that the Pd-Me and 2,6-lutidine are cis to each other with a bond angle of 90.5°. The 2Pd1 and 2Pd2 catalysts produced ethylene oligomers even at 5 bar ethylene pressure. The obtained ethylene oligomers were analyzed using 1D and 2D NMR spectroscopy. The ^{1}H NMR analysis revealed the presence of internal

and terminal double bonds, suggesting that chain termination occurred through β-hydride elimination. The ^{13}C NMR data confirmed that the oligomers contained methyl, ethyl, propyl, long-chain branches, and *sec*-butyl branches, indicating a hyperbranched structure.

Usually, traditional olefin polymerization catalysts are easily poisoned by small amounts of polar solvents or impurities. These palladium catalysts (2Pd1, 2Pd2) surprisingly produced ethylene oligomers with threefold enhanced activity with similar branches and molecular weight. Hyperbranched ethylene oligomers were post-functionalized using ozonolysis, hydroformylation, and epoxidation. The hydroxyl-functionalized ethylene oligomers were used as compatibilizers for LLDPE and Nylon 6, resulting in an enhanced strain to break compared to the uncompatibilized blend.

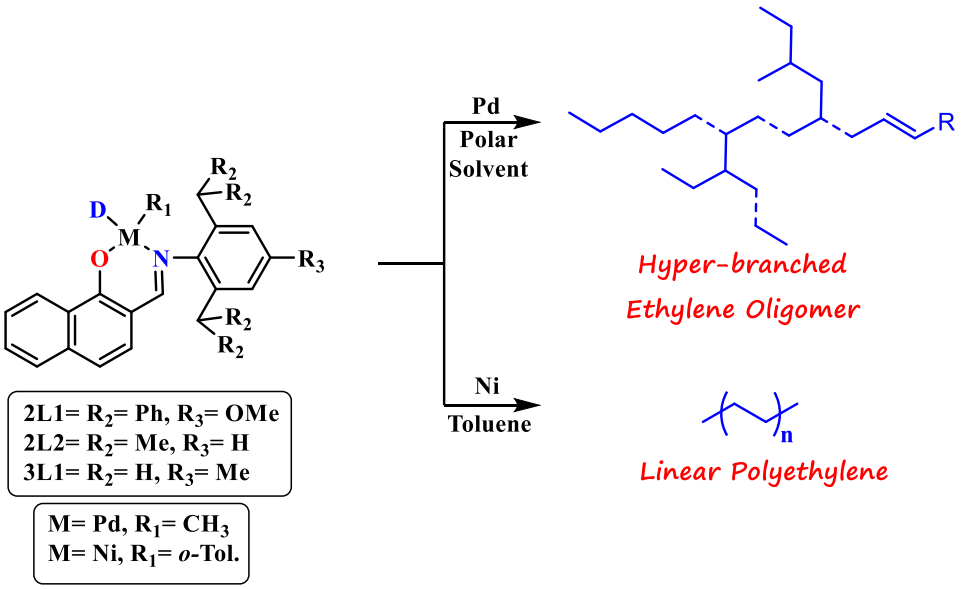

Figure 6.1: Naphthoxy imine ligated metal catalyst for the ethylene oligomerization and polymerization.

Chapter 3 reports the synthesis of sterically tuned naphthoxy imine ligands. These ligands were treated with NaH and [NiCl(oTol)(PPh_3)$_2$], yielding the corresponding nickel catalysts Ni1 to Ni3 with excellent yields. Using SambVCA 2.1 web software, the percentage of buried volume was calculated, revealing that the dibenzhydryl-substituted catalyst Ni3 showed the highest value at 49.1%. These catalysts were subjected to ethylene polymerization, where it was observed that the more sterically hindered Ni3 catalyst outperformed the Ni1 and Ni2 catalysts in activity. Proton NMR analysis of the polyethylene showed that increased steric hindrance resulted in a lower number of branches per 1000 carbon atoms (Ni1: 54, Ni2: 43, Ni3: 28). In ^{13}C NMR, the polymer obtained at 80 °C and 20 bar indicated that the Ni1 and Ni2 catalysts produced methyl, ethyl, propyl, and long-chain branches, whereas the Ni3 catalyst produced

over 99% methyl branches. The lowering in long-chain branching led to higher crystallinity and a higher melting temperature compared to the polymers produced by Ni1 and Ni2 catalysts. Additionally, the molecular weights were higher for the Ni3 catalyst compared to Ni1 and Ni2. These results conclude that the sterically more hindered Ni3 catalyst reduces β-hydride elimination and chain walking, resulting in a high molecular weight polymer with lower branches.

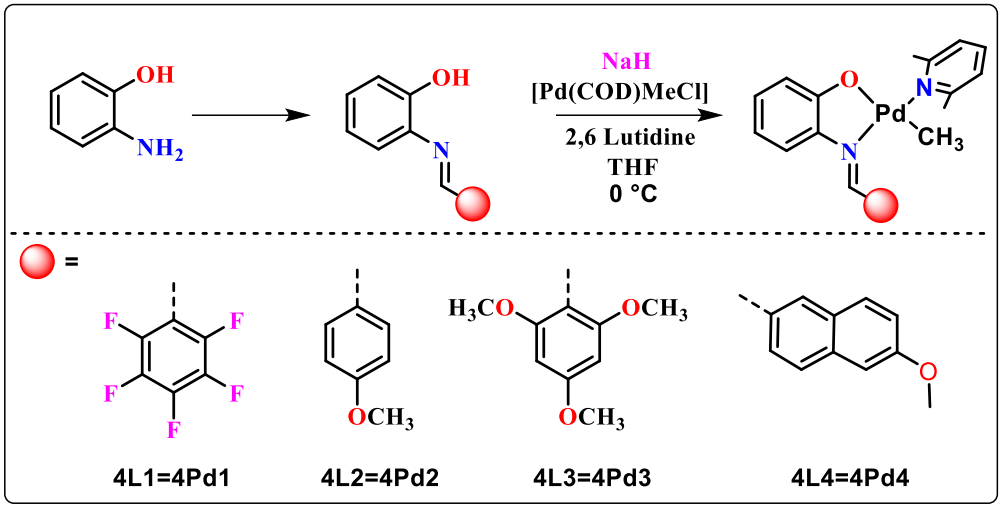

Figure 6.2: Electronically tuned imine phenoxy ligated palladium complexes.

In chapter 4, we described the synthesis of imine phenoxy ligands through condensation reactions between 2-aminophenol and various aniline derivatives (4L1–4L4). These ligands were converted to sodium salts and reacted with [Pd(COD)MeCl] and 2,6-lutidine, resulting in the formation of 4Pd1-4Pd4 complexes in a single step with excellent yields. Catalysts were characterized by using NMR, mass spectrometry, and single-crystal X-ray diffraction.

Proton NMR analysis of 4Pd1 suggested a more electronically deficient palladium center compared to the others. Using $[Ph_3C]^+[B(C_6F_5)_4]^-$ as a cocatalyst, the polymerization of norbornene produced poly(norbornene) (PNB) with high catalytic activity, reaching up to 2.97 × 10^5 g of PNB per mole of Pd. Even with low cocatalyst concentration, the system performed efficiently. When combined with MMAO as a cocatalyst, these complexes showed even higher activity (up to 63.2 × 10^5 g of PNB (mol. of Pd)$^{-1}$ h^{-1}) with over 99% conversion in norbornene homopolymerization.

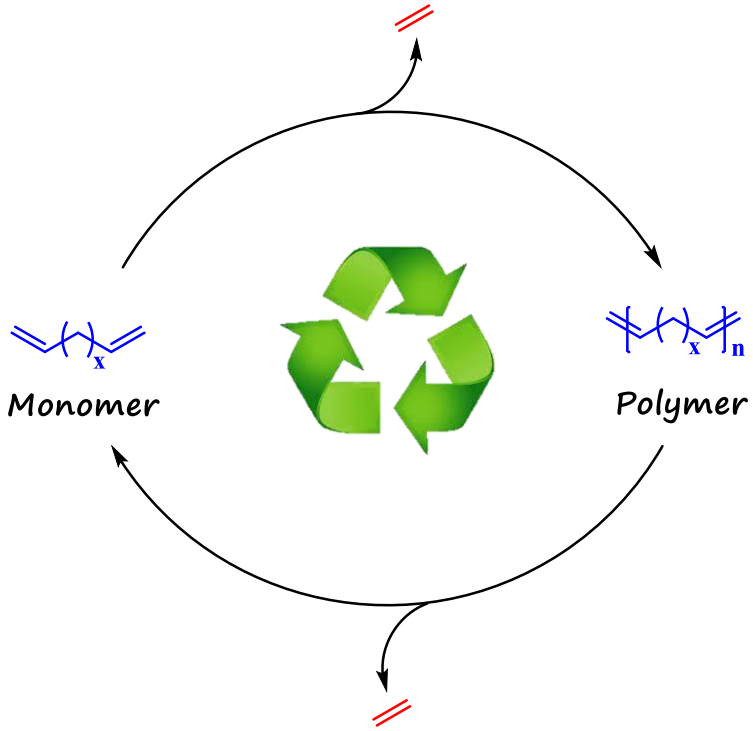

Figure 6.3: Polymerization, depolymerization and repolymerization of polyethylene-like polymer.

The significant use of polyethylene results in a substantial production of waste within a shorter time. The stable and strong C-C bonds in polyethylene prevent degradation, making it difficult to chemically recycle. To address this, the synthesis of polyethylene-like polymers has become a growing and interesting field. In chapter 1, we briefly discussed the different approaches for synthesis of chemically recyclable polyethylene-like polymers. To achieve this researchers have incorporated in-chain carbonyl groups or double bonds into the polymer backbone. At the end of life of a polymer product, these compounds can be chemically recycled into low molecular weight oligomers or their monomers.

To achieve a chemically recyclable polyethylene-like polymer, we synthesized the docosa-1,21-diene monomer and subjected it to ADMET polymerization as described in chapter 5. This process yielded a polymer with a high melting temperature of 100 °C and crystallization in an orthorhombic form, similar to HDPE crystallization. The polymer exhibited a high molecular weight of 1.8×10^4 Da. In line with circular economy principles, the polymer (P1) was subjected for cross-alkene metathesis with ethylene, producing monomers and low molecular weight oligomers, as confirmed by NMR, GC, and DSC analyses. These monomers and oligomers were then repolymerized, resulting in a repolymer (RP1) with a molecular weight of 8.2×10^3 Da. Further, polymer P1 was subjected to cross-alkene metathesis with acrylates, selectively forming α,β-unsaturated esters. These esters were hydrogenated and

condensed with ethylene glycol, resulting in a polyethylene-like material with in-chain ester functional groups (P2).

6.2. Outlook:

As ligands play an important role in olefin polymerization, the work described in this thesis contributes to designing novel ligands for ethylene oligomerization, polymerization and depolymerization. As discussed in chapter 2 and 3, by increasing the sterics around the palladium and nickel metal center, results into highly active catalyst for ethylene polymerization. As previous reports suggested, catalysts with sterically less hindered ligands are inactive in ethylene oligomerization and polymerization.[3] These results will help us to design sterically more hindered moiety in the ligand which is expected to be highly active catalyst. 8-arylnaphthyl groups integrated with dibenzosuberyl or dibenzhydrol groups will be used for the synthesis of ligands 6L1 to 6L4 (Figure 6.4). These ligands, when treated with [Pd(TMEDA)Me_2] or [NiCl(oTol)PPh_3], will produce the corresponding palladium and nickel catalyst. These catalysts are expected to be sandwich like structures.[4] The sterically hindered ligand around the metal center may reduce β-hydride elimination and chain walking. Through this catalyst, the obtained polymers are expected to be highly linear high molecular weight or UHMWPE. Additionally, these sterics help avoid the bis-ligated monometallic catalysts, which are inactive for ethylene polymerization. As a result, the catalyst remains active for a longer time during polymerization and results in high catalytic activity.

Incorporating a sterically bulky group at the C-8 position in naphthoxy has been found to significantly enhance the catalytic activity in ethylene polymerization and copolymerization with polar monomer.[5] Additionally, due to the shorter distance between peri-substituents (C1 and C8 position) in naphthalene compared to ortho-substituents in benzene, a substituent at the 8-position of naphthol will result in a more crowded catalytic center than the same substituent on the ortho-position of phenol. This increased steric congestion at the catalytic center can further influence the catalyst's performance in polymerization reactions. So, we propose the naphthoxy imine ligand with steric substituents on the C8 position (Figure 6.4, 6L7-6L10).

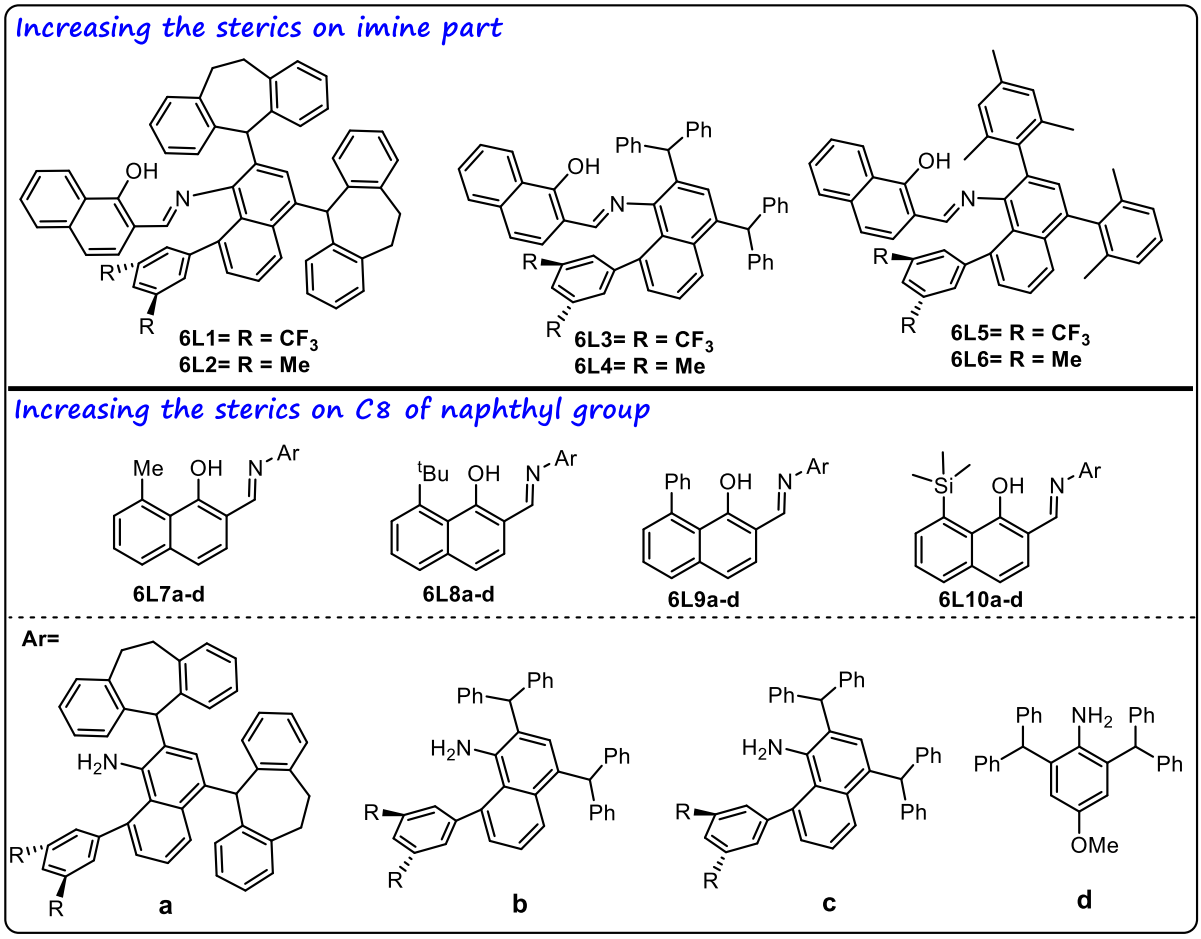

Figure 6.4: Proposed naphthoxy imine ligand library for ethylene (co)polymerization.

This newly designed catalyst can be utilized for the ethylene polymerization in polar solvent, as previous report suggest that in polar solvent the activity and molecular weight of the polymer increases drastically. Additionally, this catalyst can be used for ethylene functional olefin copolymerization with both mono- and difunctional olefins, such as acrylates and acetates.

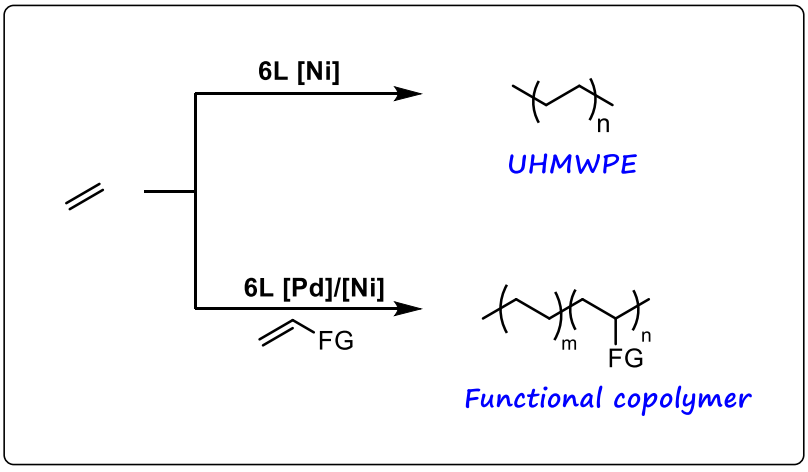

Figure 6.5: Implication of proposed naphthoxy imine ligated metal catalyst for the synthesis of UHMWPE and ethylene functional olefin copolymerization.

In addition to functional olefin copolymerization, these catalysts (derived from 6L1-6L6) can also be utilized for ethylene carbon monoxide copolymerization (Figure 6.6). It is expected that this copolymerization produces randomly distributed keto groups in polyethylene backbone. The resulting keto-polyethylene can then be converted into ester-functionalized polymer through Baeyer-Villiger oxidation. Literature reports suggest that these ester-functionalized polyethylenes can be chemically recycled.[6]

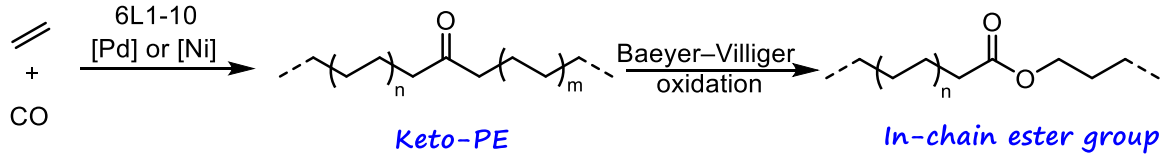

Figure 6.6: Synthesis of chemically recyclable in-chain keto functionalized polyethylene.

6.3. References:

1. Wiedemann, T.; Voit, G.; Tchernook, A.; Roesle, P.; Göttker-Schnetmann, I.; Mecking, S. Monofunctional hyperbranched ethylene oligomers. *J. Am. Chem. Soc.* **2014**, *136*, 2078-2085.
2. Li, S.; Lu, Z.; Fan, W.; Dai, S. Efficient incorporation of a polar comonomer for direct synthesis of hyperbranched polar functional ethylene oligomers. *New J. Chem.* **2021**, *45*, 4024-4031.
3. Pong, F. Y.; Mandal, S.; Sen, A. Steric and electronic effects in ethene/norbornene copolymerization by neutral salicylaldiminato-ligated palladium (II) catalysts. *Organometallics* **2014**, *33*, 7044–7051.
4. Wang, C.; Kang, X.; Mu, H.; Jian, Z. Positive effect of polar solvents in olefin polymerization catalysis. *Macromolecules* **2022**, *55*, 5441-5447.
5. Wang, X. L.; Zhang, Y. P.; Wang, F.; Pan, L.; Wang, B.; Li, Y. S. Robust and reactive neutral nickel catalysts for ethylene polymerization and copolymerization with a challenging 1, 1-disubstituted difunctional polar monomer. *ACS Catal.* **2021**, *11*, 2902−2911.
6. Schwab, S. T.; Baur, M.; Nelson, T. F.; Mecking, S. Synthesis and deconstruction of polyethylene-type materials. *Chem. Rev.* **2024**, *124*, 2327–2351.

ABSTRACT

Name of the Student: Birajdar Rajkumar S. **Registration No. :** 10CC19J26014

Faculty of Study: Chemical Science **Year of Submission:** 2024

AcSIR academic centre/CSIR Lab: CSIR-NCL **Name of the Supervisor(s):** Dr. Samir Chikkali, Dr. Ashootosh Ambade

Title of the thesis: Transition Metal Catalyzed Polymerization of Olefins and Depolymerization of Polyolefins

In metal catalyzed olefin polymerization ligands play a crucial role to control molecular weight, crystallinity, and stereo-regularity. Even after 70 years of the first catalytic process (Ziegler-Natta polymerization), the field of polyolefin catalysis remains very active. It has greatly transformed over time, evolving from intrinsically multisite catalysts to new advanced single-site catalysts, leading to increasingly advanced materials year after year. In the last three decades, significant discoveries have been made regarding ligand modifications for metal-catalyzed olefin polymerization and copolymerization to produce an *dis*-UHMWPE, Functional copolymer, hyperbranched ethylene oligomer, etc. These polymers are unique material properties, but only a handful of catalyst can produce. To achieve this polymer, designing the suitable ligands and its metal catalyst is important. In **chapter 1** we provided detailed literature review on olefin polymerization using various late transition metal-based catalysts. Additionally, we reviewed the issue of substantial waste generation due to the large-scale production of polyolefins, underscoring the importance of depolymerization and recyclability. **Chapter-2** deals with the synthesis and characterization of a naphthoxy imine ligands and its corresponding neutral palladium catalysts. These catalyst were utilized in ethylene oligomerization, and post-functionalization of these results into hyperbranched functional ethylene oligomers. These hyperbranched oligomers were then employed as compatibilizers for Nylon 6 and LLDPE. **Chapter-3** describes the synthesis and characterization of sterically tuned naphthoxy imine ligated neutral nickel complexes. It highlights the performance differences between sterically more crowded Ni3 catalysts and less crowded counterparts in terms of activity and molecular weight. Furthermore, the complex with higher steric hindrance yields lower branching and produces linear polyethylene, resulting in a highly crystalline polymer. **Chapter 4** describes the synthesis and characterization of electronically tuned four imine phenoxy-ligated palladium complexes. These complexes were utilized to produce polynorbornene through insertion polymerization, even at ambient temperature, both without and with cocatalysts [$B(C_6F_5)_3$], Trityl tetrakis(pentafluorophenyl)borate, MMAO]. **Chapter 5** delves into the synthesis and characterization of chemically recyclable polyethylene-like materials. These polymers are synthesized via ADMET and condensation polymerization, incorporating in-chain olefin and ester groups along with long hydrophobic methylene groups. **Chapter-6** concludes the work and provides future direction.

List of Publications and Patents Emanating from the Thesis Work

1. **Birajdar, R. S**.; Gonnade, R. G.; Chikkali, S. H. Regulating the polyethylene microstructure by increasing steric crowding in naphthoxy imine-ligated Ni(II) complexes. *Polym. Chem.* **2024**, *15*, 292-302.

2. **Birajdar, R. S.;** Bodkhe, D.; Gupta, P.; Shaikh, M. H.; Ramekar, R.; Chikkali, S. H. Emerging trends in olefin polymerization: a perspective. *J. Macromol. Sci. A* **2023**, *60*(11), 731-750.

3. **Birajdar, R. S**; Gonnade, R. G.; Pol, H. V.; Basava Prabhu M.; Rokade, D.; Nandimatha, S.; Chikkali, S. H. Palladium-catalyzed polar solvent empowered synthesis of hyper-branched ethylene oligomers and their applications. *Polym. Chem.* **2023**, *14*, 3239-3251.

4. **Birajdar, R. S.;** Chikkali, S. H. Insertion copolymerization of functional olefins: Quo Vadis?. *Eur. Polym. J.* **2021**, *143*, 110183.

5. Chikkali, S. H.; **Birajdar, R. S.** Synthesis of dibenzhydryl substituted phenoxy imine ligated Pd(II) and Ni (II) catalyst for ethylene (co)polymerization. **(**IN2022-NF-0181**).**

List of Publications Non-Emanating from the Thesis Work

6. Chatterjee, D.; Sajeevan, A.; Jana, S.; **Birajdar, R. S.;** Chikkali, S. H.; Sivaram, S.; Gupta, S. S. Solvent-Free Hydroxylation of Unactivated C–H Bonds in Small Molecules and Macromolecules by a Fe Complex. *ACS Catal.* **2024**, *14,* 7173–7181.

7. Gaikwad, S. R.; Patel, K.; Deshmukh, S. S.; Mote, N. R.; **Birajdar, R. S.;** Pandole, S. P.; Chugh, J.; Chikkali, S. H. Palladium-catalyzed insertion of ethylene and 1, 1-disubstituted difunctional olefins: an experimental and computational study. *ChemPlusChem* **2020**, *85*(6), 1200-1209.

8. Khopade, K. V.; Sen, A.; **Birajdar, R. S**.; Paulbudhe, U. P.; Kavale, D. S.; Shinde, P. S.; Mhaske, S. B.; Chikkali, S. H. Highly enantioselective synthesis of sitagliptin. *Asian J. Org. Chem.* **2020**, *9*(2), 189-191.

9. Chikkali, S. H.; Jawoor, S.; **Birajdar, R. S.**; Pawal, S. B.; Thenmani, N.; Chugh, P. Homogeneous single site catalyst and its use in preparing linear polyethylene. EP4157527A1; JP2023529101A; US2023201815A1; WO2021240549A1**.**

List of Oral/Poster Presented with Details

1. Attended and given flash talk along with poster in **Alexander von Humboldt Foundation Kolleg**, 2024 held at Bogmallo Beach Resort, Goa. "*Regulating the polyethylene microstructure by increasing steric crowding in naphthoxy imine-ligated Ni(II) complexes*". **Birajdar, R. S.;** Gonnade, R. G.; Chikkali, S. H.

2. **Best Oral Presentation**: Given Oral presentation in 17th International Conference on Science and Technology, **SPSI-MACRO-2023**, held from December 10–13, 2023, hosted by Indian Institute of Technology Guwahati. "*Regulating the polyethylene microstructure by increasing steric crowding in naphthoxy imine-ligated Ni(II) complexes*". **Birajdar, R. S.;** Gonnade, R. G.; Chikkali, S. H.

3. Presented poster in 19th international Conference on Modern Trends in Inorganic Chemistry (**MTIC**), was held at Banaras Hindu University (BHU) in 2022. "*Palladium-catalyzed polar solvent empowered synthesis of hyper-branched ethylene oligomers and their applications.*" **Birajdar, R. S**; Gonnade, R. G.; Pol, H. V.; Basava Prabhu M.; Rokade, D.; Nandimatha, S.; Chikkali, S. H.

4. **Best Poster Presentation**: Presented poster in 16th International Conference on Science and Technology of Polymers and Advanced Materials, **SPSI-MACRO-2022**, in CSIR-NCL, Pune. "*Palladium-catalyzed polar solvent empowered synthesis of hyper-branched ethylene oligomers and their applications.*" **Birajdar, R. S**; Gonnade, R. G.; Pol, H. V.; Basava Prabhu M.; Rokade, D.; Nandimatha, S.; Chikkali, S. H.

Rajkumar S. Birajdar

C/o Prof. Samir Chikkali

Polymer Science and Engineering Division,
CSIR-National Chemical Laboratory
Pune-411008, India
+91-9049364840

Email: *birajdarraj30@gmail.com*

An organized professional with proven research skills and looking to contribute knowledge and skills to an organization that offers a genuine opportunity for career progression

Education

Ph.D. student at the Department of Polymer Science and Engineering 2019-current
National Chemical Laboratory, Pune, Maharashtra, India
Title of Thesis- "Transition Metal Catalyzed Polymerization of Olefins and Depolymerization of Polyolefins"
Dr. Samir H. Chikkali (Research Superviser)
Dr. Ashootosh V. Ambade (Research Co-superviser)

M.Sc. Organic Chemistry 2016-2018
Solapur University, Solapur, India

B.Sc. in Chemistry 2013-2016
C. B. Khedgi's College, Akkalkot, Solapur University, Maharashtra, India

Skills and Expertise

- **Synthesis:**
  - ✓ Expertise in rational design and syntheses of ligands and complexes.
  - ✓ Good experience in homogeneous catalysis and polymerization (particularly ethylene oligomerization and polymerization).
  - ✓ Excellent knowledge in insertion polymerization reaction and polyolefin depolymerization reaction.
  - ✓ Expertise in handling highly air- and moisture-sensitive reagents/reactions.
  - ✓ Highly skilled in organic chemicals separation and purification.
- **Analytical techniques:**
  - ✓ Skilled in handling DSC (DSC Q10), GPC, IR.
  - ✓ Expertise in interpreting results from IR, UV-Vis, 1-2D NMR, DSC, TGA, FE-SEM, TEM and GPC.
  - ✓ Good knowledge of literature survey (SciFinder), Chem Draw, MestraNova, Origin, Apex 4.0, Topspin, Grapher, Mercury, SambVCA 2.1 and TA software.

Fellowships and Awards

- **Best Oral Presentation** award at the 17th International Conference on Science and Technology, "SPSI-MACRO-2023," held from December 10–13, 2023, hosted by Indian Institute of Technology Guwahati.
- **Best Poster Presentation** award at the 16th International Conference on Science and Technology of Polymers and Advanced Materials, "SPSI-MACRO-2022", held from November 2–4, 2022, in Pune, India. The conference was jointly organized by CSIR-

National Chemical Laboratory (CSIR-NCL), Pune, Indian Institute of Science Education and Research (IISER), Pune, and Savitribai Phule Pune University (SPPU).

- 2021: Awarded Senior Research Fellowship sponsored by DST-INSPIRE, India.
- 2019: Awarded Junior Research Fellowship sponsored by DST-INSPIRE, India.
- Honored with **Gold Medal** in 2019 from Solapur University, Solapur, for securing the first rank in the Master's in Chemistry.

Research Interests

- Synthesis of macromolecular materials
- Characterization of polymer with different analytical and spectroscopic method
- Utilization of polymer for the different application

Professional Experience

Ph.D. student, National Chemical Laboratory, Pune, India 01/2019-current

- In my Ph.D., I have been working on the thesis entitled "Transition Metal Catalyzed Polymerization of Olefins and Depolymerization of Polyolefins"
- Transition metal complexes: Synthesis, characterization, and its applications
- Ligands synthesized**:** Novel naphthoxy imine and imine phenoxy ligands.
- Metal Complexes: complexation with transition metals like palladium, nickel, titanium, zirconium and chromium.
- High pressure reaction: Metal catalyzed high pressure polymerization reaction.
- Synthesis of depolymerizable polyethylene like materials and its depolymerization.
- Routinely performed an 1-2D NMR, single crystal growth, IR, analysis, GPC, TGA, DSC.

Project Assistance, National Chemical Laboratory, Pune-India 07/2018-01/2019

- Transition metal catalyzed high-pressure enantioselective hydrogenation reaction.
- Synthesis of imine cyclopenatdiene ligands for ethylene polymerization.

Masters research project, National Chemical Laboratory, Pune-India 2017

- Synthesis of antimalarial drugs
- Worked on azide alkyne coupling reaction (Click chemistry)
- Synthesis of sugar based building blocks for antimicrobial drugs.

Professional Activities

- **Review of Papers:**

Date	Journal	Reviewed
03/2024	Bulletin of Materials Science	3

Research Publications

1. **Birajdar, R. S.;** Gonnade, R. G.; Chikkali, S. H. Regulating the polyethylene microstructure by increasing steric crowding in naphthoxy imine-ligated Ni(II) complexes. *Polym. Chem.*, **2024**, *15*, 292-302.
2. **Birajdar, R. S.;** Bodkhe, D.; Gupta, P.; Shaikh, M. H.; Ramekar, R.; Chikkali, S. H. Emerging trends in olefin polymerization: a perspective. *J. Macromol. Sci. A*, **2023**, *60*(11), 731-750.
3. **Birajdar, R. S**; Gonnade, R. G.; Pol, H. V.; Basava Prabhu M.; Rokade, D.; Nandimatha, S.; Chikkali, S. H. Palladium-catalyzed polar solvent empowered

synthesis of hyper-branched ethylene oligomers and their applications. *Polym. Chem.*, **2023**, *14*, 3239-3251.

4. **Birajdar, R. S**.; Chikkali, S. H. Insertion copolymerization of functional olefins: Quo Vadis?. *Eur. Polym. J.*, **2021**, *143*, 110183.
5. **Birajdar, R. S**.; Khopade, K. V.; Chikkali, S. H. Depolymerization and repolymerization of polyethylene-like polymers. (*Manuscript under preparation).*
6. **Birajdar, R. S.;** Chikkali, S. H. Norbornene polymerization catalyzed by imine-phenoxy ligated palladium complexes. (*Manuscript under preparation).*
7. Chatterjee, D.; Sajeevan, A.; Jana, S.; **Birajdar, R. S.;** Chikkali, S. H.; Sivaram, S.; Gupta, S. S. Solvent-free hydroxylation of C-H bonds by Fe-complex: A green approach for activation of small molecules and macromolecules. *ChemRxiv*. **2024**; (doi:10.26434/chemrxiv-2024-7f3dr).
8. Gaikwad, S. R.; Patel, K.; Deshmukh, S. S.; Mote, N. R.; **Birajdar, R. S.**; Pandole, S. P.; Chugh, J.; Chikkali, S. H. Palladium-catalyzed insertion of ethylene and 1, 1-disubstituted difunctional olefins: an experimental and computational study. *ChemPlusChem*, **2020**, *85*(6), 1200-1209.
9. Khopade, K. V.; Sen, A.; **Birajdar, R. S.**; Paulbudhe, U. P.; Kavale, D. S.; Shinde, P. S.; Mhaske, S. B; Chikkali, S. H. Highly enantioselective synthesis of sitagliptin. *Asian J. Org. Chem.*, **2020**, *9*(2), 189-191.
10. Shaikh, M. H.; Ramekar, R. V.; Jawoor, S.; Dash, S. R.; **Birajdar, R. S.**; Pawal, S. B.; Thenmani, N.; Vanka, K.; Chikkali, S. H. Rational sesigning of imine thiophene-ligated Cr-complex and implication in ethylene polymerization. (*Manuscript communicated).*

Research Patents

1. Chikkali, S. H.; **Birajdar, R. S.** Synthesis of dibenzhydryl substituted phenoxy imine ligated Pd(II) and Ni (II) catalyst for ethylene (co)polymerization. **(IN2022-NF-0181).**
2. Chikkali, S. H.; Jawoor, S.; **Birajdar, R. S.**; Pawal, S. B.; Thenmani, N.; Chugh, P. Homogeneous single site catalyst and its use in preparing linear polyethylene. **EP4157527A1; JP2023529101A; US2023201815A1; WO2021240549A1.**

Book Chapter

1. Chikkali, S. H.; **Birajdar, R. S**.; Sivaram S. "Chemistry of Olefin Polymerization: Early Transition Metals"

Conferences

1. Attended and given flash talk along with poster in Alexander von Humboldt Foundation Kolleg, 2024 held at Bogmallo Beach Resort, Goa. "*Regulating the polyethylene microstructure by increasing steric crowding in naphthoxy imine-ligated Ni(II) complexes*". **Birajdar, R. S.;** Gonnade, R. G.; Chikkali, S. H.
2. Attended and given Oral presentation in 17th International Conference on Science and Technology, SPSI-MACRO-2023, held from December 10–13, 2023, hosted by Indian Institute of Technology Guwahati. "*Regulating the polyethylene microstructure by increasing steric crowding in naphthoxy imine-ligated Ni(II) complexes*". **Birajdar, R. S.;** Gonnade, R. G.; Chikkali, S. H.
3. Attended and presented poster 19th international Conference on Modern Trends in

Inorganic Chemistry, was held at Banaras Hindu University (BHU) in 2022. "*Palladium-catalyzed polar solvent empowered synthesis of hyper-branched ethylene oligomers and their applications.*" **Birajdar, R. S**; Gonnade, R. G.; Pol, H. V.; Basava Prabhu M.; Rokade, D.; Nandimatha, S.; Chikkali, S. H.

4. Attended and presented poster in 16th International Conference on Science and Technology of Polymers and Advanced Materials, SPSI-MACRO-2022, in CSIR-NCL, Pune. "*Palladium-catalyzed polar solvent empowered synthesis of hyper-branched ethylene oligomers and their applications.*" **Birajdar, R. S**; Gonnade, R. G.; Pol, H. V.; Basava Prabhu M.; Rokade, D.; Nandimatha, S.; Chikkali, S. H.

Personal Information

Full name	**:**	Rajkumar Swaminath Birajdar
Date of birth	**:**	30th June 1996
Gender	**:**	Male
Nationality	**:**	Indian
Marital Status	**:**	Single
Languages known	**:**	English, Hindi, Marathi, Kannada
Email	**:**	**birajdarraj30@gmail.com**
Permanent address	**:**	At- (Bori) Rampur, Post- (Bori) Umarge, Tal- Akkalkot, Dist- Solapur, Maharashtra, India, 413216.

Referees

1. Prof. Samir H. Chikkali
Senior Principal Scientist and Professor (AcSIR)
Polymer Science and Engineering Division, CSIR-National Chemical Laboratory
Dr. Homi Bhabha Road, Pune-411008, India
Email: s.chikkali@ncl.res.in / Phone: 91-20-2590-3145
Web: http://academic.ncl.res.in/s.chikkali
Associate Editor (Bulletin of Materials Science).

2. Dr. Ashootosh V. Ambade
Senior Scientist
Polymer Science and Engineering Division, CSIR-National Chemical Laboratory
Dr. Homi Bhabha Road, Pune - 411008
Email: av.ambade@ncl.res.in / Phone: 91-20-25903221.

3. Dr. Sakya S. Sen
Principal Scientist
Inorganic Chemistry and Catalysis Division, CSIR-National Chemical Laboratory,
Dr. Homi Bhabha Road, Pashan, Pune 411008
Email: ss.sen@ncl.res.in/ Tel: 0091-20-2590-2052
web: http://academic.ncl.res.in/ss.sen

I hereby declare that the information furnished above is true and complete to the best of my knowledge and behalf.

(Rajkumar S. Birajdar)

Polymer Chemistry

ROYAL SOCIETY OF CHEMISTRY

PAPER

View Article Online
View Journal | View Issue

Published on 21 June 2023. Downloaded by National Chemical Laboratory, Pune on 5/30/2024 3:00:06 PM.

Check for updates

Cite this: *Polym. Chem.*, 2023, **14**, 3239

Palladium-catalyzed polar solvent empowered synthesis of hyper-branched ethylene oligomers and their applications†

Rajkumar S. Birajdar, [a,b] Rajesh G. Gonnade, [b,c] Harshawardhan V. Pol, [a,b] Basava Prabhu M.,[a] Dhammaraj Rokade,[a,b] Sheetal Nandimath[a] and Samir H. Chikkali *[a,b]

In this contribution, we report the synthesis of two naphthoxy imine ligands, 2-(((2,6-dibenzhydryl-4-methoxyphenyl)imino)methyl)naphthalen-1-ol (**L1**) and 2-(((2,6-diisopropylphenyl)imino)methyl)naphthalen-1-ol (**L2**), with different steric and electronic features. **L1** and **L2** were treated with [(TMEDA)PdMe$_2$] to obtain the corresponding neutral palladium(II) complexes **Cat.1** and **Cat.2** in excellent yields. The identity of **Cat.1** and **Cat.2** was unambiguously ascertained using a combination of spectroscopic and analytical methods, including single-crystal X-ray diffraction. When exposed to 5 bar ethylene pressure, **Cat.1** produced hyperbranched ethylene oligomers. The microstructure analysis of ethylene oligomers confirmed the existence of methyl, ethyl, propyl, and sec-butyl branches, with a molecular weight (M_n) of 500–1400 g mol^{-1}, a PDI of 1.46–2.10, and 67–106 branches per 1000 carbon atoms. The use of a polar solvent, tetrahydrofuran, led to a remarkable 3-fold increase in oligomerization activity without compromising the branching and molecular weight. The resultant hyperbranched ethylene oligomers were selectively monofunctionalized using industrially practiced hydroformylation, ozonolysis, and epoxidation, almost quantitatively. The hydroxy functionalized ethylene oligomer (**F4**) (5 wt%) was melt-compounded with LLDPE and Nylon-6 to produce a tough yet flexible blend with a higher strain-to-failure as compared to an uncompatibilized blend.

Received 22nd March 2023,
Accepted 16th June 2023

DOI: 10.1039/d3py00311f

rsc.li/polymers

Introduction

Metal-catalyzed polymerization of olefins to polyolefins, such as polyethylene, polypropylene, *etc*. is well established, and today the world produces ~180 million tonnes of polyolefin per year.[1–4] The current polyolefin manufacturing technologies mainly use heterogeneous Ziegler-type catalysts with donors and additives.[5] Over the years, the interest in homogeneously catalyzed olefin polymerization has attracted significant attention as these catalysts may offer an opportunity to improve specific properties of the resultant polymer.[6,7] Transition metal-catalyzed functional olefin polymerization resulting in the formation of functional polyolefins represents one of the most important reactions.[8–11] Ziegler's initial work on homogeneous alkyl aluminum catalysts and ethylene produced low molecular weight ethylene oligomers, which led to the development of an industrial process named the "Alfol" process.[12–14] Apart from aluminium, nickel has been used to prepare ethylene oligomers. The commercial SHOP-type catalysts described in 1968 are the most noteworthy examples.[15] Since then, numerous other bidentate Ni-based catalysts have been reported.[16–19] Most of these catalysts produce highly linear ethylene oligomers.

However, the synthesis of low-molecular weight (M_w) ethylene oligomers with hyperbranched microstructures was very difficult to achieve using the above catalysts. Such hyperbranched ethylene oligomers can be used as functional additives in lubricants, surface treatments, compatibilizers, waxes, *etc*. For producing hyperbranched ethylene oligomers, the choice of catalysts is decisive. Catalysts with significant chain walking abilities can produce highly branched structures.[20] In 1995 Brookhart reported late metal catalysts based on Ni(II) and Pd(II) with bidentate α-diimine ligands [N,N] as efficient catalysts for ethylene polymerization.[21,22] These cationic com-

[a]*Polymer Science and Engineering Division, CSIR-National Chemical Laboratory, Dr. Homi Bhabha Road, Pune-411008, India. E-mail: s.chikkali@ncl.res.in*
[b]*Academy of Scientific and Innovative Research (AcSIR), Sector 19, Kamla Nehru Nagar, Ghaziabad 201002, U. P., India*
[c]*Center for Materials Characterization, CSIR-National Chemical Laboratory, Dr. Homi Bhabha Road, Pune-411008, India*

† Electronic supplementary information (ESI) available: Synthesis of ligands, palladium complex, ethylene oligomerization, postfunctionalization of ethylene oligomers, NMR spectra, ESI-MS-spectra, X-ray data, GPC data, tensile test data, *etc*. Crystal data for **Cat.1**. CCDC 2225185. For ESI and crystallographic data in CIF or other electronic format see DOI: https://doi.org/10.1039/d3py00311f

Published on 21 June 2023. Downloaded by National Chemical Laboratory, Pune on 5/30/2024 3:00:06 PM.

plexes display extensive chain walking during polymerization. Though the Pd-catalyst yields a highly branched structure, the molecular weight is high and produces an amorphous rubbery material.[21,23–26] In these α-diimine ligated metal catalysts, the bulky substituents on the ligand reduce the chain transfer and yield a high molecular weight polymer,[27–30] while less bulky substituents display low activity and produce hyperbranched low molecular weight oligomers.[31,32]

In the 1990s, metal complexes with salicylaldimine (phenoxy-imine) ligands were reported to be active in olefin polymerization.[33–36] After this discovery, researchers modified this ligand and investigated olefin polymerization, and phenomenal work has been done on ligand modification with early and late transition metals.[37,38] In 2014 Mecking and co-workers reported a neutral Ni(II) salicyldiminato complex that converts ethylene into a hyperbranched low molecular weight ethylene oligomer with high activity.[20]

Ethylene oligomers or polymers with <10 branches per 1000 carbon atoms are considered as low branching materials, those with 75–100 branches per 1000 carbon atom are considered as high branching materials, and those with >150 branches per 1000 carbon atom are termed ultrahigh branching materials.[39] Producing ethylene oligomers with a hyperbranched microstructure requires the catalysts to chain walk and display a high propensity for chain transfer. Catalysts that can chain walk without chain transfer will produce highly branched but high molecular weight polyethylene. Thus, synthesizing hyperbranched ethylene oligomers is challenging, and only a handful of catalysts could achieve this feat (Fig. 1, top).

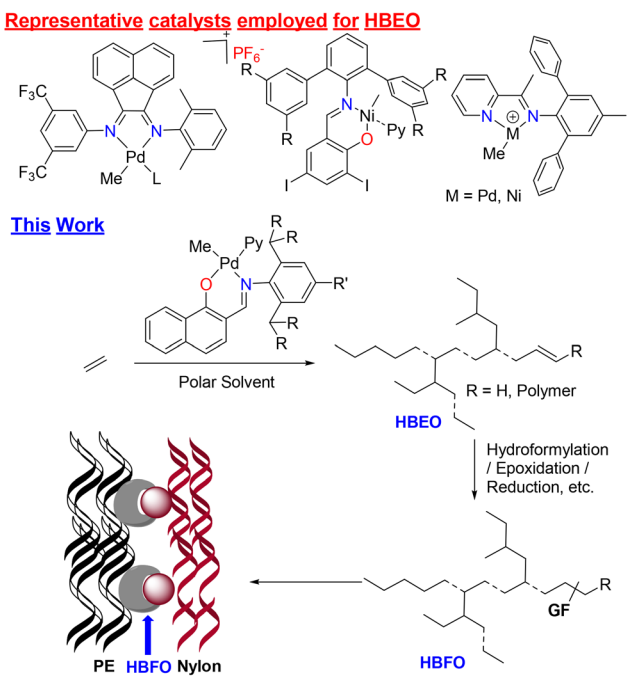

Fig. 1 Representative catalysts utilized in the synthesis of hyperbranched ethylene oligomers (HBEOs) (top) and this work (bottom), hyperbranched functionalized ethylene oligomers (HBFOs).

Herein we report a neutral Pd(II) naphthoxyimine ligated complex that produces hyperbranched ethylene oligomers (Fig. 1, bottom). Surprisingly, the use of polar solvents produced a highly active catalyst, tripling activity without affecting the branching and molecular weight. The resultant hyperbranched ethylene oligomer was functionalized using hydroformylation, epoxidation, *etc.*, and was found to be an excellent compatibilizer for two non-miscible polymers.

Results and discussion

Ligand synthesis

The synthesis of the starting aldehyde, 1-hydroxy 2-naphthaldehyde, is reported. We identified a single-step synthetic protocol, and 1-hydroxy 2-naphthaldehyde was prepared by modifying the literature procedure.[40] 1-Naphthol was treated with paraformaldehyde to obtain 1-hydroxy 2-naphthaldehyde (**1**) in 56% isolated yield (Scheme 1). The reaction between diphenyl methanol, *p*-anisidine and zinc chloride in HCl produced an aniline derivative **2**.[41]

The starting aldehyde **1** was treated with a 2,6-dibenzhydryl-4-methoxyaniline (**2**) in toluene, and the reaction mixture was refluxed for 6 hours. During the reflux, the color of the reaction mixture changed from dark brown to yellowish-brown. After completion of the reaction, the volatiles were evaporated, and the pure ligand 2-(((2,6-dibenzhydryl-4-methoxyphenyl) imino)methyl)naphthalen-1-ol (**L1**) was obtained in 69% isolated yield after column chromatography (Scheme 1). A proton NMR of the above solid revealed a characteristic singlet at 6.65 ppm (Fig. S2 and S6†), which can be easily assigned to an imine N=C–*H* proton. The proton NMR findings were further corroborated by ^{13}C NMR, which revealed an imine carbon at 168 ppm. Furthermore, the existence of **L1** was expressed using a combination of 1–2D NMR spectroscopy, and cross peaks confirmed the presence of compound **L1**. An IR of **L1** revealed the presence of an imine CN band at 1605 cm^{-1} and OH at 3385 cm^{-1}. The NMR and IR findings were corroborated by mass spectrometry analysis, which revealed a molecular ion peak at m/z = 610.27 Da $[M + H]^+$. The observed mass and isotopic pattern exactly match the simulated pattern (ESI Fig. S7†).

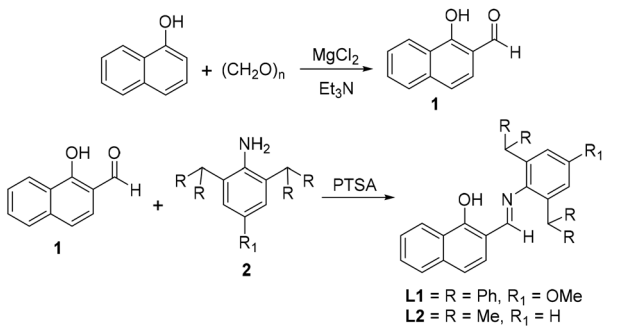

Scheme 1 Synthesis of ligands **L1** and **L2**.

This journal is © The Royal Society of Chemistry 2023

Published on 21 June 2023. Downloaded by National Chemical Laboratory, Pune on 5/30/2024 3:00:06 PM.

Along the same line, sterically less bulky ligand 2-(((2,6-diisopropylphenyl)imino)methyl)naphthalen-1-ol (**L2**) was prepared. Compound **1** was treated with 2,6-diisopropylaniline in toluene at 110 °C for 6 hours. After completion of the reaction, the desired ligand **L2** was purified by column chromatography in 51% isolated yield. The proton NMR spectrum of this compound disclosed a characteristic imine proton at 8.49 ppm, and the corresponding carbon appeared at 165 ppm in the ^{13}C NMR spectrum. The NMR data were further supported by an IR band at 1604 cm^{-1} (CN) and an ESI-MS molecular ion peak at m/z = 332.20 Da $[M + H]^+$.

Pd-complex synthesis

The naphthoxy imine ligand (**L1**) was treated with a palladium precursor [(TMEDA)PdMe$_2$] in pyridine (Scheme 2). The progress of the reaction was monitored by ^{1}H NMR, which revealed a signal at 0.44 ppm after 2 hours, indicating the completion of the reaction. The evaporation of unreacted pyridine and washing with hexane produced a solid compound with 69% isolated yield. The characteristic resonance at 0.44 ppm and the ^{13}C NMR peak at 1.9 ppm can be assigned to the Pd–Me group in **Cat.1**. The existence of **Cat.1** was further corroborated by short (HSQC) and long (HMBC) range C–H correlation spectra. ESI-MS also supported the presence of **Cat.1**, and a molecular ion peak was observed at m/z = 809.20 [**Cat.1** + H]$^+$ (ESI, Fig. S19†). The observed mass and isotopic pattern exactly match the simulated pattern. The existence of **Cat.1** was unambiguously ascertained by single crystal X-ray diffraction. Suitable crystals of **Cat.1** were obtained from a mixture of dichloromethane and hexane at 0 °C, and the structure of the resultant crystals was determined by X-ray diffraction. The palladium complex **Cat.1** crystalizes in a monoclinic unit cell in the space group $P2_{1/n}$. The single crystal consists of a central palladium atom with a bis-chelated naphthoxy imine ligand (**L1**), a coordinating pyridine, and a methyl group (Fig. 2). The geometry around the palladium is distorted square planar. The methyl group is placed *cis* to the imine nitrogen, while the pyridine is located *trans* to the imine nitrogen. The oxygen is trans to the methyl group. A Pd1–N2 (imine) distance of 2.01 Å confirms the formation of a coordinate bond, while a Pd1–O1 distance of 2.07 Å suggests the formation of a covalent bond.[42] The coordinating solvent pyridine revealed a Pd1–N1 distance of 2.03 Å. A C6–Pd1–N1 *cis* angle of 90.55° suggests that **Cat.1** can potentially initiate ethylene insertion and polymerization.

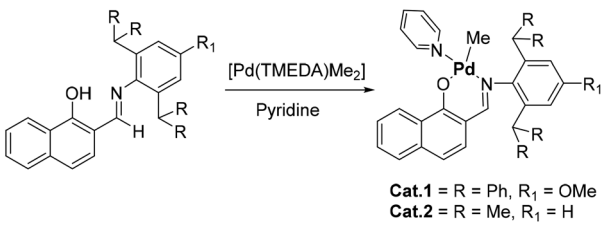

Scheme 2 Synthesis of palladium complexes **Cat.1** and **Cat.2**.

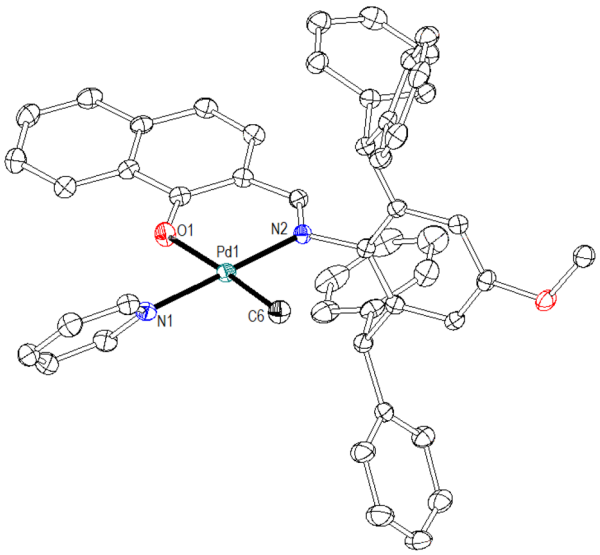

Fig. 2 Molecular structure of **Cat.1**. H-atoms have been omitted for clarity; thermal ellipsoids are drawn at the 50% probability level. Important bond distances and angles; Pd1–N2, 2.01 Å; Pd1–N1, 2.03 Å; Pd1–O1, 2.07 Å; N2–Pd1–O1, 91.70°; and C6–Pd1–N1, 90.55°; CCDC 2225185.

Along the same line, the naphthoxy imine ligand **L2** was treated with a palladium precursor [(TMEDA)PdMe$_2$] in pyridine (Scheme 2) to obtain the palladium complex **Cat.2**. **Cat.2** will allow us to investigate the effect of *ortho*-substituents on the imine arm. The existence of **Cat.2** was confirmed by spectroscopic and analytical methods. The ^{1}H NMR spectrum disclosed a singlet at 0.02 ppm which can be assigned to the Pd–Me protons. The corresponding methyl carbon was observed at 0.7 ppm. 1–2D NMR and ESI-MS data confirmed the presence of complex **Cat.2**. A similar palladium complex was reported earlier as a control catalyst. The literature protocol involves two steps; initially preparing a sodium salt of the ligand and then treating it with [Pd(COD)MeCl],[43,44] while we have used [Pd(TMEDA)Me$_2$] as a Pd-precursor and prepared **Cat.2** in one step.

Reactivity of Cat.1 with ethylene

Before we embark on polymerization, it was crucial to investigate the reactivity of **Cat.1** towards ethylene. This is especially necessary, as the previous report on a similar complex suggests that such catalysts are incapable of homopolymerizing ethylene.[44] In a high-pressure NMR tube experiment, **Cat.1** was dissolved in benzene-d$_6$, and the ^{1}H NMR spectrum was recorded. Subsequently, the NMR tube was charged with 4 bar of ethylene gas, and a proton NMR was recorded after 20 minutes, and 4 and 24 hours. As depicted in Fig. 3, the initial Pd–Me resonance at 1.00 ppm slowly disappears, with the concomitant appearance of methylene (–CH$_2$–) resonance at 1.47 ppm. These mechanistic investigations suggest that the ethylene inserts in a Pd–Me bond and **Cat.1** is capable of ethylene insertion and oligomerization or polymerization, even at room temperature.

Published on 21 June 2023. Downloaded by National Chemical Laboratory, Pune on 5/30/2024 3:00:06 PM.

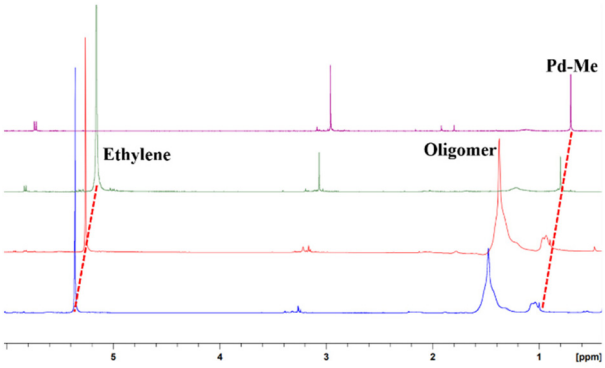

Fig. 3 Stacked high-pressure ^{1}H NMR spectra of **Cat.1** in the presence of 4 bar ethylene at 0 (top) and 20 minutes, and 4 and 24 hours (bottom) (at room temperature).

Ethylene oligomerization

As **Cat.1** was found to initiate ethylene insertion, we set out to test its performance in ethylene oligomerization. In our initial effort, **Cat.1** was exposed to 25 bar ethylene at 60 °C (Table 1, entry 1). After 90 minutes, the reaction was quenched (see the ESI† for details), and 0.171 g of highly viscous material was isolated. The ethylene oligomerization was performed at 70, 80, and 90 °C (Table 1, entries 2–4). As evident, the best yield of 0.385 g was observed at 80 °C (Table 1, entry 3), suggesting that this is an optimal reaction temperature. After optimizing the reaction temperature, we turned our attention to ethylene pressure. The same experiment as above was repeated at 25, 20, 15, 10, and 5 bars of ethylene (Table 1, entries 5–8). As the ethylene pressure decreased, the yield of the oligomer reduced. This could be due to the lower availability (concentration) of the ethylene monomer at lower pressure. Surprisingly, at 5 bar ethylene pressure, the highest yield of 0.452 g was obtained (Table 1, entry 8).

This could be due to the reduced rate of chain transfer to the monomer at lower ethylene pressure. The lower chain transfer may allow the ethylene to insert and grow into oligomers. The number of branches per 1000 carbon atom at 5 bar was found to be similar to those at a higher pressure (25–10 bars), suggesting that chain-walking is unaffected. The molecular weight was determined by NMR and GPC, and was found to be in the range of 500–1400 g mol^{-1}. The polydispersity is around 2, suggesting a well defined single-site catalyst.

The performance of **Cat.2** was examined in ethylene oligomerization. Under optimized conditions of 5 bar ethylene pressure, 80 °C temperature, and 90 minutes, **Cat.2** produced 0.194 g of ethylene oligomers (Table 1, entry 9). When ethylene pressure was increased to 10 bars, only 0.148 g of ethylene oligomer was obtained, while reducing the temperature to 60 °C further reduced the oligomer yield to 0.073 g. Interestingly, **Cat.2** disclosed higher branching (~90/1000 carbon atoms) as compared to **Cat.1** (Fig. 4). These observations suggest that **Cat.2** is susceptible to higher β-H transfer and is less active than **Cat.1**. Therefore, sterically hindered **Cat.1** potentially reduces β-H elimination and allows sufficient ethylene insertion to obtain hyperbranched ethylene oligomers. **Cat.2**, being sterically less demanding, shows higher branching than sterically hindered **Cat.1**. The electron-rich (relatively) **Cat.1** disclosed better activity and molecular weight as compared to

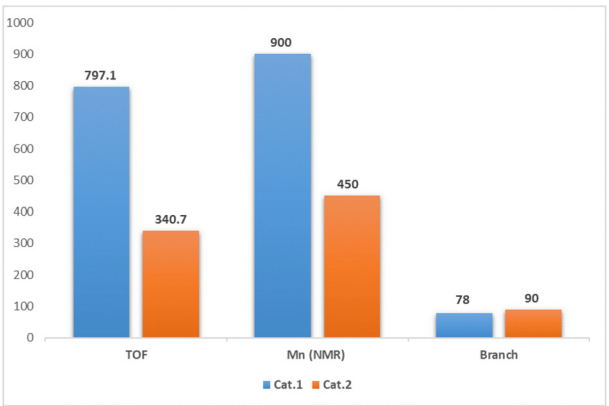

Fig. 4 Comparison of the TOF, molecular weight, and branches per 1000 carbon atoms for ethylene oligomers produced using **Cat.1** and **Cat.2**.

Table 1 Ethylene oligomerization using **Cat.1** and **Cat.2**[a]

Entry	Cat	Temperature (°C)	Pressure (bar)	Yield (g)	Branches per 1000 carbon atoms[b]	M_n[b] by NMR	TOF (h^{-1})
1	**Cat.1**	60	25	0.171	74	1350	301
2	**Cat.1**	70	25	0.206	67	1100	363
3	**Cat.1**	80	25	0.385	71	1000	679
4	**Cat.1**	90	25	0.168	76	800	296.2
5	**Cat.1**	80	20	0.298	85	950	525.5
6	**Cat.1**	80	15	0.240	87	1000	423.2
7	**Cat.1**	80	10	0.180	82	950	329.6
8	**Cat.1**	80	5	0.452	78	900	797.1
9	**Cat.2**	80	5	0.194	90	450	340.7
10	**Cat.2**	80	10	0.148	93	450	261
11	**Cat.2**	60	5	0.073	106	500	128.7

[a] Reaction conditions: toluene – 100 mL, catalyst – 13.6 μmol, time – 90 min, ethylene pressure – 5 to 25 bar, TOF in (mol of PE/mol of Pd h^{-1}); the reported yield is that obtained after subtracting the catalyst quantity from the final weight of the oligomers. [b] M_n & branches/1000 C-atoms was calculated using ^{1}H NMR (see the ESI for calculation and Fig. S31–S45† for oligomer NMR).

 This journal is © The Royal Society of Chemistry 2023

Published on 21 June 2023. Downloaded by National Chemical Laboratory, Pune on 5/30/2024 3:00:06 PM.

Cat.2. A comparative performance with respect to ToF, M_n, and branching is presented in Fig. 4.

Ethylene oligomer microstructure analysis

The microstructure of ethylene oligomers and polymers influences the properties and defines the application of the material.[45–47] Therefore, the resultant hyperbranched ethylene oligomers were subjected to detailed NMR analysis.[20] The ^{1}H NMR spectrum of an oligomer sample disclosed resonances at 5.78–5.85 ppm and 4.92–5.02 ppm. These can be assigned to terminal or chain end olefinic protons that are formed after the termination of a growing chain *via* β-H elimination (Fig. 5a). The other peak at 5.41 ppm (Fig. 5b) can be assigned to internal alkenes generated *via* the extensive chain walking of the catalyst. The minor resonances at 5.21 and 5.13 ppm can be assigned to substituted in-chain olefins such as c and d (Fig. 5). A broad resonance at 4.7 ppm may correspond to a rare olefinic peak, as depicted in e (Fig. 5).

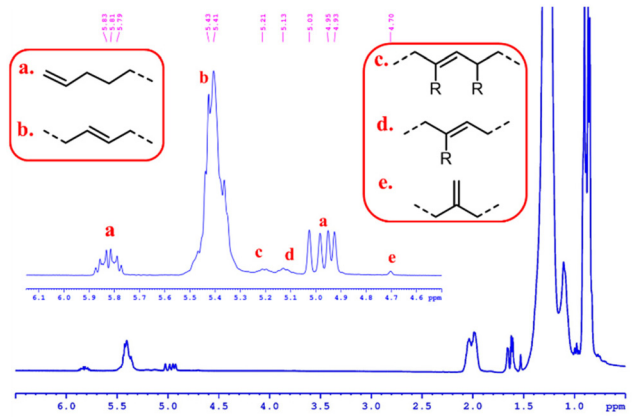

Fig. 5 ^{1}H NMR spectrum of the ethylene oligomer in $CDCl_3$ (olefinic region in sets).

^{13}C NMR spectroscopy is routinely used to determine branching in polyethylene and ethylene oligomers.[20,48–50] Therefore, the ^{13}C NMR spectra of the ethylene oligomers obtained in our studies were recorded and are depicted in Fig. 6. A resonance at 19.9 ppm can be assigned to a methyl branch, while peaks at 11.1 and 26.1 ppm can be ascribed to the ethyl branch. The ^{13}C NMR resonance at 14.8 ppm can be assigned to a methyl group in a propyl branch. Remarkably, the ^{13}C NMR spectra revealed the presence of *sec*-butyl groups at 19.4 and 11.6 ppm. The presence of these *sec*-butyl branches suggests the existence of branch-on-branch in the ethylene oligomers resulting in a hyperbranched microstructure. The ^{1}H–^{13}C HSQC NMR spectrum disclosed cross-peaks between olefinic protons and double-bond carbons, confirming the existence of internal and terminal double bonds (Fig. S32†). These hyperbranched ethylene oligomers are highly viscous fluids and do not show crystallization or melting transitions.

Ethylene oligomerization in polar solvents

Solvents or monomers that possess heteroatoms or functional groups can poison a catalyst in olefin polymerization.[37,51–57] Therefore, olefin polymerization is routinely carried out in hydrocarbon solvents without heteroatoms or functional groups. In fact, Marks and co-workers employed very nonpolar solvents to prepare highly branched ethylene oligomers.[58] However, a few recent reports suggest that the polar solvent may enable chain

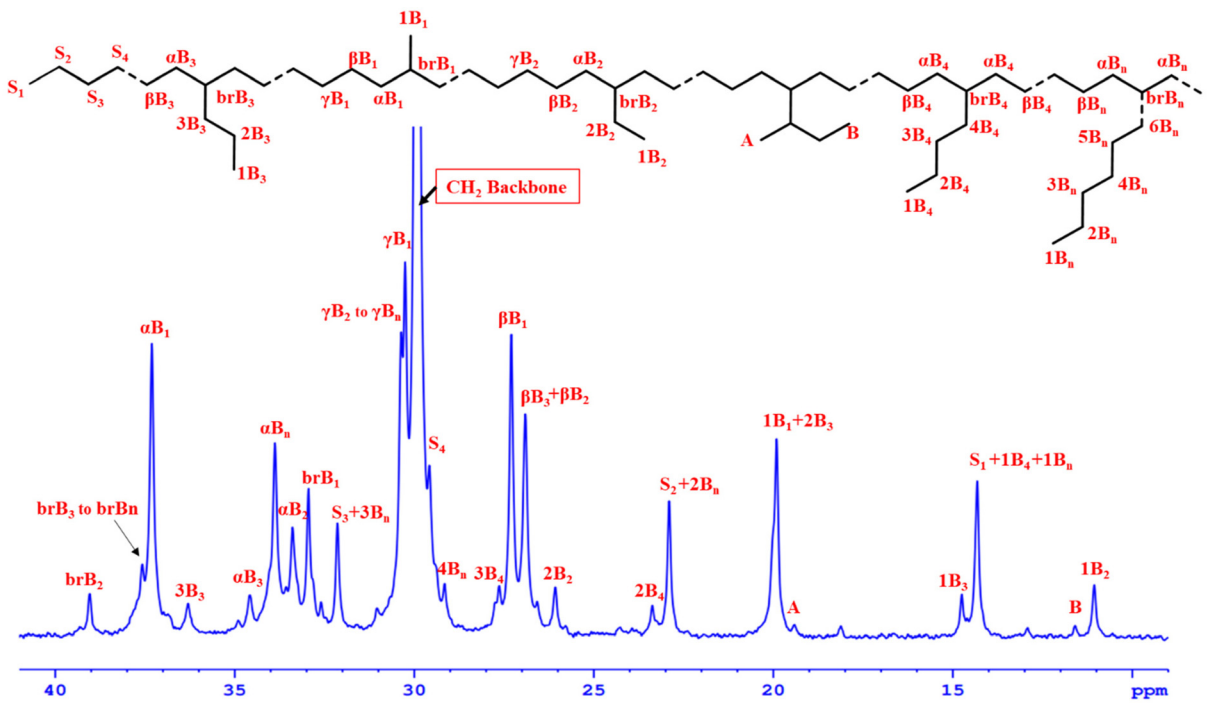

Fig. 6 ^{13}C NMR spectrum of the ethylene oligomer in $CDCl_3$.

Published on 21 June 2023. Downloaded by National Chemical Laboratory, Pune on 5/30/2024 3:00:06 PM.

growth and increase the molecular weight of polyethylene to ultrahigh molecular weight polyethylene (UHMWPE).[59–61] Although these reports do not provide a conclusive direction, the solvent seems to play a pivotal role in ethylene polymerization. In the backdrop of the above reports, we pondered if the solvent influences our ethylene oligomerization.

The effect of polar solvents on the activity, branching and molecular weight was examined, and Table 2 presents important results. When **Cat.1** was exposed to ethylene under optimized conditions in the polar solvent DME (dimethoxyethane), 0.655 g of ethylene oligomer was obtained. This is an increase of 44% yield of oligomers as compared to the highest yield achieved using nonpolar toluene (Table 1, entry 8). Similarly, **Cat.2** too displayed an increased yield in the presence of polar DME (Table 2, entry 2). Subsequently, 1,4-dioxane was used as a solvent, and a remarkable increase in the ethylene oligomer yield was observed (Table 2, entry 3).

Similar to DME and 1,4 dioxane, diethylether also produced 0.812 g of ethylene oligomer (Table 2, entry 5) while dichloromethane and acetonitrile were found to reduce the oligomer yield and TOF (Fig. 7). To our delight, the use of tetrahydrofuran (THF) as a solvent produced almost 3 times more ethylene oligomer yield under identical conditions (Table 2, entry 8). Unlike the increased molecular weight noted by Mecking and Jian in polar solvents,[60,61] the number average molecular weight remained in the ethylene oligomer range of 350–1250 g mol^{-1}, but the activity increased by multifold. The branching, too, did not change in THF and remained at 77–83 branches per 1000 C-atoms.

Understanding the effect of polar solvents

A three-fold increase in ethylene oligomerization activity in the presence of THF was unexpected. Therefore, understanding such effects is crucial for the further development of the field. To get more insight into the role of THF, we performed NMR tube experiments. An NMR tube was charged with **Cat.1** in C_6D_6, and proton NMR was recorded. The Pd–Me peak was observed at 1.00 ppm. When 50 equivalents of anhydrous THF was added to the above NMR tube, the Pd–Me resonance shifted upfield and appeared at 0.95 ppm. Although this is a small change in chemical shift, the observation suggests that THF competes with pyridine for metal coordination and might be in equilibrium (Scheme 3). To understand pyridine de-coordination further, **Cat.1** was treated with $B(C_6F_5)_3$ and 50 equivalents of THF was added to the NMR tube. Here, the Pd–Me resonance shifted further upfield and appeared at 0.92 ppm. The corresponding ^{11}B NMR disclosed a peak at −2.67 ppm, which can be assigned to the pyridine–$B(C_6F_5)_3$ adduct.[62] The formation of the pyridine–$B(C_6F_5)_3$ adduct suggests that pyridine is susceptible to de-coordination from the palladium center in the presence of an excess of polar solvent (THF), and a THF-coordinated intermediate is likely formed. The coordination of THF to the palladium center is weaker than pyridine, and therefore a [Pd·THF] adduct is proposed to be more active than the parent [Pd–Py] adduct (**Cat.1**). To validate this statement, we prepared a [Pd·THF] complex *in situ* using [Pd(COD)MeCl] and [(TMEDA)$PdMe_2$] precursors, and directly employed it for ethylene oligomerization (for details, see ESI† section 6.3). These *in situ* prepared [Pd·THF] complexes disclosed comparable activity to **Cat.1** in THF. These observations suggest that THF replaces pyridine from **Cat.1** *in situ* and generates a relatively more active [Pd·THF] catalyst. It is also proposed that the presence of an excess of THF (as a solvent) during the oligomerization reaction might stabilize the catalyst by forming a [Pd–X(THF)] species (see Scheme 3).[63]

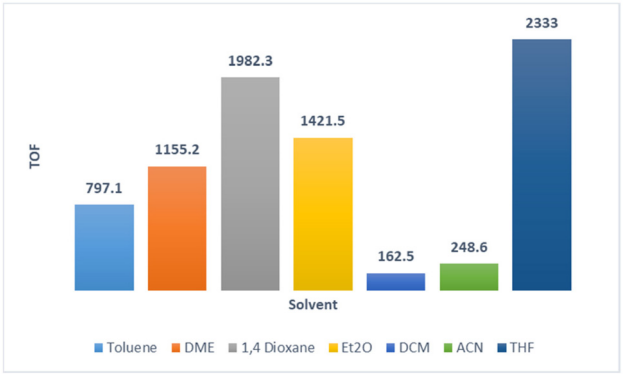

Fig. 7 Comparison of the TOF (for **Cat.1**) in polar and hydrocarbon solvents.

Table 2 Ethylene oligomerization in the presence of polar solvents[a]

Entry	Cat	Solvent	Yield (g)	Branches/1000 C-atoms	TOF (h^{-1})	M_n NMR
1	**Cat.1**	DME	0.655	78	1155.2	750
2	**Cat.2**	DME	0.466	86	821.8	350
3	**Cat.1**	1,4 Dioxane	1.124	75	1982.3	650
4	**Cat.2**	1,4 Dioxane	0.738	97	1301	350
5	**Cat.1**	Et_2O	0.812	100	1421.5	800
6[b]	**Cat.1**	DCM	0.092	100	162.5	1250
7	**Cat.1**	ACN	0.141	99	248.6	400
8	**Cat.1**	THF	1.323	77	2333	650
9	**Cat.2**	THF	0.612	83	1079	350

[a] Reaction conditions: solvent – 100 mL, catalyst – 13.6 μmol, time – 90 min, ethylene pressure – 5 bar, temperature – 80 °C, TOF in (mol of PE mol^{-1} of Pd h^{-1}), the reported yield is that obtained after subtracting the catalyst quantity from the final weight of the oligomer, branches per 1000 C-atoms was calculated using ^1H NMR (see the ESI for calculation and Fig. S49–S57† for oligomer NMR). [b] Reaction temperature was 45 °C. DME: dimethoxyethane; Et_2O: diethyl ether; DCM: dichloromethane; ACN: acetonitrile; and THF: tetrahydrofuran.

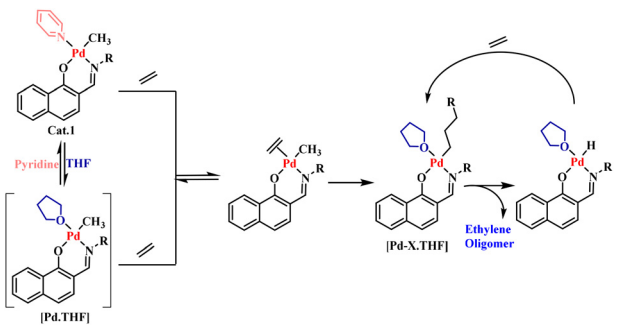

Scheme 3 Ethylene oligomerization in a polar solvent.

This journal is © The Royal Society of Chemistry 2023

Published on 21 June 2023. Downloaded by National Chemical Laboratory, Pune on 5/30/2024 3:00:06 PM.

Functionalization of the ethylene oligomer

The NMR analysis of the ethylene oligomers (Fig. 5) suggested the presence of internal and terminal double bonds. Due to extensive chain walking, internal double bonds were found to dominate the terminal double bond, and the ratio between the two was about 3 : 1, respectively. As such, a C=C double bond is an important functional group and is known to undergo several transformations. The presence of internal and terminal double bonds in ethylene oligomers offers tremendous potential for the post-polymerization functionalization of these oligomers. The resultant functionalized ethylene oligomers can be used as compatibilizers, in inks, and as interface active agents, adhesives, viscosity modifiers, nanoparticles, *etc.*[64]

Aldehydes and alcohols are versatile functional groups in organic synthesis. Therefore, the primary focus was to convert ethylene oligomers' internal and terminal double bonds into an aldehyde or alcohol. This can be easily achieved by ozonolysis, hydroformylation and epoxidation. Thus, the resultant ethylene oligomers were directly used for further functionalization without any purification. Ethylene oligomers were dissolved in dry dichloromethane and cooled to −78 °C and ozone gas was bubbled in the reaction mixture for 5 minutes. Excess ozone gas was vented, the round bottom flask was purged with argon, and the reaction was quenched by adding dimethyl sulfide.[65] Volatiles were evaporated using a high vacuum pump to yield aldehyde functionalized ethylene oligomer (**F1**) (Scheme 4).

The identity of the aldehyde product was confirmed by ^{1}H and ^{13}C NMR spectra. The proton NMR spectrum revealed a single peak at 9.76 ppm (Fig. S62†), while the ^{13}C NMR spectrum disclosed a resonance at 203.0 ppm (Fig. S63†) corresponding to the aldehydic group. The NMR findings were further corroborated by IR, which displayed a carbonyl stretching band at 1706 cm^{-1}, while THF GPC disclosed the molecular weight of the functionalized oligomer to be 1600 Da. Although ozonolysis produced an aldehyde, the molecular weight (GPC) was found to be lower than the starting HBEO. This is most likely due to the cleavage of internal double bonds in an ozonolysis reaction. Hydroformylation of the HBEO can produce the same aldehyde without sacrificing the molecular weight. Therefore, hydroformylation of ethylene oligomers was performed in the presence of [Rh(acac)(CO)$_2$] and triphenylphosphine in toluene.[66] The reaction was performed in a high-pressure autoclave at 10 bar syngas pressure and 100 °C temperature for 18 hours. This resulted in more than 99% conversion to product **F2** as observed by the ^{1}H NMR spectrum (Fig. S66A†). The ^{1}H NMR revealed three broad peaks in the deshielded region; the resonance at 9.76 ppm can be assigned to the linear aldehyde, and other peaks correspond to branched aldehydes (Fig. S66A†). As shown in Fig. S66B,† the olefinic peaks completely diminished, and new peaks were observed at 2.0–2.6 ppm, which corresponds to the C–H protons adjacent to the aldehyde. The ^{13}C NMR spectrum of the same sample displayed multiple peaks in the region of 203.2 to 205.9 ppm (Fig. S67†). These assignments are based on literature data for linear and branched aldehydes.[67–69]

The epoxide-functionalized ethylene oligomer (**F3**) was prepared by treating the ethylene oligomer with mCPBA in dichloromethane for 14 hours.[70] The conversion of an olefin into epoxide was confirmed by ^{1}H NMR spectroscopy. The protons next to epoxide–oxygen were observed between 2.48 and 3.09 ppm (Fig. S69†). While the corresponding ^{13}C NMR spectrum disclosed methylene carbon in the range of 45–60 ppm (Fig. S70†). The IR spectrum revealed an epoxide CO stretching band at 1215 cm^{-1}. Fig. 8 depicts the stacked ^{1}H NMR spectra of **F1**, **F2**, **F3**, and **F4**.

The aldehyde product (**F2**) obtained from the hydroformylation reaction was treated with sodium borohydride ($NaBH_4$) at 0 °C in methanol–toluene (1 : 1). After 14 hours of stirring at room temperature, the volatiles were evaporated, and oligomers were extracted using hexane. The aldehyde was fully (<99%) reduced to the corresponding hydroxyl functionalized

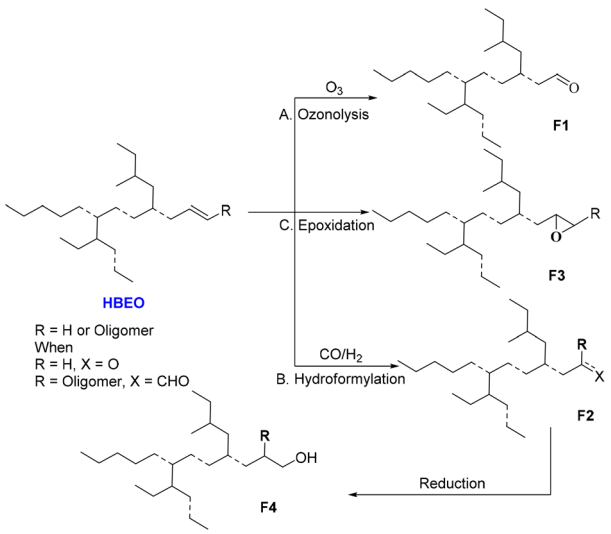

Scheme 4 Post oligomerization functionalization.

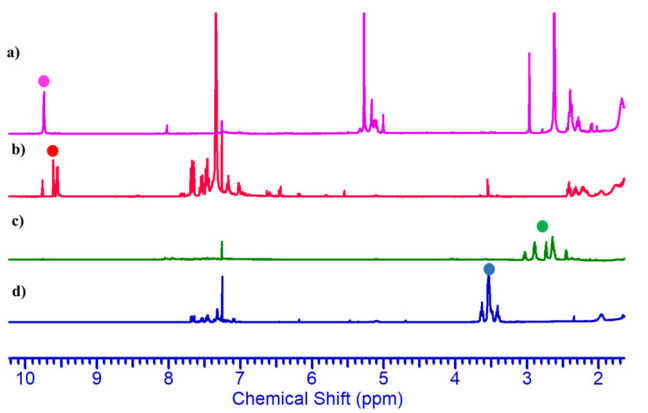

Fig. 8 Stacked ^{1}H NMR spectra of functionalized ethylene oligomers; (a) ozonolysis product (**F1**); (b) hydroformylation product (**F2**); (c) epoxide functionalized ethylene oligomer (**F3**); and (d) hydroxy functionalized oligomer (**F4**).

Published on 21 June 2023. Downloaded by National Chemical Laboratory, Pune on 5/30/2024 3:00:06 PM.

ethylene oligomer (**F4**) as confirmed by ^{1}H NMR spectroscopy (Fig. 8d). The proton NMR revealed that the aldehyde peaks disappeared, and new peaks appeared in the region of 3.39–3.77 ppm. These proton chemical shifts can be assigned to methylene groups generated after the reduction of the aldehyde to an alcohol (Fig. 8b *versus* d).

Functional oligomer as a compatibilizer

The presence of a polar functional group (OH), as well as a non-polar hydrophobic unit (methylene backbone) in the ethylene oligomer **F4**, will help to serve as a compatibilizer for two immiscible polymers, one polar and the other non-polar.[71] We choose linear low density polyethylene (LLDPE) as the non-polar polymer and Nylon-6 as a polar polymer. A DSM MICRO 5 twin screw micro-compounder was used to melt-compound the two polymers with and without the presence of the compatibilizer (**F4**) at a screw RPM of 100 at 250 °C for 5 minutes. Prior to melt compounding, the materials were dried in a vacuum oven at 80 °C for 4 hours to remove any traces of moisture. Additionally, 2000 ppm of anti-oxidant (Irganox 1010 from BASF) was added to prevent any thermal degradation during processing. The material ratios are shown in Table 3. The non-polar LLDPE was obtained from Reliance Ind. Ltd (grade: F18020), while the polar polymer Nylon-6 was obtained from Honeywell (grade Aegis H73QP). The melt mixed or compounded blends were molded into tensile specimens in a DSM micro injection molding machine and subjected to tensile testing at room temperature. Minimum 5–6 samples were tested for each blend formulation. Representative tensile test data are plotted below for the compatibilized and non-compatibilized blend samples (Fig. 9 bottom). It is clear from the tensile test data that while the uncompatibilized blend formulation displays a higher tensile strength, the compatibilized blend formulation displays equivalent Young's modulus and, more importantly, higher strain-to failure *vis-à-vis* that for uncompatibilized blend formulation. The toughness of the blends increases upon increasing the compatibilizer content and reaches an optimum at 5 wt% (see Table 3).

The small dip (around 0.5 mm/mm) in the tensile stress–strain data is the point where the clip-on extensometer was physically removed and the test was continued. It is evident that the functionalized ethylene oligomer **F4** as a compatibilizer played an important role in creating a tough yet flexible blend formulation that will also have good applications in packaging requiring a good oxygen barrier property in addition to the water vapor barrier.

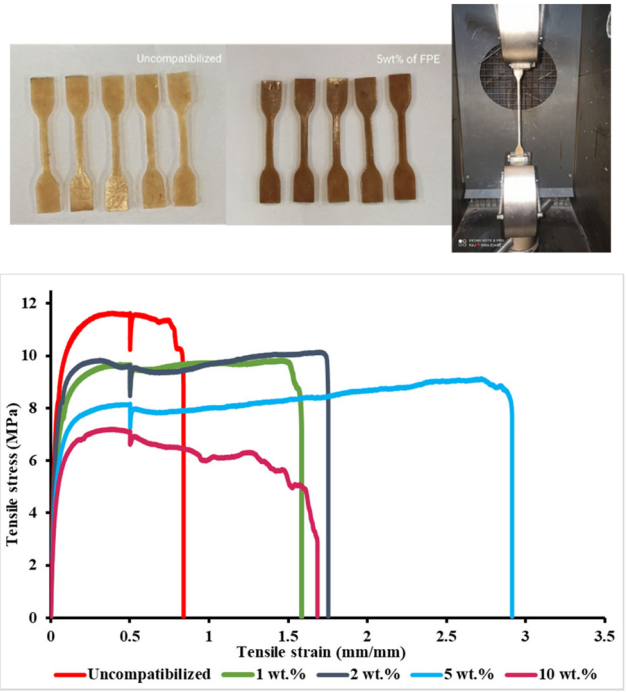

Fig. 9 Polymer compatibility study; specimen for the tensile test (top); stress *versus* strain data (bottom).

The enhanced performance of the blend can be ascribed to the compatibilizing property of the functionalized ethylene oligomer **F4**. It is proposed that the hydroxyl group in **F4** forms a hydrogen-bonding interaction with Nylon-6 and the alkyl chain mixes with LLDPE (Fig. 10 top), leading to a compatible blend. The proposed interactions are based on literature reports for PE–PLA blends with functional polyethylene.[72,73] The blend morphologies of the compatibilized (5 wt%) and uncompatibilized blends were characterized by SEM analysis (Fig. 10, bottom). The particle size of the dispersed phase is smaller in compatibilized blends (~200 nm) compared to the uncompatibilized blends (~800 to 900 nm). The void between the dispersed nylon phase and the PE matrix caused during cryofracturing due to poor interfacial adhesion is clearly visible in uncompatibilized blends. Similarly, due to poor interfacial adhesion in uncompatibilized blends, the nylon phase is pulled away from the PE matrix. In the case of compa-

Table 3 Wt% formulation of LLDPE, Nylon-6 and compatibilizer (**F4**)

Sr. no	LLDPE wt%	Nylon 6 wt%	Compatibilizer wt%	Tensile strength at break (MPa)	Young's modulus (MPa)	Strain-to-failure (mm mm^{-1})	Toughness (J mm^{-2})
1	80	20	0	9.8 ± 0.9	422 ± 13	1.0 ± 0.17	9.08
2	79	20	1	9.6 ± 0.31	327 ± 9	1.6 ± 0.19	14.77
3	78	20	2	10.5 ± 0.68	362 ± 30	1.8 ± 0.36	16.80
4	75	20	5	8.5 ± 0.15	294 ± 17	2.3 ± 0.8	24.07
5	70	20	10	2.3 ± 0.65	282 ± 21	1.4 ± 0.32	10.38

 This journal is © The Royal Society of Chemistry 2023

Published on 21 June 2023. Downloaded by National Chemical Laboratory, Pune on 5/30/2024 3:00:06 PM.

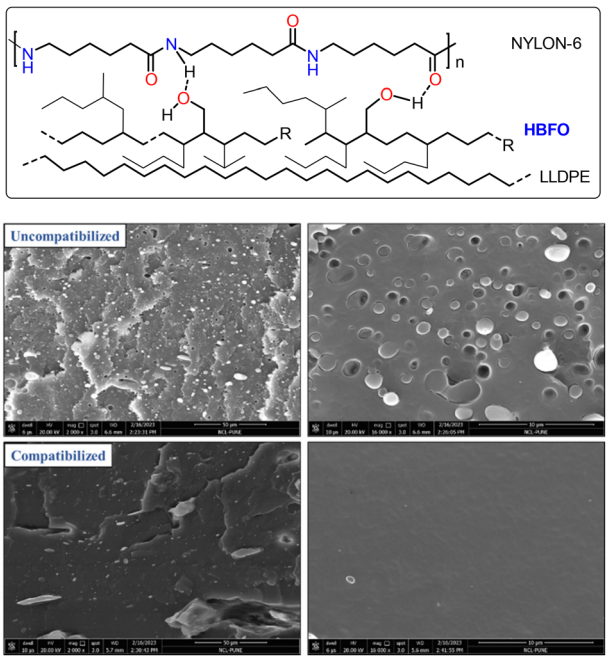

Fig. 10 Proposed hydrogen-bonding interaction between Nylon-6 and the HBFO **F4** (top); SEM images of the uncompatibilized and compatibilized polymer blend.

tibilized blends, the interfacial adhesion is increased, leading to a homogeneous phase (Fig. 10, bottom-left).

Conclusions

In summary, 1-hydroxy 2-naphthaldehyde was treated with aniline derivatives to obtain 2-(((2,6-dibenzhydryl-4-methoxyphenyl)imino)methyl)naphthalen-1-ol (**L1**) and 2-(((2,6-diisopropylphenyl)imino)methyl)naphthalen-1-ol (**L2**). Ligands **L1** and **L2** were isolated in good to excellent yields (51–69%). Ligand **L1** was treated with [Pd(TMEDA)Me_2] in pyridine to obtain the corresponding palladium complex **Cat.1** in a 69% isolated yield. The identity of **Cat.1** was established using a combination of 1–2D NMR, IR, and mass spectroscopy. Single crystal X-ray diffraction unambiguously ascertained the coordination of **L1** to palladium and the existence of **Cat.1**. **Cat.2** was prepared along the same lines and was isolated in 89% yield. **Cat.1** and **Cat.2** were treated with ethylene, and their performance in ethylene oligomerization was examined. Initial screening using **Cat.1** suggested that 5 bar ethylene pressure, 80 °C temperature, and 90 minutes are the optimal conditions to obtain the highest ToF of 797 mol of PE/mol of Pd h^{-1}. The molecular weight was found to be 500–1400 g mol^{-1}, with PDIs of 1.46–2.10 and 71–106 branches per 1000 C-atoms. Detailed microstructure analysis revealed the existence of branch-on-branch or hyperbranched ethylene oligomers. **Cat.2** was also active and produced hyperbranched ethylene oligomers but was less reactive than **Cat.1**.

To our surprise, **Cat.1** was thrice more active in polar THF than in non-polar toluene under identical conditions. Interestingly, though the productivity increased to a 3 times higher level, the molecular weight remained in the oligomer range, and the branching remained unchanged. The resultant hyperbranched ethylene oligomers were almost quantitatively functionalized to the corresponding aldehydes, alcohols, and epoxides using industrially practiced transformations. The hydroxy functionalized hyperbranched ethylene oligomer **F4** was used as a compatibilizer. The addition of 5 wt% of **F4** to non-polar LLDPE and polar Nylon-6 produced a tough yet flexible blend with higher strain-to-failure as compared to an uncompatibilized blend. This is, most likely, the first report on the use of a functionalized hyperbranched ethylene oligomer as a compatibilizing agent.

Experimental section

Methods and materials

Unless noted otherwise, all manipulations were carried out under an inert atmosphere using standard Schlenk line techniques or an M-Braun glove box. Toluene, diethyl ether, 1,4-dioxane, dimethoxyethane, and THF were distilled from sodium/benzophenone under an argon atmosphere. Acetonitrile, methylene chloride, and pyridine were distilled on calcium hydride. Ethylene (3.5 grade) was supplied by Praxiar India Ltd, India. 1-Naphthol, diisopropyl aniline, and *m*-chloroperbenzoic acid were supplied by Loba Chemie and were used as received. Sodium borohydride was supplied by Avra Synthesis Pvt. Ltd and was used as received. *p*-Anisidine and paraformaldehyde were supplied by Alfa Aesar and were used as received. [$PdMe_2$(TMEDA)],[74] 1-hydroxy 2-napthaldehyde,[40] and aniline derivatives[41] were synthesized following known procedures. The insertion polymerization was run in a Büchi Glas Uster cyclone 075 high-pressure reactor equipped with an overhead mechanical stirrer, a heating/cooling jacket, and pressure regulators.

Solution NMR spectra were recorded using Bruker Avance 200, 400 and 500 MHz instruments. Chemical shifts are referenced to the external reference TMS (^{1}H and ^{13}C). Coupling constants are given as absolute values. Multiplicities are given as follows: s: singlet, d: doublet, t: triplet, and m: multiplet. Mass spectra were recorded using a Thermo Scientific Q-Exactive mass spectrometer; column specification: a Hypersil GOLD C18 column of 150 × 4.6 mm diameter, 8 μm particle size, and the mobile phase used is 90% methanol +10% water +0.1% formic acid. Infrared (IR) spectra were recorded using a Bruker Alpha II instrument and Fourier transform infrared spectrometer as a thin film. Gel Permeation Chromatography (GPC) was performed on a system equipped with an isocratic pump (Viscotek VE 1122 pump) and a differential refractometer (DRI) detector (Viscotek VE 3580 RI). For GPC with THF as the eluent, separations were performed using serially connected size exclusion columns (two T6000M, General Mixed Organic 8 × 300 mm, from Viscotek) at 25 °C

Published on 21 June 2023. Downloaded by National Chemical Laboratory, Pune on 5/30/2024 3:00:06 PM.

and at a flow rate of 1.0 mL min^{-1}, and molecular weights were determined from the calibration curve generated from narrow polystyrene standards. A DSM MICRO 5 twin screw microcompounder was used for compounding LLDPE, Nylon-6. Tensile specimens were prepared using a DSM micro injection molding machine. Tensile testing was done using a universal testing machine (Instron 33R4204). Single crystal X-ray diffraction measurement of **Cat.1** was carried out on a Bruker D8 VENTURE Kappa Duo PHOTON II CPAD diffractometer equipped with Incoatech multilayer mirrors optics. The intensity measurements were carried out with a Mo micro-focus sealed tube diffraction source (MoKα = 0.71073 Å) at 100 K. The X-ray generator was operated at 50 kV and 1.4 mA. SEM data were recorded using an FEI-NOVA NANO 450 Field Emission Scanning Electron Microscope (FESEM).

Synthesis of 2-(((2,6-dibenzhydryl-4-methoxyphenyl)imino) methyl)naphthalen-1-ol (L1). In an oven-dried Schlenk flask, 1-hydroxy 2-naphthaldehyde (0.5 g, 2.90 mmol) and 2,6-dibenzhydryl-4-methoxyaniline (1.32 g, 2.90 mmol) were dissolved in 25 mL of toluene, and a catalytic amount of PTSA (15 mg, 0.087 mmol) was added. The resulting reaction mixture was refluxed for 6 hours at 120 °C (bath temperature). The reaction mixture was cooled to room temperature, the volatiles were evaporated, and the resultant residue was purified by column chromatography (1% ethyl acetate and 99% petroleum ether) to yield an orange-colored compound (1.22 g, 69%).

^{1}H NMR (500 MHz, $CDCl_3$) δ = 14.35 (br. s., 1 H), 8.42 (d, J = 7.6 Hz, 1 H), 7.64 (d, J = 7.9 Hz, 1 H), 7.59–7.50 (m, 1 H), 7.50–7.43 (m, 1 H), 7.25 (d, J = 7.6 Hz, 1 H), 7.21–7.12 (m, 12 H), 7.01 (d, J = 6.6 Hz, 7 H), 6.92 (d, J = 8.5 Hz, 1 H), 6.65 (br. s., 1 H), 6.45 (s, 2 H), 6.18 (s, 1 H), 5.56 (br. s., 2 H), 3.53 (s, 3 H). **^{13}C NMR (125 MHz, $CDCl_3$)** δ = 168.0, 165.3, 156.8, 143.1, 138.9, 138.3, 136.4, 129.7, 129.6, 129.2, 128.6, 128.4, 127.6, 127.4, 126.8, 126.5, 125.3, 124.3, 116.9, 114.2, 110.8, 55.2, 52.7. **ESI-MS** (positive mode): m/z = 610.27 Da $[M + H]^+$ (observed); 610.27 Da $[M + H]^+$ (calculated).

Synthesis of 2-(((2,6-diisopropylphenyl)imino)methyl) naphthalen-1-ol (L2). In an oven-dried Schlenk flask 1-hydroxy 2-naphthaldehyde (1 g, 0.0058 mol) was added along with 30 mL of toluene. 2,6-diisopropyl amine (1.02 g, 0.0058 mol) was added to the above solution along with a catalytic amount of PTSA (10 mg, 0.058 mmol). The resultant reaction mixture was refluxed for 6 hours at 110 °C. The reaction mixture was cooled to room temperature, and the volatiles were evaporated. The obtained crude product was purified using column chromatography (1% ethyl acetate and 99% petroleum ether) to produce a yellowish-color compound (872 mg, 50.57%).

^{1}H NMR (400 MHz, $CDCl_3$) δ = 14.61 (m, 1 H), 8.49 (d, J = 8.0 Hz, 1 H), 8.16 (d, J = 2.6 Hz, 1 H), 7.72 (d, J = 8.1 Hz, 1 H), 7.58 (t, J = 7.4 Hz, 1 H), 7.54–7.47 (m, 1 H), 7.25–7.15 (m, 5 H), 3.10 (td, J = 6.8, 13.7 Hz, 2 H), 1.20 (d, J = 6.9 Hz, 12 H). **^{13}C NMR (100 MHz, $CDCl_3$)** δ = 167.2, 165.0, 142.9, 140.9, 136.8, 129.8, 127.6, 127.6, 127.2, 126.6, 125.7, 124.6, 123.7, 117.5, 111.0, 28.5, 23.8. **ESI-MS** (positive mode): m/z = 332.20 Da $[M + H]^+$ (observed); 332.20 $[M + H]^+$ Da (calculated).

Synthesis of Cat.1. In an oven-dried Schlenk flask, ligand **L1** (200 mg, 0.328 mmol) and $[Pd(TMEDA)Me_2]$ (82.74 mg, 0.328 mmol) were dissolved in 5 mL of pyridine. The resulting reaction mixture was stirred at room temperature for 2 hours. The pyridine was evaporated to dryness. Next, the second batch of pyridine (5 mL) was added to the above residue, and the content was stirred for another 1 hour. Pyridine was evaporated to dryness. The above step was performed again, and finally, the resultant residue was dried under a high vacuum to pull out excess pyridine. The thus obtained crude product was washed with hexane (5 mL × 2), and dried to produce a pure yellow-colored Pd-complex, **Cat.1** (183 mg, 68.9%).

^{1}H NMR (500 MHz, $CDCl_3$) δ = 9.04 (dd, J = 1.5, 6.4 Hz, 2 H), 8.35 (d, J = 8.2 Hz, 1 H), 7.92 (s, 1 H), 7.57–7.50 (m, 3 H), 7.48 (s, 1 H), 7.33–7.27 (m, 5 H), 7.25–7.19 (m, 6 H), 7.09–7.01 (m, 10 H), 6.51 (s, 2 H), 6.45 (d, J = 8.5 Hz, 1 H), 6.29 (s, 2 H), 5.94 (s, 1 H), 5.51 (d, J = 8.9 Hz, 1 H), 3.61 (s, 3 H), 0.44 (s, 3 H). **^{13}C NMR (125 MHz, $CDCl_3$)** δ = 167.8, 166.8, 156.5, 152.8, 143.8, 143.8, 142.7, 139.7, 138.0, 137.6, 132.1, 130.1, 129.9, 129.7, 128.5, 128.3, 128.3, 127.1, 126.4, 125.7, 124.9, 123.8, 113.8, 112.4, 111.7, 55.2, 52.3, 1.9. **ESI-MS** (positive mode): m/z = 809.20 Da $[M + H]^+$ (observed); 809.23 Da $[M + H]^+$ (calculated).

Synthesis of Cat.2. In a Schlenk flask, ligand **L2** (150 mg, 0.452 mmol) and $[Pd(TMEDA)Me_2]$(114.07 mg, 0.452 mmol) were dissolved in 5 mL of pyridine. The resulting reaction mixture was stirred at room temperature for 2 hours. The pyridine was evaporated to dryness, and again 5 mL of pyridine was added and stirred for another 1 hour. Then the pyridine was evaporated to dryness. The above step was performed once again, and finally, the resultant residue was dried under a high vacuum to remove unreacted pyridine. The thus obtained crude product was washed with hexane (5 mL × 2), and dried to produce a pure green colored Pd-complex, **Cat.2** (214 mg, 89.1%).

^{1}H NMR (500 MHz, $CDCl_3$) δ = 8.91–8.89 (m, 2 H), 8.35–8.33 (m, 1 H), 7.84 (tt, J = 1.6, 7.7 Hz, 1 H), 7.75 (s, 1 H), 7.61–7.58 (m, 1 H), 7.48 (dt, J = 1.4, 7.4 Hz, 1 H), 7.44–7.40 (m, 2 H), 7.33–7.28 (m, 1 H), 7.24–7.17 (m, 3 H), 7.09–7.04 (m, 1 H), 6.84 (d, J = 8.5 Hz, 1 H), 3.68–3.54 (m, 2 H), 1.32 (d, J = 6.7 Hz, 6 H), 1.11 (d, J = 7.0 Hz, 6 H), 0.02 (s, 3 H). **^{13}C NMR (125 MHz, $CDCl_3$)** δ = 167.7, 164.8, 152.7, 149.0, 141.6, 138.0, 137.6, 131.7, 130.2, 128.9, 127.3, 126.4, 125.8, 124.8, 124.3, 123.4, 113.1, 112.3, 27.9, 25.0, 22.9, 0.7. **ESI-MS** (positive mode): m/z = 531.16 Da $[M + H]^+$ observed; 531.16 Da $[M + H]^+$, calculated.

General procedure for ethylene oligomerization

The oligomerization reaction was carried out in a 250 mL stainless steel high-pressure Büchi (Glas Uster cyclone 075) reactor equipped with a heating/cooling jacket and mechanical stirrer. Prior to the experiment, the reactor was fully dried by heating it in a vacuum at 90 °C for 1 hour, followed by cooling it to room temperature and filling it with argon. The reactor was maintained at the desired reaction temperature, and was purged with ethylene gas. To this, 100 mL of dried and freshly distilled solvent (toluene or other solvents) was added under

 This journal is © The Royal Society of Chemistry 2023

Published on 21 June 2023. Downloaded by National Chemical Laboratory, Pune on 5/30/2024 3:00:06 PM.

positive ethylene pressure. Subsequently, the solvent was stirred under ethylene pressure for 30 minutes to dissolve ethylene. A suitable amount of catalyst was injected into the reactor using a syringe under positive ethylene pressure. Next, the reactor was pressurized to the desired ethylene pressure by rapid stirring, and the desired ethylene pressure was maintained throughout the reaction. After the completion of polymerization, excess ethylene was vented, and the solvent was evaporated under a high vacuum to yield highly viscous semi-solid ethylene oligomers. The yield is determined after subtracting the initial weight of the catalyst, and the resultant oligomers were characterized by various methods. Table 1 presents a summary of the most important runs using **Cat.1** and **Cat.2**.

Synthesis of F1. In a round bottom flask, the ethylene oligomer (250 mg) was dissolved in 30 mL of DCM and cooled to −78 °C (using acetone and dry ice). Ozone gas was bubbled in the reaction mixture for 5 minutes; after that RB was purged with argon gas, and dimethyl sulfide was added dropwise to the reaction mixture with vigorous stirring. The reaction mixture was allowed to warm to ambient temperature, and DCM was evaporated using a high vacuum pump to yield a chain-end functionalized ethylene oligomer (228 mg). A single peak at 9.76 ppm in a proton NMR spectrum was observed for the chain terminal aldehyde.

Synthesis of F2. The ethylene oligomer (1.19 g), [Rh(acac)$(CO)_2$] (15 mg, 0.0581 mmol) and triphenylphosphine (30.4 mg, 0.116 mmol) were weighed in the vial, and 10 mL of toluene was added. The reaction vial was placed in a high-pressure autoclave and immediately pressurized with syngas (15 bar) after purging three times. Finally, the reactor was pressurized with 10 bar of syngas, and the temperature was increased to 100 °C for 18 hours with constant stirring. After completion of the reaction, the reactor was cooled to room temperature, and syngas pressure was released. Toluene was evaporated, and the resultant crude product was subjected to NMR analysis. 10 mL of hexane was added to the above crude reaction mixture, and the content was stirred for 5 minutes. The resultant solution was filtered, and the filtrate was evaporated. This process was repeated twice to obtain a highly viscous compound **F2** (1.2 g).

Synthesis of F3. In a round bottom flask, 200 mg of ethylene oligomer was dissolved in 20 mL of dichloromethane. The reaction mixture was cooled to 0 °C, and mCPBA [50–55% (80 mg)] was added. Subsequently, the mixture was allowed to reach ambient temperature and was further stirred for 14 hours. A saturated solution of sodium hydrogen carbonate was added to the reaction mixture and stirred for 10 minutes. The organic layer was washed three times with $NaHCO_3$ and dried over Na_2SO_4. DCM was evaporated using a rotary evaporator to obtain a colorless oil (176 mg).

Synthesis of F4. The hydroformylation product (1.2 g) obtained from the above reaction mixture was directly used in this step. Methanol (1 : 1) was added to a toluene solution of the functionalized ethylene oligomer **F2**, and the mixture was cooled to 0 °C. Next, sodium borohydride ($NaBH_4$) (110 mg) was added with vigorous stirring and was allowed to warm to room temperature. It was further stirred for 14 hours at room temperature. The solvent was evaporated, and 10 mL of hexane was added; the resultant mixture was stirred for 5 minutes. The hexane layer was decanted in another round bottom flask, and hexane was evaporated to produce **F4** (1.048 g). The formation of a hydroxyl functionalized ethylene oligomer was confirmed by ^{1}H NMR spectroscopy. It was found that the aldehyde peaks diminished, and new peaks appeared in the 3.6 ppm region.

Conflicts of interest

There are no conflicts to declare.

Acknowledgements

We gratefully acknowledge the financial support from DST-SERB (CRG/2021/005385), CSIR-NCL (HCP46), and DSIR (CRTDH@NCL) India. RSB is thankful to DST for the DST-INSPIRE fellowship (DST/INSPIRE Fellowship/2018/IF180787). We would like to thank Dr Seena Joseph for the SEM data analysis.

References

1 S. H. Chikkali, *Metal-Catalyzed Polymerization: Fundamentals to Applications*, CRC Press, Taylor and Francis Group, USA, 2017.
2 M. Stuerzel, S. Mihan and R. Muelhaupt, *Chem. Rev.*, 2016, **116**, 1398–1433.
3 K. Patel, S. H. Chikkali and S. Sivaram, *Prog. Polym. Sci.*, 2020, **109**, 101290.
4 C. Chen, *Nat. Rev. Chem.*, 2018, **2**, 6–14.
5 J. Boor Jr., *Ziegler-Natta Catalysts and Polymerization*, Academic Press, New York, 1979.
6 A. Shamiri, M. H. Chakrabarti, S. Jahan, M. A. Hussain, W. Kaminsky, P. V. Aravind and W. A. Yehye, *Materials*, 2014, **7**, 5069–5108.
7 G. Zanchin and G. Leone, *Prog. Polym. Sci.*, 2021, **113**, 101342.
8 C. Tan and C. Chen, *Angew. Chem., Int. Ed.*, 2019, **58**, 7192–7200.
9 N. M. G. Franssen, J. N. H. Reek and B. de Bruin, *Chem. Soc. Rev.*, 2013, **42**, 5809–5832.
10 R. S. Birajdar and S. H. Chikkali, *Eur. Polym. J.*, 2021, **143**, 110183.
11 A. Nakamura, S. Ito and K. Nozaki, *Chem. Rev.*, 2009, **109**, 5215–5244.
12 K. Ziegler, H. G. Gellert, K. Zosel, E. Holzkamp, J. Schneider, M. Söll and W. R. Kroll, *Justus Liebigs Ann. Chem.*, 1960, **629**, 121–166.

Published on 21 June 2023. Downloaded by National Chemical Laboratory, Pune on 5/30/2024 3:00:06 PM.

13 K. Noweck and W. Grafahrend, *Fatty alcohols.* Ullmann's encyclopedia of industrial chemistry, Wiley-VCH, Weinheim, Germany, 2006.
14 Z. Wang, *Ziegler alcohol synthesis*, John Wiley & Sons, Inc., 2010.
15 W. Keim, *Angew. Chem., Int. Ed.*, 2013, **52**, 12492–12496.
16 P. Kuhn, D. Semeril, D. Matt, M. J. Chetcuti and P. Lutz, *Dalton Trans.*, 2007, 515–528.
17 V. C. Gibson and S. K. Spitzmesser, *Chem. Rev.*, 2003, **103**, 283–316.
18 H. Mu, L. Pan, D. Song and Y. Li, *Chem. Rev.*, 2015, **115**, 12091–12137.
19 H. Olivier-Bourbigou, P. A. R. Breuil, L. Magna, T. Michel, M. F. Espada Pastor and D. Delcroix, *Chem. Rev.*, 2020, **120**(15), 7919–7983.
20 T. Wiedemann, G. Voit, A. Tchernook, P. Roesle, I. GöttkerSchnetmann and S. Mecking, *J. Am. Chem. Soc.*, 2014, **136**, 2078–2085.
21 L. K. Johnson, C. M. Killian and M. Brookhart, *J. Am. Chem. Soc.*, 1995, **117**, 6414–6415.
22 L. K. Johnson, S. Mecking and M. Brookhart, *J. Am. Chem. Soc.*, 1996, **118**, 267–268.
23 J. M. Rose, A. E. Cherian and G. W. Coates, *J. Am. Chem. Soc.*, 2006, **128**, 4186–4187.
24 D. Yan, C. Gao and H. Frey, *Hyperbranched Polymers: Synthesis, Properties, and Applications*, Wiley, Hoboken, 2011.
25 B. I. Voit and A. Lederer, *Chem. Rev.*, 2009, **109**, 5924–5973.
26 M. Calderon, M. A. Quadir, S. K. Sharma and R. Haag, *Adv. Mater.*, 2010, **22**, 190–218.
27 D. P. Gates, S. A. Svejda, E. Oñate, C. M. Killian, L. K. Johnson, P. S. White and M. Brookhart, *Macromolecules*, 2000, **33**, 2320–2334.
28 R. Wu, W. K. Wu, L. Stieglitz, S. Gaan, B. Rieger and M. Heuberger, *Coord. Chem. Rev.*, 2023, **474**, 214844.
29 Y. Zhang, Y. Zhang and Z. Jian, *Polymer*, 2023, **265**, 125578.
30 M. Qasim, M. S. Bashir, S. Iqbal and Q. Mahmood, *Eur. Polym. J.*, 2021, **160**, 110783.
31 L. Deng, T. K. Woo, L. Cavallo, P. M. Margl and T. Ziegler, *J. Am. Chem. Soc.*, 1997, **119**, 6177–6186.
32 P. Xiang, Z. Ye and R. Subramanian, *Polymer*, 2011, **52**, 5027–5039.
33 T. Fujita, Y. Tohi, M. Mitani, S. Matsui, J. Saito, M. Nitabaru, M. Sugi and H. Makio, EP-0874005, 1997.
34 L. K. Johnson, A. M. Bennett, S. D. Ittel, L. Wang, A. Parthasarathy, E. Hauptman, R. D. Simpson, J. Feldman and E. B. Coughlin, *WO Patent* 1998030609A1, 1998.
35 D. A. Bansleben, S. K. Friedriich, T. D. Younkin, R. H. Grubbs, C. Wang and R. T. Li, *WO Patent* 1998042664A1, 1998.
36 C. Wang, S. Friedrich, T. R. Younkin, R. T. Li, R. H. Grubbs, D. A. Bansleben and M. W. Day, *Organometallics*, 1998, **17**, 3149–3151.
37 H. Makio, H. Terao, A. Iwashita and T. Fujita, *Chem. Rev.*, 2011, **111**, 2363–2449.
38 M. C. Baier, M. A. Zuideveld and S. Mecking, *Angew. Chem., Int. Ed.*, 2014, **53**, 9722–9744.
39 Y. Zhang, Y. Zhang, X. Hu, C. Wang and Z. Jian, *ACS Catal.*, 2022, **12**, 14304–14320.
40 See the ESI for details.† Synthesis of 1-naphthols is reported in the following paper and reference therein. Compound **1** was synthesized based on the clues presented in this paper. L. Cai, X. Zhu, J. Chen, A. Lin and H. Yao, *Org. Chem. Front.*, 2019, **6**, 3688–3692.
41 S. Meiries, K. Speck, D. B. Cordes, A. M. Z. Slawin and S. P. Nolan, *Organometallics*, 2013, **32**, 330–339.
42 M. Kang and A. Sen, *Organometallics*, 2005, **24**, 3508–3515.
43 Y. Chen, S. Mandal and A. Sen, *Organometallics*, 2010, **29**, 3160–3168.
44 F. Y. Pong, S. Mandal and A. Sen, *Organometallics*, 2014, **33**, 7044–7051.
45 D. Meinhard, M. Wegner, G. Kipiani, A. Hearley, P. Reuter, S. Fischer, O. Marti and B. Rieger, *J. Am. Chem. Soc.*, 2007, **129**, 9182–9191.
46 L. Guo, S. Dai, X. Sui and C. Chen, *ACS Catal.*, 2016, **6**, 428–441.
47 I. D'Auria, M. Maggio, G. Guerra and C. Pellecchia, *Macromolecules*, 2017, **50**, 6586–6594.
48 Z. Guan, P. M. Cotts, E. F. McCord and S. J. McLain, *Science*, 1999, **283**, 2059–2062.
49 L. Falivene, T. Wiedemann, I. Göttker-Schnetmann, L. Caporaso, L. Cavallo and S. Mecking, *J. Am. Chem. Soc.*, 2018, **140**, 1305–1312.
50 H. Fan, G. Chang, H. Bi, X. Gui, H. Wang, G. Xu and S. Dai, *ACS Polym. Au*, 2022, **2**, 88–96.
51 J. Chen, Y. Gao and T. J. Marks, *Angew. Chem., Int. Ed.*, 2020, **59**, 14726–14735.
52 T. R. Younkin, E. F. Connor, J. I. Henderson, S. K. Friedrich, R. H. Grubbs and D. A. Bansleben, *Science*, 2000, **287**, 460–462.
53 F. A. Hicks, J. C. Jenkins and M. Brookhart, *Organometallics*, 2003, **22**, 3533–3545.
54 T. Friedberger, P. Wucher and S. Mecking, *J. Am. Chem. Soc.*, 2012, **134**, 1010–1018.
55 Y. Zhang, H. Mu, L. Pan, X. Wang and Y. Li, *ACS Catal.*, 2018, **8**, 5963–5976.
56 G. R. Jones, H. E. Basbug Alhan, L. J. Karas, J. I. Wu and E. Harth, *Angew. Chem., Int. Ed.*, 2021, **60**, 1635–1640.
57 Y. Zhang and Z. Jian, *Macromolecules*, 2021, **54**, 3191–3196.
58 Y. Gao, J. Chen, Y. Wang, D. B. Pickens, A. Motta, Q. J. Wang, Y. W. Chung, T. L. Lohr and T. J. Marks, *Nat. Catal.*, 2019, **2**, 236–242.
59 D. Guironnet, T. Rünzi, I. Göttker-Schnetmann and S. Mecking, *Chem. Commun.*, 2008, 4965–4967.
60 P. Kenyon, M. Wörner and S. Mecking, *J. Am. Chem. Soc.*, 2018, **140**, 6685–6689.
61 C. Wang, X. Kang, H. Mu and Z. Jian, *Macromolecules*, 2022, **55**, 5441–5447.
62 S. J. Geier, A. L. Gille, T. M. Gilbert and D. W. Stephan, *Inorg. Chem.*, 2009, **48**, 10466–10474.

 This journal is © The Royal Society of Chemistry 2023

Published on 21 June 2023. Downloaded by National Chemical Laboratory, Pune on 5/30/2024 3:00:06 PM.

63 P. S. Hanley and J. F. Hartwig, *J. Am. Chem. Soc.*, 2011, **133**, 15661–15673.
64 Y. Chen, L. Wang, H. Yu, Y. Zhao, R. Sun, G. Jing, J. Huang, H. Khalid, N. M. Abbasi and M. Akram, *Prog. Polym. Sci.*, 2015, **45**, 23–43.
65 V. Mamane, A. B. García, J. D. Umarye, T. Lessmann, S. Sommer and H. Waldmann, *Tetrahedron*, 2007, **63**, 5754–5767.
66 P. Dydio, R. J. Detz and J. N. Reek, *J. Am. Chem. Soc.*, 2013, **135**, 10817–10828.
67 S. S. Nurttila, P. R. Linnebank, T. Krachko and J. N. H. Reek, *ACS Catal.*, 2018, **8**, 3469–3488.
68 S. Pandey and S. H. Chikkali, *ChemCatChem*, 2015, **7**, 3468–3471.
69 S. Pandey, D. R. Shinde and S. H. Chikkali, *ChemCatChem*, 2017, **9**, 3997–4004.
70 C. Kim, T. G. Traylor and C. L. Perrin, *J. Am. Chem. Soc.*, 1998, **120**, 9513–9516 and the references therein.
71 J. Feng, G. Zhang, K. Maclnnis, Z. Li, A. Olah and E. Baer, *J. Polym. Sci., Part B: Polym. Phys.*, 2019, **57**, 281–290.
72 C. Tan, C. Zou and C. Chen, *Macromolecules*, 2022, **55**, 1910–1922.
73 Y. Na and C. Chen, *Angew. Chem., Int. Ed.*, 2020, **59**, 7953–7959.
74 W. De Graaf, J. Boersma, W. J. Smeets, A. L. Spek and G. Van Koten, *Organometallics*, 1989, **8**, 2907–2917.

Polymer Chemistry

ROYAL SOCIETY OF CHEMISTRY

PAPER

View Article Online
View Journal | View Issue

Published on 06 December 2023. Downloaded by National Chemical Laboratory, Pune on 5/30/2024 3:00:58 PM.

Check for updates

Cite this: *Polym. Chem.*, 2024, **15**, 292

Regulating the polyethylene microstructure by increasing steric crowding in naphthoxy imine-ligated Ni(II) complexes†

Rajkumar S. Birajdar, [a,b] Rajesh G. Gonnade [b,c] and Samir H. Chikkali *[a,b]

Received 6th September 2023,
Accepted 4th December 2023

DOI: 10.1039/d3py01010d

rsc.li/polymers

Ligands play a prominent role in ethylene polymerization. However, it is a highly challenging task to regulate branching through ligand modifications. Here we report the synthesis of systematically sterically tailored naphthoxy imine-ligated nickel complexes (**Ni1**, **Ni2**, and **Ni3**), their performance in ethylene polymerization, and how the ligand steric controls branching in the resultant PE. **Ni1–Ni3** were prepared in one step with an excellent yield (73–93%). The identity of these complexes was unambiguously ascertained using ^{1}H, ^{13}C, 2D NMR spectroscopy, mass analysis, and single-crystal X-ray diffraction. The molecular structure revealed a *cis* arrangement of alkyl/aryl and donor groups (C–Ni–D), which is necessary for initiating ethylene polymerization. Buried volume contours suggested **Ni3** to be sterically the most bulky among the three. When exposed to ethylene, the three nickel complexes **Ni1**, **Ni2**, and **Ni3** produced polyethylene with excellent activity. As predicted by buried volume calculations, dibenzhydryl-substituted **Ni3** outperformed sterically less crowded **Ni1** and **Ni2**. Careful analysis of the resultant PE disclosed that sterically less encumbered **Ni1** and **Ni2** produce PE with high branching (43–54 branches/1000-C atoms) density. However, the bulkiest **Ni3** revealed much lower branching (28 branches/1000-C atoms) and a high TOF of 35 400 mol of PE per mol of Ni per h, along with a high molecular weight of PE (61 000 Da). The steric bulk in **Ni3**, most likely, reduces chain-walking and thus lowers branching in the resultant PE. As compared to the literature-reported analogous **Pd1** catalyst, the **Ni3** catalyst discloses high TOF, high molecular weight, and less branched, linear polyethylene.

Introduction

Polyolefins are the largest volume polymers produced in the world and nearly 180 million tons of polyolefins are manufactured annually.[1–4] Polyethylene (PE) and polypropylene (PP) are produced on an industrial scale using Ziegler–Natta-type catalysts, with few exceptions.[5] In the Ziegler–Natta-type heterogeneous catalysts, Ti is the active metal, which is highly oxophilic in nature and gets easily poisoned even in the presence of a small amount of polar groups.[6,7] In order to address this challenge, researchers moved to late-transition metals, which are less oxophilic and show more tolerance to functional groups.[8] In 1995, Brookhart and coworkers demonstrated ethylene and α-olefin copolymerization catalyzed by Ni(II) and Pd(II) complexes bearing sterically hindered α-diimine ligands.[9,10] Also, the Pd(II) catalyst was able to incorporate polar comonomers into the polyethylene chain for the first time. The most distinctive property of these catalysts is the chain-walking process, which leads to the formation of highly branched polyolefins. This seminal work opened doors to a flood of publications and several ligand and catalyst modifications have been reported to date.[11–19]

In these late-transition metal catalysts, controlling the ratio of chain walking/chain transfer to chain propagation is crucial. This ratio determines the branching, crystallinity, and molecular weight of the resultant polyolefin.[13,20–24] The steric bulk of the ligand undisputedly plays a pivotal role in regulating chain walking and chain transfer with respect to chain propagation.[25–29] Furthermore, steric bulk has a significant influence on the thermal stability and polymerization activity of the catalyst.[16,30] Among several other sterically bulky groups, the dibenzhydryl moiety is commonly used to modify α-diimine ligated Ni(II) or Pd(II) complexes.[16,31–39]

[a]*Polymer Science and Engineering Division, CSIR-National Chemical Laboratory, Dr. Homi Bhabha Road, Pune-411008, India. E-mail: s.chikkali@ncl.res.in*
[b]*Academy of Scientific and Innovative Research (AcSIR), Sector 19, Kamla Nehru Nagar, Ghaziabad 201002, U. P., India*
[c]*Center for Materials Characterization, CSIR-National Chemical Laboratory, Dr. Homi Bhabha Road, Pune-411008, India*

†Electronic supplementary information (ESI) available: Synthesis of ligands, nickel complexes, ethylene polymerization, NMR spectra, ESI-MS-spectra, X-ray data, GPC data, and crystal data. CCDC 2285806 (**Ni1**), 2285654 (**Ni2**) and 2225186 (**Ni3**). For ESI and crystallographic data in CIF or other electronic format see DOI: **https://doi.org/10.1039/d3py01010d**

This journal is © The Royal Society of Chemistry 2024

Published on 06 December 2023. Downloaded by National Chemical Laboratory, Pune on 5/30/2024 3:00:58 PM.

The dibenzhydryl-substituted catalysts are robust and yield PE with a high molecular weight and low branch density.[40] Both the thermal stability of the α-diimine-ligated catalysts and the molecular weight of the resulting PE are significantly improved by the incorporation of a large dibenzhydryl moiety.[38,39,41] The α-diimine-ligated Pd(II) complex containing the dibenzhydryl group yields a semicrystalline polymer, with significantly reduced branching.[39,41–46] In 2016, Chen and coworkers prepared a series of sterically modified α-diimine-ligated Pd(II) complexes. It was demonstrated that with an increase in steric bulk, the molecular weight increases, activity increases, and branching reduces (see Fig. 1).[26] Along the same line, Min Chen and coworkers demonstrated the influence of ligand steric bulk on the catalytic activity, molecular weight, and polymer microstructure in *ortho*-dibenzhydryl or *ortho-sec*-phenyl-substituted α-diimine nickel catalysts.[47] It was observed that the dibenzhydryl-substituted species exhibits higher activity [(0.98–1.58) × 10^6 g per mol Ni per h], high polymer molecular weight [M_n: (8.0–13.1) × 10^5 g mol^{-1}] and low branch density (55–64 per 1000 C) compared to the methyl-substituted nickel complexes [activity ((0.63–0.44) × 10^6 g per mol Ni per h), molecular weight (M_n: (0.8–0.6) × 10^5 g mol^{-1}) and branch density (90–95 per 1000 C)]. Along with steric bulk, the ligand symmetry also plays an important role in controlling the polymer microstructure. Recently, Dai and coworkers prepared dibenzobarrelenedione and dibenzhydrylaniline-ligated α-diimine Ni(II) complexes.[48] Complexes with a quasi-centrosymmetric structure produced semi-crystalline polyethylene with a very high molecular weight and low branching densities (11–34 per 1000 C). However, a plane-symmetric complex, having similar steric bulk, produced a highly branched polymer (110–115 per 1000 C) with no obvious melting point under identical polymerization conditions.

Literature reports suggest that the bulkiness of the *N*-aryl moiety (imine) and substituents at the *ortho* position to the O-donor group play a crucial role in phenoxy imine-ligated metal catalysts. These two groups help to increase the molecular weight by retarding the chain transfer process and β-hydride elimination, and increase the polymerization activity by avoiding the formation of an inactive bis-ligated complex.[49–52] In 2014, Brookhart and coworkers produced branched ultrahigh-molecular-weight polyethylene using a sterically-hindered 2,8-diaryl naphthyl-substituted salicylaldimine ligated Ni(II) complex.[53] Along with steric bulk, the electronic effect of the ligand can considerably affect the polymerization activity. Therefore, Marks and coworkers studied the effect of fluorine substituents on ethylene polymerization and found that the CF_3-substituted catalyst shows higher stability and catalytic activity compared to the CH_3-substituted catalyst.[54] Furthermore, the resultant polymers revealed a high molecular weight and low branch density (for CF_3: M_w = 9.2 × 10^4 and branching = 7 per 1000 C; for CH_3: M_w = 1.4 × 10^3 and branching = 88 per 1000 C). The authors proposed a weak interaction between the C–F of the ligand and the C–H of the growing polymer chain, which suppresses the β-H elimination reaction. In 2022, Jian and coworkers reported a sterically-hindered sandwich-like neutral salicylaldiminato nickel catalyst having 8-aryl naphthyl and dibenzosuberyl groups as *N*-aryl moieties. This nickel catalyst yields linear UHMWPE at a high temperature of 90 °C.[55] Thus, the effect of steric bulk on ethylene polymerization has been investigated for mainly two types of ligand systems, namely, α-diamine (Fig. 1E and F) and phenoxy-imine (Fig. 1A–D). Such an in-depth understanding and analysis are missing for the naphthoxy-imine counterparts.

Here, we report the synthesis of three systematically sterically tuned naphthoxy-imine ligated Ni(II) complexes and examine their performance in ethylene polymerization. It turns out that the sterically bulky, dibenzhydryl-substituted naphthoxy-imine ligated Ni(II) catalyst outperforms its less bulky counterpart catalysts. The dibenzhydryl-substituted naphthoxy-imine ligated Ni(II) catalyst revealed the highest activity. The resultant polymer showed a high molecular weight, high melting temperature, and lowest branching among the polymers produced by the three catalysts.

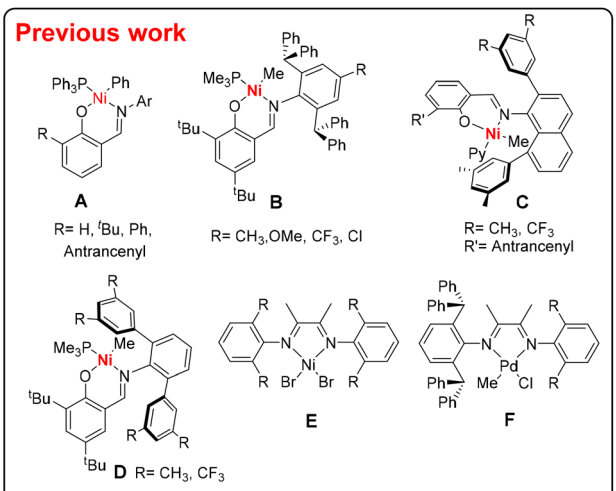

Complex E

R	Me	$CHPh_2$
Activity x 10^6	0.53-0.76	0.98-1.58
Branch	90-95	55-64
Mn x 10^5	20.6-0.8	8.0-13.1

Complex F

R	H	Me	$CHMe_2$	$CHPh_2$
Activity x 10^5	0.77-1.32	1.66-2.61	2.74-4.13	5.76-8.85
Branch	116-117	94-96	76-77	25-27
Mn x 10^4	0.23-0.42	27.3-40.3	38.4-52.8	147.1-164.6

Fig. 1 Sterically demanding catalysts (representative) for ethylene polymerization (top).

Results and discussion

Ligand synthesis

Ligand **L1** was prepared by treating 1-hydroxy 2-naphthaldehyde with commercially available 2,4,6-trimethyl aniline in the presence of a catalytic amount of *p*-toluenesulfonic acid (PTSA) (Scheme 1). After refluxing for 6 hours at 120 °C in toluene,

Published on 06 December 2023. Downloaded by National Chemical Laboratory, Pune on 5/30/2024 3:00:58 PM.

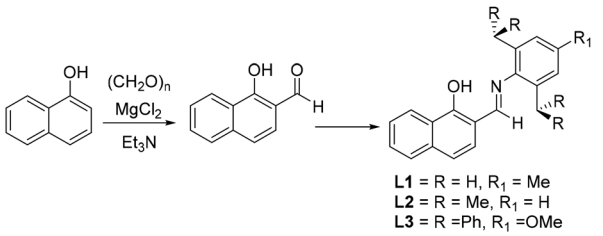

Scheme 1 Synthesis of ligands **L1**, **L2**, and **L3**.

the ^{1}H NMR spectra were recorded. The starting aldehyde peak slowly diminished with the consequent appearance of a new peak (imine proton) at 8.51 ppm (ESI, Fig. S1†), suggesting the completion of the reaction. The synthesized ligand was characterized using ^{1}H, ^{13}C, and ESI-MS analyses. The corresponding imine carbon was observed at 163.4 ppm (ESI, Fig. S2†) in the ^{13}C NMR spectrum. Sterically hindered ligands **L2** and **L3** were prepared on a gram scale using our methodology reported earlier.[56]

Synthesis of Ni complexes

The ligands were deprotonated using an excess of sodium hydride in tetrahydrofuran as a solvent. The solvent was evaporated under high vacuum, and the resultant sodium salts of ligands can be directly used for complex synthesis. The sodium salts of ligands were treated with an appropriate amount (1 equiv.) of nickel precursor (*trans* [NiCl(*o*-Tol)(PPh_3)$_2$]) leading to the formation of complexes (**Ni1–Ni3**). The formation of the Ni complex was monitored by ^{31}P NMR spectroscopy. The reduction in the ^{31}P peak intensity of the Ni precursor and concomitant appearance of a new peak for the Ni complex, along with de-coordinated triphenylphosphine (at around −6 ppm), suggested the formation of the desired Ni complex. The identity of **Ni1–Ni3** was established using 1D and 2D NMR spectroscopy along with ESI-MS. The ^{31}P NMR spectrum of **Ni1** disclosed a singlet phosphorus peak at 25.19 ppm (ESI, Fig. S5†). The ^{1}H NMR spectrum revealed an imine proton at 7.85 ppm and the corresponding imine carbon was observed at 164.8 ppm in the ^{13}C NMR spectrum. The 2D (^{1}H–^{1}H NOESY) NMR spectroscopy showed a cross-peak of the imine proton to that of the methyl group on *o*-tolyl (substituent on the ligand).

The **Ni2** complex was thoroughly characterized using ^{31}P, ^{1}H, ^{13}C, and 2D NMR spectroscopy. A singlet phosphorus peak at 25.2 ppm (ESI, Fig. S15†) was observed. The ^{1}H NMR spectrum showed an imine proton at 7.92 ppm and an imine carbon at 165.2 ppm (ESI, Fig. S16 and 17†). Also, the ^{1}H–^{1}H NOESY spectrum revealed that diisopropylic CH shows a correlation with *o*-tolyl, confirming the complex formation.

The presence of the **Ni3** complex was confirmed by 1–2D NMR spectroscopy. The ^{31}P NMR spectrum disclosed a singlet at 22.8 ppm (ESI, Fig. S24†). The ^{1}H NMR spectrum showed a singlet at 3.07 ppm (ESI, Fig. S25†) that can be assigned to the methyl of the *o*-tolyl group. The imine proton was found to be shifted to a shielded region (as compared to **L3**) and appeared at 5.67 ppm (ESI, Fig. S25†). The presence of an imine carbon was confirmed by ^{13}C NMR spectroscopy which appeared at 168.5 ppm (ESI, Fig. S26†). 2D NMR (^{1}H–^{1}H NOESY) revealed a long-range correlation between the dibenzhydrylic CH and methyl of *o*-tolyl, confirming the formation of the **Ni3** complex.

The existence of **Ni1**, **Ni2**, and **Ni3** complexes was unambiguously ascertained using single-crystal X-ray diffraction. The molecular structures of **Ni1**, **Ni2**, and **Ni3** are shown in

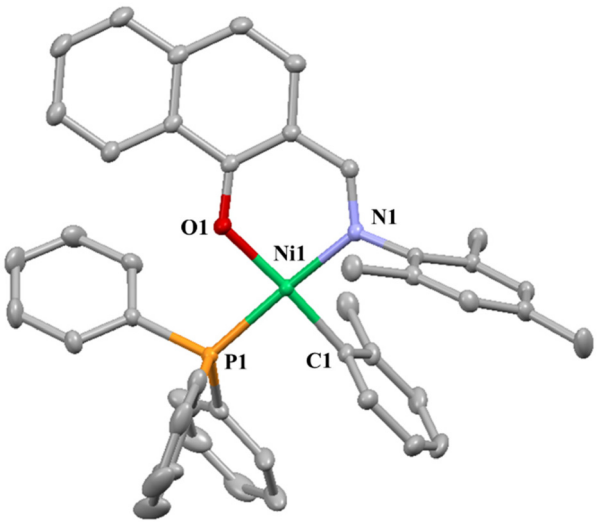

Fig. 2 Molecular structure of **Ni1**. H-atoms are omitted for clarity; thermal ellipsoids are drawn at the 50% probability level. Important bond distances and bond angles; Ni1–C1 1.89 Å, Ni1–O1 1.89 Å, Ni1–N1 1.92 Å, Ni1–P1 2.18 Å, C1–Ni1–P1 87.05°, O1–Ni1–P1 89.37°, N1–Ni1–P1 176.42°, C1–Ni1–N1 91.55°, O1–Ni1–N1 92.07°, and C1–Ni1–O1 176.33°.

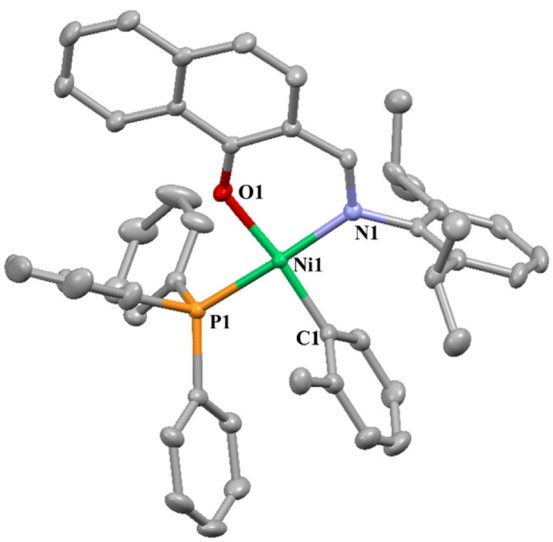

Fig. 3 Molecular structure of **Ni2**. H-atoms are omitted for clarity; thermal ellipsoids are drawn at the 50% probability level. Important bond distances and bond angles; Ni1–C1 1.89 Å, Ni1–O1 1.89 Å, Ni1–N1 1.93 Å, Ni1–P1 2.19 Å, C1–Ni1–P1 87.73°, O1–Ni1–P1 85.94°, N1–Ni1–P1 175.47°, C1–Ni1–N1 93.88°, O1–Ni1–N1 92.57°, and C1–Ni1–O1 173.38°.

This journal is © The Royal Society of Chemistry 2024

Published on 06 December 2023. Downloaded by National Chemical Laboratory, Pune on 5/30/2024 3:00:58 PM.

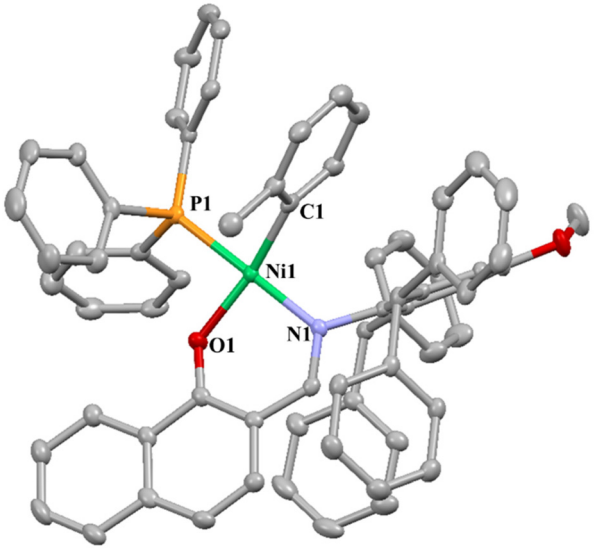

Fig. 4 Molecular structure of **Ni3**. H-atoms are omitted for clarity; thermal ellipsoids are drawn at the 50% probability level. Important bond distances and bond angles; Ni1–P1 2.19 Å, Ni1–O1 1.90 Å, Ni1–N1 1.92 Å, Ni1–C1 1.90 Å, P1–Ni1–O1 85.18°, P1–Ni1–N1 171.69°, P1–Ni1–C1 90.40°, O1–Ni1–N1 92.40°, O1–Ni1–C1 167.2°, and N1–Ni1–C1 93.6°.

Fig. 2, 3, and 4, respectively, along with selected bond distances and bond angles. Suitable crystals of **Ni1**, **Ni2**, and **Ni3** were obtained from a dichloromethane and hexane solvent mixture at room temperature. The geometry around the nickel metal center was distorted square planar. In the **Ni1** complex, the *o*-tolyl group was placed *cis* to the imine nitrogen atom with a C1–Ni1–N1 bond angle of 91.55°. Triphenylphosphine was located *trans* to the imine nitrogen with an N1–Ni1–P1 bond angle of 176.42°. The oxygen atom and triphenylphosphine are *cis* to each other with an O1–Ni1–P1 angle of 89.37° and *trans* to the *o*-tolyl group with a C1–Ni1–O1 angle of 176.33°. A nickel (**Ni1**) and imine (**N1**) bond distance of 1.92 Å suggests the coordination of imine nitrogen to nickel. A shorter Ni–O bond distance of 1.89 Å suggests the formation of a covalent bond. These observed bond distances are similar to those reported in the literature.[57,58] The bond angle between C–Ni–P was found to be 87.05° suggesting the *cis*-position of the PPh_3 and methyl groups on nickel. The *cis* arrangement is crucial for initiating ethylene polymerization.

The remaining nickel complexes, **Ni2** and **Ni3**, contain a common structural unit, *i.e.*, the naphthoxy-imine ligated nickel complex in which nickel is coordinated by four atoms and assumes a distorted square planar geometry. As observed in **Ni1**, the oxygen atom forms a covalent bond and the imine nitrogen forms a coordinate bond with the central nickel atom. As compared to **Ni1**, the P–Ni bond distance in **Ni2** and **Ni3** was found to be slightly longer. This increase in the P–Ni distance can be ascribed to the increased steric bulk in these complexes. Another noticeable difference is the N1–Ni–C1 bond angle. The N1–Ni–C1 bond angle of **Ni2** and **Ni3** is slightly larger than that in the Ni1 complex. Furthermore, the C1–Ni–P1 angle in **Ni2** and **Ni3** was found to be the *cis*-angle (<105°), suggesting that these catalysts will be able to initiate ethylene polymerization.[59]

Insights into steric bulk

As shown in Scheme 2 and Fig. 2–4, the size of the imine-substituent increases from methyl to isopropyl to dibenzhydryl in **Ni1**, **Ni2**, and **Ni3**, respectively. In our attempts to quantify the steric bulk and to correlate the effect of steric bulk on the polymerization activity, molecular weight, *etc.*, we performed buried volume measurements using readily available Cavallo's SambVca 2.1 program (Fig. 5).[60] The **Ni1** complex with a simple methyl (Me) substituent displayed a buried volume of 47.5% (V_{bur} = 47.5%), and **Ni2** with an isopropyl substituent disclosed an almost similar buried volume of 47.3. **Ni3** with the bulky dibenzhydryl substituent revealed a higher buried volume of 49.1%. Thus, the ligand covers more space around the nickel in **Ni3** and should provide higher steric bulk.[28]

Ethylene polymerization

After fully establishing the existence of **Ni1–Ni3** and their steric properties, we set out to examine their performance in ethylene polymerization. An ethylene polymerization study was carried out using **Ni1–Ni3** catalysts and $[Ni(COD)_2]$ or $B(C_6F_5)_3$ as co-catalysts (to scavenge phosphine). Ethylene polymerization was carried out in a Buchi high-pressure reactor using

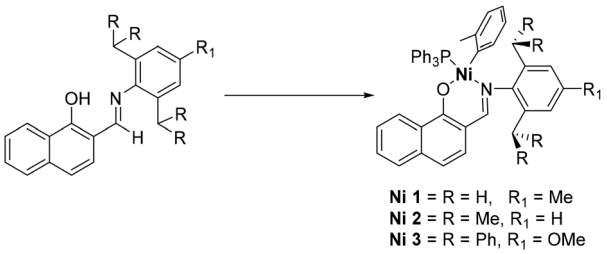

Scheme 2 Synthesis of nickel complexes **Ni1**, **Ni2**, and **Ni3**.

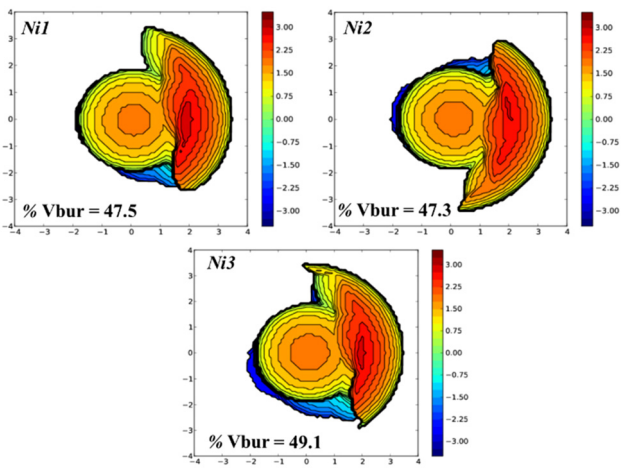

Fig. 5 Topographic steric maps of nickel complexes **Ni1**, **Ni2**, and **Ni3**.

Published on 06 December 2023. Downloaded by National Chemical Laboratory, Pune on 5/30/2024 3:00:58 PM.

Table 1 Ethylene polymerization using nickel catalysts **Ni1–Ni3**[a]

Entry	Cat.	Temp. (°C)	Pressure (bar)	Time (min.)	Yield (g)	TOF × 10^4	T_m	% of cryst.	M_n × 10^3	M_w × 10^3	PDI
1	**Ni1**	60	20	20	0.003	—	97.5	16.8	—	—	—
2	**Ni1**	70	20	20	0.026	0.028	94.4	27.8	—	—	—
3	**Ni1**	80	20	20	0.185	0.204	83.1	11.7	3.9	7.9	2
4	**Ni1**	90	20	20	0.124	0.135	75.93	12.8	—	—	—
5	**Ni2**	60	20	20	0.014	0.015	107.0	49.0	—	—	—
6	**Ni2**	70	20	20	0.528	0.578	101.7	32.3	—	—	—
7	**Ni2**	80	20	20	1.210	1.325	94.6	24.9	6.6	13.2	2
8	**Ni2**	90	20	20	2.423	2.65	80.5	10.4	—	—	—
9	**Ni3**	60	20	20	0.42	0.46	114.4	63.4	—	—	—
10	**Ni3**	70	20	20	1.748	1.95	106.3	55.1	39.0	100.0	2.5
11	**Ni3**	70	20	10	0.767	1.66	107.3	32.1	—	—	—
12	**Ni3**	70	20	30	2.265	1.65	107.6	47.7	—	—	—
13	**Ni3**	80	20	20	3.236	3.54	96.3	28.5	61.0	160.0	2.6
14	**Ni3**	90	20	20	2.235	2.4	81.4	11.5	70.0	113.0	1.6
15	**Ni3**	80	25	20	2.862	3.13	99.6	36.5	114.0	270.0	2.3
16	**Ni3**	80	15	20	3.186	3.49	89.1	23.5	—	—	—
17	**Ni3**	80	10	20	1.611	1.76	78.3	13.9	48.0	114.6	2.3
18[a]	**Ni3**	70	20	90	2.260	0.38	94.5	31.2	75.0	150.0	1.9

Reaction conditions: toluene – 100 mL, catalyst – 9.79 μmol, co-catalyst [$Ni(COD)_2$] – 2 equivalents, ethylene pressure – 10 to 25 bars, TOF (in mol of PE per mol of Ni per h), (—) – not determined. The reported yield was obtained after re-precipitating polyethylene in acidic methanol and drying under high vacuum for 4 hours. T_m and % of crystallinity were calculated by DSC. [% Crystallinity = $\Delta Hm/\Delta Hm°$ (J g^{-1}) × 100]. The molecular weight and PDI were recorded using HT-GPC in TCB at 160 °C against polystyrene standards. [a] Catalyst – 15 mg and co-catalyst ($(C_6F_5)_3B$) – 2 equivalents.

Ni1 as the catalyst and [$Ni(COD)_2$] as the cocatalyst at 60 °C and 20 bar ethylene pressure for 20 minutes (Table 1, entry 1). After completion, excess ethylene was vented and the reaction mixture was poured into acidic methanol to precipitate polyethylene. Only 3 mg of polyethylene was observed under these conditions. Next, the polymerization temperature was increased to 70 °C and 80 °C to produce 28 mg and 204 mg of polyethylene, respectively. With a further increase in the temperature to 90 °C, the polyethylene yield (124 mg) was found to reduce due to the thermal decomposition of the catalyst.[61]

Subsequently, the **Ni2** catalyst was examined in ethylene polymerization. Under similar reaction conditions to those of **Ni1** (20 bar ethylene pressure, 60 to 90 °C temperature and [$Ni(COD)_2$] as the cocatalyst to ensure a meaningful comparison), **Ni2** produced a little more (14 mg) amount of the product (Table 1, entry 5). With an increase in the polymerization temperature at constant ethylene feed, an increase in the polyethylene yield was observed (Table 1, entries 6 and 7). The highest yield of 2.42 g was observed at 90 °C with a TOF reaching 2.65 × 10^4 mol of PE per mol of Ni per h. Next, the bulkier **Ni3** complex was tested in ethylene polymerization under similar reaction conditions. At a temperature of 60 °C and 20 bar ethylene pressure, the formation of 0.42 g of polyethylene was observed. An increase in the temperature to 70 °C and 80 °C resulted in increased polyethylene production (1.74 g and 3.23 g, respectively). Further increasing the temperature to 90 °C led to a reduced polyethylene yield (2.23 g; Table 1, entry 14). Thus, **Ni3** outperformed the other catalysts and 80 °C was found to be the most optimal polymerization temperature (Fig. 6). At 80 °C, the catalyst is thermally stable and exhibits the highest activity.

After identifying the best-performing catalyst and optimal temperature, we turned our attention towards ethylene pressure. The reaction was performed between 10 and 25 bar ethylene pressure and the activity was recorded. It was found that with increasing ethylene pressure, the yield of polyethylene increased up to 20 bar. With further higher ethylene pressure (25 bar), the yield of polyethylene reduced (entries 15–17 *versus* entry 13). This could be because of the higher chain transfer to the monomer at higher ethylene pressure. The polymerization time was screened and the reaction was carried out for 10, 20, and 30 minutes (Table 1, entries 10–12). At 10 minutes, the TOF of the catalyst was 1.66 × 10^4 mol of PE per mol of Ni per h and at 20 minutes, an increase in the TOF was observed (TOF = 1.95 × 10^4 mol of PE per mol of Ni per h). A longer polymerization time of 30 minutes led to a reduced TOF of 1.65 × 10^4 mol of PE per mol of Ni per h. These observations suggest that after 20 minutes of polymerization, the catalyst slowly deactivates. When the reaction was performed

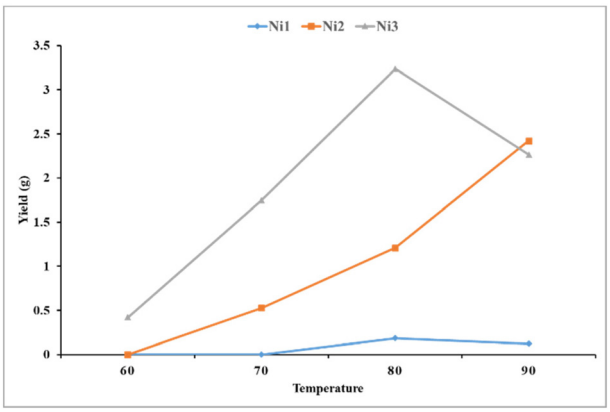

Fig. 6 Plot of the polyethylene yield *versus* polymerization temperature using catalysts **Ni1**, **Ni2**, and **Ni3**.

 This journal is © The Royal Society of Chemistry 2024

Published on 06 December 2023. Downloaded by National Chemical Laboratory, Pune on 5/30/2024 3:00:58 PM.

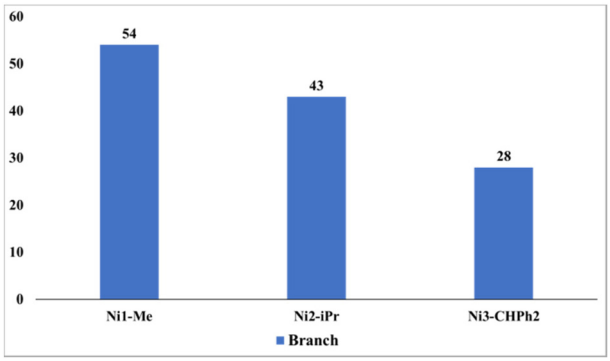

Fig. 7 Comparison of branches (per 1000 carbon atoms) in polyethylene obtained using **Ni1**, **Ni2**, and **Ni3** (entries 3, 7 and 13).

in the presence of $B(C_6F_5)_3$ as the cocatalyst, the TOF was almost comparable with the $[Ni(COD)_2]$ co-catalyst (Table 1, entry 13 *vs.* Table S2,† entry 19).

Polyethylene analysis

The polyethylene microstructure is a crucial parameter that differentiates one polyethylene from another, such as oligoethylenes or branched PE (HDPE, LLDPE, LDPE, *etc.*).[62] Therefore, the determination of the polyethylene microstructure will allow us to gauge the potential of PE. Thus, PE produced under optimal conditions was dissolved in deuterated tetrachloroethane and a high-temperature NMR (80 °C) spectrum was recorded. The chain-end methyl group, as well as the methyl branch, appeared at 0.91 ppm in the ^{1}H NMR spectrum. The ^{1}H NMR peak at 1.33 ppm corresponds to the methylene ($-CH_2-$) group from the polymer backbone

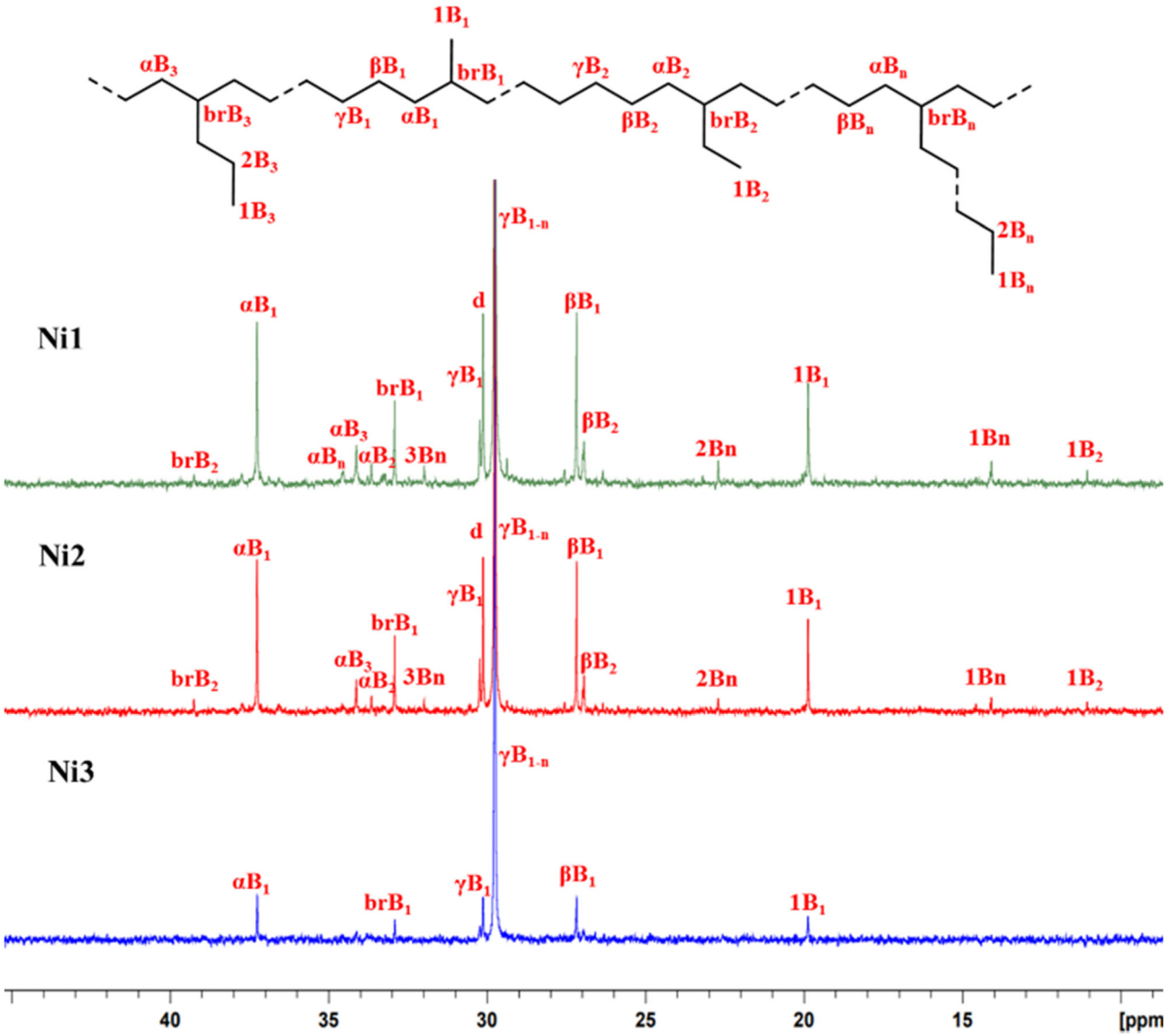

Fig. 8 ^{13}C NMR spectra of polyethylene obtained from **Ni1**, **Ni2** and **Ni3** in $C_2D_2Cl_4$ at 80 °C (entries 3, 7 and 13).

Published on 06 December 2023. Downloaded by National Chemical Laboratory, Pune on 5/30/2024 3:00:58 PM.

(Fig. S35†). The nickel catalyst **Ni1** produced polyethylene with ~54 branches per 1000 carbon atoms. The **Ni2** complex equipped with the diisopropyl substituent showed ~43 branches per 1000 carbon atoms and the **Ni3** catalysts with the sterically crowded dibenzhydryl substituent revealed only ~28 branches per 1000 C atoms (Fig. 7). It was observed that with higher steric hindrance, the number of branches per 1000 carbon atoms was reduced. These observations suggest that the steric hindrance plays a crucial role and directly controls branching in polyethylene. These results are consistent with findings in the literature about the role of steric hindrance in controlling the branching of polyethylene.[12,13,15,26,27,40,47]

In our attempts to understand the types of branches (methyl, ethyl, propyl, isopropyl, *etc.*), polyethylene produced by **Ni1–Ni3** was subjected to ^{13}C NMR analysis (Fig. 8). The presence of a methyl branch ($1B_1$) at 19.9 ppm, CH carbon (brB_1) at 32.9 ppm, and the methylene group in the backbone (γB_1) at 29.7 ppm was identified based on the literature report.[63] As evident in Fig. 8, polyethylene produced by **Ni1** and **Ni2** exhibited higher branching (like ethyl, propyl, and long chain branching). The type of branch [($1B_2$), (brB_2), (βB_2), (αB_3), ($1B_n$), ($2B_n$), *etc.*] and their chemical shifts have been mapped based on the literature reports.[64] As evident in Fig. 8, sterically less crowded **Ni1** and **Ni2** catalysts showed methyl, ethyl, propyl, and long-chain branching. However, the sterically more crowded dibenzhydryl-substituted **Ni3** catalyst revealed the presence of only methyl branch, leading to the generation of linear polyethylene.

As the polymerization temperature increases, the resulting polymer melting temperature (T_m) decreases, causing a reduction in % crystallinity due to branched structures. These trends are consistent for all three nickel catalysts (**Ni1–Ni3**).

The effect of ethylene pressure on polyethylene characteristics was investigated at 10, 15, 20, and 25 bars at 80 °C. Although drawing a direct correlation among ethylene pressure, polyethylene melting temperature and % crystallinity may not be correct, the following observations were made during our study. At a higher ethylene pressure of 25 bar, the melting temperature of the resultant PE was found to be 99.6 °C along with 36.5% crystallinity. When the pressure was lowered to 20 bar, both, the T_m (96.3 °C) and % crystallinity (28.5%) reduced. The subsequent reduction in ethylene pressure to 15 and 10 bar further lowered the melting temperature and crystallinity. The molecular weight findings suggest that with decreasing ethylene pressure, the rate of insertion decreases leading to the formation of low molecular weight polyethylene.

The molecular weight of the resultant PE was determined using high-temperature gel permeation chromatography (HT-GPC). It was observed that with increasing polymerization temperature, the number average molecular weight increases. For instance, at 70 °C, M_n was 39 000 Da (Table 1, entry 10); at 80 °C, it increased to 61 000 Da (Table 1, entry 13); at 90 °C, it further increased to 70 000 Da (Table 1, entry 14). Additionally, an increase in pressure led to higher molecular weights (Table 1, entry 14 *versus* entry 15). It was also observed that an increase in ligand steric hindrance, (**Ni1–Ni3**) results in a higher molecular weight, as indicated by the data shown in Table 1 entries 3, 7, and 13. The powder diffraction data suggest that PE chains crystallize in the orthorhombic structure. Also, it suggests that with increasing branch content, the

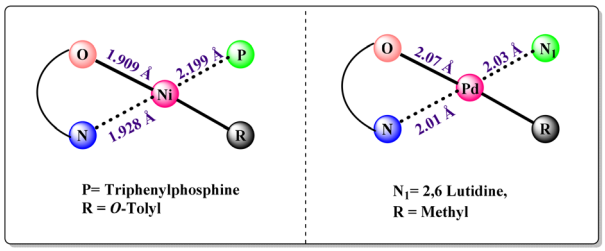

Fig. 9 Comparative single-crystal data (bond distances) for nickel (**Ni3**) and palladium (**Pd1**) catalysts.

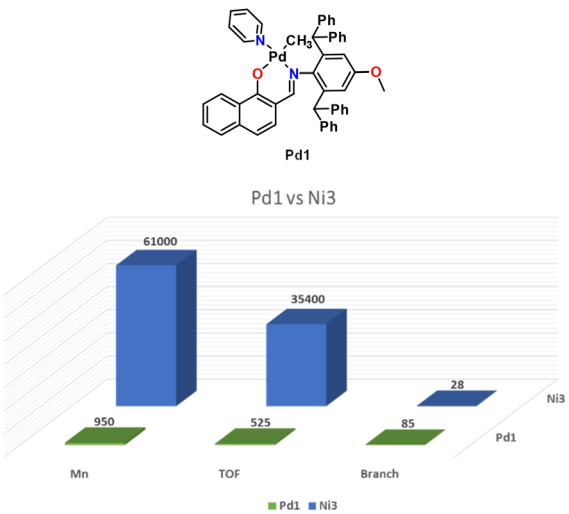

Fig. 10 L3-ligated palladium catalyst (**Pd1**) (top); comparison of TOF, molecular weight and branching between **Ni3** and **Pd1** catalyzed ethylene polymerization (bottom).

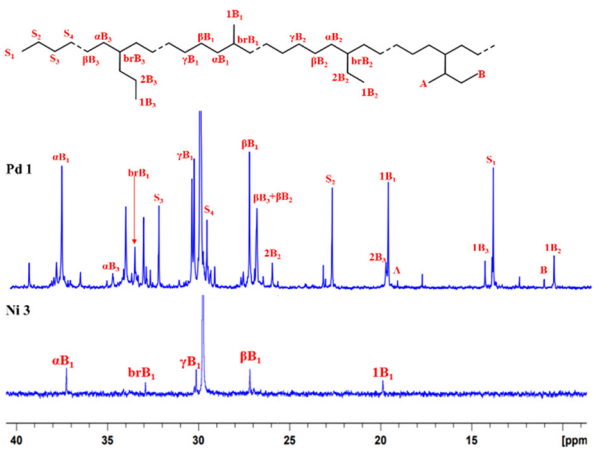

Fig. 11 Comparative ^{13}C NMR spectra of polyethylene obtained using palladium (**Pd1**) and nickel (**Ni3**) catalysts.

This journal is © The Royal Society of Chemistry 2024

Published on 06 December 2023. Downloaded by National Chemical Laboratory, Pune on 5/30/2024 3:00:58 PM.

Table 2 A comparison of properties of polyethylene produced by **Ni3** and **Pd1** catalysts

Entry[a]	Catalyst	T_m (°C)	% of Cryst.	Branch/1000 C[b]	Methyl[c] (%)	Ethyl[c] (%)	Propyl[c] (%)	LCB[d] (%)	*sec*-Butyl[c] (%)
3	**Ni1**	83.1	11.7	54	82.1	6.5	6.3	4.9	0
7	**Ni2**	94.6	24.9	43	83.1	6.0	6.3	4.4	0
9	**Ni3**	114.4	63.4	20	>99	0	0	0	0
13	**Ni3**	96.3	28.5	28	>99	0	0	0	0
17	**Ni3**	78.3	13.9	55	78.9	9.7	4.7	6.5	0
20[e]	**Pd1**	—	—	85	46.3	14.8	14.0	21.7	3.2

[a] Entries are based on Table 1. [b] Branches per 1000 carbons calculated from ^{1}H NMR. [c] Relative intensities of methyl ($1B_1$, $1B_2$, and $1B_3$), and *sec*-Bu resonances were calculated using ^{13}C NMR [in ^{13}C NMR, only methyl branches were observed for entries 9 and 13]. [d] LCB = butyl and longer branches. For entries 3, 7 and 17, the branch content was calculated using qualitative ^{13}C NMR spectra. [e] Pd catalyst produced oily oligomeric compounds which are viscous liquids at room temperature and a quantitative ^{13}C NMR spectrum was recorded.

crystallinity reduces. In the **Ni1** case, 54 branches are present per 1000 C-atoms, and therefore, it shows low crystallinity (ESI, section 8†).

Comparison with the corresponding Pd-catalysts

To know where **Ni1**–**Ni3** catalysts stand in terms of activity, molecular weight, and branching, we compared the performance of these nickel catalysts with the literature-reported corresponding palladium catalyst **Pd1** (Fig. 10).[56] Before we compare their performance in ethylene polymerization, it would be worth noting the structural similarities and differences between the two metal catalysts. Both the catalysts (**Ni3** and **Pd1**) are ligated using the same ligand, *i.e.*, **L3**. Single crystal X-ray diffraction data are depicted in Fig. 9. The geometry around Ni and Pd is distorted square-planar and bond distances (O–M and N–M) for **Ni3** were shorter than **Pd1**.

Ethylene (20 bar) polymerization using the **Pd1** catalyst at 80 °C produced a low molecular weight (950 Da) viscous oily material, with a TOF value of 525 mol of PE per mol of Pd per h and shows 85 branches per 1000 carbon atoms. However, the nickel analog, nickel catalyst (**Ni3**) revealed a TOF of 35 400 mol of PE per mol of Ni per h, along with a high molecular weight polymer (61 000 Da) with much lower branching (28 branches per 1000 carbon atoms) (Fig. 10).

Oligo/polyethylene produced by Pd1 exhibited a hyperbranched microstructure with methyl, ethyl, propyl, and *sec*-butyl (that is branch on branch) branches (Fig. 11). The palladium catalyst (**Pd1**) shows extensive chain walking during polymerization and yields a hyperbranched polymer. In the literature, it was observed that Pd catalysts produce lower molecular weight polymers with a higher degree of branching.[62,65,66] However, the nickel catalyst (**Ni3**) revealed a higher rate of insertion than chain walking and produced linear polyethylene with up to 63% crystallinity. A comparison of polyethylene produced by **Ni3** and **Pd1** is presented in Table 2.

Conclusions

In summary, the synthesis of naphthoxy imine (NI) ligands **L1**, **L2** and **L3** with increasing steric bulk has been reported. The sodium salts of the ligands (**L1**–**L3**) were treated with [NiCl(*o*-Tol)(PPh_3)$_2$] to yield the corresponding nickel complexes **Ni1**, **Ni2**, and **Ni3** in excellent yields. The identity of **Ni1**–**Ni3** has been unambiguously ascertained using 1–2D NMR, mass spectroscopy, and single-crystal X-ray diffraction. The molecular structure of **Ni1**–**Ni3** revealed that the central nickel atom assumes distorted square planar geometry. The alkyl/aryl group is situated *cis* to the donor atom, suggesting the potential of these complexes in ethylene polymerization. Indeed, the three nickel complexes (**Ni1**–**Ni3**) were found to be active in ethylene polymerization. The ligand steric bulk was quantified using buried volume calculations and was found to affect the performance of the catalyst. When exposed to ethylene, **Ni1**–**Ni3** produced polyethylene with variable degrees of branching. Various polymerization parameters such as temperature, time and pressure were optimized. The optimal polymerization conditions were found to be 20 bar ethylene pressure, 80 °C temperature, and a polymerization time of 20 minutes. Under these optimal conditions, **Ni3** outperformed **Ni1** and **Ni2**. The sterically bulkiest catalyst **Ni3** (49% buried volume) disclosed higher activity and produced linear PE with high crystallinity. The microstructure analysis of the resultant polyethylene exhibited a clear trend, *i.e.*, with increasing steric bulk around the metal, the activity increases, molecular weight increases and the branching decreases. The most successful catalyst, **Ni3**, produced high molecular weight PE with only methyl branches and exhibited the highest activity. These observations suggest that higher steric hindrance suppresses β-hydride elimination, increases the rate of propagation, and reduces chain walking.

A comparison between **Ni3** and its palladium analogs revealed that the **Ni3** catalyst outperforms **Pd1** in terms of activity, molecular weight, and branching.

Experimental section

Methods and materials

Unless noted otherwise, all manipulations were carried out under an inert atmosphere using standard Schlenk line techniques or an M-Braun glove box. Toluene, diethyl ether, 1,4 dioxane, and THF were distilled from sodium/benzophenone

Published on 06 December 2023. Downloaded by National Chemical Laboratory, Pune on 5/30/2024 3:00:58 PM.

under an argon atmosphere. Acetonitrile, methylene chloride, and pyridine were distilled on calcium hydride. Ethylene was supplied by Praxiar India Ltd, India. 1-Naphthol and diisopropyl aniline were supplied by Loba Chemie and were used as received. 2, 4, 6 trimethyl aniline, $B(C_6F_5)_3$, and $[Ni(COD)_2]$ were supplied by Sigma Aldrich and were used as received. Sodium borohydride was supplied by Avara Chemicals and was used as received. *p*-Anisidine and paraformaldehyde were supplied by Alfa Aesar and were used as received. [NiCl(*o*-Tol)$(PPh_3)_2$],[67] 1-hydroxy 2-napthaldehyde,[68] and aniline derivatives[69] were synthesized by following known procedures. The insertion polymerization was run in a Büchi Glas Uster cyclone 075 high-pressure reactor equipped with an overhead mechanical stirrer, heating/cooling jacket, and pressure regulators.

Solution NMR spectra were recorded on Bruker Avance 200, 400 and 500 MHz instruments. Chemical shifts are referenced to the external reference TMS (^{1}H and ^{13}C). Coupling constants are given as absolute values. Multiplicities are given as follows s: singlet, d: doublet, t: triplet, and m: multiplet. High-temperature NMR (HT-NMR) spectra of the polymers were recorded in $C_2D_2Cl_4$ solvent at 80 °C. Chemical shifts are referenced to the external reference TMS (^{1}H and ^{13}C). Mass spectra were recorded on a Thermo Scientific Q-Exactive mass spectrometer. Column specification: a Hypersil gold C18 column with a 150 × 4.6 mm diameter and an 8 μm particle size and the mobile phase used is 90% methanol + 10% water + 0.1% formic acid. Differential scanning calorimetry (DSC) was carried out on DSC Q-10 equipment from TA instruments with a heating and cooling rate of 10 °C min^{-1}, unless mentioned otherwise. High-Temperature Gel Permeation Chromatography (HT-GPC) of PE was performed in 1,2,4-trichlorobenzene at 160 °C on a Viscotek GPC (HT-GPC module 350A) instrument equipped with a triple detector system. The columns were calibrated with linear polystyrene standards and the reported molecular weights are with respect to polystyrene standards. The molecular weight measurements for entries 3 and 7 were performed on GPC – IR5 + Visco + LS (GPC-IR-I Polymer Char) at a flow rate of 1 ml min^{-1} on 3 × PL gel Olexis Mix-Bed columns (13 microns) and 300 × 7.5 mm + guard columns. The weight-average molecular weight (M_w), number average molecular weight (M_n) and polydispersity index (PDI) of the synthesized PE were recorded using HT-GPC.

Synthesis of L1. In an oven-dried round bottom flask, 1-hydroxy 2-naphthaldehyde (0.010 moles, 1.8 g) and 2,4,6-trimethyl aniline (0.011 moles, 1.55 g) were dissolved in 25 mL toluene. To that, a catalytic amount of PTSA (5 mg) was added and the resultant reaction mixture was refluxed for 6 hours. The color of the reaction mixture changed to yellowish and the reaction was monitored by TLC analysis. After completion of the reaction, the solvent was evaporated using a rotatory evaporator and the ligand was purified by silica gel column chromatography with pet ether (98%) and ethyl acetate (2%) as eluents (yield: 2.9 g, <99%).

^{1}H NMR (500 MHz, $CDCl_3$). δ = 14.66 (br. s., 1H), 8.51 (d, J = 8.1 Hz, 1H), 8.12 (br. s., 1H), 7.70 (d, J = 8.0 Hz, 1H), 7.59 (t, J = 7.4 Hz, 1H), 7.55–7.46 (m, 1H), 7.15 (d, J = 8.8 Hz, 1H), 7.08 (d, J = 8.8 Hz, 1H), 6.97 (s, 2H), 2.33 (s, 3H), 2.30 (s, 6H). **^{13}C NMR (125 MHz, $CDCl_3$):** δ = 170.1, 163.4, 140.8, 136.9, 135.7, 130.2, 129.8, 129.4, 127.9, 127.6, 127.4, 125.4, 124.8, 116.7, 110.5, 20.9, 18.6. **ESI-MS** (positive mode): m/z = 290.1551 Da $[M + H]^+$ (observed); 290.1545 $[M + H]^+$ (calculated).

Synthesis of Ni1. In an oven-dried Schlenk flask, NaH (13.6 mg, 0.566 mmol) and ligand **L1** (81.5 mg, 0.281 mmol) were taken. The flask was cooled to 0 °C and 5 mL THF was added. The reaction mixture was stirred at 0 °C for 2 hours, after that solvent was evaporated, the obtained compound was dissolved in 5 mL DCM and was dropwise transferred to another flask that contained precursor [NiCl(*o*-Tol)$(PPh_3)_2$] (200 mg, 0.281 mmol) at 0 °C. The content was stirred at the same temperature for 2 hours and DCM was evaporated. The resultant residue was purified by recrystallization in DCM and hexane at 0 °C (yield: 184 mg, 93%).

^{1}H NMR (500 MHz, $CDCl_3$). δ = 7.85 (d, J = 8.5 Hz, 1H), 7.55–7.43 (m, 7H), 7.37–7.29 (m, 5H), 7.23–7.19 (m, 5H), 7.07 (d, J = 8.2 Hz, 1H), 6.85 (d, J = 8.2 Hz, 1H), 6.73 (t, J = 6.7 Hz, 1H), 6.64 (d, J = 7.0 Hz, 1H), 6.56 (br. s., 1H), 6.50 (d, J = 7.6 Hz, 1H), 6.39 (br. s., 1H), 6.31–6.21 (m, 1H), 6.01 (d, J = 6.7 Hz, 1H), 5.99–5.92 (m, 1H), 2.62 (br. s., 3H), 2.48 (br. s., 3H), 2.07 (br. s., 3H), 2.02 (br. s., 3H). **^{13}C NMR (125 MHz, $CDCl_3$):** δ = 164.9, 164.8, 150.2, 143.2, 137.5, 137.1, 134.6, 134.5, 133.9, 133.8, 131.4, 131.0, 130.9, 129.9, 129.9, 129.7, 129.7, 128.8, 128.6, 128.6, 128.3, 128.1, 127.9, 127.9, 127.6, 126.7, 126.2, 126.0, 123.8, 121.8, 121.7, 113.6, 112.8, 26.4, 20.7, 19.7, 18.6. **^{31}P NMR (500 MHz, $CDCl_3$)** δ = 25.19. **ESI-MS** (positive mode): $C_{45}H_{40}NNaNiOP$ m/z = 722.15 Da $[M + Na]^+$ (observed); 722.20 $[M + Na]^+$ (calculated).

Synthesis of Ni2. In an oven-dried Schlenk flask, NaH (5.0 mg, 0.21 mmol) and ligand **L2** (35 mg, 0.10 mmol) were taken. The flask was cooled to 0 °C and 5 mL THF was added. The reaction mixture was stirred at 0 °C for 2 hours, and the solvent was evaporated. The resultant compound was dissolved in 5 mL DCM and was dropwise transferred to another flask that contained precursor [NiCl(*o*-Tol)$(PPh_3)_2$] (74.8 mg, 0.10 mmol) at 0 °C. The content was stirred at the same temperature for 2 hours and DCM was evaporated. The complex was purified by recrystallization in DCM and hexane at 0 °C (yield: 54 mg, 73%).

^{1}H NMR (500 MHz, $CDCl_3$). δ = 7.92 (d, J = 8.5 Hz, 1H), 7.50 (d, J = 8.5 Hz, 5H), 7.35–7.30 (m, 7H), 7.23–7.19 (m, 5H), 7.08–7.02 (m, J = 8.5 Hz, 1H), 7.00–6.96 (m, J = 7.6 Hz, 1H), 6.90 (t, J = 7.8 Hz, 1H), 6.87–6.82 (m, J = 8.5 Hz, 1H), 6.73 (t, J = 7.5 Hz, 1H), 6.67–6.62 (m, J = 7.3 Hz, 1H), 6.47 (d, J = 7.9 Hz, 1H), 6.42–6.36 (m, J = 7.3 Hz, 1H), 6.22–6.13 (m, 1H), 6.08–6.01 (m, J = 7.0 Hz, 1H), 5.90 (t, J = 7.3 Hz, 1H), 4.60 (td, J = 6.7, 13.4 Hz, 1H), 3.01 (td, J = 6.6, 13.4 Hz, 1H), 2.82 (s, 3H), 1.51 (d, J = 6.7 Hz, 3H), 1.03 (d, J = 6.7 Hz, 6H), 0.80 (d, J = 6.7 Hz, 3H). **^{13}C NMR (125 MHz, $CDCl_3$):** δ = 165.2, 164.8, 150.2, 145.7, 145.3, 142.6, 141.7, 140.4, 138.0, 137.1, 134.5, 134.4, 133.8, 133.7, 131.3, 130.9, 129.8, 129.7, 129.6, 128.7, 128.5, 128.5, 128.2, 127.9, 127.8, 126.8, 126.6, 125.9, 125.3, 123.7, 122.7, 122.0, 121.5, 113.7, 112.0, 29.1, 27.6, 26.0, 25.8, 22.7, 22.0. **^{31}P NMR (500 MHz, $CDCl_3$):** δ = 25.2.

 This journal is © The Royal Society of Chemistry 2024

Published on 06 December 2023. Downloaded by National Chemical Laboratory, Pune on 5/30/2024 3:00:58 PM.

Synthesis of Ni3. In an oven-dried Schlenk flask, NaH (33.8 mg, 1.40 mmol) and ligand **L3** (429 mg, 0.704 mmol) were taken. The flask was cooled to 0 °C and 25 mL THF was added. The reaction mixture was stirred at 0 °C for 1 hour and the solvent was evaporated. The resultant compound was dissolved in 20 mL DCM and transferred dropwise to another flask that contained precursor [NiCl(*o*-Tol)(PPh_3)$_2$] (500 mg, 0.704 mmol) in 5 mL of DCM at 0 °C. The content was stirred at the same temperature for 1 hour and DCM was evaporated. The complex was purified by column chromatography using pet ether (98%)/ethyl acetate (2%) (yield: 620 mg, 86%).

^{1}H NMR (500 MHz, $CDCl_3$). δ = 7.66 (s, 1H), 7.53 (t, J = 8.8 Hz, 6H), 7.40 (d, J = 7.9 Hz, 1H), 7.35–7.31 (m, 3H), 7.26 (s, 3H), 7.24 (d, J = 3.5 Hz, 3H), 7.21 (d, J = 1.9 Hz, 2H), 7.20–7.19 (m, 3H), 7.19–7.17 (m, 4H), 7.05–7.00 (m, 5H), 6.75 (d, J = 7.3 Hz, 2H), 6.72–6.62 (m, 3H), 6.60–6.53 (m, 3H), 6.49 (d, J = 2.8 Hz, 1H), 6.43 (t, J = 7.3 Hz, 1H), 6.38 (d, J = 8.5 Hz, 1H), 6.24–6.17 (m, 3H), 6.11 (t, J = 7.1 Hz, 1H), 5.97 (d, J = 2.8 Hz, 1H), 5.67 (d, J = 8.8 Hz, 1H), 5.28 (d, J = 8.8 Hz, 1H), 5.20 (s, 1H), 3.43 (s, 3H), 3.07 (s, 3H). **^{13}C NMR (125 MHz, $CDCl_3$):** δ = 168.5, 163.5, 155.8, 144.9, 143.7, 143.4, 143.3, 143.1, 139.7, 138.7, 138.6, 137.1, 134.4, 134.3, 131.3, 130.9, 130.5, 130.3, 130.2, 129.9, 129.6, 129.2, 128.5, 128.3, 128.0, 127.9, 127.7, 127.7, 127.4, 127.2, 126.4, 126.3, 126.2, 125.9, 125.8, 125.7, 123.3, 123.1, 121.8, 113.5, 113.3, 112.4, 112.1, 55.1, 53.5, 51.9, 26.5. **^{31}P NMR (500 MHz, $CDCl_3$):** δ = 22.8.

Ethylene homopolymerization procedure. The polymerization reaction was performed in a Buchi high-pressure reactor, which was connected to a high-pressure ethylene gas line. Initially, the reactor was dried at 90 °C under vacuum for 1 hour. The reactor temperature was maintained at the desired polymerization temperature and the reactor was purged with ethylene gas. To that, 100 mL of anhydrous toluene was added under positive ethylene gas flow. Furthermore, toluene was stirred under ethylene pressure for 30 minutes to dissolve ethylene in toluene. Excess ethylene was vented and the desired amount of the catalyst and cocatalyst was injected into the reactor using a syringe. The reactor was pressurized with rapid stirring and the desired pressure was maintained throughout the polymerization. After the completion of polymerization, excess ethylene was vented and polymerization was quenched by pouring the content into acidic methanol. The polymer was filtered using Whatman filter paper and dried under high vacuum to yield polyethylene. Table 1 summarizes important runs using Ni catalysts.

Conflicts of interest

There are no conflicts to declare.

Acknowledgements

We gratefully acknowledge the financial support from DST-SERB (CRG/2021/005385), CSIR-NCL (HCP46), and DSIR (CRTDH@NCL) India. R. S. B. is thankful to DST for the DST-INSPIRE fellowship. We thank D. V. B. and K. K. for the TOC figure.

References

1 S. H. Chikkali, in *Metal Catalyzed Polymerization: Fundamentals to Applications*, CRC Press, Taylor and Francis Group, USA, 2017.
2 C. Chen, *Nat. Rev. Chem.*, 2018, **2**, 6–14.
3 M. Stuerzel, S. Mihan and R. Muelhaupt, *Chem. Rev.*, 2016, **116**, 1398–1433.
4 K. Patel, S. H. Chikkali and S. Sivaram, *Prog. Polym. Sci.*, 2020, **109**, 101290/1–101290/30.
5 J. Boor Jr., in *Ziegler-Natta Catalysts and Polymerization*, Academic Press, New York, 1979.
6 S. H. Chikkali, *Resonance*, 2017, **22**, 1039–1060.
7 J. P. Claverie and F. Schaper, *MRS Bull.*, 2013, **38**, 213–218.
8 D. W. Sauter, M. Taoufik and C. Boisson, *Polymers*, 2017, **9**, 185.
9 L. K. Johnson, C. M. Killian and M. Brookhart, *J. Am. Chem. Soc.*, 1995, **117**, 6414–6415.
10 C. M. Killian, D. J. Tempel, L. K. Johnson and M. Brookhart, *J. Am. Chem. Soc.*, 1996, **118**, 11664–11665.
11 R. S. Birajdar and S. H. Chikkali, *Eur. Polym. J.*, 2021, **143**, 110183.
12 Q. Mahmood, X. Li, L. Qin, L. Wang and W. H. Sun, *Dalton Trans.*, 2022, **51**, 14375–14407.
13 Z. Wang, Q. Liu, G. A. Solan and W. H. Sun, *Coord. Chem. Rev.*, 2017, **350**, 68–83.
14 Y. Zhang, Y. Zhang, X. Hu, C. Wang and Z. Jian, *ACS Catal.*, 2022, **12**, 14304–14320.
15 M. Qasim, M. S. Bashir, S. Iqbal and Q. Mahmood, *Eur. Polym. J.*, 2021, **160**, 110783.
16 Y. Wang, R. Gao, Q. Gou, J. Lai, R. Zhang, X. Li and Z. Guo, *Eur. Polym. J.*, 2022, 111693.
17 G. Zhou, L. Cui, H. Mu and Z. Jian, *Polym. Chem.*, 2021, **12**, 3878–3892.
18 H. Mu, G. Zhou, X. Hu and Z. Jian, *Coord. Chem. Rev.*, 2021, **435**, 213802.
19 R. Wu, W. K. Wu, L. Stieglitz, S. Gaan, B. Rieger and M. Heuberger, *Coord. Chem. Rev.*, 2023, **474**, 214844.
20 H. Mu, L. Pan, D. Song and Y. Li, *Chem. Rev.*, 2015, **115**, 12091–12137.
21 Y. Zhang, Y. Zhang, X. Hu, C. Wang and Z. Jian, *ACS Catal.*, 2022, **12**, 14304–14320.
22 Z. Guan, P. M. Cotts, E. F. McCord and S. J. McLain, *Science*, 1999, **283**(5410), 2059–2062.
23 L. C. So, S. Faucher and S. Zhu, *Prog. Polym. Sci.*, 2014, **39**, 1196–1234.
24 M. Nele, J. B. Soares and J. C. Pinto, *Macromol. Theory Simul.*, 2003, **12**, 582–592.
25 D. P. Gates, S. A. Svejda, E. Oñate, C. M. Killian, L. K. Johnson, P. S. White and M. Brookhart, *Macromolecules*, 2000, **33**, 2320–2334.

Published on 06 December 2023. Downloaded by National Chemical Laboratory, Pune on 5/30/2024 3:00:58 PM.

26 S. Dai, S. Zhou, W. Zhang and C. Chen, *Macromolecules*, 2016, **49**, 8855–8862.
27 Y. Gong, S. Li, Q. Gong, S. Zhang, B. Liu and S. Dai, *Organometallics*, 2019, **38**, 2919–2926.
28 Y. Ota, S. Ito, J. Kuroda, Y. Okumura and K. Nozaki, *J. Am. Chem. Soc.*, 2014, **136**, 11898–11901.
29 L. Piche, J. C. Daigle, R. Poli and J. P. Claverie, *Eur. J. Inorg. Chem.*, 2010, 4595–4601.
30 O. B. de Oliveira, S. T. Brandao, A. J. D. de Freitas, E. P. da Silva, S. M. P. Meneghetti and M. R. Meneghetti, *Polym. Int.*, 2008, **57**, 1012–1016.
31 E. L. Yue, Q. F. Xing, L. P. Zhang, Q. S. Shi, X. P. Cao, L. Wang, C. Redshaw and W. H. Sun, *Dalton Trans.*, 2014, **43**, 3339–3346.
32 E. L. Yue, L. P. Zhang, Q. F. Xing, X. P. Cao, X. Hao, C. Redshaw and W. H. Sun, *Dalton Trans.*, 2014, **43**, 423–431.
33 S. L. Kong, C. Y. Guo, W. H. Yang, L. Wang, W. H. Sun and R. Glaser, *J. Organomet. Chem.*, 2013, **725**, 37–45.
34 K. F. Song, W. H. Li, B. X. Yang, Q. B. Liu, C. Redshaw, Y. S. Li and W. H. Sun, *Dalton Trans.*, 2013, **42**, 9166–9175.
35 S. L. Kong, K. F. Song, T. L. Liang, C. Y. Guo, W. H. Sun and C. Redshaw, *Dalton Trans.*, 2013, **42**, 9176–9187.
36 J. J. Lai, X. H. Hou, Y. W. Liu, C. Redshaw and W. H. Sun, *J. Organomet. Chem.*, 2012, **702**, 52–58.
37 Z. H. Zhou, X. Hao, C. Redshaw, L. Q. Chen and W. H. Sun, *Catal. Sci. Technol.*, 2012, **2**, 1340–1345.
38 J. L. Rhinehart, L. A. Brown and B. K. Long, *J. Am. Chem. Soc.*, 2013, **135**, 16316–16319.
39 S. Dai, X. Sui and C. Chen, *Angew. Chem., Int. Ed.*, 2015, **54**, 9948–9953.
40 X. Hu, S. Dai and C. Chen, *Dalton Trans.*, 2016, **45**, 1496–1503.
41 S. Dai and C. Chen, *Angew. Chem., Int. Ed.*, 2016, **55**, 13281–13285.
42 W. Lu, W. Fan and S. Dai, *Inorg. Chem. Front.*, 2022, **10**, 108–117.
43 L. Guo, X. Hu, W. Lu, D. Xu, Q. Liu and S. Dai, *J. Organomet. Chem.*, 2021, **952**, 122046.
44 Y. Gong, S. Li, C. Tan, W. Kong, G. Xu, S. Zhang, B. Liu and S. Dai, *J. Catal.*, 2019, **378**, 184–191.
45 H. Dau, A. Keyes, H. E. Basbug Alhan, E. Ordonez, E. Tsogtgerel, A. P. Gies, E. Auyeung, Z. Zhou, A. Maity, A. Das, D. C. Powers, D. B. Beezer and E. Harth, *J. Am. Chem. Soc.*, 2020, **142**, 21469–21483.
46 A. Keyes, H. Dau, K. Matyjaszewski and E. Harth, *Angew. Chem.*, 2022, **134**, e202112742.
47 J. Sun, F. Wang, W. Li and M. Chen, *RSC Adv.*, 2017, **7**, 55051–55059.
48 Z. Lu, X. Xu, Y. Luo, S. He, W. Fan and S. Dai, *ACS Catal.*, 2023, **13**, 725–734.
49 T. R. Younkin, E. F. Connor, J. I. Henderson, S. K. Friedrich, R. H. Grubbs and D. A. Bansleben, *Science*, 2000, **287**, 460–462.
50 C. Wang, S. Friedrich, T. R. Younkin, R. T. Li, R. H. Grubbs, D. A. Bansleben and M. W. Day, *Organometallics*, 1998, **17**, 3149–3951.
51 A. W. Waltman, T. R. Younkin and R. H. Grubbs, *Organometallics*, 2004, **23**, 5121–5123.
52 A. Berkefeld and S. Mecking, *J. Am. Chem. Soc.*, 2009, **131**, 1565–1574.
53 Z. Chen, M. Mesgar, P. S. White, O. Daugulis and M. Brookhart, *ACS Catal.*, 2015, **5**, 631–636.
54 M. P. Weberski Jr., C. Chen, M. Delferro, C. Zuccaccia, A. Macchioni and T. J. Marks, *Organometallics*, 2012, **31**, 3773–3789.
55 C. Wang, X. Kang, H. Mu and Z. Jian, *Macromolecules*, 2022, **55**(13), 5441–5447.
56 R. S. Birajdar, R. G. Gonnade, H. V. Pol, M. Basava Prabhu, D. Rokade, S. Nandimath and S. H. Chikkali, *Polym. Chem.*, 2023, **14**, 3239–3251.
57 E. Schiebel, S. Santacroce, L. Falivene, I. Goettker-Schnetmann, L. Caporaso and S. Mecking, *ACS Catal.*, 2019, **9**, 3888–3894.
58 S. S. Deshmukh, S. R. Gaikwad, R. Gonnade, S. P. Pandole and S. H. Chikkali, *Chem. – Asian J.*, 2020, **15**, 398–405.
59 For the *cis*-angle, see: S. R. Gaikwad, S. S. Deshmukh, R. G. Gonnade, P. R. Rajamohanan and S. H. Chikkali, *ACS Macro Lett.*, 2014, **4**, 933–937.
60 L. Falivene, Z. Cao, A. Petta, L. Serra, A. Poater, R. Oliva, V. Scarano and L. Cavallo, *Nat. Chem.*, 2019, **11**, 872–879.
61 D. P. Song, Y. X. Wang, H. L. Mu, B. X. Li and Y. S. Li, *Organometallics*, 2011, **30**(5), 925–934.
62 For oligoethylenes, see: N. R. Mote, S. R. Gaikwad, K. V. Khopade, R. G. Gonnade and S. H. Chikkali, *Dalton Trans.*, 2021, **50**, 3717–3723.
63 Z. Guan, *Chem. – Eur. J.*, 2002, **8**, 3086–3092.
64 T. Wiedmann, G. Voit, A. Tchernook, P. Roesle, I. Goettker-Schnetmann and S. Mecking, *J. Am. Chem. Soc.*, 2014, **136**, 2078–2085.
65 H. Fan, G. Chang, H. Bi, X. Gui, H. Wang, G. Xu and S. Dai, *ACS Polym. Au*, 2021, **2**, 88–96.
66 L. Guo, W. Liu, K. Li, M. Sun, W. Sun, L. Zhao, G. Jiang, H. Peng, Z. Liu and S. Dai, *Eur. Polym. J.*, 2019, **115**, 185–192.
67 E. A. Standley, S. J. Smith, P. Müller and T. F. Jamison, *Organometallics*, 2014, **33**, 2012–2018.
68 L. Cai, X. Zhu, J. Chen, A. Lin and H. Yao, *Org. Chem. Front.*, 2019, **6**, 3688–3692.
69 S. Meiries, K. Speck, D. B. Cordes, A. M. Z. Slawin and S. P. Nolan, *Organometallics*, 2013, **32**, 330–339.

 This journal is © The Royal Society of Chemistry 2024

European Polymer Journal 143 (2021) 110183

Contents lists available at ScienceDirect

European Polymer Journal

journal homepage: www.elsevier.com/locate/europolj

Insertion copolymerization of functional olefins: Quo Vadis?

Rajkumar S. Birajdar [a,b], Samir H. Chikkali [a,b,*]

[a] Polyolefin Lab, Polymer Science and Engineering Division, CSIR-National Chemical Laboratory, Dr. Homi Bhabha Road, Pune 411008, India
[b] Academy of Scientific and Innovative Research (AcSIR), Anusandhan Bhawan, 2 Rafi Marg, New Delhi 110001, India

ARTICLE INFO

Keywords:
Polyethylene
Functional polyethylene
Hydrophilic polyethylene
Insertion copolymerization
Catalyst
Functional polyolefins

ABSTRACT

Functional polyethylene is a specialty polymer with unique set of properties and caters to a niche market. Currently, it is manufactured using high-pressure, high-temperature radical polymerization, or post-reactor (indirect) modification methods. Insertion copolymerization of functional olefins with ethylene provides a low pressure, direct route to prepare functional polyethylenes. However, insertion copolymerization of functional olefins with ethylene poses several impediments and requires special considerations. This review presents the current strategies, examines the progress, and attempts to gauge the commercial potential of direct synthesis of functional polyethylene.

The performance of late transition metal catalysts derived from α-diimine, imine-phenolate, phosphine-sulfonate, bis-phosphine-mono-oxide, carbene-phenolate, phosphine-phenolate and their derivatives in the insertion copolymerization of functional olefins with ethylene is evaluated. While catalyst designing is crucial, incorporation of polar olefins that can serve an additional purpose is equally important. Therefore, we have organized the review in the following sections, polar alkenes with- acrylates, acrylic acids, acetates, nitriles, ethers, halides, two functional groups, cross-linking groups, dynamic interactions/self-healing properties, additional function/purpose, renewable functional olefins, and examine the progress. Among these, acrylates have been most intensively investigated and have been successfully incorporated in the polyethylene main-chain. Ethylene, methyl acrylate copolymers prepared by direct copolymerization reveal comparable melting temperature to that of LLDPE (at similar co-monomer content) and unfold the commercial potential of these materials. Recent developments on the insertion copolymerization of renewable functional olefins and di-functional olefins have elicited significant interest. This strategy is being viewed as a means of reducing environmental impact and enabling high functional group density at the same extent of incorporation. The overview thus offers a succinct account of insertion copolymerization of functional olefins, sheds light on the copolymer microstructure/material properties, and initiates a discussion on the commercial potential of functional polyethylene.

1. Introduction and scope

1.1. Functional polyolefins

Metal-catalyzed insertion polymerization of olefins to polyolefins is known for quite some time and today we produce about 180 million tons of polyolefins every year [1–3]. The scientific understanding and technological interventions have considerably simplified the industrial production of polyolefins. Polyolefins have reached every nook and corner of the planet and have become indispensable [4]. Despite this progress and the seeming maturity of the field, insertion copolymerization of functional olefins is still a formidable challenge [5–7]. Incorporation of functional olefin in a polyethylene (PE) or polypropylene (PP) backbone can confer beneficial properties such as adhesion, printability, permeability, miscibility, and compatibility on to the resultant functional polyolefin (Fig. 1). Such functional polyolefins find niche applications in paints, adhesives, coatings, printing, and nano-electronics, to name a few [8]. Thus, the commodity polyolefins could be upgraded to specialty functional polyolefins if functional groups can be incorporated in their backbone.

The early transition metals (ETM) used in the insertion or Ziegler-Natta polymerization are readily poisoned by functional olefins and polymerization is halted [9]. Late transition metals (LTM) could tolerate functional groups and could incorporate functional olefins in the

* Corresponding author at: Polyolefin Lab, Polymer Science and Engineering Division, CSIR-National Chemical Laboratory, Dr. Homi Bhabha Road, Pune 411008, India.
E-mail address: s.chikkali@ncl.res.in (S.H. Chikkali).

https://doi.org/10.1016/j.eurpolymj.2020.110183
Received 19 September 2020; Received in revised form 19 November 2020; Accepted 25 November 2020
Available online 16 December 2020
0014-3057/© 2020 Elsevier Ltd. All rights reserved.

polymer backbone [10]. Apart from insertion (co)polymerization, functional polyolefins can be prepared by Ring Opening Metathesis Polymerization (ROMP) of a cyclic-functionalized olefin (Fig. 1) [11]. However, this route requires a dedicated synthesis of functionalized cyclic olefins and is a multistep process. Similarly, Acyclic Diene Metathesis (ADMET) polymerization of functionalized diene monomers can also yield functional polyolefins [12]. This route too requires specific synthesis of diene monomer and, after the polymerization, the double bonds in the polymer backbone have to be hydrogenated. Thus, although competitive preparation routes exist, insertion copolymerization appears to be the only direct method to prepare functional polyolefins in one step.

Insertion copolymerization of functional olefins is not trivial and requires special considerations before a suitable catalyst could be identified or designed. There are at least three fundamental limitations that have to be addressed while designing a suitable catalyst. 1) The early transition metals (titanium, zirconium, chromium, etc.) regularly used on an industrial scale are highly acidic in nature and do not tolerate functional groups. Therefore, while designing catalysts, functional group tolerant metals have to be selected. Late transition metals (nickel, palladium, platinum, etc.) are known to tolerate functional groups, and metals such as nickel and palladium would be the preferred choice. 2) The second challenge is functional group coordination (σ-complex formation) to the catalytic metal, leading to catalyst poisoning. This bottleneck can be addressed by tailoring the electronic and steric properties of the catalyst, wherein ligand designing plays a crucial role. 3) The last hurdle could be chelate formation with the metal center after the insertion of functional olefin. Thus, any attempt to develop a successful catalyst for insertion copolymerization of functional olefin has to address the above limitations. The last three decades have witnessed partial success and Fig. 2 depicts representative catalysts (**C1**-**C5**) capable of functional olefin copolymerization [13].

An early breakthrough was reported by Brookhart and co-workers in the mid-'90 s [14,15]. In a rational design approach, an α-diimine ligated palladium complex **C1** (Fig. 2) was employed and insertion copolymerization of ethylene with methyl acrylate was successfully achieved for the first time. The catalyst was activated using co-catalysts such as methyl aluminoxane (MAO) or boron-based activators [16–18]. The catalytic system features two neutral imine-donors, which form coordination bonds with a cationic metal (LTM) center, and the fourth coordination is satisfied by a weakly coordinating donor solvent (D). Since its discovery in the 1990 s, this catalytic system has been rigorously tailored on several occasions and has been utilized in the insertion copolymerization of various functional olefins [19,20]. Although a large variation is reported in the ligand backbone, the metal of choice has been mainly nickel and palladium, as they tolerate various functional groups [21]. A neutral, single component phenoxy-imine nickel complex was reported by Grubbs and co-workers in 2000 (Figure 2, **C2**). It was demonstrated that **C2** could tolerate functional groups such as ester and could copolymerize functional olefins with ethylene [22]. Subsequently, the phenoxy-imine catalyst has been tested by different research groups in functional olefin copolymerization [23].

In 2002, Drent and co-workers reported a palladium complex **C3** derived from *ortho*-phosphinobenzenesulfonate ligand. **C3** has been the most successful catalytic system in polar olefin copolymerization and tolerates most functional olefins. The characteristic ligand design is credited for its success. The *ortho*-phosphinobenzenesulfonate ligand features a neutral phosphine donor and an anionic sulfonate group. There are two parameters that empower **C3** to outperform other catalytic systems; the charge effect and the orbital interactions. 1) **C3** is a neutral palladium (II) system and therefore it is a relatively electron-rich compared to catalysts with a metal center in lower oxidation state or cationic metal complexes. Since it is (**C3**) electron-rich, it has a lower affinity towards functional groups and therefore functional olefins are tolerated by **C3**. 2) Theoretical investigations point that the lone pair of the ligated oxygen (in sulfonate group) repels π-electron on palladium, which facilitates palladium back-donation to π-acceptor olefin monomer [24]. This metal back-donation further strengthens monomer-metal

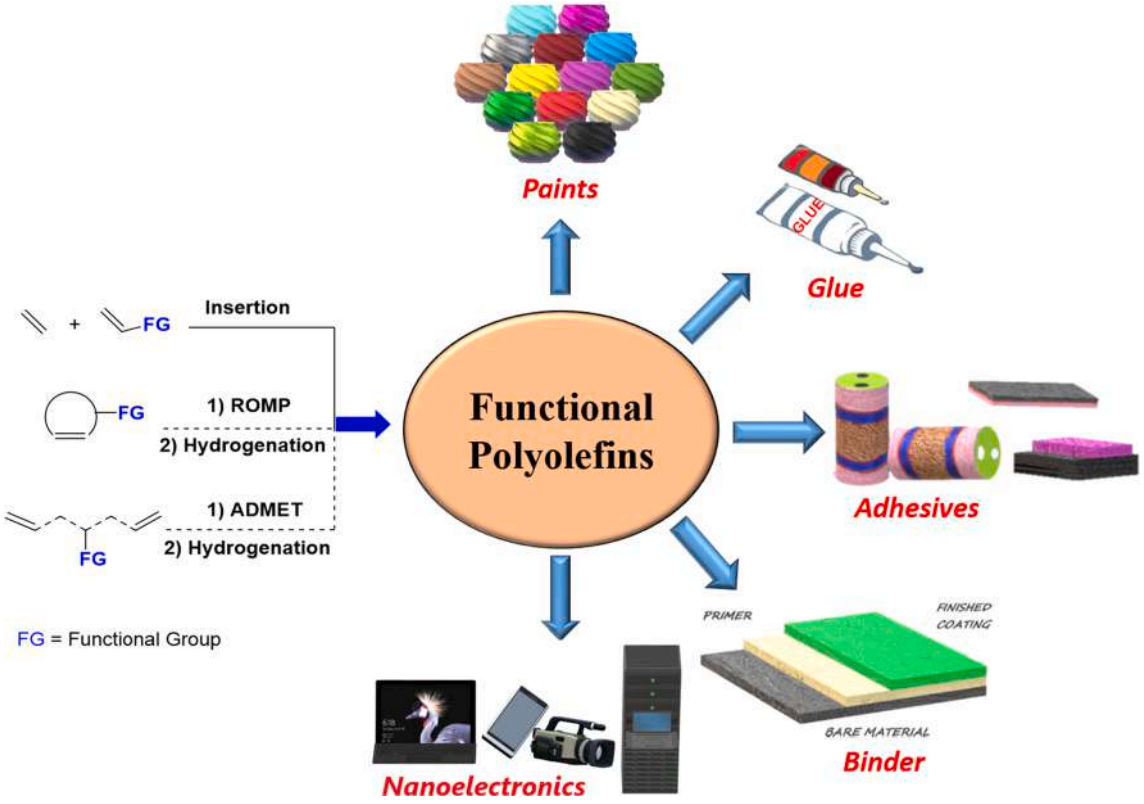

Fig. 1. Synthesis and applications of functional polyolefins.

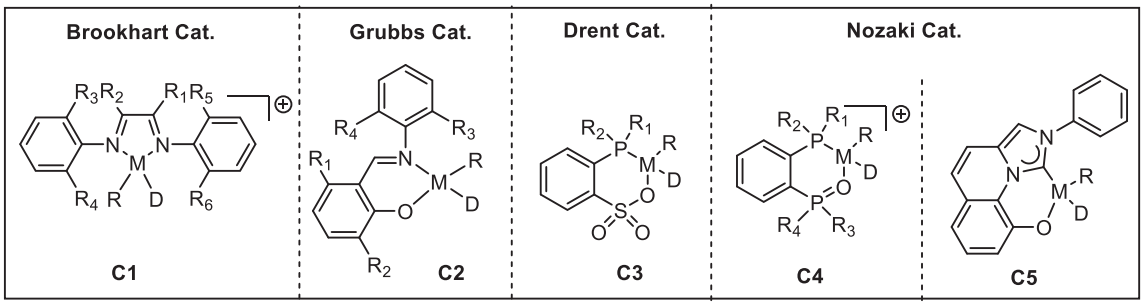

Fig. 2. Representative catalysts capable of insertion copolymerization of polar functional olefins.

π-complex formation, which promotes the insertion of olefins. Thus, the characteristic ligand feature enables **C3** for olefin insertion and functional olefin copolymerization.

In the last decade, Nozaki and coworkers introduced two catalytic systems that are capable of incorporating functional olefins in the polyolefin backbone. A bidentate ligand called bisphosphine monoxide (BPMO), disposing two neutral donors, was ligated on to LTM to produce complex **C4** [25]. Unlike **C3**, **C4** is a cationic system with a counter anion and the vacant fourth coordination is occupied by a donor solvent. The BPMO ligand with aliphatic substituents on phosphine met with limited success, subsequent ligand tailoring enabled **C4** (with aromatic substituents on phosphine) to initiate insertion copolymerization of functional olefins. Jordan and co-worker attempted replacing phosphine in **C3** with an *N*-heterocyclic-carbene (NHC) and prepared corresponding neutral palladium complex [26]. However, this palladium complex could not react with ethylene and polymerization could not take place. In a rational ligand design approach, Nozaki and co-workers reported palladium complex bearing imidazo[1,5-a]quinolin-9-olate-1-ylidene (IzQO) ligand. In the IzQO ligand, the neutral phosphine donor is replaced with isoelectronic *N*-heterocyclic-carbene (NHC) and the anionic SO_3^- is replaced by an anionic O^- donor. The orientation of NHC-plane appears to be very crucial in creating desired congestion around the active metal center. A carefully crafted, IzQO ligated, neutral, palladium complex **C5** was found to be a very active catalyst in the insertion copolymerization of functional olefins [27]. Thus, **C1**-**C5** are the work-horse catalytic systems, that are most successful in insertion copolymerization of functional olefins, among others [28,29].

1.2. Scope and objectives

Discovery of transition metal-catalyzed insertion copolymerization of functional olefins has revived the seemingly mature field of olefin polymerization and catalysts capable of incorporating functional olefins have been reported. Two curious questions drive the field, i) is it possible to design a metal catalyst that is capable of insertion copolymerization of functional olefins with high activity, molecular weight and controlled microstructure and, ii) can we prepare functional polyolefins that can replace existing binders, adhesives, primers, etc.? The former question has been partly answered, while, we don't know if we have an answer to the latter. Therefore, this review is an attempt to address the latter question and examine where is the field going, or, in Latin, "Quo Vadis"? The field of insertion copolymerization of functional olefins is completing a journey of three decades and therefore requires profound introspection by the experts and aspiring leaders to decide the future course. While ligand and catalyst design for insertion copolymerization of functional olefins is crucial, incorporation of novel polar olefins is equally important. Therefore, contemporary strategies that guide polar olefin selection to tailor specific copolymer properties, have to be identified and executed.

This review aims to identify successful strategies in insertion copolymerization of functional olefins and highlight the novelty of ligands, catalysts, and polar olefinic monomers. In order to do so, we categorize functional olefinic monomers and review the progress made in a specific category of monomer. Thus, polar olefins with acrylates, acrylic acids, acetates, nitriles, ethers, halides, 1,1-disubstituted olefins, olefins with cross-linking groups, olefins with additional function/purpose and, renewable functional olefins are reviewed. Our emphasis is on functional olefin, how these behave in presence of a particular catalyst, the challenges posed, underlying mechanistic understanding, and final properties of a copolymer. This review is predominantly polar olefin centric and therefore, for catalyst centric reviews the reader is directed to other recent literature on this topic [30,31]. In this overview, we summarize: i) insertion copolymerization of various functional olefins with ethylene, ii) present characteristic features of resultant copolymers, iii) correlate the performance of different catalytic systems in the insertion copolymerization of functional olefins, iv) a consolidated picture of the state-of-the-art and, v) critically review the path forward in our attempts to know where is the field heading. This review is limited to insertion copolymerization of functional polar olefins using LTM catalysts and excludes ETM catalysts, carbene polymerization, ethylene-CO/CO_2 copolymerization (except wherever it is related to functional olefin copolymerization), organometallic mediated radical polymerization of functional olefins or controlled radical polymerization of functional olefins, etc. Furthermore, post-functionalization of chain-end functionalized polyolefins, surface functionalization of polyolefins, other methods of functionalization of polyolefins, etc. has been summarized elsewhere and is beyond the scope of this review [32–37].

2. Insertion copolymerization: Acrylates

Acrylates constitute an important class of industrial monomers and poly(acrylates) are being industrially manufactured using emulsion, solution, etc. polymerization methods. Acrylates are typically polymerized using radical or anionic initiators, and find applications in medical products, eye lenses, coatings, textiles, adhesives, paints, paper, and pulp industry, etc. [38–40]. However, insertion polymerization or copolymerization of acrylates was not reported until recently. In this context, current state of the art in insertion copolymerization of acrylates is discussed in sections 2.1 to 2.3.

2.1. Methyl acrylate

High-pressure radical polymerization of ethylene with methyl acrylate (MA) is industrially practiced to manufacture ethylene–methyl acrylate copolymers (EMA) such as Elvaloy® (ExxonMobil) or Lotryl® (Arkema). However, radical polymerization of ethylene and methyl acrylate demands very high-pressure and high-temperature, and there is less control over incorporation, placement of MA, molecular weight, and molecular weight distribution. A paradigm shift could be achieved, if EMA copolymers could be prepared under mild conditions, at low-pressure. Due to their commercial significance, among functional olefins, acrylates were the first to be evaluated in insertion copolymerization with ethylene. In a seminal report, Brookhart disclosed the first example of insertion copolymerization of methyl acrylate with ethylene

using palladium catalyst **C1** in 1996 [14,15]. Use of α-diimine chelated late metal catalyst appears to be responsible for tolerating the ester group. The resultant copolymer was found to be highly branched (100 branches per 1000 carbon atoms) amorphous material (Scheme 1, *br*-EMA). The ester groups were located at the chain end of the branches as the Pd(II) complexes

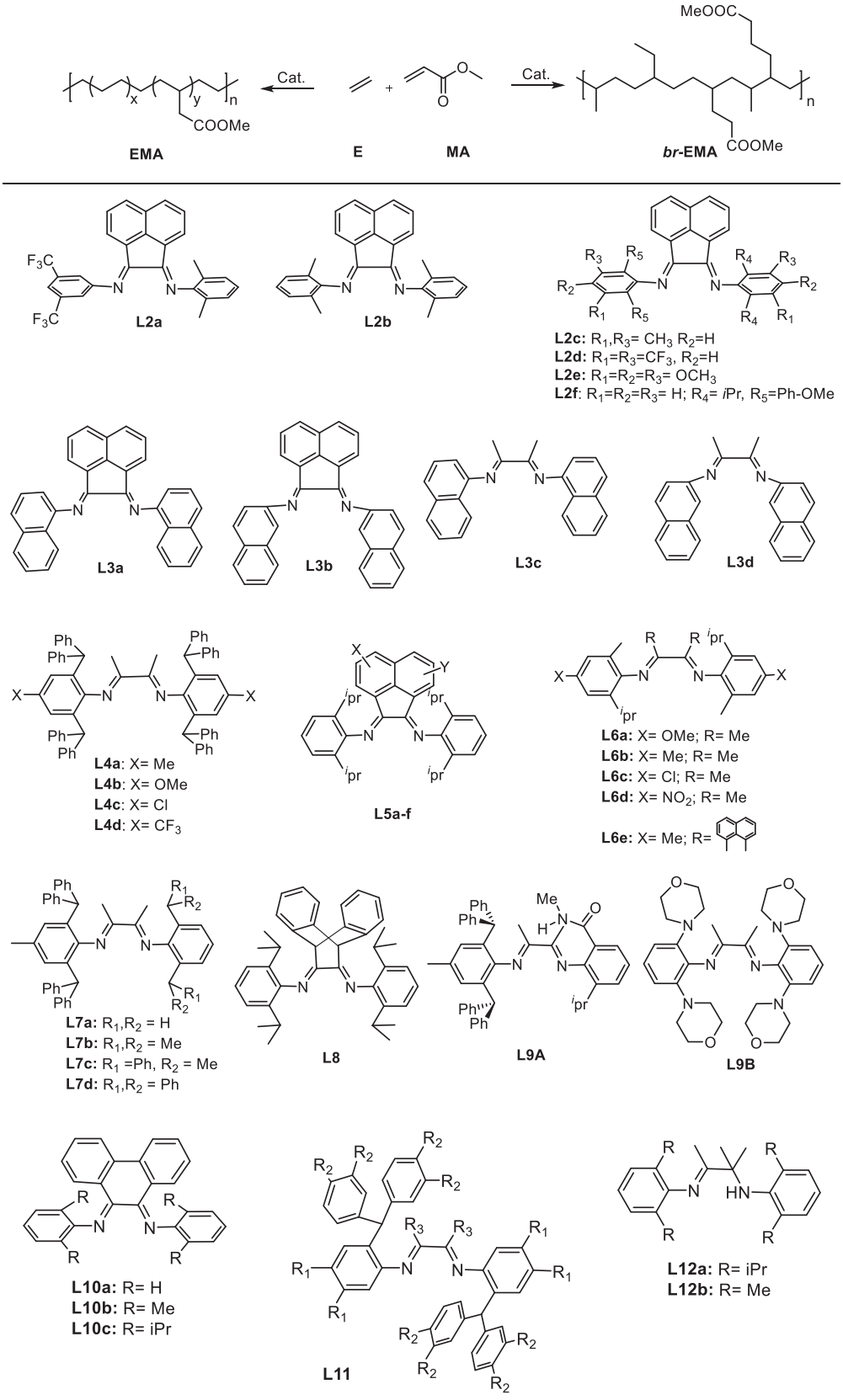

Scheme 1. Copolymerization of ethylene with methyl acrylate and modification to the α-diimine derived ligand system.

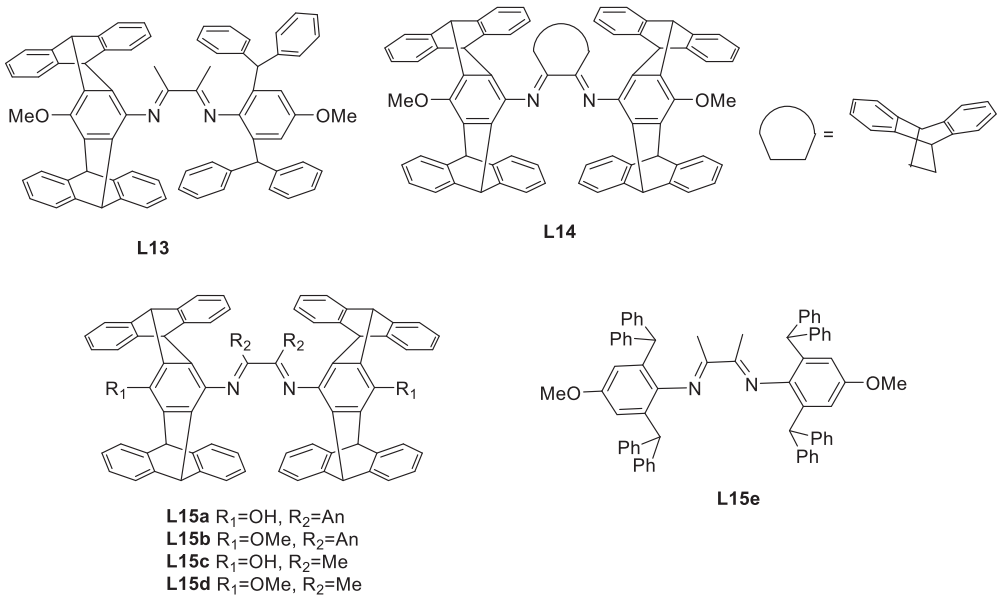

Scheme 1. (*continued*).

have the propensity to undergo β-hydride elimination and reinsertion (leading to chain-walking) of olefin. The phenomenon of chain-walking or chain-running has been extensively investigated and polyethylene with interesting properties has been prepared [41–43]. In fact, based on these findings, DuPont launched a polyethylene grade called "Versipol®" [44,45]. The discussion about chain-walking to yield Versipol® is beyond the scope of this review and the reader is referred to recent reports on this topic [46,47]. The parent Brookhart catalyst **C1** is continuously tailored to meet the increasing demand of insertion copolymerization of functional olefins. Modified **C1** has been employed in insertion copolymerization of methyl acrylate with ethylene and we summarize these developments in chronological order (Scheme 1).

Milani and co-workers reported synthesis of peculiar non-symmetrical and symmetrical substituted bis(aryl-imino)acenaphthene (Ar-BIAN) ligands **L2a-e** and corresponding neutral and cationic Pd-complexes were prepared (Scheme 1) [48]. Pd-complexes with two different donor solvents, namely, acetonitrile and dimethyl sulfoxide were also tested. The Pd-DMSO complexes revealed presence of different species in solution depending on the ligand. Ligand **L2b** displayed the complex with S-bonded DMSO. While, for **L2d**, isomers with S- and O-bonded DMSO were observed. The non-symmetric ligand **L2a** displayed existence of three species that differ in the coordination mode of DMSO and the relative position of Pd-CH_3 with respect to the two halves of Ar-BIAN. The performance of new nonsymmetric Ar-BIAN ligand (**L2a**) derived Pd–$NCCH_3$ and Pd–DMSO complexes were tested in the ethylene/methyl acrylate co-oligomerization. The resultant product was found to be a mixture of ethylene/methyl acrylate co-oligomers and higher alkenes. Pd-complexes derived from non-symmetric Ar-BIAN ligand **L2a** were found to be more active than their symmetrical counterparts (Pd-complexes derived from **L2b-e**) in the co-oligomerization. Among the two **L2a** derived palladium complexes, Pd–DMSO complex displayed higher stability and productivity than the Pd-$NCCH_3$ derivative. The reactivity of MA with Pd-complexes was investigated by treating a 10 mM (millimolar) CD_2Cl_2 solution of the Pd-complex with MA (2 equivalent) at room temperature. The ^1H NMR was recorded after every 5-minute for about 20 min. The NMR findings show that the acetonitrile is released and MA coordinates to generate five and six-membered palladacycles. An unsymmetrical version of ligands **L2a-e** i.e. **L2f**, was also reported [49]. Pan et. al prepared thermally stable α-diimine ligated palladium complexes and investigated their performance in ethylene homo-polymerization and ethylene, methyl acrylate copolymerization. The rigid naphthyl group on **L2f** backbone reduces the squeeze and push of the ligand around the palladium atom. The reduced repulsive forces increase the thermal stability of the complex. In line with this, increasing copolymerization temperature from 25 °C to 50 °C increases the methyl acrylate incorporation from 2.11% to 4.03%.

A year later, further modification to the α-diimine system was reported by the same group [50]. This time, the phenyl groups on the imine nitrogen were replaced with 1-naphthyl- and 2-naphthyl-substituents (Scheme 1, L3a-d). The corresponding neutral [Pd(CH_3)Cl(N–N)], and monocationic [Pd(CH_3)(L)(N–N)][PF_6] (L = CH_3CN, DMSO), palladium complexes were prepared and characterized using NMR, single-crystal X-ray analysis which suggested syn- and anti-isomerism with slow or fast exchange of 1 and 2 naphthyl substituted ligands. These palladium complexes were tested in ethylene, methyl acrylate copolymerization (Scheme 1). It was found that palladium complexes derived from **L3c** outperform the remaining three complexes in the copolymerization.

Sterically bulky α-diimine ligands of type **L4a-d** (Scheme 1) with electron-withdrawing and electron-donating substituents were prepared by Chen and co-workers in an excellent isolated yield [51]. Corresponding neutral palladium complexes were synthesized and fully characterized using solution NMR and single-crystal X-ray diffraction. These Pd-complexes were found to be thermally stable and displayed good activity in ethylene homo- and ethylene–methyl acrylate copolymerization. Among the four ligands, Pd-complexes derived from electron-poor ligands (**L4c** and **L4d**) were less active. Therefore, insertion copolymerization of ethylene and methyl acrylate was investigated using palladium complexes derived from **L4a** and **L4b**. Both these catalysts were active in the copolymerization and revealed highest MA incorporation of about 3%, with about 50 branches per 1000 carbon atoms. These complexes were found to be 3–4 times more active than the parent Brookhart system **C1**. Chen and co-workers investigated the effect of backbone substitution in **C1** on the copolymerization [52]. Ligands **L5a-f** (Scheme 1) with acenaphthyl backbone and various substituents on the backbone were prepared and corresponding nickel/palladium complexes were generated. The acenaphthyl ligands with two methoxy groups on the *ortho* position were active in ethylene polymerization and, produced PE with three times higher molecular weight (up to 418000 g/mol) and low degree of branching. Among the six Pd-complexes derived from **L5a-f**, sterically encumbered Pd-complex with two methoxy substituents on the acenaphthyl backbone produced E-MA

copolymer with higher activity and molecular weight. Along the same line, the palladium complexes bearing unsymmetrical α-diimine ligands **L6a-e** (Scheme 1) with different electron donating and withdrawing substituents at the para position of the aniline were tested in copolymerization [53]. The resultant copolymers displayed narrow polydispersity index (PDI). The highest MA incorporation of 3–4% was observed, except for palladium catalyst derived from electron-withdrawing NO_2 containing ligand **L6d**. It is most likely that the NO_2 substituent turns the palladium center into a more electrophilic metal-center, which is then poisoned by the incoming MA. Ligand properties (steric and electronic) can alter polymer microstructure such as branching density, molecular weight, and co-monomer incorporation. The changes in polymer microstructure can induce alteration in melting temperature, mechanical properties, and surface properties of the resultant polymer. Unsymmetrical α-diimine ligands of type **L7a-d** (Scheme 1) were prepared and the corresponding palladium complexes were synthesized [54]. When these palladium complexes were tested in the insertion copolymerization of ethylene and methyl acrylate, it was found that with increase in steric on the catalyst, MA incorporation decreases. While, sterically less bulky catalysts are more reactive towards the bulky methyl acrylate monomer. Using a series of ligands with increasing steric parameters, incorporation of MA could be tailored from 0.4% to 13.8%, and the molecular weight of copolymer could be varied from 1.1×10^3 to 79.8×10^3 g/mol. The branching density was also altered from 30 branches per 1000 C-atoms to 119 branches per 1000 C-atoms.

Gao and co-workers reported a thermally stable α-diimine ligand **L8** (Scheme 1) bearing dibenzobarrelene backbone [55]. The corresponding neutral and cationic palladium complexes were prepared and their existence was unambiguously ascertained by single-crystal X-ray diffraction. The two complexes were tested in the copolymerization of ethylene with a variety of acrylate co-monomers. The bulky dibenzobarrelene backbone provided improved selectivity towards 2,1-insertion product of methyl acrylate. This prevents the 1,2 insertion, which poisons the metal by the formation of stable five-membered palladacycle intermediate with MA. At higher ethylene pressure (300 psi) relatively linear copolymer was formed, while at lower ethylene pressure (3 psi), a hyperbranched copolymer was observed. The branching topology can be altered by changing ethylene pressure.

In small-molecule catalysis, it is known that hydrogen bonding interaction in the second coordination sphere can significantly influence catalyst properties and outcome of the reaction [56]. In this context, Jordan and co-workers installed a supramolecular/hydrogen bonding motif in the parent **C1** system and evaluated its performance in insertion copolymerization. The α-diimine ligand was mounted with secondary amide (−CONHMe) or tertiary amide ($-CONMe_2$) substituents on the N-aryl rings to produce **L9A** (Scheme 1) [57]. The existence of hydrogen-bonding interaction was demonstrated by analyzing a single crystal of the catalytic system **[(L9A)PdMeCl]**, as depicted in Fig. 3. Secondary amide is a hydrogen bond donor and acceptor but tertiary amide is only a hydrogen bond acceptor. In **[(L9A)PdMeCl]**, the Cl unit is *cis* to the amide functional group and displays a weak N-H….Cl (2.95 Å) intramolecular interaction. With an increase in steric hindrance on the ligand catalytic activity was found to increase. For a fair comparison, a non-hydrogen bonding ligand of type **L7** was prepared and corresponding Pd-complex was tested in insertion copolymerization. The secondary amide functional group-containing catalyst incorporates higher percentage of methyl acrylate during copolymerization with ethylene. Thus, insertion copolymerization of E-MA revealed a MA incorporation of 1.3 to 2.4%, and a molecular weight of 0.98 –8.1 $\times 10^3$ g/mol was obtained. The non-hydrogen bonding

ligand system displayed lower activity with 0.61% MA incorporation. Although there is no direct evidence of H-bonding interaction between incoming MA and the amide group on the catalyst, based on higher incorporation of MA and literature precedence [58], it is reasonable to assume the existence of such supramolecular interactions. Chen and co-workers independently reported α-diimine ligands bearing morpholine motifs, which are capable of forming weak interactions. Thus, ligands of type **L9B** (Scheme 1) were prepared and nickel complexes were tested in ethylene, methyl acrylate copolymerization [59]. The **L9B** ligated nickel complex initiated the copolymerization in presence of a co-catalyst (MAO) and produced EMA with 5–7.5% MA incorporation and number average molecular weight of 4500–5500 g/mol. Unlike parent **C1** system, above EMA copolymer revealed only 6–11 branches per 1000 carbon atoms. Secondary interactions between the **L9B** morpholine (N-donor) substituent and the nickel appears to be responsible for reduced chain-walking and low branching.

The α-diimine ligands **L10a-c** (Scheme 1) with phenanthrene

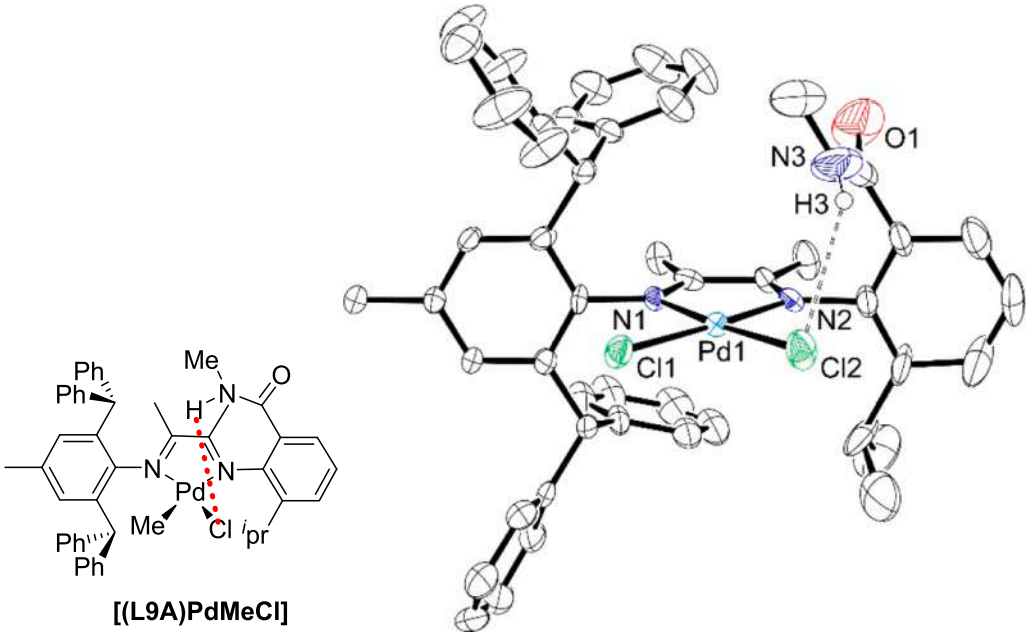

Fig. 3. Molecular structure of **[(L9A)PdMeCl]** depicting the hydrogen-bonding interaction between the amide-motif and the substituent on palladium. Reproduced with permission from Zhai et al. [57]. Copyright 2017 American Chemical Society.

backbone were synthesized and the corresponding Pd- and Ni-complexes were reported in 2019 [60]. The Pd-complexes were thermally stable and were active in ethylene homopolymerization and, ethylene–methyl acrylate copolymerization. Insertion copolymerization of E with MA using monocationic Pd-complexes derived from **L10a-c** displayed an MA incorporation of 5.3 mol%. Detailed analysis of the copolymer revealed highly branched EMA, wherein MA is located at the end of the branches and into the main chain. Unsymmetrically monosubstituted α-diimine ligands of type **L11** (Scheme 1) were reported by Jian and co-workers and, the corresponding Ni- and Pd-complexes were prepared [61]. The metal complexes produced linear high molecular weight polyethylene at low temperature and a highly branched PE was observed at high temperature. The copolymerization of ethylene/MA produced a branched EMA co-oligomer with up to 3.4% MA incorporation. In the resultant co-oligomer, the MA was observed at the chain-ends of the branches. Thus, highly branched ethylene oligomers with chain-end functionalization were obtained.

A slightly different modification to the classical α-diimine ligands was reported by Hu et. al and an amine–imine ligand of type **L12a-b** (Scheme 1) with different donating ability was prepared [62]. Corresponding cationic palladium complexes were synthesized and existence of a coordination bond between the amine donor and palladium was confirmed. The cationic complexes were active in ethylene homopolymerization and copolymerization of ethylene with methyl acrylate. As compared to the **C1**, the cationic complexes prepared using **L12a** revealed 3-fold higher incorporation of MA under identical conditions. Analysis of resultant copolymer disclosed presence of in-chain incorporated MA units, as well as, MA units at the branch/chain end.

Jian and coworkers reported sterically hindered unsymmetrical pentiptycenyl/dibenzhydryl α diimine ligands (**L13**) and corresponding Ni/Pd complex [63]. These complexes were tested in the copolymerization of ethylene with methyl acrylate. At low ethylene pressure (2 bar), up to 2.87 mol% MA incorporation was observed. While the reaction at higher pressure (8 bar) produced a copolymer with 0.83 mol % MA incorporation. The same group reported highly rigid α-diimine ligands (**L14**) and their Pd complexes [64]. The Pd(II) catalyst was active in ethylene homopolymerization as well as ethylene MA copolymerization. The copolymerization of ethylene and MA in presence of radical inhibitor (galvinoxyl) yielded a copolymer with 1.5 mol% MA incorporation. The microstructure of the copolymer was investigated by NMR spectroscopy. The functional group appears to be distributed in the polymer main chain as well as in the terminating end. In the stoichiometric reaction between [Pd(ACN)] complex with 15 equivalent of MA, formation of two insertion products was observed. ATR-IR, ESI-MS, and elemental analysis revealed that the major product is a five-membered chelate (formed by the 1,2 insertion of MA) and a minor amount of six-membered chelate (this is formed by 2,1 insertion). Sterically demanding pentiptycenyl N-aryl substituted α-diimine ligands (**L15a-e**) (which combines both dibenzhydryl substituent and a dibenzobarrelene backbone) and corresponding Ni/Pd catalysts were tested in ethylene (co)polymerization [65]. In the copolymerization reaction, pentiptycenyl-derived Ni(II) catalyst revealed higher catalytic activity up to 3.74×10^6 g $mol^{-1}h^{-1}$ and lower branching density compared to the dibenzhydryl-derived Ni(II) catalyst. The copolymerization of ethylene and MA was extensively studied using Pd-catalyst and up to 4.1 mol% of MA incorporation was observed. The parent α-diimine ligated palladium system **C1** produced highly branched *br*-EMA copolymers, while recent modifications could reduce the branching density to a large extent.

In a significant development, Drent et. al reported a neutral palladium catalyst **C3** (Fig. 2) capable of producing ethylene, methyl acrylate copolymers, with the acrylate units built into the linear polymer chain (EMA) [66]. The designing features of this system have been discussed in earlier section 1.1. The catalyst was generated in situ by treating *ortho*-phosphinobenzenesulfonate ligand with $[Pd(OAc)_2]$ or $[Pd(dba)_2]$ (dba = dibenzylideneacetone) to yield neutral palladium complex. The thus formed catalyst is capable of copolymerizing ethylene and methyl acrylate. Detailed NMR investigations revealed that the methyl ester group is incorporated in the copolymer main-chain and a maximum MA incorporation of 13% could be observed. Furthermore, ^{13}C NMR experiments of the resultant copolymer disclosed 1 methyl branch per 1000 carbon atoms, demonstrating high linearity of the EMA copolymer. Unlike **C1**, which decomposes at a higher temperature, **C3** catalysts were found to be stable until 70 °C. The characteristic features, high functional olefin incorporation, and higher thermal stability invoked considerable scientific interest and **C3** system is being rigorously investigated by many academic and industrial R&D groups around the world. The subsequent development in the insertion copolymerization of methyl acrylate with ethylene is reviewed in chronological order.

Nozaki and co-workers prepared anionic palladium complexes derived from *ortho*-phosphinobenzenesulfonate (**L16b**) and tested them in the insertion copolymerization of ethylene with methyl acrylate [67]. The anionic palladium complexes were active in the insertion copolymerization and revealed the highest MA incorporation of 16% with a number average molecular weight of 4500 g/mol. After the initial success with MA incorporation, the reactivity of palladium-phosphinobenzenesulfonate with methyl acrylate was investigated by Mecking and co-workers [68]. The neutral **L16b** ligated palladium complex reacts with MA and, the formation of 1,2-insertion and 2,1-insertion products was observed. In fact, two consecutive MA insertion products could be identified and these were characterized using single-crystal X-ray diffraction. The molecular structure revealed that the MA inserted units form a chelate with metal through the ester oxygen atom. When these MA inserted compounds were used as catalyst precursors and were exposed to ethylene, the formation of chain end functionalized polyethylene (Scheme 3, PE-ef) was observed. These results indicate that the Pd-ester chelate opens-up in the presence of ethylene and enables polymerization. The isolation of MA insertion products and chelate opening in the presence of ethylene imitates copolymerization steps and suggest that the chelate formation may retard the rate of olefin coordination to a certain extent but does not fully prohibit polymerization.

In 2011, terpolymerization of styrene and MA with CO was reported using phosphine sulfonate palladium complexes derived from ligands **L16a-c** (Scheme 2) [69]. In situ generated palladium complex derived from ligand **L16b** was used for terpolymerization of styrene, MA and carbon monoxide. The produced terpolymer (Scheme 3) displayed the random distribution of styrene, MA and CO in the polymer chain with narrow PDI. The ratio (x:y; see Scheme 3) was determined by ^{13}C NMR and could be varied in a wide range from 6:94 to 83:17 by changing the feed composition. The thermal analysis of the resultant polymer ruled out the possibility of styrene-CO and MA-CO block copolymers and supported existence of terpolymers in which the styrene-CO and MA-CO block are randomly distributed. In an attempt to establish a structure–activity relationship for **C3**, Claverie and co-workers reported different (sterically and electronically) substituents on the phosphorus atom in phosphinobenzenesulfonate. The authors systematically substituted phosphorus (9 different substituents were investigated) and ligands **L16e** and **L16f** in scheme 2 represent these variations [70]. Palladium complexes bearing ligand **L16e** with phenyl and *tert*-butyl substituent was found to incorporate 28% of MA in an ethylene MA copolymerization. Even homopolymerization of MA was attempted using **L16e** chelated Pd-complex and a homooligomer of MA with a number average molecular weight of only 600 g/mol was obtained.

Defining a structure–activity (catalyst structure which is controlled by ligand structure and its effect on activity) relationship in insertion polymerization is a challenging task and requires exhaustive investigations to come to a conclusion. It is often difficult to separate the steric and electronic parameters and drawing a conclusion becomes a risky affair. Mecking and co-workers prepared 13 different symmetric and asymmetric phosphinobenzenesulfonate ligands

and few of them have been listed as **L17a-f** (Scheme 2) [71]. The phosphinobenzenesulfonate ligands were treated with palladium and,

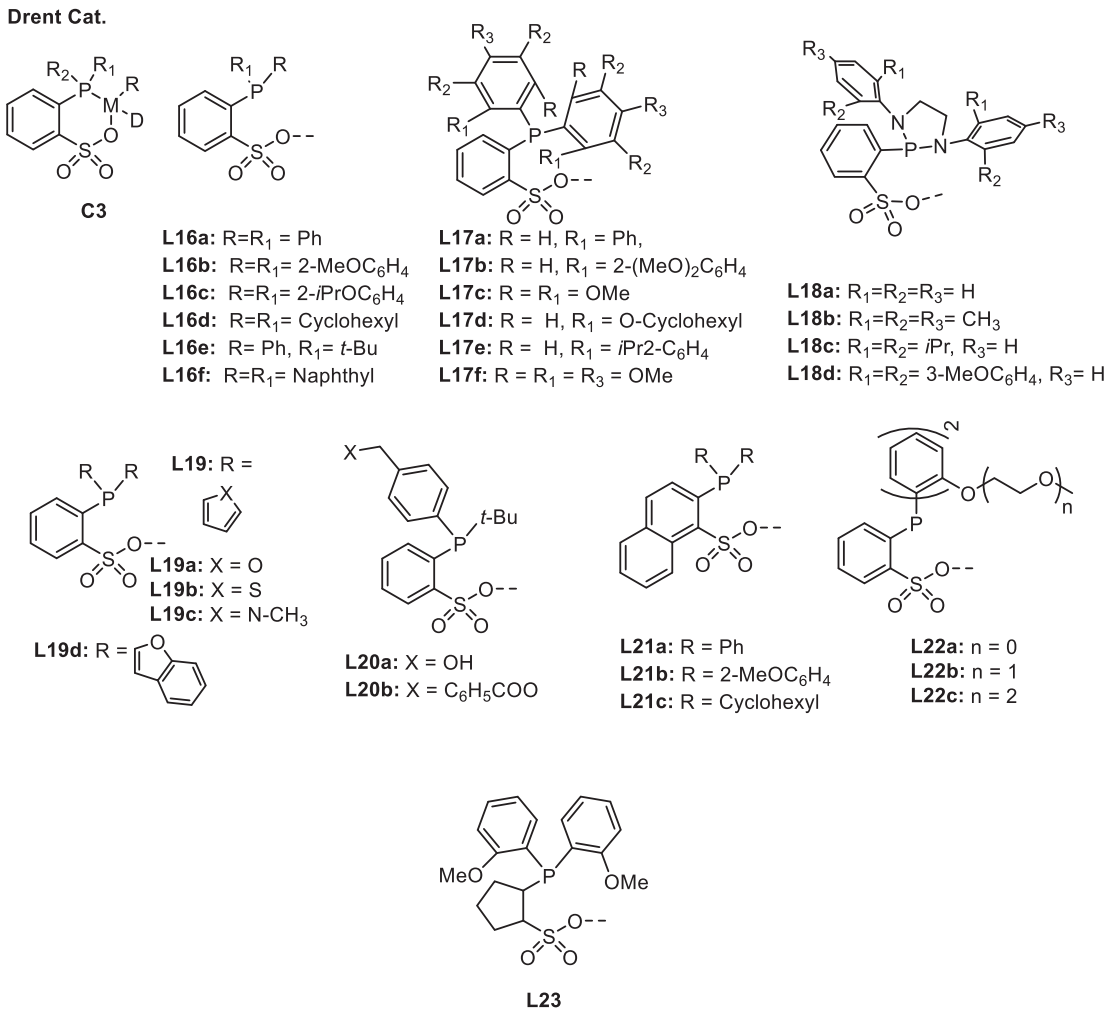

Scheme 2. Modifications reported for the phosphinobenzenesulfonate derived ligand system.

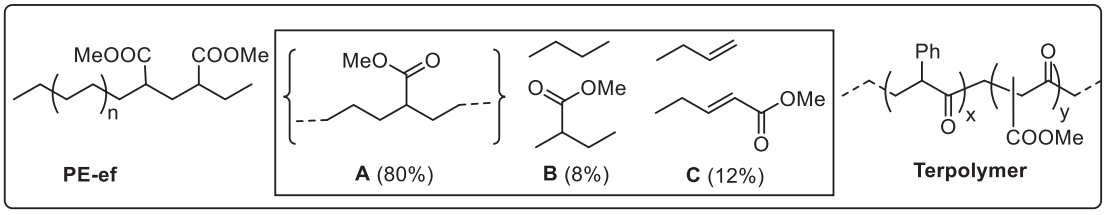

Scheme 3. Functional polyolefins: chain-end functionalized PE (PE-ef, left), types of end functionalization's (A, B, C, center), and Terpolymer (right).

were *in-situ* activated by using $AgBF_4$. These complexes displayed consecutive MA insertion along with decomposed products and β-H eliminated products, which were characterized by the NMR spectroscopy. The palladium complexes derived from twelve ligands of type **L17** (Scheme 2) were tested in the insertion copolymerization of ethylene with MA and the influence of ligand structure on polymerization activity, MA incorporation, and molecular weight was investigated. It was observed that 1) electron-deficient catalysts displayed higher activity, but fast deactivation/catalyst poisoning occurred. 2) Electron rich palladium complex derived from **L17f** revealed the highest MA incorporation of 33%. It is speculated that in a coordination competition between ethylene and MA, electron-deficient MA wins to coordinate the electron-rich Pd-complex (derived from **L17f**); while, π-coordination with electron-rich double bond is denounced. 3) In E, MA copolymerization reaction, the steric shielding leads to a pronounced increase in polymer molecular weight. Thus, a systematic investigation allowed the authors to conclude the influence of ligand substitution on E, MA copolymerization and Fig. 4 depicts the outcome.

C3 catalyzed MA insertion generally favors 2,1-insertion mode and changing substituents did not make a big difference in stereo-control. Therefore, Mecking and co-workers introduced a completely different ligand motif and synthesized Diazaphospholidine-sulfonato ligands **L18a-d** (Scheme 2) in order to control MA insertion mode [72,73]. Insertion of MA using Pd(II) complexes derived from Diazaphospholidine-sulfonato ligands was investigated. The sterically hindered substituents on the Diazaphospholidine moiety yields the rare 1,2-insertion product with > 95% selectivity. While sterically less hindered substituent produced an electronically favored 2,1-inserted products with > 95% selectivity. MA insertion into diazaphospholidine hydride or deuteride complexes follows the common 2,1-insertion pathway even for sterically bulky complexes (**L18c**, $R_1 = R_2 = i$Pr). Theoretical studies suggest that insertion into the hydride or

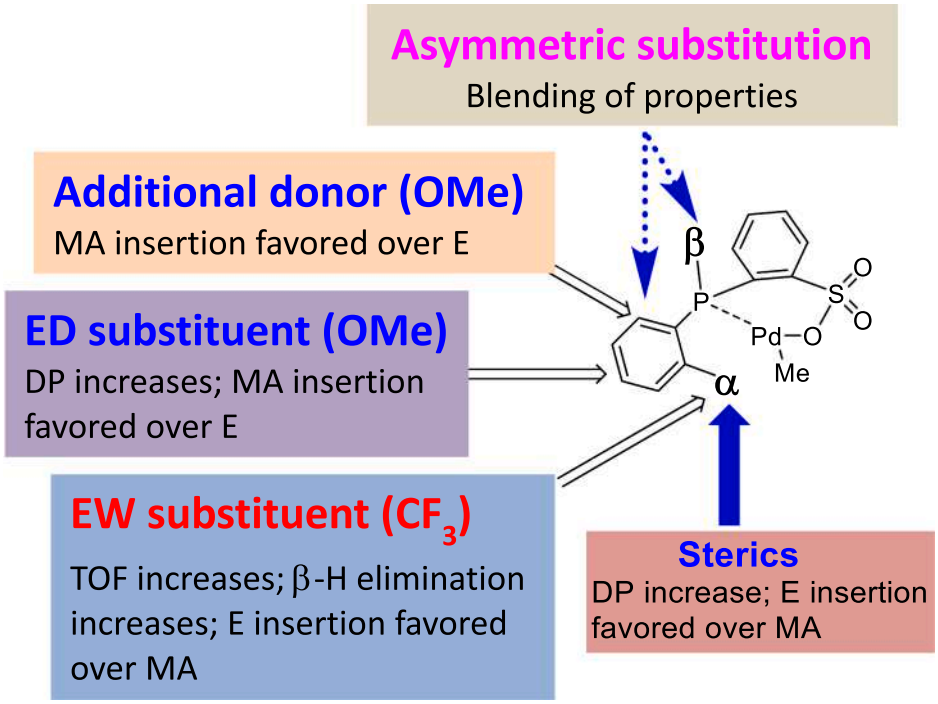

Fig. 4. Catalyst structure and E-MA copolymerization properties (DP: Degree of polymerization; ED: Electron-donating; EW: Electron-withdrawing; E: Ethylene; MA: Methyl acrylate). Reproduced with permission from Neuwald et al. [71]. Copyright@ 2013 John Wiley and Sons Inc.

deuterium occurs from the species in which the π-coordinated acrylate is *trans* to the P-donor. Therefore, the olefin is more remote from the P-donor and has less influence on the insertion step. Although 1,2-insertion of MA in an E, MA copolymer can produce interesting stereochemistry in the resultant copolymer; Pd-complexes derived from Diazaphospholidine-sulfonato ligands were not very active in the copolymerization. Only 0.1% MA incorporation was observed with a number average molecular weight of only 1000 g/mol.

The impact of heterocyclic-substituents in phosphinobenzenesulfonate ligand on ethylene methyl acrylate copolymerization was investigated by Jian et. al [74]. It was anticipated that the heterocyclic substituent may nurture weak electrostatic interactions with the catalytic palladium center and may influence the copolymerization. Thus, phosphinobenzenesulfonate ligands **L19a-d** with -furyl, -thienyl, -(N-methyl)pyrrolyl and -benzofuryl substituent (Scheme 2) were prepared. Subsequently, corresponding Pd(II) complexes with pyridine or DMSO as donor solvent were prepared. In the stoichiometric MA insertion experiments, the thienyl substituted phosphinesulfonato Pd-complex was found to be more active. The thienyl-substituted Pd(II) complex revealed MA insertion in a primary 2,1-fashion. The DMSO complexes show a higher insertion rate due to the weakly coordinating DMSO molecule. These investigations revealed that the heterocyclic substituents have very little influence on insertion copolymerization of E-MA.

The heterogeneous version of catalyst **C3** was reported by Mecking and co-workers [75]. The phosphine sulfonate ligand with hydroxyl or acid linker (**L20a-b**) at the non-chelating P-aryl moiety was synthesized and adsorbed on the clay or on silica. These heterogeneous neutral palladium complexes were active in ethylene homopolymerization and ethylene/methyl acrylate copolymerization and do not require any co-catalyst. The resultant EMA revealed low MA incorporation, but the copolymer microstructure was not very different from EMA produced using the homogeneous analogous. It is most likely that heterogenization of catalyst induces steric congestion around palladium, rendering reduced access to the catalytic site and the consequent lower MA incorporation. To the best of our knowledge, this is the only report on heterogeneous version of **C3**. Therefore, there is huge scope to develop a recyclable catalyst of Drent type and use the heterogenization to improve the performance of **C3** type catalysts.

Guided by buried volume calculations, Nozaki and co-workers synthesized sterically demanding alkyl phosphine sulfonate palladium complexes, and their performance was investigated in the insertion copolymerization of E-MA [76]. Menthyl substituents on the phosphine appear to play a decisive role and higher molecular weight EMA copolymers could be prepared (compared to previously reported aryl-substituted phosphine). The copolymerization of ethylene and methyl acrylate produced a high molecular weight copolymer ($M_n = 6.1 \times 10^3$ – 72×10^3 g/mol), along with MA incorporation of 1.4–11%. As can be judged by the discussion so far, most of the ligand tinkering was around the phosphine phosphorus. Chen and co-worker investigated the effect of naphthalene-bridged phosphine-sulfonate ligands of type **L21a-c** (Scheme 2) and the corresponding Pd(II)/Ni(II) complexes were prepared [77]. Insertion copolymerization of ethylene and methyl acrylate was investigated using these complexes. In the copolymerization, these complexes showed lower activity than the classical palladium phosphine sulfonate complex **C3**. While higher MA incorporation and higher copolymer molecular weight was observed. At lower ethylene pressure (5 bar) up to 40% MA incorporation was observed. The resultant copolymer was found to contain a linear polymer chain and similar micro-structure as that of an EMA copolymer produced by **C3**.

To investigate the influence of second coordination sphere interactions on insertion copolymerization of polar olefins, polyethylene glycol units were installed on the parent phosphinobenzenesulfonate to produce ligands **L22a-c** (Scheme 2). Palladium and nickel complexes derived from **L22a-c** were prepared and implicated in ethylene, methyl acrylate copolymerization [78]. It was observed that, as the number (n) of ethylene glycol units in the ligand backbone increases, activity, MA incorporation, and copolymer molecular weight increases. It is speculated that the weak interactions between the ethylene–glycol units and the monomer (MA) lead to increased activity, incorporation, and molecular weight.

The aromatic backbone in the phosphinobenzenesulfonate was replaced by an aliphatic cyclic backbone by Jordan and co-workers. The authors designed and synthesized cyclopentanesulfonate ligands (**L23**) and their Pd(II) complexes [79]. Insertion copolymerization of ethylene

with methyl acrylate was investigated. The phosphinobenzenesulfonate chelated Pd-complexes catalyze the copolymerization at 80 °C and a low molecular weight EMA copolymer with MA incorporation of 3.3–3.8 mol % was observed. Detailed analysis of the resultant EMA copolymer revealed that majority of MA is incorporated in the main chain (80% (**A**) (Scheme 3, A, B, C)). While about 8% and 12% MA is incorporated at the chain ends. These results suggest that the chain growth is favored rather than chain transfer following a methyl acrylate insertion.

Inspired by the superb performance of phosphinobenzenesulfonate in the insertion copolymerization of functional olefins, Nozaki and co-workers designed bisphosphine monoxide (BPMO) ligands **L24a-d** (Scheme 4) [25]. The phosphine serves as a strong σ-donor, while the phosphine-oxide behaves as a weak σ-donor in BPMO ligand system. The structural features of BPMO have been discussed in section 1.1. Corresponding cationic palladium complexes were prepared and examined in the insertion copolymerization of functional olefins. The use of BPMO ligands in insertion copolymerization of ethylene and methyl acrylate is discussed sequentially. Cationic palladium complex derived from **L24d** failed to incorporate MA and EMA could not be produced. The BPMO ligand framework was further customized and the aliphatic substituent on the phosphine was replaced with aromatic group. Thus, new BPMO ligands **L25a-f** (Scheme 4) were synthesized. The palladium bisphosphine monoxide catalyst bearing diarylphosphino moiety (**L25c**) revealed improved activity and MA incorporation as compared to the alkyl BPMO catalyst [80]. Electron-donating **L25c** displayed better performance than electron-withdrawing **L25d**. A mechanistic investigation revealed that the diarylphosphino containing complexes exclusively undergo 2,1-insertion by avoiding a more stable 1,2-inserted palladacycle.

Similar to steric and electronic effects, ligand backbone plays an important role in insertion polymerization. Backbone structure can alter the bite angle of a bidentate ligand, introduce flexibility, vary the distance between coordination sites, manipulate electronic effect, and thus control selectivity and reactivity of the catalysts. In order to investigate the impact of backbone, the backbone of bisphosphine monoxide ligand was tailored and a methylene linker was introduced to prepare ligands **L26a-f** [81] (Scheme 4). **L26a-f** were treated with palladium, corresponding cationic complexes were prepared and examined in ethylene, methyl acrylate copolymerization. The copolymerization of ethylene with methyl acrylate at 30 bar ethylene pressure revealed up to 7.2% MA

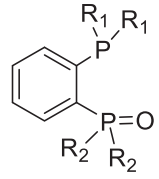

L24a: R_1=R_2= Ph
L24b: R_1= Ph, R_2= *t*Bu
L24c: R_1= *i*Pr, R_2= Ph
L24d: R_1=*i*Pr, R_2= *t*Bu

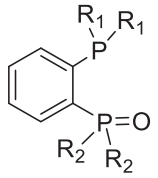

L25a: R_1= *i*Pr, R_2= *t*Bu
L25b: R_1= Ph, R_2= *t*Bu
L25c: R_1= *2*-$MeOC_6H_4$, R_2= *t*Bu
L25d: R_1= *2*-$CF_3C_6H_4$, R_2= *t*Bu
L25e: R_1= *2*-$CF_3C_6H_4$, R_2= *i*Pr
L25f: R_1= *2*-$CF_3C_6H_4$, R_2= Me

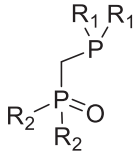

L26a: R_1= *2*-$MeOC_6H_4$, R_2= *t*Bu
L26b: R_1= *2*-$CF_3C_6H_4$, R_2= *t*Bu
L26c: R_1= *i*Pr, R_2= *t*Bu
L26d: R_1= *t*Bu, R_2= *t*Bu
L26e: R_1= *t*Bu, R_2= Me
L26f: R_1= Menthyl, R_2= Me

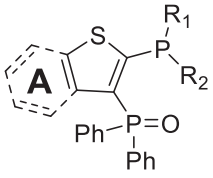

L27a: R_1=R_2 = 2-$OMeC_6H_4$
L27b: A = Ph, R_1=R_2 = 2-$OMeC_6H_4$
L27c: A = Ph, R_1=R_2= Cy
L27d: A = Ph, R_1= Ph, R_2= 2-(2',6'-OMe_2-C_6H_3)C_6H_4

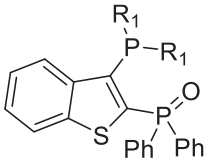

L28a: R_1= R_2= Ph
L28b: R_1= R_2=$MeOC_4H_4$
L28c: R_1= R_2= 2CF_3-C_4H_4
L28d: R_1= Ph, R_2= 2-(2',6'-$(OMe)_2$-C_4H_3)-C_6H_4

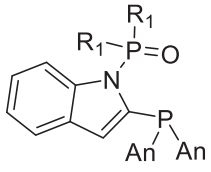

L29a:R_1=Ph
L29bR_1=NMe_2

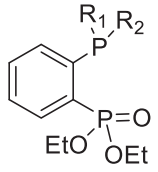

L30a: R_1=R_2= Ph
L30b: R_1=R_2= *2*-$MeOC_6H_4$
L30c: R_1= R_2= *i*Pr
L30d: R_1= *4*-*t*Bu-C_6H_4,
R_2= *2*-$(OEt)_2(O)PC_6H_4Me$

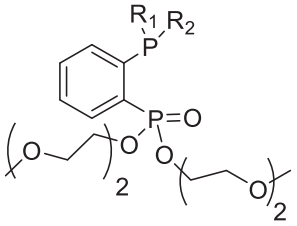

L31a: R_1=R_2= Ph
L31b: R_1=R_2= *2*-$MeOC_6H_4$

Scheme 4. Bisphosphine monoxide and phosphine-phosphonate ligands used in ethylene, methyl acrylate copolymerization (Cy = cyclohexyl).

incorporation, although at the expense of reduced molecular weight. Analysis of EMA copolymer disclosed that majority of the MA was incorporated into the polymer main chain (78%) and a small amount was found at the polymer chain ends (22%). In the subsequent year, Ye et. al reported the synthesis of bisphosphine monoxide supported on a heteroaryl backbone (**L27a-d**) (Scheme 4) [82]. Palladium complex derived from **L27b** revealed 7.1 mol% MA incorporation in ethylene, methyl acrylate copolymerization with a number average molecular weight of 6600 g/mol. The resultant EMA copolymer is highly linear with negligible branching (1 per 1000 carbon atoms).

Jian and coworkers reported BPMO ligands with asymmetric benzothiophene backbone (**L28a-d)** and corresponding Pd (II) complexes [83]. The Pd complexes show higher activity (up to 2.0 × 10^7 g $mol^{-1}h^{-1}$) in ethylene homopolymerization. Palladium complexes ligated with **L28b-d** were active for the ethylene MA copolymerization. Using **L28b** derived catalyst, E, MA copolymer with up to 3.6 mol% MA insertion and 2.7 × 10^4 g $mol^{-1}h^{-1}$ activity was observed. Along the same line copolymerization of ethylene and polar monomers using BPMO **(L29a-b)** ligated Pd (II) complexes was reported [84]. An indole was used to bridge to BPMO ligands that allow Csp^2 atom and Nsp^2 atom as the C-N linker to the BPMO Pd six-membered chelate. The resultant Pd(II) complexes were used in ethylene MA copolymerization and copolymer with 3.3 mol% MA incorporation was observed.

Jordan and co-workers anticipated that phosphine-phosphonate ligands offer a combination of strong and weak σ-donors, and will mimic the behavior of BPMO ligands in insertion copolymerization of functional olefins. The authors prepared benzo-linked phosphine- phosphonate ligands **L30a-d** (Scheme 4) and corresponding cationic palladium complexes [85]. These complexes are active in ethylene, methyl acrylate co-oligomerization. The MA incorporation was found to be 1.5–2.6% and the number average molecular weight was low (800–1500 g/mol). Detailed analysis of resultant oligomers revealed that catalyst derived from **L30b** incorporates 95% MA in the main-chain. While **L30d** derived catalyst showed only 60% in chain incorporation, and remaining MA is located at the chain-ends of EMA copolymer.

The design was further extended and phosphine-phosphonate ligands **L31a-b** (Scheme 4) bearing polyethylene glycol units were synthesized by Do and co-workers [86]. Mono- and di-cationic palladium complexes were prepared and tested in insertion copolymerization of ethylene and methyl acrylate. It was observed that the polyethylene glycol (PEG) substituent forms an adduct (these palladium – alkali complexes) with sodium, potassium, and lithium and the resultant complexes were more active. Presence of alkali ions with transition metal led to significant enhancement in the catalytic activity and thermal stability of the complex. The copolymerization of ethylene, MA with Pd-complex derived from **L31b** produced linear poly(ethylene-co-methyl acrylate) EMA containing 1.4 mol % of MA.

The phosphine oxide arm of the parent BPMO type ligand was further tweaked by Chen and co-workers and a series of phosphine-phosphonic amide ligands **L32a-d** (Scheme 5) were synthesized [87]. The ligand design offers additional substituents on phosphorus and nitrogen atoms, and these substituents can exert necessary control on the catalyst properties. Corresponding mono-cationic palladium complexes were prepared and their performance in ethylene, methyl acrylate copolymerization was investigated. The Pd-complex derived from anisole substituted ligand **L32b** displayed the best performance in ethylene, methyl acrylate copolymerization. At 100 °C copolymerization temperature, an increase in acrylate incorporation (7.1%), activity (14 × 10^3 g/mol/h) and molecular weight (M_n = 32000 g/mol) was observed. When methyl acrylate concentration was increased to 3 mol/L, increased MA incorporation of 33% along with number average molecular weight of 12000 g/mol was observed. The copolymer molecular weight is approximately 3 times higher than the EMA copolymer produced using Drent system **C3**. Analysis of resultant copolymer by NMR spectroscopy revealed in chain MA incorporation.

Next to these developments, Carrow and co-workers envisioned that installing two amine groups on the phosphine oxide arm of the BPMO would allow both steric and electronic tuning and would thus enable the production of functionalized polyethylene with even higher molecular weight. A series of phosphonic diamide-phosphine (PDAP) ligand **L33a-i** (Scheme 5) was synthesized and corresponding single component mono-cationic palladium complexes were prepared [88]. **L33a-i** feature highly polarized P(V) – P(III) chelating ligands that manifest unique space-filling and electrostatic effects within the coordination sphere of single component cationic Pd-complexes. Among the nine ligands, the palladium complex derived from **L33i** was found to outperform other ligands and influenced MA incorporation and EMA molecular weight. The EMA copolymer analysis revealed 5.1% MA incorporation, along with a weight average molecular weight of 28000 g/mol. NMR analysis of the copolymer revealed that 97% of the MA groups were positioned in the main chain, and only 3% of MA groups were located at the ends of branches or chain ends.

Understanding the material properties of the final copolymer is important in the context of developing an application. As depicted in Fig. 5, a comparison between the functionalized polyethylene produced by **L33i** and a regular LLDPE containing similar amount of non-polar co-monomer was presented. A drop in melting temperature (Tm) versus co-monomer content was examined. As it is evident from Fig. 5, the lowering of Tm with increasing MA content in the EMA copolymer closely matches with traditional LLDPE prepared from ethylene, 1-

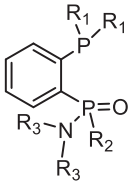

L32a: R_1=R_2= Ph, R_3= *i*Pr
L32b: R_1= 2-$OMeC_6H_4$, R_2= Ph, R_3= *i*Pr
L32c: R_1= Cy, R_2= Ph, R_3= *i*Pr
L32d: R_1=R_2= Ph, R_3= Et

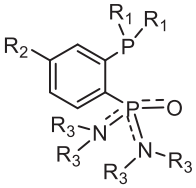

L33a: R_1= *i*Pr, R_2= H, R_3= Me
L33b: R_1= *i*Pr, R_2= H, R_3= *i*Pr
L33c: R_1= iC_5H_{11}, R_2= H, R_3= *i*Pr
L33d: R_1= Ph, R_2= H, R_3= *i*Pr
L33e: R_1= 2-$OMeC_6H_4$, R_2= H, R_3= Me
L33f: R_1= 2-$OMeC_6H_4$, R_2= H, R_3= Et
L33g: R_1= 2-$OMeC_6H_4$, R_2= H, R_3= *i*Pr
L33h: R_1= 2,6-$F_2C_6H_3$, R_2= H, R_3= *i*Pr
L33i: R_1= 2,4-$(OMe)_2C_6H_3$, R_2= NMe_2, R_3= Me

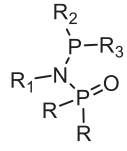

L34a: R= Ph, R_1= Ph, R_2= R_3= 2-$OMeC_6H_4$
L34b: R= Ph, R_1= Ph, R_2= Ph, R_3= 2-[2',6'-$(OMe)_2$-C_6H_3]C_6H_4
L34c: R= *i*Pr, R_1= Ph, R_2= Ph, R_3= 2-[2',6'-$(OMe)_2$-C_6H_3]C_6H_4
L34d: R= Ph, R_1= 4-$OMeC_6H_4$, R_2= Ph, R_3= 2-[2',6'-$(OMe)_2$-C_6H_3]C_6H_4
L34e: R= Ph, R_1= 4-$CF_3C_6H_4$, R_2= Ph, R_3= 2-[2',6'-$(OMe)_2$-C_6H_3]C_6H_4

Scheme 5. Ligands utilized in the insertion copolymerization of ethylene with methyl acrylate.

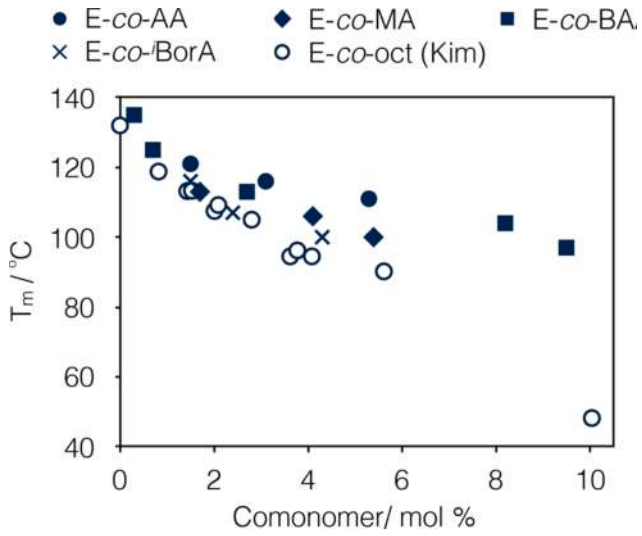

Fig. 5. Melting temperature versus comonomer content of a regular LLDPE and functionalized polyethylene prepared using catalyst derived from PDAP ligands. Reproduced with permission from Zhang et al. [88]. Copyright@ 2018 American Chemical Society.

octene. This is due to exclusive placement of functional olefin along the main chain of the copolymer, which mimics the microstructure of LLDPE. Thus, the microstructure of EMA copolymer appears to be similar to LLDPE. Such insights on the material properties of the copolymers are very much sought after and will guide future commercialization of functional polyethylene.

To reduce the bite angle that the phosphine and phosphine-oxide make at the metal, Chen and co-workers introduced diphosphazane monoxide ligands **L34a-e** (Scheme 5) [89]. These ligands were treated with palladium and nickel precursors and corresponding complexes were obtained in excellent yields (80–90%). The molecular structure of these complexes unambiguously proved the formation of 5-membered Pd and Ni complexes with the P-M−O(=P) bite angle of 88-91°. The cationic palladium complexes initiate insertion copolymerization of E, MA to produce a copolymer with 6.8% MA incorporation and a number average molecular weight of 6100 g/mol. Interestingly, the corresponding nickel complexes were equally good in the insertion copolymerization and an EMA copolymer with 6.5% MA incorporation was produced. The narrow bite angle, strong σ-donation from the phosphine, and weakly σ-donating phosphine-oxide is believed to be responsible for the better performance of **L34a-e**.

Nozaki and co-workers meticulously designed a N-heterocyclic-carbene ligand called imidazo- [1,5-a]quinolin-9-olate-1-ylidene (IzQO) (Scheme 6a; **L35a-c**). The principles of ligand design have been discussed in section 1.1. The IzQO ligated palladium complexes were found to be active in the insertion copolymerization of ethylene/propylene with polar monomers [90]. Regular NHC-ligated complexes decompose rapidly, whereas the IzQO derived catalyst is robust and the NHC-plane appears to be a crucial factor for this stabilization. The Pd/IzQO catalysts initiate copolymerization at 100 °C and produced an EMA copolymer with 1.5% MA incorporation. The scope of the work was extended and nickel complexes derived from IzQO ligands were prepared [91]. Although these nickel complexes were active in ethylene and polar allylic monomers copolymerization; ethylene, MA copolymerization was not very successful. It is stated that 1,2-insertion of MA in-situ produces a chelate complex, which retards copolymerization.

The group combined their experience in BPMO ligand design and IzQO ligand design to synthesize a hybrid ligand system carrying a neutral carbene donor and a neutral phosphine oxide donor. Thus, ligands **L36a-b/L37** (Scheme 6a) were synthesized and corresponding mono-cationic palladium complexes were prepared [92]. Copolymerization of ethylene with MA using Pd-complex derived from **L36a** revealed better activity and 0.61 mol% MA incorporation. The N-heterocyclic carbene (NHC) based ligand was further tailored and ligands **L38a-b** (Scheme 6a) were prepared [93]. The NHC-sulfonamide bidentate ligands were treated with palladium precursors to obtain neutral

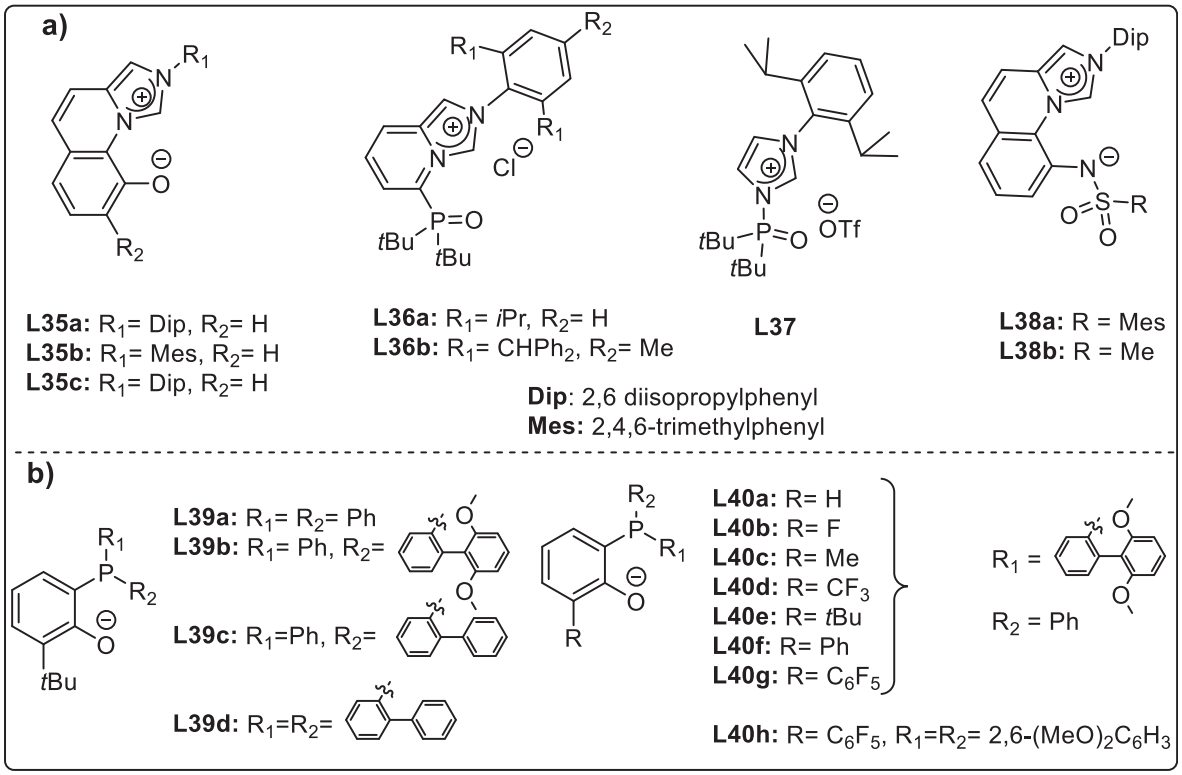

Scheme 6. a) N-heterocyclic carbene based ligands (**L35** to **L38**) and, b) phosphine-phenolate ligands (**L39-L40**) for ethylene, MA copolymerization.

complexes. In the ethylene/MA insertion copolymerization reaction, co-oligomers with 2.8% MA incorporation were observed. NMR analysis of the co-oligomers suggested that the MA units were located at the chain end rather than in the main-chain.

To overcome the in-situ chelation effect, Zhang et. al reported the synthesis of sterically bulky phosphino-phenolate ligands **L39a-d** (Scheme 6b). Corresponding neutral Ni (II) complexes were prepared and were found to be highly active in ethylene homopolymerization [94]. At higher temperatures, a high catalytic activity of up to 10^7 g mol_{Ni}^{-1} h^{-1} of polyethylene was observed. It was observed that the nickel catalysts derived from **L39a-d** tolerates polar additives (ethyl alcohol, diethyl ether, acetone, and water) and produces high molecular weight (6.53×10^5 g/mol) linear polymers. Furthermore, the nickel complexes were found to catalyze the insertion copolymerization of ethylene with functional olefins. The bulkier substituents (**L39b-d**) on the phosphorous show higher catalytic activity with a high molecular weight copolymer (up to 1.08×10^5 g/mol). It is proposed that the bulky axial substituent not only prevents the chain transfer reaction but also inhibits the chelate interaction between the ester group (of MA) and metal (Ni) center. Under mild conditions, up to 5.4 mol% of MA incorporation was observed with a high molecular weight copolymer. The resultant EMA copolymer was thoroughly analyzed. The inserted MA was located in the main-chain, as well as chain ends. Bulky ligands such as **L39d** revealed up to 93% main-chain MA incorporation. While the phenyl substituted (less bulky) ligand **L39a** revealed only 37% in-chain MA incorporation. Thus, the ligand structure plays an important role and dictates copolymer microstructure. A detailed investigation to understand the steric and electronic effect on the phosphino-phenolate system was reported by the same group [95]. Phosphino-phenolate ligands **L40a-g** (Scheme 6b) with electron-donating- as well as electron-withdrawing substituents, and sterically bulky substituents were prepared. Thermally stable neutral nickel complexes were prepared and their performance in ethylene, MA (co)polymerization was investigated. These nickel complexes were thermally robust and displayed high catalytic activity (up to 10^7 g mol_{Ni}^{-1} h^{-1}) even at 120 °C. It was found that in ethylene, MA copolymerization, the presence of the electron-withdrawing substituent (F, CF_3 or C_6F_5) on *ortho*-phenoxy position significantly increases the catalytic activity and molecular weight of the resultant copolymer. Stoichiometric NMR experiment revealed that the nickel complexes bearing an electron-withdrawing substituent at the *ortho*- position are a relatively more functional group (MA) tolerant. While complexes bearing electron-donating group on the P-R_1 moiety increases the catalytic activity and produces high molecular weight copolymer. Analysis of resultant E, MA copolymer by NMR spectroscopy disclosed that the obtained copolymer is highly linear with MA incorporated in the main-chain. Xin et al. reported neutral nickel complex derived from ligand **L40h** (Scheme 6b) and tested the same in insertion copolymerization ethylene and methyl acrylate [96]. An MA incorporation of 4.5% was noted with a high molecular weight of 68000 g/mol. Jian and co-workers very recently reported a N-bridged version of BPMO ligand and examined its performance in E, MA copolymerization [97]. Cationic Ni and Pd complexes derived from N-bridged phosphine–carbonyl ligand revealed MA incorporation of up to 3.3%, but with limited molecular weight of 600 g/mol.

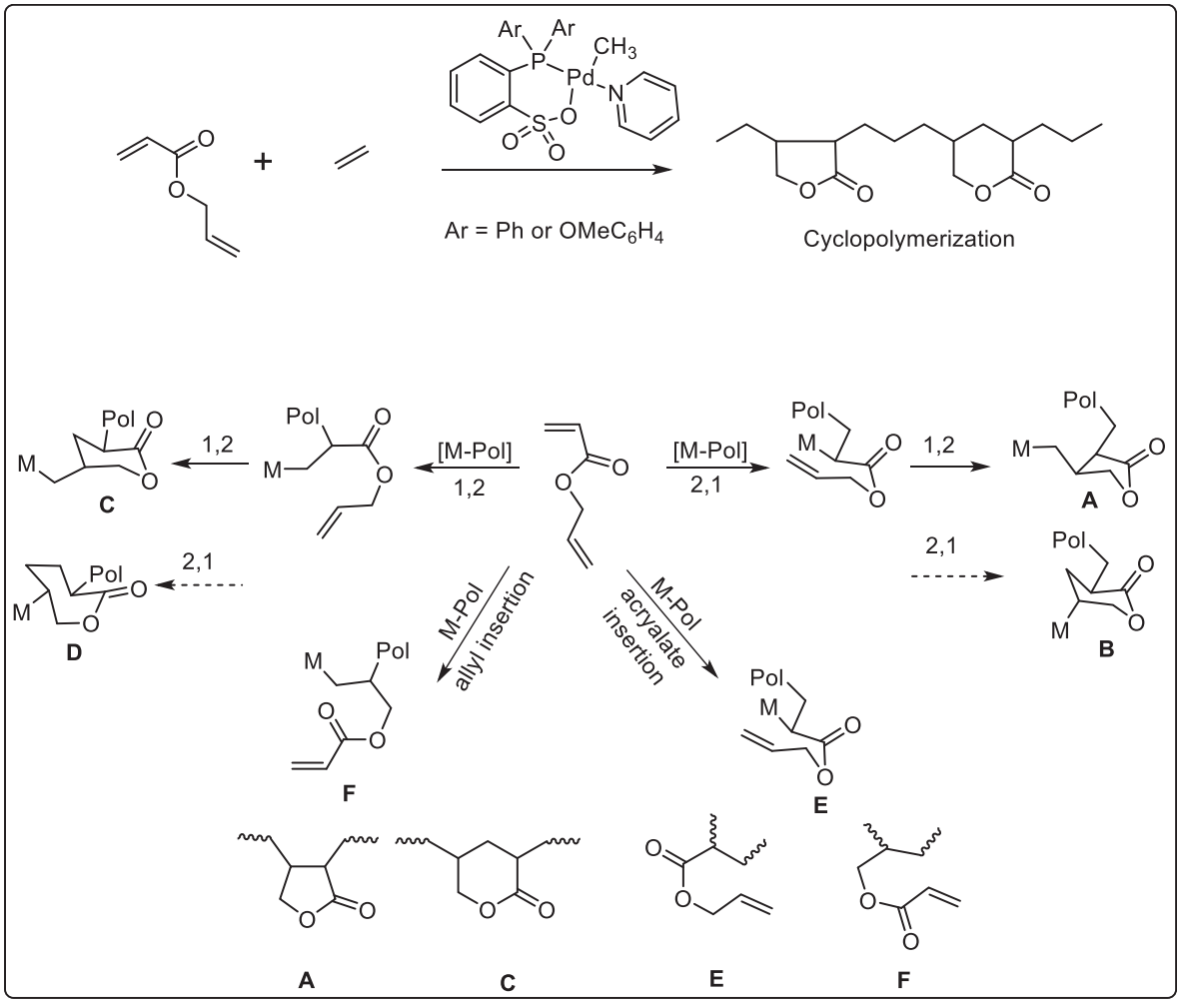

Scheme 7. Insertion copolymerization of ethylene and allyl acrylate using Drent type catalyst.

2.2. Allyl acrylates

The scope of ethylene functional olefin copolymerization was widened to incorporate allylic acrylates by Claverie and co-workers. Traditional Drent catalyst **C3** with phenyl or o-Anisole substituents on the phosphine was used for catalyzing the copolymerization (Scheme 7) [98]. The phenyl substituted **C3** displayed allylic acrylate incorporation of 6.4%, along with number average molecular weight of 6000 g/mol. The resultant copolymers were characterized by using NMR and FTIR spectroscopy. It was found that the copolymers contain two lactone moieties in the chain and complete characterization revealed presence of δ-valerolactone and γ-butyrolactones in the main-chain. This was a little surprising and the authors proposed a mechanism to explain formation of such cyclic lactones. It appears that the allyl group inserts in 1,2 fashion, while the acrylate follows 2,1-insertion leading to cyclization as shown in scheme 7. Thus, insertion cyclopolymerization takes place to yield copolymers with in-chain cyclic structures.

Recently Jian and coworkers reported the copolymerization of ethylene with allyl acrylate and its derivatives [99]. Using Drent type catalyst system, the authors were able to incorporate up to 6% allyl acrylate.

2.3. Long-chain ester olefins

Insertion copolymerization of long-chain functional α-olefins was investigated using two catalytic systems, the Brookhart type **C1** and the Drent type **C3** (Fig. 2). These catalysts were tailored to incorporate functional α-olefins with high molecular weight and activity. A rigid and sterically bulky dibenzobarrelene-bridged, α-diimine **L41** (Scheme 8) was prepared by Coates and co-workers and corresponding Ni(II) complexes were evaluated in the insertion copolymerization of ethylene with Methyl 10-undecenoate [100]. These nickel complexes were found to be active in the copolymerization and an increase in incorporation was observed with increasing concentration of methyl 10-undecenoate. At 7 bar ethylene pressure and −25 °C temperature, the formation of highly linear (T_m = 128 °C) copolymer, with 1% Methyl 10-undecenoate incorporation, was observed. The linearity of the copolymer is believed to be enforced by the barrelene backbone, which restricts chain-walking and allows the formation of a linear polymer chain. While Chen and co-workers installed a hetero-atom in the classical Brookhart type ligand to prepare **L42** (Scheme 8) [101]. Corresponding mono-cationic nickel complexes catalyzed the insertion copolymerization of ethylene with Methyl 10-undecenoate to produce highly branched (46/1000 carbon atoms) copolymer. The comparison of these copolymers allowed the authors to conclude that the microstructure of the copolymer is similar to LDPE, with densities ranging 0.92–0.94 g/cm^3. The Methyl 10-undecenoate incorporation could be raised to 6.8%, along with a number average molecular weight of 6000 g/mol and a melting temperature of just 68 °C.

Wang et. al reworked on the α-diimine backbone and reported pyridazine-imine based ligands **L43a-b** (Scheme 8) [102]. Corresponding mono-cationic nickel complexes were tested in ethylene, methyl 10-undecenoate copolymerization. These complexes displayed low activity and low methyl 10-undecenoate incorporation. However, the activity

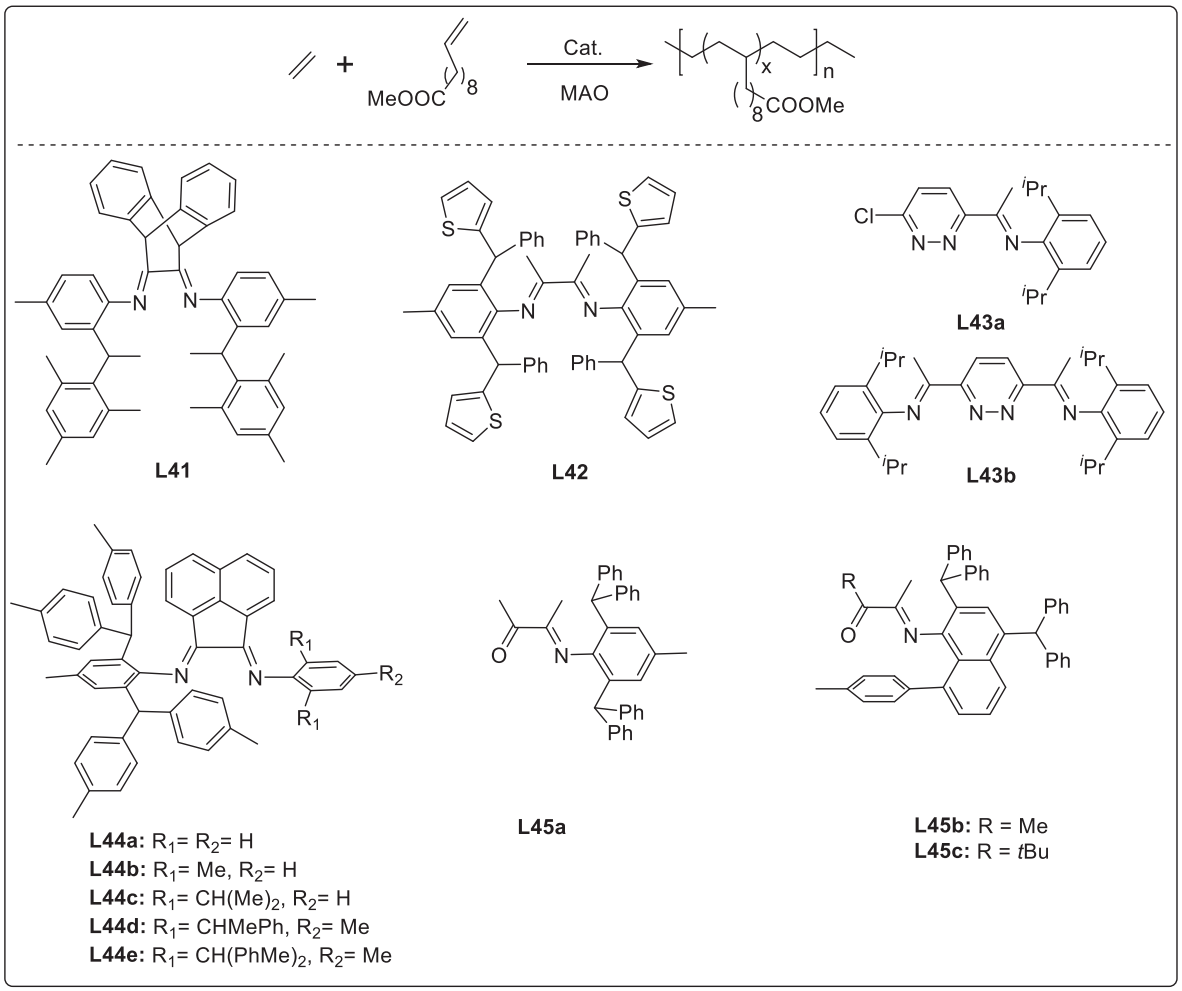

Scheme 8. Brookhart and Drent type ligands used in the insertion copolymerization of ethylene with Methyl 10-undecenoate.

and incorporation was found to increase (up to 2.0 mol%) after the addition of Lewis acid such as BF_3 or $B(C_6F_5)_3$. The increased activity can be attributed to the interaction of Lewis acid (with pyridazine-N), which reduces the electron density at the nickel center. It is known in the literature that Lewis acid coordinates to the lone pair on O- or N-atom in the ligand and generates zwitterionic species which shows higher catalytic activity [103]. Bulky diarylmethyl substituted α-diimine ligands **L44a-e** (Scheme 8) were reported by Gong et. al and corresponding nickel complexes were prepared [104]. Nickel complexes activated by Et_2AlCl were examined in the copolymerization of ethylene and methyl 10-undecenoate. The copolymerization activity was 104.8 $\times$ 10^4 g of PE (mol of Ni)$^{-1}$h^{-1} and incorporation of 0.43 mol% was observed. When the concentration of methyl 10-undecenoate was increased, an increase in percentage incorporation of 2.12 mol% was observed.

In an effort to ease synthetic protocols for well-known Brookhart's α-diimine ligand synthesis, Chen and co-workers reported α-imino-ketone ligands **L45a-c** (Scheme 8) [105]. The α-imino-ketone moieties are in fact, precursors to α-diimines and can be readily prepared in one step with good to excellent yields. Subsequently, **L45a-c** were treated with nickel allyl precursors to prepare single component cationic complexes. In ethylene, methyl 10-undecenoate copolymerization, these complexes disclosed high catalytic activity (up to 2.5 $\times$ 10^5 g mol^{-1}h^{-1}), high copolymer molecular weight (M_n up to 165200 g/mol), and high comonomer incorporation (1.8–6.3%). These cationic nickel allyl complexes revealed higher incorporation of methyl 10-undecenoate even at a lower concentrations. It is proposed that due to open space (sterically less crowded) around the nickel center, higher incorporation of methyl 10-undecenoate could be achieved.

The insertion copolymerization of methyl 10-undecenoate was also carried out in the presence of a Drent type catalyst. Chen and co-workers reported phosphine sulfonate nickel catalyst decorated with sterically bulky substituents. The electronic properties of the ligands were also modulated and ligands **L46a-e** (Scheme 9) were synthesized [106]. The Ni-catalysts were found to copolymerize ethylene with functional olefins. The copolymerization of ethylene with methyl 10-undecenoate at 80 °C produced copolymers with 2.5–6.0% incorporation and a number average molecular weight of 3600–12000 g/mol. Along the same line, ligand **L46a** was treated with palladium precursor to produce neutral palladium complex, which was tested in ethylene, methyl 10-undecenoate copolymerization [101]. Copolymerization of ethylene with methyl 10-undecenoate proceeds with high catalytic activity and 2.7% incorporation of methyl 10-undecenoate. The copolymer properties were comparable with that of regular LLDPE and therefore, the authors labeled this material as polar LLDPE or P-LLDPE.

Along the same line, Xia et. al reported the synthesis of sterically demanding phosphine sulfonate ligands **L47a-d** (Scheme 9) [107]. The nickel (II) complexes derived from **L47a-d** were examined in the ethylene, polar monomer copolymerization. Among the four, nickel complexes derived from **L47d** were used for ethylene, methyl 10-undecenoate copolymerization. The nickel catalyst revealed higher catalytic activity (17.8 $\times$ 10^4 g mol^{-1}h^{-1}) with high molecular weight (165.5 $\times$ 10^3 g/mol.) but at meager incorporation of 0.04% of methyl 10-undecenoate.

3. Acetates

Acetate containing polymers such as poly(vinyl acetate) are industrially important polymers and are widely used in paint and adhesive industries [108–110]. Poly(vinyl acetate)s are used directly or after the hydrolysis of the acetate group, as poly(vinyl alcohol) polymers. A copolymer of vinyl acetate and ethylene called EVA (Ethylene-Vinyl Acetate) is also a commercial product and is sold world over. The EVA copolymers are conventionally synthesized by radical polymerization at high temperatures (exceeding 180 °C) and very high pressures [111–113]. Apart from lesser control over the reaction, the operating conditions pose additional challenges and safety concerns. Therefore, a low-pressure process to manufacture EVA copolymers is highly desirable. Acetates are challenging monomer for the low-pressure metal-catalyzed coordination insertion polymerization. The reactivity of vinyl acetate (VA) was thoroughly investigated using Pd and Ni complexes [114–116]. Brookhart and co-workers examined a stoichiometric reaction between vinyl acetate and α-diimine Pd/Ni catalyst (Scheme 10) and concluded the following [117]. a) The binding affinity of VA to the metal center is lower than ethylene. b) 2,1-insertion of VA with palladium leads to the formation of a stable five-membered chelate complex. c) While nickel complex revealed 1,2- and 2,1-insertion of VA and formation of five and six-membered chelate complexes. d) At higher temperatures, chelates readily undergo β-OAc elimination to yield a decomposed catalyst containing Pd/Ni-OAc complex, which poisons the catalyst, and activity is lost. Despite these challenges, progress has been made in the insertion copolymerization of acetate containing monomers with ethylene, and sections 3.1 to 3.3 will present the current status.

3.1. Vinyl acetates

The Drent type catalyst **C3** and BPMO catalyst **C4** (Fig. 2) have been tested in VA, ethylene copolymerization. In 2009 Nozaki and co-workers reported Pd-alkyl phosphine sulfonate catalyzed copolymerization of VA with ethylene [118]. Isolated Pd-complexes derived from **L16d** (Scheme 2), **L47a**, **L47d** (Scheme 9), and **L48** (Scheme 11) and in-situ generated catalysts (by mixing [Pd(dba)$_2$] and ligand) were examined in the copolymerization to yield a copolymer with 0.6–1.9% VA incorporation. The isolated complexes outperformed the *in-situ* generated catalysts and revealed higher activity. From the NMR data analysis, it is concluded that the copolymer is highly linear with < 1 branch/1000 carbon atoms. The inserted acetate group was located in the main chain as well as at the initiating and terminating chain ends. The presence of sterically hindered menthyl substituent (**L48**) on the phosphine, in neutral Pd phosphine sulfonate catalyst, revealed incorporation of 1.3% of the vinyl acetate in the copolymerization with ethylene [76]. Replacing one menthyl substituent by other sterically bulky groups (**L47a** and **L47d**) did not improve vinyl acetate incorporation (0.1–0.3%) [119].

The cationic bisphosphine monoxide ligated Pd-complexes were also tested in the ethylene, vinyl acetate copolymerization [25]. Palladium complexes derived from **L24d** (Scheme 4) revealed 1.4% vinyl acetate

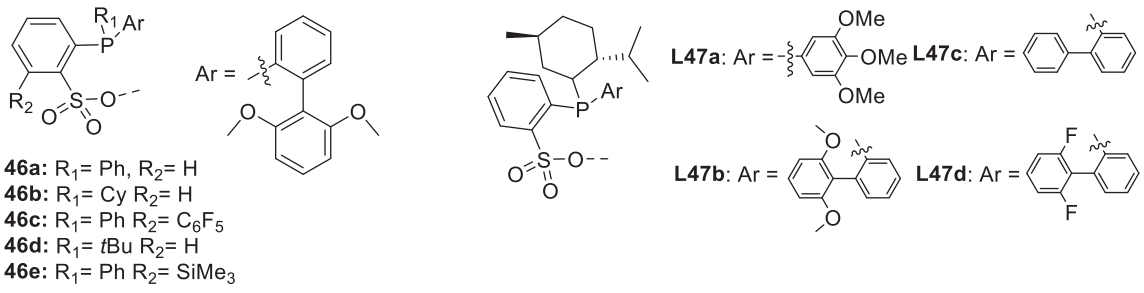

Scheme 9. Phosphine sulfonate ligands for ethylene, methyl 10-undecenoate copolymerization.

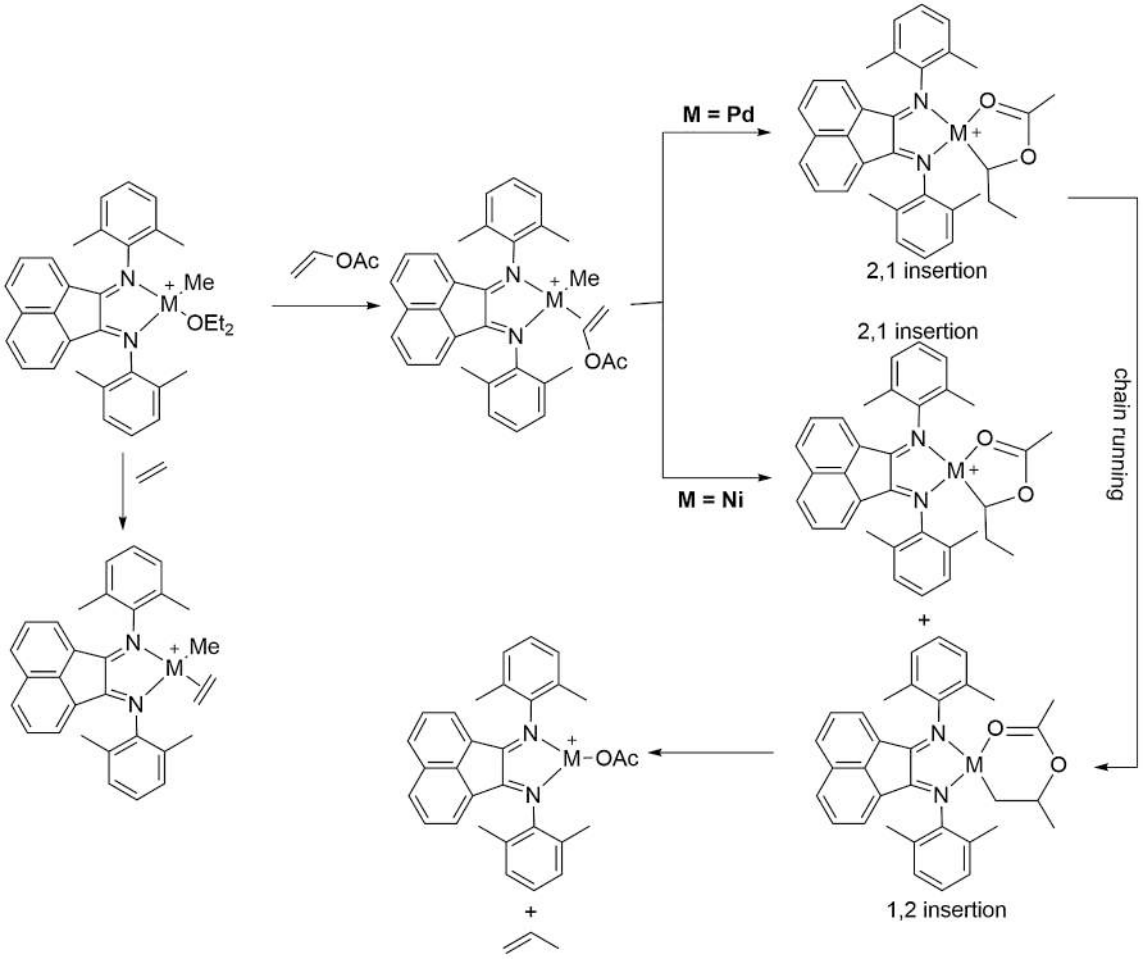

Scheme 10. Reactivity of vinyl acetate with α-diimine Pd/Ni-complexes.

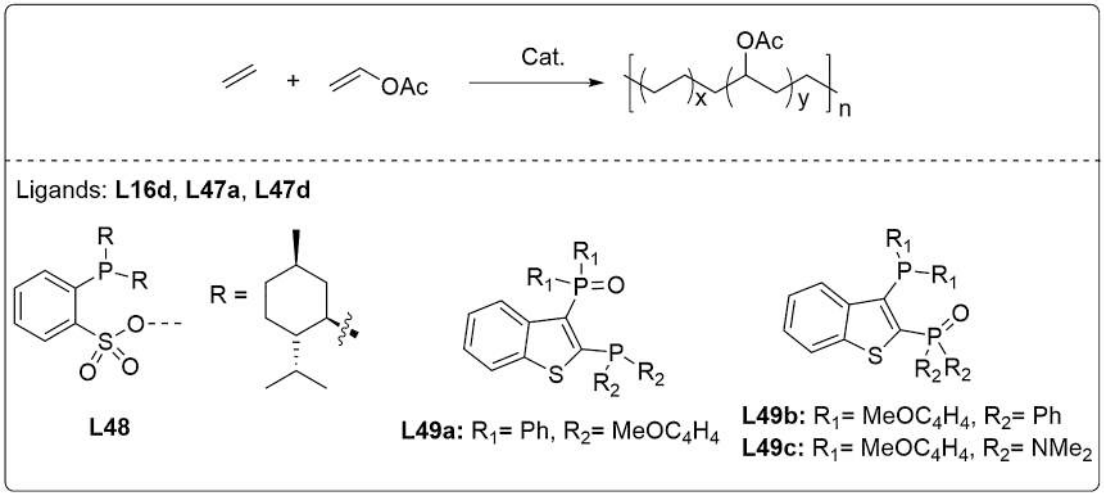

Scheme 11. Copolymerization of VA with ethylene using Pd alkyl phosphine sulfonate and BPMO complexes.

incorporation. Analysis of EVA copolymer suggested that the vinyl acetate is incorporated into the main chain, as well as at the initiating and terminating chain ends. Recently Zhou et. al reported benzothiophene derived BPMO ligands **L49a-c** (Scheme 11) [120]. Corresponding cationic palladium complexes were prepared and were evaluated in the ethylene, vinyl acetate copolymerization reaction. In the copolymerization reaction, palladium complexes derived from ligands **L49a-b** did not show any vinyl acetate incorporation, while **L49c** disclosed 0.3% incorporation. The resultant copolymer was found to be highly linear with only 1 branch/1000 carbon atoms and a number average molecular weight of 8.2×10^3 g/mol.

3.2. Allyl acetates

Allyl acetates (AA) are traditionally copolymerized using radical polymerization methods, although only low molecular weight co-polymers are obtained due to "degradative chain transfer" [121]. Similar to vinyl acetate, allyl acetates can be also copolymerized with ethylene using catalytic systems of type **C1**, **C3**, **C4**, and **C5**. Nozaki and co-workers evaluated ethylene, allyl acetate copolymerization using palladium complexes derived from phosphine-sulfonate ligands **L16b** and **L16d** (Scheme 2) [122]. The copolymerization of ethylene with allyl acetate was carried out at 80 °C and 30 bar ethylene pressure. Under these conditions and at a lower allyl acetate concentration (3 mL), the formation of a copolymer with lower AA incorporation (1.2%) was observed. An increase in the concentration of allyl acetate led to an increase in the incorporation of AA (up to 7–9%) but with a concomitant decrease in catalytic activity. The resultant copolymer was analyzed by NMR spectroscopy, which revealed the formation of highly linear functional polyethylene with AA groups incorporated in the main chain. The major chain ends in the copolymer were found to be n-alkyl and/or vinyl groups. The n-alkyl chain end can be anticipated if the initiation occurs through ethylene insertion, while, vinyl chain ends could be the result of β-hydride elimination after ethylene insertion. The copolymer was deprotected using KOH to obtain hydroxy-functionalized copolymers.

The scope of the reaction was extended and neutral nickel complexes derived from ligands **L16d** (Scheme 2), **L25c**, **L25d** (Scheme 4), were tested in ethylene, AA copolymerization [123]. At 80 °C 30 bar ethylene pressure, above nickel catalyst could not produce any oligomer/polymer (only a trace amount of material was observed). However, at a lower temperature of 30/0 °C, the formation of ethylene, AA co-oligomers was observed with 0.19–0.24% AA incorporation and Mn of about 900–1000 g/mol. Analysis of co-oligomers by NMR spectroscopy revealed a highly linear (3 branches/1000 carbon) structure with CH_2OAc incorporated in the main chain. Similar to their palladium counterparts, the nickel complexes initiate the oligomerization by inserting ethylene into the Ni-Me bond and termination occurs through β-hydride or β-OAc elimination. In order to understand low activity and formation of low molecular weight co-oligomers, a mechanistic investigation was attempted and two pathways were evoked. The possible catalyst deactivation pathways in the presence of allyl acetate are

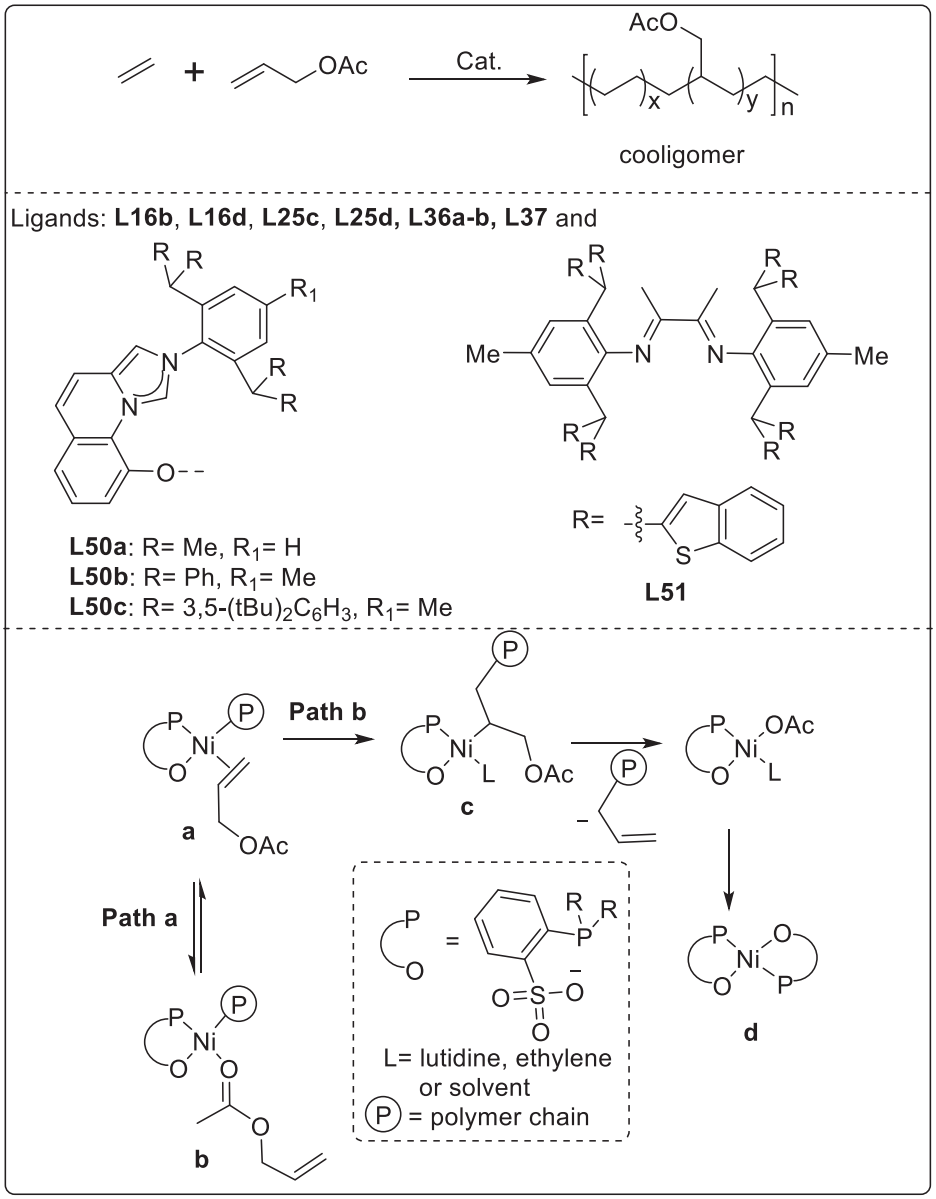

Scheme 12. Copolymerization of ethylene with allyl acetate using metal complexes derived from ligands **L16**, **L25**, **L50**, **L51** and deactivation pathways (bottom).

depicted in scheme 12 (bottom). Existence of path a (Scheme 12) was ruled out by performing homooligomerization of ethylene in the presence and absence of propyl acetate. Similar ethylene oligomerization activity was observed in the presence and absence of propyl acetate, ruling out the possibility of direct intermolecular σ-coordination of the acetate functional group to the metal center (**path a**). Therefore, it is proposed that the deactivation possibly follows path b. The 2,1-insertion of allyl acetate into the nickel-methyl bond produces complex **c**, which undergoes β-OAc elimination followed by disproportionation to yield inactive nickel species **d**.

The mono-cationic palladium complexes derived from **L32a-d** (Scheme 5) were found to be active in ethylene and allyl acetate copolymerization [87]. The copolymerization reaction at 80 °C and at low ethylene pressure (5–9 bars) revealed activity of 2.7×10^3 g mol^{-1}h^{-1} and 0.5–1.8% AA incorporation. The lower activity stems from the cationic nature of the palladium center.

Imidazo[1,5-a]quinolin-9-olate-1-ylidene (IzQO) (**L50a-c**) (Scheme 12) ligated nickel complexes were found to be active in ethylene, allyl acetate copolymerization [91]. When the Ni/IzQO complex was activated by [Ni(COD)$_2$], an ethylene-allyl acetate copolymer was obtained. The copolymer revealed a molecular weight of 8500 g/mol with 0.20% of allyl acetate incorporation. In absence of an activator, a copolymer with a low molecular weight of 600 g/ mol and 0.49% AA incorporation was observed. Along the same line, NHC–phosphine oxide ligands **L36a-b** and **L37** (Scheme 6) were treated with palladium to obtain monocationic palladium complexes, and these were found to be active in ethylene, allyl acetate copolymerization [92]. When the copolymerization was carried out at 30 °C, AA incorporation of 0.58% was observed. The cationic bisphosphine monoxide (**L25c-d**) ligated-palladium catalysts were active in ethylene, allyl acetate copolymerization and displayed AA incorporation of 0.9% [80]. Benzothiophene substituted α-diimine (**L51**) (Scheme 12) ligated Pd complexes perform well in ethylene and polar monomer (acetate, acrylates, nitrile, ether, halogen, etc.) copolymerization [124]. The copolymerization of ethylene and allyl acetate at lower ethylene pressure (8 bars) produced a copolymer with number average molecular weight of 3.96×10^5 g/mol, although with low AA incorporation of 0.56%. Analysis of the copolymer revealed 15 branches/1000 carbon atoms, suggesting linear copolymer.

3.3. Long-chain acetates

Fu et. al reported copolymerization of ethylene with 5-hexene-1-yl acetate (HAc) and allyl acetate using anilinonaphthoquinone (**L52a-c**) (Scheme 13) ligated nickel complexes [125]. The copolymerization of ethylene and 5-hexene-1-yl acetate using a catalyst derived from **L52a** disclosed higher activity of 3000 kg mol^{-1}h^{-1} as compared to **L52c** derived catalyst (110 kg mol^{-1}h^{-1}). It is proposed that the higher activity by **L52a** is due to the steric hindrance at the axial position of the metal. The anilinonaphthoquinone (**L52a**) ligated nickel catalyst produced 5-hexene-1-yl acetate, ethylene copolymer with number average molecular weight of 7700 g/mol and a lower HAc incorporation of 0.76%. A detailed analysis of resultant copolymer revealed the formation of a highly linear copolymer with acetates groups incorporated in the main-chain. The HAc incorporation could be increased to 1.60% by increasing the concentration of the co-monomer and by reducing ethylene pressure (from 10 bars to 5 bars).

The best catalyst system from above ligands (**L52a**) was chosen and a heterogeneous version was prepared (Scheme 13, right). The heterogeneous cationic nickel catalyst (Ni-MMAO/SiO$_2$) disclosed higher activity (4700 kg mol^{-1}h^{-1}) compared to its homogenous counterpart. The heterogeneous catalytic system produced ethylene, HAc copolymer with higher number average molecular weight of 31100 g/mol at the incorporation of 0.94%.

4. Nitriles

A copolymer of butadiene, acrylonitrile called “Nitrile rubber” is a household name. Copolymerisation of acrylonitrile and ethylene produces a copolymer analogous to that of hydrogenated nitrile butadiene rubber (HNBRs), which shows excellent heat, oil, and chemical resistance [126,127]. The incorporation of polar acrylonitrile into the polymer significantly changes the physical and chemical properties of the material. Currently, the homopolymer (Polyacrylonitrile: PAN) of acrylonitrile and copolymers of ethylene acrylonitrile are being produced using radical polymerization methods [128,129]. As compared to radical copolymerization, insertion copolymerization offers better control over comonomer incorporation, PDI, and copolymer architecture [21,130]. Thus, insertion copolymerization of nitrile containing

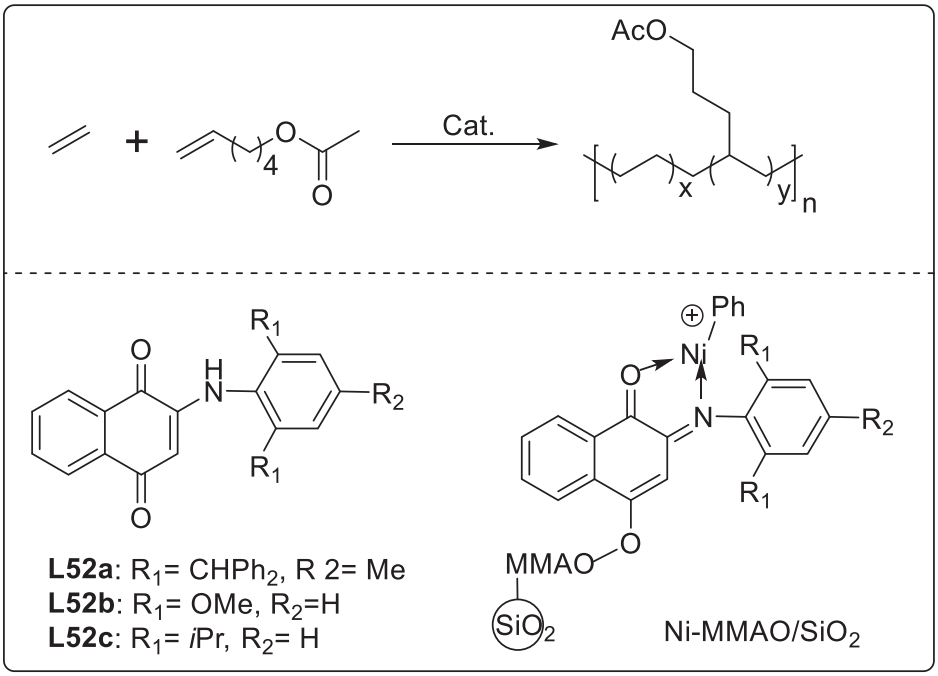

Scheme 13. Anilinonaphthoquinone (**L52a-c**) ligated Ni complexes for long chain acetate, ethylene copolymerization.

monomers with olefins has attracted recent scientific interest and the development of this topic is reviewed in sections 4.1 to 4.2 in chronological order.

4.1. Acrylonitrile

Acrylonitrile is a highly challenging monomer for metal-catalyzed coordination insertion copolymerization as it can coordinate to the metal through the double bond, or nitrogen lone pair (–CN: group) or by bridging modes (Scheme 14). The former mode will enable insertion polymerization, while the latter two modes will poison the metal catalyst. Jordan and Baird's group independently investigated stoichiometric reactions between the cationic palladium-diimine type complexes and acrylonitrile (AN). It was observed that the acrylonitrile forms an N-bonded adduct **A** or a catalytically inactive 2,1-inserted product **B** that readily aggregates through bridging nitrile group to **C** [129,131] (Scheme 14). The insertion of acrylonitrile was also investigated using different bidentate ligand (**L16b**, **L53-L54**) (Scheme 14) containing Pd-complexes and similar results were reported by other groups [132,133].

The first successful insertion copolymerization of ethylene with AN was reported by Nozaki and co-workers using neutral phosphine sulfonate complexes of type **C3** (**L16b**) (Scheme 2) [134]. The neutral palladium complexes produced a copolymer with number average molecular weight of 2900–12300 g/mol, along with 2–9% of AN incorporation. Analysis of resultant copolymers using high-temperature NMR revealed the formation of a highly linear copolymer with the acrylonitrile units located in the copolymer main-chain, as well as at the initiating and terminating chain ends.

A detailed investigation was reported by the same group and the performance of three representative bidentate ligands **L16b** (phosphine sulfonate (P-SO_3)), **L53** (diphosphine (P-P)), and **L54** (imine phenolate (N-O)) was evaluated. Ligand **L16b** and **L54** produced neutral palladium complexes, while **L53** yielded a mono-cationic palladium complex. Insertion copolymerization of ethylene and acrylonitrile was carried out using these palladium complexes and their experimental and theoretical behavior was reported [24]. A theoretical comparison between anionic (**L16b**) and neutral (**L53**) ligand allowed the authors to conclude that in both cases, the π-acrylonitrile complex [(L)PdPr(π-AN)] is less stable than the corresponding σ-complex [(L)PdPr(σ-AN)]. In case of the phosphine sulfonate system, the energetic difference between the π-complex and the σ-complex is smaller than in the case of neutral **L53**. Furthermore, as compared to the diphosphine (**L53**) complexes, the phosphine sulfonate (**L16b**) derived complexes revealed lower activation energy for both AN insertion and subsequent insertion of ethylene, relative to the most stable species [(L)PdPr(σ-AN)]. While similar theoretical investigation for phosphine sulfonate (**L16b**) and imine phenolate (**L54**) did not show any major energy difference in AN insertion and subsequent ethylene insertion. Therefore, the authors performed additional copolymerization experiments and it was found that the imine-phenolate derived Pd-complexes are susceptible to β-hydride elimination and terminate the copolymerization. The *in-situ* formed Pd-H species reacts with the ligand to produce N-OH and Pd(0) particles. Thus, based on above theoretical and experimental evidence, it is proposed that phosphine-sulfonate (**L16b**) derived palladium complex destabilize the σ-AN complex **A** and stabilizes the π-AN complex (Scheme 14). This π-AN complex is an important intermediate for insertion copolymerization and thus can catalyze the ethylene, acrylonitrile copolymerization.

Similar to palladium phosphine sulfonate catalyst [24], bisphosphine monoxide (BPMO) (**L24d**) (Scheme 4) derived mono-cationic palladium complexes were also found to be active in ethylene/AN copolymerization and revealed 2.1–2.5% AN incorporation [25]. The resultant copolymer was found to be highly linear with a random distribution of AN in the polymer main-chain. Another BPMO ligand **L25c** (Scheme 4) derived mono-cationic palladium complex copolymerized AN with ethylene and revealed 2.4% AN incorporation [80]. Bisphosphine monoxide ligand **L26f** (Scheme 4) with a methylene linker displayed up to 1.0 mol% AN insertion [81]. Thus, the phosphine-sulfonate derived Drent system appears to be the most successful catalyst for the insertion copolymerization of acrylonitrile with ethylene.

4.2. Allylic nitrile

The parent phosphine sulfonate ligand reported by Drent was tailored to obtain bulky ligands **L55a-e** (Scheme 15) and the corresponding palladium complexes were evaluated in the copolymerization of propylene with allylic/vinylic polar monomers [135]. Among these,

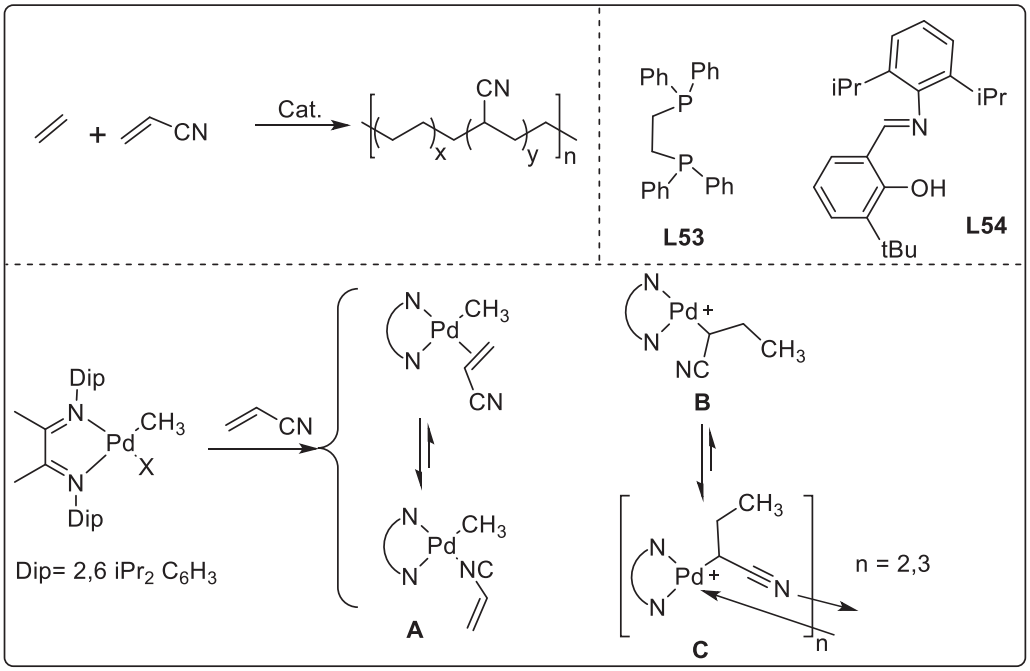

Scheme 14. Reactivity of acrylonitrile with late transition metal complexes.

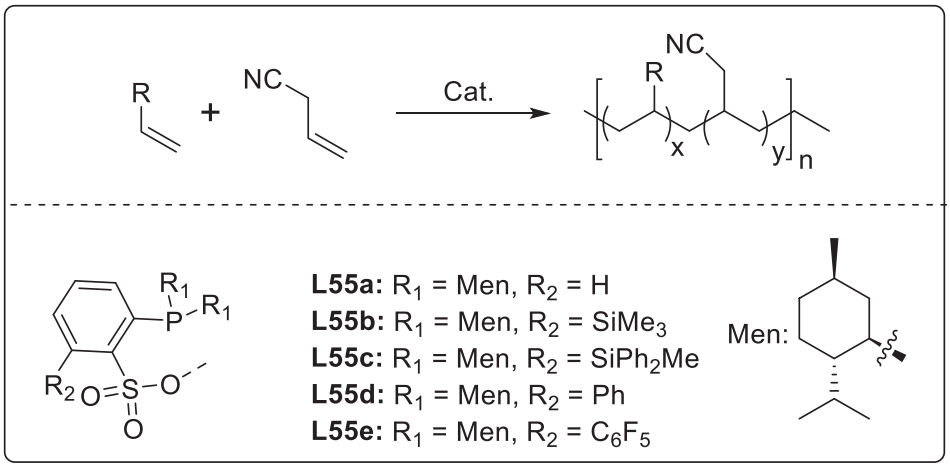

Scheme 15. Copolymerization of ethylene with allylic nitrile (allyl cyanide) using phosphine sulfonate derived Pd and Ni complexes.

the menthyl-, and trimethylsilyl -substituted phosphine-sulfonate ligand **L55b** was found to outperform other ligands. Insertion copolymerization of propylene and allylic nitrile using corresponding palladium complexes revealed 1.3–1.6% incorporation of allylic nitrile along with number average molecular weight of 10000 g/mol. Along the same line, sterically bulky phosphine sulfonate ligands **L46a** and **L46c** (Scheme 9) were treated with Ni(II) and the corresponding neutral catalysts were evaluated in ethylene, allylic nitrile copolymerization [106]. The nickel

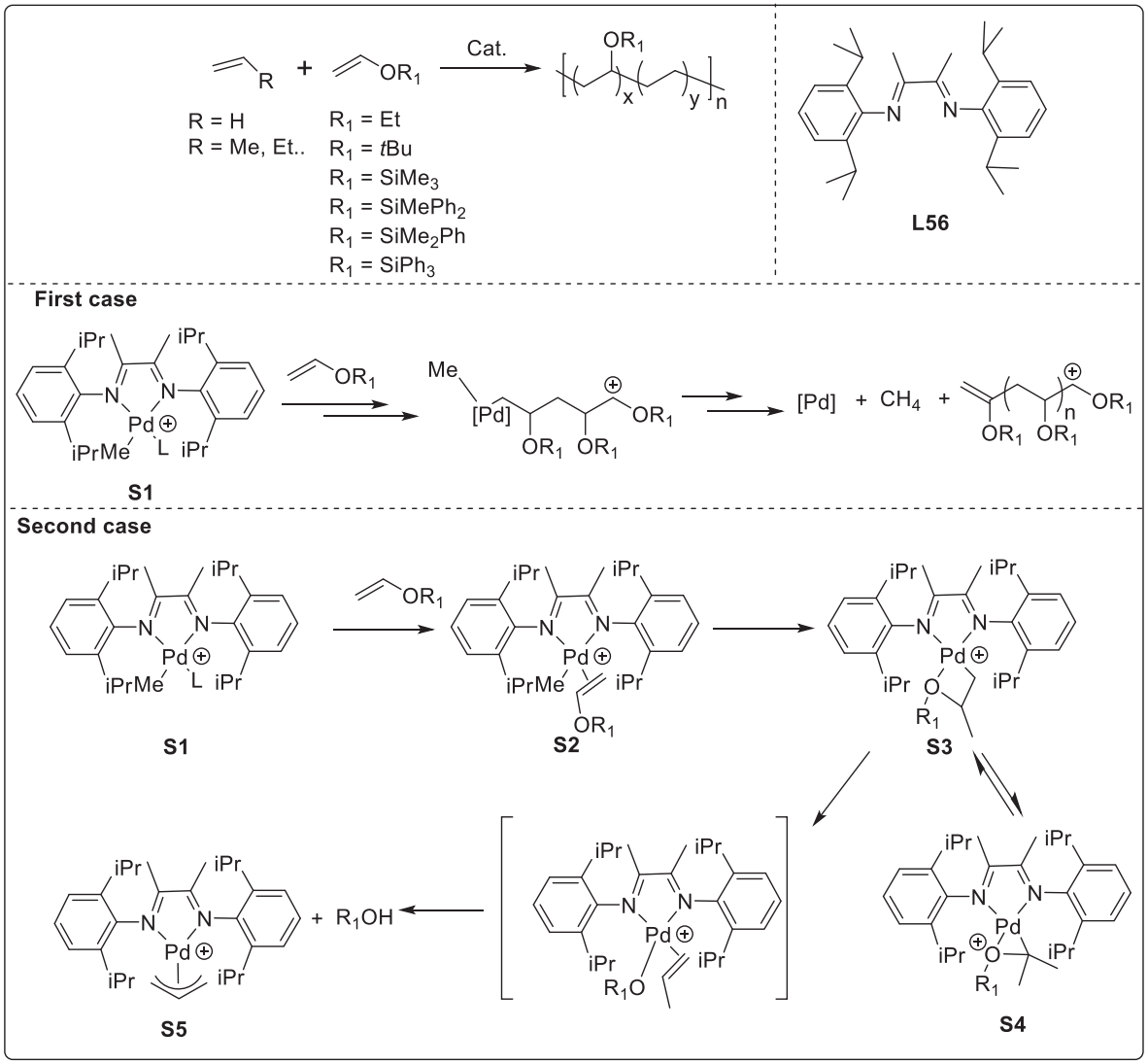

Scheme 16. Insertion copolymerization of ether containing monomers and reactivity of vinyl ether with Pd α-diimine complexes.

catalysts containing *ortho*-penta fluorobenzene substituent (**L46c**) revealed higher activity, allylic nitrile incorporation of 1.2%, and a number average molecular weight of 5400 g/mol.

5. Ethers

Homopolymers, as well as copolymers of alkyl vinyl ether are commercial products and serve various engineering applications [136–138]. The alkyl vinyl ether monomers are traditionally polymerized by radical or cationic polymerization and cannot control the tacticity of monomer addition to the growing polymer chain [139]. Therefore, coordination insertion copolymerization alkyl vinyl ethers would be an attractive strategy to precisely control monomer insertion and produce stereoselective copolymers. However, alkyl vinyl ethers are challenging monomers for insertion copolymerization and pose following challenges. i) The coordination of the ether monomer to the metal center is not only through olefin but also the oxygen (ether group) lone pair coordinates. ii) Ethers are electron-donating groups due to which insertion barrier is high [140]. iii) After the vinyl ether insertion, the resultant intermediate readily decomposes via β-OR elimination [141]. Due to aforementioned impediments, only a few catalytic systems are capable of catalyzing insertion copolymerization of ether containing polar monomers, which will be reviewed in sections 5.1 and 5.2.

5.1. Vinyl ethers

Insertion copolymerization of silyl vinyl ethers with ethylene and other α-olefins using cationic palladium catalysts derived from classical α-diimine ligands (**L56**) (Scheme 16) was first reported by Jordan and co-workers [142]. The mono-cationic [(**L56**)PdMe]$^+$ complex catalyzed insertion copolymerization of 1-hexene with triphenyl(vinyloxy)silane to produce a copolymer containing 20% vinyl ether. Detailed analysis of the copolymer revealed a number average molecular weight of 18000 g/mol, with 90–100 branches per 1000 carbon atoms. The final material was desilylated to obtain a copolymer containing hydroxyl groups in the polymer main-chain. Subsequently, the same group reported a detailed investigation on the reactivity and insertion copolymerization of alkyl vinyl ethers using same (classical) Brookhart catalyst [(**L56**)PdMe]$^+$ [143]. In the first case (Scheme 16), the **S1** $[B(C_6F_5)_4]$ reacts with an excess of *tert*-butyl vinyl ether at 20 °C to yield a quantitative amount of polymer. Analysis of the resultant material by NMR spectroscopy revealed a polymer similar to that obtained via cationic polymerization. Rapid formation of [Pd^0] species was observed during the reaction. In the second case scenario (Scheme 16), the reaction between **S1**$[SbF_6]$ or **S1**$[B(C_6F_5)_4]$ and 1 equivalent of vinyl ether proceeds via formation of species **S2** which is followed by 1,2-insertion to form a species **S3**. The reversible isomerization of **S3** leads to the formation of **S4.** This mixture of species **S3** and **S4** at 20 °C undergoes rapid OR_1 elimination to form a $[Pd(\eta^3\text{-}C_3H_5)]^+$ (**S5**) and R_1OH. Thus, there appears to be stiff competition between a cationic polymerization and insertion polymerization for vinyl ether monomers. Furthermore, kinetic data suggest that the rate of cationic polymerization is higher than insertion polymerization for vinyl ether with Et, *t*Bu substituents. While, rate of insertion polymerization is higher than cationic polymerization for vinyl ethers with $SiPh_3$, $SiMePh_2$, etc. Therefore, 1-hexene, silyl vinyl ether could be readily copolymerized [142].

Similarly, dimerization of vinyl ethers to acetals using [(**L56**)PdCl]$^+$ as a catalyst has been reported by the same group [144,145]. Treatment of divinyl ethers with [(**L56**)PdCl]$^+$ produces cyclic acetals. Such in-situ reaction between vinyl ethers might play an important role in the insertion copolymerization of olefins. Having learned that Brookhart type catalyst dimerizes vinyl ethers to acetals; Chen and co-workers explored the possibility of incorporating these in-situ generated acetals in ethylene copolymerization [146]. The α-diimine palladium mediated copolymerization of ethylene with ethyl vinyl ether yields a high molecular weight (M_n = 27000 g/mol) copolymer with low comonomer incorporation (0.72%). The comonomer incorporation could be increased to 1.57%, but at the cost of reduced activity and molecular weight. The resultant copolymer was found to be highly branched (100 branches/1000 carbon atoms) with acetal groups located at the branch end.

Thus, α-diimine palladium system was successful in incorporating silyl vinyl ethers, but the catalyst failed to incorporate a reasonable amount of ethyl or butyl vinyl ether in an ethylene–vinyl ether copolymerization. To address this bottleneck, Jordan and co-workers evaluated the performance of neutral Drent type system [147]. Unlike the α-diimine system, the neutral pyridine ligated palladium complex [(**L57a**)PdMe(Py)] (Scheme 17) catalyzed insertion copolymerization of ethyl, *tert*-butyl, and butyl vinyl ether with ethylene. The highest incorporation of 6.9% was observed for butyl vinyl ether, along with a number average molecular weight of 3100 g/mol. Detailed analysis of the copolymer revealed the formation of a linear copolymer (only 3–7 branches/1000 carbon atoms) with in-chain and chain-end incorporated vinyl ether groups.

The scope of this copolymerization was widened and insertion copolymerization of divinyl formal (DVF) was reported by Mecking and co-workers using [(**L16b**)PdMe(DMSO)] (Scheme 2) catalyst [148]. The copolymerization with divinyl formal revealed an enhanced activity, molecular weight, and comonomer incorporation compared to butyl vinyl ether. The better performance with divinyl formal can be ascribed to the secondary intramolecular insertion to form a more reactive alkyl intermediate. Under identical conditions, enhanced incorporation of 12.5% divinyl ether was observed, along with a number average molecular weight of 1200 g/mol. The resultant copolymer was analyzed to understand the copolymer microstructure and it was found that the E/DVF copolymer shows the non-cyclic and cyclic structures (Scheme 17, bottom). The formation of such unusual microstructure was deeply investigated and a mechanism as in scheme 17 has been proposed. It has been observed that the 2,1-insertion of DVF produces a five-membered ring structure, while, 1,2-insertion generates a six-membered ring structure in the copolymer backbone. Inclusion of such oxygen-containing ring structures in the polymer backbone imparts different properties to the material.

Neutral palladium complexes derived from sterically bulky menthyl substituted phosphine-sulfonate ligand **L47a-d** (Scheme 9) and **L48** (Scheme 11) were found to be active in the insertion copolymerization of butyl vinyl ether [76,119]. **L47** derived Pd-catalyst showed minor incorporation (0.1–0.2%), while the **L48** ligated Pd-catalyst revealed 7.7% incorporation along with a number average molecular weight of 11000 g/mol.

Nozaki and co-workers investigated the copolymerization of butyl vinyl ether with ethylene using BPMO ligands **L24d**, **L25c**, **L25d**, and **L25f** (Scheme 4) [25,80]. The cationic Pd-catalysts promote copolymerization reaction with butyl vinyl ether incorporation ranging between 0.1 and 4.1%. NMR spectroscopy revealed that ether groups are incorporated in the main-chain and at the initiating chain end of the copolymer. Mono-cationic palladium complexes derived from modified BPMO ligands **L27b**, **L27d** (Scheme 4), **L49c** (Scheme 11) with heteroaryl backbone were also active in ethylene butyl vinyl ether copolymerization [82,120]. However, the incorporation of butyl vinyl ether was only 0.4% with very low branching (3–4 branches/ 1000 carbon atoms). The phosphine phosphonic amide **L32d** (Scheme 5) ligated monocationic palladium complex catalyzes copolymerization of ethylene with butyl vinyl ether [87]. The cationic Pd-complexes at 9 bar ethylene pressure produced a copolymer with number average molecular weight of 13000 g/mol, with low (0.4%) BVE incorporation. The BVE incorporation could be increased to 2.2% by reducing the ethylene pressure to 5 bars.

Chen and co-workers examined phosphine phosphazene monoxide (**L34a-e**) (Scheme 5) ligated Pd/Ni complexes in the insertion copolymerization of BVE and ethylene [89]. Both Pd and Ni complexes were found to be active in ethylene and BVE copolymerization. The cationic

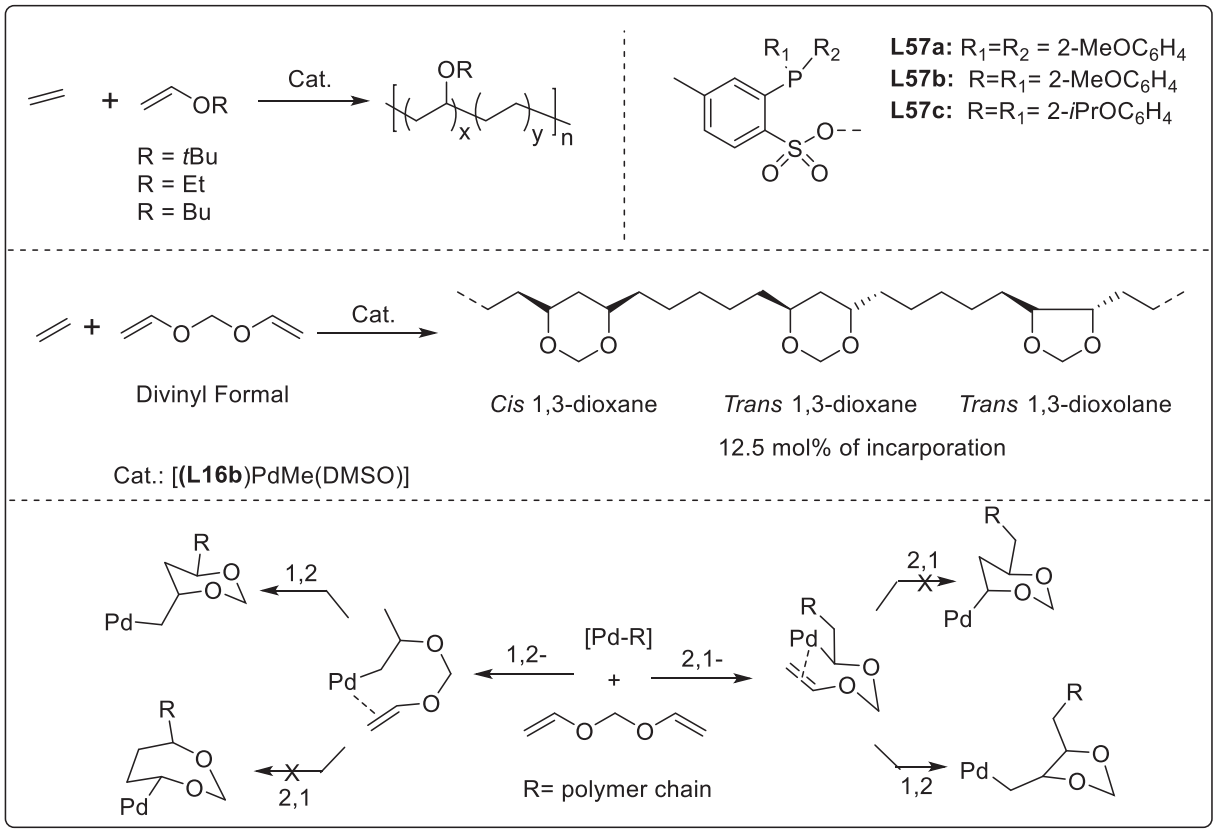

Scheme 17. Insertion copolymerization of alkyl vinyl ethers and divinyl formal.

palladium complex could yield ethylene BVE copolymer with 4.4% BVE incorporation and a number average molecular weight of 9200 g/mol. Under identical conditions, the Ni complex revealed 2.0% BVE incorporation and number average molecular weight of 8000 g/mol. The cationic phosphine phosphonic diamide (**L33a-f**) (Scheme 5) ligated Pd complexes were also tested in the copolymerization of ethylene with BVE [88]. The copolymerization reaction was performed at 30 bar ethylene pressure in toluene to produce a copolymer with only 0.5% BVE incorporation. About 90% of the incorporated BVE was located in the main-chain while remaining 10% was found at the chain-ends.

5.2. *Allyl ethers*

The scope of insertion copolymerization of ether was widened and copolymerization of allyl ethers with olefins was evaluated using late transition metal catalysts. Mecking and co-workers reported the copolymerization of allyl ethyl ether (AEE) and diallyl ether (DAE) with ethylene using Drent type catalyst [(**L16b**)PdMe(DMSO)] [149]. The

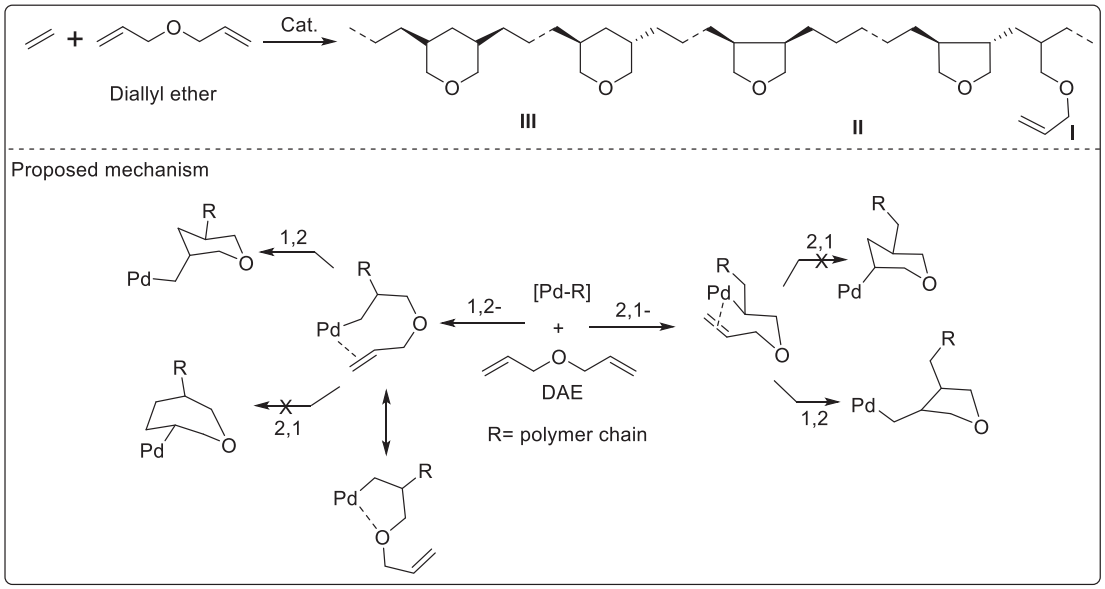

Scheme 18. Copolymerization of ethylene, diallyl ether and proposed mechanism.

copolymerization of allyl ethyl ether with ethylene at 80 °C yields a copolymer with 0.8 mol% of AEE incorporated. While increasing comonomer concentration led to higher incorporation of 4.0 mol% with a concomitant decrease in the catalytic activity. On the other hand copolymerization of diallyl ether with ethylene revealed higher activity and higher comonomer incorporation. Copolymerization of ethylene with DAE disclosed 20.4 mol% DAE incorporation along with number average molecular weight of 2300 g/mol. Apart from very high incorporation, the copolymer microstructure appears to be unique. Detailed analysis of the copolymer by 1-2D NMR revealed linear copolymer with cyclic and noncyclic motifs as presented in scheme 18. A deuterium-labeled ethylene (C_2D_4) was used in an NMR investigation and formation of 5 and 6 membered ring structures was elucidated. The intramolecular insertion of second double bond plays an important role in determining the ring structure. 2,1-insertion of the second double bond of DAE generates 5-membered ring, while, 1,2-insertion produces a 6-membered ring (Scheme 18). Analysis of the E-DAE copolymer suggests the predominant formation of 5-membered tetrahydrofuran rings (two-fold higher than a 6-membered ring). Not only copolymerization but also homopolymerization of DAE was catalyzed by the Drent catalyst and DAE homopolymer (i.e. poly-diallyl ether) with a number average molecular weight of 4400 g/mol was obtained.

Along the same line, Chen and co-workers designed sterically bulky phosphine sulfonate (**L46a-d**) (Scheme 9) ligated nickel complexes and investigated insertion copolymerization of 3-(*tert*-butoxy)prop-1-ene (ABE) with ethylene [106]. An ABE incorporation of 1.6 mol% along with number average molecular weight of 19600 g/mol was observed. The Ni complexes bearing menthyl substituents on the phosphinesulfonato ligand (**L47a-d**) (Scheme 9) were also investigated in the ethylene ABE copolymerization by Xia et. al [107]. Although high molecular weight (55600 g/mol) copolymer was obtained, the ABE incorporation was limited to only 0.6% and PDI was broad (3.5).

Theoretical understanding of the insertion of allyl ethers such as AEE and DAE using a Drent system (phosphinesulfonato-palladium) was reported by Falivene [150]. The DFT investigations revealed that 2,1-insertion is favored over 1,2-insertion for both monomers. But, in case of AEE, both 2,1- and 1,2-insertion lead to a stable O-chelate product and therefore the incorporation of AEE is limited. While, in case of DAE, after the first 2,1-insertion, the second DAE bond coordination and subsequent 2,1-/1,2-insertion is possible. The intramolecular insertion of second double bond in DAE leads to Pd-alkyl cyclic unit, which is stabilized by a β-agostic interaction. This cyclic unit can be easily opened by ethylene and thus favor ethylene, DAE insertion copolymerization.

The Ni/IzQO **(L35a-c)** system was found to be active in the ethylene and allyl ether copolymerization [91]. Upon activation with [Ni$(COD)_2$], the neutral nickel complex copolymerizes diallyl ether and allyl ethyl ether with ethylene. Resultant copolymers revealed 1.9% DAE and 0.68% AEE incorporation. The complexes bearing sterically hindered substituents on the IzQO nitrogen generate higher molecular weight copolymer but at the cost of lower comonomer incorporation. The microstructure of the copolymer revealed linear structure **I**, 3,4-disubstituted tetrahydrofuran structure **II**, and 3,5-disubstituted tetrahydropyran structure **III** (Scheme 18). However, 7-membered ring structure could not be observed in the copolymer. Sterically bulky α-diimine (**L51**) ligated Pd complexes were found to be active in the copolymerization of ethylene and allyl ether [124]. The copolymerization reaction at 8 bar ethylene pressure yields a copolymer with moderate 3-methoxyprop-1-ene incorporation of 0.56 mol% and a number average molecular weight of 75400 g/mol. The formation of a linear copolymer with low branching density (16 branches /1000 carbon atom) was observed.

6. Acid containing olefins

Carboxylic acid-functionalized polymers are one of the largely synthesized industrial products. The presence of carboxylate moiety in a copolymer or its ionomer provides enhanced adhesion, toughness, and stiffness to the polymer [151]. Ethylene, acrylic acid copolymers, such as Nucrel® by DuPont, are industrially produced using free radical polymerization which operates under harsh conditions and does not allow control on polymer microstructure. To obtain some control on the copolymer microstructure and properties, Wagner and co-workers prepared ethylene/acrylic acid [poly(ethylene-co-acrylic acid)] copolymer in two steps by two different techniques [152]. a) A diene monomer was subjected to Acyclic Diene METathesis (ADMET) and subsequent hydrogenation. b) In the second case, a cyclic olefin was polymerized by Ring Opening Metathesis Polymerization (ROMP) followed by hydrogenation. The carboxylic group was masked during the above polymerization to avoid catalyst poisoning. Although above metathesis polymerization provides great control over functional group placement and polymer microstructure, the method requires special monomers and dedicated monomer synthesis. Insertion copolymerization of ethylene with acrylic acid-containing monomers would provide direct access to poly(ethylene-co-acrylic acid). However, carboxylic acid-containing monomers are notoriously difficult to incorporate using insertion copolymerization. The presence of acidic proton can deactivate the catalyst via protonation reaction, while, the carboxylate will coordinate to the metal center and poison the catalyst. Despite these challenges, last decade has witnessed successful insertion copolymerization of acid-containing monomers with ethylene and the subsequent sections 6.1 and 6.2 will present the current state of the art.

6.1. Acrylic acid

The first successful insertion copolymerization of acrylic acid with ethylene was reported by Mecking and co-workers using a [(**L16b**)PdMe(DMSO)] catalyst [153]. The authors investigated the effect of an acidic additive such as propanoic acid on ethylene polymerization and it was concluded that, though the activity decreases with increasing concentration of additive, the catalyst was active and ethylene polymer could be obtained. It was found that the catalyst retains its activity over a time of 30 min. The data suggests that there is reversible retardation of polymerization, due to co-ordination of acid moiety to the catalyst but there is no catalyst decomposition by propanoic acid. A stoichiometric reaction between [(**L16b**)PdMe(DMSO)] and 20 equivalents of acrylic acid was investigated and facile 2,1-insertion of acrylic acid was observed. Subsequently, insertion copolymerization of acrylic acid with ethylene was performed and a poly(ethylene-co-acrylic acid) with 9.6% acrylic acid incorporation ($M_n = 6100$ g/mol) was obtained. The acrylic acid content is comparable to the commercial poly(ethylene-co-acrylic acid) copolymer. Thus, the strategy holds immense potential for commercial-scale synthesis, if the catalyst activity and molecular weight can be improved to meet the techno-economic feasibility.

The classical Brookhart type catalyst with different substituents on the phenyl rings was also tested in ethylene acrylic acid copolymerization [154]. The α-diimine ligands (**L58a-c**) (Scheme 19) with the bulkier group on the *para*-positions of the aniline were synthesized and corresponding palladium complexes were prepared. The cationic palladium complexes produced a poly(ethylene-co-acrylic acid) copolymer with 2.7% acrylic acid incorporation. With increasing steric hindrance on the *ortho*-position (R-substituent), acrylic acid incorporation was found to decrease. The resultant copolymer was analyzed by NMR spectroscopy and it was observed that the acrylic acid units are located at the end of the branches. The α-diimine ligated Pd and Ni catalyst containing benzhydryl and multiple methoxy/fluoro groups (**L59a-b**) (Scheme 19) was reported by Chen and co-workers [155]. The presence of large *ortho*-substituents and six methoxy/fluoro groups in **L59a-b** alters the ligand electronics and steric at the same time. The **L59a** ligated palladium catalyst copolymerizes acrylic acid with ethylene and the resultant copolymer revealed 1.2% acrylic acid incorporation along with a high molecular weight (48800 g/mol).

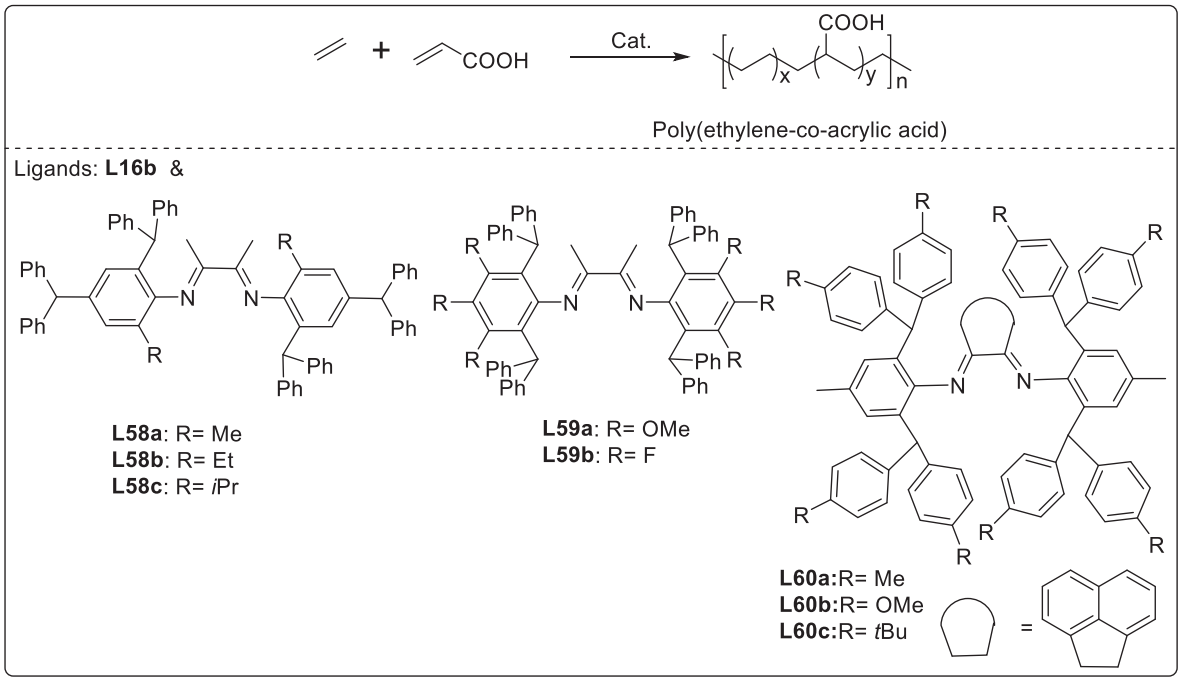

Scheme 19. Insertion copolymerization of ethylene with acrylic acid.

Chen and coworkers reported ethylene–acrylic acid copolymerization using Brookhart type catalyst [156]. The copolymerization of ethylene and acrylic acid using Brookhart type catalyst yields copolymer with moderate activity (up to 4.1 × 10^4 g/mol Pd h), appreciable incorporation (0.1–7.3%) and high molecular weight (Mn up to 5.6 × 10^5). The incorporation of the carboxylic group into the polymer backbone significantly changed the surface properties of the material, which is evidenced by a reduced water contact angle and enhanced affinity for the azo dye compound. The obtained copolymer was converted into the sodium, zinc and iron-based inomers and the metal ions act as physical crosslink, which improved the mechanical property of the copolymer.

Dai and coworkers reported acenaphthene-based diimine ligands (**L60a-c**) and corresponding Pd(II) complexes [157]. The complexes were active in ethylene homopolymerization and ethylene polar monomer copolymerization. The metal complexes displayed π-π interaction in acenaphthene moiety and the phenyl on diarylmethyl moiety. This interaction plays a critical role in ethylene copolymerization. The presence of π-π interaction freezes the N aryl bond rotation at room temperature, which enhances the axial steric bulk and reduces the branching density of the polymer. An ethylene AA copolymerization reaction yields a copolymer with 0.34–0.58 mol% AA incorporation. The resultant copolymer with moderate activity (up to 0.83 × 10^4 g/mol Pd h^{-1}) and low branching density (19–50 branches per 1000 carbon) was observed.

The hetero-aryl backbone BPMO (**L27a-d**) (Scheme 5) ligated Pd-complexes were active in ethylene acrylic acid copolymerization [82]. The resultant copolymer revealed up to 4.7% acrylic acid incorporation, but a number average molecular weight of 800 g/mol only. At 0.2% acrylic acid incorporation, the molecular weight was 9100 g/mol. The linear copolymer was produced with 1–2 branches/1000 carbon atoms.

6.2. Long-chain carboxylic acid

The Brookhart and Drent type catalysts were also evaluated in the insertion copolymerization of long-chain carboxylic acids with ethylene [101]. Chiral phosphine sulfonate **L46a** (Scheme 9) ligated palladium catalyst copolymerized ethylene with 10-undecanoic acid (m-COOH) to yield a copolymer with 10.7% m-COOH incorporation and melting temperature of 114 °C. While thienyl phenyl substituted α-diimine (**L42**) (Scheme 8) ligated Pd-complex copolymerized ethylene with 10-undecanoic acid to produce a copolymer with moderate (0.90%) m-COOH incorporation. The pentiptycenyl-substituted bowl-shaped α-diimine ligand (**L61a-b**) (Scheme 20) with Ni were active in ethylene 10-undecanoic acid copolymerization [158]. The resultant copolymer revealed 4.2% m-COOH incorporation and a melting temperature of 77 °C. The activity of the catalyst was found to depend on the ratio of the polar monomer and Et_2AlCl. This is most likely due to higher oxophilicity of Al than the Ni, leading to polar monomer coordination to the Al and Ni remain free for copolymerization.

Recently Chen and co-workers reported the terpolymeization of ethylene, carboxylic acid and norbornene derived monomer using biaryl derived phosphine-sulfonate ligated palladium (Drent type) catalyst [159]. Terpolymers with number average molecular weight between 2000 and 20000 g/mol and with different compositions were prepared. The incorporation of ethylidene norbornene (ENB) was higher (5.7–22.3%) than 10-undecanoic acid (1.0–2.6%). The earlier reports were limited to determining the incorporation of functional olefin and at the most water contact angle. This report deeply investigated the properties offered by the terpolymer for the first time and shed light on the processing of the material, surface, mechanical, elastic, photo-responsive, and self-healing properties. Fig. 6 depicts the versatility of this material. The incorporation of m-COOH could tailor the surface properties of the terpolymer, while, inserted ENB efficiently modulates the elastic property and crystallinity of the terpolymer. The presence of ENB allows easy vulcanization to permanently crosslinked polymer and the dynamic crosslinking can tailor the self-healing and mechanical/elastic properties of the material. Controlling the weak and strong chemical interactions through hydrogen bonding and crosslinking can modulate the material properties from elastomer to a thermoset. Thus, the material properties offered by this terpolymer open-up new avenues and may find an entirely different application.

7. Halide containing monomers

Incorporation of a halide group into polymer chain significantly

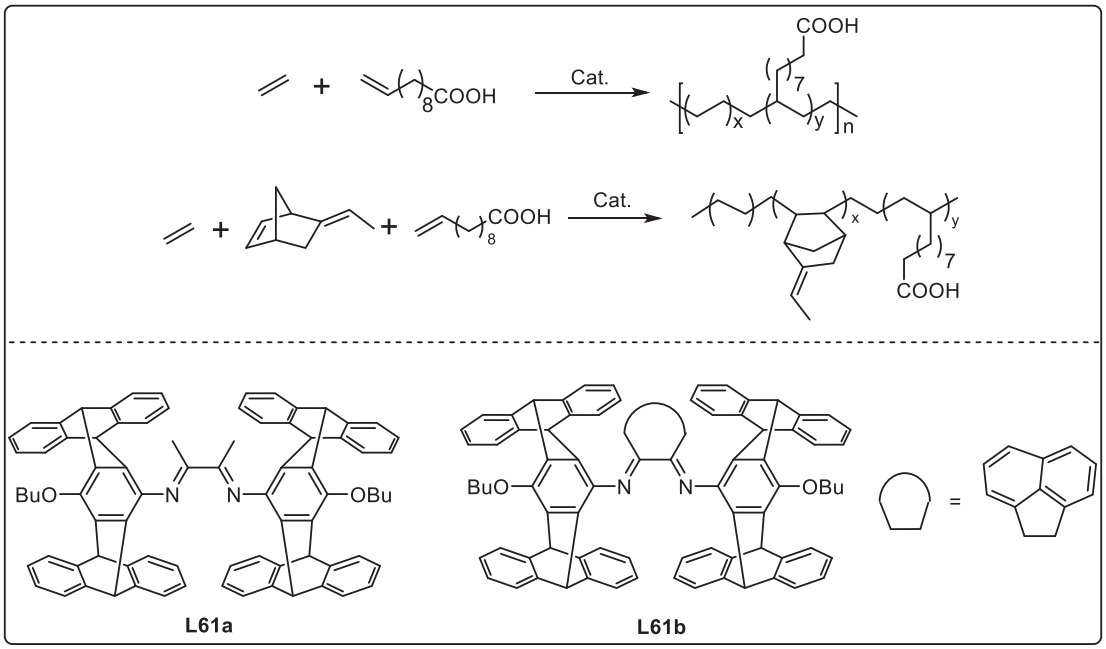

Scheme 20. Copolymerization of ethylene with undec-10-enoic acid using P-O and α-diimine Pd complexes.

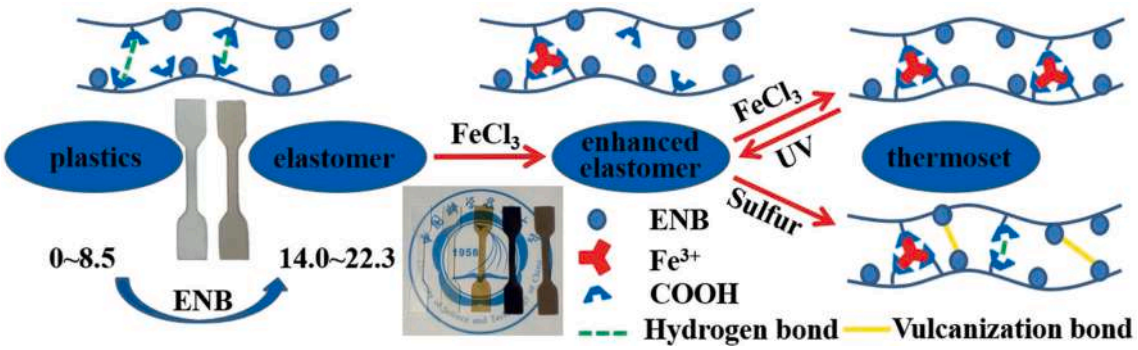

Fig. 6. Tailoring terpolymer properties through weak (H-bonding) and strong (crosslinking) chemical interactions. Reproduced with permission from Zou et al. [159]. Copyright@ 2020 John Wiley and Sons Inc.

alters the polymer properties [160]. Halogenated polymers find a wide range of applications and display material properties such as chemical resistance, thermal stability, gas permeability, and adhesion [161]. Because of the wide range of applications, halide containing monomers such as vinyl halide are industrially attractive. Traditionally, halogenated polyethylene is synthesized by two routes. a) Halogenation of polyethylene or its analog polymers [162,163]. b) Dehalogenation of a homopolymer of vinyl halides [164]. The resultant polymer from above two routes has its own limitations (reaction conditions, etc.) and produces undefined polymer microstructure. Radical polymerization has been industrially used to polymerize vinyl chloride to polyvinyl chloride (PVC). Copolymerization of ethylene and vinyl halide using free radical polymerization was also explored but the approach suffers from precise placement of halogenated monomer, uncontrolled molecular weight, and molecular weight distribution, etc. [165,166]. Above limitations can be addressed by insertion copolymerization of vinyl halide monomers and good control over the polymer microstructure and properties can be obtained [167]. The subsequent sections 7.1 and 7.2 will take a stock of progress made in the insertion copolymerization of halide containing monomers, in the last decade.

7.1. Vinyl chloride

The reactivity of vinyl chloride with late transition metal complexes was investigated by Jordan and co-workers, and the existence of different insertion modes of vinyl chloride into the metal complex was established [168]. The coordination ability of the electron-deficient olefin (vinyl chloride) to the cationic palladium complexes is lower than ethylene or propylene. The lower coordination ability of vinyl chloride could be due to the absence of metal-olefin d-π* back-donation over the predominance of olefin to metal σ donation. The insertion rate for $[(Me_2bipy)Pd(Me)(olefin)]^+$ complex were found to be in the order of, vinyl chloride > ethylene > propylene [168]. The Pd/bipyridine vinyl chloride complex and Pd/α-diimine vinyl chloride complexes undergo net 1,2 vinyl chloride insertion followed by β-Cl elimination to produce Pd-Cl species and propylene. From the DFT studies, it was observed that 2,1-insertion was more favorable than 1,2-insertion. It is predicted that the 2,1-inserted product undergoes isomerization via rapid β-hydride elimination/reinsertion step and the resultant intermediate species undergoes facile β-Cl elimination. The cationic Pd/bipyridine or bisphosphine acyl species undergoes the facile vinyl chloride 2,1-insertion [169]. Thus, the mechanistic investigations by Jordan laid a solid foundation for the insertion copolymerization of vinyl halides with ethylene. Cationic Palladium complexes derived from the

ligand **L24d** (Scheme 4) were tested in ethylene–vinyl chloride copolymerization [25]. Reduced catalytic activity and absence of chloromethine moiety (-CHCl-) resonance indicated negligible vinyl chloride incorporation.

The neutral, Drent type catalyst **C3** was examined in the insertion copolymerization of ethylene, vinyl chloride by Mecking, and co-workers [170]. The authors used **L16e** (Scheme 2) derived Pd-complex and formation of a chlorinated copolymer with 0.1% of vinyl chloride incorporation was observed. A detailed NMR analysis suggested that the -CHCl unit is not incorporated in the main-chain, but it is observed at chain-ends ($CH_3CHClCH_2$-P). The palladium catalyst was isotopically labeled (see Scheme 21) to understand the origin and placement of vinyl chloride. The authors examined two possibilities; i) 1,2-insertion of vinyl chloride into Pd-methyl bond and subsequent ethylene insertion (Scheme 21, top) and ii) 2,1-insertion of vinyl chloride into the Pd-H and subsequent ethylene insertion. Among these two pathways, the authors could not observe 1,2-insertion product but could observe 2,1-insertion product as depicted in scheme 21 (center). This was further supported by control experiments using ^{13}C labeled palladium catalysts. The 2,1-insertion was also supported by the reaction between the deuterium-labeled [(**L16e**)PdD(P*t*Bu$_3$)] complex with vinyl chloride leading to a 2-deuterated vinyl chloride due to the 2,1-insertion of vinyl chloride followed by the β-hydride elimination. In line with these observations, when Pd-H catalyst was employed in the copolymerization, the formation of ethylene homopolymer and monochlorinated polyethylene (mCPE) chains was observed. Furthermore, the [(**L16e**)Pd-H(P*t*Bu$_3$)] catalyst produced a copolymer with increased vinyl chloride incorporation of 0.4%. Thus, only one vinyl chloride unit was inserted and incorporated at the chain-end.

7.2. Vinyl fluoride

Vinyl fluoride (VF) is less susceptible to radical polymerization compared to other vinyl halides and β-F elimination is relatively less favorable due to higher C-F bond energy [171]. In 2007 Jordan and co-workers reported copolymerization of ethylene and vinyl fluoride using a Drent type **C3** catalyst [172]. Ethylene-vinyl fluoride copolymerization reaction at 80 °C produces a linear copolymer with low vinyl fluoride incorporation (0.1–0.5 mol%). The low incorporation suggests that the vinyl fluoride competes poorly with ethylene in the Pd-catalyzed coordination insertion copolymerization. An enhanced VF incorporation was observed at higher vinyl fluoride in feed, but a consequent reduction in the copolymer yield and molecular weight was noted. Detailed NMR investigations displayed two characteristic fluorine resonances at 179.4 and 171.8 ppm. The former signal originates from an in-chain incorporated fluorine atom, while the latter is ascribed to chain-end fluorine. The above ^{19}F NMR findings were further corroborated by 2D C-H correlation-NMR spectroscopy.

A tetrameric neutral phosphinesulfonate-PdMe complex was tested in ethylene VF copolymerization by Jordan and co-workers in 2010 [173]. Higher VF incorporation of 3.6% was observed and the resultant polymer was highly linear with < 5 branches/1000 carbon atoms. The concentration of vinyl fluoride affects the polymer yield; with increasing VF feed, reduced copolymer yield was reported. It was observed that copolymer yield increases linearly with reaction time. This observation suggests that VF does not deactivate the catalyst but it inhibits the polymerization. The inhibition of polymerization is most likely due to the formation of α-fluoro-alkyl intermediate [LPdCHFR (R = H or polymer chain] after VF insertion. The electron-withdrawing effect of fluoro-substituent increases the barrier for subsequent ethylene or vinyl fluoride insertion and thus leads to inhibition. Microstructure analysis by NMR spectroscopy, suggests in -chain vinyl fluorine (-CH_2CHFCH_2-) units with cis and trans (–CH_2CH = CHF) chain end. Above chain ends originate from 2,1 VF insertion into the metal alkyl or growing chain, followed by β-H elimination. Along the same line, a palladium catalyst derived from cyclopentane phosphine-sulfonate ligand **L23** (Scheme 2) copolymerizes ethylene and vinyl fluoride and a VF incorporation of 0.4 mol% was observed [28].

Apart from β-H elimination, the β-F elimination is also a major side reaction in the insertion copolymerization of ethylene with VF. This β-F elimination leads to the in-situ formation of Pd-F complex. A metal halide (M−X) bond is usually considered as “inert” for the insertion of olefins. In contrast to all earlier assumptions, insertion of ethylene in a Pd-F bond has been recently reported by Jordan and co-workers [174]. Catalyst [(**L62d**)PdMe(lut)] (Scheme 22) was exposed to ethylene, VF and corresponding fluorine functionalized PE was obtained. Microstructure analysis of the resultant polymer revealed the presence of two new chain ends. The ^{19}F NMR spectrum displayed two characteristic singlets at −115.2 and −217 ppm. While, the corresponding fluorine coupled proton NMR revealed a triplet of triplets at 5.63 (J_{HF} = 57, J_{HH} = 4 Hz) ppm and a doublet of triplets at 4.28 (J_{HF} = 48, J_{HH} = 6 Hz) ppm. After a detailed analysis. the former ^{19}F resonance at −115.2 ppm and ^{1}H peak at 5.63 ppm has been assigned to a -CH_2CHF_2 chain-end. The latter fluorine and proton signal is ascribed to CH_2CH_2F group.

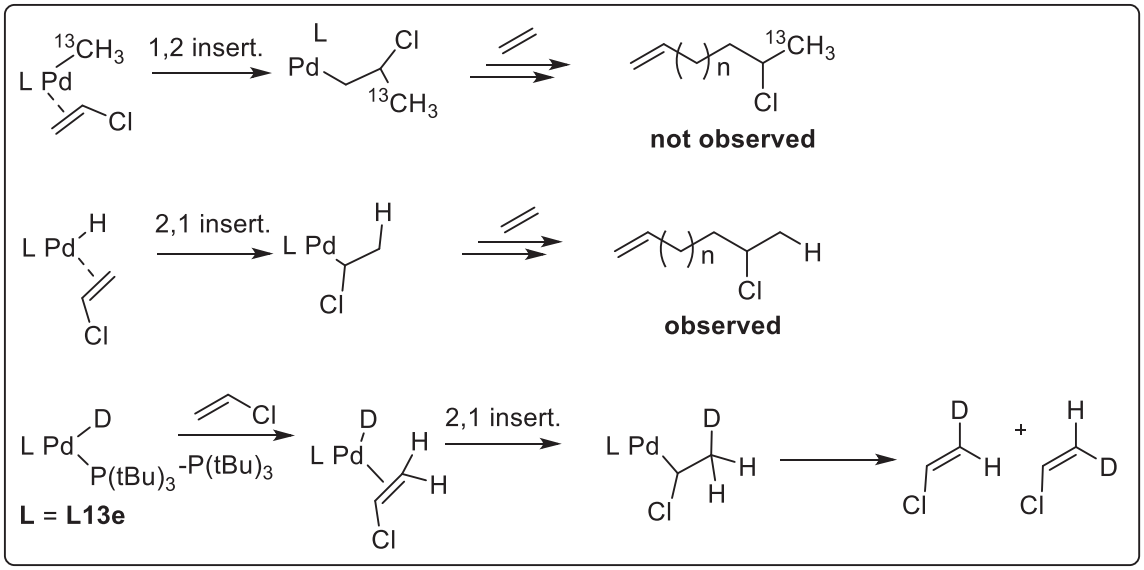

Scheme 21. Reactivity of vinyl chloride and ethylene with [(**L16e**)PdMe(donor)] catalyst.

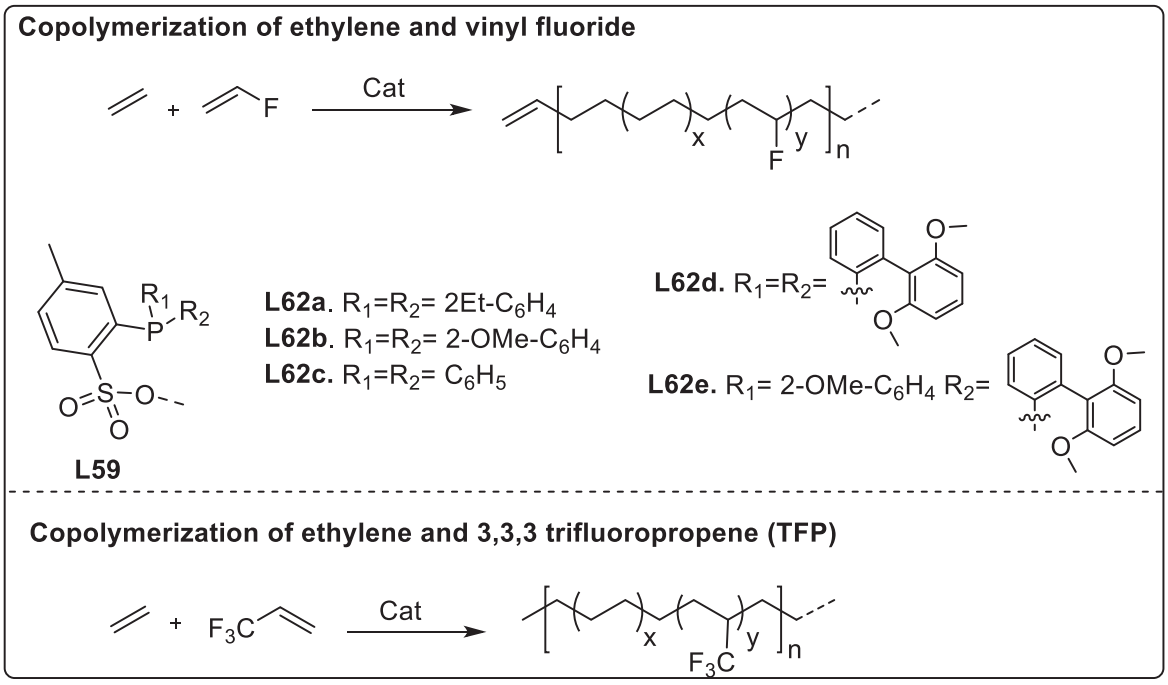

Scheme 22. Copolymerization of ethylene and vinyl fluoride or TFP using Pd phosphine sulfonate catalyst.

The possible route to these chain-ends could be the vinyl fluoride insertion, β-F elimination, and ethylene insertion into the Pd-F bond and subsequent chain growth. This hypothesis was authenticated by an on-purpose synthesis of [(**L62d**)PdF(lut)] complexes and exposure to vinyl fluoride in DCM, to observe 1,2-insertion of vinyl fluoride into the metal fluoride bond to produce (Pd-CH_2CHF_2) (Scheme 23). This species subsequently inserts ethylene to produce a polymer with -CH_2CHF_2 units at the chain-end. Similarly, when above [(**L62d**)PdF(lut)] complex was treated with ethylene, the formation of a polymer with -CH_2CH_2F chain-ends was observed. Thus, above mechanistic investigations suggest that β-F elimination does not deactivate the catalyst, rather, a [Pd-F] species is amenable to ethylene insertion and polymerization.

The Jordan group continues to contribute significantly in the area of insertion copolymerization of vinyl halides and their recent mechanistic investigations shed light on the reactivity of two isomers of a [Pd-F] complex [cis(P-F) and trans(P-F)] [175]. On purpose prepared cis and trans complexes react quantitatively with vinyl fluoride to yield an inserted product [Pd(CH_2CHF_2)(lut)]. In-situ NMR investigations revealed that cis(P-F) complexes react faster than the trans(P-F) complexes with vinyl fluoride. Theoretical DFT studies indicate that the reaction goes via substitution of lutidine by vinyl fluoride and subsequent migratory insertion into the metal fluoride bond (Scheme 24).

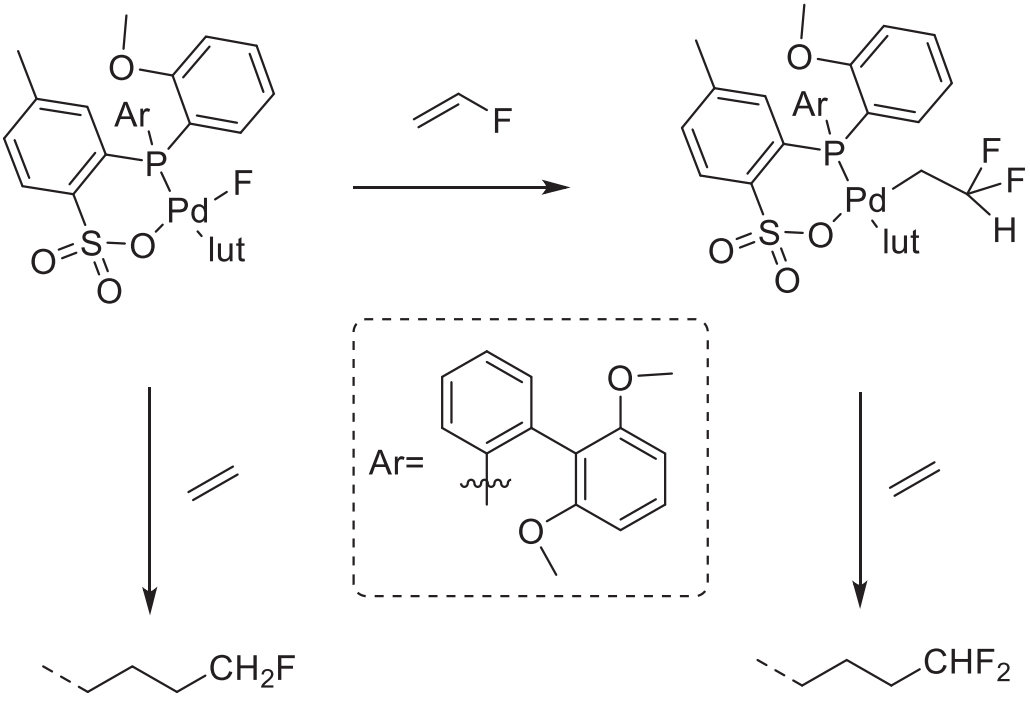

Scheme 23. Reactivity of [Pd-F] complex with ethylene and vinyl fluoride.

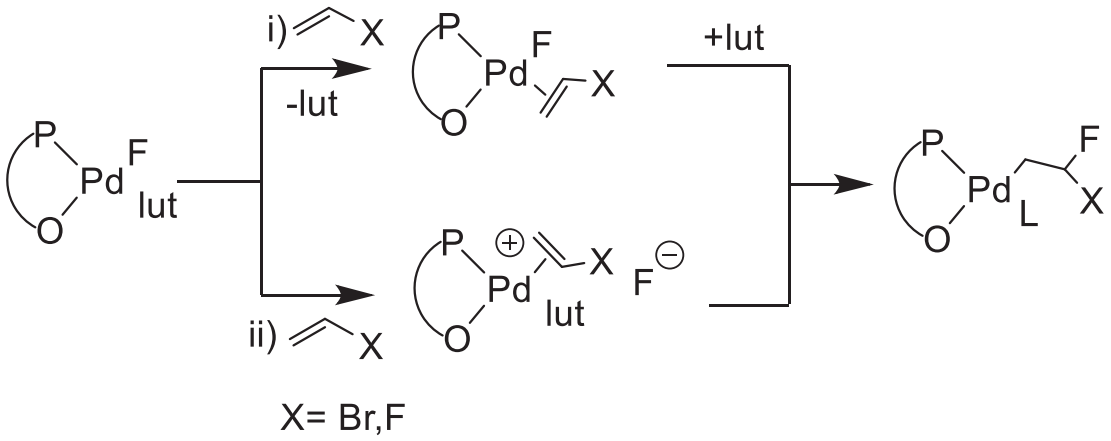

Scheme 24. Proposed mechanism for fluoro-palladation of vinyl halide.

Rieger and coworkers reported insertion copolymerization of ethylene and 3,3,3 trifluoropropene (TFP) using phosphine-sulfonate ligated palladium complex [176]. A linear copolymer with high fluorine content of up to 15 wt% (8.9 mol% of TFP) was observed. ^{13}C and ^{19}F NMR analysis revealed that most of the TFP units were located in the polymer backbone. Copolymerization of ethylene with C_2D_4 revealed that the insertion of TFP in Pd-D occurs via both 1,2- and 2,1-insertion but 1,2-regioselective insertion is slightly preferred.

8. Disubstituted monomers

From the previous sections, it is very clear that the major emphasis in the area of functional olefins copolymerization has been new catalyst development. Although catalyst development is crucial, insertion copolymerization of "novel monomers" with added "features, functionality and purpose" is equally important. Insertion copolymerization of 1,1-disubstituted olefin with ethylene can double the functional group density on polymer backbone at the same amount of functional olefin incorporation. Such increased functional group density can lead to enhanced adhesion even at same or lower incorporation. However, as compared to mono-substituted olefins reviewed in the previous sections, 1,1- and 1,2-disubstituted olefins are highly challenging monomers for metal-catalyzed insertion copolymerization. Additional substitution in the disubstituted olefin increase the steric hindrance around the double bond and concomitantly reduces the coordination ability of the olefin. This cumulative challenge has been taken up by a few research groups in the recent past and sections 8.1–8.3 will review the progress in this area.

8.1. 1,1-disubstituted monofunctional olefins

Based on the number of functional groups, 1,1-disubstituted olefins can be further classified as i) di-substituted monofunctional olefins and ii) di-substituted difunctional olefins. A very well-known example of a di-substituted monofunctional would be methyl methacrylate (MMA). MMA is an industrially important monomer and the polymer, PMMA, has been widely investigated and finds various applications [177]. PMMA is regularly manufactured using anionic and radical polymerization pathways [178,179]. MMA bears a -Me and a -COOMe group on the same carbon and therefore the steric hindrance around the double bond is much higher as compared to ethylene. This increased steric hindrance decreases the coordination ability of MMA towards the metal center and poses an additional challenge for insertion copolymerization.

The insertion copolymerization of ethylene and MMA has been studied using almost all known functional olefin polymerization catalyst systems **C1, C2, C3, C4** and **C5** (Fig. 2). Sen and coworkers reported stoichiometric reaction between **C1** type, α-diimine ligated, Pd-complex, and MMA to yield a stable five-membered cationic chelate complex [180]. The MMA insertion occurs in a 1,2-fashion and the resultant palladium chelate species did not contain any β-hydrogen. The copolymerization reaction between ethylene and MMA was investigated using a four silylated substituent containing α-Diimine nickel complexes by Matos et al. [181]. The introduction of silyl group at the para position of imine reduced the oxophilicity of the metal and stabilized the metal towards the functional monomer. The silylated complex activated by MAO yields a copolymer with up to 60% of MMA incorporation. Although such high incorporation raises questions about the polymerization mechanism. Gibson et al. used neutral phosphine-enolato Ni(II) catalysts and formation of a copolymer with low molecular weight was observed [182]. The copolymer was formed by 2,1-insertion of MMA into the growing polyethylene chain and subsequent β-hydride elimination to yield an enolate-terminated polyethylene.

An in-situ MMAO activated [(β-ketoiminato)Ni(II)Ph(PPh_3)] complex was employed in the copolymerization of ethylene and MMA by Hu and co-workers [183]. The Ni/ketoiminato complex efficiently copolymerized ethylene and MMA with a molecular weight of 2500–7700 g/mol and displayed up to 16.7% MMA incorporation. The authors proposed an insertion mechanism. In contrast, a similar catalytic system [Bis(β-ketoiminato)Ni(II)]/MAO was reported to initiate radical catalyzed MMA polymerization [184]. A year later, Monteil and coworkers proposed that the nickel(II) salicylaldiminato complex plays a dual role during the copolymerization reaction [185,186]. Thus, the picture of MMA insertion copolymerization was not very clear until Mecking and co-workers reported a detailed mechanistic investigation. The authors performed ethylene polymerization in the presence of MMA using a Salicylaldiminato Ni(II) complex (Scheme 25) to yield a mixture of homopolymers of ethylene and MMA [187]. It was found that in the presence of MMA, the polymer productivity decreases as MMA acts as a weak coordinating solvent. Detailed mechanistic investigations using a combination of labeling studies, NMR, and EPR spectroscopy allowed the authors to conclude that the migratory insertion of ethylene does not affect the simultaneous radical polymerization of MMA. The insertion and radical polymerization proceed simultaneously and both cycles are independent of each other. In stoichiometric reactions, it was observed that Ni-Me complex doesn't insert MMA, but Ni-H species (which is obtained by β-H elimination from Ni-alkyl species) are capable of MMA insertion in 1,2-fashion at low (-35 °C) temperature. The Ni-Ph complexes insert MMA in 2, 1-fashion at 70 °C. These stoichiometric reactions suggest catalyst decomposition via a bimolecular coupling of two Ni complexes, i. e. [Ni(II)R] and [Ni(II)R'] couple to yield an R-R' and Ni(I) species which is characterized by EPR analysis.

Based on this investigation, it has been proposed that Ni(II) leads to insertion polymerization of ethylene, while, radical polymerization of MMA is catalyzed by homolytic cleavage of P-C (PPh_3) bond. The source of radicals is believed to be the donor group triphenyl phosphine and the

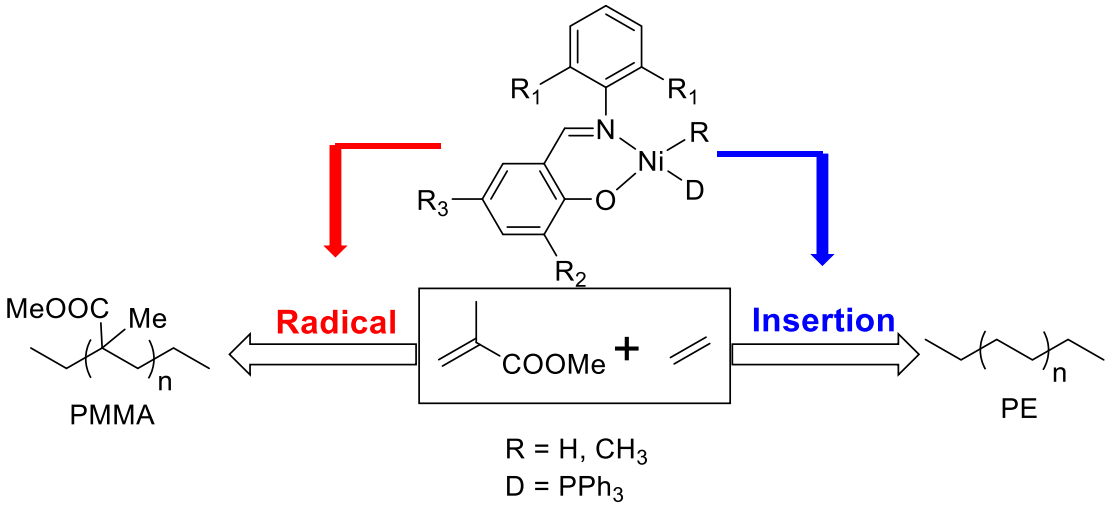

Scheme 25. Interplay between an insertion and a radical polymerization of MMA and ethylene.

existence of organic radicals was detected using EPR spectroscopy. Detailed analysis of resultant polymer microstructure allowed the authors to conclude that there is an interplay between a radical and insertion mechanism and the ethylene and MMA blocks are produced via coordination insertion mechanism and radical mechanism, respectively.

Reactivity of MMA and ethylene copolymerization using a palladium phosphine-sulfonate type catalyst **C3** was investigated by Mecking and co-workers [188]. The polymerization reaction produced a highly linear ethylene homopolymer, even in the presence of a considerable amount of MMA. With increasing concentration of MMA catalytic activity decreased, but without any MMA incorporation. In order to understand the reactivity of MMA, a stoichiometric reaction between complex **1** (Scheme 26) and MMA was investigated. In the stoichiometric reaction, the formation of species **3**–**6** was observed. Compound **3** was found to be the major product (62%) in this reaction, which is formed by 1,2-insertion of MMA. First 2,1-insertion, followed by β-H elimination and 1,2-insertion into the Pd-H species produces compound **4** (30%). While the same sequence of steps and 2,1-insertion of MMA into the Pd-H yields species **5** in a minor quantity (8%).

Apart from the Brookhart and Drent type catalyst, the Nozaki type, methylene bridged Pd-bisphosphine monoxide catalysts were found to be active in ethylene MMA copolymerization [81]. The Pd(BPMO) complexes derived from **L26a-f** (Scheme 4) successfully incorporate MMA into the polyethylene chain along with high molecular weight. The thus obtained copolymer was a statistical copolymer with up to 0.6 mol% MMA incorporation. At higher ethylene pressures, reduced MMA incorporation was observed. Similar to BPMO, diphosphazene monoxide (**L34a-e**) (Scheme 5) derived Pd-catalyst copolymerized ethylene with MMA [89]. The neutral Pd-catalyst at 1 bar ethylene pressure produced a copolymer with only 0.2 mol% MMA incorporation.

Nozaki and coworkers investigated the copolymerization of ethylene with 1,1 disubstituted functional olefins using an imidazo[1,5-a] quinolin-9-olate-1-ylidene (IzQO) (**C5** type catalyst) [189]. The copolymerization reaction with variable MMA concentrations produced a copolymer with up to 0.85 mol% MMA incorporation. While, under reduced ethylene pressure, significant increase in MMA incorporation (up to 2.5 mol%) was observed. The copolymer microstructure was analyzed by 1-2D NMR spectroscopy, which suggested the formation of statistical copolymer and MMA was inserted into the polymer main chain. A stoichiometric reaction between complex **1** (Scheme 27) and MMA revealed 1,2-insertion of MMA into the Pd-Me to yield a five-membered chelate complex. The identity of the chelate complex was unambiguously established using NMR analysis and single crystal. This MMA inserted product **2** was further treated with ethylene at 100 °C to produce a mixture of two types of polymer (**3** and **4**). Chelate opening of the complex **2** and subsequent coordination-insertion of ethylene produces product **3**. An in-situ generated (after β–hydride elimination) Pd-H complex initiates polymerization of ethylene to form a polyethylene **4**. The scope of the reaction was widened and the same catalyst was utilized for insertion copolymerization of 1,1 disubstituted monofunctional monomer with ethylene. Methallyl phenyl ether was found to insert and an ethylene copolymer with 0.41 mol% incorporation was observed. The 3-methylbut-3-en-1-yl acetate was found to insert with moderate catalytic activity and up to 0.23 mol% incorporation.

8.2. *1,1-disubstituted difunctional olefins*

In continuation with the foregoing discussions, it is restated that

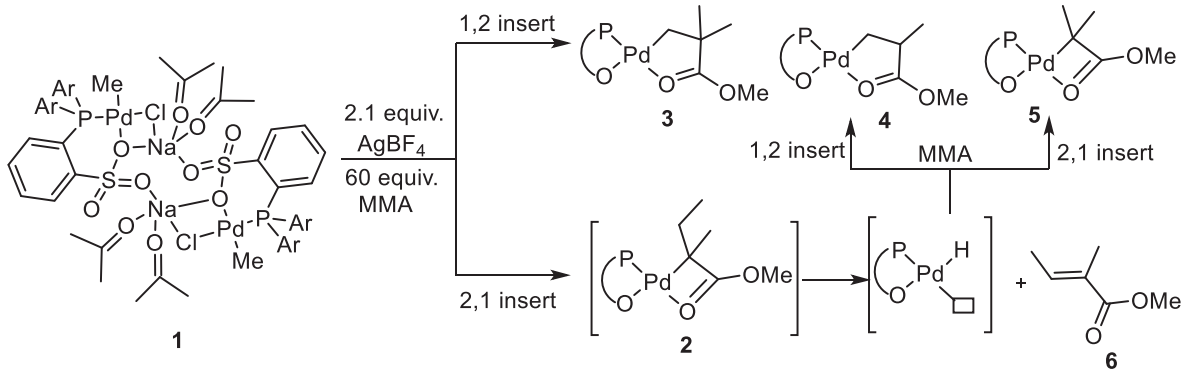

Scheme 26. Reactivity of MMA with phosphinesulfonato Pd(II) complexes.

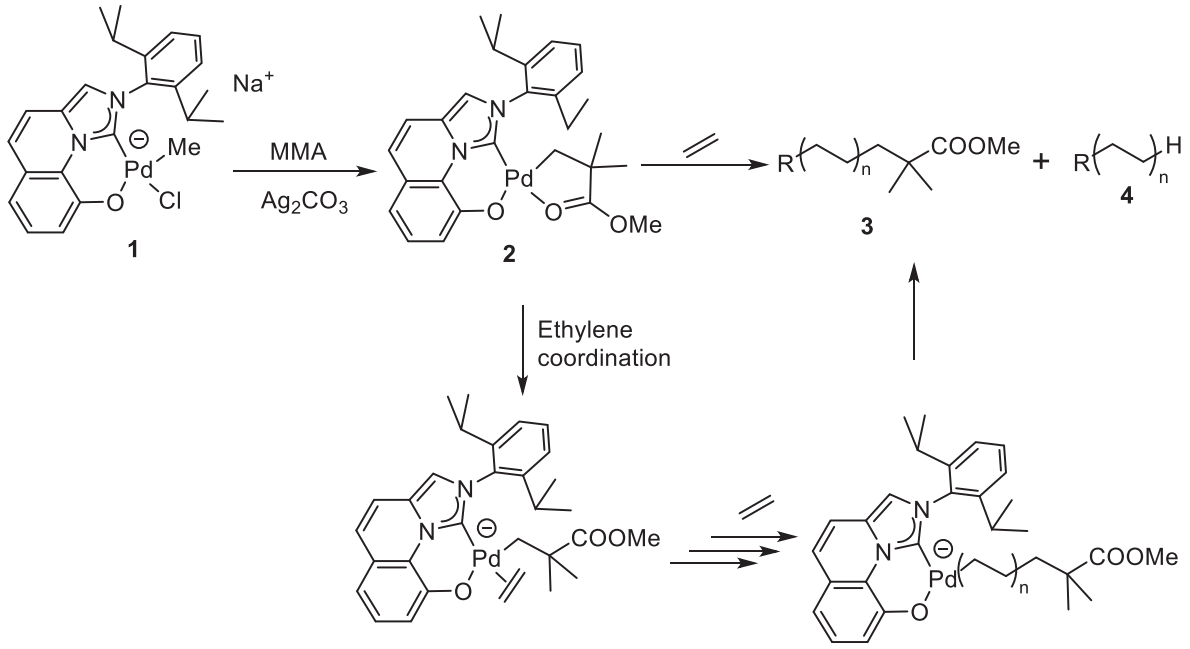

Scheme 27. Reactivity of [Pd(II)(IzQO)] catalyst with MMA.

insertion copolymerization of disubstituted difunctional monomers is highly challenging and requires specific issues to be addressed. The substitution around the double bond increases the steric bulk and thereby reduces coordinating ability of the olefins (Fig. 7, top). However, electronic properties of the substituents can be manipulated to create electronic differentiation between the substituted carbon of the double bond and non-substituted carbon. Highly electron-withdrawing, sterically less bulky substituents may encourage a nucleophilic attack by metal-bound carbon on an electrophilic olefinic carbon atom, in a 4-member transition state, in Cossee-Arlman type mechanism [2]. This will lead to a net 1,2-insertion of a 1,1-disubstituted difunctional olefin (DDO). A generic interplay between the steric versus electronics of the substituents is depicted Fig. 7. It should be noted that steric and electronic parameters can not be decoupled and both of them will be at play for any given monomer. Therefore, Fig. 7 is only for understanding the two effects and the insertion mode will depend on which parameter (steric or electronic) dominates the overall process. While preparing Fig. 7, it is assumed that catalyst/ligand parameters do not interfere with the insertions modes. In reality, even the ligand/catalyst parameters can reverse the insertion modes. Previously discussed MMA would be a good example of non-polarized sterically bulky olefin, while ethyl cyanoacrylate (ECA) would represent polarized olefin with electron-withdrawing, less bulky substituents.

ECA is known for its adhesive properties and is being commercially

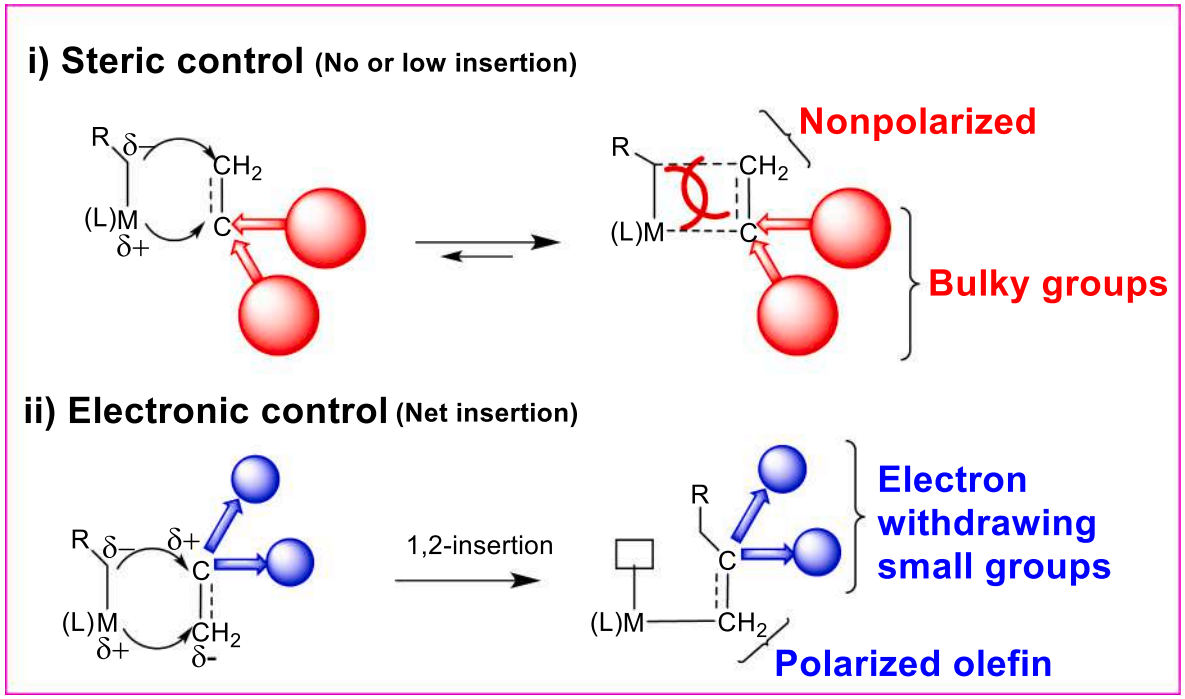

Fig. 7. A representative picture of steric versus electron control in the insertion copolymerization of 1,1-disubstituted difunctional olefin.

used (Krazy glue or super glue) for a long time [190,191]. We envisioned that incorporation of ECA would imbibe hydrophilicity to the resultant copolymer and will change the material properties. Insertion copolymerization of ECA with ethylene was first attempted in 2015 using Drent type- acetonitrile coordinated palladium complex [192]. At an ethylene pressure of 1 bar, 6.5% ECA incorporation was observed. The resultant copolymer was analyzed using high-temperature 1-2D NMR, high-temperature GPC, MALDI-ToF-MS, and incorporation of ECA in the polymer backbone was established. Similarly, insertion copolymerization trifluoromethyl acrylic acid (TFMAA) with ethylene was reported and a 3% incorporation was observed.

Subsequently, the reactivity of 1,1-disubstituted difunctional olefin was investigated using two representative monomers, namely, methyl 2-acetamido acrylate (MAAA) and 2-(trifluoromethyl) acrylic acid and Scheme 28 presents the possible products [193]. In a stoichiometric reaction, 2 equivalents of MAAA was treated with Pd-DMSO complex, and presence of both 1,2- and 2,1-inserted products was detected. The insertion products were characterized using various spectroscopic and analytical methods, including 1-2D NMR and single-crystal X-ray diffraction. Single crystal X-ray diffraction analysis unambiguously confirmed the preferential formation of amide carbonyl coordinated chelate **8** (Fig. 8). While, TFMAA displayed 2,1-insertion and subsequent elimination, re-insertion products. After establishing that 1,1-disubstituted olefins are amenable to insertion, the scope of this

reaction was widened and various difunctional monomers were copolymerized with ethylene (Scheme 28, bottom). The incorporation spanned from 1 to 6% for olefins to 6–12% for allylic monomers. Water contact angle (WCA) measurements suggested that the resultant copolymer, with 11.8% DMAM incorporation, was relatively hydrophilic and displayed a lower angle of 76° (compared to 112° by neat PE).

However, a complete understanding was still missing, which warranted further investigations [189]. In our attempts to address the incorporation of DDO and present a comprehensive picture, we recently reported a detailed study [194]. DDO inserted species were isolated and

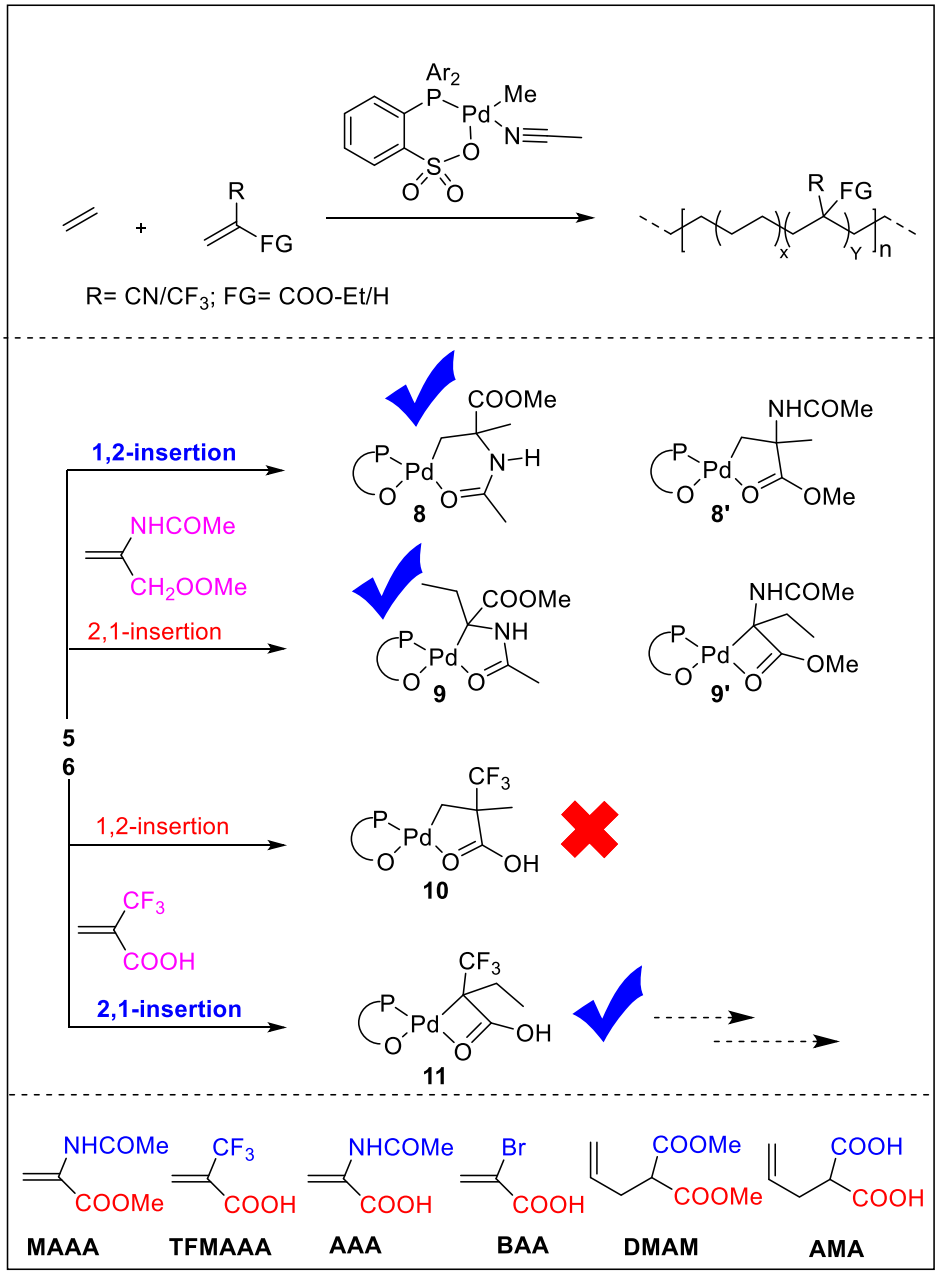

Scheme 28. Insertion copolymerization of 1,1-disubstituted difunctional olefin and mechanistic investigations.

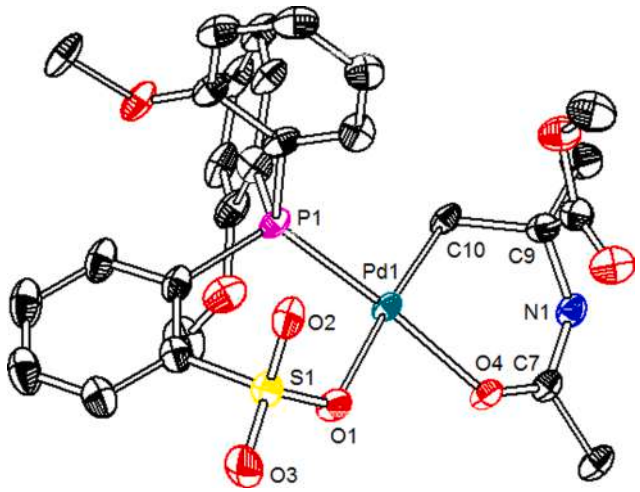

Fig. 8. Molecular structure of MAAA insertion intermediate 8. Reproduced with permission from Gaikwad et al. [193]. Copyright@ 2017 American Chemical Society.

subjected to ethylene insertion. The thus formed, multiple ethylene inserted, low molecular weight polymers were characterized and their structure was fully established. Further, model compounds were prepared on purpose and the characteristic chemical shifts were compared with ethylene inserted low molecular weight polymers. The characteristic features of on purpose prepared model compounds were found to closely match with the ethylene inserted low molecular weight compounds. Additionally, DFT was employed to examine the insertion barriers and predict the feasibility of insertion of DDO's. These combined experimental and theoretical investigations suggested that DDO's are amenable to insertion and ethylene polymerization.

8.3. 1,2-disubstituted olefins

1,2-disubstituted olefins are equally challenging monomers for insertion copolymerization but will have added advantages. Recently Chen and coworkers reported palladium-catalyzed copolymerization of 1,2 di-substituted functional olefins with ethylene [195]. Di-substituted difunctional olefins, such as dimethyl fumarate and dimethyl maleate were examined in ethylene copolymerization. It was observed that the cis isomer, i. e. dimethyl maleate is efficiently incorporated (1.1 mol%) into the polyethylene chain but trans isomer (dimethyl fumarate) could not be enchained. Mechanistic investigations suggest that the rate of insertion of cis isomer (dimethyl maleate) is slow and the resultant 5-membered intermediate is less stable due to *cis*-geometry. These two aspects provide enough room for ethylene insertion and copolymerization of dimethyl maleate. While insertion of *trans*-isomer (dimethyl fumarate) is fast and the resultant 5-membered intermediate with trans geometry is highly stable. Due to these impediments, insertion copolymerization of dimethyl fumarate is halted. Although the overall incorporation of difunctional monomer was a major challenge, the authors addressed this by combing olefin metathesis with insertion polymerization in one pot. Thus, tandem ethenolysis of dimethyl maleate using **Ru1**/**Ru2** (Scheme 29) and subsequent insertion polymerization produced a reasonable molecular weight of copolymer (Mn = 8700 Da) with high incorporation (8.3 mol%).

9. Renewable functional olefins

An overview of earlier sections 1–8 will convince that almost all functional olefins used in these investigations are derived from fossil resources. On the contrary, fossil resources are on fast decline and may not be able to meet our future needs. Therefore, it is worth an effort to incorporate renewable functional olefins in a polyethylene backbone. Incorporation of renewable functional olefins offers two advantages, i) it partly reduces our dependence on fossil resources, ii) the renewable functional olefins might be amenable to microbial/enzymatic degradation. Thus, insertion copolymerization of renewable functional olefins with ethylene opens up new avenues and offers distinct advantages. Plant oils and sugars are the most suitable candidates for insertion copolymerization with ethylene, as these are readily and abundantly available.

Although highly desirable, insertion copolymerization of renewable functional olefins has been largely overlooked and to the best of our knowledge, there are only three reports. Section 9.1 presents recent developments in this upcoming area.

9.1. Catechol and sugar-derived monomers

Insertion copolymerization of ethylene with essential oil derivatives, renewable catechols, sugar derivatives using palladium-phosphinesulfonate (**C3**, Drent type) catalyst has been recently reported. Miri and coworkers investigated insertion copolymerization of ethylene with eugenol using palladium complex derived from the ligand

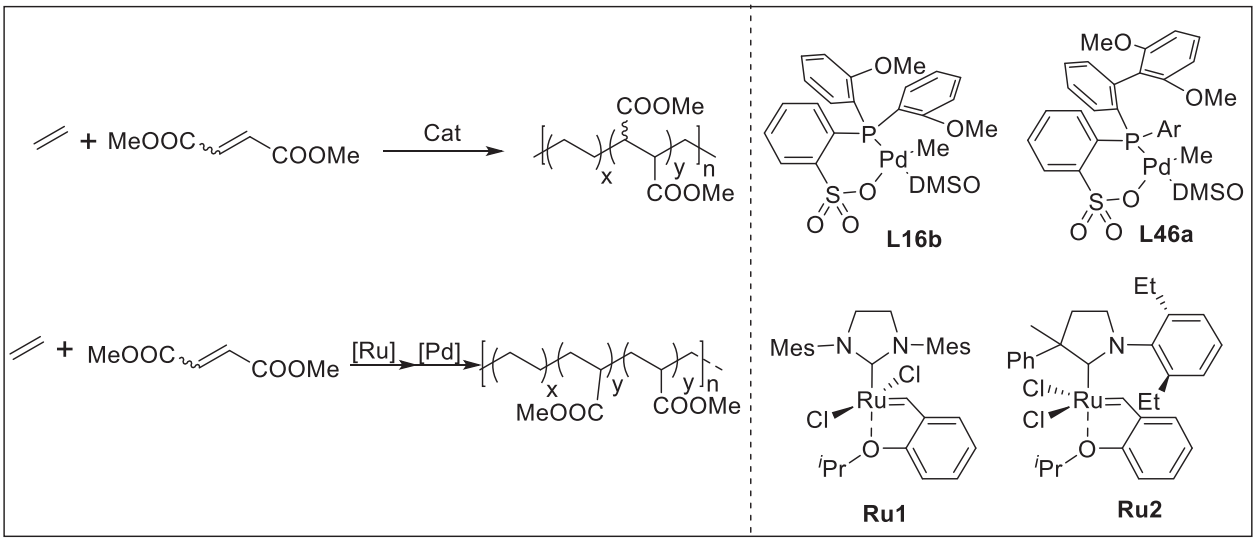

Scheme 29. Direct (top) and tandem (bottom) copolymerization of ethylene with 1,2 difunctional olefins.

L16b (Scheme 2) [196]. The resultant copolymer revealed weight average molecular weight of ~ 3400–15300 g/mol and eugenol incorporation of 1.4–13.5%. Detailed NMR analysis of the copolymer confirmed in-chain incorporation of eugenol and both 2,1- and 1,2-insertion modes were noted. Interestingly, the copolymer displayed antibacterial activity, a characteristic feature of molecular eugenol. The antibacterial activity displayed by eugenol-ethylene copolymer opens up new avenues for "active packaging (PE)" materials. The existing method of preparing "active packaging PE" requires post-reactor modification, while above copolymerization provides a direct route to manufacture active PE material. Similarly, non-renewable allylbenzene based monomers have been recently reported [197].

Chen and co-workers reported insertion copolymerization of ethylene with eugenol, catechol, and related bio-sourced monomers using a sterically bulky **L46a** (Scheme 29) ligated palladium catalyst (Scheme 30) [198]. The catalyst [(**L46a**)PdMe(DMSO)] revealed efficient co– and ter-polymerization and produced copolymers with high molecular weights (~50000 g/mol). The incorporation of eugenol varied from 0.4 to 3.1%. Direct use of comonomer Eug-OH led to significant decrease in the copolymer molecular weight. While, the $SiEt_3$ protected comonomer displayed enhanced activity, molecular weight, and comonomer incorporation (2.3 mol%). Terpolymerization reaction of ethylene, hexene, eugenol, and its derivatives produced copolymers with high-molecular-weight and high incorporation. The Eug-Si copolymer or terpolymer was hydrolyzed under mild reaction conditions to obtain the hydroxyl functional groups [199]. The incorporation of catechol derivatives was found to significantly influence mechanical, adhesive, and self-healing properties of the copolymer. The co- and terpolymer interact with various metal ions and thereby endure better material performance. Thus, the interaction of above copolymers with Fe^{+3} ion leads to increased mechanical strength and self-healing properties. The ethylene-hexene-Eug-Si/HCl terpolymer was found to blend LLDPE with PLA, a highly sought after application in industry. Thus, the co– and terpolymers derived from renewable resources can considerably influence the material properties and hold great potential for commercialization.

Recently, Chikkali and co-workers reported insertion copolymerization of ethylene with sugar derived isohexide mono-enes using Drent type catalyst [(**L16b**)PdMe(CH_3CN)] (Scheme 31) [200]. The insertion copolymerization of ethylene and sugar-based monomer isomannide mono-ene (**Sa**) and isosorbide mono-ene (**Sb**) produced copolymers with poor to moderate incorporation (0.2–0.44%). The copolymer of ethylene with isoidide mono-ene (**Sc**) revealed the highest incorporation of 1.45%, which can be ascribed to the *exo*-exo stereochemistry of comonomer. NMR analysis of the copolymer displayed in-chain incorporation of the sugar derived monomers. While the bulky disubstituted functional olefin **Sd** and trifunctional allylic monomer **Se** showed lower incorporation of 0.48% and 0.41% respectively. The water contact angle of the ethylene, isoidide mono-ene **Sc** was found to be 104° (Fig. 9), which confirms increased hydrophilicity of copolymer, as compared to neat PE.

10. Summary and outlook

Insertion copolymerization of functional olefins with ethylene offers a direct route to prepare functional polyethylene. However, insertion of functional olefins in polyethylene backbone is not trivial and several limitations have to be addressed. The challenges include, i) designing functional group tolerant catalysts, ii) identifying olefins that serve additional function/purpose and, iii) inventing strategies to enhance functional group density.

Several of these limitations have been addressed and catalytic systems capable of insertion copolymerization of functional olefins with ethylene have been discovered over the last two decades. The initial focus was on judicious choice of ligand and metal, which led to the discovery of Brookhart's α-diimine, Drent's phosphine-sulfonate, Grubbs imine-phenolate, and Nozaki's BPMO and IzQO catalytic systems. Subsequently, the scope of functional olefins was widened and several functional olefins were subjected to insertion-copolymerization. As presented in this review, olefins with various functional groups such as acrylates, acrylic acids, acetates, nitriles, ethers, and halides were copolymerized with ethylene. The purpose of these initial studies was limited to demonstrating insertion of functional olefins and did not extensively look at the properties of resultant copolymer. Recent reports

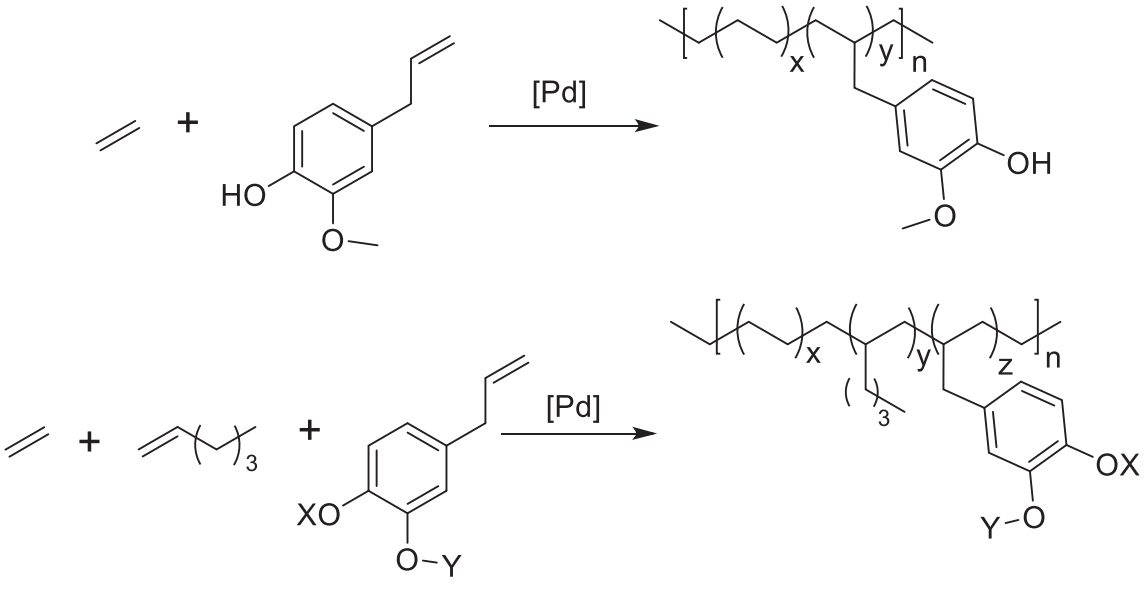

Scheme 30. Copolymerization and terpolymerization of ethylene with eugenol.

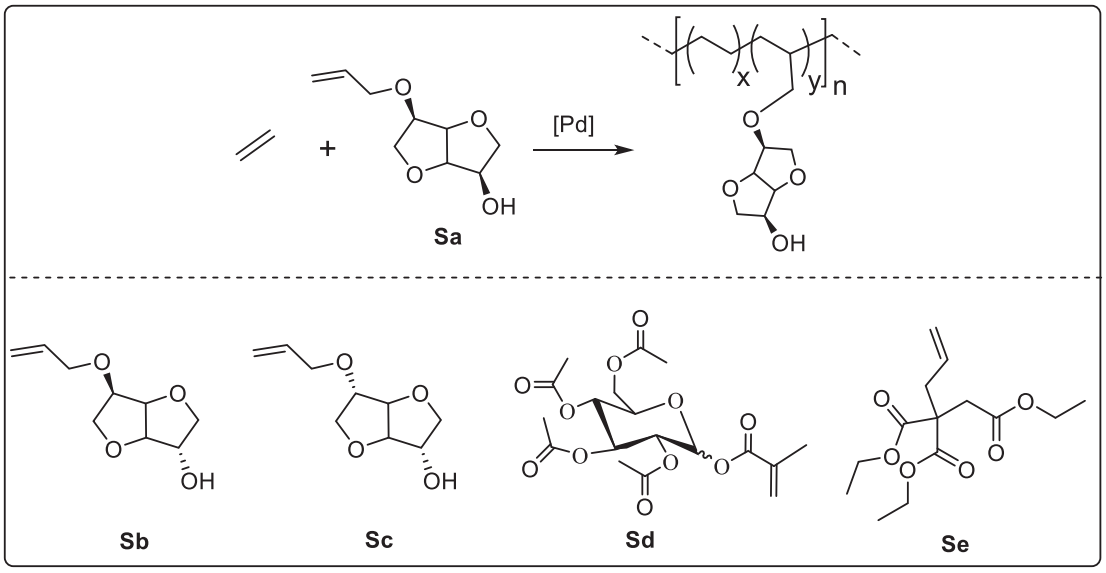

Scheme 31. Copolymerization of ethylene with sugar derived isohexide mono-enes.

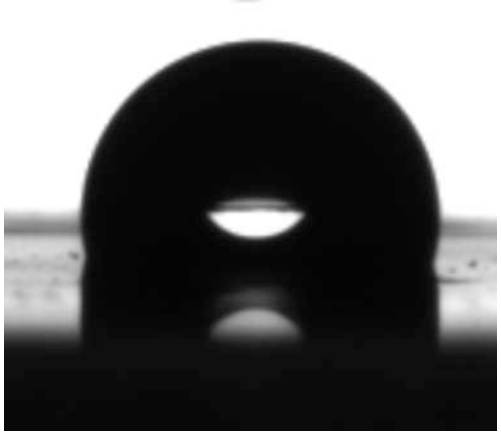

Fig. 9. Water contact angle image for isoidide derived copolymer (104° (±2); an average of 3 measurements). Reproduced with permission from Rajput et al. [200]. Copyright@ 2020 Elsevier B. V.

analyze the microstructure of the functional copolymers and provide a comparative property profiling with commercial functional polyolefins [88,159]. In the last five years, the focus is slowly shifting from merely incorporating a functional group in a polymer backbone to, insertion of functional olefins that can serve an additional purpose or function. In this context, insertion copolymerization of olefins with dynamic/interactive functional groups, di-functional olefins and renewable functional olefins has been achieved [159,192,193,198,200].

Thus, the review attempts to capture the essence of major developments and poses a question about the future of a quarter of a century's intellectual investment. In fact, the last section of this review partly answers this and forecasts the potential of the functional polyolefins. No doubt that catalyst development is going to be the key enabler, but the focus is going to shift to produce functional polyolefins that can either replace existing functional PE or serve a niche application/market. Tailoring the copolymer properties using an existing catalyst to match the features of commercial functional polyethylene (produced by high pressure radical polymerization method), can exploit the full potential of the insertion copolymerization. Incorporation of renewable functional olefins adds another dimension to the field. It may not be an exaggeration to anticipate a fully renewable functional polyethylene (derived from bio-ethylene and renewable functional olefin), that can serve a conscious customer who is willing to pay extra cost. Thus, although significant progress has been made, a lot of ground has to be covered to bridge the gap between the current state of the field and a commercial product. This gap will drive the field and will catalyze further research and development activities across academic and industrial laboratories.

Declaration of Competing Interest

The authors declare that they have no known competing financial interests or personal relationships that could have appeared to influence the work reported in this paper.

Acknowledgements

We are indebted to DST-SERB (EMR/2016/005120), CSIR-National Chemical Laboratory (HCP0011), India and AvH foundation Bonn, Germany for financial support. RSB is grateful to DST-INSPIRE for fellowship. We would like to thank Mr. Kishor Khopade for table of contents figure.

Data availability

This is a review article and hence no additional data is available.

References

[1] M. Stürzel, S. Mihan, R. Mülhaupt, From Multisite Polymerization Catalysis to Sustainable Materials and All-Polyolefin Composites, Chem. Rev. 116 (2016) 1398–1433.
[2] S.H. Chikkali, Ziegler-Natta Polymerization and the Remaining Challenges, Resonance 22 (2017) 1039–1060.
[3] K. Patel, S.H. Chikkali, S. Sivaram, Ultrahigh molecular weight polyethylene: Catalysis, structure, properties, processing and applications, Prog. Polym. Sci. 109 (2020) 101290/1-30.
[4] P.D. Hustad, Frontiers in Olefin Polymerization: Reinventing the World's Most Common Synthetic Polymers, Science 325 (2009) 704–707.
[5] C. Chen, Designing catalysts for olefin polymerization and copolymerization: Beyond electronic and steric tuning, Nat. Rev. Chem. 2 (2018) 6–14.
[6] A. Nakamura, T.M.J. Anselment, J. Claverie, B. Goodall, R.F. Jordan, S. Mecking, B. Rieger, A. Sen, P.W.N.M. van Leeuwen, K. Nozaki, *Ortho*-Phosphinobenzenesulfonate: A superb ligand for palladium-catalyzed coordination-insertion copolymerization of polar vinyl monomers, Acc. Chem. Res. 46 (2013) 1439–1449.

[7] S.R. Gaikwad, S.S. Deshmukh, S.H. Chikkali, Pd-Phosphinesulfonate bravely battles the "vinyl halide insertion copolymerization" barricade, J. Polym. Sci. Part A: Polym. Chem. 52 (2014) 1–6.
[8] T.C.M. Chung, Functional Polyolefins for Energy Applications, Macromolecules 46 (2013) 6671–6698.
[9] J. Chen, Y. Gao, T.J. Marks, Early Transition Metal Catalysis for Olefin-Polar Monomer Copolymerization, Angew. Chem. Int. Ed. 59 (2020) 14726–14735.
[10] Z. Chen, M. Brookhart, Exploring Ethylene/Polar Vinyl Monomer Copolymerizations Using Ni and Pd α-Diimine Catalysts, Acc. Chem. Res. 51 (2018) 1831–1839.
[11] H. Martinez, N. Ren, M.E. Matta, M. Hillmyer, Ring-opening metathesis polymerization of 8-membered cyclic olefins, Polym. Chem. 5 (2014) 3507–3532.
[12] Y. Chen, M.M. Abdellatif, K. Nomura, Olefin metathesis polymerization: Some recent developments in the precise polymerizations for synthesis of advanced materials (by ROMP, ADMET), Tetrahedron 74 (2018) 619–643.
[13] A. Nakamura, S. Ito, K. Nozaki, Coordination-Insertion Copolymerization of Fundamental Polar Monomers, Chem. Rev. 109 (2009) 5215–5244.
[14] L.K. Johnson, S. Mecking, M. Brookhart, Copolymerization of Ethylene and Propylene with Functionalized Vinyl Monomers by Palladium(II) Catalysts, J. Am. Chem. Soc. 118 (1996) 267–268.
[15] S. Mecking, L.K. Johnson, L. Wang, M. Brookhart, Mechanistic Studies of the Palladium-Catalyzed Copolymerization of Ethylene and α-Olefins with Methyl Acrylate, J. Am. Chem. Soc. 120 (1998) 888–899.
[16] E.Y.X. Chen, T.J. Marks, Cocatalysts for metal-catalyzed olefin polymerization: Activators, activation processes, and structure-activity relationships, Chem. Rev. 100 (2000) 1391–1434.
[17] H.S. Zijlstra, S. Harder, Methylalumoxane-History, Production, Properties, and Applications, Eur. J. Inorg. Chem. 2015 (2015) 19–43.
[18] M.E.Z. Velthoen, A. Munoz-Murillo, A. Bouhmadi, M. Cecius, S. Diefenbach, B. M. Weckhuysen, The Multifaceted Role of Methylaluminoxane in Metallocene-Based Olefin Polymerization Catalysis, Macromolecules 51 (2018) 343–355.
[19] D.H. Camacho, Z. Guan, Designing late-transition metal catalysts for olefin insertion polymerization and copolymerization, Chem. Commun. 46 (2010) 7879–7893.
[20] For a recent review on Brookhart catalyst in olefin copolymerization see: F. Wang, C. Chen, A continuing legend: The Brookhart-type α-diimine nickel and palladium catalysts Polym. Chem. 10 (2019) 2354–2369.
[21] S.D. Ittel, L.K. Johnson, M. Brookhart, Late-Metal Catalysts for Ethylene Homo- and Copolymerization, Chem. Rev. 100 (2000) 1169–1204.
[22] T.R. Younkin, E.F. Connor, J.I. Henderson, S.K. Friedrich, R.H. Grubbs, D. A. Bansleben, Neutral, Single-Component Nickel (II) Polyolefin Catalysts That Tolerate Heteroatoms, Science 287 (2000) 460–462.
[23] For a recent review on Ni-based systems in olefin copolymerization, please see: H. Mu, L. Pan, D. Song, Y. Li, Neutral Nickel Catalysts for Olefin Homo- and Copolymerization: Relationships between Catalyst Structures and Catalytic Properties Chem. Rev. 115 (2015) 12091–12137.
[24] K. Nozaki, S. Kusumoto, S. Noda, T. Kochi, L.W. Chung, K. Morokuma, Why Did Incorporation of Acrylonitrile to a Linear Polyethylene Become Possible? Comparison of Phosphine-Sulfonate Ligand with Diphosphine and Imine-Phenolate Ligands in the Pd-Catalyzed Ethylene/Acrylonitrile Copolymerization, J. Am. Chem. Soc. 132 (2010) 16030–16042.
[25] B.P. Carrow, K. Nozaki, Synthesis of Functional Polyolefins Using Cationic Bisphosphine Monoxide−Palladium Complexes, J. Am. Chem. Soc. 134 (2012) 8802–8805.
[26] X. Zhou, R.F. Jordan, Synthesis, cis/trans Isomerization, and Reactivity of Palladium Alkyl Complexes That Contain a Chelating N-Heterocyclic-Carbene Sulfonate Ligand, Organometallics 30 (2011) 4632–4642.
[27] R. Nakano, K. Nozaki, Copolymerization of Propylene and Polar Monomers Using Pd/IzQO Catalysts, J. Am. Chem. Soc. 137 (2015) 10934–10937.
[28] R.E. Black, R.F. Jordan, Synthesis and Reactivity of Palladium(II) Alkyl Complexes that Contain Phosphine-cyclopentanesulfonate Ligands, Organometallics 36 (2017) 3415–3428.
[29] N.D. Contrella, J.R. Sampson, R.F. Jordan, Copolymerization of Ethylene and Methyl Acrylate by Cationic Palladium Catalysts That Contain Phosphine-Diethyl Phosphonate Ancillary Ligands, Organometallics 33 (2014) 3546–3555.
[30] B.P. Carrow, K. Nozaki, Transition-metal-catalyzed Functional Polyolefin Synthesis: Effecting Control through Chelating Ancillary Ligand Design and Mechanistic Insights, Macromolecules 47 (2014) 2541–2555.
[31] L. Guo, S. Dai, X. Sui, C. Chen, Palladium and Nickel Catalyzed Chain Walking Olefin Polymerization and Copolymerization, ACS Catal. 6 (2016) 428–441.
[32] E. Passaglia, S. Coiai, F. Cicogna, F. Ciardelli, Some recent advances in polyolefin Functionalization, Polym. Int. 63 (2014) 12–21.
[33] S.B. Amin, T.J. Marks, Versatile Pathways for In Situ Polyolefin Functionalization with Heteroatoms: Catalytic Chain Transfer, Angew. Chem. Int. Ed. 47 (2008) 2006–2025.
[34] D.J. Walsh, M.G. Hyatt, S.A. Miller, D. Guironnet, Recent Trends in Catalytic Polymerizations, ACS Catal. 9 (2019) 11153–11188.
[35] A. Keyes, H.E.B. Alhan, E. Ordonez, U. Ha, D.B. Beezer, H. Dau, Y.S. Liu, E. Tsogtgerel, G.R. Jones, E. Harth, Olefins and Vinyl Polar Monomers: Bridging the Gap for Next Generation Materials, Angew. Chem. Int. Ed. 58 (2019) 12370–12391.
[36] P.D. Goring, C. Morton, P. Scott, End-functional polyolefins for block copolymer synthesis, Dalton Trans. 48 (2019) 3521–3530.
[37] N.M.G. Franssen, J.N.H. Reek, B. de Bruin, Synthesis of functional 'polyolefins': state of the art and remaining challenges, Chem. Soc. Rev. 42 (2013) 5809–5832.
[38] "Polyacrylates": E. Penzil in Ullmann's encyclopaedia of industrial chemistry, Wiley-VCH, Weinheim, 2000, pp. 515-536.
[39] K. Matyjaszewski, J. Xia, Atom Transfer Radical Polymerizatoin, Chem. Rev. 101 (2001) 2921–2990.
[40] M. Kamigaito, T. Ando, M. Sawamoto, Metal-Catalyzed Living Radical Polymerization, Chem. Rev. 101 (2001) 3689–3746.
[41] H. Xu, P.B. White, C. Hu, T. Diao, Structure and Isotope Effects of the β-H Agostic (α-Diimine) Nickel Cation as a Polymerization Intermediate, Angew. Chem. Int. Ed. 56 (2017) 1535–1538.
[42] O. Daugulis, A.H.R. MacAruthur, F.C. Rix, J.L. Templeton, A Career in Catalysis: Maurice Brookhart, ACS Catal. 6 (2016) 1518–1532.
[43] A. Michalak, T. Ziegler, Stochastic Simulations of Polymer Growth and Isomerization in the Polymerization of Propylene Catalyzed by Pd-Based Diimine Catalysts, J. Am. Chem. Soc. 124 (2002) 7519–7528.
[44] J.M. Malinoski, M. Brookhart, Polymerization and Oligomerization of Ethylene by Cationic Nickel(II) and Palladium(II) Complexes Containing Bidentate Phenacyldiarylphosphine Ligands, Organometallics 22 (2003) 5324–5335.
[45] S. Plentz-Meneghetti, J. Kress, F. Peruch, A. Lapp, M. Duval, R. Muller, P.J. Lutz, Solution and bulk rheological behavior of poly(ethylenes) based on VERSIPOL™ catalysts, Polymer 46 (2005) 8913–8925.
[46] Z. Guan, Control of Polymer Topology by Chain-Walking Catalysts, Chem. Eur. J. 8 (2002) 3086–3092.
[47] Z. Dong, Z. Ye, Hyperbranched polyethylenes by chain walking polymerization: synthesis, properties, functionalization, and applications, Polym. Chem. 3 (2012) 286–301.
[48] A. Meduri, T. Montini, F. Ragaini, P. Fornasiero, E. Zangrando, B. Milani, Palladium-Catalyzed Ethylene/Methyl Acrylate Cooligomerization: Effect of a New Nonsymmetric α-Diimine, ChemCatChem 5 (2013) 1170–1183.
[49] H. Pan, L. Zhu, J. Li, D. Zang, Z. Fu, Z. Fan, A thermal stable α-diimine palladium catalyst for copolymerization of ethylene with functionalized olefins, J. Mol. Catal. A: Chem. 390 (2014) 76–82.
[50] V. Rosar, A. Meduri, T. Montini, F. Fini, C. Carfagna, P. Fornasiero, B. Milani, Analogies and Differences in Palladium-Catalyzed CO/Styrene and Ethylene/Methyl Acrylate Copolymerization Reactions, ChemCatChem 6 (2014) 2403–2418.
[51] S. Dai, X. Sui, C. Chen, Highly Robust Palladium (II) α-Diimine Catalysts for Slow-Chain-Walking Polymerization of Ethylene and Copolymerization with Methyl Acrylate, Angew. Chem. Int. Ed. 54 (2015) 9948–9953.
[52] W. Zou, C. Chen, Influence of backbone substituents on the ethylene (co) polymerization properties of α-diimine Pd (II) and Ni (II) catalysts, Organometallics 35 (2016) 1794–1801.
[53] X. Sui, C. Hong, W. Pang, C. Chen, Unsymmetrical α-diimine palladium catalysts and their properties in olefin (co) polymerization, Mater. Chem. Front. 1 (2017) 967–972.
[54] S. Dai, S. Zhou, W. Zhang, C. Chen, Systematic investigations of ligand steric effects on α-diimine palladium catalyzed olefin polymerization and copolymerization, Macromolecules 49 (2016) 8855–8862.
[55] S. Zhong, Y. Tan, L. Zhong, J. Gao, H. Liao, L. Jiang, Q. Wu, Precision synthesis of ethylene and polar monomer copolymers by palladium-catalyzed living coordination copolymerization, Macromolecules 50 (2017) 5661–5669.
[56] N.R. Mote, S.H. Chikkali, Hydrogen-Bonding-Assisted Supramolecular Metal Catalysis, Chem. Asian J. 13 (2018) 3623–3646.
[57] F. Zhai, J.B. Solomon, R.F. Jordan, Copolymerization of ethylene with acrylate monomers by amide-functionalized α-diimine Pd catalysts, Organometallics 36 (2017) 1873–1879.
[58] V.S. Koshti, A. Sen, D. Shinde, S.H. Chikkali, Self-assembly of P-chiral supramolecular phosphines on rhodium and direct evidence for Rh-catalyst-substrate interactions, Dalton Trans 46 (2017) 13966–13973.
[59] M. Li, X. Wang, Y. Luo, C. Chen, A Second-Coordination-Sphere Strategy to Modulate Nickel- and Palladium-Catalyzed Olefin Polymerization and Copolymerization, Angew. Chem. Int. Ed. 56 (2017) 11604–11609.
[60] A. Dall'Anese, V. Rosar, L. Cusin, T. Montini, G. Balducci, I. D'Auria, B. Milani, Palladium-Catalyzed Ethylene/Methyl Acrylate Copolymerization: Moving from the Acenaphthene to the Phenanthrene Skeleton of α-Diimine Ligands, Organometallics 38 (2019) 3498-3511.
[61] X. Ma, X. Hu, Y. Zhang, H. Mu, L. Cui, Z. Jian, Preparation and in situ chain-end-functionalization of branched ethylene oligomers by monosubstituted α-diimine nickel catalysts, Polym. Chem. 10 (2019) 2596–2607.
[62] H. Hu, D. Chen, H. Gao, L. Zhong, Q. Wu, Amine–imine palladium catalysts for living polymerization of ethylene and copolymerization of ethylene with methyl acrylate: incorporation of acrylate units into the main chain and branch end, Polym. Chem. 7 (2016) 529–537.
[63] X. Hu, Y. Zhang, Y. Zhang, Z. Jian, Asymmetrical Strategy Makes Significant Differences in α-Diimine Nickel and Palladium Catalyzed Ethylene (co) Polymerizations, ChemCatChem. 12 (2020) 2497–2505.
[64] Y. Zhang, C. Wang, S. Mecking, Z. Jian, Ultrahighly Branched Main-Chain-Functionalized Polyethylenes via Inverted Insertion Selectivity, Angew. Chem. Int. Ed. 59 (2020) 14296–14302.
[65] Y. Liao, Y. Zhang, L. Cui, H. Mu, Z. Jian, Pentiptycenyl substituents in insertion polymerization with α-diimine nickel and palladium species, Organometallics 38 (2019) 2075–2083.
[66] E. Drent, R. van Dijk, R. van Ginkel, B. van Oort, R.I. Pugh, Palladium catalysed copolymerisation of ethene with alkylacrylates: polar comonomer built into the linear polymer chain, Chem. Commun. 7 (2002) 744–745.

[67] T. Kochi, K. Yoshimura, K. Nozaki, Synthesis of anionic methylpalladium complexes with phosphine–sulfonate ligands and their activities for olefin polymerization, Dalton Trans. 25–27 (2006).
[68] D. Guironnet, L. Caporaso, B. Neuwald, I. Göttker-Schnetmann, L. Cavallo, S. Mecking, Mechanistic Insights on Acrylate Insertion Polymerization, J. Am. Chem. Soc. 132 (2010) 4418–4426.
[69] T. Kageyama, S. Ito, K. Nozaki, Vinylarene/CO Copolymerization and Vinylarene/Polar Vinyl Monomer/CO Terpolymerization Using Palladium/Phosphine-Sulfonate Catalysts, Chem. Asian J. 6 (2011) 690–697.
[70] L. Piche, J.-C. Daigle, G. Rehse, J.P. Claverie, Structure-Activity Relationship of Palladium Phosphanesulfonates: Toward Highly Active Palladium-Based Polymerization Catalysts, Chem. Eur. J. 18 (2012) 3277–3285.
[71] B. Neuwald, L. Falivene, L. Caporaso, L. Cavallo, S. Mecking, Exploring electronic and steric effects on the insertion and polymerization reactivity of phosphinesulfonato Pd^{II} catalysts, Chem. Eur. J. 19 (2013) 17773–17788.
[72] P. Wucher, P. Roesle, L. Falivene, L. Cavallo, L. Caporaso, I. Göttker-Schnetmann, S. Mecking, Controlled acrylate insertion regioselectivity in diazaphospholidine-sulfonato palladium (II) complexes, Organometallics 31 (2012) 8505–8515.
[73] P. Wucher, L. Caporaso, P. Roesle, F. Ragone, L. Cavallo, S. Mecking, I. Göttker-Schnetmann, Breaking the regioselectivity rule for acrylate insertion in the Mizoroki-Heck reaction, Proc. Natl. Acad. Sci. U. S. A. 108 (2011) 8955–8959.
[74] Z. Jian, P. Wucher, S. Mecking, Heterocycle-Substituted Phosphinesulfonato Palladium (II) Complexes for Insertion Copolymerization of Methyl Acrylate, Organometallics 33 (2014) 2879–2888.
[75] P. Wucher, J.B. Schwaderer, S. Mecking, Solid-supported single-component Pd (II) catalysts for polar monomer insertion copolymerization, ACS Catal. 4 (2014) 2672–2679.
[76] Y. Ota, S. Ito, J.I. Kuroda, Y. Okumura, K. Nozaki, Quantification of the steric influence of alkylphosphine–sulfonate ligands on polymerization, leading to high-molecular-weight copolymers of ethylene and polar monomers, J. Am. Chem. Soc. 136 (2014) 11898–11901.
[77] Z. Wu, M. Chen, C. Chen, Ethylene polymerization and copolymerization by palladium and nickel catalysts containing naphthalene-bridged phosphine–sulfonate ligands, Organometallics 35 (2016) 1472–1479.
[78] D. Zhang, C. Chen, Influence of Polyethylene Glycol Unit on Palladium- and Nickel-Catalyzed Ethylene Polymerization and Copolymerization, Angew. Chem. Int. Ed. 56 (2017) 14672–14676.
[79] For details, see reference 28.
[80] Y. Mitsushige, B.P. Carrow, S. Ito, K. Nozaki, Ligand-controlled insertion regioselectivity accelerates copolymerisation of ethylene with methyl acrylate by cationic bisphosphine monoxide-palladium catalysts, Chem. Sci. 7 (2016) 737–744.
[81] Y. Mitsushige, H. Yasuda, B.P. Carrow, S. Ito, M. Kobayashi, T. Tayano, Y. Watanabe, Y. Okuno, S. Hayashi, J. Kuroda, Y. Okumura, K. Nozaki, Methylene-bridged bisphosphine monoxide ligands for palladium-catalyzed copolymerization of ethylene and polar monomers, ACS Macro Lett. 7 (2018) 305–311.
[82] J. Ye, H. Mu, Z. Wang, Z. Jian, Heteroaryl backbone strategy in bisphosphine monoxide palladium-catalyzed ethylene polymerization and copolymerization with polar monomers, Organometallics 38 (2019) 2990–2997.
[83] H.L. Mu, J.H. Ye, G.L. Zhou, KK. Li, ZB. Jian, Ethylene polymerization and copolymerization with polar monomers by benzothiophene-bridged BPMO-Pd catalysts, Chinese J. Polym. Sci. 38 (2020) 579–586.
[84] K. Li, J. Ye, Z. Wang, H. Mu, Z. Jian, Indole-bridged bisphosphine-monoxide palladium catalysts for ethylene polymerization and copolymerization with polar monomers, Polym. Chem. 11 (2020) 2740–2748.
[85] Cationic palladium complexes derived from phosphine-phosphonate ligands were employed in the copolymerization, for details, see reference 29.
[86] Z. Cai, LH. Do, Thermally Robust Heterobimetallic Palladium-Alkali Catalysts for Ethylene and Alkyl Acrylate Copolymerization, Organometallics 37 (2018) 3874–3882.
[87] X. Sui, S. Dai, C. Chen, Ethylene polymerization and copolymerization with polar monomers by cationic phosphine phosphonic amide palladium complexes, ACS Catal. 5 (2015) 5932–5937.
[88] W. Zhang, P.M. Waddell, M.A. Tiedemann, C.E. Padilla, J. Mei, L. Chen, B. P. Carrow, Electron-rich metal cations enable synthesis of high molecular weight, linear functional polyethylenes, J. Am. Chem. Soc. 140 (2018) 8841–8850.
[89] M. Chen, C. Chen, A Versatile Ligand Platform for Palladium- and Nickel-Catalyzed Ethylene Copolymerization with Polar Monomers, Angew. Chem. Int. Ed. 57 (2018) 3094–3098.
[90] For details, see reference 27.
[91] W. Tao, R. Nakano, S. Ito, K. Nozaki, Copolymerization of Ethylene and Polar Monomers by Using Ni/IzQO Catalysts, Angew. Chem. Int. Ed. 55 (2016) 2835–2839.
[92] W. Tao, S. Akita, R. Nakano, S. Ito, Y. Hoshimoto, S. Ogoshi, K. Nozaki, Copolymerisation of ethylene with polar monomers by using palladium catalysts bearing an N-heterocyclic carbene–phosphine oxide bidentate ligand, Chem. Commun. 53 (2017) 2630–2633.
[93] W. Tao, X. Wang, S. Ito, K. Nozaki, Palladium complexes bearing an N-heterocyclic carbene–sulfonamide ligand for cooligomerization of ethylene and polar monomers. J. Polym. Sci. Part A, Polym. Chem. 57 (2019) 474–477.
[94] Y. Zhang, H. Mu, L. Pan, X. Wang, Y. Li, Robust bulky [P, O] neutral nickel catalysts for copolymerization of ethylene with polar vinyl monomers, ACS Catal. 8 (2018) 5963–5976.
[95] Y. Zhang, H. Mu, X. Wang, L. Pan, Y. Li, Elaborate tuning in ligand makes a big difference in catalytic performance: bulky nickel catalysts for (co)polymerization of ethylene with promising vinyl polar monomers, ChemCatChem 11 (2019) 2329–2340.
[96] B.S. Xin, N. Sato, A. Tanna, Y. Oishi, Y. Konishi, F. Shimizu, Nickel catalyzed copolymerization of ethylene and alkyl acrylates, J. Am. Chem. Soc. 139 (2019) 3611–3614.
[97] L. Cui, Z. Jian, N-bridged strategy enables hemilabile phosphine–carbonyl palladium and nickel catalysts to mediate ethylene polymerization and copolymerization with polar vinyl monomers, Polym. Chem. 11 (2020) 6187–6193.
[98] J. Daigle, L. Piche, A. Arnold, J.P. Claverie, Probing the Regiochemistry of Acrylate Catalytic Insertion Polymerization via Cyclocopolymerization of Allyl Acrylate and Ethylene, ACS Macro Lett. 1 (2012) 343–346.
[99] Y. Zhang, J. Xia, J. Song, J. Zhang, X. Ni, Z. Jian, Combination of ethylene, 1, 3-butadiene, and carbon dioxide into ester-functionalized polyethylenes via palladium-catalyzed coupling and insertion polymerization, Macromolecules 52 (2019) 2504–2512.
[100] B.K. Long, J.M. Eagan, M. Mulzer, G.W. Coates, Semi-Crystalline Polar Polyethylene: Ester-Functionalized Linear Polyolefins Enabled by a Functional-Group-Tolerant, Cationic Nickel Catalyst, Angew. Chem. Int. Ed. 55 (2016) 7106–7110.
[101] Y. Na, S. Dai, C. Chen, Direct synthesis of polar-functionalized linear low-density polyethylene (LLDPE) and low-density polyethylene (LDPE), Macromolecules 51 (2018) 4040–4048.
[102] G. Wang, M. Li, W. Pang, M. Chen, C. Tan, Lewis acids in situ modulate pyridazine-imine Ni catalysed ethylene (co) polymerisation, New J. Chem. 43 (2019) 13630–13634.
[103] Z. Cai, Z. Shen, X. Zhou, R.F. Jordan, Enhancement of chain growth and chain transfer rates in ethylene polymerization by (phosphine-sulfonate) PdMe catalysts by binding of B(C6F5)3 to the sulfonate group, ACS Catal. 2 (2012) 1187–1195.
[104] Y. Gong, S. Li, Q. Gong, S. Zhang, B. Liu, S. Dai, Systematic investigations of ligand steric effects on α-diimine nickel catalyzed olefin polymerization and copolymerization, Organometallics 38 (2019) 2919–2926.
[105] T. Liang, S.B. Goudari, C. Chen, A simple and versatile nickel platform for the generation of branched high molecular weight polyolefins, Nat. Commun. 11 (2020) 372, https://doi.org/10.1038/s41467-019-14211-0.
[106] M. Chen, C. Chen, Rational design of high-performance phosphine sulfonate nickel catalysts for ethylene polymerization and copolymerization with polar monomers, ACS Catal. 7 (2017) 1308–1312.
[107] J. Xia, Y. Zhang, J. Zhang, Z. Jian, High-performance neutral phosphine-sulfonate nickel (II) catalysts for efficient ethylene polymerization and copolymerization with polar monomers, Organometallics 38 (2019) 1118–1126.
[108] K.W. Doak, In Encyclopaedia of Polymer Science and Engineering, 2nd ed.; H.F. Mark, N.M. Bikales, C.G. Overberger, G. Menges, Eds.; Wiley: New York, (1986) Vol. 6, pp 386-429.
[109] W. Daniels, in: Encyclopaedia of Polymer Science and Engineering, 2nd ed.; H.F. Mark, N.M. Bikales, C.G. Overberger, G. Menges, Eds.; Wiley: New York, (1989) Vol. 17, pp 393-455.
[110] K.S. Whiteley, T.G. Heggs, K. Koch, R.L. Mawer, W. Immel, Ullmann's Encyclopedia of Industrial Chemistry Vol. 28 (2003) 393–495.
[111] H. Rinno, Ullmann's Encyclopedia of Industrial Chemistry Vol. 29 (2003) 49–59.
[112] C. Schneider, R. Langer, D. Loveday, D. Hair, Applications of ethylene vinyl acetate copolymers (EVA) in drug delivery systems, J. Control. Release 262 (2017) 284–295.
[113] F. Yang, Y. Zhao, J. Sjoblom, C. Li, K.G. Paso, Polymeric Wax Inhibitors and Pour Point Depressants for Waxy Crude Oils: A Critical Review, J. Disper. Sci. Technol. 36 (2015) 213–225.
[114] U. Klabunde, S.D. Itten, Nickel catalysis for ethylene homo- and co-polymerization, J. Mol. Catal. 41 (1987) 123–134.
[115] H.W. Boone, P.S. Athey, M.J. Mullins, D. Philipp, R. Muller, W.A. Goddard, Copolymerization studies of vinyl chloride and vinyl acetate with ethylene using a transition metal catalyst, J. Am. Chem. Soc. 124 (2002) 8790–8791.
[116] E.F. Conner, T.R. Younkin, J.I. Henderson, S. Hwang, R.H. Grubbs, W.P. Roberts, J.I. Litzau, Linear functionalized polyethylene prepared with highly active neutral Ni(II) complexes, J. Polym. Sci. Part A: Polym. Chem. 40 (2002) 2842–2854.
[117] B.S. Williams, M.D. Leatherman, P.S. White, M. Brookhart, Reactions of vinyl acetate and vinyl trifluoroacetate with cationic diimine Pd(II) and Ni(II) alkyl complexes: identification of problems connected with copolymerizations of these monomers with ethylene, J. Am. Chem. Soc. 127 (2005) 5132–5146.
[118] S. Ito, K. Munakata, A. Nakamura, K. Nozaki, Copolymerization of vinyl acetate with ethylene by palladium/alkylphosphine-sulfonate catalysts, J. Am. Chem. Soc. 131 (2009) 14606–14607.
[119] J. Xia, Y. Zhang, X. Hu, X. Ma, L. Cui, J. Zhang, Z. Jian, Sterically very bulky aliphatic/aromatic phosphine-sulfonate palladium catalysts for ethylene polymerization and copolymerization with polar monomers, Polym. Chem. 10 (2019) 546–554.
[120] G. Zhou, H. Mu, Z. Jian, A comprehensive picture on catalyst structure construction in palladium catalyzed ethylene (co) polymerizations, J. Catal. 383 (2020) 215–220.
[121] A. Matsumoto, Polymerization of multiallyl monomers, Prog. Polym. Sci. 26 (2001) 189–257.
[122] S. Ito, M. Kanazawa, K. Munakata, J.I. Kuroda, Y. Okumura, K. Nozaki, Coordination-insertion copolymerization of allyl monomers with ethylene, J. Am. Chem. Soc. 133 (2011) 1232–1235.
[123] S. Ito, Y. Ota, K. Nozaki, Ethylene/allyl monomer cooligomerization by nickel/phosphine-sulfonate catalysts, Dalton Trans. 41 (2012) 13807–13809.

[124] S. Dai, C. Chen, Direct synthesis of functionalized high-molecular-weight polyethylene by copolymerization of ethylene with polar monomers, Angew. Chem. Int. Ed. 55 (2016) 13281–13285.
[125] X. Fu, L. Zhang, R. Tanaka, T. Shiono, Z. Cai, Highly robust nickel catalysts containing anilinonaphthoquinone ligand for copolymerization of ethylene and polar monomers, Macromolecules 50 (2017) 9216–9221.
[126] D.M. Kulich, J.E. Pace, L.W. Fritch Jr., A. Brisimitzakis. In Kirk-Othmer Encyclopaedia of Chemical Technology, 4th Ed.; J.I. Kroschwitz, M. Howe-Grant, Eds.; Wiley: New York, 1991; Vol. 1, p. 370.
[127] F.M. Peng. In Encyclopaedia of Polymer Science and Engineering, 2nd Ed.; H.F. Mark, N.M. Bikales, C.G. Overberger, G. Menges, Eds.; Wiley: New York, 1985; Vol.1, p. 426.
[128] J.C. Randall, C..J. Ruff, M. Kelchtermans, B.H. Gregory, Carbon-13 NMR characterization of ethylene-acrylonitrile copolymers prepared by high-pressure free-radical polymerizations, Macromolecules 25 (1992) 2624–2633.
[129] F. Wu, S.R. Foley, C.T. Burns, R.F. Jordan, Acrylonitrile Insertion Reactions of Cationic Palladium Alkyl Complexes, J. Am. Chem. Soc. 127 (2005) 1841–1853.
[130] L.S. Boffa, B.M. Novak, Copolymerization of Polar Monomers with Olefins Using Transition-Metal Complexes, Chem. Rev. 100 (2000) 1479–1493.
[131] G. Stojcevic, E.M. Prokopchuk, M.C. Baird, Coordination insertion reactions of acrylonitrile into Pd–H and Pd–methyl bonds in a diimine-palladium (II) system, J. Organomet. Chem. 690 (2005) 4349–4355.
[132] F. Wu, R.F. Jordan, Acrylonitrile insertion reactions of palladium alkyl complexes that contain neutral or anionic bidentate phosphine ligands, Organometallics 25 (2006) 5631–5637.
[133] L.F. Groux, T. Weiss, D.N. Reddy, P. . Chase, W.E. Piers, T. Ziegler, M. Parvez, J. Benet-Buchholz, Insertion of acrylonitrile into palladium methyl bonds in neutral and anionic Pd (II) complexes, J. Am. Chem. Soc. 127 (2005) 1854–1869.
[134] T. Kochi, S. Noda, K. Yoshimura, K. Nozaki, Formation of linear copolymers of ethylene and acrylonitrile catalyzed by phosphine sulfonate palladium complexes, J. Am. Chem. Soc. 129 (2007) 8948–8949.
[135] Y. Ota, S. Ito, M. Kobayashi, S. Kitade, K. Sakata, T. Tayano, K. Nozaki, Crystalline Isotactic Polar Polypropylene from the Palladium-Catalyzed Copolymerization of Propylene and Polar Monomers, Angew. Chem. Int. Ed. 55 (2016) 7505–7509.
[136] R.B. Login, Vinyl Ether Monomers and Polymers, Kirk-Othmer Encyclopedia of Chemical Technology (2000).
[137] W.G.S. Reyntjens, E.J. Goethals, New materials from poly(vinyl ethers), Polym. Adv. Technol. 12 (2001) 107–122.
[138] A.J. Teator, F.A. Leibfarth, Catalyst-controlled stereoselective cationic polymerization of vinyl ethers, Science 363 (2019) 1439–1443.
[139] J.C. Foster, R.K. O'Reilly, How to better control polymer chemistry, Science 363 (2019) 1394.
[140] H. Schenck, S. Strömberg, K. Zetterberg, M. Ludwig, B. Åkermark, M. Svensson, Insertion Aptitudes and Insertion Regiochemistry of Various Alkenes Coordinated to Cationic (σ-R)(diimine) palladium (II)(R=$-CH_3$,$-C_6H_5$), A Theoretical Study, Organometallics 20 (2001) 2813–2819.
[141] S.A. Strazisar, P.T. Wolczanski, Insertion of H_2C=CHX (X= F, Cl, Br, OiPr) into (tBu_3SiO) $3TaH_2$ and β-X-Elimination from (tBu_3SiO)$_3HTaCH_2CH_2X$ (X= OR): Relevance to Ziegler– Natta Copolymerizations, J. Am. Chem. Soc. 123 (2001) 4728–4740.
[142] S. Luo, R.F. Jordan, Copolymerization of silyl vinyl ethers with olefins by (α-diimine) PdR^+, J. Am. Chem. Soc. 128 (2006) 12072–12073.
[143] C. Chen, S. Luo, R.F. Jordan, Cationic polymerization and insertion chemistry in the reactions of vinyl ethers with (α-diimine) $PdMe^+$ species, J. Am. Chem. Soc. 132 (2010) 5273–5284.
[144] C. Chen, R.F. Jordan, Palladium Catalyzed Dimerization of Vinyl Ethers to Acetals, J. Am. Chem. Soc. 132 (2010) 10254–10255.
[145] Along the same lines, cross-coupling between vinyl ether and α-olefin is also reported, see: WH. Chen, Y. Li, Y. Chen, C.-Y. Ho, (NHC)NiH-Catalyzed Regiodivergent Cross-Hydroalkenylation of Vinyl Ethers with α-Olefins: Syntheses of 1,2- and 1,3- Disubstituted Allyl Ethers, Angew. Chem., Int. Ed. 57 (2018) 2677-2681.
[146] C. Hong, X. Wang, C. Chen, Palladium-catalyzed dimerization of vinyl ethers: mechanism, catalyst optimization, and polymerization applications, Macromolecules 52 (2019) 7123–7129.
[147] S. Luo, J. Vela, G.R. Lief, R.F. Jordan, Copolymerization of Ethylene and Alkyl Vinyl Ethers by a (Phosphinesulfonate) PdMe Catalyst, J. Am. Chem. Soc. 129 (2007) 8946–8947.
[148] Z. Jian, S. Mecking, Insertion polymerization of divinyl formal, Macromolecules 49 (2016) 4395–4403.
[149] Z. Jian, S. Mecking, Insertion Homo- and Co-polymerization of Diallyl Ether, Angew. Chem. Int. Ed. 54 (2015) 15845–15849.
[150] F.P. Wimmer, L. Caporaso, L. Cavallo, S. Mecking, L. Falivene, Mechanism of insertion polymerization of allyl ethers, Macromolecules 51 (2018) 4525–4531.
[151] The industrial significance of acid containing polymers is described in Ullmann's Encyclopedia of Industrial Chemistry; for details see reference 110 and 111.
[152] T.W. Baughman, C.D. Chan, K.I. Winey, K.B. Wagener, Synthesis and Morphology of Well-Defined Poly (ethylene-co-acrylic acid) Copolymers, Macromolecules 40 (2007) 6564–6571.
[153] T. Rünzi, D. Fröhlich, S. Mecking, Direct synthesis of ethylene−acrylic acid copolymers by Insertion polymerization, J. Am. Chem. Soc. 132 (2010) 17690–17691.
[154] L. Guo, Y. Liu, W. Sun, Q. Du, Y. Yang, W. Kong, D. Chen, Synthesis, characterization, and olefin (co)polymerization behavior of unsymmetrical α-diimine palladium complexes containing bulky substituents at 4-position of aniline moieties, J. Organomet. Chem. 877 (2018) 12–20.
[155] Q. Muhammad, C. Tan, C. Chen, Concerted steric and electronic effects on α-diimine nickel- and palladium-catalyzed ethylene polymerization and copolymerization, Science Bulletin 65 (2020) 300–307.
[156] S. Dai, C. Chen, Palladium-catalyzed direct synthesis of various branched, carboxylic acid-functionalized polyolefins: characterization, derivatization, and properties, Macromolecules 51 (2018) 6818–6824.
[157] Y. Gong, S. Li, C. Tan, W. Kong, G. Xu, S. Zhang, S. Dai, π–π interaction effect in insertion polymerization with α-Diimine palladium systems, Journal of Catalysis 378 (2019) 184–191.
[158] Y. Kanai, S. Foro, H. Plenio, Bispentiptycenyl–Diimine–Nickel Complexes for Ethene Polymerization and Copolymerization with Polar Monomers, Organometallics 38 (2019) 544–551.
[159] C. Zou, C. Chen, Polar-Functionalized, Crosslinkable, Self-Healing, and Photoresponsive Polyolefins, Angew. Chem. Int. Ed. 59 (2020) 395–402.
[160] A.P. Kharitonov, R. Taege, G. Ferrier, V.V. Teplyakov, D.A. Syrtsova, G.-H. Koops, Direct fluorination-useful tool to enhance commercial properties of polymer articles, J. Fluorine Chem. 126 (2005) 251–263.
[161] D.L. Beach, Y.V. Kissin, in: Encyclopedia of Polymer Science and Engineering, 2nd ed.; H.F. Mark, N.M. Bikales, C.G. Overberger, G. Menges, Eds.; Wiley: New York, 1986; Vol. 6, pp. 383.
[162] E. Boz, K.B. Wagener, Progress in the Development of Well-Defined Ethylene-Vinyl Halide Polymers, Polym. Rev. 47 (2007) 511–541.
[163] Insertion copolymerization of vinyl halides with ethylene has been reviewed, see reference 7 for details.
[164] X.L. He, Q. Zhou, X.Y. Li, P. Yang, J.M.N. van Kasteren, Y.Z. Wang, Dechlorination of poly(vinyl chloride) by 1-butyl-3-methylimidazoliumhydroxide, Polym. Degrad. Stabil. 97 (2012), 145–148 and the references therein.
[165] G.P. Belov, T.I. Solovyova, V.I. Smirnov, Copolymerization of ethylene and vinyl chloride in the presence of Ziegler-Natta catalysts, Acta Polymerica 41 (1990) 178–185.
[166] R.D. Burkhart, N.L. Zutty, Copolymerization studies. III. Reactivity ratios of model ethylene copolymerizations and their use in Q–e calculations, J. Polym. Sci., Part A 1 (1963) 1137–1145.
[167] H. Shen, R.F. Jordan, Molecular Structure and Vinyl Chloride Insertion of a Cationic Zirconium(IV) Acyl Carbonyl Complex, Organometallics 22 (2003) 2080–2086.
[168] SR. Foley, R.A. Jr, Stockland, H. Shen, R.F. Jordan, Reaction of vinyl chloride with late transition metal olefin polymerization catalysts, J. Am. Chem. Soc. 125 (2003) 4350–4361.
[169] H. Shen, R.F. Jordan, Reaction of vinyl chloride with cationic palladium acyl complexes, Organometallics 22 (2003) 1878–1887.
[170] H. Leicht, I. Goettker-Schnetmann, S. Mecking, Incorporation of vinyl chloride in insertion polymerization, Angew. Chem. Int. Ed. 52 (2013) 3963–3966.
[171] D. Sianesi, G.J. Caporiccio, Polymerization and copolymerization studies on vinyl fluoride, J. Polym. Sci., Part A-1 6 (1968) 335–352.
[172] W. Weng, Z. Shen, R.F. Jordan, Copolymerization of ethylene and vinyl fluoride by (phosphine-sulfonate) Pd (Me)(py) catalysts, J. Am. Chem. Soc. 129 (2007) 15450–15451.
[173] Z. Shen, R.F. Jordan, Copolymerization of ethylene and vinyl fluoride by (phosphine-bis (arenesulfonate)) PdMe (pyridine) catalysts: Insights into inhibition mechanisms, Macromolecules 43 (2010) 8706–8708.
[174] S. Wada, R.F. Jordan, Olefin Insertion into a Pd–F Bond: Catalyst Reactivation Following β-F Elimination in Ethylene/Vinyl Fluoride Copolymerization, Angew. Chem., Int. Ed. 56 (2017) 1820–1824.
[175] R.E. Black, S.M. Kilyanek, E.D. Reinhart, R.F. Jordan, Olefin Insertion Reactivity of a (Phosphine-arenesulfonate) Palladium (II) Fluoride Complex, Organometallics 38 (2019) 4250–4260.
[176] D. Lanzinger, M.M. Giuman, T.M.J. Anselment, B. Rieger, Copolymerization of Ethylene and 3,3,3-Trifluoropropene Using (Phosphine-sulfonate)Pd(Me)(DMSO) as Catalyst, ACS Macro Lett. 3 (2014) 931–934.
[177] M. Stickler, T. Rhein, Ullmann's Encyclopedia of Industrial Chemistry Vol. 28 (2003) 377.
[178] K. Hatada, T. Kitayama, K. Ute, Stereoregular polymerization of α-substituted acrylates, Prog. Polym. Sci. 13 (1988) 189–276.
[179] K. Matyjaszewski, Inner sphere and outer sphere electron transfer reactions in atom transfer radical polymerization, Macromol. Symp. 134 (1998) 105–118.
[180] S. Borkar, H. Yennawar, A. Sen, Methacrylate Insertion into Cationic Diimine Palladium (II)– Alkyl Complexes and the Synthesis of Poly (alkene-block-alkene/carbon monoxide) Copolymers, Organometallics 26 (2007) 4711–4714.
[181] I. Matos, S.N. Fernandes, H.R. Liu, A.K. Tevtia, R.P. Singh, M.A.N.D.A. Lemos, MM. Marques, Copolymerization of ethylene with unsaturated alcohols and methylmethacrylate using a silylated α-diimine nickel catalyst: Molecular modeling and photodegradation studies, J. Appl. Poly. Sci. 129 (2013) 1820–1832.
[182] V.C. Gibson, A. Tomov, Functionalised polyolefin synthesis using [P, O] Ni catalysts, Chem. Commun. 19 (2001) 1964–1965.
[183] X.F. Li, Y.G. Li, Y.S. Li, Y.X. Chen, N.H. Hu, Copolymerization of ethylene with methyl methacrylate with neutral nickel (II) complexes bearing β-ketoiminato chelate ligands, Organometallics 24 (2005) 2502–2510.
[184] X. He, Q. Wu, Polymerization of methyl methacrylate using bis (β-ketoamino) nickel (II)–MAO catalytic systems, Appl. Organomet. Chem. 20 (2006) 264–271.
[185] A. Leblanc, E. Grau, J.-P. Broyer, C. Boisson, R. Spitz, V. Monteil, Homo-and copolymerizations of (meth) acrylates with olefins (styrene, ethylene) using neutral nickel complexes: a dual radical/catalytic pathway, Macromolecules 44 (2011) 3293–3301.

[186] A. Leblanc, J.-P. Broyer, C. Boisson, R. Spitz, V. Monteil, Synthesis of copolymers of ethylene and (meth) acrylates or styrene by an original dual radical/catalytic mechanism, Pure Appl. Chem. 84 (2012) 2113–2120.
[187] F. Ölscher, I. Göttker-Schnetmann, V. Monteil, S. Mecking, Role of Radical Species in Salicylaldiminato Ni (II) Mediated Polymer Chain Growth: A Case Study for the Migratory Insertion Polymerization of Ethylene in the Presence of Methyl Methacrylate, J. Am. Chem. Soc. 137 (2015) 14819–14828.
[188] T. Rünzi, D. Guironnet, I. Göttker-Schnetmann, S. Mecking, Reactivity of methacrylates in insertion polymerization, J. Am. Chem. Soc. 132 (2010) 16623–16630.
[189] H. Yasuda, R. Nakano, S. Ito, K. Nozaki, Palladium/IzQO-catalyzed coordination–insertion copolymerization of ethylene and 1, 1-disubstituted ethylenes bearing a polar functional group, J. Am. Chem. Soc. 140 (2018) 1876–1883.
[190] HW. Coover Jr., In Handbook of adhesives; Skeist, J., Eds.; Reinhold Publishing Corporation Chapman and Hall Ltd.: London, 1962; pp. 409−414.
[191] G.T. Schueneman, S. Attarwala, K.R. Brantl, Cyanoacrylate compositions incorporating organic micropulp, U. S. Patent 8,287,687, Oct. 16, 2012.
[192] S.R. Gaikwad, S.S. Deshmukh, R.G. Gonnade, P.R. Rajamohan, S.H. Chikkali, Insertion copolymerization of difunctional polar vinyl monomers with ethylene, ACS Macro Lett. 4 (2015) 933–937.
[193] S.R. Gaikwad, S.S. Deshmukh, V.S. Koshti, S. Poddar, R.G. Gonnade, P. R. Rajamohanan, S.H. Chikkali, Reactivity of difunctional polar monomers and ethylene copolymerization: A comprehensive account, Macromolecules 50 (2017) 5748–5758.
[194] S.R. Gaikwad, K. Patel, S.S. Deshmukh, N.R. Mote, R.S. Birajdar, S.P. Pandole, J. Chugh, S.H. Chikkali, Palladium-catalyzed insertion of ethylene and 1,1-disubstituted difunctional olefins: An experimental and computational study, ChemPlusChem 85 (2020) 1200–1209.
[195] M. Chen, C. Chen, Direct and Tandem Routes for the Copolymerization of Ethylene with Polar Functionalized Internal Olefins, Angew. Chem. Int. Ed. 59 (2020) 1206–1210.
[196] L.R. Parisi, D.M. Scheibel, S. Lin, E.M. Bennett, J.M. Lodge, M.J. Miri, Eugenol as renewable comonomer compared to 4-penten-1-ol in ethylene copolymerization using a palladium aryl sulfonate catalyst, Polymer 114 (2017) 319–328.
[197] X. Hu, X. Ma, Z. Jian, Coordination-insertion polymerization of polar allylbenzene monomers, Polym. Chem. 10 (2019) 1912–1919.
[198] Y. Na, C. Chen, Catechol Functionalized Polyolefins, Angew. Chem. Int. Ed. 59 (2020) 7953–7959.
[199] H. Takeshima, K. Satoh, M. Kamigaito, Scalable synthesis of bio-based functional styrene: protected vinyl catechol from caffeic acid and controlled radical and anionic polymerizations thereof, ACS Sustainable Chem. Eng. 6 (2018) 13681–13686.
[200] B.S. Rajput, S.B. Pawal, D.V. Bodkhe, N. Rao, A.V. Sesha Sainath, S.H. Chikkali, Renewing polyethylene: Insertion copolymerization of sugar derived hydrophilic monomers with ethylene, Eur. Poly. J. 134 (2020) 109775/1–6.

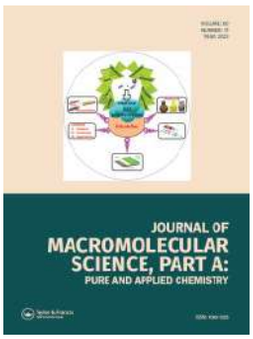

Journal of Macromolecular Science, Part A
Pure and Applied Chemistry

ISSN: (Print) (Online) Journal homepage: www.tandfonline.com/journals/lmsa20

Emerging trends in olefin polymerization: a perspective

Rajkumar S. Birajdar, Dnyaneshwar Bodkhe, Poonam Gupta, Maulali H. Shaikh, Rohan Ramekar & Samir H. Chikkali

To cite this article: Rajkumar S. Birajdar, Dnyaneshwar Bodkhe, Poonam Gupta, Maulali H. Shaikh, Rohan Ramekar & Samir H. Chikkali (2023) Emerging trends in olefin polymerization: a perspective, Journal of Macromolecular Science, Part A, 60:11, 731-750, DOI: 10.1080/10601325.2023.2269971

To link to this article: https://doi.org/10.1080/10601325.2023.2269971

Published online: 22 Oct 2023.

Submit your article to this journal

Article views: 605

View related articles

View Crossmark data

Full Terms & Conditions of access and use can be found at
https://www.tandfonline.com/action/journalInformation?journalCode=lmsa20

JOURNAL OF MACROMOLECULAR SCIENCE, PART A: PURE AND APPLIED CHEMISTRY
2023, VOL. 60, NO. 11, 731–750
https://doi.org/10.1080/10601325.2023.2269971

Taylor & Francis
Taylor & Francis Group

Check for updates

Emerging trends in olefin polymerization: a perspective

Rajkumar S. Birajdar[a,b], Dnyaneshwar Bodkhe[a,b], Poonam Gupta[a,b], Maulali H. Shaikh[a], Rohan Ramekar[a], and Samir H. Chikkali[a,b]

[a]Polymer Science and Engineering Division, CSIR-National Chemical Laboratory, Pune, MH, India; [b]Academy of Scientific and Innovative Research (AcSIR), Ghaziabad, U.P., India

ABSTRACT

The seemingly matured field of olefin polymerization still poses several challenges and holds enormous potential to meet contemporary material requirements. In this feature article, we examine the progress of olefin polymerization in the last two decades. Among the several emerging trends, we identify four most impactful discoveries, namely, (i) disentangled ultra-high molecular weight polyethylene (dUHMWPE), (ii) disubstituted functional olefin copolymerization, (iii) incorporation of bioderived comonomers in polyolefins, and (iv) application of above (ii, iii) functional polyolefins as compatibilizers. The dUHMWPE has attracted significant attention and heterogeneous Ziegler-type catalysts, homogenous metallocene, and post-metallocene catalysts have been reported to produce disentangled ultrahigh molecular weight polyethylene. Insertion copolymerization of difunctional disubstituted olefins has been reported only recently and ortho-phosphinobenzene sulfonate palladium catalyst outperforms the other catalysts. Interestingly, insertion copolymerization of bioderived olefins has witnessed a surge in the number of reports. Sugar and plant oil-derived olefins have been copolymerized with ethylene to obtain relatively hydrophilic polyethylene. The functional polyethylene is finding a new application as compatibilizer or displays better adhesion to surfaces. Thus, the feature article offers a succinct account of emerging trends in polyolefins, identifies the most impactful contributions, and debates the application potential of these new materials.

GRAPHICAL ABSTRACT

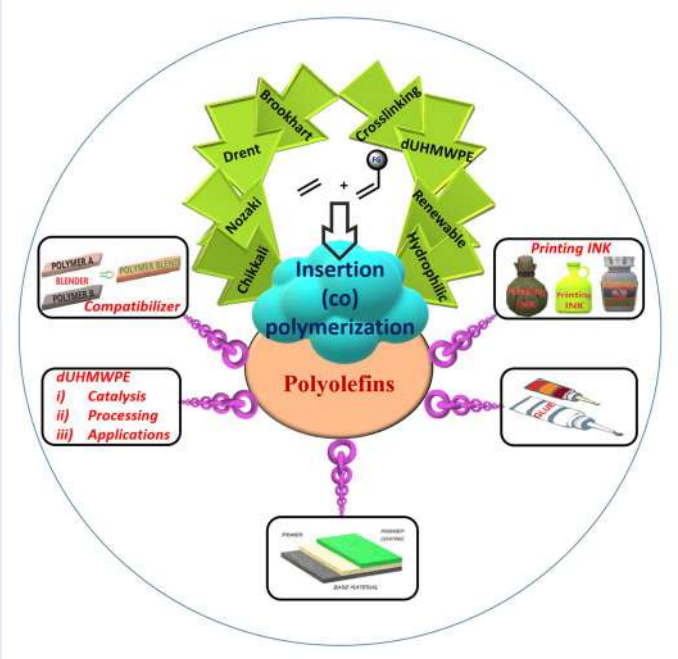

ARTICLE HISTORY
Received September 2023
Accepted September 2023

KEYWORDS
Insertion (co)polymerization; uHMWPE; functional polyethylene; renewable monomers; compatibilizer

CONTACT Samir H. Chikkali s.chikkali@ncl.res.in Polymer Science and Engineering Division, CSIR-National Chemical Laboratory, Dr. Homi Bhabha Road, Pune, 411008, MH, India.

This article has been corrected with minor changes. These changes do not impact the academic content of the article.

© 2023 Taylor & Francis Group, LLC

1. Introduction

1.1. Early years in olefin polymerization

Olefin polymerization is known for several decades.[1] Among various polymers, polyethylene (PE) and polypropylene (PP) are two of the most widely used polymers in the world.[2] These versatile materials have revolutionized various industries, including packaging, automotive, construction, and textiles. Polyethylene and polypropylene offer exceptional properties and therefore are widely used.[3] These polymers possess a unique combination of strength, flexibility, chemical resistance, and thermal stability, making them ideal for a wide range of applications. Their low cost, lightweight, and ease of processing further contribute to their popularity. Polyethylene is widely used for packaging materials, including plastic bags, films, and bottles. It is also employed in the manufacturing of pipes, wire insulation, and automotive components. Polypropylene, on the other hand, finds applications in food packaging, textiles, medical devices, and automotive parts. The demand for these polymers continues to grow as industries seek lightweight, durable, and sustainable materials. The global production of polyolefins is close to 200 million tons per annum and it is bound to increase in the near future.

Moving back in time, we may follow the history of the synthesis of polyethylene and polypropylene, which has an intriguing tale before we take stock of the most recent advancements in olefin polymerization. Around the end of the nineteenth century, for the first time, traces of polyethylene were observed during a thermal decomposition reaction of diazomethane, which was named "polymethylene."[1] During that period, the field of polymer science was underdeveloped and was not accepted by the community. German chemist Hermann Staudinger proposed that polymers consist of long chains, connected through covalent bonds.[1] This theory was initially met with skepticism, but it was eventually widely accepted and laid the foundation of rational polymer science. In 1933, Fawcett and Gibson at the Imperial Chemical Industry (ICI) found a white powdery material on the reactor wall while performing a high-pressure condensation reaction of ethylene and benzaldehyde (Figure 1, top).[1] When they were repeating the experiment without benzaldehyde, the reactor exploded and the project was halted. It took a couple of years to understand this and develop radical polymerization of ethylene to polyethylene.[1] The ICI process operates at high pressure (1000–4000 bars) and high temperature (200–300 °C).[1] After this discovery, several academic groups initiated research programs on ethylene polymerization to make polyethylene.

The major breakthroughs were reported in the early 1950s. The first one was by Hogan and Banks at the Phillips Petroleum Company who reported low molecular weight oligomer from gaseous olefin using nickel oxide supported on silica or alumina.[1] In 1951, while studying the effect of nickel oxide and chromium oxide supported on silica or alumina they found solid HDPE in their reactor.[1] In the 1950s, Ziegler, at the Max Planck Institute in Mülheim, Germany, made a significant breakthrough in ethylene polymerization. Before embarking on the journey of polyethylene, he was investigating the reactivity of alkyl lithium/alkyl aluminum compounds with ethylene.[1] These organometallic reagents formed the foundation for his development of the "Aufbaureaktion," a process enabling the synthesis of 1-olefins, aliphatic alcohols (known as alfol synthesis), and high-purity alumina through the oxidation of alkyl aluminum compounds. By a stroke of luck, Ziegler discovered that the presence of nickel had a profound effect on the "Aufbaureaktion" by favoring chain termination, leading to the formation of 1-butene. This unexpected phenomenon, known as "the nickel effect," was attributed to the presence of nickel in the autoclave resulting from previous hydrogenation reactions. This discovery marked the beginning of significant metal screening conducted by Ziegler's students to investigate the behavior of different metal precursors when associated with alkyl aluminum compounds.[1] In 1953, Ziegler's team evaluated the combination of triethyl aluminum with various transition metal compounds, including chromium, vanadium, manganese, and platinum. The most notable result was achieved by combining zirconium acetylacetonate with triethyl aluminum, resulting in a conversion rate of over 90% for the introduced ethylene. The patent application claimed "a process for the production of a high molar mass polyethylene" which involved the association of triethyl aluminum with complexes containing metals from group 4 (Ti, Zr, Hf), 5 (V, Nb, Ta), and 6 (Cr, Mo).[1] This process operates at lower temperatures and with ethylene pressure below 55 bars and is widely known as the "Mülheim Atmospheric Process."[1] In March 1954, Natta, an Italian chemist, successfully achieved the stereospecific polymerization of propylene using a Ziegler catalyst composed of titanium trichloride and triethyl aluminum.[1] For this groundbreaking discovery, Ziegler and Natta were bestowed with the Nobel Prize in 1963. Subsequent to this discovery, several developments, such as metallocene, MAO, post-metallocenes, etc. have been reported.[4,5]

1.2. State-of-the-art and scope

The preparation of polyethylene and polypropylene involves a complex and fascinating journey, starting from the discovery of the raw materials to the development of an efficient manufacturing process. In the ever-evolving landscape of polymer science, researchers are continuously pushing the boundaries of material engineering to develop innovative solutions with enhanced properties and sustainability in mind. Among the several frontiers in polyolefins, the most impactful discoveries in the last two decades have been in the realm of (i) ultra-high molecular weight polyethylene (UHMWPE),[6] (ii) incorporation of bioderived comonomers in polyolefins, (iii) functional olefin copolymerization, and (iv) application of some of i–iii as compatibilizers.[7,8] A polyethylene with a viscosity average molecular weight of 2.5 million g/mol is considered as UHMWPE (ultra-high molecular weight polyethylene).[9] UHMWPE is known for its exceptional mechanical properties, chemical resistance,

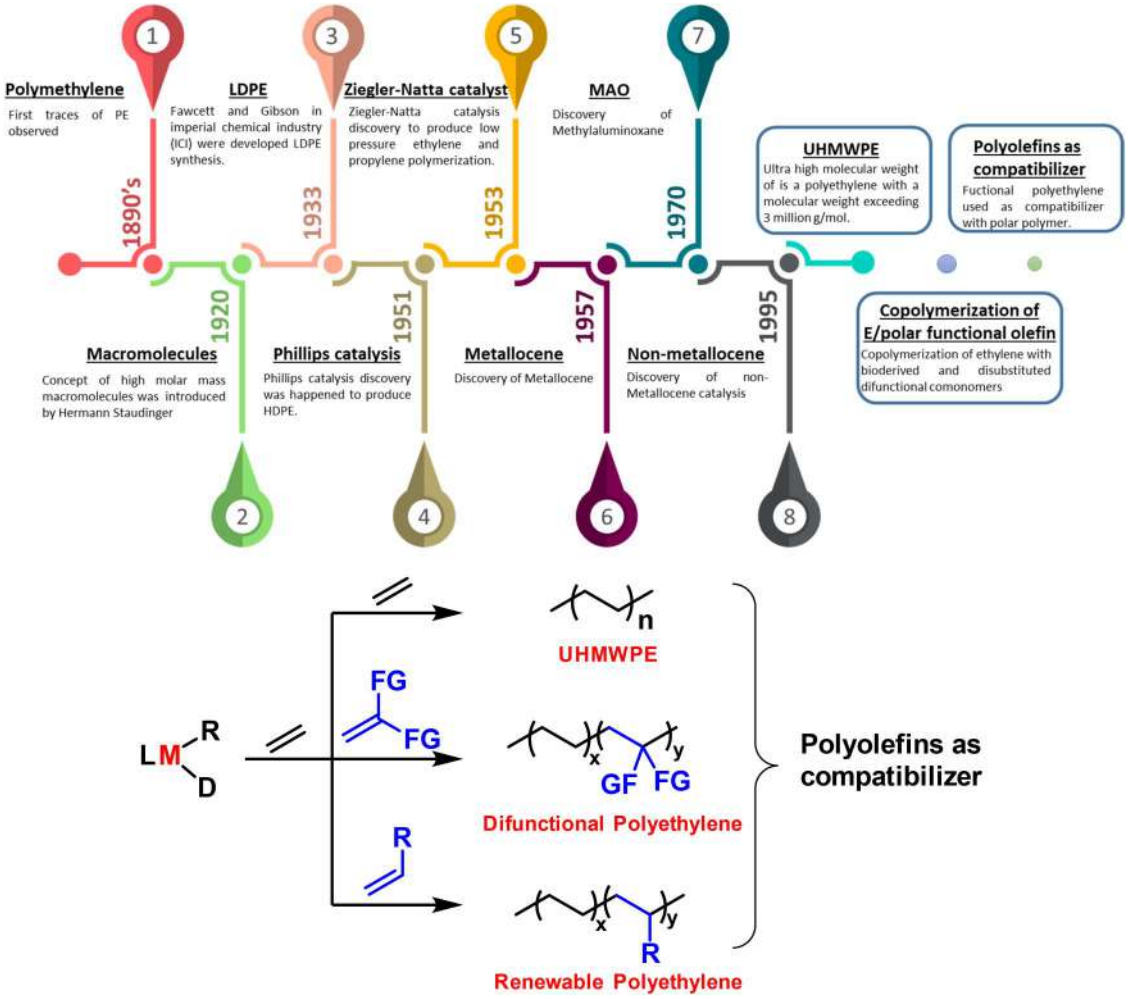

Figure 1. Significant advancements in the development of polyolefins (top) and emerging polyolefins (bottom).

and low coefficient of friction. This material has established itself as a key player in various industries, including automotive, medical, bulletproof vests, industrial parts, and sports equipment.[6,10,11] Ziegler catalyst can be suitably modified to produce UHMWPE. Synthesis and processing present significant challenges due to its unique characteristics and requirements.

Polyethylene or UHMWPE is made up of ethylene repeating units, which are hydrophobic in nature. It does not contain any functional group in its backbone. The lack of functional groups leads to certain limitations in the application of polyethylene. For example, polyethylene cannot be used in printing inks, adhesives, binders, paints, dyeing, flame retardancy, barrier, etc.[12] Incorporating a small amount of functional groups in the polymer backbone can open up a new application window for polyethylene.[13–15] One promising approach involves the insertion copolymerization of bioderived and substituted difunctional comonomers with ethylene.[7] However, the insertion copolymerization of ethylene and functional olefin remains a highly challenging area of research even today. The metal catalysts are readily poisoned in the presence of polar functional groups and form a stable σ-complex or chelate, or there is no incorporation of functional comonomer into the polyethylene backbone. Considering these challenges, late transition metal complexes-based catalysts have been developed for functional olefin copolymerization.[5] Comonomers derived from renewable resources, such as plant-based feedstocks, present an eco-friendly alternative to traditional petrochemical-based comonomers. Their incorporation into polyethylene not only imparts improved properties but also enables the development of relatively sustainable polyolefins with a reduced environmental footprint.

Two functional groups per insertion can be built into the polyethylene backbone by copolymerization of disubstituted polar olefins with ethylene. These polar olefins, characterized by their distinct dipolar and functional groups, introduce additional functionalities and tune the copolymer's chemical, thermal, and mechanical attributes. This strategic incorporation can fine-tune polyethylene surface energy, adhesion, and overall performance, expanding its applications into previously unexplored domains. The introduction of a polar functional group will enhance the polar nature and hydrophilicity of the resultant polyethylene. The hydrophilic polyethylene opens up new opportunities to use this material with polar polymer (Nylon-6, PLA, etc.). These polymers can be used as additives to promote miscibility and blend uniformity between two different polyolefins. By judiciously selecting and optimizing compatibilizer formulations, researchers can

effectively overcome the immiscibility barrier and enhance the mechanical and thermal properties of the resulting copolymer materials.

In this feature article, we delve into the emerging areas of olefin polymerization. This feature article aims to identify successful strategies in olefin polymerization that allow access to polyolefins with significantly different properties than traditional polyolefins. To do so, we focus on four frontiers of olefin polymerization, (i) UHMWPE, (ii) disubstituted difunctional olefin copolymerization, (iii) renewable/bioderived functional olefin copolymerization, and (iv) functional PE as a compatibilizing material (Figure 1, bottom). The perspective debates these concepts that might drive further scientific explorations and presents an overview of exciting advancements in these chosen areas. The other areas in olefin polymerization, such as (mono)functional olefin copolymerization, olefin polymerization, etc. have been reviewed elsewhere and are beyond the scope of this feature article.[5–7,16–21]

2. UHMWPE (ultra-high molecular weight polyethylene)

As defined in ASTM D4020, a polyethylene with a viscosity average molecular weight of 2.5 million g/mol or higher is considered as ultrahigh molecular weight polyethylene (UHMWPE).[9] The synthesis of UHMWPE is highly challenging and the following 4 key aspects have to be addressed. (i) Designing appropriate metal catalysts and co-catalysts is crucial to achieve high molecular weights. (ii) Identifying suitable reaction conditions is essential to enhance the rate of propagation while minimizing the rate of chain transfer reactions. (iii) Manipulating the steric and electronic properties of the metal center is crucial in minimizing transfer and termination reactions. (iv) Moderating the Lewis acidity of the metal catalyst is important to reduce β-hydride elimination, which can lead to chain termination and the production of lower molecular weight polymers. Despite these difficulties, researchers have made significant progress in developing catalytic systems capable of producing UHMWPE. The two commercial grades of UHMWPE, Spectra, and Dyneema, are produced using Ziegler-type catalysts. However, the UHMWPE reactor powder cannot be processed using standard melt processing techniques and requires a special gel-spinning facility. To address this bottleneck, Rastogi et al. attempted to understand the processing challenge and introduced a new state of the same material and named it "disentangled" ultrahigh molecular weight polyethylene (dUHMWPE).[22]

There are three main classes of catalysts used for UHMWPE production: (i) heterogeneous Mg-Ti catalysts, (ii) homogeneous metallocene complexes, and (iii) homogenous/heterogeneous post-metallocene catalysts. The following section gets into details of each of the above three broad types of catalysts and covers the recent advances in the dUHMWPE synthesis.

2.1. Heterogeneous Mg-Ti catalysts

Heterogeneous Ziegler-type catalysts are known to produce entangled UHMWPE. It is believed that the multiple sites available in Ziegler-type catalysts are responsible for entanglement. In a recent advancement, Chikkali et al. attempted to prepare a single-site heterogeneous Ziegler-type catalyst and tested it in ethylene polymerization. The authors reported a one-pot two-step synthesis of a $MgCl_2$ supported $[Ti(OEt)_4]$ derived catalyst and controlled reduction of Ti center to +3 (Ti^{3+}) as a single oxidation state. This Ziegler-type, heterogeneous catalyst, with a two-stage activation strategy produced disentangled ultrahigh molecular weight polyethylene (Figure 2, top).[23] The catalyst demonstrated quasi-living behavior and allowed the synthesis of dUHMWPE with a molecular weight range of 1.0–13.0×10^6 g · mol^{-1} and a polydispersity index (PDI) of ~3. The catalyst disclosed moderate activity, and the polymer had a storage modulus of up to 1.82 MPa. The resultant dUHMWPE displayed the first melting temperature at 141.3–144.1 °C. The entangled *vs.* disentangled nature of UHMWPE was probed using two techniques, namely, DSC and rheology. Rastogi et al. have developed a DSC method that allows access to the two states of UHMWPE.[24] This method was employed and the melting temperature was recorded at a time interval of 5, 15, 30, and 60 min (Figure 2, center). As depicted in Figure 2 bottom, the 5-min DSC thermogram disclosed two melting temperatures, one at 134 and another at 139.5 °C. These two curves indicate the T_m of the entangled and the disentangled domain, respectively. As the hold time (Figure 2, center, step B–C) increases, the disentangled domain starts to convert to an entangled domain, which is a thermally stable state. In line with the DSC findings, the rheological measurements revealed that an equilibrium storage modulus of 1.82 MPa is attained after 37 h.

2.2. Homogeneous metallocene catalysts

In 2021, O'Hare et al. reported permethylindenyl-phenoxide (PHENI*) ligated ansa-metallocene complexes as catalysts in ethylene polymerization (Figure 3, top).[25] Catalyst **1** (Figure 3) was found to exhibit high activity and produced disentangled ultrahigh molecular weight polyethylene (dUHMWPE) with excellent strength and wear resistance. The PHENI* catalyst **1** was activated using polymethylaluminoxane. The thus activated catalyst **1** displayed an excellent activity of 3.7×10^6 g_{PE} $mol_{Ti}^{-1}h^{-1}bar^{-1}$ in ethylene polymerization and produced dUHMWPE (Mw: 3.4 million g/mol). Additionally, these PHENI* complexes are more active than indenyl-PHENICS analogs in the polymerization of ethylene. Overall, the use of PHENI* ansa-metallocene titanium complexes as catalysts has shown a great potential for producing high-quality dUHMWPE.

Cui et al. reported binuclear half-sandwich scandium complexes to polymerize ethylene under high temperatures and pressures, producing disentangled ultra-high molecular weight polyethylene (dUHMWPE) with excellent mechanical properties, including high tensile strength and modulus (Figure 3, bottom).[26] The **C1-Sc$_2$** complex was particularly effective in

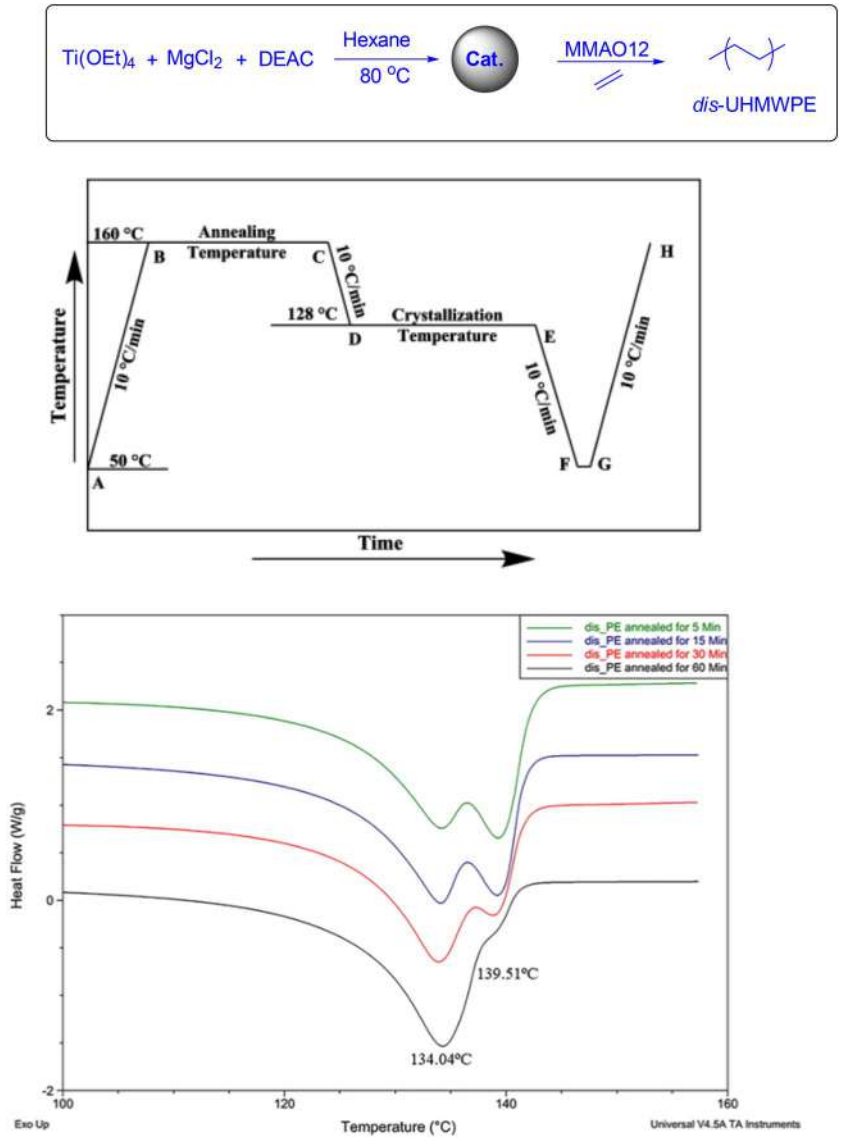

Figure 2. Synthesis of $MgCl_2$ supported $[Ti(OEt)_4]$ catalyst and its application in the preparation of UHMWPE (top), DSC method employed to study entangled *vs.* disentangled UHMWPE (center) and DSC plots of the dUHMWPE samples (bottom) (obtained during final G–H stage). Reproduced with permission from Gote et al.[23] Copyright 2018 American Chemical Society.

producing dUHMWPE. While the mononuclear $\mathbf{Sc_1}$ and the relatively flexible binuclear $\mathbf{C2\text{-}Sc_2}$ could not meet the performance of $\mathbf{C1\text{-}Sc_2}$. Based on the DFT inputs, the success of $\mathbf{C1\text{-}Sc_2}$ complex is believed to be due to the binuclear synergistic effect and agostic interaction between the active center and the growing polymer chain. Another contributing factor is the conformational ordering of the polymer chains due to the steric effect. The existence of dUHMWPE was proved using DSC and rheology, which displayed tensile strength and modulus of up to 149.2 MPa and 1.5 GPa, respectively. This study represents an important advancement in the production of dUHMWPE and has the potential to lead to new and improved materials for a variety of applications.

2.3. Homogenous/heterogeneous post-metallocenes catalysts

In 2001, Fujita et al. reported a substituted phenoxy-imine (which they named as "FI" catalyst) ligated titanium complex **3** (Figure 4).[27,28] The authors demonstrated that complex **3** catalyzes the living polymerization of ethylene upon activation with methyl aluminoxane (MAO). Although the catalyst displayed living behavior, high molecular weight, etc., the ability of the catalyst to produce dUHMWPE was overlooked. The potential of the FI system to produce dUHMWPE was recognized by Rastogi et al. almost a decade later.[24,29] The performance of FI catalyst **3** in ethylene polymerization was investigated in great detail and the resultant polymer was meticulously characterized. Optimized polymerization conditions allowed the authors to prepare UHMWPE and DSC, solid-state NMR and rheological measurements allowed the authors to demonstrate the disentangled nature of UHMWPE. This study is considered the early breakthrough in the field of disentangled ultrahigh molecular weight polyethylene and is a current "benchmark" for dUHMWPE. The tensile properties of dUHMWPE produced by catalyst **3**, were compared with those of entangled UHMWPE produced using a standard heterogeneous Ziegler

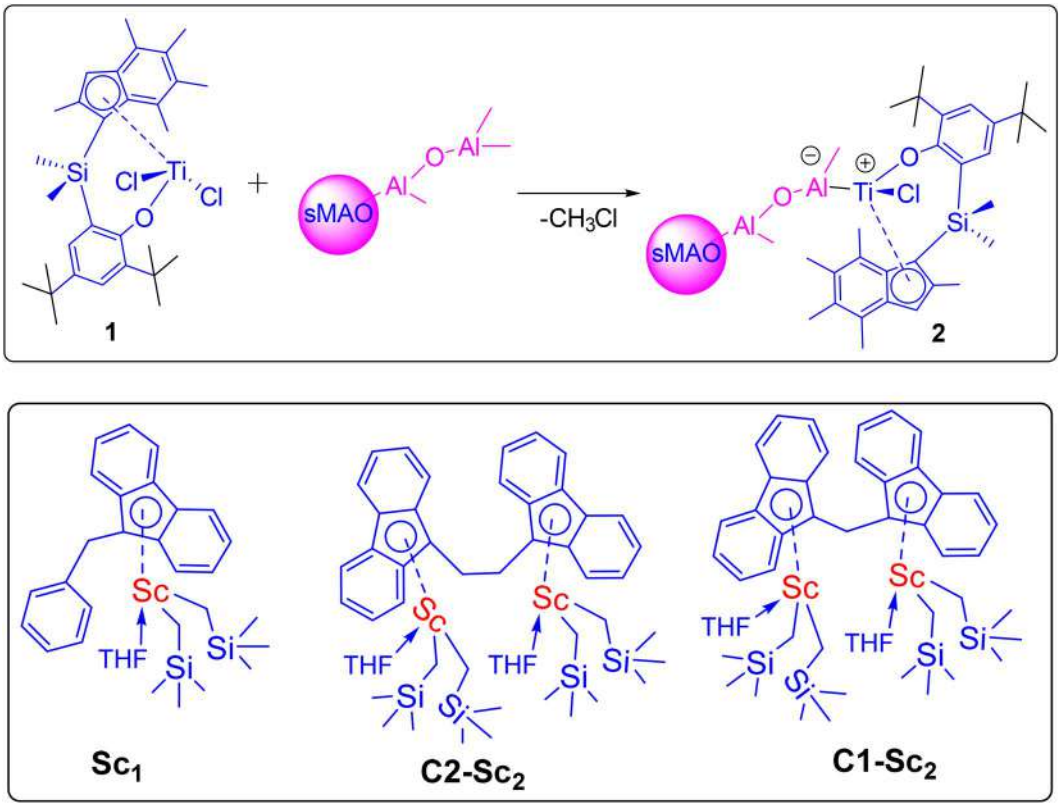

Figure 3. Permethylindenyl-phenoxide and binuclear scandium complexes for UHMWPE.

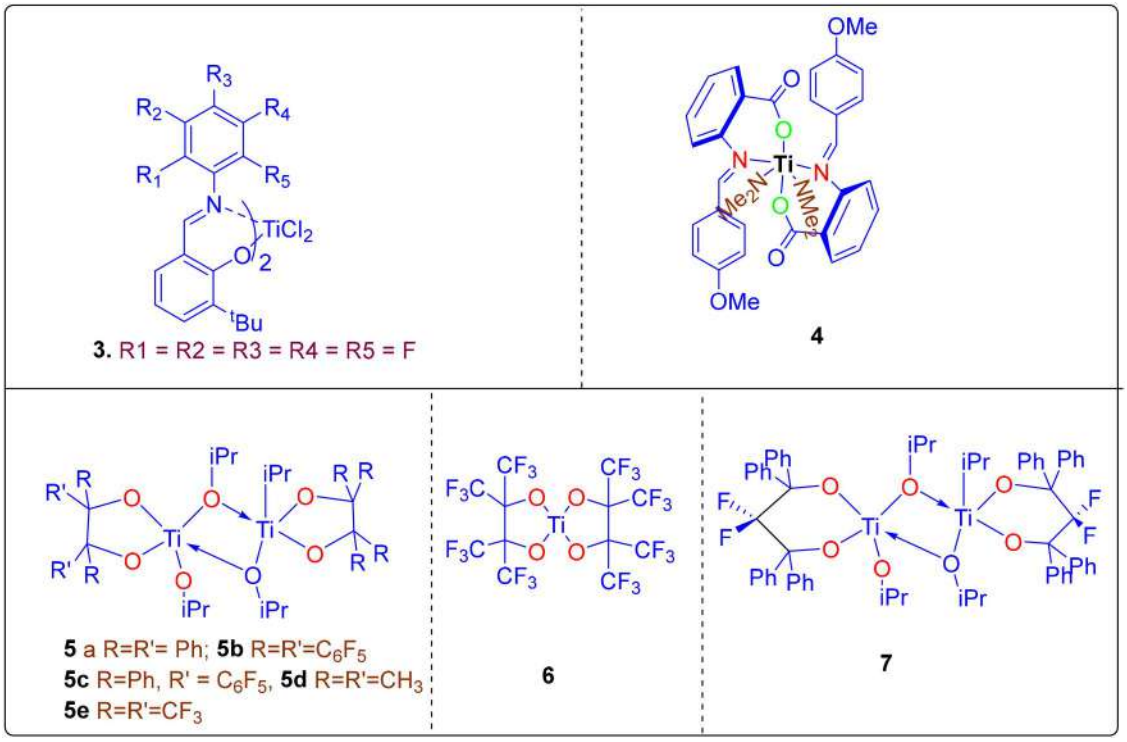

Figure 4. Ti-based catalysts for ethylene polymerization to UHMWPE.

catalyst. Rastogi, Romano, et al. have described the development of dUHMWPE in several reports.[30] The impact of the co-catalyst modification on the catalytic performance and material properties was investigated.[31] A similar investigation was carried out by employing catalyst **3** and other co-catalysts made of aluminoxane, modified methyl aluminoxane (MMAO12, MMAO3), and polymethyl aluminoxane (PMAO).[32] However, no discernible improvements in the properties of UHMWPE were observed. Using **3**/MAO to improve the polymerization conditions Ivanchev et al. and

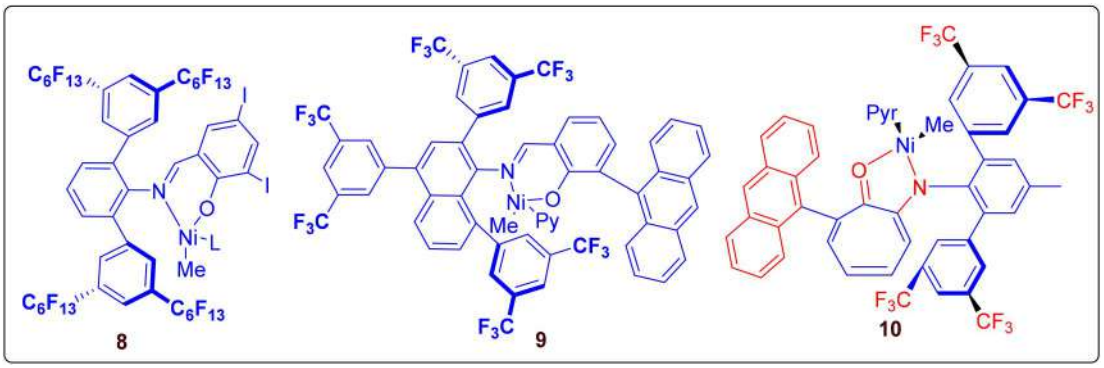

Figure 5. Ni-based catalysts 8–10 employed in ethylene polymerization to produce UHMWPE.

Forte et al. both reported the same information.[33,34] The effects of catalyst concentration and solvent type (toluene), on the catalytic activity, molecular weight, and shape of the resulting UHMWPE were meticulously examined.

Disentangled UHMWPE offers several advantages over entangled UHMWPE. This includes the ability of dUHMWPE to be treated and pulled with ease throughout a large temperature range below the equilibrium melting point. Disentangled UHMWPE showed better tensile strength, higher tensile modulus, and the ability to draw biaxially without any solvent.[35] The polymerization of ethylene with **3**/MAO (1100 equiv. of MAO) in toluene was carefully controlled by Rastogi et al. in an additional effort to reduce the number of entanglements. The authors thoroughly investigated the effect of experimental parameters, including temperature, time, and solvent volume, on the final entanglement number and molecular weight. The molecular weight and number of entanglements per unit chain revealed an increase/decrease as polymerization time increased. Consequently, it is opined that the majority of the entanglements are generated in the early stages of the polymerization process. The catalyst activity spanned from 620 to 10,330 kg of PE (mol Ti).h^{-1}. Along the same line, Rastogi et al. made an effort to stabilize the disentangled state of UHMWPE by adding linear low-density polyethylene (LLDPE) to the reaction mixture to prevent UHMWPE aggregation/entanglement.[36] It was demonstrated that the LLDPE can prevent entanglements and stabilize UHMWPE in a disentangled state.

Tuskaev et al. synthesized $[OOOO]^{4-}$ ligated titanium complexes **5**, **6**, **7** (Figure 4) for ethylene polymerization using cheaper co-catalysts (Et_2AlCl/Bu_2Mg or $Et_3Al_2Cl_3/Bu_2Mg$).[37] The resulting dUHMWPE exhibited Mn of $(0.34–7.73) \times 10^6$ g · mol^{-1}, a melting temperature of 136–144 °C, and crystallinity of 59–80%. The catalysts demonstrated high activity of $(0.24–4.05) \times 10^6$ g PE · $mol^{-1}Ti{\cdot}h^{-1}{\cdot}bar^{-1}$. The synthesized UHMWPE showed a broad PDI range of 3.3–11.5, highlighting the multi-center nature of these catalysts. Catalysts **6** and **7** maintained stable catalytic activity and polymer molecular weight increased with increasing temperature from 30 to 80 °C, indicating high thermal stability. The titanium concentration in the solvent was considerably higher (1.66–10.00 µmol Ti/100 mL toluene) compared to previous studies. The synthesized UHMWPE exhibited excellent solid-phase processing performance, with draw ratios of 20–44, tensile strength of 1.83–2.81 GPa, tensile modulus of 85–145 GPa, and breaking elongation of 1.96–3.09%. However, it still fell short compared to solid-phase processed dUHMWPE obtained from "living" FI catalysts.

Recently, Chikkali et al. reported Ti-iminocarboxylate complex **4** and its performance in ethylene polymerization (Figure 4).[38] The titanium precursor tetrakis (dimethyl amido-titanium) $[Ti(NMe_2)_4]$ was treated with 2 equivalents of 2-((4-methoxybenylidene) amino) benzoic acid to give the new titanium complex **4** [bis-dimethyl amido-Ti-(bis-mono-carboxylate)] in good yield. Complex **4** was activated using various cocatalysts and MMAO (modified methyl aluminoxane) outperformed the others. The best polymerization conditions were determined by screening the polymerization parameters. Thus, the optimal conditions were found to be an Al/Ti ratio of 1000, 4 bar ethylene pressure, 35 °C temperature, and a polymerization period of 30 min. Catalyst **4** polymerizes ethylene to ultrahigh molecular weight polyethylene with a weight average molecular weight (Mw) of 2.5×10^6 g/mol under the optimal polymerization conditions. The thus prepared UHMWPE revealed a high crystallinity of 96% and the existence of strictly linear polyethylene. A specially created DSC method unambiguously ascertained the existence of a disentangled state of UHMWPE. Sun et al. reported aroylhydrazine-arylolates ligated vanadium(V) complexes as catalysts for the synthesis of ultra-high molecular weight polyethylene (UHMWPE).[39] When the vanadium complex was activated with MAO, the resultant polymer revealed a molecular weight (Mw) of 3300 kg/mol and qualifies to be considered as UHMWPE.

There has been a substantial increase in the number of reports on nickel-catalyzed synthesis of high molecular weight and ultra-high molecular weight polyethylene (UHMWPE).[40–43] In 2019, Mecking et al. employed water-soluble catalysts (**8**) (Figure 5) in the mini emulsion coordination polymerization of ethylene to UHMWPE.[44] This approach enabled the synthesis of UHMWPE within oil droplets dispersed in an aqueous phase. The catalysts exhibited remarkable "living" characteristics, including a narrow molecular weight distribution ($M_w/M_n < 1.4$), minimal branching (up to 1.0 branch/1000C), and nearly one nickel center per chain. Interestingly, the nascent UHMWPE formed aggregates consisting of lozenge-shaped single crystals with a size distribution of <100 nm. This finding

challenges the conventional notion that polyethylene aggregates primarily consist of spherulites or lamellae. The nascent UHMWPEs demonstrated typical disentangled UHMWPE properties, such as a higher melting point (140–143 °C) and higher crystallinity (64–73%) as compared to the melt crystallized component (melting point of 133–136 °C and crystallinity of 41–48%). Along the same line, **Cat.9** (Figure 5) was found to have a low propensity for β-H elimination, as a result, **Cat.9** produced a highly linear polymer even at high temperatures (60 °C).[45] The UHMWPE was produced in polar organic solvents (THF and diethyl ether), the molecular weight was around 1.1×10^6 g/mol, and $M_w/M_n = 1.2$. Wang et al. reported a neutral, sandwich-like, salicylaldiminato nickel catalyst consisting of 8-arylnaphthyl and dibenzos beryl groups.[46] It was found that the above catalyst, in polar solvents, at a high temperature of 90 °C, enables controlled, living ethylene polymerization and produces nearly linear UHMWPE ($M_w = 6020$ kDa, $M_w/M_n = 1.10$). A UHMWPE with a molecular weight of 1002 kDa was obtained. To increase TOF and Mw in olefin polymerization, suppressing chain transfer and stimulating chain propagation is a crucial yet challenging task. The key to regulating these essential steps is designing a transition-metal catalyst, such as **10** (Figure 5).[47] Jian et al. employed **Cat.10** in ethylene polymerization, which produced a highly linear UHMWPE with a molecular weight of 212.4×10^4 g/mol and having 2 branches per thousand carbon atoms.

Thus, synthesis of entangled and disentangled UHMWPE is a challenging task and the field is being revived after the initial commendable contributions from Rastogi et al. The entangled UHMWPE is well explored and there are two commercial grades produced by DSM (Dyneema) and Honeywell (Spectra). While the disentangled UHMWPE is a new kid on the block with great potential. The disentangled UHMWPE has attracted significant attention in the recent past. The commercial exploitation of dUHMWPE has begun and the first announcement to introduce dUHMWPE in the market was made by "Teijin Aramid" around 2015. The company offers a dUHMWPE grade named "Endumax®." Thus, the field of dUHMWPE is witnessing revived interest in the academic and industrial world and is bound to grow in the coming years.

3. Copolymerization of ethylene with disubstituted difunctional olefins

Commodity polyethylenes, such as LDPE, LLDPE, and HDPE are made up of ethylene repeating units which are highly hydrophobic in nature. It does not contain any functional group in its backbone. The lack of functional groups in the PE backbone limits its application in printing inks, adhesives, paints, binders, dyeing, etc.[12] While catalyst development is crucial, it is equally important to explore the insertion copolymerization of "novel monomers" with added features, functionality, and purpose.[7] Incorporating a small amount of functional groups in the polymer backbone can open up new avenues for polyethylene applications. Insertion copolymerization of disubstituted olefins with ethylene offers an opportunity to double the functional group density in the polymer backbone while incorporating the same number of olefins. This increased functional group density can result in enhanced adhesion, even with the same incorporation. However, compared to mono-substituted olefins, 1,1- and 1,2-disubstituted olefins pose significant challenges for metal-catalyzed insertion copolymerization. The additional substitution in disubstituted olefin increases steric hindrance around the double bond, thereby reducing the coordination ability of the olefin.

The classical Zeigler-Natta type catalysts use early transition metals which are highly oxophilic in nature. Due to the high oxophilicity of early transition metals (such as Ti, Zr), the functional group on polar monomer coordinates to the vacant site on metal which poisons the catalyst. Various strategies, such as post-functionalization of PE,[48] OMRP of polar vinyl monomers with ethylene,[49] or ADMET polymerization of functionalized dienes have been developed.[50] Nevertheless, these methods have their own advantages and limitations. Therefore, it has been a dream for organometallic chemists to incorporate functional groups in the PE backbone in a single step. There are three features associated with this transformation that hinder the insertion of polar monomer and makes it a challenging task.[7] (i) One of the main obstacles is the coordination of the functional group on the polar monomer with the metal to form an σ-complex. This coordination often results in catalyst poisoning and decreases the overall activity of the catalyst. (ii) The electron-deficient nature of functional olefin leads to the formation of a weak π-complex compared to ethylene, resulting in lower or no incorporation of polar monomer into the polymer backbone. (iii) The formation of a stable chelate complex after the insertion of polar monomer or β-X elimination represents the final bottleneck. The late transition metals are less oxophilic in nature and more tolerant to the polar groups. Late transition metals, such as Pd and Ni have been widely employed in ethylene, functional olefin copolymerization. A breakthrough was reported in the early 90s when Brookhart et al. copolymerized ethylene and methyl acrylate.[51] The rationally designed α-diimine ligated Pd-complex (Figure 6(A)) successfully achieved the insertion copolymerization of ethylene with methyl acrylate for the first time. Along with variation in late transition metal, ligand designing to tolerate functional groups was explored. The major catalytic systems that have been tested in ethylene-functional-olefin copolymerization are depicted in Figure 6. Out of these, the most successful system is *ortho*-phosphinobenzenesulfonate or Drent catalyst **C**. The ligand consists of a neutral phosphine donor and an anionic sulfonate group that coordinates with the metal. This unique ligand structure makes the palladium complex tolerate a wide range of functional groups.[52]

As compared to mono-functional olefin, the use of disubstituted difunctional olefin increases the complexity by one order of magnitude. Due to this uphill task, only a handful of research groups have taken on the cumulative challenge posed by disubstituted difunctional olefins and have made

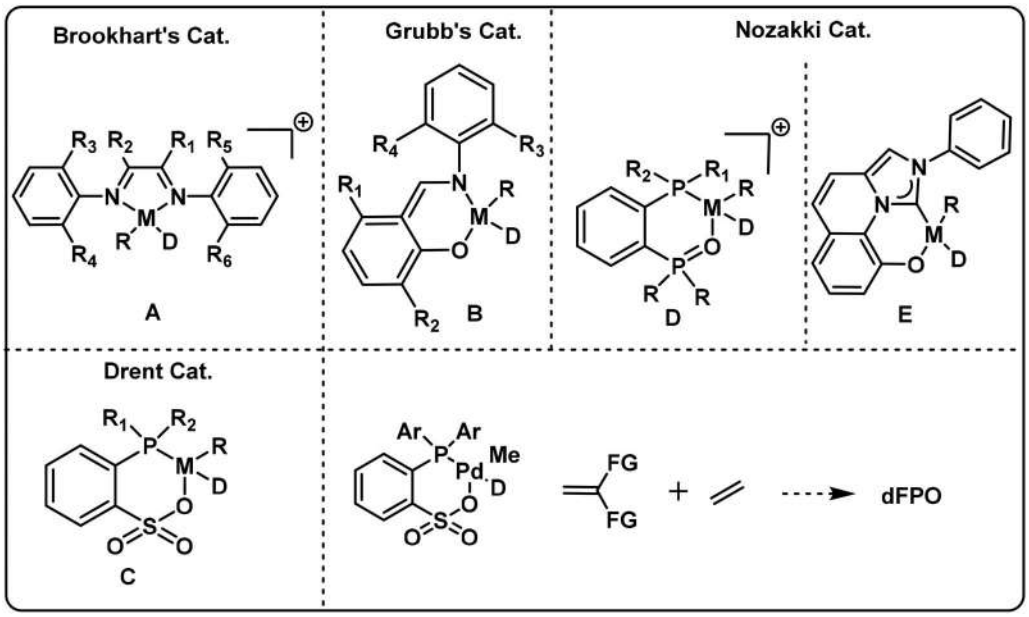

Figure 6. Typical catalysts for polar functional olefin insertion copolymerization.

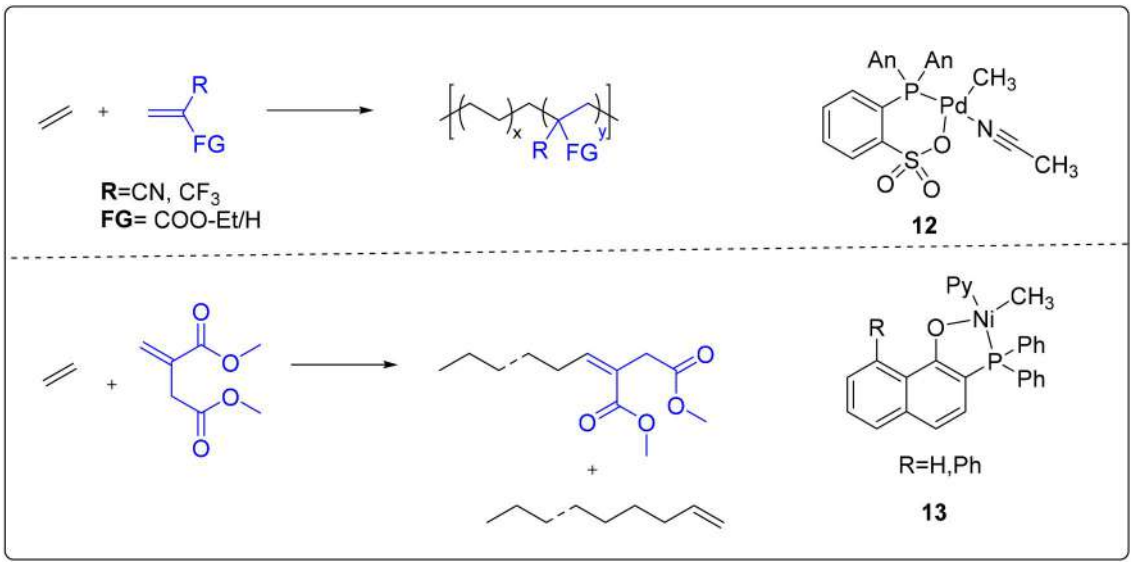

Figure 7. Insertion copolymerization of ethylene with 1,1-disubstituted difunctional olefin.

progress in this area. Among all the catalysts, the phosphine sulfonate system's exceptional performance further raised scientific hopes, and the following research concentrated on the catalyst's structural fine-tuning. Three major sites were identified, and substantial research has been done on the impact of the donor group "D" in each of them.[53] 1,1-disubstituted olefins can be further divided into two groups based on the number of functional groups: (i) di-substituted monofunctional olefins, and (ii) di-substituted difunctional olefins. The first report on the insertion copolymerization of 1,1-disubstituted difunctional olefins appeared in 2015.[12] The authors reported the synthesis of Pd-phosphinobenzene sulfonate acetonitrile complex (**12**) (Figure 7) and its implications in the insertion copolymerization of ethylene with 1,1-disubstituted difunctional vinyl monomers (see Figure 6; dFPO-difunctional polyolefin). The effectiveness of catalyst **12** in the copolymerization of ethylene with difunctional olefin was examined. The commonly known "Krazy glue" contains a monomer called ethyl-2-cyanoacrylate (ECA), has cyano- and acrylate- groups, and was chosen as a model 1,1-disubstituted difunctional olefin. It should be noted that cyanoacrylates are frequently marketed under the name "Super Glue" and their polymers are commercial adhesives. It is one of the most widely made adhesives worldwide. At 95 °C, the Pd-catalyst **12** (Figure 7) catalyzed the copolymerization of ethylene with ECA and disclosed the highest incorporation of 6.5%. The existence of the copoly(ethylene-ECA) was unambiguously ascertained using a combination of 1-2D NMR, GPC, and MALDI-TOF-MS.

Insertion copolymerization of another 1,1-disubstituted difunctional monomer, trifluoromethyl acrylic acid (TFMAA) was investigated and an incorporation of 3% was achieved.

The resultant copolymer was fully characterized using spectroscopic and analytical methods. After the initial success, Chikkali et al. investigated the insertion mechanism of 1,1-disubstituted functional olefins, and a comprehensive understanding of the mode of insertion of the disubstituted difunctional olefin was reported in 2017 (Figures 8(A,B)).[54] The methyl 2-acetamidoacrylate (MAAA) can undergo 1,2 insertion to produce **15** and **15′**, while 2,1 insertion can yield **16** and **16′**. The authors observed 1,2 and 2,1-insertion products **15** and **16**, respectively. Product **15** was isolated and fully characterized, including single-crystal X-ray diffraction. A similar study for TFMAA insertion produced only 2,1-insertion product **18**. The way polar vinyl monomers are inserted into a metal–carbon bond involves striking the right balance between electronic effects and steric constraints. Careful tuning of these parameters can allow access to 1,2-insertion products or the insertion can be reversed to 2,1-insertion.[55]

The above investigation provides direct evidence for the insertion of MAAA and TFMAA, which allowed the authors to install these into the polymer backbone without difficulty. The researchers also examined the polymerization of ethylene with several difunctional olefins, including MAAA and TFMAA, and discovered that dimethyl allyl malonate (DMAM) had the highest incorporation (11.8%). By monitoring the water contact angle, the researchers assessed how the surface characteristics of the copolymers changed after the incorporation of difunctional olefins into the polyethylene backbone. With a reduced water contact angle of 76°, the copolymer containing maximum DMAM incorporation was found to be the most hydrophilic.

In 2018, Nozaki et al. examined the insertion copolymerization of disubstituted functional olefins with ethylene (Figure 9).[56] The authors designed a new ligand named imidazo[1,5-*a*]quinolin-9-olate-1-ylidene (IzQO) and prepared the corresponding palladium complex **20** (Figure 9). The complex **20** was found to be active in ethylene, 1,1-disubstituted functional olefin copolymerization, and produced statistical copolymers of ethylene and methyl methacrylate (MMA). The resultant copolymers were thoroughly characterized and the incorporation was determined. Further, the authors investigated the insertion mechanism and successfully isolated the MMA-inserted complex. Isolation of MMA inserted product suggests that complex **20** is amenable to the insertion of 1,1-disubstuted olefins. The isolated complex was exposed to ethylene and polyethylene with MMA chain-end was obtained. These investigations reaffirm that the insertion of 1,1-disubstituted difunctional olefin is feasible and holds great potential.

Later in 2020, the insertion copolymerization of various 1,1-disubstituted difunctional monomers was reported using

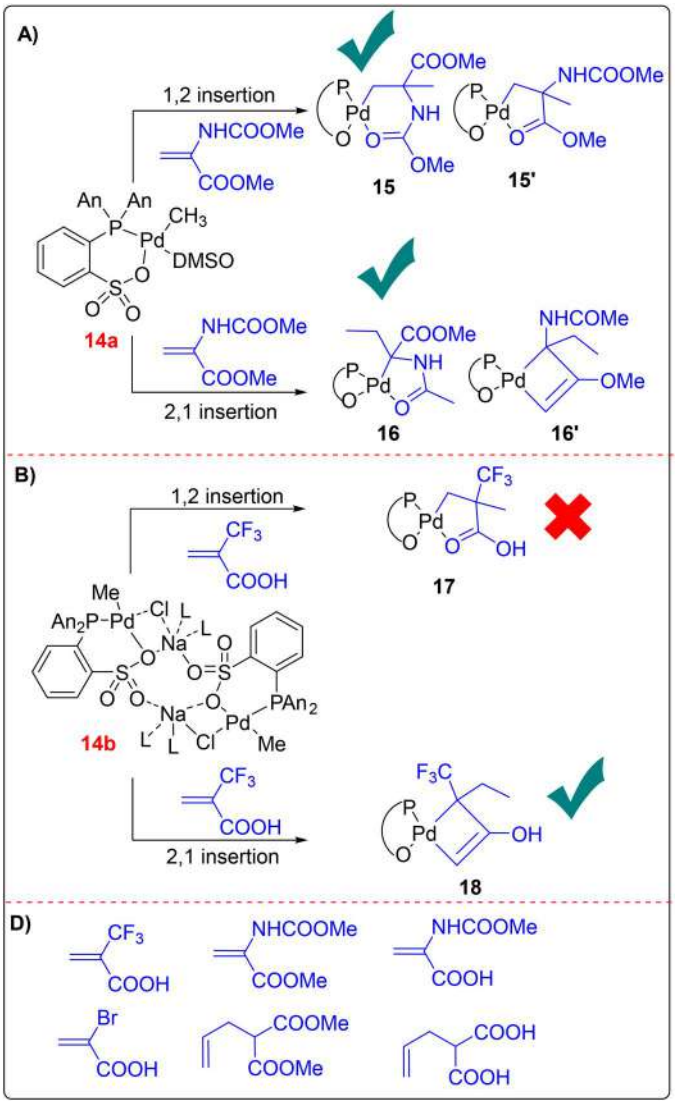

Figure 8. Possible insertion products of MAAA and TFMAA.

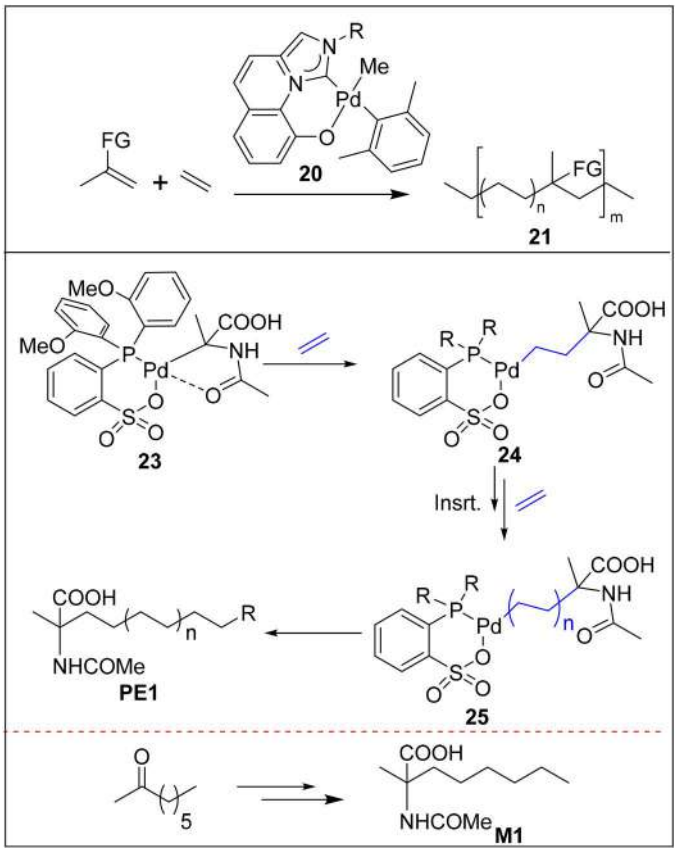

Figure 9. Insertion copolymerization of ethylene with methyl methacrylate catalyzed by imidazo[1,5-*a*]quinolin-9-olate-1-ylidene ligated Pd complex **20** (top) and insertion of 2-acetamidoacrylic acid and corresponding AAA functionalized PE1 (bottom).

phosphine sulfonate complex.[57] The article presents the challenges associated with the copolymerization of ethylene and disubstituted olefins through insertion or coordination mechanisms. Specifically, the researchers focused on difunctional olefins, such as 2-acetamido acrylic acid, methyl 2-acetamidoacrylate, and ethyl 2-cyanoacrylate. They demonstrated that these difunctional olefins can undergo ethylene insertion and polymerization when treated with a palladium complex called [{P^O}PdMe (L)]. The researchers were able to establish the presence of insertion intermediates (Figure 9 bottom) with moderate yields (up to 37%) and were successful in isolating and characterizing the corresponding products **23/24** (Figure 9 bottom). When **23** was exposed to ethylene, **PE1** was produced with 2-acetamido acrylic acid (AAA). This observation demonstrates that the AAA-inserted species is amenable to ethylene insertion and copolymerization. The existence of **PE1** was authenticated by preparing model compound M1 and comparing the NMR data. The research team combined experimental investigations with computational studies and presented a comprehensive understanding of the insertion of 1,1-disubstituted difunctional olefin copolymerization.

In 2021, Li et al. reported the design, synthesis, and characterization of a series of methyl nickel(II) complexes with phosphino-naphtholate chelate ligands (Figure 7, **13**).[58] These complexes exhibited high activity in ethylene polymerization and copolymerization with unsaturated acid ester and challenging 1,1-disubstituted difunctional polar monomers. The diphenylphosphino-8-phenylnaphtholate ligated nickel catalyst was optimized and displayed unprecedented activity for ethylene polymerization (3.0×10^7 g PE mol Ni^{-1} h^{-1}). The copolymers produced through this process consist of functional groups incorporated within the polymer chain as well as at the chain ends. Remarkably, end-functionalized polyethylene was directly obtained. The copolymerization of ethylene and 1,1-disubstituted difunctional dimethyl itaconate (Figure 7) was successfully conducted and up to 1.8 mol % incorporation was achieved. The ^{13}C NMR spectrum disclosed a signal at 145.6 and 125.9 ppm, which can be assigned to a carbon-carbon double bond (Figure 7), which is formed by the 2,1 insertion of dimethyl itaconate and subsequent β-hydride elimination.

Similar to 1,1 disubstituted olefin, 1,2-disubstituted olefins are equally challenging. In 2020, Chen et al. studied the copolymerization of ethylene with 1,2 di-substituted difunctional olefins (dimethyl fumarate and dimethyl maleate).[59] It was found that the trans isomer (dimethyl fumarate), could not be enchained but the cis isomer, or dimethyl maleate, was successfully inserted (1.1 mol%) into the polyethylene chain. Also, in recent study, copolymerization of difunctional olefins long spacers (5,6-disubstituted norbornenes) revealed high polymerization activity, copolymer molecular weight, and comonomer incorporation.[60]

4. Copolymerization of ethylene with bioderived/ renewable functional comonomer

Renewable resource-derived functional olefins are of current interest and are important for the sustainable future of the planet.[61] Therefore, in this section, we examine the recent developments in the area of insertion copolymerization of ethylene and bioderived/renewable functional monomers.

Miri et al. reported the copolymerization of ethylene with two bioderived comonomers, eugenol, and 4-penten-1-ol, using a palladium aryl phosphine sulfonate (**27**) catalyst in a toluene solution (Figure 10, top).[62] The co-polymerizations were carried out at 80 °C for 1 h, and the reactions were quenched with methanol. To characterize the resulting copolymers, various analytical techniques were employed. The ^1H and ^{13}C NMR analysis revealed that eugenol exhibited higher tolerance as compared to 4-penten-1-ol. Both co-monomers were predominantly inserted into the polymer chains rather than added as end groups. Despite the fact that the lengths between the terminal alkene group and the hydroxyl group are comparable in both monomers, the aromatic group works as a more effective spacer group. Eugenol is incorporated extensively into the copolymer chains by both 2,1 and 1,2 insertion mechanisms, whereas 4-penten-1-ol was mainly polymerized by 2,1-insertion and contributes significantly to end groups. Furthermore, the antibacterial efficiency of the copolymers was studied and it was observed that copolymers containing more than 3.1% eugenol exhibited a significant reduction in bacterial growth, surpassing 90%. These findings provide a new twist to known material and demonstrate the untapped potential functional polyolefins. Later in 2020 Chen et al. reported the synthesis of polymeric materials from renewable monomers, by using a phosphine-sulfonate palladium catalyst (**28**) (Figure 10).[63] Apart from copolymers of ethylene (E) with eugenol (Eug), terpolymers of E, Eug with other bioresourced comonomers were investigated. The copolymerization activity was found to decrease with the direct use of Eug-OH, but the use of protected comonomer, Eug-Si, improved copolymerization activity. Terpolymerization of ethylene with Eugenol and 1-hexene (Hex) displayed reduced molecular weight, while, E/Eug-Si/Hex terpolymer disclosed increased comonomer incorporation. The resulting terpolymer could be fully hydrolyzed to E/Eug-Si/Hex-HCl. Copolymers E/Eug (0.5) and E/Eug-Si(0.5) showed ductile behavior, while hydrolyzed E/Eug-Si(0.5)-HCl revealed improved stress-at-break. In addition, the introduction of Fe^{3+} ions enhanced mechanical properties, especially in Fe^{3+} functionalized E/Eug-Si(0.1)/Hex-HCl-Fe^{3+} terpolymer. Chain flexibility and Fe^{3+} catechol interactions played vital roles in improving polymer properties. By incorporating eugenol and catechol functionality, the researchers observed improvements in the mechanical properties of the resulting polyolefin materials. The influence of metal ions on these materials was investigated which led the authors to discover the self-healing properties of these co/ter-polymers. Additionally, the incorporation of catechol functionality allowed the authors to modulate the surface properties, adhesion, and compatibilizing capabilities in immiscible polyolefin blends. These findings highlight the potential of these bioresourced polymers in biomedical applications. Such an application of polyolefins was probably unthought of a few decades ago. Along the same line, Liu et al. synthesized functionalized isotactic poly(1-butene) (*i*PB)

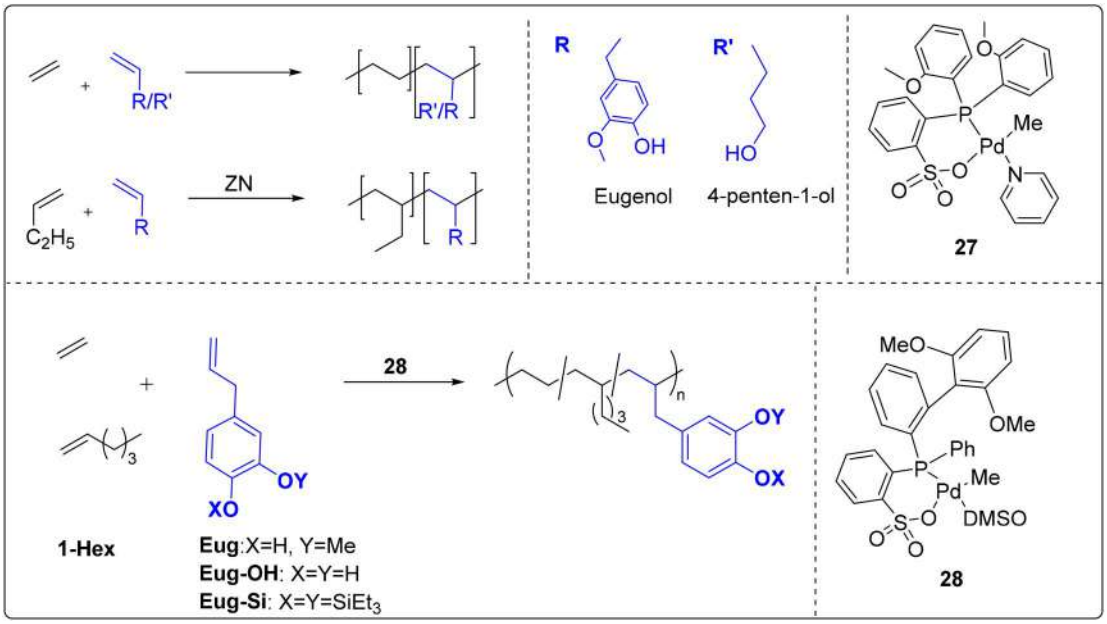

Figure 10. Ethylene copolymerization with eugenol and 4-penten-1-ol (top) terpolymerization of ethylene with 1-hexene and eugenol derivatives (bottom).

copolymers bearing natural antioxidant eugenol (Eug) using a Ziegler-type catalytic system.[64] By carefully adjusting comonomer concentration and reaction parameters, authors could successfully incorporate Eug units into the *i*PB chain, although the maximum incorporation was limited to only 0.62 mol%. The Eug-functionalized *i*PB copolymers show enhanced thermal-oxidative stability. This improvement in thermal stability is of great interest in various applications where heat and oxidation resistance are crucial factors. Remarkably, *i*PB copolymers with 0.62 mol% Eug units displayed an oxidation induction time (OIT) that was 25 times longer than that of copolymers without Eug. This substantial increase in OIT demonstrates the effectiveness of Eug units in retarding the oxidation process, effectively prolonging the lifespan of the copolymer.

Gao et al. reported the insertion copolymerization of petroleum-based ethylene and bio-based polar monomers.[65] The authors introduced a series of dibenzobarrelene-derived α-diimine palladium complexes (**30**) for the (co)polymerization of ethylene and bio-based furfuryl acrylate(FA) (Figure 11, top). Increasing the steric bulk on the ligand backbone enhanced the tolerance of palladium catalysts toward the polar monomer FA. This finding indicated that the structural modifications in the catalyst can improve its ability to accommodate polar monomers. Furthermore, the authors focused on the living (co)polymerizations of ethylene and furfuryl acrylate using the dibenzobarrelene-derived α-diimine palladium catalysts. A mechanistic study revealed that furfuryl acrylate inserts into a Pd–Me bond in a 2,1-mode, without any significant interactions between the furyl ring and the palladium center. The primary product undergoes rapid isomerization, leading to the formation of a six-membered chelate palladium complex. The incorporation of furan-based monomers in a polyethylene backbone offers the advantage of post-functionalization through thermoreversible Diels-Alder reactions.

Chikkali et al. investigated the insertion copolymerization of ethylene with various sugar-derived functional olefins (Figure 11, bottom).[66] The copolymerization reactions were carried out using a Pd-phosphinesulfonate acetonitrile catalyst (Figure 11, **31**). The renewable functional monomers, such as isomannide mono-ene (SDa), isosorbide mono-ene (SDb), isoidide mono-ene (SDc), and methacryl-2,3,4,6-tetra-O-acetyl-D glucopyranoside (SDd) were copolymerized with ethylene resulting into functional polyethylene. The copolymerization of ethylene with isosorbide mono-ene (SDb) and isoidide mono-ene (SDc), was performed at a high temperature of 95 °C which showed improved incorporations of 0.44 and 1.45%, respectively. The results indicate that the stereochemistry of the isohexide monomers influences their incorporation. The exo-endo and exo-exo configurations revealed better incorporation. Copolymerization of a 1,1-disubstituted functional olefin (SDd) and a tri-functional allyl monomer (SDe) resulted in relatively low incorporations of 0.48 and 0.41%, respectively. The copolymers exhibited melting temperatures ranging from 117 to 126 °C. The water contact angle of the copolymer derived from SDc with the maximum incorporation was 104°, indicating improved hydrophilicity.

Jian et al. successfully synthesized bio-based monomers through a carefully designed telomerization process (Figure 12).[67] By employing 1,3-butadiene and three renewable alcohols, namely furfuryl alcohol, tetrahydrofurfuryl alcohol, and solketal, the team was able to produce three distinct 2,7-octadienyl ether monomers, namely OC8-FUR, OC8-THF, and OC8-SOL (Figure 12). These novel monomers possessed intriguing structural features, consisting of a terminal double bond, an internal double bond, and a terminal polar cyclic group in a linear molecule. After preparing the renewable polar monomers, the authors examined the insertion copolymerization of OC8 with ethylene in the presence of phosphine–sulfonate palladium catalysts (**27**, **28**, **32**). This strategic choice enabled the successful creation of polar-

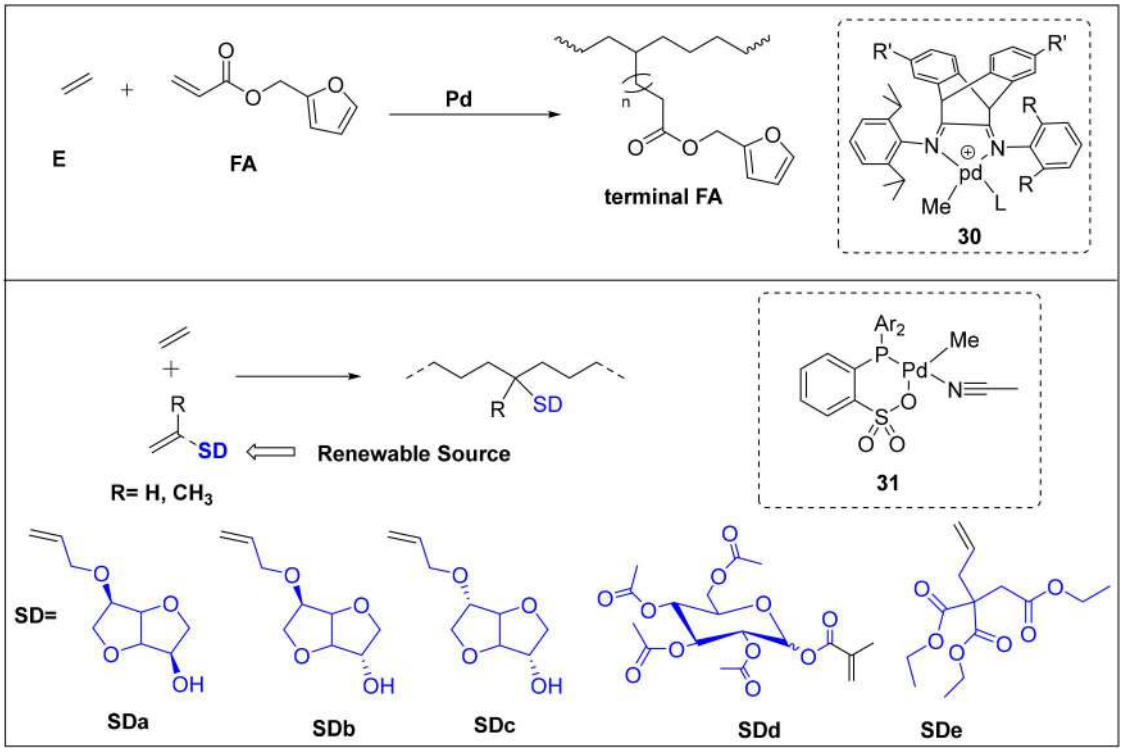

Figure 11. Copolymerization with ethylene and furfuryl acrylate (FA) with α-diimine palladium catalyst (**30**) (top) and insertion copolymerization of sugar-derived functional olefins with ethylene (bottom).

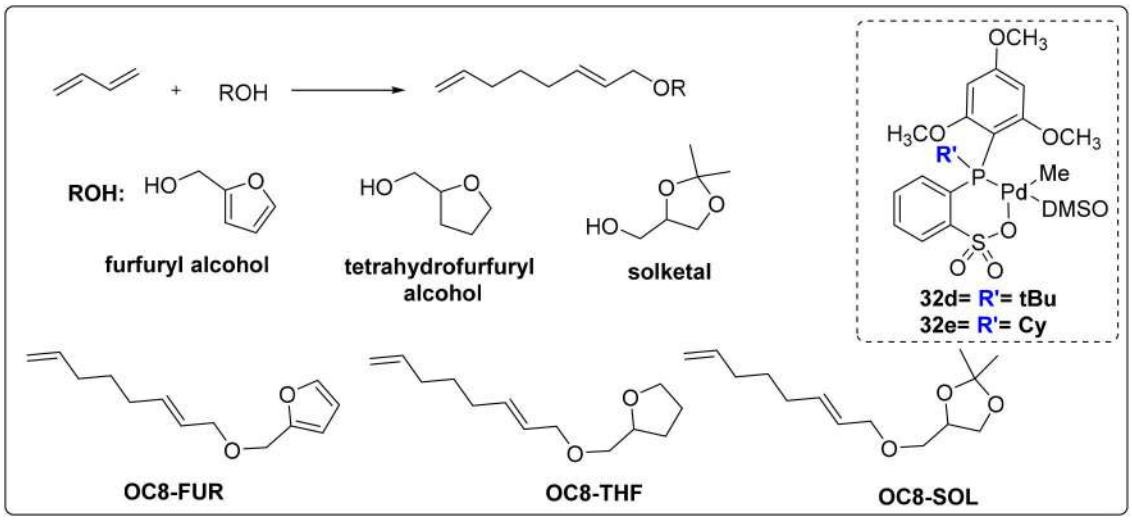

Figure 12. Synthesis of bio-derived 2,7-octadienyl ether monomers and copolymerization with ethylene.

functionalized polyethylenes with improved properties. Analysis of the resultant copolymers using NMR revealed linear structures with the incorporation of long-side chains. These side chains exhibited a unique combination of allyl ether units and polar cyclic groups, conferring the copolymers with enhanced functional motifs. These copolymers displayed superior strain-at-break as compared to non-polar polyethylene. Among the various copolymers synthesized, the one with the incorporation of 0.3 mol% OC8-FUR monomers, revealed exceptional performance. It exhibited the highest strain-at-break of 940% and a remarkable stress-at-break of 35.9 MPa.

Chen et al. reported the synthesis of polar functionalized polyolefins with high biomass content through insertion copolymerization reactions.[68] Two bioresourced oleyl and cinnamyl groups were installed on a norbornyl ring and were incorporated into polyolefins using phosphine-sulfonate palladium catalysts (**33** and **34**) (Figure 13). The use of a norbornene-based comonomer in the reaction allows efficient copolymerization with ethylene, resulting in high catalytic activities, polymer molecular weights, and comonomer incorporations. Additionally, the presence of internal carbon-carbon double bonds in the biomass groups provides reactive sites for vulcanization, which can enhance the tensile strength of the copolymers. The carbon-carbon double bonds also enable the creation of reversible dynamic cross-linked networks, for remodeling applications. The copolymerization results show that the choice of catalyst (**33** and

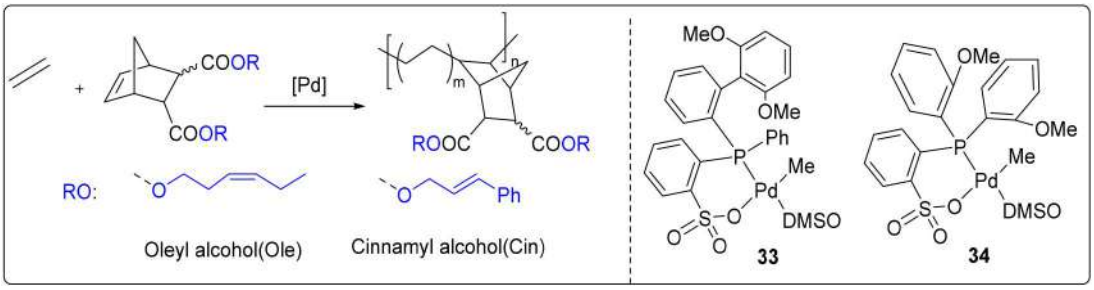

Figure 13. Copolymerization of ethylene with bioresourced disubstituted norbornene-based comonomers using phosphine-sulfonate palladium-catalysts.

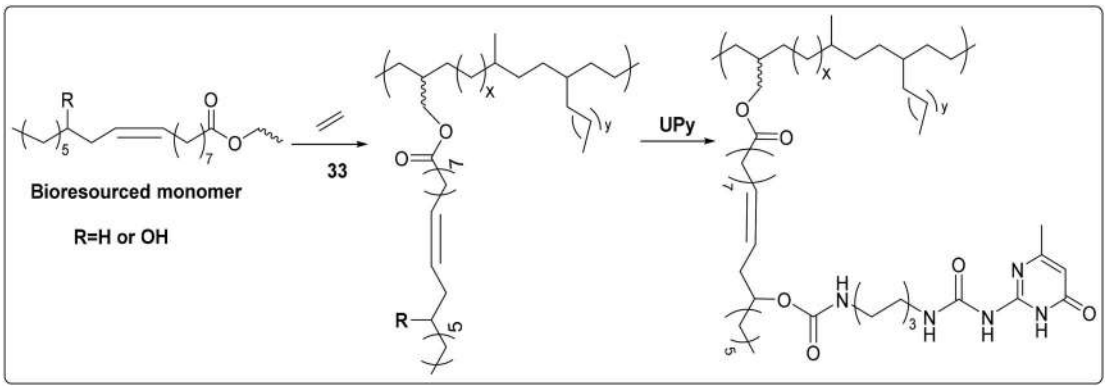

Figure 14. The bioresourced comonomers copolymerization with ethylene with phosphine-sulfonate palladium catalyst **33**.

34) and comonomer configuration (endo or trans) influences the copolymerization outcome. The trans-configurations of the comonomers lead to higher activities, comonomer incorporations, and copolymer molecular weights as compared to the endo-configurations. The sterically less bulky catalyst, **34** exhibits higher polymerization activities and comonomer incorporations.

Chen et al. reported direct insertion copolymerization of plant oils derived monomers with ethylene using a palladium catalyst (**33**) (Figure 14).[69] The researchers also examined the possibility of ureido-pyrimidinone (UPy) functionalization by leveraging the hydroxyl group in the polymer structure. The researchers could successfully tailor the surface and mechanical properties of the developed materials. These polymers effectively served as toughners for gutter oil, addressing waste management and environmental sustainability challenges. The UPy functionalization enabled a self-complementary hydrogen bonding network, allowing applications in multifunctional smart materials. The polar nature and exceptional elastic properties, render them highly suitable as toughening components in polymer blends. One of the standout features of UPy is its dynamic equilibrium nature, which engenders a polymer network with unconventional mechanical properties, such as strain rate dependence and remarkable mechanical damping. The diverse combinations and interactions of these properties hold immense potential for the development of novel applications. Furthermore, the optimization of the dynamic exchange of UPy promises to expand the horizons of polymer applications, unlocking greater possibilities and offering extensive application potential in various industries.

5. Functional polyolefins as compatibilizer

Polymer compatibilization refers to the process of improving the compatibility between two or more polymers that are immiscible or exhibit poor interfacial adhesion. The importance of polymer compatibilizer lies in its ability to enhance the performance and properties of polymer blends or composites. When two or more polymers are blended together, their individual properties can be combined to create a material with enhanced polymer characteristics. However, if the polymers are immiscible, phase separation and weak interfacial adhesion can occur, leading to a reduction in mechanical strength, toughness, and other properties. By introducing a compatibilizer, which is a third polymer or a reactive agent, the interfacial adhesion between the polymers can be improved, resulting in a homogeneous blend with enhanced properties. Polymer blends often face challenges during processing due to the differences in melt viscosity and melt temperature of the constituent polymers. Incompatibility can lead to phase separation, melt fracture, or poor dispersion of fillers, additives, or reinforcements. Compatibilization can help to overcome these issues by improving the melt flow, reducing melt viscosity mismatch, and promoting uniform dispersion, leading to better processability and stability of the blend.

The third application of compatibilizers is in plastic recycling. Compatibilizers can be added to different types of post-consumer polymers, such as polyethylene and polypropylene, to blend them together and create a recycled material with improved properties. This promotes the reuse of polymer waste and reduces the amount of plastic going to

landfills, contributing to a more sustainable and environmentally friendly approach to plastics. Overall, polymer compatibilization is essential for improving the processability, properties, and versatility of polymer blends.

Chen et al. reported the compatibilization of two immiscible polymers, such as polyethylene-isotactic polypropylene (PE-iPP) and polyethylene-polystyrene (PE-PS) using bis(phenylsulfonyl)ethylene (BPSE) (Figure 15).[70] The modified polyethylene samples (PE-gBPSE) were examined as a compatibilizer with polystyrene. The PE-PS ratio of 80/20 was used to obtain a binary blend, and PE/PE-g-BPSE/PS ratio of 78/8/18 was used to create a ternary blend (Figure 16). As evidenced in Figures 16(A,B), the PE/PS binary blend displayed significant voids (about 20–30 µm) that result from phase separation. Figure 16(B) shows a large cavity that may arise when small volumes of PS merge. The area outside of these cavities has a smooth and homogenous morphology indicating that they were formed from relatively pure PE. While, Figures 16(C,D) (PE/PE-g-BPSE/PS ternary blend) displayed a surface consisting of spherulites surrounded by amorphous regions, with no sizeable cavities. Thus, a significant enhancement in the blend's properties was achieved by the addition of the modified polymer.

Tang et al. reported the ethylene/styrene interpolymer (E-SI) as a compatibilizer for the LDPE/PS blends.[71] Polystyrene (PS) is a typical brittle polymer that exhibits high strength, high modulus, and excellent dimensional stability. It was highlighted that by fine-tuning the molecular structure of the compatibilizers, it is possible to produce PS/LDPE blends with finer phase structure and better mechanical properties. As a result of the compatibilization of PS/E-SI, LDPE/E-SI binary, and PS/LDPE/E-SI ternary blends the Izod impact strength and elongation at break were greatly improved. Adding 10 wt % E-SI improved the ductility and hardness of all blends. Along similar lines, Xie et al. reported the compatibilization of immiscible polypropylene/polystyrene and polypropylene/polyamide-6.[72,73] A multiphase compatibilizer (PP-g-(MAH-co-St) prepared from maleic anhydride (MAH) and styrene (St) monomers melt grafted on polypropylene(PP), was utilized. It is well known that a maleic anhydride (MAH) functional group can readily react with an amine end group of a polyamide, which leads to a significant improvement in the state of PA6 phase dispersion and particle size. The compatibilized blends exhibit very fine particle sizes and appear to have good interfacial adhesion between the phases.

Chen et al. reported the synthesis of high-molecular-weight polar-polyolefins using eugenol and related comonomers through the utilization of a sterically bulky phosphine-sulfonate palladium catalyst (**Cat.28**).[63] Because of the polar nature and good adhesion, these catechol-functionalized polyolefins can be a great candidate to serve as compatibilizers. E/Eug-Si(0.5)/Hex-HCl represents a polar counterpart of the widely used LLDPE material. Therefore, commercially available LLDPE ($Mn = 7.8 \times 10^4$) and PLA ($Mw = 1.0 \times 10^5$) were blended together using an internal mixer at a set temperature of 180 °C and with a rotor speed of 80 rpm, for 10 min. Clear phase separation was observed for this sample. The addition of 5 wt% E/Eug-Si(0.5)/Hex-HCl led to a more homogeneous distribution of the LLDPE and PLA. It was observed that the un-compatibilized LLDPE and PLA blend show reduced tensile strength and strain at break, but the addition of 5 wt% E/Eug-Si(0.5)/Hex-HCl improved the mechanical properties. Recently, Chen et al. reported polar functionalized polyethylenes containing ionic clusters and their composites.[74,75] The addition of these polyethylene composites with polar functional groups to the recycled waste HDPE/PET led to a significant enhancement in mechanical properties (Tensile-strength: from 17 ± 2 to 42 ± 2 MPa; Elongation at break: from 9 ± 2 to 17 ± 3%).

In 2023 Chikkali et al. reported the synthesis of hyperbranched functional ethylene oligomer (HBFO) as a compatibilizer for linear low density polyethylene (LLDPE) and Nylon-6.[76] As the HBFO contains a polar functional group (OH) and non-polar hydrophobic unit (methylene backbone), they can lend themselves to compatibilize two immiscible polymers (one polar and the other non-polar). The hydroxyl group in HBFO forms a hydrogen-bonding interaction with Nylon-6 (Figure 17(b)) and the alkyl chain mixes with LLDPE, leading to a compatible blend. The tensile test data shows that, while the un-compatibilized blend formulation displays a higher tensile strength, the compatibilized blend formulation displays equivalent Young's modulus and, more importantly, higher strain to failure vis-à-vis that for un-compatibilized blend formulation (Figure 17(a)). The toughness of the blends increases upon increasing the compatibilizer content and reaches an optimum at 5 wt%. The functionalized ethylene oligomer as a compatibilizer played an important role in creating a tough yet flexible blend formulation. The potential applications could be in the packaging sector requiring a good oxygen barrier property in addition to the water vapor barrier. SEM images

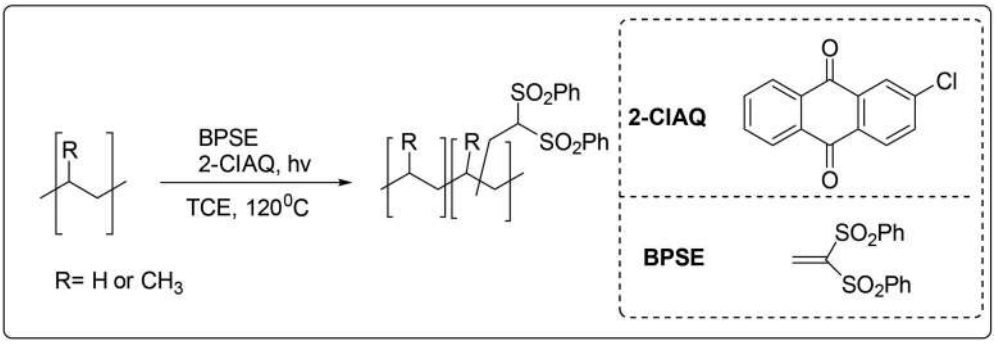

Figure 15. The preparation of modified polyethylene (HBPE/PE-g-BPSE) and isotactic polypropylene (iPP-*g*-BPSE).

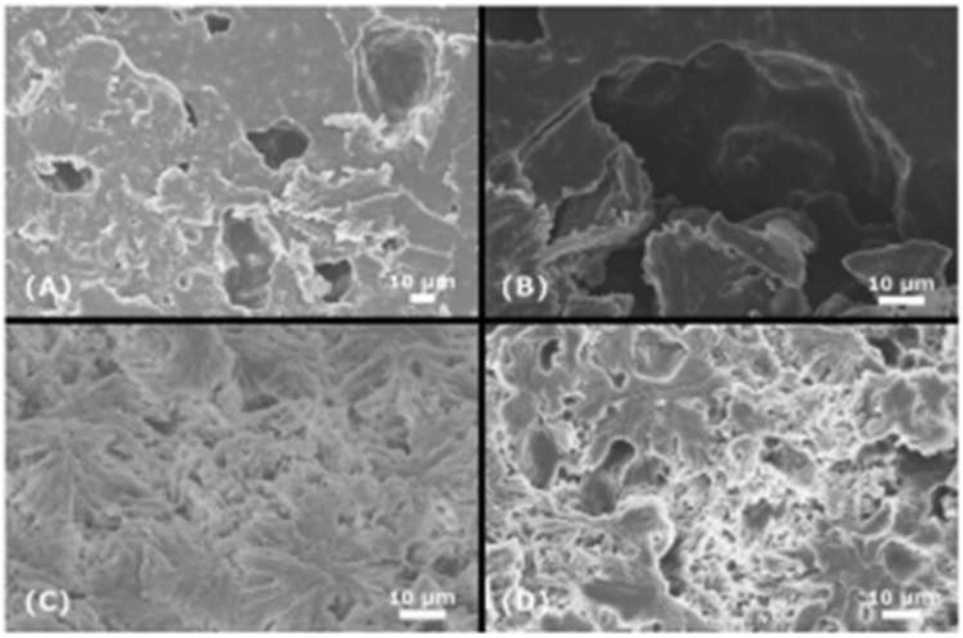

Figure 16. SEM Micrographs of fractured surfaces etched by acetone. (A,B) PE/PS (80/20), (C,D) PE/PE-g-BPSE/PS (74/8/18). Reproduced from Ref.[59] with permission from the Royal Society of Chemistry.

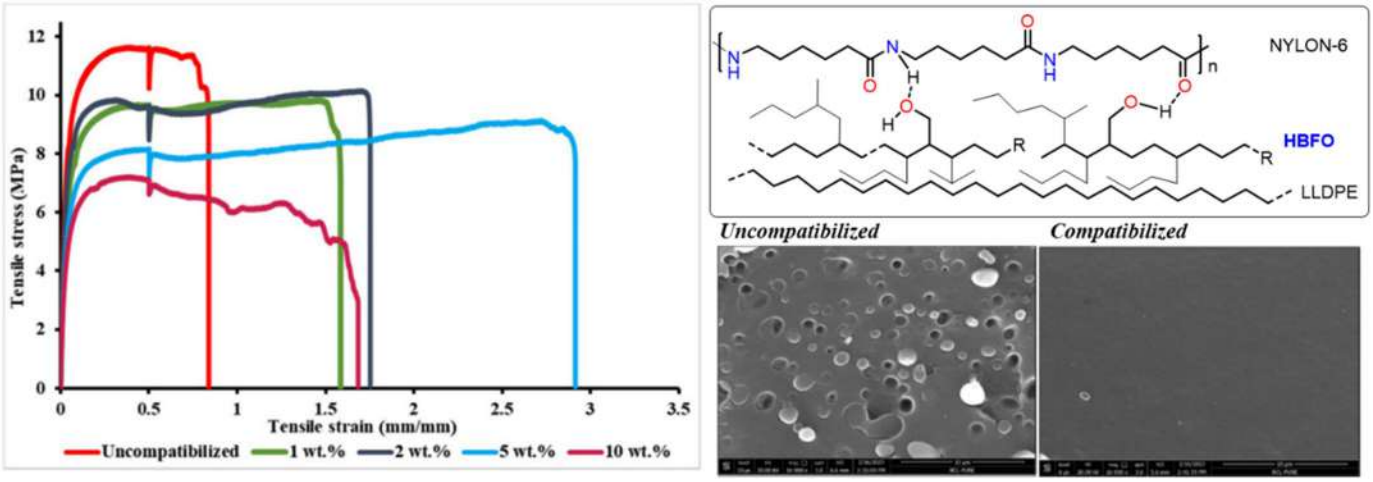

Figure 17. (a) Tensile plot for uncompatibilized and compatibilized blends. (b) Proposed hydrogen-bonding interaction between Nylon-6 and the HBFO F4. (c) SEM images of the un-compatibilized and compatibilized polymer blend.

(Figure 17(c)) clearly display a dispersed phase for compatibilized blends compared to the uncompatibilized blends.

Kumaraswamy et al. reported nanocomposites comprising polyethylene covalently grafted onto sheet-like silsesquioxanes by ring-opening metathesis polymerization (ROMP) of cyclooctene using the second-generation Grubbs catalyst.[77] This catalyst was covalently tethered to a sheet-like norbornenyl-Mg-silsesquioxane. The ROMP reaction led to the formation of poly(cyclooctene) chains. Subsequently, the poly(cyclooctene) chains were subjected to catalytic hydrogenation. The obtained polyethylene nano-composite shows extraordinary adhesion to metals and glass (Figure 18). The adhesion observed in this nanocomposite is ~100 times greater than that found in pure polyethylene and 10 times higher than what is typically observed in polyethylene copolymers or surfaces treated with corona treatment.

6. Conclusion and outlook

The feature article provides an overview of the recent developments in the area of olefin polymerization and pins down the four most impactful trends. These include (a) disentangled ultra-high molecular weight polyethylene (dUHMWPE), (b) disubstituted difunctional olefin copolymerization, (c) incorporation of bioderived comonomers in polyolefins, and (d) application of above (b, c) functional polyolefins as compatibilizers. The remaining challenges in

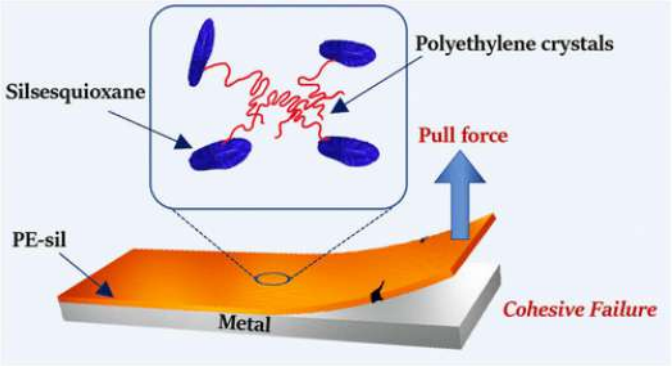

Figure 18. Adhesion property of polyethylene nanocomposite to metal. Reproduced with permission from Sharma et al.[77] Copyright 2023 American Chemical Society.

the insertion polymerization of ethylene to disentangled ultra-high molecular weight polyethylene (dUHMWPE) and the most successful catalytic systems to produce dUHMWPE have been discussed in detail. It turns out that, with suitable modification, even the Ziegler-type catalyst can produce dUHMWPE. While, homogeneous metallocene and post-metallocene catalysts produce dUHMWPE with much better activity, molecular weight, and polydispersity index (PDI). Characterization of dUHMWPE has been streamlined and rheology, DSC methods, and solid-state NMR can be employed to prove the existence of entangled *vs.* disentangled states of UHMWPE.

Insertion copolymerization of 1,1-disubstituted difunctional olefins offers a direct route to prepare hydrophilic polyethylene but remained a distant dream until 2015. The first report demonstrated that 1,1-disubstituted difunctional olefin, such as 2-ethyl cyanoacrylate can be inserted and incorporated into the PE chain. Subsequently, detailed mechanistic investigations have been reported by Chikkali and Nozaki groups, and access to functional polyethylene has been secured. The authors were able to isolate 1,2-inserted intermediates of MAAA and AAA. These intermediates were exposed to ethylene and produced end-functionalized (AAA) polyethylene. The scope has been expanded and about 10–12 disubstituted difunctional olefins have been incorporated in a polyethylene chain. Although the percentage incorporation is limited, the functional group density doubles and produces a hydrophilic polyethylene. Insertion copolymerization of bioresourced olefins with ethylene was almost missing from the scene until 2017. Several reports started surfacing in the recent past and insertion copolymerization of bioresourced olefins has been examined. Plant-derived molecules, such as catechol, isohexides, furfural, eugenol, oleic acid derivatives, etc. have been suitably modified and incorporated in polyethylene chains using late transition metal catalysts. Incorporation of these monomers increases the bio-content (green content) of the polyethylene and improves several properties, such as hydrophilicity, degradability, etc., and opens up new application avenues. The last part of the feature article delved into developing new applications for functional polyethylene. In this section, the use of functional polyethylene as a compatibilizer for two immiscible polymers was examined. As the reports suggest, the functional polyethylene can serve as a compatibilizer between a hydrophobic and a hydrophilic polymer. A polyethylene grafted on a sheet-like clay shows extraordinary adhesion to metals. The adhesion observed in this nanocomposite is ~100 times greater than that found in pure polyethylene.

Thus, the feature article captures the most significant developments in the area of polyolefins and debates the progress and future. As witnessed throughout the article, catalyst development has been at the core of the progress and it is anybody's guess that it will play a pivotal role in the coming years. The development of disentangled ultra-high molecular weight polyethylene has been driven by the catalyst discovery and tailoring of polymerization conditions. Teijin has already launched a grade "Endumax" that covers certain applications. It is anticipated that new applications will be developed and dUHMWPE will see spectacular growth in the years to come. A proof of concept for the insertion copolymerization of disubstituted difunctional olefins has been demonstrated. However, the activity and incorporations are still low. Therefore, focused efforts to increase the catalyst activity, incorporation of functional olefin, and molecular weight are necessary to meet the minimum threshold for any commercialization effort. It is reasonable to assume that new catalyst developments will drive this area and exploit the potential. The tried and tested recipe of ligand modification, steric and electronic tuning, etc. may not be sufficient and one may have to resort to a precise catalyst designing feature, such as hydrogen bonding, secondary interactions, etc. Insertion copolymerization of renewable monomers with ethylene opens up a completely new area of research. This does not merely incorporate the bioresourced monomers but also meets the growing demand to shift to sustainable polymers. These bioderived functional polyolefins disclose several properties, such as degradability that are uncommon for a regular polyolefin. The untapped potential of these bioresourced polyolefins will catalyze further research across academic and industrial laboratories. Application development for functional polyolefins has been on the back burner for decades. This could be due to the small volume of these functional polyolefins. However, with increasing demand for specialty polyolefins, there will be a renewed emphasis on application development and functional polyolefins will see the light of the day. Thus, this several decade-old field offers enough opportunities even today and is full of potential to meet future material demands.

Disclosure statement

No potential conflict of interest was reported by the author(s).

Funding

We gratefully acknowledge the financial support from DST-SERB (CRG/2021/005385), CSIR-NCL (HCP46), and DSIR (CRTDH@NCL)

India. RSB is thankful to DST for the DST-INSPIRE fellowship. DVB and PG are thankful to UGC for the fellowship.

Notes on contributors

Rajkumar Birajdar was born in 1996 in Maharashtra, India. He earned his Bachelor of Science degree in 2016 from C.B. Khedgi's College, Akkalkot, Maharashtra. Subsequently, in 2018, he attained a Master of Science degree from Solapur University, Maharashtra. During his Master's studies, he secured the first rank in the university for his field of study. His exceptional achievement led to him being honored with a gold medal in 2019, recognizing his outstanding academic performance. Rajkumar Birajdar was granted the DST-INSPIRE research fellowship in 2019. Following this, he joined to Dr. Samir H. Chikkali's group in National Chemical Laboratory, Pune, India to pursue his Ph.D. Currently, his research focus is in the field of designing and synthesizing ligands and it's corresponding metal catalyst for olefin (co)polymerization and he is also involved in the study of the de/re-polymerization processes of polyolefin.

Dnyaneshwar V. Bodkhe was born in Maharashtra, India. In 2013, he achieved his B.Sc. from S. B. College at Dr. B. A. M. U University. Following his M.Sc. at the same university, he became a part of Dr. Samir Chikkali's research team at CSIR-National Chemical Laboratory in Pune, India, taking on the role of a Junior Research Fellow (JRF) in July 2015. His current focus lies in the synthesis of ligands and early transition metal complexes for the purpose of UHMWPE synthesis.

Poonam Gupta was born in Haryana, India. Her academic journey began in Haryana, India, where she was born. She pursued her undergraduate studies and earned a B.Sc degree from IIS University, Jaipur, which she completed in 2016. After her bachelor's degree, Poonam Gupta pursued further education by enrolling in a Master of Science (M.Sc) program at the University of Delhi. In the year 2021, she achieved a significant accomplishment by clearing the National Eligibility Test (NET) for Junior Research Fellowship (JRF) with a remarkable rank of 91. Subsequently she joined the research group of Dr. Samir H. Chikkali at CSIR- National Chemical Laboratory, Pune, India, as a Junior Research Fellow (JRF) in 2021. Currently she is working on the design and synthesis of Transition metal catalyzed olefin-insertion copolymerization.

Maulali H. Shaikh was born in Solapur, India. He Completed his B.Sc. at D.B.F. Dayanand college of Arts and Science Solapur in (2018). After completing his M.Sc. at KBC- North Maharashtra University of Jalgaon, India, (2020). He joined the research group of Dr. Samir H. Chikkali at CSIR-National Chemical Laboratory Pune, India, As a Project Associate-I (2022). Currently he is working on the synthesis of ligands and early transition metal complexes for the ethylene polymerization.

Rohan V. Ramekar was born in Amravati, India. He completed his B.Sc. at Shri Shivaji Science College Amravati, affiliated with Sant Gadge baba Amravati University in 2020. After completing his M.Sc. at MIT-World Peace University, he joined the research group of Dr. Samir H. Chikkali at CSIR-National Chemical Laboratory Pune, India, As a Project Associate-I (2022). Currently he is working on the synthesis of ligands and early transition metal complexes for the ethylene polymerization.

Samir Chikkali earned his Ph.D. under the supervision of Prof. Dietrich Gudat from the University of Stuttgart, Germany. Subsequently, he did postdoctoral research with Prof. Joost Reek at the University of Amsterdam, the Netherlands, and Prof. Stefan Mecking at the University of Konstanz, Germany. In 2012 he returned to India and joined CSIR-National Chemical Laboratory (CSIR-NCL), Pune, to start his independent research career. He has guided 8 Ph.D. students, 6 post-docs, and 15 project assistants. Currently, he leads a team of 18 highly motivated researchers in organometallics, polyolefins, and renewable/degradable polymers. His honours and awards include a summer fellowship from the Indian Academy of Science, DPI (Dutch Polymer Institute) postdoctoral fellowship, AvH (Alexander von Humboldt) postdoctoral fellowship, the Ramanujan (DST) Fellowship, Best Scientist Award by North Maharashtra University, the Scientist of the Year Award 2016–2017 & 2022–2023 by NCL-RF, Young Associate of Maharashtra Academy of Sciences 2017, Professor Kaushal Kishore Memorial Award 2020 by Society of Polymer Science, India (SPSI), and 10th National Award 2020, by Ministry of Chemicals and Fertilizers, Government of India. He has published over 68 papers in international journals of high repute, he is an inventor on 11 patents and has edited a book on metal-catalyzed polymerization. He has served as guest editor of "Journal of Chemical Sciences" in the past (July 2018 issue) and has been appointed as an "Associate Editor" of "Bulletin of Materials Science" recently.

References

[1] Chikkali S. H., Ed. *Metal Catalyzed Polymerization: Fundamentals to Applications*; CRC Press; Taylor and Francis Group: Boca Raton, FL, 2017 and the references therein.

[2] Hustad, P. D. Frontiers in Olefin Polymerization: Reinventing the World's Most Common Synthetic Polymers. *Science* **2009**, *325*, 704–707. DOI: 10.1126/science.1174927.

[3] Severn, J. R.; Chadwick, J. C., Eds. *Tailor-Made Polymers*; Wiley-VCH Verlag GmbH & Co. KGaA: Weinheim, 2008.

[4] Sauter, D. W.; Taoufik, M.; Boisson, C. Polyolefins, a Success Story. *Polymers* **2017**, *9*, 185. DOI: 10.3390/polym9060185.

[5] Nakamura, A.; Ito, S.; Nozaki, K. Coordination-Insertion Copolymerization of Fundamental Polar Monomers. *Chem. Rev.* **2009**, *109*, 5215–5244. DOI: 10.1021/cr900079r.

[6] Patel, K.; Chikkali, S. H.; Sivaram, S. Ultrahigh Molecular Weight Polyethylene: Catalysis, Structure, Properties, Processing and Applications. *Prog. Polym. Sci.* **2020**, *109*, 101290. DOI: 10.1016/j.progpolymsci.2020.101290.

[7] Birajdar, R. S.; Chikkali, S. H. Insertion Copolymerization of Functional Olefins: Quo Vadis? *Eur. Polym. J.* **2021**, *143*, 110183. DOI: 10.1016/j.eurpolymj.2020.110183.

[8] Hippi, U. 2005. *Novel Functionalized Polyolefins as Compatibilizers in Polyolefin/Polyamide 6 Blends and Polyethylene/Metal Hydroxide Composites*; Helsinki University of Technology: Espoo, Finland.

[9] Anonymous. ASTM D4020-18, 2018. https://compass.astm.org/document/?contentCode=ASTM%7CD4020-18%7Cen-US&proxycl=https%3A//secure.astm.org&fromLogin=true (accessed Sep 2, 2023).

[10] Wu, S. L.; Qiao, J.; Guan, J.; Chen, H. M.; Wang, T.; Wang, C.; Wang, Y. Nascent Disentangled UHMWPE: Origin, Synthesis, Processing, Performances and Applications. *Eur. Polym. J.* **2022**, 184, 111799.

[11] Padmanabhan, S.; Sarma, K. R.; Rupak, K.; Sharma, S. Synthesis of Ultra High Molecular Weight Polyethylene: A Differentiate Material for Specialty Applications. *Mater. Sci. Eng. B* **2010**, *168*, 132–135. DOI: 10.1016/j.mseb.2009.10.026.

[12] Gaikwad, S. R.; Deshmukh, S. S.; Gonnade, R. G.; Rajamohanan, P. R.; Chikkali, S. H. Insertion Copolymerization of Difunctional Polar Vinyl Monomers with Ethylene. *ACS Macro Lett.* **2015**, *4*, 933–937. DOI: 10.1021/acsmacrolett.5b00562.

[13] Zou, C.; Tan, C.; Chen, C. Heterogenization Strategies for Nickel Catalyzed Synthesis of Polyolefins and Composites. *Acc. Mater. Res.* **2023**, *4*, 496–506. DOI: 10.1021/accountsmr.2c00263.

[14] Tan, C.; Zou, C.; Chen, C. Material Properties of Functional Polyethylenes from Transition-Metal-Catalyzed Ethylene–Polar Monomer Copolymerization. *Macromolecules* **2022**, *55*, 1910–1922. DOI: 10.1021/acs.macromol.2c00058.

[15] Zou, C.; Wang, Q.; Si, G.; Chen, C. A Co-anchoring Strategy for the Synthesis of Polar Bimodal Polyethylene. *Nat. Commun.* **2023**, *14*, 1442. DOI: 10.1038/s41467-023-37152-1.

[16] Chen, C. Designing Catalysts for Olefin Polymerization and Copolymerization: Beyond Electronic and Steric Tunning. *Nat. Rev. Chem.* **2018**, *2*, 6–14. DOI: 10.1038/s41570-018-0003-0.

[17] Guo, L.; Dai, S.; Sui, X.; Chen, C. Palladium and Nickel Catalyzed Chain Walking Olefin Polymerization and Copolymerization. *ACS Catal.* **2016**, *6*, 428–441. DOI: 10.1021/acscatal.5b02426.

[18] Chen, Z.; Brookhart, M. Exploring Ethylene/Polar Vinyl Monomer Copolymerizations Using Ni and Pd–α-Diimine Catalysts. *Acc. Chem. Res.* **2018**, *51*, 1831–1839. DOI: 10.1021/acs.accounts.8b00225.

[19] Mecking, S.; Schnitte, M. Neutral Nickel (II) Catalysts: From Hyper Branched Oligomers to Nano-Crystal Based Materials. *Acc. Chem. Res.* **2020**, *53*, 2738–2752. DOI: 10.1021/acs.accounts.0c00540.

[20] Tan, C.; Chen, M.; Chen, C. 'Catalyst + X' strategies for Transition Metal-Catalyzed Olefin-Polar Monomer Copolymerization. *Trends Chem.* **2023**, *5*, 147–159. DOI: 10.1016/j.trechm.2022.12.007.

[21] Tan, C.; Chen, C. Emerging Palladium and Nickel Catalysts for Copolymerization of Olefins with Polar Monomers. *Angew. Chem. Int. Ed.* **2019**, *58*, 7192– 7200. DOI: 10.1002/anie.201814634.

[22] Lippits, D. R.; Rastogi, S.; Talebi, S.; Bailly, C. Formation of Entanglements in Initially Disentangled Polymer Melt. *Macromolecules* **2006**, *39*, 8882–8885. DOI: 10.1021/ma062284z.

[23] Gote, R. P.; Mandal, D.; Patel, K.; Chaudhuri, K.; Vinod, C. P.; Lele, A. K.; Chikkali, S. H. Judicious Reduction of Supported Ti Catalyst Enables Access to Disentangled Ultrahigh Molecular Weight Polyethylene. *Macromolecules* **2018**, *51*, 4541–4552. DOI: 10.1021/acs.macromol.8b00590.

[24] Talebi, S.; Duchateau, R.; Rastogi, S.; Kaschta, J.; Peters, G. W. M.; Lemstra, P. J. Molar Mass and Molecular Weight Distribution Determination of UHMWPE Synthesized Using a Living Homogeneous Catalyst. *Macromolecules* **2010**, *43*, 2780–2788. DOI: 10.1021/ma902297b.

[25] Collins Rice, C. G.; Buffet, J.-C.; Turner, Z. R.; O'Hare, D. Supported Permethylindenyl Titanium Catalysts for the Synthesis of Disentangled Ultra-High Molecular Weight Polyethylene (Dis UHMWPE). *Chem. Commun.* **2021**, *57*, 8600–8603. DOI: 10.1039/D1CC03418A.

[26] Zhang, Z.; Kang, X.; Jiang, Y.; Cai, Z.; Li, S.; Cui, D. Access to Disentangled Ultrahigh Molecular Weight Polyethylene via a Binuclear Synergic Effect. *Angew. Chem.* **2023**, *135*, e202215582. DOI: 10.1002/ange.202215582.

[27] Saito, J.; Mitani, M.; Mohri, J.; Yoshida, Y.; Matsui, S.; Ishii, S.; Kojoh, S.; Kashiwa, N.; Fujita, T. Living Polymerization of Ethylene with Titanium Complex Containing Two Phenoxy-Imine Chelate Ligands. *Angew. Chem. Int. Ed.* **2001**, *40*, 2918–2920. DOI: 10.1002/1521-3773(20010803)40:15<2918::AID-ANIE2918>3.0.CO;2-S.

[28] Mitani, M.; Mohri, J.; Yoshida, Y.; Saito, J.; Ishii, S.; Tsuru, K.; Matsui, S.; Furuyama, R.; Nakano, T.; Tanaka, H.; et al. Living Polymerization of Ethylene Catalyzed by Titanium Complex Having Fluorine-Containing Phenoxy-Imine Chelate Ligands. *J. Am. Chem. Soc.* **2002**, *124*, 3327–3336. DOI: 10.1021/ja0117581.

[29] Rastogi, S.; Yao, Y.; Ronca, S.; Bos, J.; Van Der Eem, J. Unprecedented High-Modulus High-Strength Tapes and Films of Ultrahigh Molecular Weight Polyethylene via Solvent-Free Route. *Macromolecules* **2011**, *44*, 5558–5568. DOI: 10.1021/ma200667m.

[30] Yang, H.; van Ingen, Y.; Blom, B.; Rastogi, S.; Romano, D. Structural Modification of Phenoxyimine Titanium Complexes and Activation Studies with Alkyl Aluminum Compounds. *ChemCatChem* **2020**, *12*, 5209–5220. DOI: 10.1002/cctc.202000731.

[31] Romano, D.; Andablo-Reyes, E. A.; Ronca, S.; Rastogi, S. Effect of a Cocatalyst Modifier in the Synthesis of Ultrahigh Molecular Weight Polyethylene Having Reduced Number of Entanglements. *J. Polym. Sci. A Polym. Chem.* **2013**, *51*, 1630–1635. DOI: 10.1002/pola.26534.

[32] Romano, D.; Andablo-Reyes, E.; Ronca, S.; Rastogi, S. Aluminoxane Co-catalysts for the Activation of a Bis Phenoxyimine Titanium (IV) Catalyst in the Synthesis of Disentangled Ultra-High Molecular Weight Polyethylene. *Polymer* **2015**, *74*, 76–85. DOI: 10.1016/j.polymer.2015.07.039.

[33] Ivanchev, S. S.; Ruppel', E. I.; Ozerin, A. N. Optimization of the Conditions of Ethylene Polymerization into Reactor Powders of Ultra-High-Molecular-Weight Polyethylene Suitable for Solid-Phase Formation into Oriented Ultra-High-Strength and Ultra-High-Modulus Film Yarns. *Dokl. Phys. Chem.* **2016**, *468*, 89–92. DOI: 10.1134/S0012501616060026.

[34] Forte, G.; Ronca, S. Synthesis of Disentangled Ultra-High Molecular Weight Polyethylene: Influence of Reaction Medium on Material Properties. *Int. J. Polym. Sci.* **2017**, *2017*, e7431419. DOI: 10.1155/2017/7431419.

[35] Romano, D.; Tops, N.; Andablo-Reyes, E.; Ronca, S.; Rastogi, S. Influence of Polymerization Conditions on Melting Kinetics of Low Entangled UHMWPE and Its Implications on Mechanical Properties. *Macromolecules* **2014**, *47*, 4750–4760. DOI: 10.1021/ma5008122.

[36] Ronca, S.; Forte, G.; Ailianou, A.; Kornfield, J. A.; Rastogi, S. Direct Route to Colloidal UHMWPE by Including LLDPE in Solution during Homogeneous Polymerization of Ethylene. *ACS Macro Lett.* **2012**, *1*, 1116–1120. DOI: 10.1021/mz300369x.

[37] Tuskaev, V. A.; Gagieva, S. C.; Kurmaev, D. A.; Bogdanov, V. S.; Magomedov, K. F.; Mikhaylik, E. S.; Golubev, E. K.; Buzin, M. I.; Nikiforova, G. G.; Vasil'ev, V. G.; et al. Novel Titanium(IV) Diolate Complexes with Additional O-Donor as Precatalyst for the Synthesis of Ultrahigh Molecular Weight Polyethylene with Reduced Entanglement Density: Influence of Polymerization Conditions and Its Implications on Mechanical Properties. *Appl. Organom. Chem.* **2021**, *35*, e6256. DOI: 10.1002/aoc.6256.

[38] Bodkhe, D. V.; Chikkali, S. H. Ti-Iminocarboxylate Catalyzed Polymerization of Ethylene to Highly Crystalline, Disentangled, Ultrahigh Molecular Weight Polyethylene. *Eur. Polym. J.* **2023**, *182*, 111725. DOI: 10.1016/j.eurpolymj.2022.111725.

[39] Suo, H.; Faisca Phillips, A. M.; Satrudhar, M.; Martins, L. M. D. R. S.; da Silva, G. M. d F.; Pombeiro, A. J. L.; Han, M.; Sun, W.-H. Achieving Ultra-High Molecular Weight Polyethylenes by Vanadium Aroylhydrazine-Arylolates. *J. Polym. Sci.* **2023**, *61*, 482–490. DOI: 10.1002/pol.20220592.

[40] Tan, C.; Chen, C. Nickel Catalysts for the Synthesis of Ultra-High Molecular Weight Polyethylene. *Sci. Bull.* **2020**, *65*, 1137–1138. DOI: 10.1016/j.scib.2020.04.009.

[41] Liang, T.; Goudari, S. B.; Chen, C. A Simple and Versatile Nickel Platform for the Generation of Branched High Molecular Weight Polyolefins. *Nat. Commun.* **2020**, *11*, 372. DOI: 10.1038/s41467-019-14211-0.

[42] Zou, C.; Si, G.; Chen, C. A General Strategy for Heterogenizing Olefin Polymerization Catalysts and the Synthesis of Polyolefins and Composites. *Nat. Commun.* **2022**, *13*, 1954.

[43] Ma, Z.; Xu, M.; Zhu, N.; Tan, C.; Chen, C. Heterogeneous α-Diimine Nickel Catalysts with Improved Catalytic Performance in Ethylene Polymerization. *Chin. J. Chem.* **2023**, *41*, 1155–1162. DOI: 10.1002/cjoc.202200785.

[44] Schnitte, M.; Staiger, A.; Casper, L. A.; Mecking, S. Uniform Shape Monodisperse Single Chain Nanocrystals by Living

Aqueous Catalytic Polymerization. *Nat. Commun.* **2019**, *10*, 2592. DOI: 10.1038/s41467-019-10692-1.

[45] Kenyon, P.; Wörner, M.; Mecking, S. Controlled Polymerization in Polar Solvents to Ultrahigh Molecular Weight Polyethylene. *J. Am. Chem. Soc.* **2018**, *140*, 6685–6689. DOI: 10.1021/jacs.8b03223.

[46] Wang, C.; Kang, X.; Mu, H.; Jian, Z. Positive Effect of Polar Solvents in Olefin Polymerization Catalysis. *Macromolecules* **2022**, *55*, 5441–5447. DOI: 10.1021/acs.macromol.2c00472.

[47] Li, K.; Mu, H.; Kang, X.; Jian, Z. Suppression of Chain Transfer and Promotion of Chain Propagation in Neutral Anilinotropone Nickel Polymerization Catalysis. *Macromolecules* **2022**, *55*, 2533–2541. DOI: 10.1021/acs.macromol.2c00091.

[48] Boaen, N. K.; Hillmyer, M. A. Post-Polymerization Functionalization of Polyolefins. *Chem. Soc. Rev.* **2005**, *34*, 267. DOI: 10.1039/b311405h.

[49] Watson, M. D.; Wagener, K. B. Quantitative Ring-Closing Metathesis of Polyolefins. *Macromolecules* **2000**, *33*, 8963–8970. DOI: 10.1021/ma0010332.

[50] Kermagoret, A.; Debuigne, A.; Jerome, C.; Detrembleur, C. Precision Design of Ethylene and Polar Monomer-Based Copolymers by Organometallic Mediated Radical Polymerization. *Nat. Chem.* **2014**, *6*, 179–187. DOI: 10.1038/nchem.1850.

[51] Mecking, S.; Johnson, L. K.; Wang, L.; Brookhart, M. Mechanistic Studies of the Palladium-Catalyzed Copolymerization of Ethlyene and α-Olefins with Methyl Acrylate. *J. Am. Chem. Soc.* **1996**, *118*, 267–268.

[52] Nakamura, A.; Anselment, T. M. J.; Claverie, J.; Goodall, B.; Jordan, R. F.; Mecking, S.; Rieger, B.; Sen, A.; van Leeuwen, P. W. N. M.; Nozaki, K. Ortho-Phosphinobenzenesulfonate: A superb Ligand for Palladium-Catalyzed Coordination-Insertion Copolymerization of Vinyl Monomers. *Acc. Chem. Res.* **2013**, *46*, 1438–1449. DOI: 10.1021/ar300256h.

[53] Neuwald, B.; Olscher, F.; Gottker-Schnetmann, I.; Mecking, S. Limits of Activity: Weakly Coordinating Ligands in Arylphosphinesulfoanto Palladium (II) Polymerization Catalysts. *Organometallics* **2012**, *31*, 3128–3137. DOI: 10.1021/om3000339.

[54] Gaikwad, S. R.; Deshmukh, S. S.; Koshti, V. S.; Poddar, S.; Gonnade, R. G.; Rajamohanan, P. R.; Chikkali, S. H. Reactivity of Difunctional Monomers and Ethylene Copolymerization: A Comprehensive Account. *Macromolecules* **2017**, *50*, 5748–5758. DOI: 10.1021/acs.macromol.7b01356.

[55] Wucher, P.; Caporaso, L.; Roesle, P.; Ragone, F.; Cavallo, L.; Mecking, S.; Göttker-Schnetmann, I. Breaking the Regioselectivity Rule for Acrylate Insertion in the Mizoroki-Heck Coupling. *Proc. Natl. Acad. Sci. U.S.A.* **2011**, *108*, 8955–8959. DOI: 10.1073/pnas.1101497108.

[56] Yasuda, H.; Nakano, R.; Ito, S.; Nozaki, K. Palladium/IzQO-Catalyzed Coordination-Insertion Copolymerization of Ethylene and 1,1-Disubstituted Ethylenes Bearing a Polar Functional Groups. *J. Am. Chem. Soc.* **2018**, *140*, 1876–1883. DOI: 10.1021/jacs.7b12593.

[57] Gaikwad, S. R.; Patel, K.; Deshmukh, S. S.; Mote, N. R.; Birajdar, R. S.; Pandole, S. P.; Chugh, J.; Chikkali, S. H. Palladium-Catalyzed Insertion of Ethylene and 1,1-Disubstituted Difunctional Olefins: An Experimental and Computational Study. *ChemPlusChem* **2020**, *85*, 1200–1209.

[58] Wang, X.; Zhang, Y.; Wang, F.; Pan, L.; Wang, B.; Li, Y. Robust and Reactive Neutral Nickel Catalysts for Ethylene Polymerization and Copolymerization with a Challenging 1,1-Disubstituted Difunctional Polar Monomer. *ACS Catal.* **2021**, *11*, 2902–2911. DOI: 10.1021/acscatal.0c04450.

[59] Chen, M.; Chen, C. Direct and Tandem Routes for the Copolymerization of Ethylene with Polar Functionalized Internal Olefins. *Angew. Chem. Int. Ed.* **2020**, *59*, 1206–1210. DOI: 10.1002/anie.201913088.

[60] Xu, M.; Chen, C. A Disubstituted-Norbornene-Based Comonomer Strategy to Address Polar Monomer Problem. *Sci. Bull.* **2021**, *66*, 1429–1436. DOI: 10.1016/j.scib.2021.03.012.

[61] Pandey, S.; Rajput, B. S.; Chikkali, S. H. Refining of Plant Oils and Sugars to Platform Chemicals, Monomers and Polymers. *Green Chem.* **2021**, *23*, 4255–4295. DOI: 10.1039/D1GC00955A.

[62] Parisi, L. R.; Scheibel, D. M.; Lin, S.; Bennett, E. M.; Lodge, J. M.; Miri, M. J. Eugenol as Renewable Comonomer Compared to 4-Penten-1-Ol in Ethylene Copolymerization Using a Palladium Aryl Sulfonate Catalyst. *Polymer* **2017**, *114*, 319–328. DOI: 10.1016/j.polymer.2017.03.009.

[63] Na, Y.; Chen, C. Catechol-Functionalized Polyolefins. *Angew. Chem. Int. Ed.* **2020**, *59*, 7953–7959. DOI: 10.1002/anie.202000848.

[64] Cui, X.; Gu, G.; Li, C.; Liu, N.; Gong, Y.; Liu, B. Synthesis and Properties of Biomass Eugenol-Functionalized Isotactic Poly(1-Butene)S. *Polymer* **2020**, *202*, 122739. DOI: 10.1016/j.polymer.2020.122739.

[65] Du, C.; Zhong, L.; Gao, J.; Zhong, S.; Liao, H.; Gao, H.; Wu, Q. Living (Co)Polymerization of Ethylene and Bio-Based Furfuryl Acrylate Using Dibenzobarrelene Derived α-Diimine Palladium Catalysts. *Polym. Chem.* **2019**, *10*, 2029–2038. DOI: 10.1039/C9PY00126C.

[66] Rajput, B. S.; Pawal, S. B.; Bodkhe, D. V.; Rao, IN.; Sainath, A. V. S.; Chikkali, S. H. Renewing Polyethylene: Insertion Copolymerization of Sugar Derived Hydrophilic Monomers with Ethylene. *Eur. Polym. J.* **2020**, *134*, 109775. DOI: 10.1016/j.eurpolymj.2020.109775.

[67] Zong, Y.; Wang, C.; Zhang, Y.; Jian, Z. Polar-Functionalized Polyethylenes Enabled by Palladium-Catalyzed Copolymerization of Ethylene and Butadiene/Bio-Based Alcohol-Derived Monomers. *Polymers* **2023**, *15*, 1044. DOI: 10.3390/polym15041044.

[68] Xu, M.; Chen, A.; Li, W.; Li, Y.; Zou, C.; Chen, C. Efficient Synthesis of Polar Functionalized Polyolefins with High Biomass Content. *Macromolecules* **2023**, *56*, 1372–1378. DOI: 10.1021/acs.macromol.3c00086.

[69] Chen, J.; Wang, W.; Pan, Y.; Peng, D.; Li, Y.; Zou, C. Palladium-Catalyzed Synthesis of Oil-Based Functionalized Polyolefins. *Polym. Chem.* **2023**, *1*, 1103–1109. DOI: 10.1039/d3py00012e.

[70] Plummer, C. M.; Zhou, H.; Li, S.; Zhong, H.; Sun, Z.; Bariashir, C.; Sun, W. H.; Huang, H.; Liu, L.; Chen, Y. A Direct Functionalization of Polyolefins for Blend Compatibilization by an Insertion of 1,1-Bis (Phenylsulfonyl) Ethylene (BPSE). *Polym. Chem.* **2019**, *10*, 3325–3333. DOI: 10.1039/C9PY00599D.

[71] Tang, W.; Tang, J.; Yuan, H.; Jin, R. The Compatibilization Effect of Ethylene/Styrene Interpolymer on Polystyrene/Polyethylene Blends. *J. Polym. Sci. B Polym. Phys.* **2007**, *45*, 2136–2146. DOI: 10.1002/polb.21218.

[72] Wang, D.; Li, Y.; Xie, X. M.; Guo, B. H. Compatibilization and Morphology Development of Immiscible Ternary Polymer Blends. *Polymer* **2011**, *52*, 191–200. DOI: 10.1016/j.polymer.2010.11.019.

[73] Li, H.; Xie, X. M. Morphology Development and Superior Mechanical Properties of PP/PA6/SEBS Ternary Blends Compatibilized by Using a Highly Efficient Multi-Phase Compatibilizer. *Polymer* **2017**, *108*, 1–10. DOI: 10.1016/j.polymer.2016.11.044.

[74] Tan, C.; Zou, C.; Chen, C. An Ionic Cluster Strategy for Performance Improvements and Product Morphology Control in Metal-Catalyzed Olefin-Polar Monomer Copolymerization. *J. Am. Chem. Soc.* **2022**, *144*, 2245–2254.

[75] Li, J.; Peng, D.; Tan, C.; Chen, C. Outer-Shell Self-Supported Nickel Catalysts for the Synthesis of Polyolefin Composites. *Angew. Chem. Int. Ed.* **2023**, *62*, e202300359. DOI: 10.1002/anie.202300359.

[76] Birajdar, R. S.; Gonnade, R. G.; Pol, H. V.; Prabhu, B. M.; Rokade, D.; Nandimath, S.; Chikkali, S. H. Palladium Catalyzed Polar Solvent Empowered Synthesis of Hyper-Branched Ethylene Oligomers and Their Application. *Polym. Chem.* **2023**, *14*, 3239–3251. DOI: 10.1039/D3PY00311F.

[77] Sharma, V.; Paulbudhe, U.; Bachhar, N.; Chikkali, S. H.; Kumaraswamy, G. Polyethylene-Grafted Sheet-like Silsesquioxane Nanocomposites with Unprecedented Adhesion to Polar Substrates. *ACS Appl. Polym. Mater.* **2023**, *5*, 5972–5983. DOI: 10.1021/acsapm.3c00649.